Development of Alkali-Metal-Mediated Metallation: Advances with Potassium and Aluminium

by

Ben Conway

A thesis submitted to the Department of Pure and Applied Chemistry, University of Strathclyde, in part fulfilment of the requirements for the degree of Doctor of Philosophy.

February 2010

Acknowledgements

First and foremost I would like to thank Cassandra, who supported my desire to undertake a PhD project and who has constantly been a source of encouragement and wisdom throughout. Also, my mum, dad, brothers and sisters deserve a special mention as they are always there for me no matter what, which I appreciate immensely.

Another person I have a huge amount of thanks for is Professor Mulvey (Rab, as he's known in these parts!). I've known Rab since the 2nd year of my undergraduate studies when he kindly allowed me to undertake a summer placement within his research group. I have a great deal of respect for what he has achieved professionally, and I appreciate the fact that he strives to help you achieve your career goals, as long as you work hard for him in return of course!

Life would not be complete without Pablo (so he says, and I have to agree), but I have to say that throughout my time within Rab's research group, I've had the pleasure to be surrounded by a great bunch of people. Whether it's been the enjoyable lab banter, endless questions which make no sense (Ross), questionable attire (Liam) or crazy lookalikes (Stuart, Shaggy from Scooby Doo), everyone has made this experience unforgettable. Those members also include Matt (my favourite fatty undergraduate, apparently), Jan, Joaquin, Charlie, David, Ben F., Gemma, Sharon, Elaine, Emma and Zoe. I will miss our amazing "fimosis 5" and "los foyadores" football teams (three wins in sixteen games!), however, I will not miss Pablos flatulence problem (I'm pretty sure I've got diseases from him). Special mentions go to: Lorna, we'll always have New Orleans; Eva, my co-mentor who always has time for a wee chat; Allison, my source of guidance; and Vicki, after eight and a half years of being your sort of lab partner, I'm free!

Alan Kennedy, Luca Russo and Bill Clegg must also get a mention, as well as Pablo, Jan and Stuart, for the numerous X-ray analyses that they have made for me.

Finally, I would like to thank my higher chemistry teacher Mr Boal for his infectious excitement over chemistry, and his blunt career views, because if it wasn't for him I could have been a geologist!

Abstract

To date alkali-metal-mediated metallation (AMM*M*) chemistry has focused mainly on lithium and sodium methodologies. This project sought to develop the meagrely studied concepts of potassium-mediated zincation, magnesiation, and alumination.

Five potassium dialkyl TMP-zincate bases [PMDETA·K(μ-TMP)(μ-A)Zn(A)] {A = Me (**3a**), Et (**3b**), ^{i}Pr, ^{n}Bu, or ^{t}Bu (**3e**)} have been synthesised by a cocomplexation procedure. Reactions of **3b** with a series of substituted 4-R-pyridines (R = Me$_2$N, H, Et, ^{i}Pr, ^{t}Bu, Ph) gave 2-zincated products of formulation [{PMDETA·K[2-Zn(Et$_2$)-4-R-C$_5$H$_3$N]}$_2$] (**3j-3o**, respectively). X-ray crystallographic and NMR spectroscopic characterisation of **3j–3o** revealed a novel structural motif comprising a dianionic dihydroanthracene-like tricyclic ring with a central diazadicarbadizinca (NCZn)$_2$ ring, face-capped on either side by PMDETA-wrapped K$^+$ cations. All the new zincated pyridine complexes share this dimeric arrangement. **3b** selectively deprotonates 4-methoxypyridine at the 3-position affording a complex with a remarkably different, step-ladder structure *catena*-{PMDETA·K[3-Zn(Et)$_2$-4-MeO-C$_5$H$_3$N]}$_\infty$]. These studies established the importance of Zn–N bonds for efficient zincation.

Direct zincation of ferrocene (FcH) and ruthenocene (RcH) by the synergic base **3a** produced the monozincated complexes [PMDETA·K(μ-Me)$_2$Zn(Fc)]$_\infty$ and [{PMDETA·K(μ-Me)$_2$Zn(Rc)}$_2$] respectively. Dizincation of ferrocene can be achieved with base **3e** to yield the complex [THF·{(PMDETA)K}$_2$·(C$_5$\{1-Zn(^{t}Bu)$_2$\}H$_4$)Fe(C$_5$\{1′-Zn(^{t}Bu)$_2$\}H$_4$)].

Potassium-mediated magnesiation of anisole *via* [PMDETA·K(μ-TMP)(μ-CH$_2$SiMe$_3$)Mg(TMP)] was followed by a combination of X-ray crystallographic and NMR spectroscopic studies. Departing from the behaviour of other heteroleptic alkyl-amido bases, the reaction stops first at an *ortho*-magnesiated anisole intermediate with elimination of amine, but finally ends at an *ortho*-magnesiated anisole complex with reincorporatation of amine ligand and elimination of alkane.

Amide enriched ^{i}Bu$_2$Al(TMP)$_2$Li acts as a single-fold amido base towards TMEDA or PMDETA to afford [Li{Me$_2$NCH$_2$CH$_2$N(Me)CH$_2$}(TMP)Al(^{i}Bu)$_2$] and [Li{Me$_2$NCH$_2$CH$_2$N(Me)CH$_2$CH$_2$N(Me)CH$_2$}(TMP)Al(^{i}Bu)$_2$] respectively. Long utilised as a strong Brønsted base, the TMP anion converts to a Brønsted acid under the persuasion of a potassium aluminate KTMP, TMEDA, ^{i}Bu$_2$Al(TMP) mixture, in the most remarkable reaction of the project.

Publications

Papers arising from work carried out in this project

1. *Structurally Stimulated Deprotonation/Alumination of the TMP Anion*: B. Conway, A. R. Kennedy, R. E. Mulvey, and S. D. Robertson, *Angew. Chem. Int. Ed*. **2010**, DOI: 10.1002/anie.201000181.

2. *cis-2,6-Dimethylpiperidide: a structural mimic for TMP (2,2,6,6-tetramethylpiperidide) or DA (diisopropylamide*: R. Campbell, B. Conway, G. S. Fairweather, P. García-Álvarez, A. R. Kennedy, J. Klett, R. E. Mulvey, C. T. O'Hara, and G. M. Robertson, *Dalton Trans*. **2010**, *39*, 511.

3. *Potassium-mediated zincation of ferrocene and ruthenocene: potassium, the architect behind supramolecular structural variations:* W. Clegg, B. Conway, P. García-Álvarez, A. R. Kennedy, J. Klett, R. E. Mulvey, and L. Russo, *Dalton Trans*. **2010**, *39*, 62.

4. *Closer Insight into the Reactivity of TMP–Dialkyl Zincates in Directed ortho-Zincation of Anisole: Experimental Evidence of Amido Basicity and Structural Elucidation of Key Reaction Intermediates:* W. Clegg, B. Conway, E. Hevia, M. D. McCall, L. Russo, and R. E. Mulvey, *J. Am. Chem. Soc.* **2009**, *131*, 2375.

5. *Structural Tracking of the Potassium-Mediated Magnesiation of Anisole*: W. Clegg, B. Conway, P. García-Álvarez, A. R. Kennedy, R. E. Mulvey, L. Russo, J. Sassmannshausen, and T. Tuttle, *Chem. Eur. J.* **2009**, *15*, 10702.

6. *Structurally Defined Potassium-Mediated Zincation of Pyridine and 4-R-Substituted Pyridines (R = Et, iPr, tBu, Ph and Me$_2$N) by Using Dialkyl–TMP–Zincate Bases:* W. Clegg, B. Conway, D. V. Graham, E. Hevia, A. R. Kennedy, R. E. Mulvey, L. Russo, and D. S. Wright, *Chem Eur. J.* **2009**, *15*, 7074.

7. *Contacted Ion-Pair Lithium Alkylamidoaluminates: Intramolecular Alumination (Al–H Exchange) Traps for TMEDA and PMDETA:* B. Conway, J. García-Álvarez, E. Hevia, A. R. Kennedy, R. E. Mulvey, and S. D. Robertson, *Organometallics* **2009**, *28*, 6462.

8. *Tuning the Basicity of Synergic Bimetallic Reagents: Switching the Regioselectivity of the Directed Dimetalation of Toluene from 2,5- to 3,5- Positions:* V. L. Blair, L. M. Carrella, W. Clegg, B. Conway, R. W. Harrington, L. M. Hogg, J. Klett, R. E. Mulvey, E. Rentschler, and L. Russo, *Angew. Chem. Int. Ed.* **2008**, *47*, 6208.

9. *Alkali-Metal-Mediated Manganation(II) of Functionalized Arenes and Applications of ortho-Manganated Products in Pd-Catalyzed Cross-Coupling Reactions with Iodobenzene:* V. L. Blair, W. Clegg, B. Conway, E. Hevia, A. R. Kennedy, J. Klett, R. E. Mulvey, and L. Russo, *Chem. Eur. J.* **2008**, *14*, 65.

10. *Structurally-defined potassium-mediated regioselective zincation of amino- and alkoxy-substituted pyridines:* B. Conway, D. V. Graham, E. Hevia, A. R. Kennedy, J. Klett, and R. E. Mulvey, *Chem. Commun.* **2008**, 2638.

11. *Isolation and structural elucidation of a key aluminoaromatic intermediate and evidence for dismutation phenomena in TMP–alumination chemistry:* B. Conway, E. Hevia, J. García-Álvarez, D. V. Graham, A. R. Kennedy, and R. E. Mulvey, *Chem. Commun.* **2007**, 5241.

12. *Structurally-defined direct C-magnesiation and C-zincation of N-heterocyclic aromatic compounds using alkali-metal-mediated metallation:* B. Conway, E. Hevia, A. R. Kennedy, and R. E. Mulvey, *Chem. Commun.* **2007**, 2864.

Other papers from the author

13. *A Convenient Method to Aniline Compounds Using Microwave-Assisted Transfer Hydrogenation:* N. Chapman, B. Conway, F. O'Grady, and M. D. Wall, *Synlett* **2006**, 1043.

14. *Synthesis and characterisation of a series of alkylmagnesium amide and related oxygen-contaminated "alkoxy" compounds:* B. Conway, E. Hevia, A. R. Kennedy, R. E. Mulvey, and S. Weatherstone, *Dalton Trans.* **2005**, 1532.

Conference Presentations

1. *Alkali-Metal-Mediated Metallation: Application to Cross-Coupling Reactions.* Ben Conway and Robert E. Mulvey.

   Oral presentation at the 41st Universities of Scotland Inorganic Conference (USIC), The University of Edinburgh, 6-7th September 2007. Awarded prize for the best oral presentation.

2. *Alkali-Metal-Mediated Manganation(II) of Functionalized Arenes and Applications of Ortho-Manganated Products in Pd-Catalyzed Cross-Coupling Reactions with Iodobenzene.* Victoria L. Blair, William Clegg, Ben Conway, Eva Hevia, Jan Klett, Robert E. Mulvey, and Luca Russo.

   Poster presentation at the 41st Universities of Scotland Inorganic Conference (USIC), The University of Edinburgh, 6-7th September 2007. Awarded prize jointly with Victoria L. Blair for one of the best posters.

3. *New heterobimetallic chemistry of potassium: synthesis, structures and reactivity.* Ben Conway and Robert E. Mulvey.

   Poster presentation at the ACS Spring Meeting, New Orleans, USA, April 2008.

4. *Synergic Synthesis: Potassium-mediated Zincation.* Ben Conway and Robert E. Mulvey.

   Oral presentation at University of Strathclyde Inorganic Section Conference, Ross Priory, 13th June 2008.

5. *New heterobimetallic chemistry of potassium: synthesis, structures and reactivity.* Ben Conway and Robert E. Mulvey.

   Poster presentation at the 42nd Universities of Scotland Inorganic Conference (USIC), The University of Strathclyde, 11-12th September 2008.

Abbreviations

AMMAl	Alkali-Metal-Mediated Alumination
AMMM	Alkali-Metal-Mediated Metallation
AMMMg	Alkali-Metal-Mediated Magnesiation
AMMMn	Alkali-Metal-Mediated Manganation
AMMO	Alkali-Metal-Mediated Organotransitionmetallation
AMMZn	Alkali-Metal-Mediated Zincation
^{n}Bu	n-butyl
^{t}Bu	t-butyl
Bz	Benzyl
bcp	Bond critical point
CSD	Cambridge Structural Database
C_6D_6	Deuterated benzene
d_{12}-Cy	Deuterated cyclohexane
COSY	Correlated Spectroscopy
Cp	Cyclopentadienide
DA	Diisopropylamide
DA(H)	Diisopropylamine
DFT	Density Functional Theory
Dipp	Diisopropylphenyl
DMAE	Dimethylaminoethanol
DMAP	Dimethylaminopyridine
DMP	2,6-Dimethylpiperidide
DMP(H)	2,6-Dimethylpiperidine
DoM	Directed *ortho* Metallation
D_2O	Deuterated water
Et	Ethyl
HMDS	1,1,1,3,3,3-hexamethyldisilazide
HMDS(H)	1,1,1,3,3,3-hexamethyldisilazane
HMPA	hexamethylphosphoramide

HSQC	Heteronuclear Single Quantum Coherence
ICE	Inverse Crown Ether
KMMg	Potassium-mediated Magnesiation
KMZn	Potassium-mediated Zincation
LDA	Lithium Diisopropylamide
LICKOR	Alkyllithium/potassium alkoxide superbase
Me	Methyl
Mes	Mesityl
MMA	Methyl methacrylate
NMR	Nuclear Magnetic Resonance
NADP	Nicotinamide Adenine Dinucleotide Diphosphate
NBO	Natural Bond Orbital
^{n}Pe	neo-pentyl
Ph	Phenyl
PMDETA	*N,N,N',N'',N''*-pentamethylethylenediamine
PMP	2,2,4,6,6-pentamethylpiperidide
PMP(H)	2,2,4,6,6-pentamethylpiperidine
ppm	Part per million
^{i}Pr	*iso*-propyl
pyr	Pyridine
RMSD	Root Mean Square Deviation
THF	Tetrahydrofuran
TM	Transition Metal
TMCDA	*N,N,N',N'*-tetramethylcyclohexane-1,2-diamine
TMEDA	*N,N,N',N'*-tetramethylethylenediamine
TMP	2,2,6,6-tetramethylpiperidide
TMP(H)	2,2,6,6-tetramethylpiperidine
TMTAC	1,3,5-trimethyl-1,3,5-triazacyclohexane

Table of Contents

XIII

Chapter 1: Introduction to Organometallic Chemistry

1.1)   Background to s-Block Organometallics

Organometallic reagents, very occasionally referred to as organo-inorganics, metallo-organics or metalorganics, are defined as chemical compounds containing a direct bond between a carbon and a metal. These types of compounds combine aspects from both inorganic and organic chemistry and are a genre in their own right. The nature of the carbon-metal bond in these types of compounds is generally between ionic and covalent, with the carbon residing a negative charge and the metal holding a degree of positive character. In regard to s-block organometallic reagents, the metal is very electropositive and hence the metal-carbon bond becomes more ionic than covalent, especially more so in the case of the alkali-metals, and therefore these types of reagents are often referred to as the 'polar organometallic compounds'.

Wilhelm Schlenk, the man who pioneered the development of inert gas techniques to handle air-sensitive compounds, first reported the synthesis of organoalkali metal complexes in 1914.[1] This was soon followed up by his ground-breaking paper on the discovery of methyl-, ethyl- and phenyllithium in 1917, a landmark account which set the basis of modern organolithium chemistry.[2]

Slightly later in the 1930's, Gilman,[3,4] Wittig [5] and Ziegler [6] led a resurgence of the use of organolithium compounds after several years of relative neglect in the area. Organolithium compounds were found to be extremely useful in preparative chemistry, and the work of these scientists allowed the lithium-based reagents to reach the same status enjoyed by the earlier established, very important organomagnesium Grignard compounds (pioneered in 1900 by Victor Grignard, who shared the Nobel Prize for Chemistry in 1912 with Paul Sabatier "for the

discovery of the so-called Grignard reagent, which in recent years has greatly advanced the progress of organic chemistry").

It was not until the 1960's when the first definitive structural studies of organometallic complexes were made. The structure-reactivity relationship is key to understanding how organometallic compounds react with organic substrates, especially in the case of organolithium compounds. The knowledge of their molecular structures is crucial when elucidating reaction mechanisms and rationalising selectivities observed, hence structure-determining techniques are very useful in synthetic chemistry. It is also important to study the solvent adducts of these organometallic compounds as these reagents are typically used in solution.

1.2)   *Organolithium Compounds*

Organolithium reagents are perhaps the most utilised organometallic compounds in synthetic laboratories worldwide, both in industry, for the manufacture of fine chemicals and in academia, for all round general research purposes. These utility compounds have numerous applications, for example: as very successful deprotonating agents; as initiators for anionic polymerisation reactions; as nucleophilic addition agents for carbolithiations; and also as reagents for asymmetric synthesis.[7] A statistic to show the high regard for organolithiums can be found in the realm of natural product synthesis, where as many as 95% of natural product syntheses rely on the use of a lithium reagent at some stage of their development. Organolithiums, although very reactive in their own right, tend to be proportionately less reactive compared to organosodium or organopotassium compounds, making them relatively easier to handle. They are also soluble in common organic solvents, typically hydrocarbons for alkyllithium reagents and ethers for aryllithiums, and can be stored at subambient temperatures (to avoid self-mutilation and decomposition of the solvent, which their heavier alkali-metal congeners are prone to). These attractive attributes of organolithiums make them very useful to synthetic

chemists and, along with compounds such as Grignard reagents, have become the choice reagents for many organic and organometallic syntheses.

Based in the University of Jena, Germany, Schlenk and Holtz first prepared alkyl- and aryllithium compounds by reacting metallic lithium with dialkyl- or diarylmercury in a metal displacement reaction [Schlenk was nominated for the Nobel Prize for Chemistry twice, partly for his work in this area, however at the time of the first consideration (1918) of the award it was thought that the organolithium reagents would be too unstable to be of much use. He never won the prize in the end having come so close].[2] This highly challenging synthesis had its major drawback in the form of using exceptionally toxic mercury compounds. In 1930, Ziegler and Colonius discovered a less hazardous route to these types of organolithiums by pioneering the use of metallic lithium with organic halides.[6] Gilman modified this second route to organolithiums so that it was possible to synthesise secondary alkyl and tertiary-butyllithium reagents.[3,4]

In 1938, Wittig described one of the most significant finds in the pursuit of improving and broadening the scope of the synthesis of organolithium compounds. Thus, the lithium-halogen exchange reaction was introduced to the literature using the reagent phenyllithium, which is the simplest aryllithium compound.[5] This reaction provided the key to the synthesis of numerous aryl, vinylic and heterocyclic lithium reagents and the reaction has been studied in great detail ever since, resulting in its wide use in synthesis today.[8,9]

Currently there are three main methods to synthesise organolithium reagents (**figure 1.1**): i) deprotonation (lithiation or lithium-hydrogen exchange) reactions; ii) metal-halogen exchange; and iii) reductive elimination. Methods i and ii both require the use of an organolithium starting material to react with the substrate, usually an alkyllithium, whereas method iii requires lithium metal.
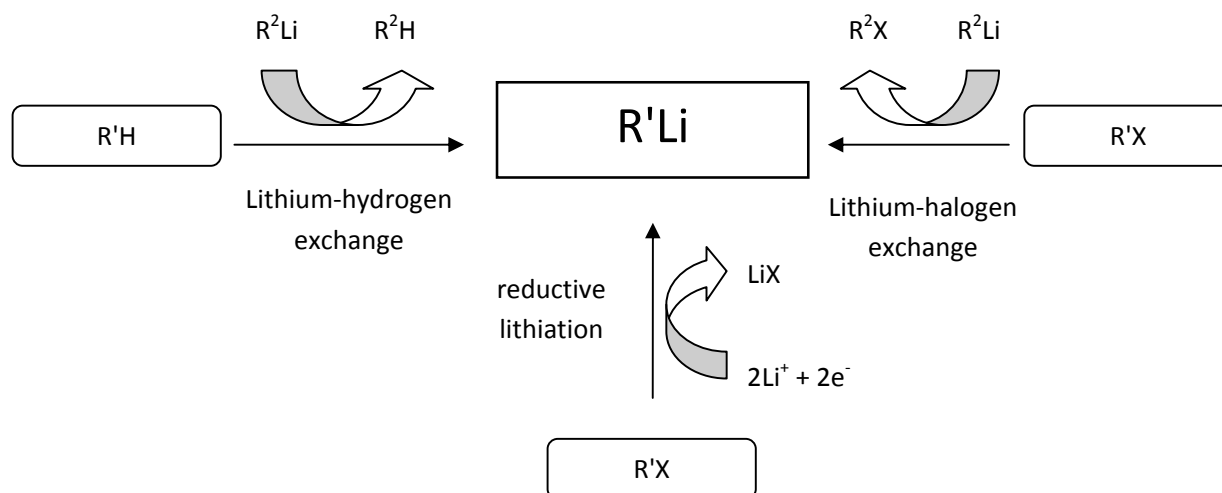
Figure 1.1: Three common methods of forming organolithium compounds.

Organolithium complexes are generally strong Brønsted bases. However, donor solvents and Lewis base adducts have a great effect on the extent of the basicity of these reactive compounds. For example, when *n*-butyllithium is reacted with benzene in tetrahydrofuran (THF) solution, the rate of the reaction is much faster compared to when diethyl ether is used as the solvent. Also, when TMEDA (TMEDA = *N,N,N',N'*-tetramethylethylenediamine) is added to a n-butyllithium/benzene reaction mixture, metallation of the arene is very fast.[7] Therefore, the study of the effect of donor molecules on the reactivity of organolithiums is of paramount importance.

To gather understanding behind the reactivity of these organolithium reagents, analysing the structures of these compounds, investigating their degree of aggregation and the extent of solvation are all vital to this process. The first structural data of organolithium reagents was provided in 1963 by Dietrich in the form of the solid-state characterisation of the tetramer ethyllithium, which was better refined two decades later.[10,11] Weiss followed this report a year later on the now classical structure of the smallest alkyllithium compound, the tetramer of methyllithium, $(MeLi)_4$.[12] In this predominately ionic compound, the $(MeLi)_4$ tetrahedra are linked to each other through $Li_3-C\cdots Li$ long range intermolecular contacts between the

4

carbanions and the lithium atom of an adjacent tetramer (**figure 1.2**). Due to the three-dimensional network produced by these intermolecular interactions, methyllithium has a low volatility. Ethyllithium, in comparison, has weaker contacts between the tetrahedra, and for organolithiums with larger organic units, this interaction is negligible, for example in the hexamer (^{n}BuLi)$_6$, which exists as a liquid.
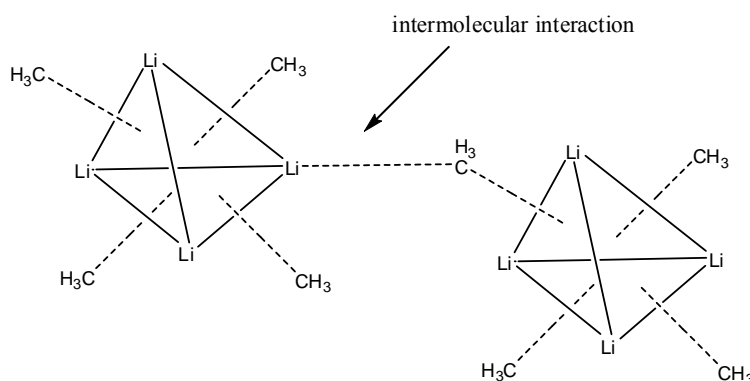
Figure 1.2: Intermolecular interaction between individual (MeLi)$_4$ tetrahedra to form the polymer [(MeLi)$_4$]$_\infty$.

As discussed within the next chapters of this thesis, the silyl-stabilised, neo-pentyl type ligand, trimethylsilylmethyl, Me$_3$SiCH$_2^-$, is an important component in the subsequent synthesis of several bases. Therefore, it is important to provide some background to it in this section. The molecular structure of trimethylsilylmethyllithium was elucidated by Oliver and co-workers in 1986 as the hexamer (LiCH$_2$SiMe$_3$)$_6$.[13] This organolithium reagent has excellent storage properties and can be utilised in silyl transfer reactions.[14,15] Recently, the deaggregation of trimethylsilylmethyllithium has been studied using a series of bi- and tri-dentate ligands (**figure 1.3**).[16] Using the bidentate ligands TMEDA and (-)-sparteine, hexameric (LiCH$_2$SiMe$_3$)$_6$ breaks down to the dimeric complexes (TMEDA·LiCH$_2$SiMe$_3$)$_2$ and [{(-)-sparteine}·LiCH$_2$SiMe$_3$]$_2$ respectively. However, the tridentate donor ligand PMDETA (PMDETA = *N,N,N',N'',N''*-pentamethyldiethylenetriamine) deaggregates the hexamer even further to produce the monomeric structure (PMDETA·LiCH$_2$SiMe$_3$). Investigations on these organolithium complexes found that the PMDETA-solvated monomer is more reactive compared to its dimeric counterparts due to the improved accessibility of the carbanion and the lithium atom.[17-19]
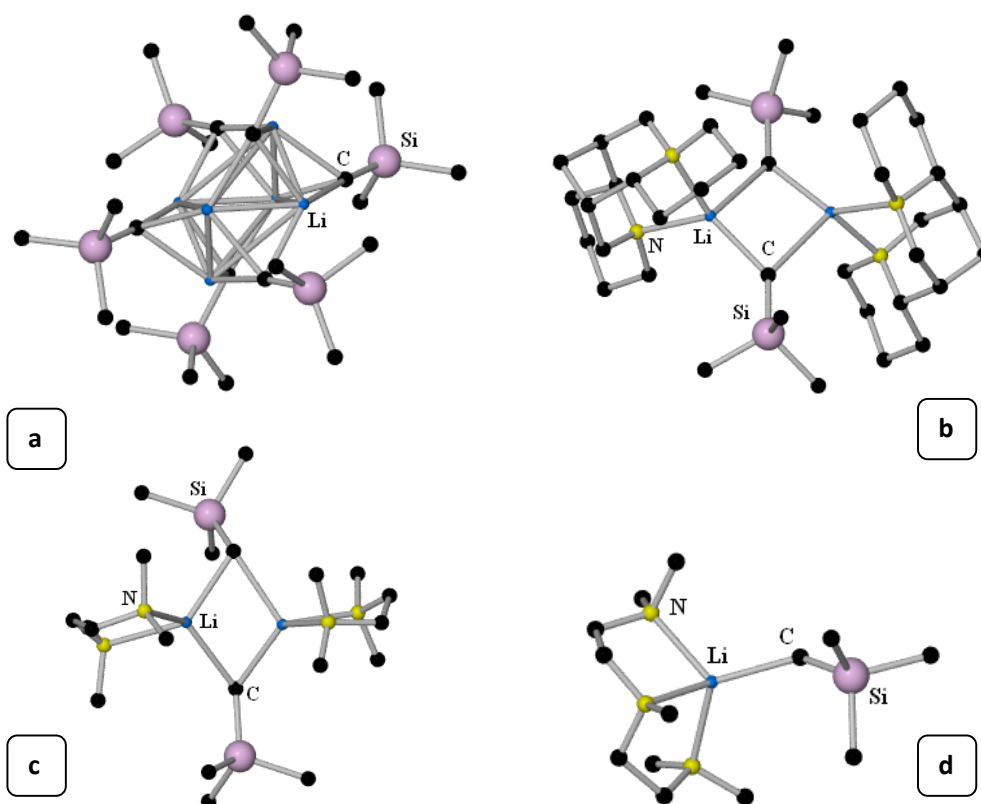
Figure 1.3: Molecular structures of: a) Unsolvated hexamer (LiCH$_2$SiMe$_3$)$_6$; b) dimeric [{(-)-sparteine}·LiCH$_2$SiMe$_3$]$_2$; c) dimeric (TMEDA·LiCH$_2$SiMe$_3$)$_2$; d) monomeric (PMDETA·LiCH$_2$SiMe$_3$).

The contribution of alkyllithium reagents to modern synthesis has been immense; however, the importance of their closely related organonitrogen compounds, lithium amide, [(R$_2$NLi)$_n$], cannot be overlooked. Titherly reported the first lithium amide, (LiNH$_2$)$_n$,[20] strictly an inorganic salt, in the late 1800's, however the first lithium amide organic-based compound to be structurally characterised was the silylamide LiHMDS.[21,22] Alkali-metal nitrogen bonds are predominately ionic in nature due to the large degree of electronegativity of the nitrogen atom and the strong electropositive character of the s-block metal. The majority of lithium amides, as well as many other alkali-metal amides, are synthesised by reacting the corresponding amine with the alkali-metal reagent of choice (**equation 1.1**). The deprotonation of the amine generates an alkane by-

product, usually a gas, which is eliminated from the reaction mixture. This type of reaction is generally fast with high yields achievable.

$$R^1M \; + \; NHR^2R^3 \longrightarrow R^1H \; + \; MNR^2R^3 \qquad \textbf{1.1}$$

alkali-metal **alkyl**
secondary amine
alkane
Alkali-metal **amide**
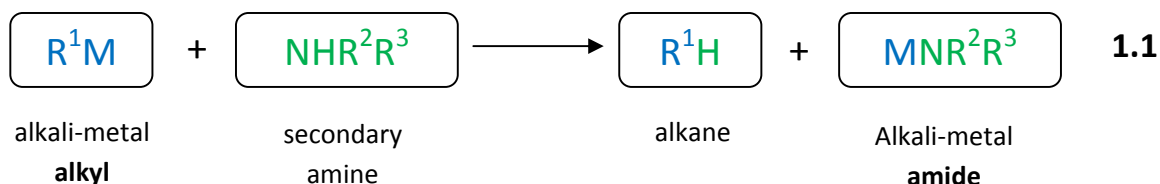
In synthetic chemistry, organolithium reagents are used as either highly reactive nucleophiles or strong bases. Sterically hindered lithium amides (**figure 1.4**) possess certain advantages over conventional alkyllithium compounds, especially in metal-hydrogen exchange reactions. Though less powerful bases than their alkyl counterparts, lithium amides can react with high regio- and stereoselectivity and they are relatively more tolerant of functional groups due to their high basicity and low nucleophilicity.

LDA   **LiHMDS**   **LiTMP**
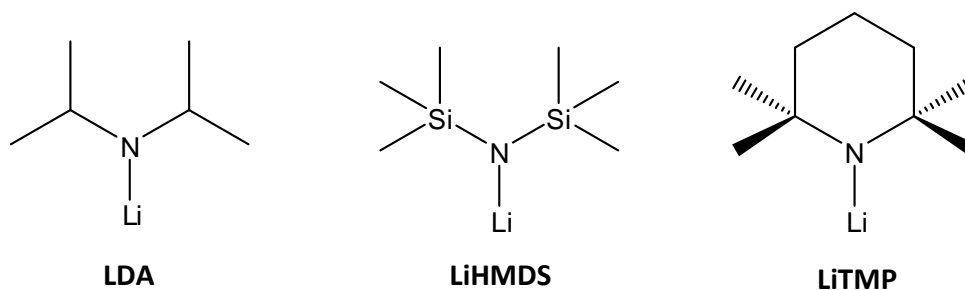
Figure 1.4: The common utility lithium amides in their empirical formulations.

Many organolithiums are often schematically depicted inaccurately as monomeric species with one positively charged lithium atom and a counter organic anion. For lithium amides, the highly polar Li−N bond combined with the additional lone pair of electrons on the amido nitrogen atom allow enable Li−N monomeric building blocks to aggregate both in solution and in the solid state. There are several factors that effect the degree of aggregation. These include: i) the steric

bulk of the organic fragment; ii) the metal ion size and its polarisability and; iii) the donor solvation of the metal centre. There are comparatively few structures of solvent-free lithium amide complexes, however it is clear to see that the mode of aggregation can change dramatically when considering the anionic amide moiety as now illustrated.

Lithium diisopropylamide (LDA) is the most widely utilised amide reagent in synthetic chemistry. LDA can be used to deprotonate esters,[23] nitriles,[24] nitrosamines[25,26] and various other organic substrates.[27] The non-solvated structure of LDA exists as a single strand helical polymer and is still to date the only polymeric non-solvated lithium amide to be crystallographically characterised (**figure 1.5**).[28]
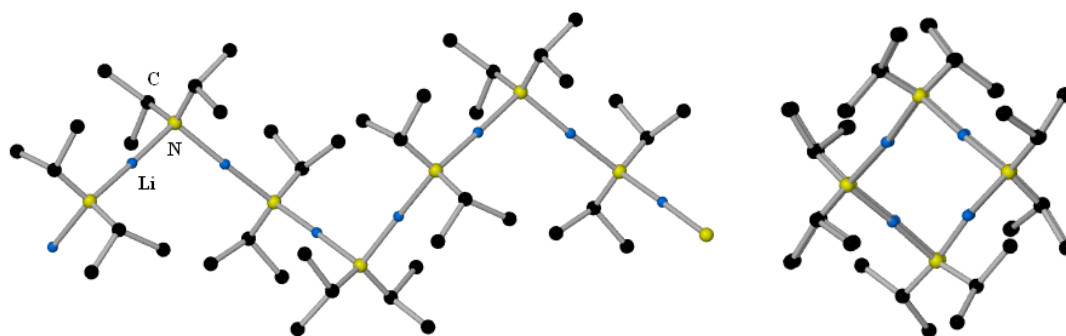
Figure 1.5: Left, a section of the helical structure of [LiN{CH(Me)₂}₂]∞; Right, a view down the centre of the helix.
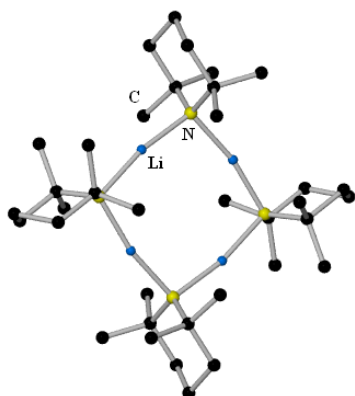
Figure 1.6: Tetrameric molecular structure of LiTMP.

In contrast to the polymeric aggregation of LDA, the lithium derivatives of the bulkier secondary amines HMDS(H) and TMP(H) produce six-membered trimeric [LiHMDS]₃ [21,22] and eight-membered tetrameric [LiTMP]₄ [29] structures respectively (**figure 1.6**). Lithiated dicyclohexylamide also forms a tetrameric ring analogous to (LiTMP)₄.[30] Other tetrameric lithium amides, such as the sterically

crowded cubane [{LiNH(Si^{t}BuMe$_2$)}$_4$] [31] or the complex [{LiN(SiMe$_3$)Ph}$_4$] [32] for example, have been crystallographically characterised by X-ray diffraction. Higher aggregates of lithium amides, such as hexamers are also known,[33] for example the lithium amide ladder motif in [{LiN(CH$_2$)$_5$CH$_2$}$_6$].[34]

Within the literature, the structures of solvated lithium amides are much more common. On addition of TMEDA to the helical polymer of LDA, its structure is broken down but rearranges itself to form another type of polymeric complex consisting of LDA dimers connected through bridging, though non-chelating, TMEDA molecules (**figure 1.7**).[35] The non-solvated helical metal-organic framework can also be deaggregated to discrete molecules by for example using THF to generate the solvated dimer [THF·LiN{CH(Me)$_2$}$_2$]$_2$.[36]
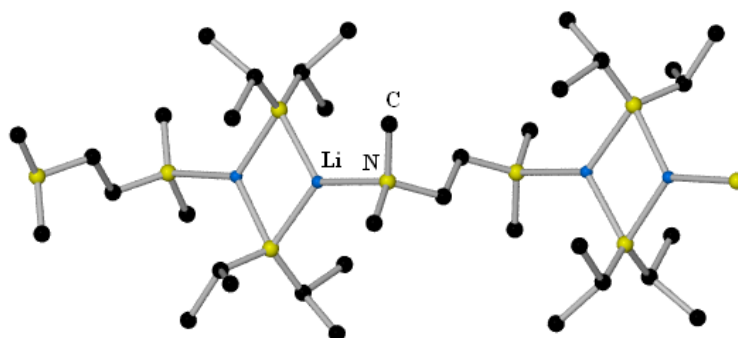
Figure 1.7: A section of the polymeric chain arrangement of TMEDA-solvated LDA.

In contrast to the TMEDA solvated LDA polymer, LiTMP is broken down from a tetramer in the unsolvated state, to the novel hemi-solvated open dimer (LiTMP)$_2$.TMEDA (**figure 1.8**).[37] In 1997, Collum confirmed the presence of this dimeric complex in solution by carrying out ^{6}Li and ^{15}N NMR spectroscopic experiments using LiTMP and the conformational locked surrogate, LiPMP (LiPMP = lithium 2,2,4,6,6-pentamethylpiperidide), together with bidentate ligands.[38] The structure of the TMEDA-solvated HMDS lithium amide is different to both the DA and TMP lithium reagents, as it forms the discrete monomeric complex (TMEDA·LiHMDS).[39]
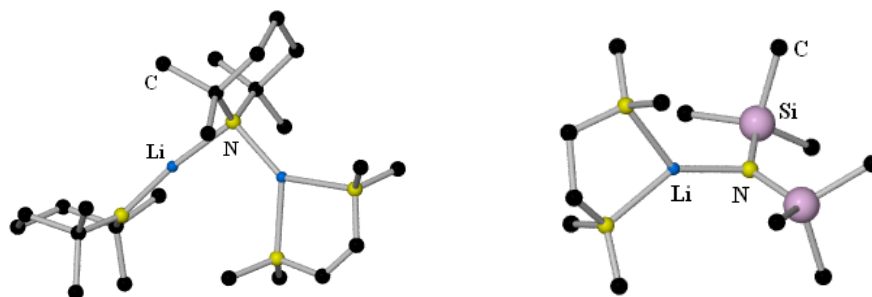
Figure 1.8: Open dimeric complex of [Li(TMP)]$_2$·TMEDA (LHS) and monomeric TMEDA.LiHMDS (RHS).

1.3) *Organosodium Compounds*

In comparison to organolithiums, there is relatively less structural information available on sodium metal organometallics due to their extreme reactivity, which makes them extremely challenging to manipulate. In the 1800's organosodium compounds were only known as intermediates, few attempts having been made to try to isolate such materials. Initial investigations into organosodium compounds began in 1858 with Wanklyn's report of the sodium zincate NaZnEt$_3$.[40] Morton subsequently attempted to 'trap' intermediates from the reaction of sodium and organic halides, but his investigations led to limited progress due to the basis of low yielding reactions and the poor stability of the resultant compounds.[41] In 1931, however, the simplest arylsodium compound, phenylsodium was isolated in a high yield by Bockmühl and Ehrhart by reacting sodium wire with chlorobenzene, in benzene solution.[42] By heating phenylsodium in toluene, Nobis and Moormeier (1959) isolated benzylsodium in a near quantitative yield.[43]

In the early 1940's, Morton announced the preparation of *n*-butylsodium, which was quickly followed by the reporting of higher alkylsodium reagents.[44,45] Alkylsodium compounds can be employed as effective Brønsted bases and highly reactive nucleophiles. One of the earliest examples of sodiation (sodium−hydrogen exchange) with organometallic reagents was the

deprotonation of benzene by ethylsodium. Reported in 1908 by Schorigin, expecting the product ethylsodium, the reaction of diethylmercury with sodium metal, in benzene solution, yielded the surprising product phenylsodium.[46] With increased reactivity brings problems as these largely ionic compounds cannot be prepared in ethereal solvents due to ether fragmentation. The principle pathway for ether cleavage is *via* metallation α to the oxygen,[47] though other pathways including β-metallation are occasionally observed.[48]

Due to the high reactivity of these compounds and the difficulties involved in crystallising them, there is a dearth of structural information of unsolvated organosodium complexes. One of the compounds central to the research performed by our group is *n*-butylsodium. The molecular structure of this compound has still yet to be elucidated, however in a report on the general preparation and NMR characterisation of this alkylsodium, Schleyer describes that *n*-butylsodium can be solubilised by the addition of the donor ligands TMEDA or THF.[49] The new solvated compounds can then be utilised in metallation reactions at low temperatures. Although the structure of *n*-butylsodium is unknown, methyl- and ethyl-sodium have been successfully characterised by X-ray crystallography as a low-symmetry tetramer [50] and a layered tetramer [51] respectively.

It is noteworthy to mention here that as far as the author can ascertain trimethylsilylmethylsodium has not been reported, in either unsolvated or solvated form, nor has it been used in subsequent synthetic reactions.

As in the case of lithium amides, amido sodium reagents are also useful in synthetic chemistry. The first sodium secondary amide to be crystallographically characterised was that of solvent-free NaHMDS, a polymeric chain.[52] A second polymorph was identified around twenty years later as the six-membered cyclic trimer (NaHMDS)$_3$ (**figure 1.9**),[53,54] isostructural with that of the solid-state complex of (LiHMDS)$_3$.

A search of the literature reveals that sodium amides are reported mostly as solvated (Lewis acidic−Lewis basic) complexes. Strong donors are required when breaking down the highly ionic nature of the polymeric amides. Using a strongly coordinating bidentate ligand, the TMEDA-solvated structures of NaDA and NaTMP have been published as the dimeric species [TMEDA·NaDA]$_2$ [55] and [TMEDA·NaTMP]$_2$ [56] respectively (**figure 1.10**). These dimeric compounds have planar (Na–N)$_2$ rings but other dimers have been reported with non-planar rings. For example, the

Figure 1.9: Molecular structure of a NaHMDS polymorph, the cyclic trimer (NaHMDS)$_3$.

mixture of PhNa, PhCH$_2$(Me)NH and TMEDA in hexane solution yields the dimeric complex [PhCH$_2$(Me)NNa(TMEDA)]$_2$, which adopts a non-planar, slightly-folded (Na-N)$_2$ cyclic ring with a *cisoid* arrangement of benzyl-methyl amido-attached ligands.[57]
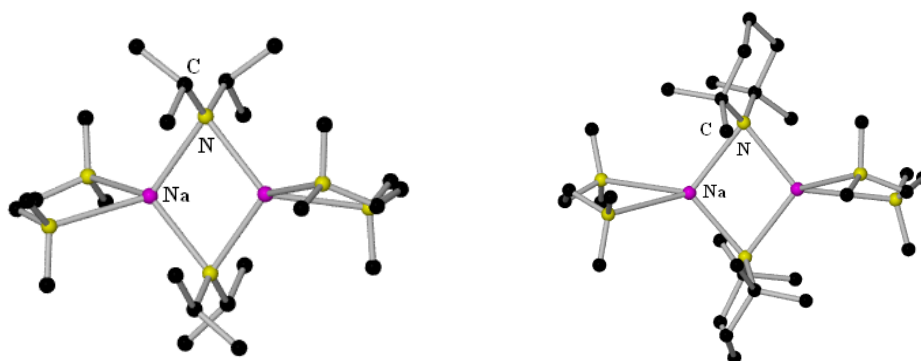
Figure 1.10: Molecular structures of the dimeric sodium amide solvates [TMEDA·NaDA]$_2$ (left) and [TMEDA·NaTMP]$_2$ (right).

1.4) *Organopotassium Compounds*

Orders of magnitude more reactive than their sodium congeners, potassium organometallics have also had considerably less investigation than organolithiums. Trimethylsilylmethylpotassium is

the compound that is the crux of this PhD research investigation, as all the potassium-mediated metallation work reported herein stems from this starting material. Unfortunately, however, its molecular structure remains elusive. From the same family of compounds, the unsolvated structure of silyl-rich tris(trimethylsilyl)methylpotassium, $[(Me_3Si)_3CK]_\infty$, is known and was found to have a polymeric arrangement in the solid state (**figure 1.11**) with C—K—C bonds exceedingly close to linearity [178.5(3)°].[58]
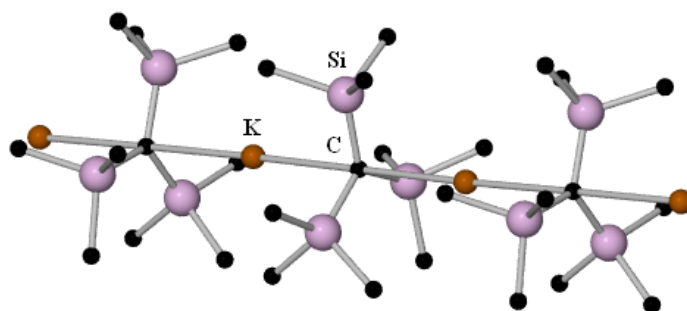
Figure 1.11: A section of the polymeric near-linear chain of unsolvated $[KC(SiMe_3)_3]_\infty$.

On addition of the bidentate donor TMEDA, deaggregation of the polymer takes place to form a very pyrophoric, polymeric aggregate (**figure 1.12**).[59] Here, on every potassium atom lies a chelating TMEDA molecule, and the monomers interact with neighbouring units by the way of K−C interactions from one of the methyl groups of a trimethylsilyl fragment. The high reactivity of this compound toward air and moisture was stated to be due to the exposed positions of the potassium and the carbanion.
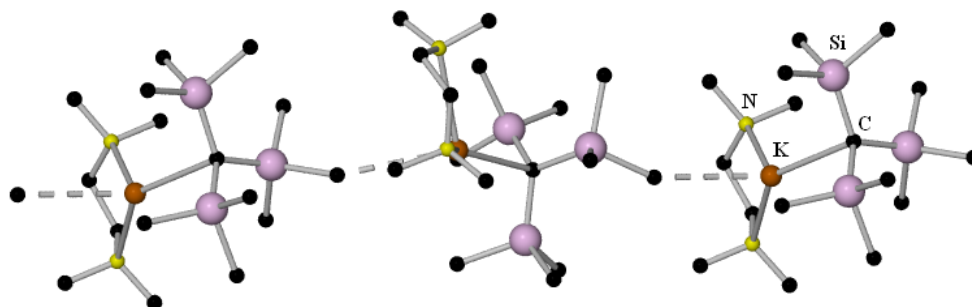
Figure 1.12: Three monomeric unit section of polymeric $[TMEDA \cdot KC(SiMe_3)_3]_\infty$ linked to one another via K•••C_{Me} interactions (depicted as dashed lines).

The PMDETA-solvated structure of the organopotassium derivative of the bis(silyl) member of this family, bis(trimethylsilyl)methylpotassium [KCH(SiMe₃)₂], was reported by Lappert in 2000 (**figure 1.13**) as [PMDETA·{KCH(SiMe₃)₂}]₂.[60] This complex was synthesised using a 0.5:1 ratio of the tridentate ligand to the potassium reagent in hexane solvent.
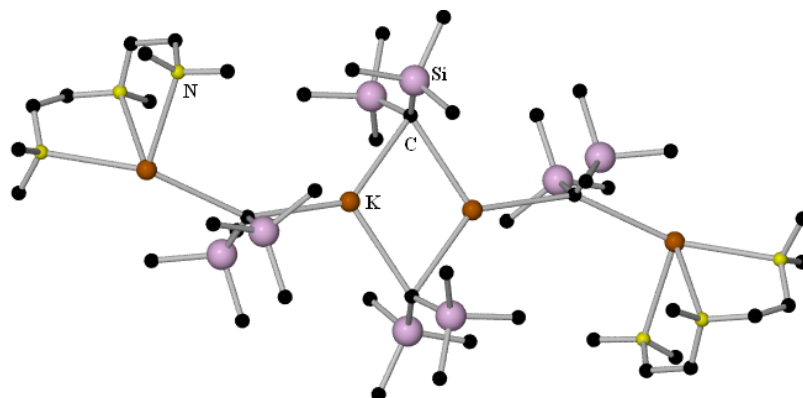
Figure 1.13: Molecular Structure of [PMDETA·{KCH(SiMe₃)₂}]₂.
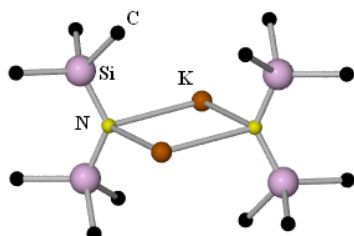
Figure 1.14: Four-membered (K−N)₂ ring dimer structure of KHMDS.

With respect to amido-potassium compounds, the unsolvated complex of KHMDS has been solved as a dimer (**figure 1.14**),[61] unlike its lithium and sodium congeners, which both form trimeric arrangements. As commonly observed in many alkali metal amide structures, the cental metal (K)−N ring in (KHMDS)₂ is planar. The potassium also forms agostic interactions with the trimethylsilyl groups to stabilise its coordination sphere. The TMEDA-solvated TMP [56] and DA potassium amides [62] have also been successfully characterised as dimeric compounds (**figure 1.15**), analogous to the sodium amides of the same secondary amines. These two dimeric potassium amide complexes are centrosymmetric in nature.
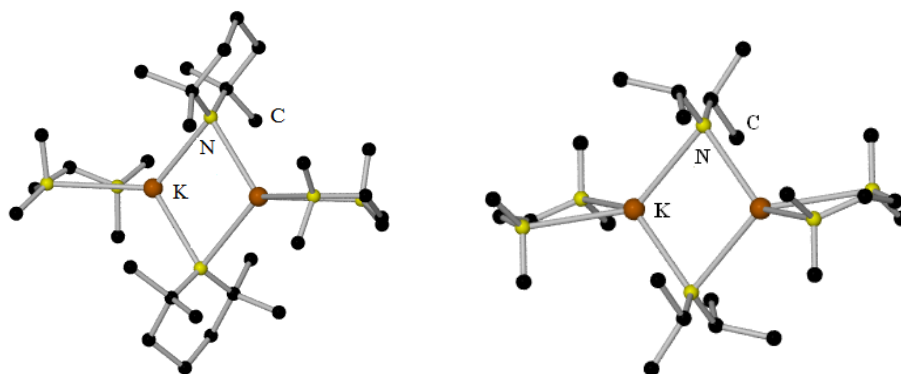
Figure 1.15: Molecular structures of the TMEDA-solvated dimers of KTMP (left) and KDA (right).

1.5) *Organozinc Compounds*

Found in group 12 of the periodic table, zinc tends not to exhibit the same properties as the other transition metals. This is due to its stable completely filled d shell, hence zinc is, in several respects, chemically similar to magnesium. One can cite a long list of similarities between the two metals: obvious examples include: their reactivity is based on their s^2 valence shell configuration; both elements have a similar ion size; both have stable +2 oxidation states; they each engage in strong σ bonds to carbon; and both can assume trigonal planar arrangements. One of the main distinctions between Zn and Mg are that the former metal is more carbophilic, and therefore forms stronger, shorter bonds to carbon atoms than does magnesium.

Organozinc reagents have been studied for over one hundred and fifty years. Pioneered by Frankland in 1849, diethylzinc, the first organozinc compound,[63] was also noteworthy for being the first compound to possess a metal−carbon sigma bond. Diethylzinc was synthesised through the study of ethyl iodide with zinc metal with hydrogen gas utilised as a "protective" blanket. This reaction produces ethylzinc iodide and diethylzinc. Although these products are formed from the reaction, Frankland missed the dialkylzinc co-product at the time. However, he went on

to report the deliberate preparation and characterisation of dimethylzinc, the simplest diorganozinc reagent. Wanklyn (1861),[64] Gladstone and Tribe (both 1873) [65] all reported improvements on the synthesis of dialkylzincs by modifying the solvent system and employing additional metals in the reaction mixture.

Although significantly less reactive than organolithium and organomagnesium compounds, most organozinc compounds are pyrophoric and therefore difficult to handle. Dimethyl- and diethylzinc have proved useful in the alkylation reactions of inorganic and organometallic halides due to the nucleophilicity of their alkyl groups. One of the main advantages organozinc reagents possess is that of their increased tolerance to functional groups. Where reagents such as Grignards and alkyllithiums would generally have the problem of undesirable side reactions, alkylzinc reagents, with their stronger Zn—C bonds, can generally avoid these issues. Alkylzincs are normally regarded as "soft" compounds, in contrast to the "hard" s-block metal organometallics.

The use of organozinc reagents in deprotonation reactions has been severely hampered due to the slow kinetics involved with this type of soft base. Metallation of relatively non-acidic C–H bonds is usually carried out by stronger bases, such as organolithiums or lithium amides. Studies of zinc-amides with respect to their use as bases have been made, highlighting the need for the more reactive and more polar Zn–N bond.[66,67]
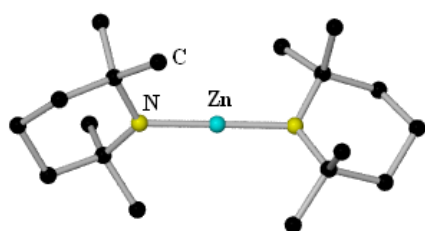
Figure 1.16: The molecular structure of Zn(TMP)₂.

Whereas LiTMP and NaTMP have been known for many years, the zinc analogue, Zn(TMP)$_2$ was reported by Rees in 1998.[68] It was prepared by the simple transmetallation reaction between ZnCl$_2$ and two molar equivalents of LiTMP. The molecular structure of this zinc reagent was also disclosed as a linear monomer (**figure 1.16**). It is important to note

here that Mg(TMP)$_2$ is not known in the solid form as it exists as an oil.

Despite their aforementioned limitations as bases, different organozinc reagents have recently been investigated to see if their performance as deprotonating agents could be improved. Of particular note, Hagadorn compared the bisamides Zn(TMP)$_2$ and Zn(HMDS)$_2$, along with the mixed alkyl/amido zinc reagents ethylzinc diisopropylamide (EtZnN^{i}Pr$_2$) and ethylzinc diphenylamide (EtZnNPh$_2$).[67] Hagadorn noted that the performance of the bases increased in the order mixed-ligand zinc species is less than Zn(HMDS)$_2$ which in turn is less than that of Zn(TMP)$_2$. This study revealed that the bulky TMP group was an effective base for deprotonating a wide range of substrates that included *tert*-butyl acetate, *N,N*–diethylacetamide, 2-methylpyridine and (methylsulfonyl)methane under mild conditions.

1.6)   *Organomagnesium Compounds*

The literature of organomagnesium reagents covers a vast area and these compounds have become some of the most widely utilised organometallic compounds since Victor Grignard published his seminal first paper of compounds in which magnesium is bonded to a carbon way back in 1900.[69] Given the vast wealth of information on Grignard reagents (RMgX) and Hauser bases (R$_2$NMgX)[70] (where R = an alkyl or aryl group and X = a halide), for brevity this section will mainly focus on organomagnesium amides, in particular magnesium Mg(TMP)$_2$.

Several routes have been developed over the years to synthesise magnesium bis(amide) complexes. The most popular route is the simple reaction of one molar equivalent of a dialkylmagnesium reagent (usually ether-free di-*n*-butylmagnesium) with two equivalents of an amine. With this reaction the first amine can be easily deprotonated but the metallation of the second amine is sometimes slow so the reaction mixture requires gentle heat to release the second alkyl group.[71] Magnesium bis(amide) complexes can also be achieved by the following

methods: direct reaction of an amine and magnesium metal; transamination reactions; transmetallation pathways; and from the disproportionation of alkylmagnesium amides (see **figure 1.17**).
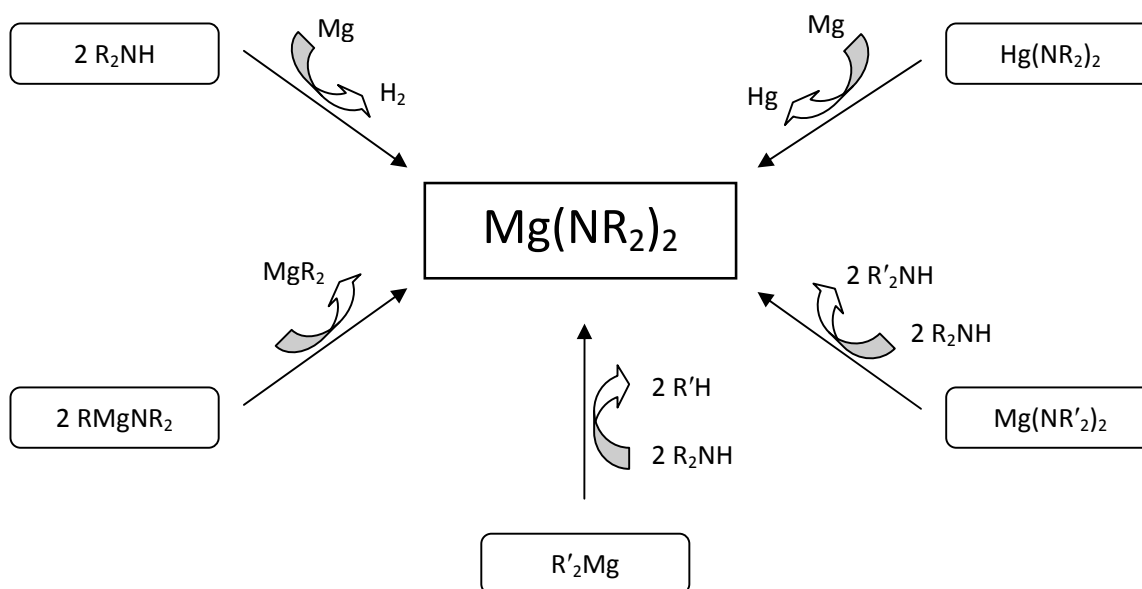
Figure 1.17: Five common methods of forming bis(amido)magnesium compounds.

Although magnesium bis(amides) were known beforehand, Eaton's clever employment of the amidomagnesium compound $[Mg(TMP)_2]$ for executing direct *ortho*-magnesiation of representative aromatic amides and esters (**scheme 1.1**) showed these types of bases could act as selective proton abstracting reagents.[72] Within this study, the ester methylbenzoate was shown to be selectively *ortho*-deprotonated by $[Mg(TMP)_2]$ with the resulting aryl/amido intermediate [2-(MgTMP)-1-methylbenzoate] staying apparently quite unreactive; however, this intermediate compound was never isolated. The amide fragment can co-exist with the ester group for some time, in the reaction mixture, without any further reaction until subsequent quenching with carbon dioxide took place. The mild reactivity of $Mg(TMP)_2$ was also highlighted with the successful magnesiation of carbocubane systems.[72]
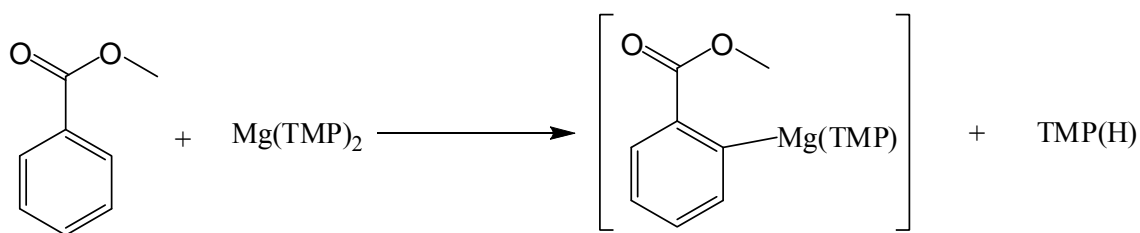
Scheme 1.1: *Ortho*-**magnesiation of methylbenzoate with Mg(TMP)₂.**

The relative stability of certain magnesium bis(amides) in THF solution allowed reactions to take place that alkali-metal reagents could not handle due to their exceedingly high (uncontrollable) reactivity with common ethereal solvents. For example, at ambient temperature and in THF solvent, a range of indoles can be metallated (magnesiated) directly at the 2–position with the magnesium reagent $Mg(N^iPr_2)_2$. Subsequent electrophilic quenching of these heteroaryl/amido magnesium intermediates can produce high yields of various 2-substituted indoles (**scheme 1.2**).[73]
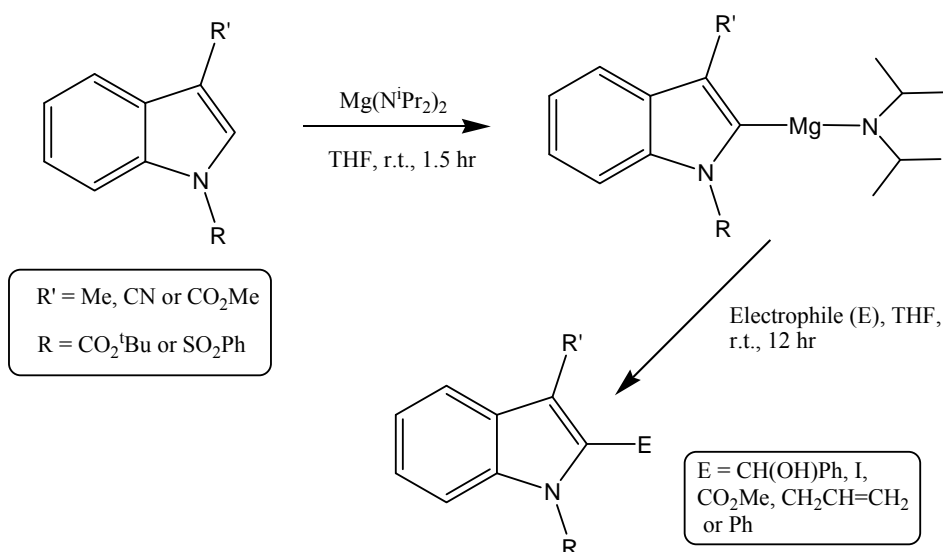
Scheme 1.2: Direct magnesiation of substituted indoles at the 2-position by the bisamide $Mg(N^iPr_2)_2$.

1.7) *Organoaluminium Compounds*

Organoaluminium reagents have found many applications in synthetic organic chemistry,[74] for example in the area of hydro- and carboalumination chemistry. The Lewis acidic nature of aluminium allows reactions with unique chemo-, regio- [75] and enantioselectivity [76] to be undertaken. There are many molecular structures in the literature of three-coordinate aluminium amides, mostly discovered in the past 30 or so years. A search of the CSD [77] results in no structural data on tris(tetramethylpiperidino)aluminium, (TMP)$_3$Al. However, Nöth has developed neutral aluminium compounds containing two tetramethylpiperidino units. Initially reporting the synthesis of (TMP$_2$AlH)$_2$,[78] Nöth has expanded this area of aluminium chemistry by subsequently revealing the monomeric complexes TMP$_2$Al(X) [X = Cl, Br, I] and the dimeric compound [TMP$_2$Al(X)]$_2$ [X = F].[79] These mixed amido/halide alumanes can undergo nucleophilic displacement reactions to form the monomeric series of compounds TMP$_2$Al(X) [where X = OR, SR, NR$_2$, PR$_2$, AsR$_2$, CR$_3$, Si(SiMe$_3$)$_3$] (**scheme 1.3**).[80-82] This section will narrowly focus on homometallic dialkylaluminium amide chemistry based on the amine 2,2,6,6-tetramethylpiperidine, due to the significance of this specific amine to this investigation. Unfortunately, the molecular structures of the reagent type R$_2$Al(TMP) [where R is an alkyl group] have not been determined to date.
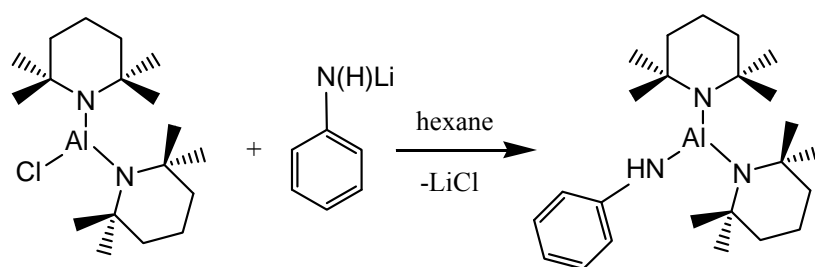
Scheme 1.3: Nucleophilic displacement reaction of the monomeric complex (TMP)$_2$AlCl with mono-lithiated aniline.

Yamamoto first reported the use of the mixed alkyl/amido aluminium reagent Et$_2$Al(TMP) as a regiospecific base in 1974.[83] The preparation of this compound (**scheme 1.4**) is achieved by

reacting diethylaluminium chloride with preformed LiTMP in a routine transmetallation step. It is noteworthy that the solvent mixture in this synthetic step is benzene, and as no metallation of the solvent is witnessed then this neutral aluminium reagent can be said to be a weak base.
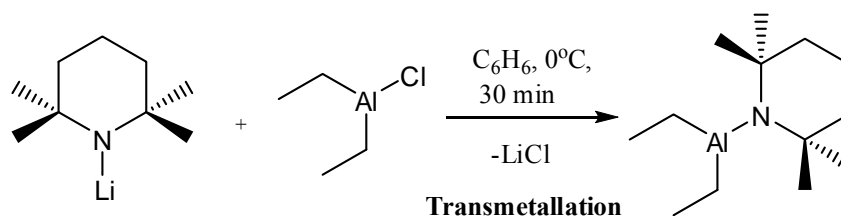
Scheme 1.4: Synthetic route to the dialkylaluminium amide, Et$_2$Al(TMP).

In a reaction where LiTMP was unsatisfactory, several dialkylamido aluminium compounds were tested as potential deprotonation agents against (*E*)-cyclododecene oxide under fixed conditions (**scheme 1.5, table 1.1**). Under the conditions of 1 hr reaction time, at 0°C in benzene solution, the bulky TMP amide aluminium reagent Et$_2$Al(TMP) generated the greatest yield (80%) of the alcohol product (*E*)-2-cyclododecen-1-ol from the deprotonation of the starting material, (*E*)-cyclododecene oxide. The diisopropylamide analogue (45% yield) was less effective than the TMP base, however, it was more capable than the dicyclohexylamide and diethylamide bases (36 and 5% yield respectively) as a deprotonative reagent. Yamamoto found
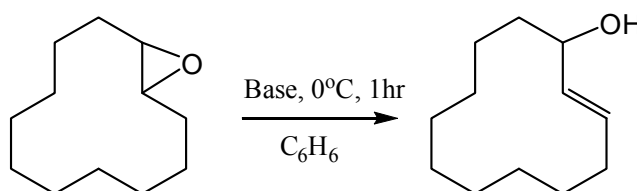
Scheme 1.5: Deprotonation of (*E*)-cyclododecene oxide to form (*E*)-2-cyclododecen-1-ol.

Table 1.1: Yields obtained by deprotonating (*E*)-cyclododecene oxide with various bases.

Reagent	Et$_2$Al(NEt$_2$)	Et$_2$Al(NcHex$_2$)	Et$_2$Al(N^{i}Pr$_2$)	Et$_2$Al(TMP)	LiTMP
Yield of Product (%)	5	36	45	80	<5

that several other epoxide species could be deprotonated using Et$_2$Al(TMP) and that this aluminum reagent showed great regioselective properties towards both *E* and *Z* epoxides.

In 1979, Nokazi reported that Et$_2$Al(TMP) can be used to deprotonate ketones and esters in THF solvent at subambient temperatures to yield diethylaluminum enolates (**scheme 1.6**), which were not isolated but quenched with benzaldehyde at -78°C.[84]
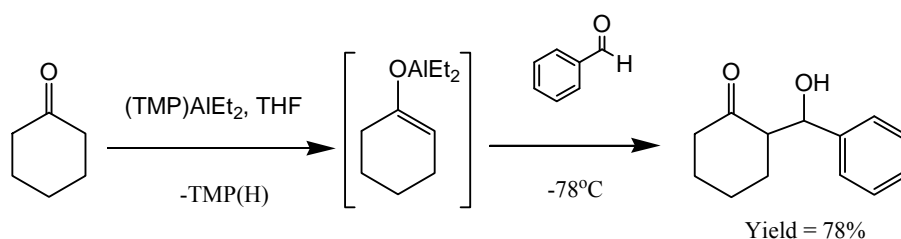
Scheme 1.6: Use of Et$_2$Al(TMP) for the deprotonation of cyclohexanone.

Over ten years later, Yamamoto reported a new use for the base Et$_2$Al(TMP).[85] Several types of dialkyl/monoamido aluminium compounds were revealed to be highly effective in the promotion of the Fischer indole synthesis. The diethyl complex Et$_2$Al(TMP) was found to be the best aluminium base to use for this methodology (**scheme 1.7**) producing the product 1,3-dimethyl-2-
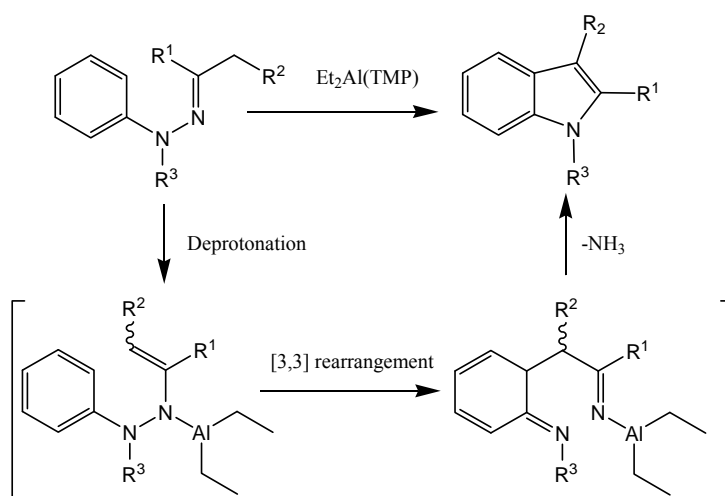
Scheme 1.7: Postulated mechanism for the Et$_2$Al(TMP)-promoted Fischer indole synthesis.

22

ethyl indole in a high yield of 78%. The isobutyl analogue, ^{i}Bu$_2$Al(TMP), was not far behind in its ability to act as a good base, producing the desired indole in a yield of 76%.

1.8) *Mixed-Metal Complexes*

The topic of mixed-metal chemistry spans a huge area of literature and its origins can be traced back over 150 years. In 1858, Wanklyn discovered that sodium and potassium triethylzincate, "M$^+$Et$_3$Zn$^-$" [M = Na or K], could be made by the reaction of the relevant alkali metal with diethylzinc.[40] The term 'ate' arose almost a century later, with Wittig coining the term [86] after realising that special anionic compounds could be generated from the addition of anionic species to Lewis acidic organometallic reagents.

Wittig and Bickelhaupt, among other scientists, pushed the advancement of ate chemistry by investigating the mixed alkali metal complexes of empirical formula [RLi·RM] (where M is a heavier alkali metal). For example, the *n*-butyl complex [C$_4$H$_9$Li·C$_4$H$_9$Na] was studied in 1958 and it was deduced that this compound was only stable for only a short period of time and therefore could not be isolated.[87] These types of compounds were only starting to be structurally characterised 30 years later when Weiss reported the formation of the ate complex [{Na(TMEDA)}$_3$][LiPh$_4$], confirmed by X-ray diffraction studies.[88] Towards the later part of the 20th century it was recognised that mixtures of organolithium derivatives, such as alkyl- or amidolithiums, and heavier alkali-metal alkoxides (e.g. *tert*-butoxide or *tert*-pentoxides) presented a type of reactivity that solely the lithium reagents themselves could not replicate.[89-93] The increased basicity of these types of combinations led to the term "superbases". One of the most commonly used superbases in synthesis, pioneered independently by Schlosser and Lochmann (though several years earlier, Morton [94,95] made similar formulations for polymer research using the combination of potassium isopropoxide and *n*-amylsodium), is the mixed formulation of *n*-butyllithium (^{n}BuLi) with potassium *tert*-butoxide (KO^{t}Bu). This concoction has become known as the Lochmann-Schlosser superbase and is generally abbreviated to

LICKOR (LIC denoting the alkyllithium and KOR denoting the potassium alkoxide).[96] The exact nature of this base, in structural terms, is still uncertain and the definite identification of the metallo-products produced upon deprotonation with this superbase is complicated by the vast number of structural permutations involved – they could be organolithiums, organopotassiums or mixed organolithium-potassium species.

The superbase LICKOR can be used as a very successful, but harsh, deprotonating agent against relatively non-acidic substrates. Metallation of benzene is a good example of this as the arene can be deprotonated without the use of a donor ligand, and can be subsequently quenched with carbon dioxide to give benzoic acid after protonation. This contrasts with the same metallation using *n*-butyllithium, where the bidentate ligand TMEDA is required before the reaction can proceed. LICKOR can also achieve regiospecific metallations in different positions to that achieved by lithium alkyls and amides on the same substrates. The example of 1,3-bis(triflouromethyl)benzene highlights this point perfectly (**figure 1.18**).[97,98]

Figure 1.18: Difference in regioselectivity between *n*BuLi, LiTMP and LICKOR towards 1,3-bis(triflouromethyl)benzene (arrows represent metallation site).

One of the problems associated with the superbasic LICKOR mixture is that sometimes it can react with poor regioselectivity. For example, with the case of benzene, the products of attempted dimetallation were monosubstituted and *meta-* and *para*-substituted compounds.[99] Attempted dimetallation of polycyclic aromatic naphthalene yields an astonishing ten disubstituted isomers albeit all in very small yields.[99] Therefore although LICKOR and other related superbasic reagents possess the reactivity of a strong base, their poor regioselectivity hampers their use.

Knochel has pioneered the use of Grignard regeants coupled with lithium chloride (LiCl) to make so-called "turbo-Grignards".[100,101] The addition of the salt LiCl to reaction mixtures enhances the reactivities of these turbo bases compared to that of conventional Grignard reagents. For example, inactivated aryl bromides react poorly with the Grignard reagent *i*PrMgCl, even at elevated temperatures. The simple addition of one equivalent of LiCl, forming, *in situ* in THF solution, the turbo base *i*PrMgCl·LiCl, to the reaction mixture results in a completely opposite reactivity as metal-halogen exchange proceeds smoothly and yields of the quenched products are excellent (**scheme 1.8**).[100] A major advantage of these reagents is their tolerance to a wide range of functional groups, such as esters, ethers, halides, nitriles, tosylate and triazine groups for example.[102] The reasoning behind the increased reactivity of this type of reagent is that LiCl increases the solubility of this reagent by breaking up the aggregated *i*PrMgCl dimer to the highly reactive monomeric *i*PrMgCl·LiCl compound (**scheme 1.9**). Such is the ever growing popularity of turbo-Grignards in synthetic chemistry these reagents are now commercially available from companies such as Aldrich and Chemetall GmbH.
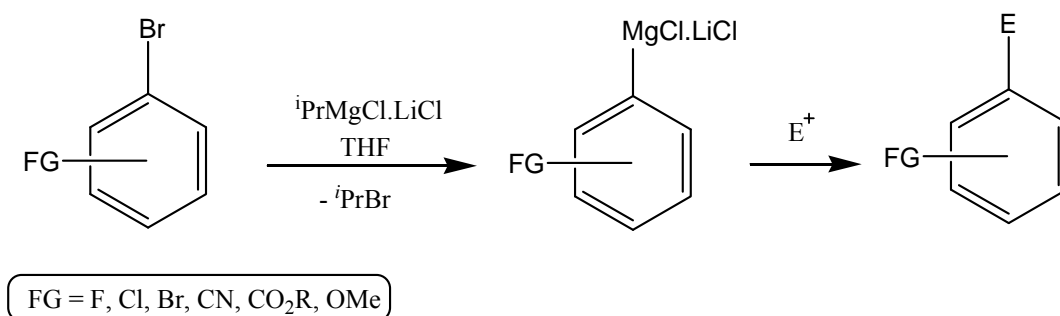
Scheme 1.8: Metal-halogen exchange of substituted arylbromides with a turbo-Grignard reagent.
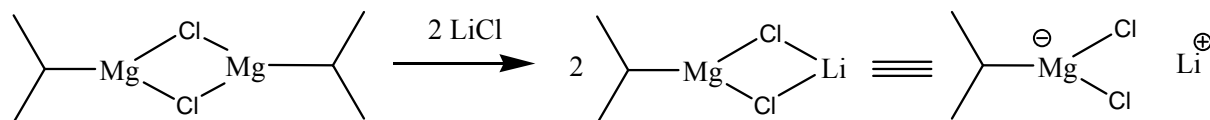
Scheme 1.9: Simplistic view of the generation of "turbo-Grignard" [*i*PrMgCl·LiCl].

As well as metal–halogen exchange reactions, Knochel has published many reports on deprotonation reactions with turbo-Grignard reagents.[103-105] The use in synthetic chemistry of conventional lithium amides or alkyllithiums has been slightly hampered by their intolerance of several commonly encountered functional groups. The low solubility of amides of type R_2NMgCl, R_2NMgR' and $(R_2N)_2Mg$ has led to their relatively limited use as a result. Knochel has reported, however, that the reagents of general formula $R_2NMgCl \cdot LiCl$ are highly soluble mixed magnesium/lithium amides, which react with a high degree of regiospecificity.[106] To form these amides, $^iPrMgCl \cdot LiCl$ is reacted with the desired bulky secondary amine, such as TMPH (**scheme 1.10**), to generate bases that exhibit high kinetic activity, extremely good solubility and that can be stored in THF solutions.
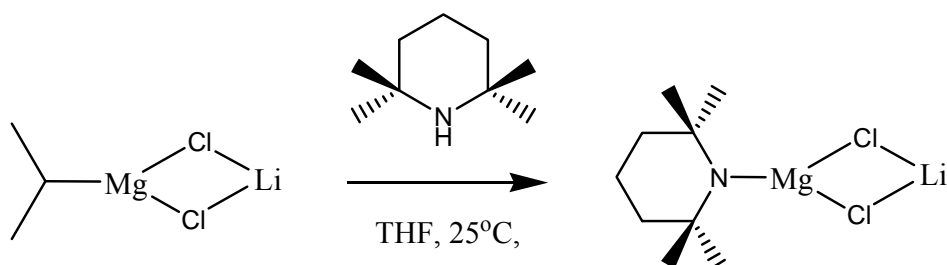
Scheme 1.10: Synthesis of the sterically hindered Mg/Li amide (TMP)MgCl·LiCl.

The amide TMPMgCl·LiCl has been found to be an extremely effective regioselective base.[106-108] Various heteroaromatics and aromatic compounds can be functionalised with it (in THF solutions), with even multiple functionalisation of a bisubstituted aromatic compound being possible. Thus these reagents allow access to new magnesium species not previously reported in the literature. Other formulations of related reagents investigated by Knochel include $Mg(TMP)_2 \cdot 2LiCl$,[103] $(TMP)_2Zn \cdot 2MgCl_2 \cdot 2LiCl$ [109] and $(TMP)_2Mn \cdot 2MgCl_2 \cdot 4LiCl$ [110] and $(TMP)ZnCl \cdot LiCl$,[111] which have all been used *in situ* without any type of crystallographic or solution analysis on the bases themselves being discussed.

The molecular structure of a turbo-Grignard reagent has only very recently been elucidated. This significant breakthrough in this area came from within our own group in 2008, manifested in the

heavily-solvated compound [(THF)$_2$Li(μ-Cl)$_2$Mg(THF)TMP] (**figure 1.19**).[112]
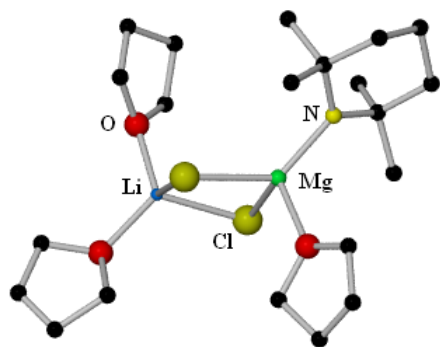
Figure 1.19: Molecular structure of the turbo-Grignard [(THF)$_2$Li(μ-Cl)$_2$Mg(THF)TMP].

Knowledge of this structure allowed a number of conclusions to be drawn about the high reactivity and exceptional regioselectivity that these turbo-bases possess. Most obviously it established that the turbo-Grignard is a molecular halide, not salt-like. Furthermore the active base, the sterically hindered TMP ligand sits in the terminal position and therefore it only binds to Mg and not to Li. This allows only one bond to be broken, the Mg-N(TMP) bond, to release the active base. Another note to consider is that a potentially labile THF molecule is bonded to the four coordinate Mg centre, geminal to the active TMP ligand. The loss of this THF molecule could lead to a vacant coordination site opening up on Mg where a substrate could potentially dock prior to its metallation. A final point to make is that the ate complex motif is retained, that is Li$^+$MgR$_3^-$, and the presence of strongly electronegative ligands could help to rationalise the enhanced magnesiating ability that these compounds can have.

To help support that the isolated compound is an active base, the solid [(THF)$_2$Li(μ-Cl)$_2$Mg(THF)TMP] was dissolved in THF and was found to successfully deprotonate ethyl 3-chlorobenzoate to furnish the final product ethyl-3-chloro-2-iodobenzoate in an isolated yield of 68% (**scheme 1.11**).
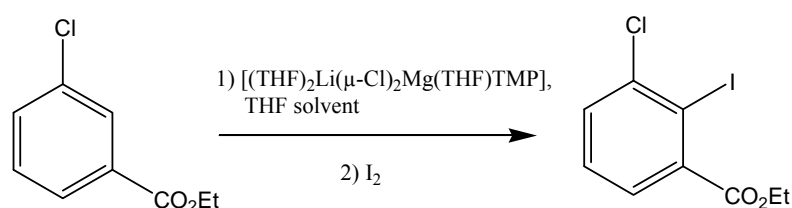
Scheme 1.11: Metallation/electrophilic quenching reaction of ethyl 3-chlorobenzoate.

Mongin has also reported successful direct magnesiation applications with the mixed-metal lithium/magnesium ate derivatives $LiMgR_3$ and Li_2MgR_4.[113] Since 1951 when Wittig introduced the first lithium magnesiate, $LiMgPh_3$, several structural studies of these types of compounds have been carried out. For example, Weiss has reported the dimeric lithium magnesiate $[Li\{Mg(C{\equiv}CPh)_3.TMEDA\}]_2$ [114] and the highly-coordinated ate complex $[(TMEDA)_2Li_2MgMe_4]$ [115] in the early 1980s. However, it was only recently that the synthetic applications of lithium magnesiates have been investigated. By mixing a 1:1 or 2:1 ratio of an organolithium to a diorganomagnesium compound, stoichiometric variants lithium trialkyl and lithium tetraalkyl magnesiates can be generated.

Castaldi and Borsotti reported the first use of a magnesiate as a deprotonating agent towards aromatic substrates in 1992, reacting (trifluoromethyl)benzene derivatives with the lithium magnesiate Bu_3MgLi (**scheme 1.12**).[116] This type of reaction is an inefficient way to deprotonate substrates as only one of the three potentially basic limbs of the base is utilised, and the other two are discarded.
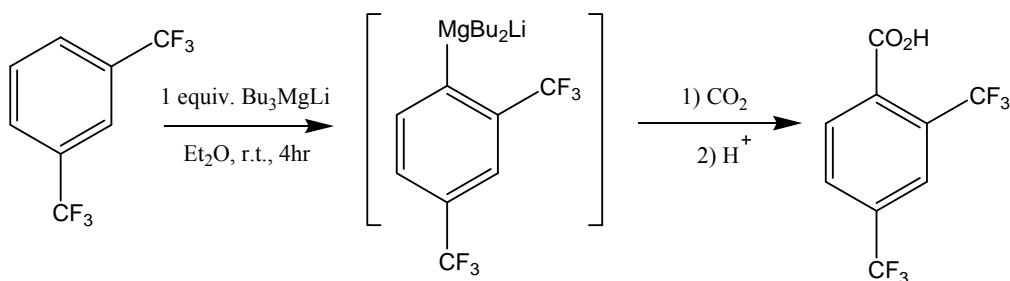
Scheme 1.12: Magnesiation of 1,3-bis(trifluoromethyl)benzene with LiMgBu₃ and subsequent trapping.

Mongin and co-workers have developed the use of standard magnesiates and highly coordinated magnesiates with respect to the deprotonation of functionalised heterocyclic compounds such as pyridines,[117] furans,[118] benzofurans,[118] thiophenes,[119] oxazoles [120] and benzoxazoles.[120] Within these metallation steps, depending on the magnesiate involved, either a third (for $LiMgR_3$) or a quarter (for Li_2MgR_4) of a molar equivalent of the base is reacted with one

equivalent of the substrate to maximise the use of the anionic ligands, presenting an efficient method of metallation. Mongin very recently applied this methodology to lithium cadmates and lithium zincates, though in all her reports no structural properties of the metal reagent or metal products (prior to quenching) have been eluciated.[121]

In the 1990's, Kondo and Uchiyama introduced a notable study of mixed–metal chemistry, mainly pairing lithium with zinc in an ate complex (**figure 1.20**). These types of compound were known to behave in a special way that their monometallic counterparts could not.[122,123] Initial studies were focused on triorganozincates, such as trimethylzincate, and their use in metal-exchange reactions.[124,125] Harada had already reported metal-halide exchange reactions of triorganozincates with bromide and iodide containing substrates for the preparation of alkenyl-, alkyl-, phenyl- and indolylzinc compounds a few years beforehand.[113] In the late '90s, attention

zincate   *highly coordinated zincate*
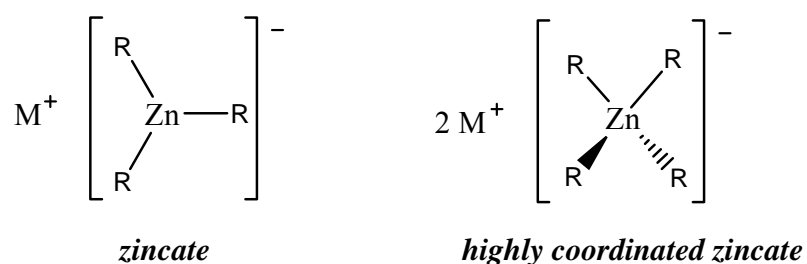
Figure 1.20: Common trigonal planar and tetrahedral zincate motifs.

turned on attempts to use zincate compounds as novel bases. Harada recorded the first deprotonation reactions with organozincates involving metallation of alkynyl mesylates and chlorides with a variety of triorganozincates (**scheme 1.13**).[126] The lithium zincate deprotonates the terminal alkynyl proton to form the corresponding alkynyl zincate, which subsequently undergoes a 1,2-migration to generate the allenyl zinc compound. This intermediate can be subsequently quenched *in situ* with a range of electrophiles, giving selective substitution at the γ–position in good-to-high yields of 51-98%. Using the monoamido-dialkyl zincate reagent

"^{t}Bu$_2$Zn(TMP)Li" [generally referred to as "TMP-zincate"] (**scheme 1.14**), Kondo and Uchiyama carried out selective deprotonations of substituted aromatic rings with a high degree of chemo- and regioselectivity (for example metallation of aromatic amides, esters and nitriles

X = MeSO$_2$O, Cl
R^1 = Me, Bu, ^{t}Bu, C$_8$H$_{17}$, hexyl
R^2 = Ph, Me, Bu
E = I$_2$, NCS, Me$_3$SiCl, RCOCl, RCHO
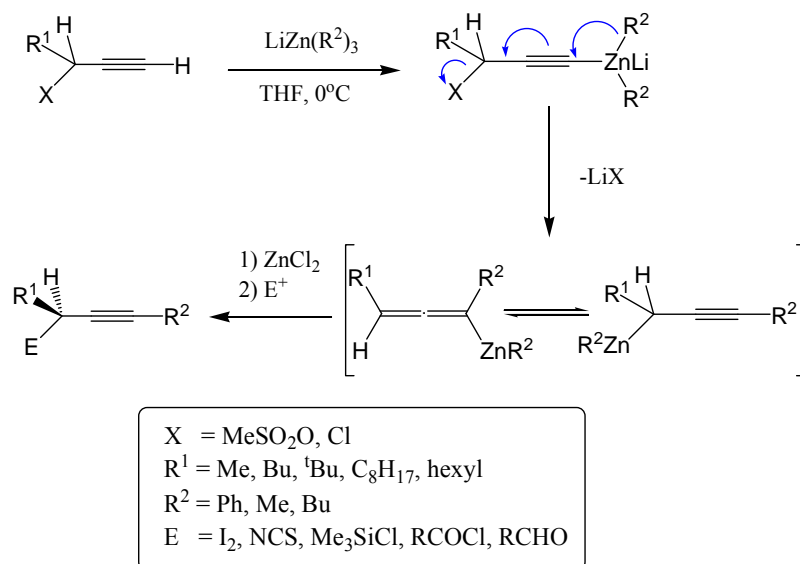
Scheme 1.13: Deprotonative metallation of alkynes, followed by 1,2-migration and further reaction with an electrophile.

with TMP-zincate proceeds almost exclusively on the ring, *ortho* to the functional group which itself is left untouched).[127] However, in their several reports of substrate metallation no mentions were made of the solid-state or solution structures of the bimetallic base or metallated intermediates.

1) 2 eq.^{t}Bu$_2$Zn(TMP)Li, THF, r.t., 3hr

2) I$_2$

R = CO$_2$Me, CO$_2$Et, CO$_2$^{i}Pr, CO$_2$^{t}Bu, CON^{i}Pr$_2$, CN
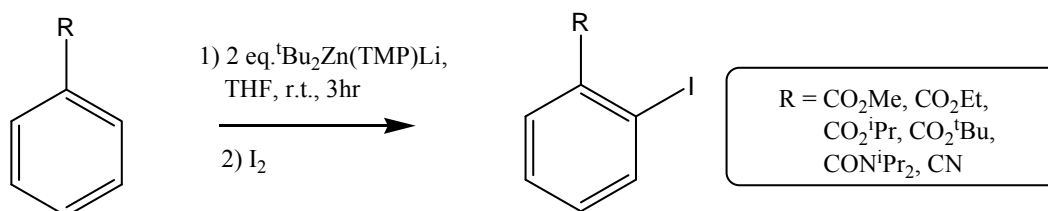
Scheme 1.14: Examples of zincation using TMP-zincate.

TMP-zincate can also deprotonate various nitrogen-, oxygen- and sulfur-containing heterocyclic compounds including pyridines, furans and thiophenes respectively.[127] Bromobenzene derivatives containing either a OMe, Cl, F, CN or CON^{i}Pr$_2$ group at the 3-position can be successfully deprotonated with very high regioselectivity in good to excellent yields.

Recently, Uchiyama revealed theoretical calculations (at the B3LYP/631SVP level) which suggest, using the model zincate of Me$_2$Zn(NMe$_2$)Li as a simplified replacement for TMP-zincate, that depending on the substrate to be metallated, different transition states can be adopted (**figure 1.21**). These calculations hence show the high substrate compatibility that these bases hold.[128]
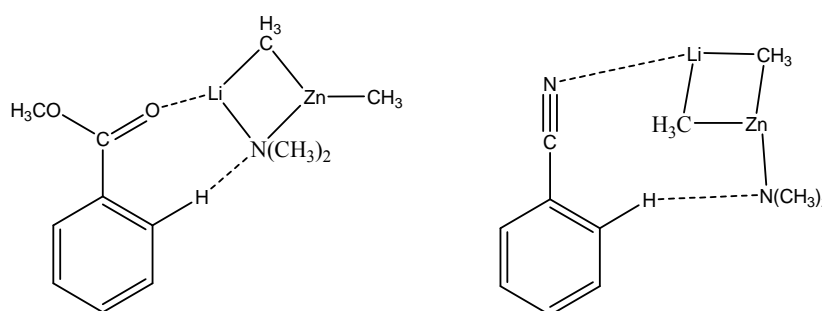
Figure 1.21: Proposed transition states for TMP-zincate deprotonation of methylbenzoate and benzonitrile.

Uchiyama and Morokuma,[129] as well as our own group in independent studies,[130] published in 2006 the X-ray molecular structure of the THF adduct of TMP-zincate in the form [THF·Li(μ-TMP)(μ-^{t}Bu)Zn(^{t}Bu)] (**figure 1.22**). The reactivity characteristics of this base were called into question, specifically regarding whether the amido arm or the alkyl ligand promoted deprotonation of an aromatic substrate. Reported by the Mulvey group, the sodium analogue of lithium-TMP-zincate, [TMEDA·Na(μ-TMP)(μ-^{t}Bu)Zn(^{t}Bu)] (Na-TMP-zincate) (**figure 1.22**), was shown to ultimately react as an alkyl base towards benzene, with the loss of one ^{t}Bu group liberated as *iso*-butane.[131] Uchiyama and Morokuma also undertook a theoretical study on the directed-*ortho* metallation (DoM) of anisole using the simplified base

31

Me$_2$O·Li(NMe$_2$)ZnMe$_2$.[129] The computational results concluded that it is kinetically more favourable for the TMP ligand to deprotonate anisole, not the alkyl component.
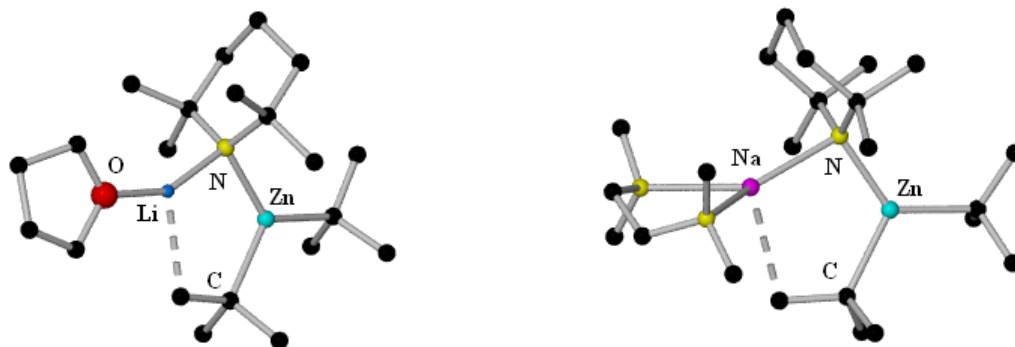
Figure 1.22: Molecular structures of [THF·Li(μ-TMP)(μ-^{t}Bu)Zn(^{t}Bu)] (left) and [TMEDA·Na(μ-TMP)(μ-^{t}Bu)Zn(^{t}Bu)] (right) respectively.

Uchiyama and Nobuto carried out a subsequent theoretical study on the metallation of benzene using the Na-TMP-zincate that our group had reported (**figure 1.22**).[132] A one-step reaction mechanism, where the base would react in a straight deprotonation *via* the alkyl group, was ruled out due to the very high values of Gibbs energy of activation that would be required. The idea of a two-step mechanism was introduced, where the TMP ligand would deprotonate benzene releasing free amine into the reaction mixture in an initial step. The next move would be the metallation of the free TMP(H) by the alkyl group to reincorporate a TMP anion and at the same time to release *iso*-butane (**scheme 1.15**). Their calculations showed that the two-step mechanism was the preferred option as the activation energy for the first step was relatively small (+25.1 kcal/mol). It must be mentioned, however, these calculations used the significantly simplified model of NMe$_2$, and not the full structure of the sterically demanding TMP amide ligand. Further to these theoretical studies of Uchiyama *et al*, we obtained direct experimental evidence of this two-step mechanism, revealing that step 1 can also go backwards to regenerate the starting base substrate, and that the course of these reactions critically depends on the identity of the alkyl ligand (for example, Me versus ^{t}Bu) and solvent.[133]
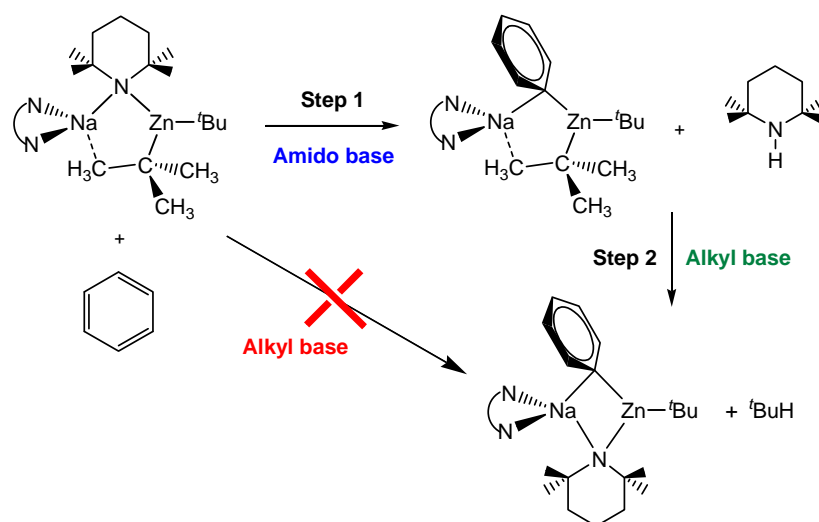
Scheme 1.15: Proposed reaction pathways for the reaction of Na-TMP-zincate with benzene.
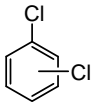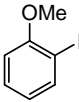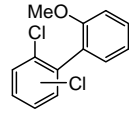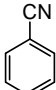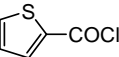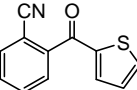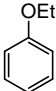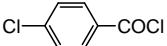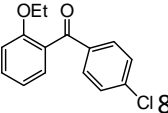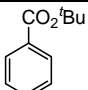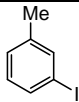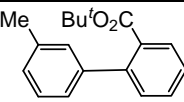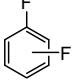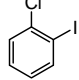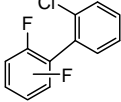
As well as making important contributions to lithium zincate chemistry, Uchiyama has also investigated mixed lithium/aluminum ate compounds with regard to their application in synthesis. In 2004, he reported the lithium triisobutyl(tetramethylpiperidino) aluminate [^{i}Bu$_3$Al(TMP)Li, known as TMP-aluminate] by the addition of preformed LiTMP to the homometallic reagent ^{i}Bu$_3$Al. This aluminate acts as an amido base and was found to be a very successful chemoselective base in the deprotonation of functionalised arenes.[134-136] This TMP-aluminate also has the additional property of being able to tolerate both electron-withdrawing (the amide group in *N,N*-diisopropybenzamide) and electron-donating (the methoxy group in aniosole) substituents. A more detailed discussion on aluminate chemistry will be covered later in this PhD thesis.

Very recently, Knochel has revealed that the addition of three molar equivalents of the salt LiCl to a *neutral* aluminum trisamide results in a base mixture that undergoes highly regioselective direct alumination of aromatic and heteroaromatic compounds.[75] The capabilities of this base Al(TMP)$_3$·3LiCl and closely related Al(N^{t}Bu$_3$)$_3$·3LiCl were tested (**table 1.2**), with the results

concluding that these reagents are highly tolerable of a number of functional groups, including chloride, cyano, ester and ether and fluoride groups.

Table 1.2: Metallation/quenching reactions of Al(N^{t}Bu$_3$)$_3$·3LiCl with aromatic substrates.

Substrate	Electrophile	Product / Yield
		78%
		71%
		85%
		77%
		89%

The number of studies into mixed-metal formulations, not just from inorganic chemists, but from scientists with organic and theoretical backgrounds, highlights how important the area of mixed-metal chemistry is in the synthetic community.

1.9)   *Alkali-Metal-Mediated Metallation – The Synergic Effect*

Within our research group, various studies have been carried out on heterobimetallic (ate) combinations, involving the pairing of an alkali metal (Li, Na or K) with either magnesium, zinc,

aluminium, manganese (II), chromium (II) or iron (II). A special synergic reactivity has been found with these types of mixed-metal compounds, as they can react in unique ways that cannot be replicated by their homometallic (non-ate) counterparts. [113,137,138] Selective deprotonations and polydeprotonations can be carried out on various substrates, including arenes, aromatic heterocycles, metallocenes and metal π-arene compounds. The terms alkali-metal-mediated magnesiation (AMM*Mg*), alkali-metal-mediated zincation (AMM*Zn*), alkali-metal-mediated alumination (AMM*Al*), alkali-metal-mediated manganation (AMM*Mn*) and alkali-metal-mediated organotransitionmetallation (AMMO) [for Cr and Fe] have been coined to describe these new types of deprotonative metallations. This section will focus on this topic of special synergic reactivity.

One of the ways in which the concept of synergy can be displayed is in the area of "inverse crown" chemistry. These types of structures formally comprise cationic "host" rings and anionic "guests". The term inverse crown is used as the host/guest Lewis acid–Lewis base sites have been reversed in comparison to those in traditional crown ether complexes (**figure 1.23**).
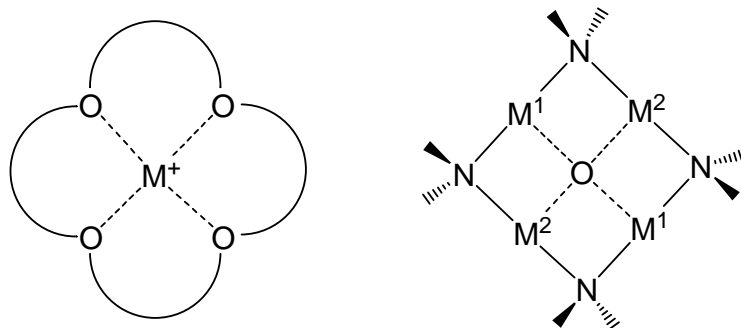
Figure 1.23: Structural motifs of a typical crown "ether" complex (left) and a typical inverse crown ether (right).

Reported in 1998, the concept of an inverse crown ether (ICE) was introduced through the lithium-magnesium formulation $[Li_2Mg_2(HMDS)_4(O)_x(O_2)_y]$.[139] This compound is constructed with an anionic core, comprising of either a single oxide or a peroxide ion, surrounded by an 8-membered ring where the metals are connected by the anionic nitrogen atom of the HMDS

ligands. Subsequently several ICE complexes have been published pairing the alkali metals lithium, sodium or potassium with magnesium,[140] zinc [141] or manganese.[142] The mechanism (or mechanisms) of the insertion of the oxy-anion is still unknown and has initially been ascribed to the presence of adventitious oxygen or moisture. Suitable amides involved in holding the framework together have been noted as 2,2,6,6-tetramethylpiperidide (TMP), 1,1,1,3,3,3-hexamethyldisilazide (HMDS) and diisopropylamide (DA). As well as peroxide and oxide ICE complexes, "guests" can also include alkoxides or hydrides, trapped within eight-membered "host" rings. With these types of mixed-metal compounds regioselectivity is not an issue, as either a simple deprotonation has taken place (for example, alcohol deprotonation [143]) or no deprotonative metallation occurs in the first instance (as in the case of hydrido inverse crown complexes [144]).

When considering the synthesis of inverse crowns, the identities of the metals and the amides involved are critical factors. The same can be said of the choice of solvent. ICE's were generated when the solvent used to carry out the reactions was a hydrocarbon. To a hexane solution of butylsodium, dibutylmagnesium and three molar equivalents of TMP(H), the addition of an arene co-solvent (benzene or toluene) produced the remarkable result of the encapsulation of a new guest, a regioselective, twofold deprotonated arene (1,4-positions for benzene and 2,5-positions for toluene, **scheme 1.16**).[145] The fact that benzene can be magnesiated at all by this reaction mixture was a major surprise as Grignard reagents, dialkyl (e.g. $^{n}Bu_2Mg$) and diamido (e.g. TMP_2Mg) magnesium reagents are inert towards this arene. Monometallation of benzene can be achieved using nBuLi·TMEDA, however, attempts of dimetallation using this reagent invariably results in a mixture of compounds.[146,147] For the case of toluene dideprotonation, the fact that the most acidic (in terms of pK_a) protons (on the methyl group) remain untouched is particularly significant, as conventional organometallics would be expected to attack this position first to generate resonance stabilised benzyl ($PhCH_2^-$) products. From the structural data obtained on these complexes, the arene ring lies orthogonal to the mean plane of the host ring and the Mg atoms have filled in the cleaved H sites, forming short, strong Mg–C σ bonds. In contrast, the sodium atoms are nearly perpendicular to the arene ring plane, forming Na–(π-arene) electrostatic interactions. Thus these reactions can be said to be magnesiations and not

sodiations, resulting in a reversal of the reactivity known for conventional organometallic reagents. The special reactivity of this sodium/magnesium brew towards benzene and toluene can thus be best thought of as alkali-metal-mediated magnesiations (AMM*Mg*).

BuNa + Bu$_2$Mg + 3 TMP(H)

hydrocarbon solvent
-2 BuH

"NaMg(Bu)(TMP)$_2$"

R = H or CH$_3$

excess

R
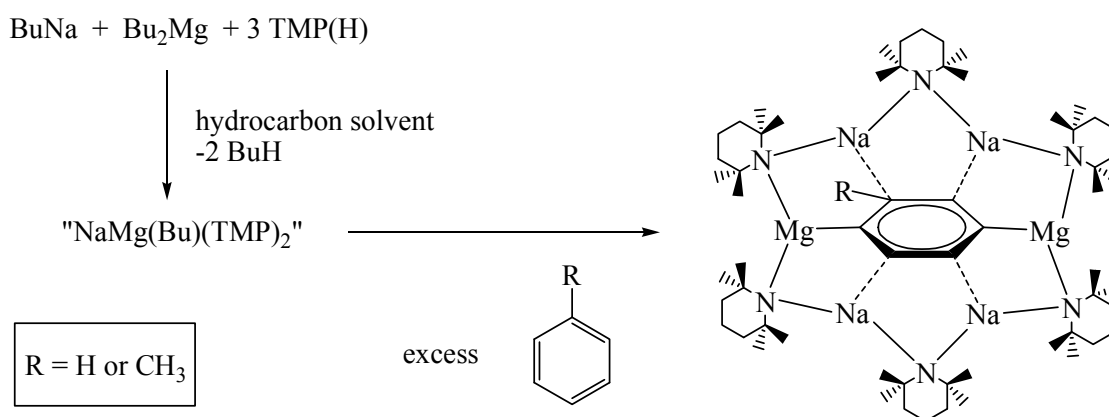
Scheme 1.16: Twofold deprotonation of benzene (R = H) and toluene (R = Me) to synthesise arenediide "guest" anions within a 12-membered inverse crown ring.

An investigation into elucidating the nature of the base responsible for the deprotonations in **scheme 1.16**, led to the isolation of the monoalkyl-bis(amido) complex [TMEDA·Na(μ-TMP)(μ-*^{n}*Bu)Mg(TMP)] (**1a**) after the addition of the chelating ligand TMEDA into the base reaction mixture.[148] This fully characterised base was subsequently found to be a very effective magnesiator. On addition of benzene to the bimetallic base, the butyl group is replaced by a monodeprotonated benzene molecule to make the compound [TMEDA·Na(μ-TMP)(μ-C$_6$H$_5$)Mg(TMP)]. Substituting benzene with toluene, regioselectivity comes into play and a *meta*-substituted toluene complex is produced, again with the loss of *n*-butane (**figure 1.24**).[149] This result was very surprising as homometallic bases cannot repeat this regioselectivity to any significant extent. Dimetallation of benzene can again be achieved using the even more reactive *t*-butyl variant of this mixed-metal reagent. Subjecting superfluous benzene to two molar equivalents of the mixture NaTMP/*^{t}*BuMgTMP/TMEDA leads to an open inverse crown where
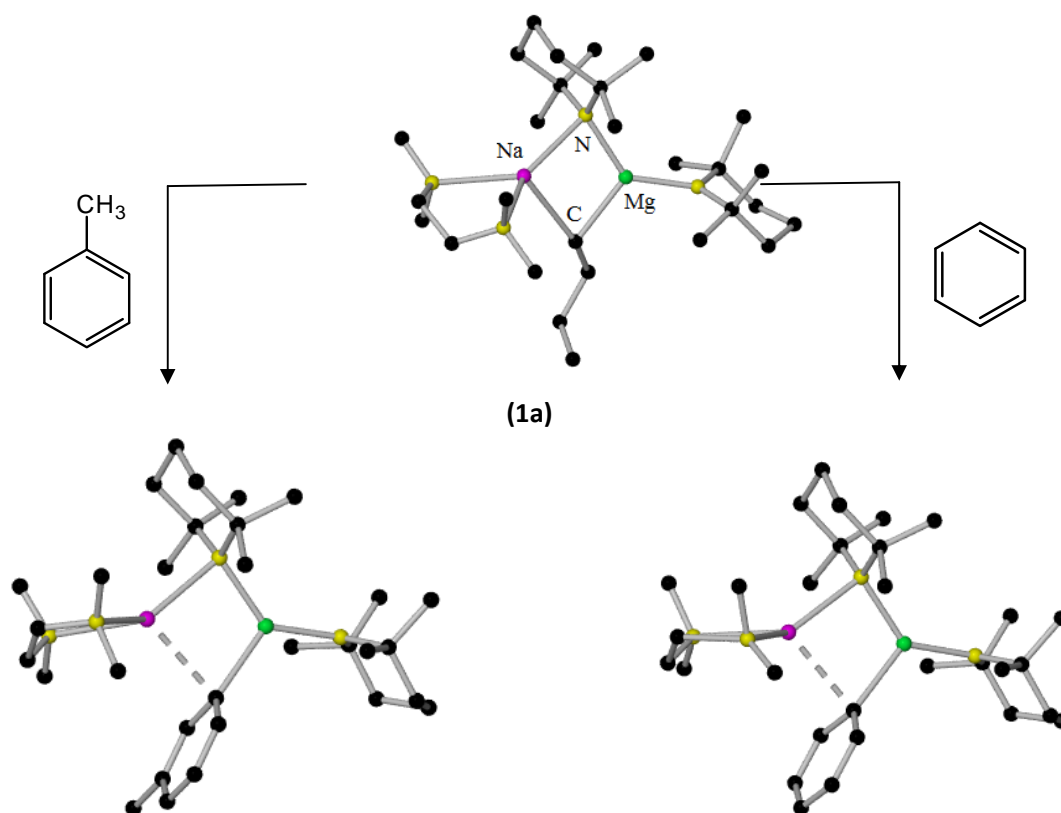
Figure 1.24: AMM*Mg* of benzene and toluene via magnesiate 1a. The interactions between sodium and the π-arene are indicted by a dashed line.

benzene is again twofold metallated at the 1,4-positions in which Mg engages in a σ-manner and Na interacts with the arenediide ring *via* its π-surface (**figure 1.25**).[150]

An investigation of the deprotonating ability of this sodium-magnesium mixed alkyl-amido base **1a** toward aromatic heterocycles has also been undertaken. The cyclic ether furan (C_4H_4O) undergoes alkali-metal-mediated α-magnesiation, giving rise to the unusual 12-membered inverse crown ring complex [{{(THF)$_3$.Na$_2$}{(TMEDA)·Mg$_2$}(2-C$_4$H$_3$O)$_6$}$_\infty$]. This macrocycle differs to previous inverse crown structures as the α-deprotonated furan is found in both the "host" and "guest" sites.[151]
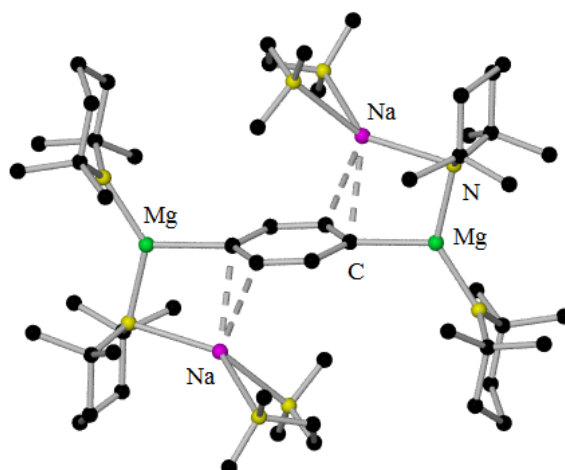
Figure 1.25: Molecular structure of the open inverse crown complex of dideprotonated benzene. The interactions between sodium and the π-arene are indicted by a dashed line.

AMM*Mg* has also been applied to the metal π-arene complexes bis(benzene)chromium [152] and bis(toluene)chromium [153] (**figure 1.26**). Though the metallation of one of the classical molecules in organometallic chemistry, bis(benzene)chromium, is not a new concept (as it can be dimetallated with conventional homometallic reagents such as BuLi·TMEDA)[154],
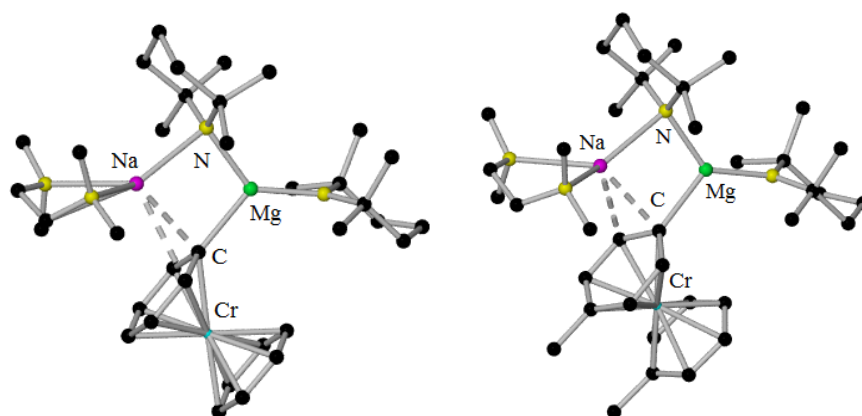
Figure 1.26: Molecular structures of the products of AMM*Mg* of bis(benzene)chromium [left] and bis(toluene)chromium [right].

monometallated products can usually only be obtained in a low yield (5-10%) and are always contaminated with some of the dimetallated product. However, using this mixed-metal approach, base **1a** can selectively mono-metallate the metallocene to afford [(TMEDA)·NaMg(TMP)$_2${(C$_6$H$_5$)Cr(C$_6$H$_6$)}] in good yields as a pure crystalline solid. Similar attempts to mono-metallate bis(benzene)chromium with butylsodium, butylpotassium or dibutylmagensium failed; however sodium–magnesium and potassium–magensium mixtures succeeded, thus demonstrating these monodeprotonations are synergic in nature. It is noteworthy that the AMM*Mg* of bis(toluene)chromium results in *para*-regioselectivity only.

Arguably the finest example of molecular synergy can be found in the field of metallocene deprotonation. Mono- or dideprotonation of metallocenes can be carried out by alkyllithium reagents in the presence of a donor ligand,[155,156] but controllable higher levels of deprotonation cannot be achieved to a synthetically useful extent. By applying AMM*Mg* to the Group 8 homologous series of ferrocene, ruthenocene and osmocene by the way of the sodium-magnesium tris(diisopropylamide) base, a remarkable four-fold deprotonation of these metallocenes can be achieved (**scheme 1.17**).[157,158] This selective tetramagnesiation results in 16-membered inverse crown ring complexes of general formula [{TM-(C$_5$H$_3$)$_2$}Na$_4$Mg$_4$(DA)$_8$] (where TM = Fe, Ru, or Os), where the Mg atoms substitute for the cleaved H atoms in the 1,1',3,3'-positions, hence, as a result these reactions can be classed as magnesiations. The mediation of the sodium is massively important and highlights the concept of synergic metallations, as direct magnesiation of any kind is not possible using conventional organomagnesium bases, such as Grignards or bisalkyl reagents. Knochel, however, has shown recently that ferrocene can be metallated more than once with the more reactive turbo-Grignard compound (TMP)MgCl·LiCl, although only a single deprotonation occurs at a time followed by an electrophilic quench.[159] It also has to be noted that even sodium diisopropylamide is a completely uneffective base towards these metallocenes.

Potassium-mediated magnesiation, which has revealed several impressive structures in the aromatic substrate area, will be discussed further on in this thesis.
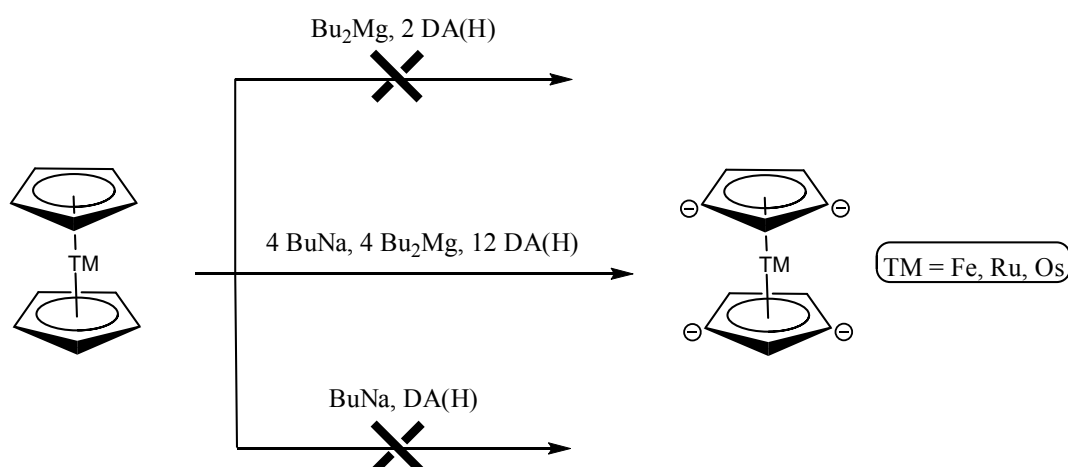
Scheme 1.17: Synergic AMM*Mg* fourfold deprotonation of the Group 8 metallocenes.

Due to the success of alkali-metal-mediated magnesiation, questions were asked as whether other metals could be paired with an alkali-metal to similarly enhance their reactivity. The group 12 metal zinc exhibits many properties similar to magnesium. For example it can assume a stable +2 oxidation state and it has a propensity to form trigonal planar ate geometries. Also, due to its increased electronegativity compared to magnesium, zinc generally forms stronger bonds with carbon, an ideal property which could be utilised when a post-metallation compound is generated, forming a strong Zn-carbon bond to the carbon-based substrate.

As mentioned earlier in this chapter, Na-TMP-zincate can be generated by the addition of ^{t}Bu$_2$Zn and NaTMP in the presence of one molar equivalent of TMEDA. The addition of TMEDA is crucial as the homometallic reagents do not form a cocomplex in hexane solution without it (**scheme 1.18**). Structurally, the sodium-zincate in **scheme 1.18** and the sodium-magnesiate in **figure 1.24** are closely related, with the main difference being that the magnesiate has a monoalkyl-bisamido formulation, whereas the zincate has a bisalkyl-monoamido template design.
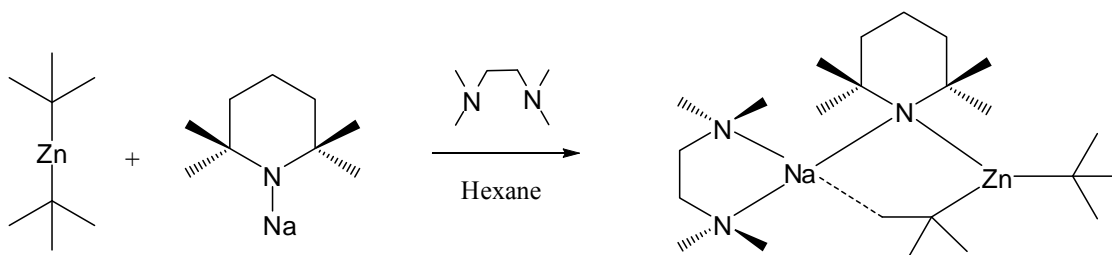
Scheme 1.18: Cocomplexation synthesis of the synergic Na-TMP-zincate base.

A host of other organic substrates can be zincated by this versatile base. Na-TMP-zincate regioselectively monozincates 1-methylpyrrole at the α-position,[160] *N,N*-diisopropylbenzamide at the *ortho* position [161] and *N,N*-dimethylaniline at the *meta* position (**figure 1.27**).[162] In all of these examples, the zincate acts as an alkyl base overall. The *meta*-metallation of *N,N*-dimethylaniline is particularly special as *ortho*-metallation would normally be expected with conventional reagents, and direct metallation of a tertiary aniline is not possible at any ring position when utilising mainstream alkylzinc reagents on their own.
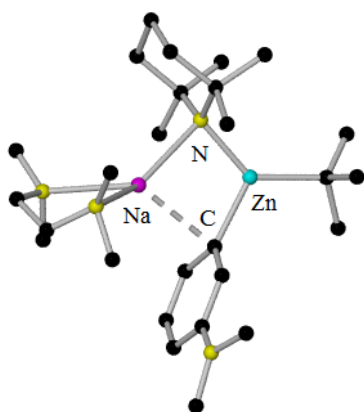
Figure 1.27: Molecular structure of [TMEDA·Na(µ-TMP)(µ-C$_6$H$_4$NMe$_2$)Zn(^{t}Bu)].

Na-TMP-zincate is also a very efficient zincator of polycyclic aromatic compounds, producing zincated compounds that conventional organozinc reagents just cannot access. Reacting Na-TMP-zincate with naphthalene in a 1:1 stoichiometric ratio affords the complex [(TMEDA)·Na(µ-TMP)(µ-2-C$_{10}$H$_7$)Zn(^{t}Bu)] where the polycyclic aromatic has been metallated in the 2-position, whereas reacting naphthalene and the base in a 1:2 ratio proceeds to the dizincated compound [TMEDA]$_2$Na$_2$(µ-2,6-C$_{10}$H$_6$)Zn$_2$(^{t}Bu)$_2$], where zinc atoms have replaced hydrogen atoms at the

2- and 6-positions (**scheme 1.19**).[163] This high degree of regioselectivity of the zincate base marks a huge improvement compared to the known reactions of ^{n}BuLi [164] or the superbasic LICKOR reagent [165] with naphthalene. These reagents produce non-selective mixtures of 1- and 2-substituted isomers, and even ten disubstituted isomers all in very poor yields.
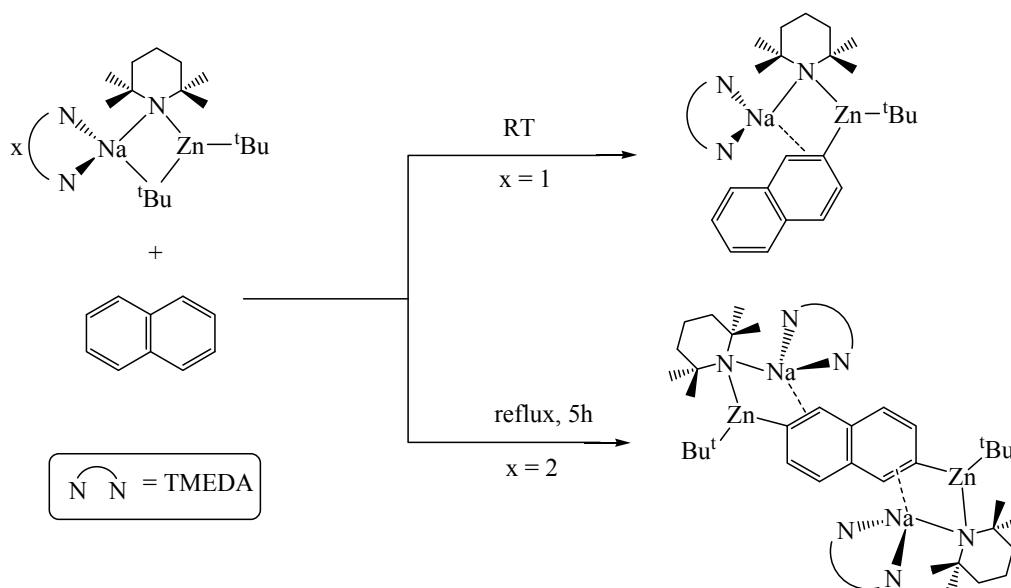
Scheme 1.19: Regioselective monozincation and dizincation of naphthalene with Na–TMP–zincate.

With respect to the metallation of toluene, Na-TMP-zincate behaves differently to that of the sodium bisamido-monoalkyl magnesiate which is selective to the sole deprotonation of the *meta* position of the arene ring. Though avoiding deprotonation of the methyl substituent, direct zincation of toluene can be achieved, however, generating a mixture of isolable *meta-* and *para-* zincated products (64.5% and 35.5% respectively).[166] The reason for this combination of products was established by DFT calculations [performed at the Hartree-Fock (HF) level using the 6-31G* basis set] that show that of the four possible regioisomeric products that can form, those of the *meta-* and *para-* substituted variety are the most energetically favourable, to almost the same degree. Hence these special zincations are thermodynamic in origin.

With alkali-metal-mediated magnesiation and alkali-metal-mediated zincation as established concepts, other metals have been introduced to this growing idea of molecular synergy. One of these metals was the group 13 element aluminium.[167-170] However, given the importance of aluminium to this PhD project, it will be discussed separately in further chapters of this thesis. In 2006, our own group started to investigate the pairing of an alkali-metal with the early transition metal manganese. By combining lithium and sodium amides with the generally inert homometallic manganese (II) reagent bis(trimethylsilylmethyl)manganese [(Me$_3$SiCH$_2$)$_2$Mn], a new cohort of bases started to emerge, starting with the dialkyl-monoamido lithium–manganese complex [TMEDA·Li(µ-TMP)(µ-CH$_2$SiMe$_3$)Mn(CH$_2$SiMe$_3$)] (Li-TMP-manganate, **figure 1.28**).[171] The trimethylsilylalkyl group was picked due to its advantageous properties of being thermally stable and insusceptibility to undergo decompoisition *via* β-hydride elimination.
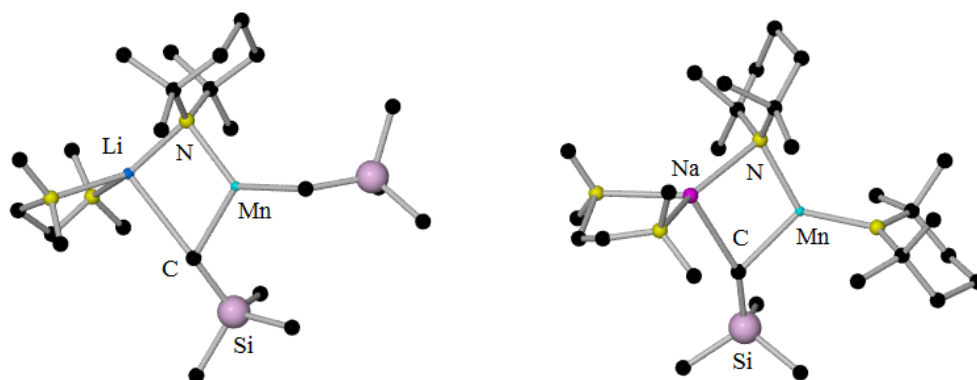
Figure 1.28: Molecular structures of [TMEDA·Li(µ-TMP)(µ-CH$_2$SiMe$_3$)Mn(CH$_2$SiMe$_3$)] (left) and [TMEDA·Na(µ-TMP)(µ-CH$_2$SiMe$_3$)Mn(TMP)] (right).

The idea of alkali-metal-mediated manganation was boosted by the 1,1' twofold deprotonation of ferrocene with Li-TMP-manganate to form the dilithium-dimanganese(II) trinuclear ferrocenophane [(TMEDA)$_2$Li$_2$Mn$_2${Fe(C$_5$H$_4$)$_2$}$_3$].[171] However, metallation of toluene failed with this base.

A stronger manganator, in the form of [TMEDA·Na(µ-TMP)(µ-CH$_2$SiMe$_3$)Mn(TMP)], was then introduced.[172] The effectiveness of this base was displayed in its manganating ability towards

N,N-diisopropylbenzamide and anisole, which delivered the isolable *ortho*-substituted products [TMEDA·Na(TMP){*o*-[C(O)N-^{i}Pr$_2$}C$_6$H$_4$}Mn(CH$_2$SiMe$_3$)] and TMEDA·Na(TMP)(o-C$_6$H$_4$OMe)Mn(TMP)] respectively.[173] The synthetic application of these isolated intermediates was highlighted through palladium-catalysed cross-coupling with iodobenzene under [PdCl$_2$(dppf)] catalysis to yield unsymmetrical biaryl compounds in good to excellent yields.

An interesting aspect of incorporating a transition metal into these mixed-metal systems is the possibility of the additional property of magnetism. Benzene can be directly dimanganated regioselectively in the 1,4-positions by the *in situ* mixture [Na$_4$Mn$_2$(TMP)$_6$(CH$_2$SiMe$_3$)$_2$], mimicking the previous reaction with magnesium (refer to **scheme 1.16**).[172] This double manganese-hydrogen exchange process yields the inverse crown [(TMP)$_6$Na$_4$(1,4-Mn$_2$C$_6$H$_4$)] which represents the first inverse crown in which a transition metal is incorporated into the host ring, and also the first paramagnetic inverse crown. Applying the same *in situ* base mixture to toluene resulted in a 3,5-dideprotonated toluene inverse crown [(TMP)$_6$Na$_4$(3,5-Mn$_2$C$_6$H$_3$CH$_3$)].[174] From this finding, the magnesium variant was synthesised by substituting ^{n}Bu to CH$_2$SiMe$_3$ (in **scheme 1.16**) to yield the *in situ* base mixture of [NaMg(CH$_2$SiMe$_3$)(TMP)$_2$]. This change of alkyl group in the sodium magnesiate base resulted in a change of regioselectivity from 2,5- to 3,5-positioned dimagnesiation, establishing that the reactivity of these bases can be tuned to metallate arenes selectively at different positions.

In 2009, the alkali-metal-mediated organotransitionmetallation involving Fe (II) or Cr (II), the nearest neighbours of manganese, was reported. The newest addition to the synergy family paired Cr(R)$_2$ (a tetranuclear structure) [R = Me$_3$SiCH$_2$$^-$] and Fe(R)$_2$ [an unstable molecule that needs a Lewis acid support] with sodium tetramethylpiperidide. The reaction of the base mixtures ½[Cr(CH$_2$SiMe$_3$)$_2$]$_4$/4NaTMP/2TMP(H) and 2[(TMEDA·Fe(CH$_2$SiMe$_3$)$_2$]/4NaTMP/2TMP(H) with benzene produced the 1,4-dimetallated inverse crowns [(TMP)$_6$Na$_4$(1,4-Cr$_2$C$_6$H$_4$)] and [(TMP)$_6$Na$_4$(1,4-Fe$_2$C$_6$H$_4$)] respectively [175] (**scheme 1.20**), akin to those of AMM*Mg* and AMM*Mn* of benzene. These results were remarkable, as CrR$_2$ was deemed chemically inert to even strongly acidic molecules such as

carboxylic acids and phenols,[176] while FeR_2 requires prechelation with TMEDA before the addition of the rest of the reaction mixture, which asked questions over whether mixed-metal products would be possible to generate in this system.
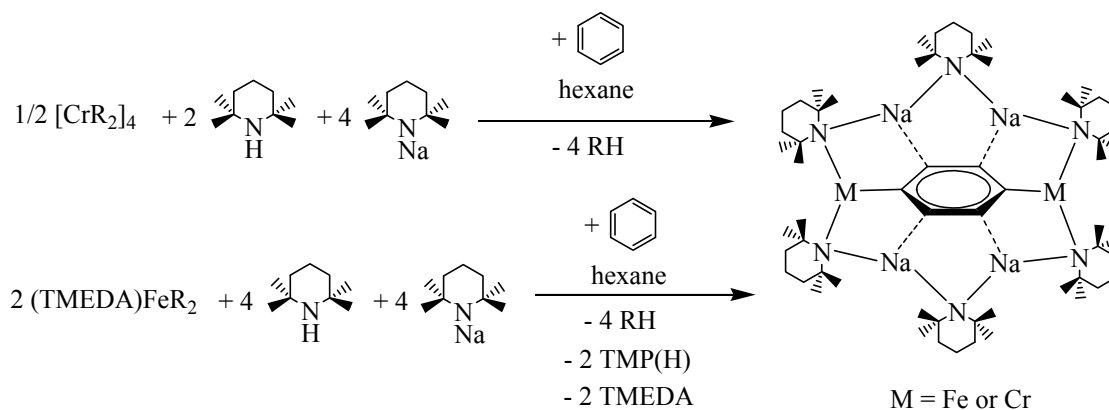
Scheme 1.20: Preparation of the sodium ferrate and sodium chromate inverse crowns.

This brief description of the research performed with the Mulvey group shows that alkali-metal-mediated metallation in general offers a wide application of these types of bases to a variety of substrates. The large programme of work carried out independently by Mulvey, Knochel and Uchiyama, as well as a host of other groups, have shown that mono- and multifunctionalisation of many compounds can be achieved and that these mixed-metal reagents have a leading role to play in synthesis. This study aims to build on the topic of alkali-metal-mediated metallation by introducing structures, reactivity and mechanisms of several new potassium zincates, magnesiates and aluminates, all generated by the alkali-metal reagent KCH_2SiMe_3 which is central to the synthesis of these ate complexes.

Chapter 1 – References:

[1]   W. Schlenk, J. Appenrodt, A. Michael, A. Thal, *Ber. Dtsch. Chem. Ger*. **1914**, *47*, 473.

[2]   W. Schlenk, J. Holtz, *Ber. Dtsch. Chem. Ger*. **1917**, *50*, 272.

[3]   H. Gilman, E. A. Zollner, W. M. Selby, *J. Am. Chem. Soc*. **1932**, *54*, 1957.

[4]   H. Gilman, F. W. More, O. Baine, *J. Am. Chem. Soc*. **1941**, *63*, 2479.

[5]   G. Wittig, U. Pockels, H. Droge, *Ber. Dtsch. Chem. Ger*. **1938**, *71*, 1903.

[6]   K. Zeigler, H. Colonius, *Liebigs Ann. Chem*. **1930**, *476*, 135.

[7]   J. Clayden, *Organolithiums: Selectivity for Synthesis*, *Vol. 23*, Pergamon, Oxford, **2002**.

[8]   W. F. Bailey, J. J. Patricia, *J. Organomet. Chem*. **1988**, *352*, 1.

[9]   B. J. Wakefield, *The Chemistry of Organolithium Compounds*, Pergamon, Oxford, **1974**.

[10]   H. Dietrich, *Acta. Crystallogr*. **1963**, *16*, 681.

[11]   H. Dietrich, *J. Organomet. Chem*. **1981**, *205*, 291.

[12]   E. Weiss, A. C. Lucken, *J. Organomet. Chem*. **1964**, *2*, 197.

[13]   B. Tecle, A. F. M. M. Rahman, J. P. Oliver, *J. Organomet. Chem*. **1986**, *317*, 267.

[14]   A. Douhdou, C. Woltermann, P. C. Gros, *J. Org. Chem*. **2007**, *72*, 4978.

[15]   G. G. Skvortsov, G. K. Fukin, A. A. Trifonov, A. Noor, C. Döring, R. Kempe, *Organometallics* **2007**, *26*, 5770.

[16]   T. Tatic, H. Ott, D. Stalke, *Eur. J. Inorg. Chem*. **2008**, 3765.

[17]   C. Strohmann, V. H. Gessner, *Angew. Chem. Int. Ed*. **2007**, *46*, 4566.

[18]   C. Strohmann, V. H. Gessner, *Angew. Chem. Int. Ed*. **2007**, *46*, 8281.

[19]   C. Strohmann, V. H. Gessner, *J. Am. Chem. Soc*. **2007**, *129*, 8952.

[20]   A. W. Titherly, *J. Chem. Soc*. **1894**, *65*, 504.

[21]   D. Mootz, A. Zinnius, B. Bottcher, *Angew. Chem. Int. Ed*. **1969**, *8*, 378.

[22]   R. D. Rogers, J. L. Atwood, R. Gruning, *J. Organomet. Chem*. **1978**, *157*, 229.

[23]   M. Hammell, R. Levine, *J. Am. Chem. Soc*. **1950**, *72*, 162.

[24]   G. Stork, L. Maldonado, *J. Am. Chem. Soc*. **1971**, *93*, 5286.

[25]   D. Seebach, D. Enders, *Angew. Chem. Int. Ed.* **1972**, *11*, 301.

[26]   D. Seebach, D. Enders, *Angew. Chem. Int. Ed.* **1975**, *14*, 15.

[27]   D. B. Collum, A. J. McNeill, A. Ramirez, *Angew. Chem. Int. Ed.* **2007**, *46*, 3002.

[28]   N. D. R. Barnett, R. E. Mulvey, W. Clegg, P. A. O'Neil, *J. Am. Chem. Soc.* **1991**, *113*, 8187.

[29]   M. F. Lappert, M. J. Slade, A. Singh, J. L. Atwood, R. D. Rogers, R. Shakir, *J. Am. Chem. Soc.* **1983**, *105*, 302.

[30]   J. Jubb, P. Berno, S. Hao, S. Gambarotta, *Inorg. Chem.* **1995**, *34*, 3563.

[31]   L. Ruwisch, U. Klingebeil, S. Rudolph, R. Herbst-Irmer, M. Noltemeyer, *Chem. Ber.* **1996**, *129*, 823.

[32]   F. Antolini, P. B. Hitchcock, M. F. Lappert, P. G. Merle, *Chem. Commun.* **2000**, 1301.

[33]   R. Snaith, D. Barr, D. S. Wright, W. Clegg, S. M. Hodgson, G. R. Lamming, A. J. Scott, R. E. Mulvey, *Angew. Chem. Int. Ed.* **1989**, *28*, 1241.

[34]   D. R. Armstrong, D. Barr, R. Snaith, W. Clegg, R. E. Mulvey, K. Wade, D. Reed, *J. Chem. Soc., Dalton. Trans.* **1987**, 1071.

[35]   M. P. Bernstein, F. E. Romesburg, D. J. Fuller, A. T. Harrison, D. B. Collum, Q. Y. Liu, P. G. Williard, *J. Am. Chem. Soc.* **1992**, *114*, 5100.

[36]   P. G. Williard, J. M. Salvino, *J. Org. Chem.* **1993**, *58*, 1.

[37]   P. G. Williard, Q. Y. Liu, *J. Am. Chem. Soc.* **1993**, *115*, 3380.

[38]   J. F. Remenar, B. L. Lucht, D. Kruglyak, F. E. Romesburg, J. H. Gilchrist, D. B. Collum, *J. Org. Chem.* **1997**, *62*, 5748.

[39]   K. W. Henderson, A. E. Dorigo, Q. Y. Liu, P. G. Williard, *J. Am. Chem. Soc.* **1997**, *119*, 11855.

[40]   J. A. Wanklyn, *Justus Liebigs Ann. Chem.* **1858**, *44*, 6018.

[41]   A. A. Morton, J. B. LeFevre, I. Heckenblieker, *J. Am. Chem. Soc.* **1936**, *58*, 754.

[42]   M. Bockmühl, G. Ehrhart, U. S. Patent 2,012,372, 8/27/1935.

[43]   J. F. Nobis, L. F. Moormeier, R. E. Robinson, *Metal-Organic Compounds*, American Chemical Society, Washington D.C., **1959**.

[44]   A. A. Morton, J. B. Davidson, R. J. Best, *J. Am. Chem. Soc.* **1942**, *64*, 2239.

[45]   R. N. Meals, *J. Org. Chem.* **1944**, *9*, 211.

[46]   P. Schorigin, *Ber. Dtsch. Chem. Ger.* **1908**, *41*, 2711.

[47]   R. E. Bates, L. M. Kroposki, D. E. Potter, *J. Org. Chem.* **1972**, *37*, 560.

[48]   I. Fleming, S. R. Mack, B. P. Clark, *J. Chem. Soc., Chem. Commun.* **1998**, 713.

[49]   P. v. R. Schleyer, C. Schade, W. Bauer, *J. Organomet. Chem.* **1985**, *295*, C25.

[50]   E. Weiss, S. Corbelin, J. K. Cockroft, A. N. Fitch, *Angew. Chem. Int. Ed.* **1990**, *29*, 650.

[51]   E. Weiss, G. Sauermann, *J. Organomet. Chem.* **1970**, *21*, 1.

[52]   R. Gruning, J. L. Atwood, *J. Organomet. Chem.* **1977**, *137*, 101.

[53]   M. Dreiss, H. Pritzkow, M. Skipinski, U. Winkler, *Organometallics* **1997**, *16*, 5108.

[54]   J. Knizek, I. Krossing, H. Nöth, H. Schwenk, T. Seifert. *Chem. Ber. / Recl.* **1997**, *130*, 1053.

[55]   P. C. Andrews, N. D. R. Barnett, R. E. Mulvey, W. Clegg, P. A. O'Neil, D. Barr, L. Cowton, A. J. Dawson, B. J. Wakefield, *J. Organomet. Chem.* **1996**, *518*, 85.

[56]   D. R. Armstrong, D. V. Graham, A. R. Kennedy, R. E. Mulvey, C. T. O'Hara, *Chem. Eur. J.* **2008**, *14*, 8025.

[57]   P. C. Andrews, D. R. Armstrong, W. Clegg, M. MacGregor, R. E. Mulvey, *J. Chem. Soc., Chem. Commun.* **1991**, 497.

[58]   C. Eaborn, P. B. Hitchcock, K. Izod, A. J. Jagger, J. D. Smith, *Organometallics* **1994**, *13*, 753.

[59]   C. Eaborn, W. Clegg, P. B. Hitchcock, M. Hopman, K. Izod, P. N. O'Shaughnessy, J. D. Smith, *Organometallics* **1997**, *16*, 4728.

[60]   W. M. Boesveld, P. B. Hitchcock, M. F. Lappert, D.-S. Liu, S. Tian, *Organometallics* **2000**, *19*, 4030.

[61]   K. F. Tesh, T. P. Hanusa, J. C. Huffman, *Inorg. Chem.* **1990**, *29*, 1584.

[62]   W. Clegg, S. Kleditzsch, R. E. Mulvey, P. N. O'Shaughnessy, *J. Organomet. Chem.* **1998**, *558*, 193.

[63]   E. Frankland, *Ann.* **1849**, *71*, 171.

[64]   J. A. Wanklyn, *J. Chem. Soc.* **1861**, *13*, 124.

[65]   J. H. Gladstone, A. Tribe, *J. Chem. Soc.* **1873**, *26*, 455.

[66]   M. L. Hlavinka, J. F. Greco, J. R. Hagadorn, *Chem. Commun.* **2005**, 5304.

[67]   M. L. Hlavinka, J. R. Hagadorn, *Organometallics* **2007**, *26*, 4105.

[68]   W. S. Rees, O. Just, H. Schumann, R. Weinmann, *Polyhedron* **1998**, *17*, 1001.

[69]   V. Grignard, *Compt. Rend. Acad. Sci. Paris* **1900**, *130*, 1322.

[70]   Halomagnesium amides of empirical formula R_2NMgX were first introduced by Meunier: L. Meunier, *C. R. Hebd. Seances Acad. Sci*. **1903**, *136*, 758.

[71]   K. W. Henderson, W. S. Kerr, *Chem. Eur. J*. **2001**, *7*, 3430.

[72]   P. E. Eaton, C. H. Lee, Y. Xiong, *J. Am. Chem. Soc*. **1985**, *111*, 8016.

[73]   Y. Kondo, A. Yoshida, T. Sakamoto, *J. Chem. Soc., Perkin Trans. 1* **1996**, 2331.

[74]   H. Yamamoto, K. Oshima, *Main Group Metals in Organic Synthesis, Vol. 1,* Wiley-VCH, Weinheim, **2004**, chap. 6.

[75]   S. H. Wunderlich, P. Knochel, *Angew. Chem. Int. Ed*. **2009**, *48*, 1501.

[76]   B. Liang, T. Novak, Z. Tan, E. Negishi, *J. Am. Chem. Soc*. **2006**, *128*, 2770.

[77]   F. H. Allen, *Acta Crystallogr., Sect. B: Struct. Sci*. **2002**, *58*, 380.

[78]   C. Klein, H. Nöth, M. Tacke, M. Thomann, *Angew. Chem. Int. Ed*. **1993**, *32*, 886.

[79]   I. Krossing, H. Nöth, C. Tacke, M. Schmidt, H. Schwenk, *Chem. Ber*. **1997**, *130*, 1047.

[80]   I. Krossing, H. Nöth, H. Schwenk, *Eur. J. Inorg. Chem*. **1998**, 927.

[81]   K. Knabel, I. Krossing, H. Nöth, H. Schwenk, M. Schmidt, T. Seifert, *Eur. J. Inorg. Chem*. **1998**, 1095.

[82]   T. Habereder, H. Nöth, R. T. Paine, *Eur. J. Inorg. Chem*. **2007**, 4298.

[83]   A. Yasuda, S. Tanaka, K. Oshima, H. Yamamoto, H. Nozaki, *J. Am. Chem. Soc*. **1974**, *96*, 6513.

[84]   H. Nozaki, K. Oshima, K. Takai, S. Ozawa, *Chem. Lett*. **1979**, 379.

[85]   K. Maruoka, M. Oishi, H. Yamamoto, *J. Org. Chem*. **1993**, *58*, 7638.

[86]   G. Wittig, F. J. Meyer, G. Lange, *Ann*. **1951**, *571*, 167.

[87]   G. Wittig, F. Bickelhaupt, *Chem. Ber*. **1958**, *91*, 865.

[88]   E. Weiss, U. Schumann, *Angew. Chem*. **1988**, *100*, 573.

[89]   L. Lochmann, J. Pospíšil, J. Vodnansky, J. Trekoval, D. Lim, *Collect. Czech. Chem. Commun*. **1965**, *61*, 2187.

[90]   L. Lochmann, J. Pospíšil, D. Lim, *Tetrahedron Lett*. **1966**, *7*, 257.

[91]   M. Schlosser, *J. Organomet. Chem*. **1967**, *8*, 9.

[92]   M. Schlosser, F. Faigl, L. Franzini, H. Geneste, G. Katsoulos, G.-F. Zhong, *Pure Appl. Chem*. **1994**, *66*, 1439.

[93]   L. Lochmann, *Eur. J. Inorg. Chem*. **2000**, 1115.

[94]   A. A. Morton, C. E. Claff, *J. Am. Chem. Soc*. **1954**, *76*, 4935.

[95]   A. A. Morton, C. E. Claff, F. W. Collins, *J. Org. Chem*. **1955**, *20*, 428.

[96]   M. Schlosser, *Mod. Synth. Methods* **1992**, *6*, 227.

[97]   M. Schlosser, G. Katsoulos, S. Takagashi, *Synlett* **1990**, 747.

[98]   M. Schlosser, F. Mongin, J. Porwisiak, W. Dmowski, H. H. Büker, N. M. M. Nibbering, *Chem. Eur. J.* **1998**, *4*, 1281.

[99]   M. Schlosser, J. H. Choi, S. Takagishi, *Tetrahedron* **1990**, *46*, 5633.

[100] A. Krasovskiy, P. Knochel, *Angew. Chem. Int. Ed*. **2004**, *43*, 3333.

[101] H. Ren, A. Krasovshiy, P. Knochel, *J. Org. Chem*. **2004**, *6*, 4215.

[102] Z. Rappoport, I. Marek, *The Chemistry of Organomagnesium Compounds, Part 2,* Wiley-VCH, Weinheim, **2008**, chap. 12.

[103] C. J. Rohbogner, G. C. Clososki, P. Knochel, *Angew. Chem. Int. Ed*. **2008**, *47*, 1503.

[104] L. Shi, Y. Chu, P. Knochel, H. Mayr, *Angew. Chem. Int. Ed*. **2008**, *47*, 202.

[105] S. H. Wunderlich, P. Knochel, *Angew. Chem. Int. Ed*. **2007**, *46*, 7681.

[106] C. J. Rohbogner, S. H. Wunderlich, G. C. Clososki, P. Knochel, *Eur. J. Org. Chem*. **2009**, 1781.

[107] W. Lin, O. Baron, P. Knochel, *Org. Lett*. **2006**, *8*, 5673.

[108] A. Krasovskiy, V. Krasovskaya, P. Knochel, *Angew. Chem. Int. Ed*. **2006**, *45*, 2958.

[109] S. H. Wunderlich, P. Knochel, *Chem. Commun*. **2008**, 6387.

[110] S. H. Wunderlich, M. Kienle, P. Knochel, *Angew. Chem. Int. Ed*. **2009**, *48*, 7256.

[111] M. Mosrin, G. Monzon, T. Bresser, P. Knochel, *Chem. Commun*. **2009**, 5615.

[112] P. García-Álvarez, D. V. Graham, E. Hevia, A. R. Kennedy, J. Klett, R. E. Mulvey, C. T. O'Hara, S. Weatherstone, *Angew. Chem. Int. Ed*. **2008**, *47*, 8079.

[113] R. E. Mulvey, F. Mongin, M. Uchiyama, Y. Kondo, *Angew. Chem. Int. Ed*. **2007**, *46*, 3802.

[114] B. Schubert, E. Weiss, *Chem. Ber*. **1984**, *117*, 366.

[115] T. Greiser, J. Kopf, D. Thoennes, E. Weiss, *Chem. Ber*. **1981**, *114*, 209.

[116] G. Castaldi, G. Borsotti, Eur. Patent 491326A2, **1992**. [*Chem. Abstr*. **1992**, *117,* 150667].

[117] H. Awad, F. Mongin, F. Trécourt, G. Quéguiner, F. Marsais, *Tetrahedron Lett*. **2004**, *45*, 7873.

[118]   F. Mongin, A. Bucher, J. P. Bazureau, O. Bayh, H. Awad, F. Trécourt, *Tetrahedron Lett.* **2005**, *46*, 7989.

[119]   O. Bayh, H. Awad, F. Mongin, C. Hoarau, F. Trécourt, G. Quéguiner, F. Marsais, F. Blanco, B. Abarca, R. Ballesteros, *Tetrahedron* **2005**, *61*, 4779.

[120]   O. Bayh, H. Awad, F. Mongin, C. Hoarau, L. Bischoff, F. Trécourt, G. Quéguiner, F. Marsais, F. Blanco, B. Abarca, R. Ballesteros, *J. Org. Chem.* **2005**, *70*, 5190.

[121]   K. Snégaroff, J.-M. L'Helgoual'ch, G. Bentabed-Ababsa, T. T. Nguyen, F. Chevallier, M. Yonehara, M. Uchiyama, A. Derdour, F. Mongin, *Chem. Eur. J.* **2009**, *15*, 10280.

[122]   M. Uchiyama, M. Kameda, O. Mishima, N. Yokoyama, M. Koike, Y. Kondo, T. Sakamoto, *J. Am. Chem. Soc.* **1998**, *120*, 4934.

[123]   Y. Kondo, M. Fujinami, M. Uchiyama, T. Sakamoto, *J. Chem. Soc., Perkin Trans. 1* **1997**, 799.

[124]   Y. Kondo, N. Takazawa, C. Yamazaki, T. Sakamoto, *J. Org. Chem.* **1994**, *59*, 4717.

[125]   M. Uchiyama, M. Koike, M. Kameda, Y. Kondo, T. Sakamoto, *J. Am. Chem. Soc.* **1996**, *118*, 8733.

[126]   T. Katsuhira, T. Harada, K. Maejima, A. Osada, A. Oku, *J. Org. Chem.* **1993**, *58*, 6166.

[127]   Y. Kondo, M. Shilai, M. Uchiyama, T. Sakamoto, *J. Am. Chem. Soc.* **1999**, *121*, 3539.

[128]   M. Uchiyama, Y. Matsumoto, K. Morokuma, S. Usai, Y. Hashimoto, *Angew. Chem. Int. Ed.* **2007**, *46*, 926.

[129]   M. Uchiyama, Y. Matsumoto, D. Nobuto, T. Furuyama, K. Yamaguchi, K. Morokuma, *J. Am. Chem. Soc.* **2006**, *128*, 8748.

[130]   W. Clegg, S. H. Dale, E. Hevia, G. Honeyman, R. E. Mulvey, *Angew. Chem. Int. Ed.* **2006**, *45*, 2370.

[131]   P. C. Andrikopoulos, D. R. Armstrong, H. R. L. Barley, W. Clegg, S. H. Dale, E. Hevia, G. W. Honeyman, A. R. Kennedy, R. E. Mulvey, *J. Am. Chem. Soc.* **2005**, *127*, 6184.

[132]   D. Nobuto, M. Uchiyama, *J. Org. Chem.* **2008**, *73*, 1117.

[133]   W. Clegg, B. Conway, E. Hevia, M. D. McCall, L. Russo, R. E. Mulvey, *J. Am. Chem. Soc.* **2009**, *131*, 2375.

[134]   M. Uchiyama, H. Naka, Y. Matsumoto, T. Ohwada, *J. Am. Chem. Soc.* **2004**, *126*, 10526.

[135]   H. Naka, M. Uchiyama, Y. Matsumoto, A. E. H. Wheatley, M. McPartlin, J. V. Morey, Y. Kondo, *J. Am. Chem. Soc.* **2007**, *129*, 1921.

[136]   H. Naka, J. V. Morey, J. Haywood, D. J. Eisler, M. McPartlin, F. Garcia, H. Kudo, Y. Kondo, M. Uchiyama, A. E. H. Wheatley, *J. Am. Chem. Soc.* **2008**, *130*, 16193.

[137]   R. E. Mulvey, *Organometallics* **2006**, *25*, 1060.

[138]   R. E. Mulvey, *Acc. Chem. Res.* **2009**, *42*, 743.

[139]   A. R. Kennedy, R. E. Mulvey, R. B. Rowlings, *J. Am. Chem. Soc*. **1998**, *120*, 7816.

[140]   A. R. Kennedy, R. E. Mulvey, C. L. Raston, B. A. Roberts, R. B. Rowlings, *Chem. Commun*. **1999**, 353.

[141]   G. C. Forbes, A. R. Kennedy, R. E. Mulvey, R. B. Rowlings, W. Clegg, S. T. Liddle, C. C. Wilson, *Chem. Commun*. **2000**, 1759.

[142]   A. R. Kennedy, L. Klett, R. E. Mulvey, S. Newton, D. S. Wright, *Chem. Commun.* **2008**, 308.

[143]   K. J. Drewette, K. W. Henderson, A. R. Kennedy, R. E. Mulvey, C. T. O'Hara, R. B. Rowlings, *Chem. Commun*. **2002**, 1176.

[144]   D. J. Gallagher, K. W. Henderson, A. R. Kennedy, C. T. O'Hara, R. E. Mulvey, R. B. Rowlings, *Chem. Commun*. **2002**, 376.

[145]   D. R. Armstrong, A. R. Kennedy, R. E. Mulvey, R. B. Rowlings, *Angew. Chem. Int. Ed.* **1999**, *38*, 131.

[146]   C. D. Broaddus, *J. Org. Chem*. **1970**, *35*, 10.

[147]   C. D. Broaddus, *J. Am. Chem. Soc*. **1966**, *88*, 4174.

[148]   E. Hevia, D. J. Gallagher, A. R. Kennedy, R. E. Mulvey, C. T. O'Hara, C. Talmard, *Chem. Commun*. **2004**, 2422.

[149]   P. C. Andrikopoulos, D. R. Armstrong, D. V. Graham, E. Hevia, A. R. Kennedy, R. E. Mulvey, C. T. O'Hara, C. Talmard, *Angew. Chem. Int. Ed*. **2005**, *44*, 3459.

[150]   D. R. Armstrong, W. Clegg, S. H. Dale, D. V. Graham, E. Hevia, L. M. Hogg, G. W. Honeyman, A. R. Kennedy, R. E. Mulvey, *Chem. Commun*. **2007**, 598.

[151]   D. V. Graham, E. Hevia, A. R. Kennedy, R. E. Mulvey, C. T. O'Hara, C. Talmard, *Chem. Commun*. **2006**, 417.

[152]   E. Hevia, G. W. Honeyman, A. R. Kennedy, R. E. Mulvey, D. C. Sherrington, *Angew. Chem. Int. Ed.* **2005**, *44*, 68.

[153]   P. C. Andrikopoulos, D. R. Armstrong, E. Hevia, A. R. Kennedy, R. E. Mulvey, *Organometallics*, **2006**, *25*, 2415.

[154]   C. J. Eisenbroch, *J. Organomet. Chem*. **1968**, *14*, 157.

[155]   F. Rebiere, O. Samuel, H. B. Kagan, *Tetrahedron Lett*. **1990**, *31*, 3121.

[156]   I. R. Butler, W. R. Cullen, J. Ni, S. J. Rettig, *Organometallics* **1985**, *4*, 2196.

[157] W. Clegg, K. W. Henderson, A. R. Kennedy, R. E. Mulvey, C. T. O'Hara, R. B. Rowlings, D. M. Tooke, *Angew. Chem. Int. Ed.* **2001**, *40*, 3902.

[158] P. C. Andrikopoulos, D. R. Armstrong, W. Clegg, C. J. Gilfillan, E. Hevia, A. R. Kennedy, R. E. Mulvey, C. T. O'Hara, D. M. Tooke, J. A. Parkinson, *J. Am. Chem. Soc.* **2004**, *126*, 11612.

[159] A. H. Stoll, P. Mayer, P. Knochel, *Organometallics* **2007**, *26*, 6694.

[160] B. Conway, E. Hevia, A. R. Kennedy, R. E. Mulvey, *Chem. Commun.* **2007**, 2864.

[161] W. Clegg, S. H. Dale, R. W. Harrington, E. Hevia, G. W. Honeyman, R. E. Mulvey, *Angew. Chem. Int. Ed.* **2006**, *45*, 2374.

[162] D. R. Armstrong, W. Clegg, S. H. Dale, E. Hevia, L. M. Hogg, G. W. Honeyman, R. E. Mulvey, *Angew. Chem. Int. Ed.* **2006**, *45*, 3775.

[163] W. Clegg, S. H. Dale, E. Hevia, L. M. Hogg, G. W. Honeyman, R. E. Mulvey, C. T. O'Hara, *Angew. Chem. Int. Ed.* **2006**, *45*, 6548.

[164] H. Gilman, R. L. Bebb, *J. Am. Chem. Soc.* **1939**, *61*, 109.

[165] E. Baston, R. Maggi, K. Friedrich, M. Schlosser, *Eur. J. Org. Chem.* **2001**, 3985.

[166] D. R. Armstrong, J. García-Álvarez, D. V. Graham, G. W. Honeyman, E. Hevia, A. R. Kennedy, R. E. Mulvey, *Chem. Eur. J.* **2009**, *15*, 3800.

[167] J. Garcia-Álvarez, D. V. Graham, A. R. Kennedy, R. E. Mulvey, S. Weatherstone, *Chem. Commun.* **2006**, 3208.

[168] J. Garcia-Álvarez, E. Hevia, A. R. Kennedy, J. Klett, R. E. Mulvey, *Chem. Commun.* **2007**, 2402.

[169] B. Conway, E. Hevia, J. García-Álvarez, D. V. Graham, A. R. Kennedy, R. E. Mulvey, *Chem. Commun.* **2007**, 5241.

[170] B. Conway, J. García-Álvarez, E. Hevia, A. R. Kennedy, R. E. Mulvey, S. D. Robertson, *Organometallics*, **2009**, *28*, 6462.

[171] J. García-Álvarez, A. R. Kennedy, J. Klett, R. E. Mulvey, *Angew. Chem. Int. Ed.* **2007**, *46*, 1105.

[172] L. M. Carrella, W. Clegg, D. V. Graham, L. M. Hogg, A. R. Kennedy, J. Klett, R. E. Mulvey, E. Rentschler, L. Russo, *Angew. Chem. Int. Ed.* **2007**, *46*, 4662.

[173] V. L. Blair, W. Clegg, B. Conway, E. Hevia, A. R. Kennedy, J. Klett, R. E. Mulvey, L. Russo, *Chem. Eur. J.* **2008**, *14*, 65.

[174] V. L. Blair, L. M. Carrella, W. Clegg, B. Conway, R. W. Harrington, L. M. Hogg, J. Klett, R. E. Mulvey, E. Rentschler, L. Russo, *Angew. Chem. Int. Ed.* **2008**, *47*, 6208.

[175] P. Alborés, L. M. Carrella, W. Clegg, P. García-Álvarez, A. R. Kennedy, J. Klett, R. E. Mulvey, E. Rentschler, L. Russo, *Angew. Chem. Int. Ed*. **2009**, *48*, 3317.

[176] C. Schulzke, D. Enright, H. Sugiyama, G. LeBlanc, S. Gambarotta, G. P. A. Yap, *Organometallics* **2002**, *21*, 3810.

Chapter 2: Homometallic Potassium Reagents – Precursors to bimetallics

2.1) Introduction

The starting point of this study required the use of a clean, easy to handle compound of potassium. It should be able to react cleanly with secondary amines to form stable potassium amide complexes. This chapter will reveal the source of this potassium reagent and its successful transformation to an excellent potassium amide starting material, which will be used in conjunction with other organometallic compounds in subsequent chapters to showcase the new concept of potassium-metal-mediated metallation.

2.2) Organopotassiums in synthesis

Homometallic potassium compounds, though not as well established as lithium reagents, have been utilised as bases in a handful of deprotonation reactions. However, many potassium compounds are not made directly but instead a substrate is prelithiated and then reacted onwards with for example potassium *t*-butoxide, to yield the desired potassium compound and lithium *t*-butoxide in a transmetallation reaction. There are examples where direct potassiations of organic substrates are possible. Organopotassium reagents tend to be considerably more reactive than their smaller group 1 congeners. For example, as a comparison *n*-butylsodium can react with cyclopentene and cyclohexene, in ether, deprotonating these species at the olefinic position exclusively. *n*-Butylpotassium (*n*BuK) on the other hand deprotonates cyclopentene at the olefinic and allylic positions with very little discrimination between the two sites, highlighting its superior reactivity.[1] With cyclohexene, however, a degree of regioselectivity is witnessed as the potassium reagent deprotonates solely at the allylic position, in total contrast to the sodium product, 1-cyclohexenylsodium (**scheme 2.1**). An advantageous property that *n*-butylpotassium

holds is that butane is released as a gas in a metallation reaction, meaning that no back reaction can take place as can occur with metal amides for example.

no regioselectivity

exclusive
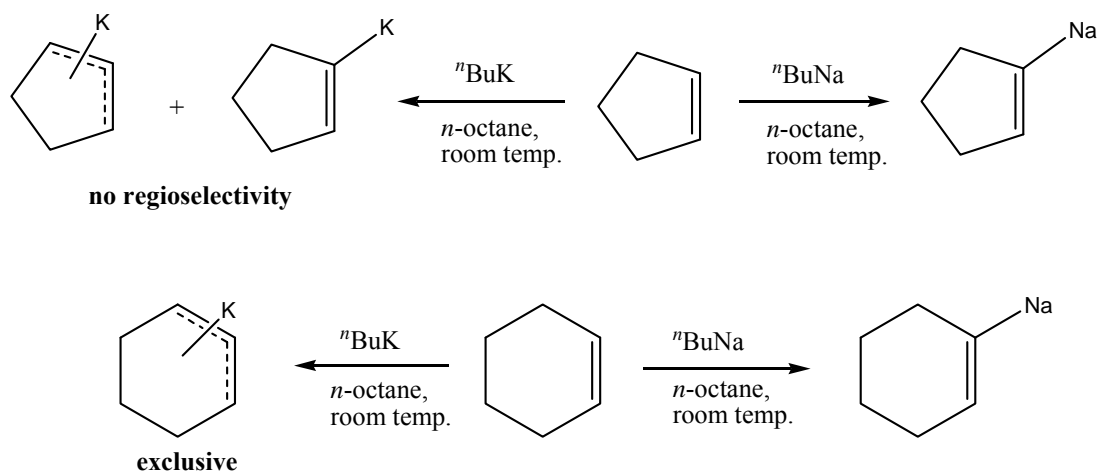
Scheme 2.1: Deprotonation products of cyclopentene and cyclohexene with *n*-butylsodium or *n*-butylpotassium.

At extremely low temperatures, *n*-butylpotassium has been shown to be an effective base towards acyclic and cyclic ethers (at -75°C), where deprotonation occurs at the α-position adjacent to the oxygen heteroatom.[2]

Potassium reagents have also been employed in the metallation of alkylarenes. With these types of substrates, the issue arises of lateral deprotonation versus ring deprotonation. Isopropylbenzene (cumene) represents this competition perfectly. A very selective and relatively mild-mannered potassium reagent was found during this investigation. Trimethylsilylmethylpotassium [$KCH_2Si(Me)_3$], at subambient temperatures, can selectively deprotonate cumene in the exocyclic α-position (**scheme 2.2**) leading to the least basic cumylmetal isomer,[3] a feat not even the superbasic mixture of *n*-butyllithium and potassium *t*-butoxide can match.[4] Ethylpotassium, in contrast, is completely unselective towards cumene as it abstracts hydrogen atoms simultaneously from the *ortho*, *meta*, *para* and α-positions in a ratio

of 7:23:25:45.[5-8] Trimethylsilylmethylpotassium can also laterally metallate ethylbenzene and toluene at the benzylic positions cleanly, with the same reactivity as the LICKOR base, unlike the previous example (**scheme 2.2**).[9] In contrast, metallation of these two alkylarenes with alkylpotassiums,[8-10] alkylsodiums [8] and butyllithium [11,12] is well known to be difficult to control, even if the alkyl alkali-metal reagent is complexed with TMEDA.
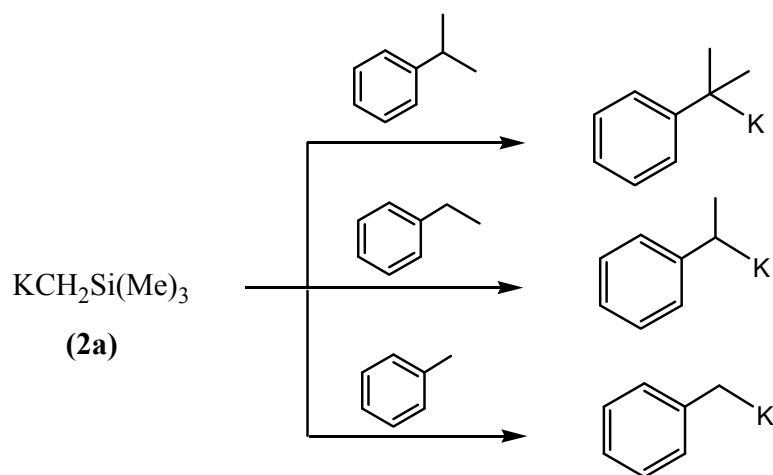
Scheme 2.2: Lateral potassiation of alkylarenes with trimethylsilylmethylpotassium.

One literature method of synthesising *n*-butyl- and trimethylsilylmethylpotassium (**scheme 2.3**) involves taking the dialkylmercury compounds [*n*Bu$_2$Hg [13] or (CH$_2$SiMe$_3$)$_2$Hg [14,15]] and reacting them with a mixed K/Na alloy under subambient conditions. These reactions have a major disadvantage in a very toxic mercury amalgam by-product. Hence, if these types of potassium compounds are to be of any use to this investigation, a new synthetic method had to be devised. This is now discussed.
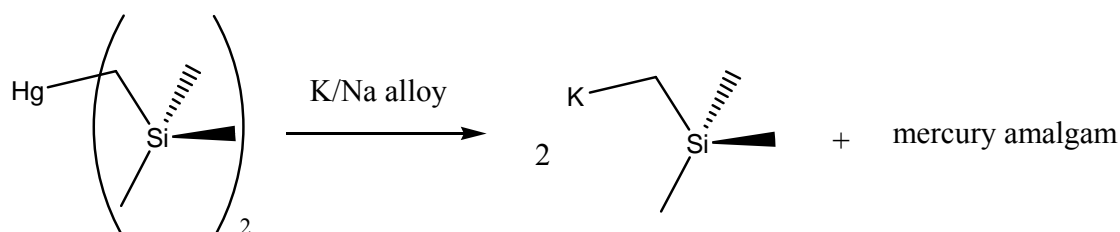
Scheme 2.3: Earlier synthetic method to generate trimethylsilylmethylpotassium.

2.3) *Synthesis of alkylpotassium precursors*

Many organic substrates undergo lithiation followed by transmetallation reactions to replace lithium with a different metal of choice. Therefore, as potassium reagents such as ^{n}BuK rely on reactions like the transmetallation of dibutylmercury with a K/Na alloy, for example, the commercially available compound trimethylsilylmethyllithium should react in with KO^{t}Bu in a metathetical reaction step, with the added bonus of no toxic by-products compared to the literature preparation.

A safer, ambient temperature approach was attempted *via* the metathetical precipitation reaction between the lithium congener LiCH$_2$SiMe$_3$ and the alkoxide ^{t}BuOK in an alkane solution, from which the insoluble, key compound KCH$_2$SiMe$_3$ was successfully obtained as a white solid in a high isolated yield of 93% (**scheme 2.4**). This compound is essentially insoluble in hexane, thus its ^{1}H NMR spectroscopic characterisation was carried out in a deuterated THF (d$_8$-THF) solution (**figure 2.1**). The resonance of the Si−CH_2−K protons comes at a very upfield value of −2.24ppm reflecting the predominately ionic nature of the K−C bond. The Si(CH_3)$_3$ resonance of **2a** appears as a singlet slightly less upfield at −0.20ppm.
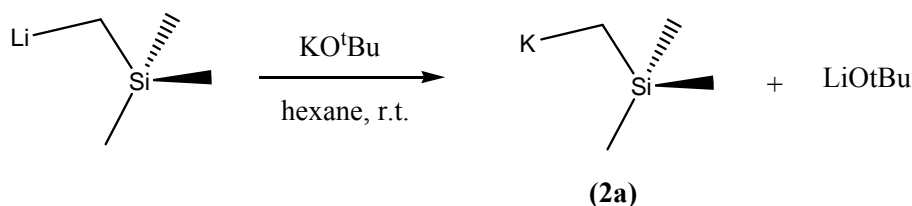
Scheme 2.4: Metathetical synthesis of (KCH$_2$SiMe$_3$).

Having achieved the goal of isolating a pure potassium starting material, the next stage of the study was to solvate **2a** by the addition of donor ligands. A recent search of the Cambridge Structural Database (CSD) [16] revealed no structural data regarding the homometallic compound KCH$_2$SiMe$_3$ or indeed any of its solvated compounds. The closest related hits found were the
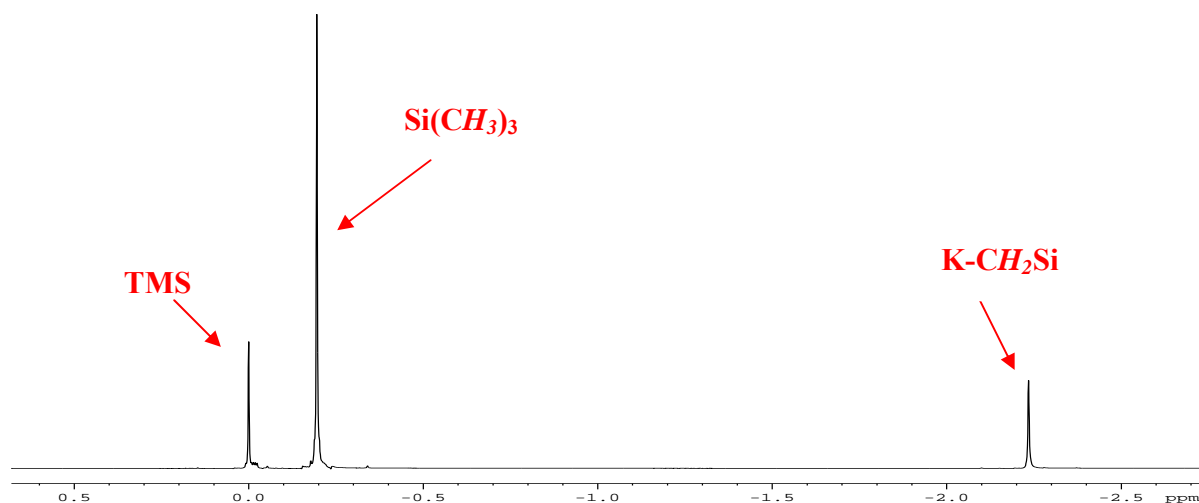
Figure 2.1: ^{1}H NMR spectrum of KCH$_2$SiMe$_3$ in d$_8$-THF solution. TMS is present as a result of hydrolysis.

unsolvated lithium hexamer, (LiCH$_2$SiMe$_3$)$_6$, and its (-)-sparteine, TMEDA and PMDETA solvates (see **figure 1.3**).[17] It was therefore decided to prepare the PMDETA analogue of KCH$_2$SiMe$_3$. Thus, by suspending **2a** in hexane solution, followed by addition of three molar equivalents of the tridentate donor solvent PMDETA, a clear solution deposited a batch of isolated crystalline [PMDETA·KCH$_2$SiMe$_3$]$_\infty$ (**2b**) at -72$^{\text{o}}$C, in a 53.5% yield. X-ray crystallographic analysis (**figure 2.2**) confirmed the polymeric structure of this highly reactive compound (it fully degrades in the glovebox overnight). The coordination sphere of the potassium atom in the asymmetric unit consists of three K−N contacts [lengths, 2.9250(18), 2.9265(16) and 2.9512(16) Å] and a K–CH$_2$ [K(1)−C(1)] bond length of 2.9151(19) Å. A further K(1)−C(1') interaction with a neighbouring unit, which facilitates polymerisation, is slightly longer at 3.0358(19) Å. This polymeric arrangement of **2b** contrasts with that of the trimethylsilylmethyllithium/PMDETA compound, which is found to be a monomer in the solid state. The Li−C bond length in PMDETA·LiCH$_2$Si(Me)$_3$ is 2.113(2) Å, a large 0.802 Å difference in bond distance compared to that in **2b**. The coordination sphere of the potassium atom in the asymmetric unit is not satisfied enough and therefore K interacts with the CH$_2$ carbon of a neighboring trimethylsilylmethyl ligand to complete a full coordination sphere, resulting in the polymeric complex in **figure 2.2**. ^{1}H and ^{13}C NMR spectroscopy of **2b** was

carried out in deuterated cyclohexane (C_6D_{12}) solution. The K−CH_2−Si and Si(CH_3)$_3$ proton resonance appears in the ^{1}H NMR spectrum at -2.27 and -0.11 ppm respectively. The resonance for the central and terminal N−CH$_3$ of the PMDETA ligand come at 2.21 ppm, with the N-CH$_2$ resonance peaks appearing within the range 2.32−2.40 ppm.

The synthesis of a TMEDA-solvated trimethylsilylmethylpotassium complex was attempted by Dr. Jan Klett of this research group. Its congener TMEDA-solvated trimethylsilylmethyllithium was reported as a dimer. However, Dr. Klett revealed that the reaction of an excess of TMEDA (5 molar equivalents) towards KCH$_2$SiMe$_3$ produced the more complicated, donor-deficient compound [(TMEDA)$_3$(KCH$_2$SiMe$_3$)$_4$] **2c** (**figure 2.3**). Complex **2c** can be thought of as a distorted cube built from K−C bonds, with an individual TMEDA molecule *N,N*–chelating three of the four potassium atoms. Each potassium centre forms bonds to three carbon atoms, while one unique potassium atom lies 'naked' as its coordination sphere is satisfied by electrostatic interactions with three trimethylsilylmethyl ligands and hence does not require an additional bidentate ligand. This structural motif contrasts considerably with the TMEDA-solvated trimethylsilylmethyllithium dimer, all due to the change of alkali-metal. K−C bond lengths in complex **2c** range from 2.922(3)−3.247(3) Å, all longer than the K1−C1 bond length of 2.9151(19) Å in polymer **2b**. As expected from cation size considerations, these metal−carbon
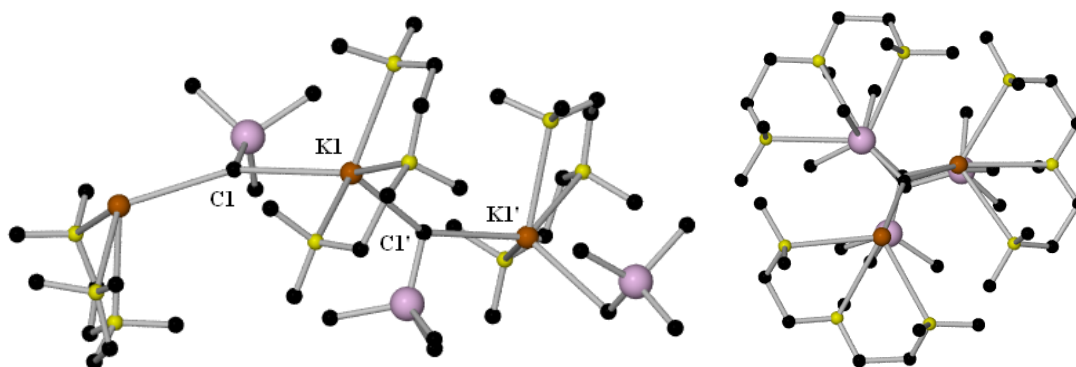
Figure 2.2: Molecular structure of a small section of the polymeric chain of 2b (left) and a view down the centre of the polymer (right).

bond lengths are also much longer than the Li−C bond lengths in the dimeric complex (TMEDA·LiCH$_2$SiMe$_3$)$_2$ [2.317(4) and 2.253(4) Å].
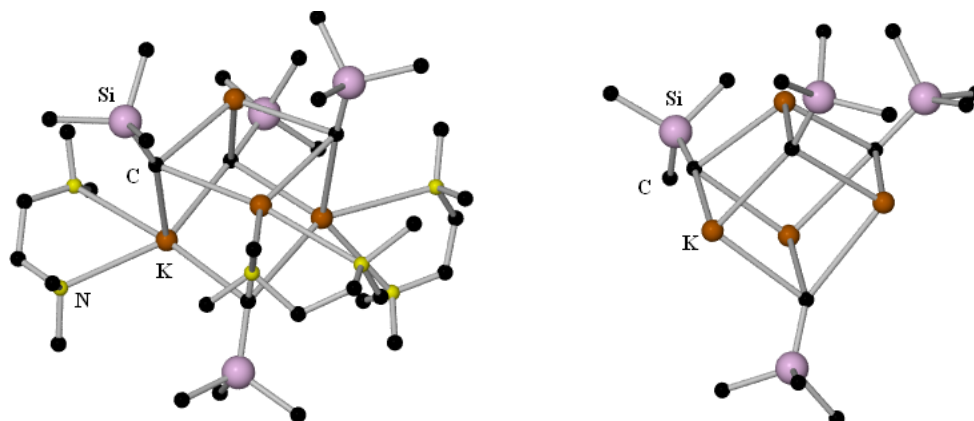
Figure 2.3: Molecular structure of [(TMEDA)$_3$(KCH$_2$SiMe$_3$)$_4$] 2c (left) and the carbon/metal skeleton of the distorted cube without TMEDA ligands (right).

2.4) Synthesis of amidopotassium precursors

Potassium amides ["KN(H)R" or "KNRR'"] can be generated *via* three main routes, namely through: i) a transmetallation reaction of a lithium amide with potassium *t*-butoxide; ii) a transamination reaction between an amine and the potassium amide KN(SiMe$_3$)$_2$; or iii) the direct reaction of elemental potassium (K), potassium hydride (KH), *n*-butylpotassium (^{n}BuK) or benzylpotassium (KBz) with an amine. As noted in the empirical formulae above, the amine can be a primary or secondary type.[18]

The sterically encumbered amine TMP(H) is the amine of choice with regard to mixed-metal chemistry (see Chapter 1), therefore to apply potassium-mediated metallations, a good source of potassium-TMP was required. Work reported by Mulvey and O'Hara had already uncovered the TMEDA-solvates of sodium-TMP and potassium-TMP, which exist in the solid state as the dimers, [TMEDA·Na(TMP)]$_2$ and [TMEDA·K(TMP)]$_2$.[19] The unsolvated forms of these

secondary amine bases were synthesised by pre-forming lithium TMP by the reaction of the parent amine TMP(H), in hexane, with *n*-butyllithium (*ⁿ*BuLi) and then reacting the lithium amide in a transmetallation step with either sodium or potassium *t*-butoxide. Potassium 2,2,6,6-tetramethylpiperidide (KTMP), a brown suspension, formed which was then solvated with one molar equivalent of TMEDA.

In a repeat of the literature procedure, the isolation of unsolvated KTMP (**2d**) was attempted. The problem with this method was the relatively poor yields (46%) of the insoluble potassium amide and the hazardous nature of the extremely air sensitive solid KTMP. This meant a new method of synthesising KTMP had to be devised. Utilising the pure potassium reagent **2a** as a suspension in hexane solution, one molar equivalent of TMP(H) was added, which resulted in a tan-coloured suspension of **2d**. No attempts were made to isolate this solid as the colour of the suspension of **2d** was similar to that reported in the TMEDA-solvated KTMP synthesis. Addition of one molar equivalent of PMDETA to this tan suspension resulted in a homogeneous solution of which pale yellow crystals of the dimeric complex [PMDETA·K(TMP)]₂ (**2e**) could be grown at -28ºC in an excellent isolated yield of 78.0%. It is important to note that the synthesis of **2e** can be achieved by the initial addition of one molar equivalent of PMDETA to **2a** (which also forms a suspension), then subsequently introducing TMP(H) (**scheme 2.5**).
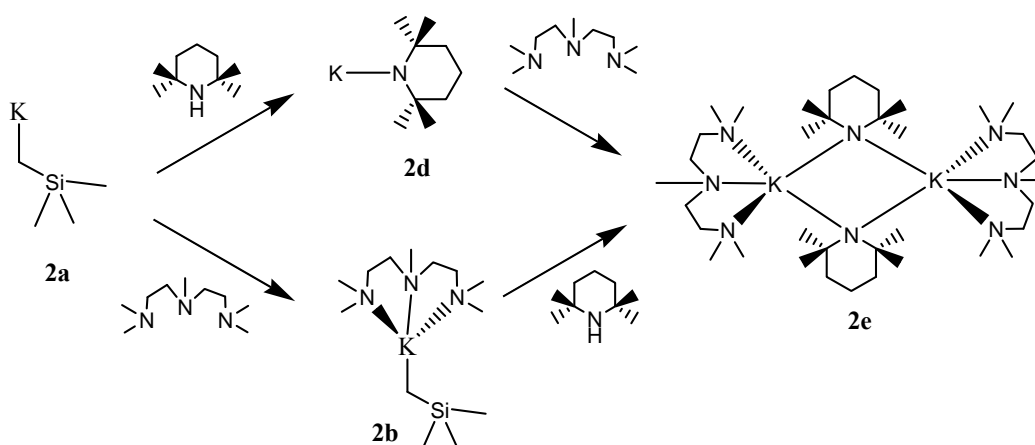
Scheme 2.5: Synthesis of [PMDETA·K(TMP)]₂ *via* two possible methods.

X-ray crystallography was used to confirm the structure as a dimeric complex (**figure 2.4**), mirroring the same structural core of the crystalline TMEDA-solvated KTMP compound. Featuring a central four-membered KNKN ring, the molecular structure contains two potassium atoms where each K has a coordination environment of five K–N contacts consisting of three K–N_{PMDETA} and two K–N_{TMP} bonds. The central nitrogen of the tridentate ligand forms the closest bond to potassium from the ligand [bond distances: K(1)–N(7) {3.0613(9) Å} and K(2)–N(4) {3.0443(9) Å}] compared to the terminal nitrogen atoms [K–$N_{terminal}$ range: 3.1671(10)–3.2610(10) Å]. Each potassium atom makes a shorter, stronger bond the TMP nitrogen anion [bond lengths: K(1)–N(1) {2.7732(9) Å} and K(2)–N(2) {2.7800(8) Å}] and dimerisation is complete through a longer metal–nitrogen interaction to a TMP anion of a second molecule [bond distances: K(1)–N(2) {3.0029(9) Å} and K(2)–N(1) {3.0028(9) Å}]. A comparison of bond distances to those of the recently reported dimer [TMEDA·K(TMP)]$_2$ (**figure 2.5**) can be made. The TMEDA potassium–nitrogen bonds [range: 2.882(2)–2.934(2) Å] are at least 0.11 Å
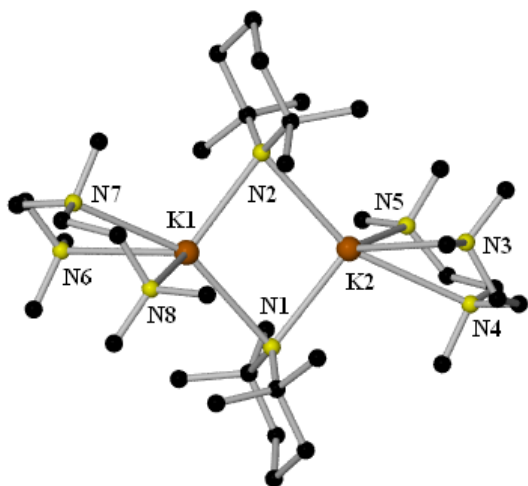
Figure 2.4: Molecular structure of the solvated potassium amide [PMDETA·K(TMP)]$_2$, 2e.
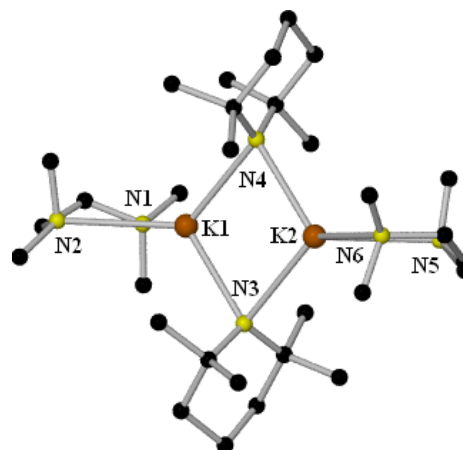
Figure 2.5: Molecular structure of the published TMEDA-solvated KTMP compound.

shorter than those of K–N_{PMDETA} [shortest bond is 3.0443(9) Å in length, though longest is 3.2610(10) Å]. The K–N_{TMP} bond distances in the TMEDA-solvate are also slightly more

contracted [K–N_{TMP} bond range: 2.744(2)–2.836(2) Å] in comparison to those in the PMDETA-solvate [K–N_{TMP} bond range: 2.7732(9)–3.0029(9) Å].

^1H and ^{13}C NMR spectroscopic analysis was carried out on amide **2e** in d_{12}-cyclohexane (d_{12}-Cy) solution (**figure 2.6**). The ^1H NMR resonances associated with the CH_3 and the βCH_2 of the TMP anion modestly shift upfield from 1.06 and 1.29 ppm to 1.04 and 1.21 ppm respectively compared to those of the free amine. Conversely, those peaks associated with the γCH_2 of TMP, and all of the PMDETA peaks, move, to a small extent, towards the downfield direction from 1.62 (γCH_2 of TMP), 2.14 (4 x CH_3, PMDETA), 2.19 (1 x CH_3, PMDETA), 2.29 (2 x CH_2, PMDETA) and 2.41 (2 x CH_2, PMDETA) ppm to 1.68, 2.18, 2.25, 2.33 and 2.42 ppm respectively.
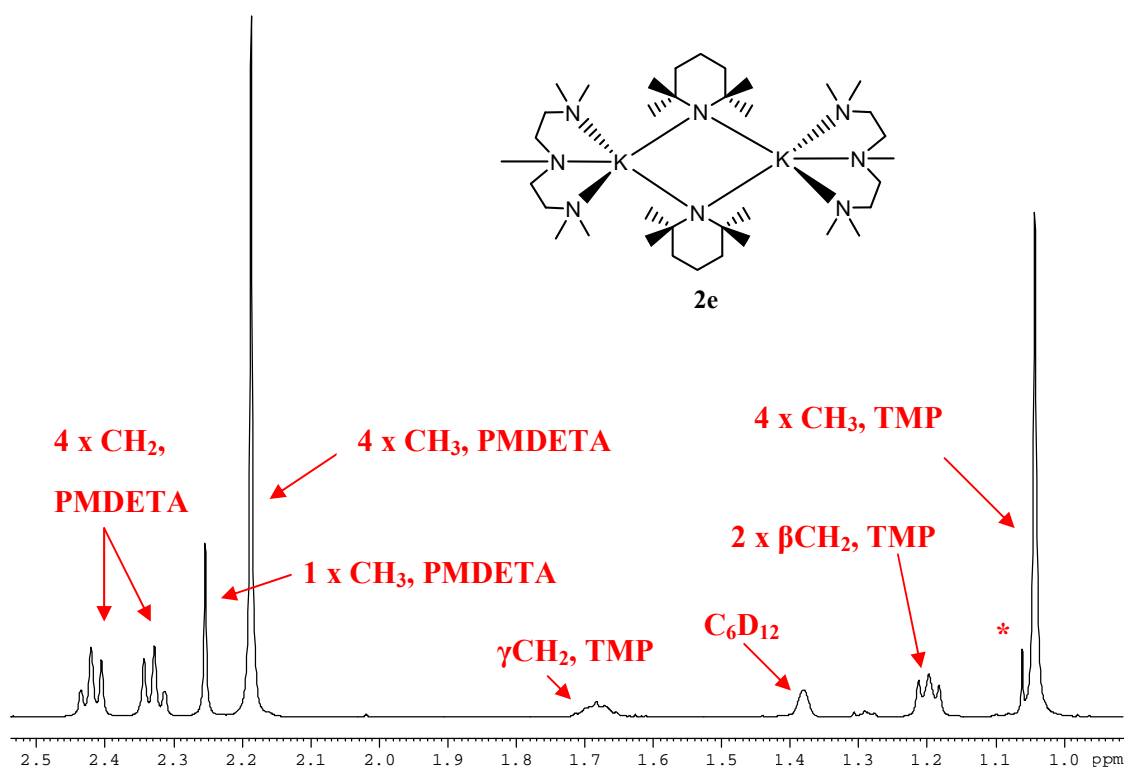
Figure 2.6: ^1H NMR spectrum of [PMDETA·K(TMP)]$_2$ in d_{12}-Cy solution. * = TMP(H).

With the isolation of the alkylpotassium reagent [PMDETA·K(CH_2SiMe_3)]$_\infty$ and the amido-

potassium base [PMDETA·K(TMP)]$_2$, potassium-mediated zincation, magnesiation and alumination could now be investigated in depth. The progress made in these areas will now be covered in turn for each metal, providing a new perspective on alkali-metal-mediated metallation chemistry.

2.5) Experimental Section

Synthesis of KCH$_2$SiMe$_3$ (2a)

2.75 g (25 mmol) of KO^{t}Bu was dissolved in 50 mL of hexane in a Schlenk tube. To this solution, 25 mL (25 mmol) of 1M LiCH$_2$SiMe$_3$ solution was added, and the reaction mixture was left to stir overnight to form an off-white suspension. The solid was filtered, washed with hexane (2 x 20 mL) and dried under vacuum to afford a white solid (2.80 g, 93.0 % yield). ^{1}H NMR (400.13 MHz, 298K, d$_8$-THF): δ -0.20 (s, 9H, 3 × CH_3), -2.24 ppm (s, 2H, CH_2-K).

Synthesis of [PMDETA·KCH$_2$SiMe$_3$]$_∞$ (2b)

0.24g (2 mmol) of KCH$_2$Si(Me)$_3$ was suspended in 10 mL of hexane. To this suspension 1.26 mL (6 mmol) of PMDETA was added to yield a homogeneous yellow solution. The Schlenk tube was placed in the freezer at -72°C to generate a batch of colourless crystals (0.32 g, 53.5 % yield). ^{1}H NMR (400.13 MHz, 298K, C$_6$D$_{12}$): δ = 2.32−2.40 (m, 8H, 4 × CH$_2$ PMDETA), 2.21 (s, 15H, 5 × CH3 PMDETA), -0.11 (s, 9H, 3 × CH$_3$), -2.27 ppm (s, 2H, CH$_2$-K); ^{13}C{^{1}H} (100.62 MHz, 298K, C$_6$D$_{12}$): δ = 58.6 (2 × CH$_2$ PMDETA), 57.2 (2 × CH$_2$ PMDETA), 46.1 (4 × CH$_3$ PMDETA), 43.1 (1 × CH$_3$ PMDETA), 6.5 (3 × CH$_3$), 1.1 ppm (1 × K-CH$_2$).

Synthesis of [PMDETA·K(TMP)]$_2$ (2e)

0.24g (2 mmol) of KCH$_2$SiMe$_3$ was suspended in 10 mL of hexane. To this suspension 0.42 mL (2 mmol) of PMDETA, followed by 0.34 mL (2 mmol) of TMP(H) was injected into the reaction mixture to yield a homogeneous yellow solution. The Schlenk tube was next placed in the freezer at -28°C resulting in a crop of pale yellow crystals (0.55 g, 78.0 % yield). ^{1}H NMR (400.13 MHz, 298K, C$_6$D$_{12}$): δ = 2.40-2.44 (m, 4H, 2 × CH$_2$ PMDETA), 2.30-2.34 (m, 4H, 2 × CH$_2$ PMDETA), 2.25 (s, 3H, 1 × CH$_3$ PMDETA), 2.18 (s, 12H, 4 × CH$_3$ PMDETA), 1.68 (m, 2H, γCH$_2$ TMP), 1.21 (t, 4H, *J* = 6.0 Hz, 2 × βCH$_2$ TMP), 1.04 ppm (s, 12H, 4 × CH$_3$ TMP); ^{13}C{^{1}H} (100.62 MHz, 298K, C$_6$D$_{12}$): δ = 58.0 (2 × CH$_2$ PMDETA), 56.7 (2 × CH$_2$ PMDETA), 45.7 (4 × CH$_3$ PMDETA), 42.8 (1 × CH$_3$ PMDETA), 42.9 (2 × βCH$_2$ TMP), 37.6 (4 × CH$_3$ TMP), 21.3 (1 × γCH$_2$ TMP).

Chapter 2 – References

[1]   C. D. Broaddus, D. L. Muck, *J. Am. Chem. Soc.* **1967**, *89*, 6533.

[2]   R. Lehmann, M. Schlosser, *Tetrahedron Lett.* **1984**, *25*, 745.

[3]   J. Hartmann, M Schlosser, *Helv. Chim. Acta* **1976**, *59*, 453.

[4]   M. Schlosser, S. Strunk, *Tetrahedron Lett.* **1984**, *225*, 741.

[5]   D. Bryce-Smith, *J. Chem. Soc.* **1954**, 1079.

[6]   D. Bryce-Smith, *J. Chem. Soc.* **1963**, 5983.

[7]   R. A. Benkeser, T. V. Liston, *J. Am. Chem. Soc.* **1960**, *82*, 3221.

[8]   R. A. Benkeser, A. E. Trevillyan, J. Hooz, *J. Am. Chem. Soc.* **1962**, *84*, 4971.

[9]   M. Schlosser, *J. Organomet. Chem.* **1967**, *8*, 9.

[10]   C. D. Broaddus, *J. Am. Chem. Soc.* **1966**, *88*, 4174.

[11]   A. J. Chalk, T. J. Hoogeboom, *J. Organomet. Chem.* **1968**, *11*, 615.

[12]   C. D. Broaddus, *J. Org. Chem.* **1970**, *35*, 10.

[13]   F. Leroux, M. Schlosser, unpublished results, see: M. Schlosser, *Organometallics in Synthesis,* 2nd edn, VCH, Weinheim, Germany, **2002**.

[14]   J. Hartmann, M Schlosser, *Synthesis* **1975**, 328.

[15]   M. Stähle, J. Hartmann, M Schlosser, *Helv. Chim. Acta* **1977**, *60,* 1730.

[16]   F. H. Allen, *Acta Crystallogr., Sect. B: Struct. Sci.* **2002**, *58*, 380.

[17]   T. Tatic, H. Ott, D. Stalke, *Eur. J. Inorg. Chem.* **2008**, 3765.

[18]   M. Lappert, P. Poer, A. Protchenko, A. Seeber, *Metal Amide Chemistry*, VCH, Weinheim, Germany, **2009**.

[19]   D. R. Armstrong, D. V. Graham, A. R. Kennedy, R. E. Mulvey, C. T. O'Hara, *Chem. Eur. J.* **2008**, *14*, 8025.

Chapter 3: Developing the New Concept of Potassium-Mediated Zincation

3.1) Introduction

Though a member of one of the oldest known organometallic dynasties, alkali zincate compounds of a mixed alkyl-amido formulation are among the youngest established potent organometallic bases. Many aromatic and heteroaromatic substrates generally inert to familiar neutral organozinc compounds ("R_2Zn") can now be selectively metallated with this new improved generation of bisalkyl-monoamido zincate reagent ["$M^+\{(R_2NZnR_2)\}^-$"].[1-3] Often superior in terms of functional group tolerance, compatibility with more organic substrates, and milder experimental conditions than classical lithiation methods, these new metallations, being zinc-hydrogen exchange reactions assisted by the presence of a charge-balancing alkali metal cation, can be interpreted as alkali-metal-mediated zincations (AMMZn).[4-8] Two widely studied reagents in the context of AMMZn are TMP (2,2,6,6-tetramethylpiperidide) based in the lithium dialkyl zincate "$Li(TMP)Zn(^tBu)_2$" originally made by Kondo and Uchiyama,[6,9,10] and its sodium big brother [TMEDA·Na(μ-^tBu)(μ-TMP)Zn(^tBu)] (TMEDA = *N,N,N',N'*-tetramethylethylenediamine) made by the Mulvey group,[5] while Knochel has recently introduced an efficient zincating concoction mixing the lithium magnesiate "$(TMP)_2Mg·2LiCl$" with the halide $ZnCl_2$.[11]

A founder member of the organometallic community, potassium zincate chemistry first began 150 years ago through Wanklyn's epochal report of the synthesis of "potassium ethyl", ($KZnEt_3$), and its sodium congener.[12,13] The first structural determination of a potassium zincate, a powder diffraction study of the tetraethynyl zincate salt, [$K_2Zn(C\equiv CH)_4$], by Weiss, also appeared early in the history of organometallic structural chemistry in 1968.[14] Surprisingly, in the intervening years to the present, conspicuously few potassium zincates have been crystallographically characterised.[15] Underlining this underdevelopment, potassium tris-cyclopentadienylzincate, [$KZn(C_5H_5)_3$], which one might have predicted (erroneously) was a known, classical zincate compound was actually only synthesised and its crystal structure elucidated as recently as 2007.[16] Taken from the Cambridge Structural Database,[17] a selective

list of potassium zincate structures unveiled since the first X-ray of this type of ate complex appeared in 1966 is shown in **table 3.1**.

There are three types of aggregation states that potassium zincates tend to arrange themselves in; namely monomeric, dimeric or polymeric states. Monomeric potassium zincate structures are rarely found and, from examining those in the CSD, form when the coordination site of potassium is filled by either heteroatom dative bonding from donor compounds such as THF, a mix of dative bonding and π-electron stabilisation from the substrate, or by π-electron stabilisation alone (**figure 3.1**). A communication by Darensbourg showed that reacting the potassium salt of 2,6-di-*tert*-butylphenol with the neutral zinc complex of the same phenol, in THF, resulted in the solvent-separated structure of $[K(THF)_6][Zn(O-2,6-^tBu_2C_6H_3)_3]$.[18] Containing one zinc atom with three anionic phenoxide ligands, the potassium counterion is surrounded by six molecules of THF, thus satisfying the alkali metals coordinating sphere and blocking its ability to polymerise. Van Koten and Spek found that *via* a one electron reduction of the complex $Zn\{(t\text{-BuNCHCHN-}t\text{-Bu})^{\bullet}\}_2$ with exactly one molar equivalent of potassium metal, in THF, the product $[K(THF)_3]^+[Zn(t\text{-BuNCHCHN-}t\text{-Bu})(t\text{-BuNCHCHN-}t\text{-Bu})^{\bullet}]^-$ can be synthesised in crystalline form.[19] In this monomeric complex, the $[K(THF)_3]^+$ cation is coordinated to the π-electrons of the dianionic *t*-BuNCHCHN-*t*-Bu ligand and also to three THF molecules. Very recently, Hanusa reported a monomeric potassium zincate, $K^+[Zn(1,3\text{-}(SiMe_3)_2C_3H_3)_3]^-$, where intra π-electron stabilisation from the anionic ligands were sufficient to prevent the potassium cation from seeking donor molecule dative bonding or any other types of inter-molecular interaction.[20] Dimeric and polymeric potassium zincates structures tend to grow as a result of the alkali-metal requiring more electron density to complete its coordination sphere than it can get from within a monomeric architecture. This means that there is also insufficient donor interactions or π-stabilisation available to the potassium cation, therefore it must interact with a neighbouring unit, or several units, to achieve its desired high coordination number state.

Surprisingly, after the outstanding success of lithium and sodium zincates as deprotonation reagents,[1-3] comparatively little effort has gone into studying whether potassium can replicate its smaller alkali Group 1 members when also paired with the Group 12 metal zinc. Unplanned,

70

unexpected metallation reactions have been reported using potassium ate chemistry. For example, Purdy and George observed that when synthesising the potassium trialkylzincate

Table 3.1 Selected potassium zincate structures from the CSD and their aggregation states.

Structure	Aggregation State	Ref. Number
$[K(THF)_6][Zn(O-2,6-^tBu_2C_6H_3)_3]$	Monomeric	[18]
$K(THF)_3[Zn(t\text{-BuNCHCHN-}t\text{-Bu}) (t\text{-BuNCHCHN-}t\text{-Bu})^{\bullet}]$	Monomeric	[19]
$K[Zn(1,3-(SiMe_3)_2C_3H_3)_3]$	Monomeric	[20]
$[(THF)_2KZnMe(OSiMe_3)_2]_2$	Dimeric	[21]
$[(TMEDA)KZn(OSiMe_3)_3]_2$	Dimeric	[21]
$[KZnEt_2O^tBu]_2$	Dimeric	[22]
$[KZn(O^tBu)_3]_2$	Dimeric	[23]
$[K_2Zn_2\{OC(=CH_2)Mes\}_6(CH_3Ph)_2]$	Dimeric	[24]
$[\{K(o\text{-xylene})_2\}\{Zn(HMDS)_3\}]_2$	Dimeric	[25]
$[KZn(CH_2CMe_3)_3.C_6H_6]_2$	Dimeric	[26]
$[KZn(CH_2SiMe_3)_3]_2$	Dimeric	[26]
$[KZn(CH_2SiMe_3)_2Ph]_\infty$	Polymeric	[26]
$[K_2Zn(C_2H)_4.2NH_3]_\infty$	Polymeric	[27]
$[K_2\{Zn(CH_2Ph)(t\text{-BuNCHCHN-}t\text{-Bu})\}_2.OEt_2]_\infty$	Polymeric	[28]
$[\{KZn(CH_2Ph)(t\text{-BuNCHCHN-}t\text{-Bu})\}.THF]_\infty$	Polymeric	[28]
$[\{KZn(Me)(t\text{-BuNCHCHN-}t\text{-Bu})\}.THF]_\infty$	Polymeric	[28, 29]
$[\{K_2Cp\}\{Zn(HMDS)_3\}]_\infty$	Polymeric	[25]
$[KZn(HMDS)_2(CH_2Ph)]_\infty$	Polymeric	[30]
$[KZn(C_5H_5)_3]_\infty$	Polymeric	[16]

$[KZn(CH_2SiMe_3)_3]_2$, metallation of the arene solvent benzene occurs to yield the phenyl byproduct $[\{KZn(CH_2SiMe_3)_2Ph\}_\infty]$.[26] Exchanging the alkyl ligand, trimethylsilylmethyl for the amide 1,1,1,3,3,3-hexamethyldisilazide (HMDS), metallation of toluene (as the solvent) has been

reported   by   our   own   group,   yielding   the   unplanned   benzyl   product
[{KZn(HMDS)$_2$(CH$_2$Ph)}$_\infty$].[30]
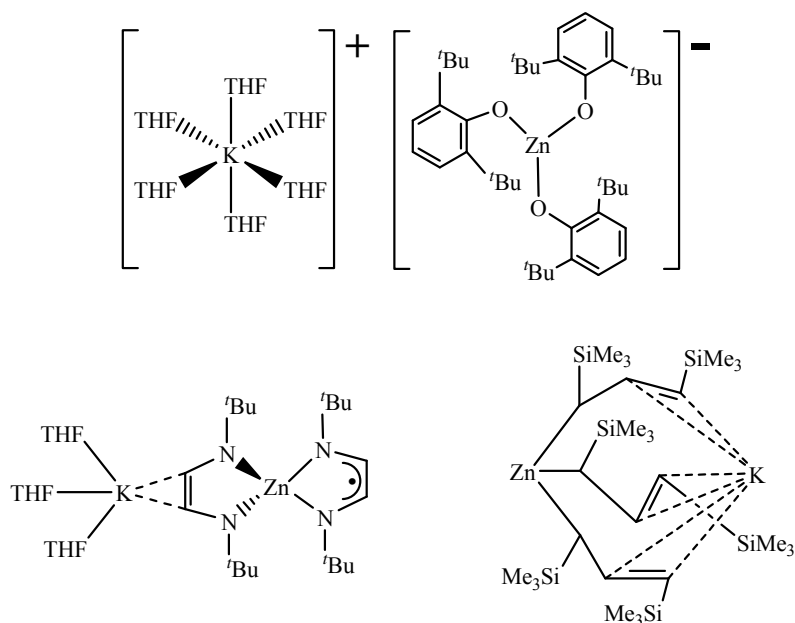
Figure 3.1: Structures of the monomeric ates [K(THF)$_6$]$^+$[Zn(O-2,6-^{t}Bu$_2$C$_6$H$_3$)$_3$]$^-$ (top), [K(THF)$_3$]$^+$[Zn(t-BuNCHCHN-t-Bu)(t-BuNCHCHN-t-Bu)$^\bullet$]$^-$ (bottom left) and K$^+$[Zn(1,3-(SiMe$_3$)$_2$C$_3$H$_3$)$_3$]$^-$ (bottom right).

While synthetically, structurally, and mechanistically the use of these lithium and sodium TMP-zincate reagents in AMM*Zn* applications is largely well understood, little comparable information is available on potassium TMP-zincate chemistry. Since the alkali metal plays a pivotal, albeit supporting, role in AMM*Zn* methodology, and given that major distinctions exist between certain lithium, sodium, and potassium congeners in other classes of organometallic compound, one of the objectives of this work was to develop a complementary TMP-zincate chemistry of potassium. To the best our knowledge, the idea that potassium/zincate mixed-metal compounds could be utilised as reagents for executing direct zincation of C-H bonds within a range of aromatic substrates has hitherto never been explicitly proposed. Hence, this chapter will address this issue with the report of attempted potassium-mediated zincation reactions of heterocyclic substrates and metallocenes.

72

3.2)   *Synthesis of Potassium Zincate Bases*

A co-complexation methodology, where distinct components interlock to form the zincate complex, was applied to prepare each of the desired different alkyl containing potassium TMP-zincate bases [PMDETA·K(μ-TMP)(μ-R)Zn(R)] (**3a**, R = Me; **3b**, R = Et; **3c**, R = ^{i}Pr, **3d**, R = ^{n}Bu; **3e**, R = ^{t}Bu) (**scheme 3.1**) in isolated yields of 60% (**3a**), 61% (**3b**), 20% (**3d**) and 70% (**3e**). The low yield of **3d** can be attributed to its high solubility in hydrocarbon solvents, thus making it difficult to crystallise in substantial yields (even at -72°C). ^{1}H NMR spectroscopic analysis of the filtrates for zincates **3a-3e** suggests that these complexes form near quantitative yields. An isolated crystalline yield for **3c** was not measured as this reaction was a trial with very few experiments, with only one set of crystals isolated and investigated by X-ray analysis. Trimethylsilylmethylpotassium, Me$_3$SiCH$_2$K (**2a**), provided a convenient potassium source. It was converted to [PMDETA·K(TMP)]$_2$ (**2e**) by initial addition of the amine TMP(H), followed by PMDETA (or vice versa) and the interlocking co-complexation process (**scheme 3.1**) was

$R = Me, {}^i Pr, {}^n Bu$ or ${}^t Bu$
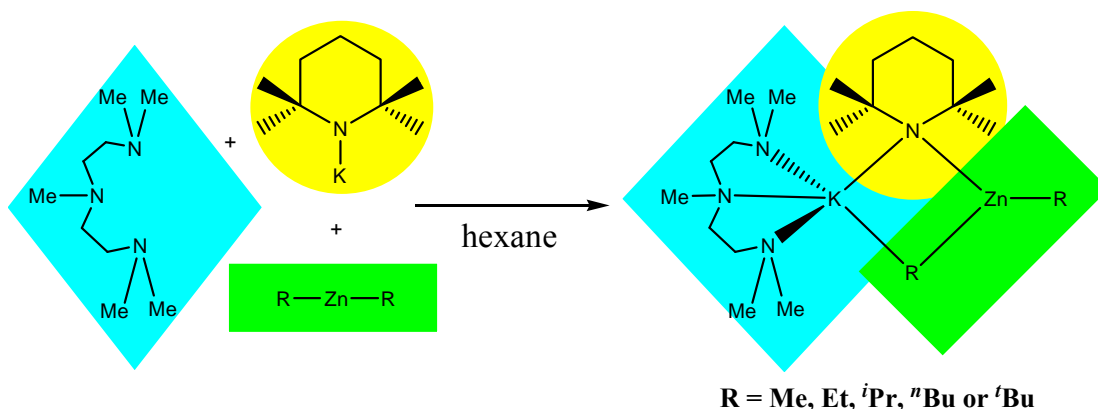
Scheme 3.1: Interlocking co-complexation synthesis of the new potassium-TMP-dialkyl zincates.

completed by addition of the appropriate dialkylzinc (Me$_2$Zn, Et$_2$Zn, ^{i}Pr$_2$Zn, ^{n}Bu$_2$Zn or ^{t}Bu$_2$Zn) reagent. It is important to note here that dimethylzinc must be taken from an alkane solution, not from toluene, as an insoluble concoction is produced with the arene solvent. Utilising bidentate TMEDA instead of tridentate PMDETA, addition of the ligand to a mixture of KTMP and Et$_2$Zn resulted in the dimeric complex [TMEDA·K(μ-TMP)(μ-Et)Zn(Et)]$_2$ (**3f**), which can be isolated

in a good crystalline yield of 70 %. Replacing TMP for HMDS, the mixture of PMDETA, KHMDS and Me$_2$Zn (in hexane solution) results in the crystalline complex [PMDETA·K(μ-HMDS)(μ-Me)Zn(Me)] (**3g**) in an isolated yield of 58 %.

3.2.1) Solid-State Analysis

X-ray crystallographic analysis of these compounds established a series of closely related potassium TMP-zincate structures (**figure 3.2**). All five structures show that introduction of
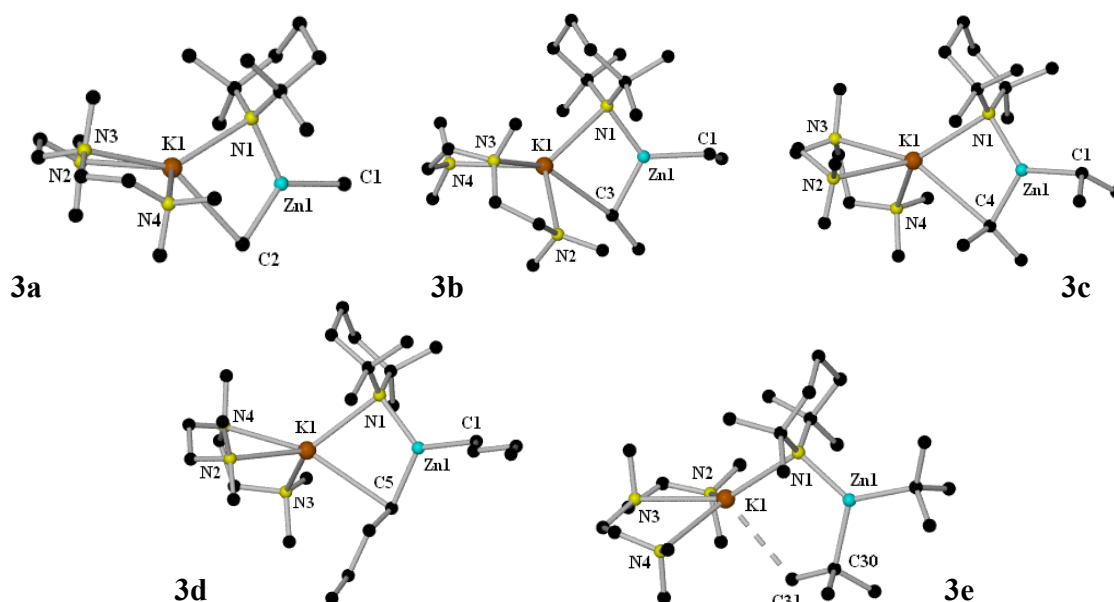
Figure 3.2: Molecular structures of the family of potassium dialkyl zincates, [PMDETA·K(μ-TMP)(μ-R)Zn(R)] (3a, R = Me; 3b, R = Et; 3c, R = ^{i}Pr; 3d, R = ^{n}Bu; 3e, R = ^{t}Bu).

dialkylzinc breaks the dimeric arrangement of the PMDETA-solvated potassium amide to form monomeric mixed-metal complexes. The precision of the molecular structures of **3a** and **3b** are relatively low, limiting any detailed comparison of bond lengths and angular dimensions; however, the molecular connectivity of these two structures is definite. With regards to **3c**, **3d**,

and **3e**, a comparison of key bond lengths is given in **tables 3.2** and **3.3**. Compounds **3a-3d** are designed around a KNZnC ring of four different elements, with terminal PMDETA (three nitrogen atoms) and alkyl ligands (one carbon atom) on K and Zn, respectively, to complete the

Table 3.2 Comparison of K–N and K–C bond lengths in potassium TMP-dialkyl zincate structures.

[PMDETA·K(TMP)(R)Zn(R)]	K–C$_{ring}$ (Å)	K–N$_{ring}$ (Å)	mean K–N$_{pmdeta}$ (Å)
R = ^{i}Pr (**3c**)	3.103(2)	2.8171(19)	2.860
R = ^{n}Bu (**3d**)	3.1356(18)	2.8141(13)	2.887
R = ^{t}Bu (**3e**)	3.061(6) to CH$_3$ of ^{t}Bu	2.7989(14)	2.880

Table 3.3 Comparison of Zn–N and Zn–C bond distances in potassium TMP-dialkyl zincate structures.

[PMDETA·K(TMP)(R)Zn(R)]	Zn–C$_{ring}$ (Å)	Zn–C$_{terminal}$ (Å)	Zn–N$_{ring}$ (Å)
R = ^{i}Pr (**3c**)	2.063(3)	2.034(3)	2.0190(17)
R = ^{n}Bu (**3d**)	2.0487(17)	2.0227(18)	2.0179(13)
R = ^{t}Bu (**3e**)	2.0877(16)	2.0964(11)	2.0617(13)

structures. In both structures **3c** and **3d,** as expected from size considerations, the K–N$_{tmp}$ bond [2.8171(19) and 2.8141(13) Å respectively] is significantly shorter than the K–C bond [3.103 and 3.1356(18) Å respectively]. The same pattern is seen with the Zn–N$_{tmp}$ bonds [2.0190(17) and 2.0179(13) Å], as they appear more contracted compared to the Zn–C$_{terminal}$ [2.034(3) and 2.0227(18) Å] and Zn–C$_{ring}$ bond lengths [2.063(3) and 2.0487(17) Å]. Compound **3e**, however, is unique as it forms a central 5-membered (KNZnCC) ring, with the potassium interacting with a methyl group, C(31), from the *t*-butyl ligand instead of the zincated quaternary carbon atom. This type of agostic interaction [length, K(1)–C(31), 3.061(6) Å] has been observed before in the THF-lithium, [THF·Li(TMP)Zn^{t}Bu$_2$],[6,9,10] and TMEDA-sodium, [TMEDA·Na(TMP)Zn^{t}Bu$_2$],[5] analogues (see **figure 1.22,** page 32). Of the three *t*-butyl zincate bases, this alkali-metal–carbon

bond distance is the largest, 0.311Å longer than the TMEDA-Na compound [2.750(10) Å] and 0.651 Å greater in distance compared to Kondo's Li/THF complex [2.410(6) Å], which lies roughly in line with the relative differences in ionic radii of the alkali metals (Na^+ and K^+, Δ 0.32 Å; Li^+ and K^+, Δ 0.58 Å).[31] A comparison of selected bond angles can be found in **figure 3.3**. In the lithium-zinc base, the agostic interaction of lithium to the methyl group pulls the *t*-butyl fragment closer to the alkali-metal, distorting the trigonal planar arrangement of zinc, mainly at the N_{ring}–Zn–$C_{tertiary(ring)}$ bond angle [111.72(9)°]. The larger the alkali-metal, the more closely a restoration of the trigonal plane becomes, as the N_{ring}–Zn–$C_{tertiary(ring)}$ angle increases sequentially to 116.9(3)° and 117.70(6)° for the sodium and potassium complexes respectively,
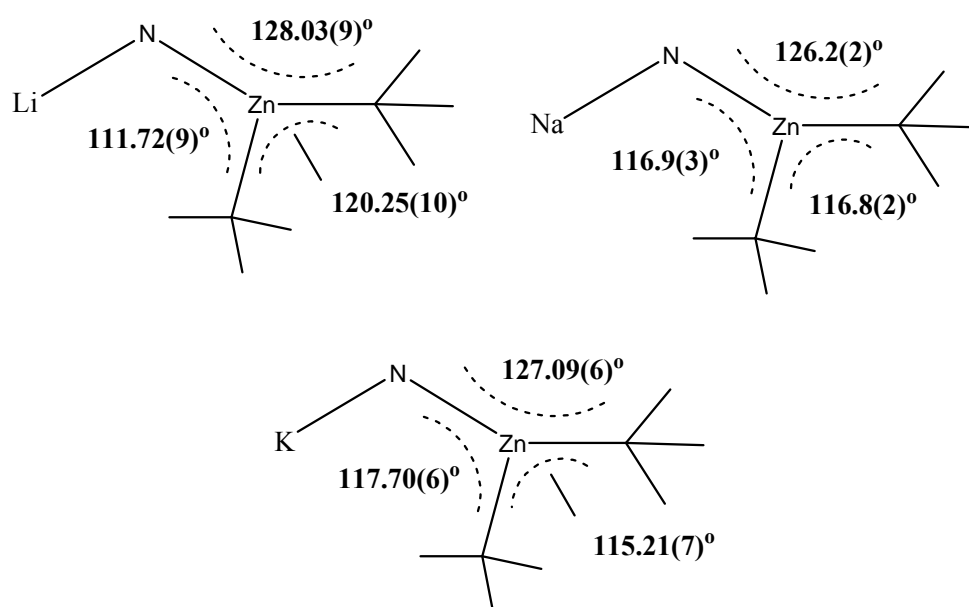
Figure 3.3: Angles subtended at zinc in Li, Na and K TMP-dialkyl zincate bases

highlighting the elongating of the agostic contact. To counter this change in bond angle, the C_{tBu}–Zn–C_{tBu} bond angle compensates for this by becoming narrower [bond angle: 120.25(10)° for Li; 116.8(2)° for Na; 115.21(7)° for K], retaining the distorted trigonal planar geometry on Zn [the sum of the angles around the Zn center for each zincate is 360° (359.9° for the sodium zincate)]. Although this comparison of bond angles gives us an insight into the effect the alkali

metal has on structure dimensions, this is not an exact comparison as the donor changes from THF to TMEDA to PMDETA.

A change in the donor ligand in these bases can also induce a change in their aggregation state. The dimeric, centrosymmetric complex [TMEDA·K(μ-TMP)(μ-Et)Zn(Et)]$_2$ (**3f**) contains a monomeric unit which consists of a four-membered (KNZnC) ring, with TMP and ethyl bridges and a terminal ethyl group on zinc. To complete the asymmetric unit, TMEDA engages in a (N)$_2$ bidentate fashion to the potassium atom. The reduction in ligand denticity from tridentate to bidentate means that the coordination requirements of potassium becomes unfulfilled and it therefore needs more stabilisation. This is achieved intermolecularly by the interaction of the potassium cation of one monomer with the bridging ethyl group on a second, resulting in a two-rung ladder structure (**figure 3.4**). Laddering was first described by Snaith and co-workers with the complex [PMDETA·{LiN(CH$_2$)$_3$CH$_2$}$_3$]$_2$.[32] The concept of the ring-laddering principle involves the self-assembly of (LiN)$_2$ dimers, with the extent of association reliant on the size and stereochemistry of the organo-substituents on the nitrogen, as well as the type of solvating medium being used. In addition, a lower degree of solvation is crucial in the generation of the polymeric (LiN)$_n$ ladder-type complexes, as a high level of solvation can lead to isolated dimers.[33] The ladder structure **3f** is an example of a heterometallic derivative, where the (KNZnC) acts like a (LiN)$_2$ dimer, and two of these rings associates to form a complex consisting ring three fused rings [(KNZnC) × 2; (KCKC)], joined at the K(1)–C(12) and K(1')–C(12') junctions. The lower level of solvation that bidentate TMEDA gives to K (*cf.* PMDETA solvated monomer **3b**) follows the rules regarding the formation of ladder structures. The K(1)-N(1) bond [2.772(2) Å] in **3f** is again shorter than the K(1)-C(12) bond [3.200(3) Å] by a notable 0.428Å and the potassium atom actually forms a slightly shorter K-C bond to the carbon of the neighbouring monomer [K(1)-C(12)', 3.173(3) Å]. Analysis of the Zn–C bonds reveals that the terminal Zn(1)-C(10) bond [2.015(3) Å] is marginally shorter than the Zn(1)-C(12) and Zn(1)-N(1) bond distances [2.045(3) Å and 2.039(2) Å, respectively].

A change in the amine has also been shown to have an interesting effect on the complexes produced. Replacing TMP for HMDS, the mixture of PMDETA, KHMDS and Me$_2$Zn (in hexane solution) results in the crystalline complex [PMDETA·K(μ-HMDS)(μ-Me)Zn(Me)] (**3g**) (**figure
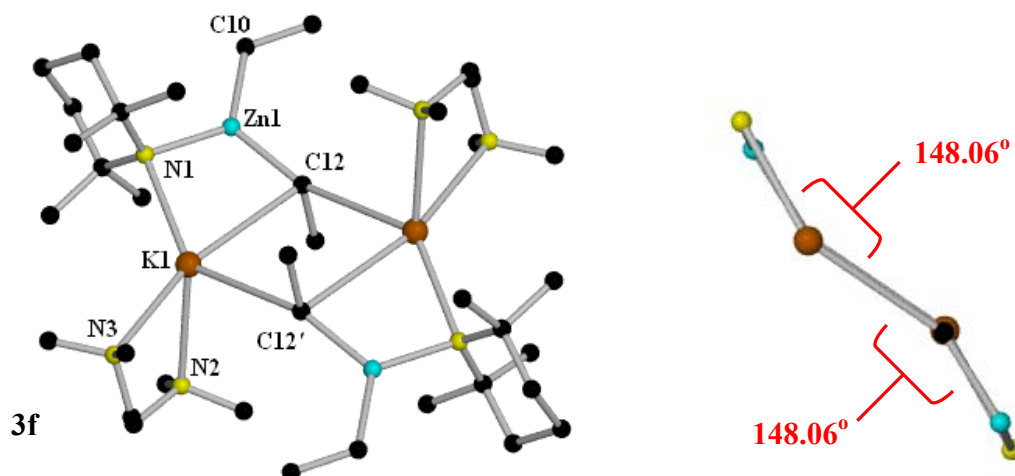
Figure 3.4: Molecular structure of the dimeric potassium TMP-zincate [TMEDA·K(μ-TMP)(μ-Et)Zn(Et)]₂ (3f).

3.5). Although compound **3g** is isostructural with the TMP analogue **3a**, comparisons with work published by our group the lithium HMDS–zincate [PMDETA·Li(μ-Me)Zn(Me)(HMDS)] (**3h**) reveals a change in the structural framework.[34] In complex **3h**, HMDS occupies a terminal position and only one methyl group bridges the two metal centres. For potassium zincate **3g**, the HMDS ligand and one methyl group are now bridging between the alkali-metal and zinc. This forces the second methyl group into a terminal site. A reason for this structural distinction could be due to the different sizes of the alkali-metals. Lithium seems to be content to have four contacts (3 × N and 1 × C) and therefore does not require any additional stabilisation from the second methyl group or the HMDS ligand, resulting in the open cyclic structure. Potassium, on the other hand, prefers more interactions (see **figure 3.2**), thus resulting in a closed cyclic structure with five (4 × N and 1 × C) contacts to the alkali-metal. The terminal Zn-N$_{hmds}$ bond [Zn(1)-N(1)] in **3h** is 1.9851(10) Å, shorter than the bridging Zn(1)-N(1) bond in **3g** [2.053(7) Å]. The bridging Zn-C bond is actually longer, albeit marginally, in the open complex [Zn(1)-C(2) 2.0361(15) Å] compared to that in the closed structure [Zn(1)-C(2) 2.007(9) Å]. This pattern is also seen in the remaining Zn-C bond length [**3g**, Zn(1)-C(1) 1.994(10) Å; **3h**, Zn(1)-C(1) 2.0074(14) Å]. The distance between the lithium atom and the non-bridged methyl group [Li(1)···C(1) 3.083(3) Å] is too long to suggest any significant secondary agostic interaction, thus resulting in the open cyclic motif; whereas the K(1)-C(1) bond [3.036(9) Å] is within the

acceptable region for sigma potassium-carbon bonds [mean Li–C and K–C bond lengths from the CSD [17], 2.265 Å and 3.206 Å respectively], producing the closed cyclic arrangement.
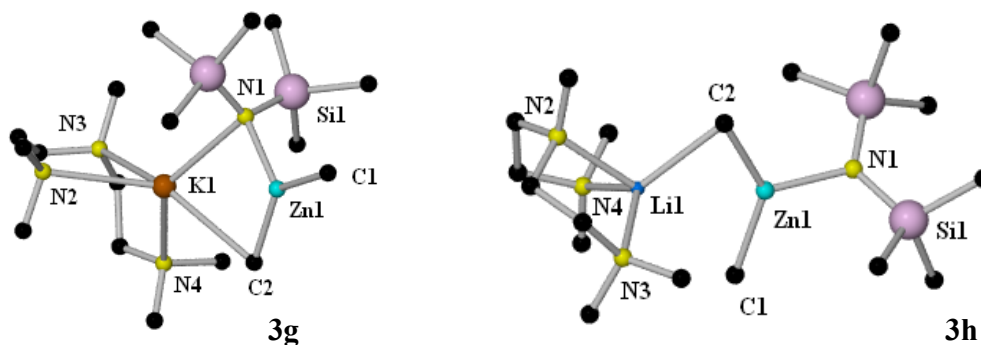
Figure 3.5: Contrasting molecular structures of the PMDETA-solvated potassium HMDS zincate [PMDETA·K(μ-HMDS)(μ-Me)Zn(Me)] (3g) and the literature lithium congener [PMDETA·Li(μ-Me)Zn(Me)(HMDS)] (3h).

3.2.2) Solution Studies

Potassium zincate bases **3a-3g** are soluble in both hydrocarbon and arene solvents, enabling their ^{1}H and ^{13}C NMR spectra to be recorded (**3a-3d** and **3g** in C_6D_6 solution; **3e** in d_{12}-cyclohexane {d_{12}-Cy} solution), at room temperature. In all cases only one set of resonances, consistent with the crystallographically determined formulae, were observed. **Table 3.4** compares the ^{1}H NMR chemical shifts of complexes **3a-3d** and **3g**, plus those of the free amines PMDETA and TMP(H). Without exception, the TMP resonances for the five bases **3a-3d** and **3g**, all shift to higher frequency (in the range 1.31-2.06 ppm) compared with those of the free amine (δ = 1.06-1.53 ppm). In contrast, the resonances associated with the PMDETA ligand move in the opposite direction, as they shift to a lower frequency (in the range δ = 1.77-1.91 ppm) compared to the free ligand resonances (2.11-2.46 ppm) which is indicative of PMDETA-K$^+$ chelation as observed in the crystal structures. Compound **3a**, [PMDETA·K(μ-TMP)(μ-Me)Zn(Me)], was found to have the most upfield Zn-CH$_{2/3}$ chemical shift of -0.35 ppm, which represents a downfield shift of 0.17 ppm compared to the spectrum of the homometallic reagent Me$_2$Zn (δ = -0.52 ppm) in C_6D_6 solution. The HMDS analogue of **3a**, **3g**, shows a methyl resonance at a

higher frequency (-0.28 ppm) compared to the TMP congener, highlighting that the amide group can have a substantial effect on the chemical shift of other ligands surrounding the Zn atom.

Table 3.4 Selected ^{1}H NMR chemical shifts (in ppm) of zincates 3a-3d and 3g and free amines PMDETA and TMP(H) in C_6D_6 solutions.

Compound	Alkyl	Amide	M-$CH_{2/3}$	TMP (CH_3)	TMP (βCH_2)	TMP (γCH_2)	PMDETA $(4 \times CH_2)$	PMDETA $(4 \times CH_3)$	PMDETA $(1 \times CH_3)$
PMDETA	-	-	-	-	-	-	2.46, 2.35	2.11	2.18
TMP(H)	-	-	-	1.06	1.22	1.53	-	-	-
3a	Me	TMP	-0.35	1.41	1.57	2.01	1.86	1.88	1.82
3b	Et	TMP	0.47	1.36	1.58	2.03	1.77	1.81	1.74
3c	^{i}Pr	TMP	0.41	1.31	1.59	1.98	1.91	1.88	1.83
3d	^{n}Bu	TMP	0.41	1.36	1.58	2.01	1.78-1.87	1.76	1.78-1.87
3g	Me	HMDS	-0.28	-	-	-	1.81	1.85	1.81

The *t*-butyl base **3e** was dissolved in d$_{12}$-Cy solution instead of C$_6$D$_6$ solution due to the high probability of benzene metallation occurring in the latter solvent which has been witnessed with the TMEDA-sodium analogue.[5] This ^{1}H NMR spectrum of **3e** is shown in **figure 3.6**. A comparison to the related published complex [TMEDA·Na(μ-TMP)(μ-^{t}Bu)Zn(^{t}Bu)] **(3i)** can be made as its ^{1}H and ^{13}C NMR spectra were also reported in d$_{12}$-Cy solution (**table 3.5**). In both bases, the TMP-associated resonances move to higher frequency compared to that of the free amine, though the degree of movement is different in each case. An example of this is seen with the methyl resonances of the amide, as they have moved downfield from 1.06 ppm (in the free amine) to 1.11ppm (**3e**) and 1.29 ppm (**3i**). The chemical shifts of the resonance attributed to the *t*-butyl groups in the ^{1}H NMR spectra are, however, quite similar in each base. In the ^{1}H NMR spectrum of **3e** the peak is rather narrow (at δ 1.02 ppm), though in the associated ^{1}H NMR spectrum of **3i** the peak is more broad in nature (from 0.95-1.19 ppm). At room temperature, the two ^{t}Bu groups seem to be equivalent in d$_{12}$-Cy solution (as seen by a single resonance in the ^{1}H NMR attributed to these ligands), a marked contrast to the two different ^{t}Bu groups identified in the X-ray structures of these zincates. This observation hints that a dynamic process involved

with regards to these alkyl groups (that is, the switching between bridging and terminal modes) could be occurring in solution, commencing at a slower rate in complex **3i** than in zincate **3e** in
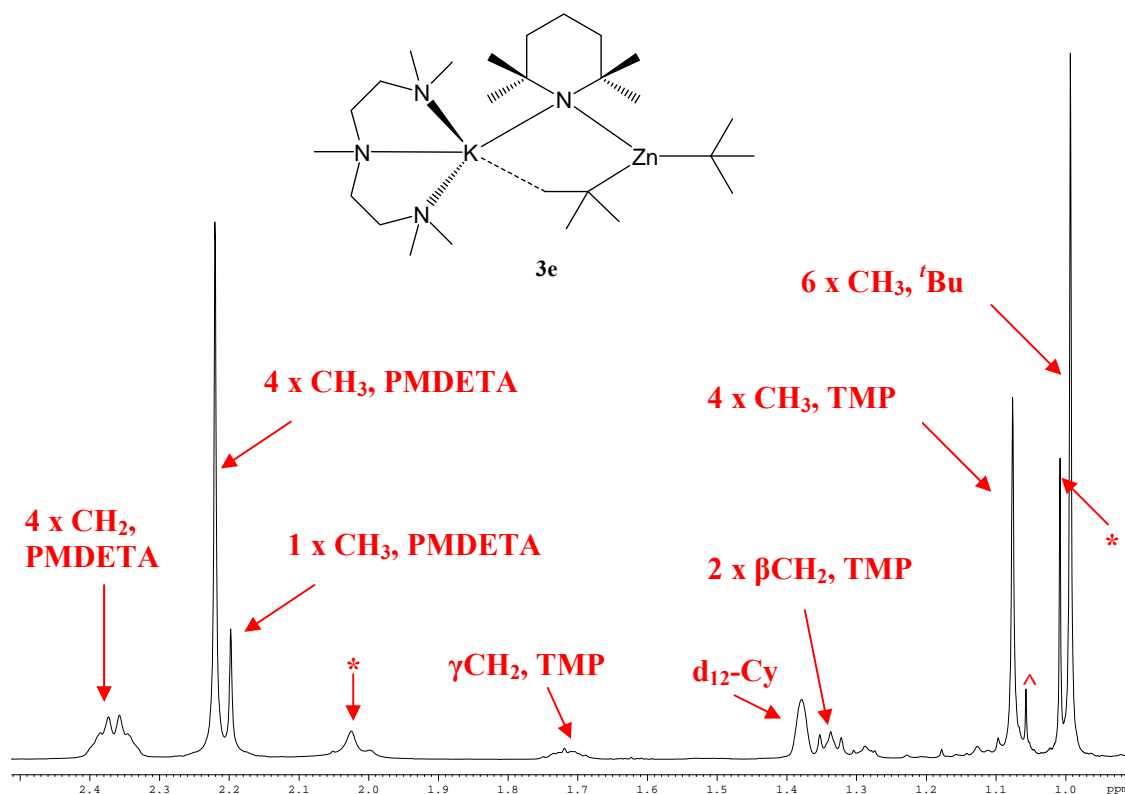
Figure 3.6: ^{1}**H NMR spectrum of [PMDETA·K(μ-TMP)(μ-^{t}Bu)Zn(^{t}Bu)] (3e) in deuterated cyclohexane solution. * = unknown protic impurity, ^ = TMP(H).**

the NMR timescale (as judged by the broadness of their associated ^{t}Bu resonance). It can be deduced from the comparative analysis of the ^{1}H NMR spectra of **3e** and **3i** that [(TMP)Zn(^{t}Bu)$_2$]$^-$ cannot be solvent-separated here as different shifts are found for the potassium and sodium examples. This is good evidence for the retention of the contacted ion pairs in solution. Cyclohexane is a poor solvating medium, therefore different results may occur in benzene for example.

The ^{13}C NMR spectra of zincates **3a**, **3b**, **3d**, **3e** and **3g** were fully assigned using ^{1}H-^{13}C HSQC correlation spectroscopy. Some of the biggest comparative resonance shifts can be seen with the

carbon of the alkyl groups attached to Zn, which appears at a relatively higher frequency the longer the alkyl chain becomes [Me, -2.9 ppm; Et, 9.0 ppm; ^{n}Bu, 19.3 ppm]. A comparison of the ^{13}C NMR methyl resonance of the ^{t}Bu groups in **3e** and **3i** (**table 3.5**) show a 4.9 ppm difference in chemical shift, with the resonance associated with **3e** residing at a higher frequency [35.5 ppm for **3e**; 30.6 ppm for **3i**]. Although not an exact comparison, the ^{13}C methyl (of ^{t}Bu) resonance in the Li/THF congener resides at a lower frequency (22.0 ppm in d$_8$-THF solution). Coupled with the similar ^{13}C NMR TMP resonance values, the change in alkali-metal [K, **3e**; Na, **3i**] appears to have an effect on the ^{t}Bu groups, which was also seen in the solid state structures with regard to bond lengths and angular dimensions.

Table 3.5 Selected ^{1}H and ^{13}C NMR chemical shifts (in ppm) of the K/Zn base 3e, the Na/Zn zincate 3i and the free amine TMP(H) in solutions of C$_6$D$_{12}$.

NMR expt.	Compound	$4 \times CH_3$, TMP	$2 \times \beta CH_2$, TMP	$1 \times \gamma CH_2$, TMP	$6 \times CH_3$, ^{t}Bu
^{1}H	**3e**	1.11	1.37	1.74	1.02
^{1}H	**3i**	1.29	1.72	1.72	0.95-1.19
^{1}H	TMP(H)	1.06	1.29	1.62	-
^{13}C	**3e**	34.2	39.4	19.5	35.5
^{13}C	**3i**	35.7	40.1	20.4	30.6
^{13}C	TMP(H)	32.3	39.2	19.3	-

3.3) Potassium-mediated Zincation of Pyridines

3.3.1) *Introduction*
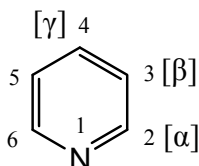
Figure 3.7: Structure of pyridine.

Pyridines (**figure 3.7**) are one of the most important classes of heterocyclic compounds in chemistry.[35,36] These heterocycles have several applications in synthesis, including being used as solvents, Lewis base catalysts or as bases. Important derivatives of pyridine are found in biological systems, such as

82

nicotine, nicotinamide (niacin) and nicotinamide adenine dinucleotide diphosphate (NADP) or pyridoxine (vitamin B_6) (**figure 3.8**). Many pyridine-based compounds are registered as having agriculturally [37] or pharmaceutically [38] active properties, and as such functionalising these heterocyclic species is a very desirable process. To isolate pyridine, and its simple alkyl derivatives (picolines), the old method of choice was to extract these compounds from coal tar (in which they occur abundantly). Pyridine itself can be synthesised nowadays by condensation of formaldehyde and crotonaldehyde with ammonia in the presence of air.[35]
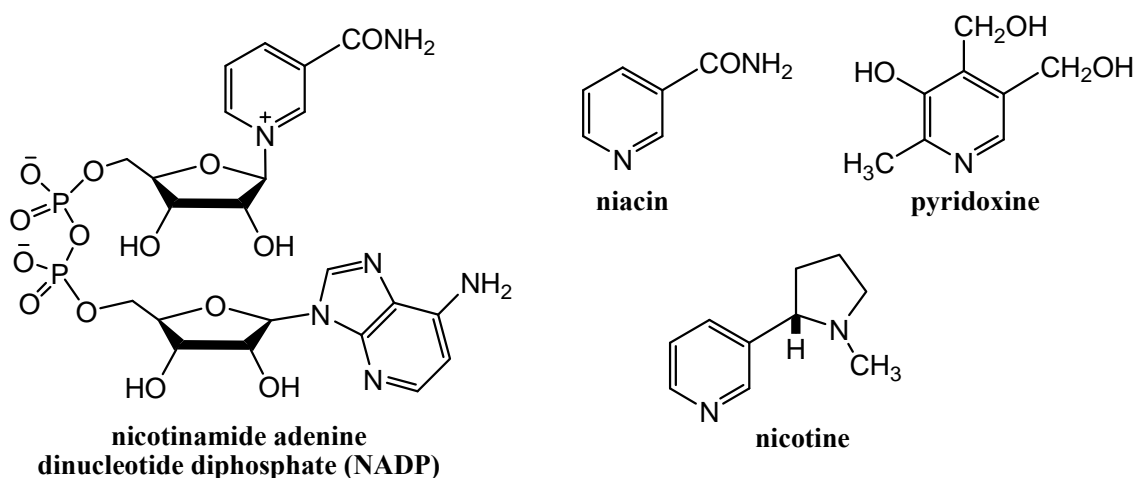
Figure 3.8: Biologically active compounds containing a pyridine sub-unit.
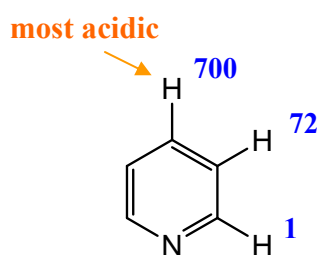
Figure 3.9: Relative acidities of the hydrogen atoms in pyridine.

Pyridine is classed as an electron-deficient, six-membered aromatic heterocycle. By formally replacing one CH unit in benzene by nitrogen, these compounds become much more acidic than their carbocyclic analogues. The relative acidities of the hydrogen atoms of the parent pyridine are shown in **figure 3.9**. In 1983 Quéguiner published a review on the metallation of π-deficient hetroaromatic compounds involving numerous pyridines and lithium bases.[39] This study highlighted that the relative stabilities of the lithiopyridines, where lithium occupies the 4-, 3- or 2- positions on the heterocyclic ring of pyridine, are linked to the relative acidities of the hydrogen

atoms.

In terms of the deprotonation of pyridine substrates, regioselectivity is more often determined by the stability of the anion produced, than the rate of deprotonation, that is thermodynamic effects outweigh kinetic effects. In this case, the coordination effect becomes less important than the acidifying effect of the substrate in question. This situation strongly influences the regiochemistry of lithiation: the nitrogen lone pair can act as a directing group, coordinating to lithium, and facilitating deprotonation of the carbon adjacent to N, but the lone pair then has a destabilising effect on the anion produced because of repulsion with the developing C–Li bond (**scheme 3.2**). The most stable pyridinyllithiums are those where the lithium resides on the 3- or
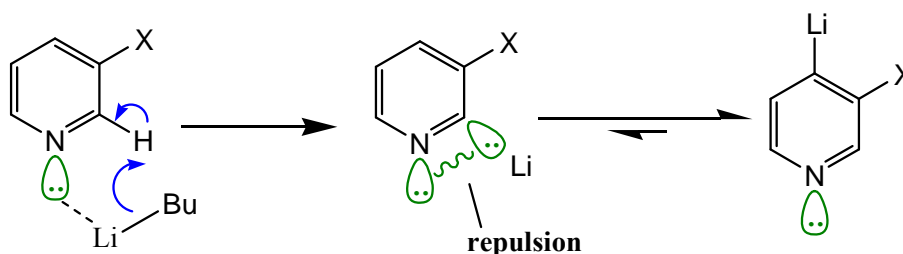
Scheme 3.2: Accelerated deprotonation due to the N directing group, followed by destabilisation of the product due to electronic repulsion.

4-position. 2-pyridinyllithiums can form faster, however these compounds can readily isomerise, given appropriate conditions, to the product where the 4-position carbon holds the alkali metal.
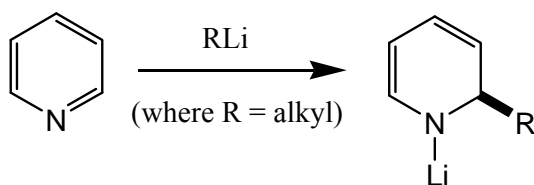
Scheme 3.3: Addition of an alkyllithium to the azomethine C=N bond of pyridine.

A competitive reaction using alkyllithium reagents as deprotonating agents toward pyridines is their tendency to add across the C=N double bond (**scheme 3.3**) rather than to deprotonate the substrate.[40] A way of circumventing this problem involves the use of ligands with donor groups to enhance the basicity of the alkyllithium reagent. For example, the reagent LiDMAE [LiDMAE = $Me_2N(CH_2)_2OLi$] can be utilised with two molar

equivalents of *n*-butyllithium (at -78°C), in a hexane solution, to successfully lithiate pyridine at the 2-position.[41] This was confirmed indirectly by the electrophilic quenching of the reaction mixture to produce a series of 2-substituted pyridines in yields ranging from 25-80%.

Lithium amides, in particular LDA and LiTMP, can be used to deprotonate pyridines in good yields.[42] However, even though successful lithiations can be achieved with these amido bases, the addition of the lithiated product to unreacted starting material can occur. In a representative example, LDA can directly lithiate pyridine at the 2-position at -70°C in diethylether solution in the presence of HMPA (HMPA = hexamethylphosphoramide). The lithiated pyridine then adds across the azomethine bond of unreacted pyridine to generate, after an aqueous quench, the coupled product 2,2′-bipyridine in a yield of 50% (**scheme 3.4**).[43]

The lone pair of the nitrogen on pyridine can be blocked by synthesising pyridine oxides [44] or pyridine borates.[45-47] This allows deprotonation to occur at the 2-position without the destabilising effect from the lone pair. For example, pyridine and hexafluoroacetone combine together to form the zwitterionic β-oxidopyridinium betaine compound, and this resultant
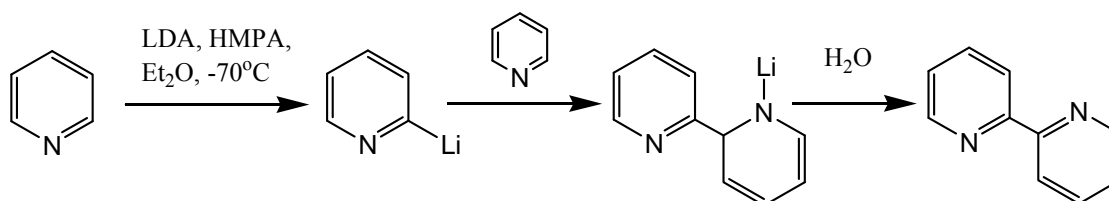
Scheme 3.4: Initial 2-lithiation of pyridine followed by addition to the C=N bond of a second pyridine molecule.

substrate can be metallated with LiTMP in THF solution at -107°C.[44] Subsequent quenching with several electrophiles resulted in the isolation of 2-substituted products (**scheme 3.5**). The additional inductive and chelation effect from the lone pair of the oxygen helps direct the regioselectivity of this reaction by interaction with the lithium. Boron trifluoride adducts of pyridine, 4-methylpyridine and 4-(dimethylamino)pyridine all react with LiTMP in diethyl ether at -75°C to produce 2-substituted products.[45-47] It is interesting to note that without the

cocomplexation of boron trifluoride to 4-methylpyridine, the site of metallation moves from the 2-position of the ring to the lateral deprotonation of the methyl substituent.
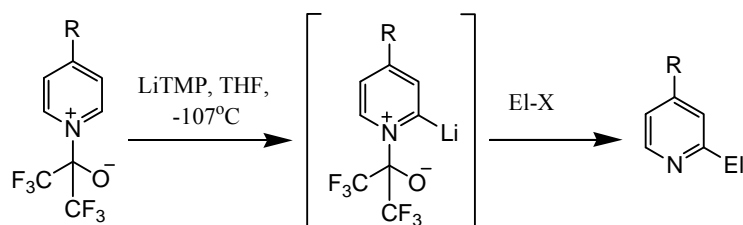
Scheme 3.5: Lithiation of pyridine/hexafluoroacetone adducts (R = ^{t}Bu or H; El-X = H$_5$C$_6$CH=O, (F$_3$C)$_2$C=O, I$_2$, ClSiMe$_3$).

Mixed–metal bases have also been utilised to deprotonate pyridine. The superbasic, bimetallic, Lochmann-Schlosser LICKOR reagent was used in slight excess (1.5 molar equivalents) compared to the heterocycle at -105°C.[48,49] This method of deprotonation results in a mixture of 2-, 3-, and 4-substituted pyridines after quenching with the electrophiles deuteriomethanol, dimethyldisulphide or trimethylchlorosilane (3, 1.2 and 1.2 molar equivalents added respectively) in hexane/THF solvent mixtures.

In 1999, Kondo reported the direct α-metallation of π-deficient heteroaromatic compounds using the bimetallic mixed amido/alkyl zincate "(TMP)Zn(^{t}Bu)$_2$Li".[9] At room temperature (unlike most of the lithiation reactions which must be performed at very low temperatures to avoid unwanted side-reactions), in a THF solution, pyridine, quinoline and isoquinoline were are all subjected to the lithium zincate base. In what was perceived at the time to be a challenging reaction on paper, in fact the α-metallation of pyridine proceeded rather smoothly, generating 2-iodo-pyridine in a 76% yield following a iodine quench (**scheme 3.6**). It should be stressed that no structural information nor any NMR spectroscopic characterisation was gathered on the metallated pyridine intermediate.
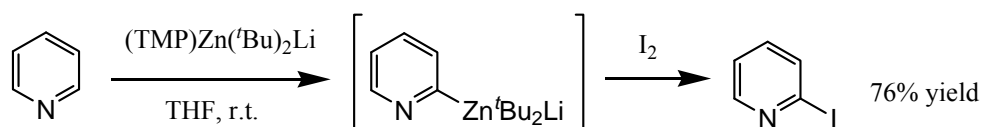
Scheme 3.6: α-Metallation of pyridine with the lithium zincate "(TMP)Zn(^{t}Bu)$_2$Li".

3.3.2) *Direct zincation of pyridine and 4-(R)-substituted pyridines (R = Et, ^{i}Pr, ^{t}Bu, Ph, OMe and Me$_2$N) using dialkyl-TMP-zincate bases*

Given the fact that there is a dearth of zincated pyridine complexes in the CSD (only one hit of zincation at any position of the ring was found) [50], our initial objective was to accumulate definitive information on the zincated intermediates formed from this series of reactions, so the focus was on growing, from solution, suitable crystals for single-crystal X-ray crystallographic characterisation. Note, however, that the reaction filtrates obtained following isolation of the crystalline products were also probed by NMR spectroscopic studies (see later, page 93). The base chosen to study the potassium-mediated zincation (KMZn) of the selected pyridines was the diethyl-TMP zincate [PMDETA·K(μ-TMP)(μ-Et)Zn(Et)] **3b**. In the preparative procedure, base **3b**, prepared *in situ* in hexane solution, was treated with one molar equivalent of pyridine, 4-dimethylamidopyridine (4-DMAP), 4-ethylpyridine, 4-isopropylpyridine, 4-*tert*-butylpyridine, or 4-phenylpyridine. These reactions yielded [{2-Zn(Et)$_2$-μ-4-R-C$_5$H$_3$N}$_2$·2{K(PMDETA)}] {R = H (**3j**), Me$_2$N (**3k**), Et (**3l**), ^{i}Pr (**3m**), ^{t}Bu (**3n**) and Ph (**3o**)} in isolated yields of 16, 53, 7, 23, 67 and 51% respectively. The reaction of 4-methoxypyridine formed [*catena*-{PMDETA·K[3-Zn(Et)$_2$-4-MeO-C$_5$H$_3$N]}$_\infty$], **3p**, in a crystalline yield of 52% (**scheme 3.7**). In addition, reaction

Scheme 3.7: Zincation reactions of pyridine and 4-substituted derivatives.

of the closely related dibutyl reagent [PMDETA·K(μ-TMP)(μ-*^{n}*Bu)Zn(*^{n}*Bu)] **3d** with 4-*tert*-butylpyridine afforded a 58% crystalline yield of [{2-Zn(*^{n}*Bu)$_2$-μ-4-*^{t}*Bu-C$_5$H$_3$N}$_2$·2{K(PMDETA)}], **3q**. Owing to the close similarity between **3q** and the family of diethyl analogues, no attempts were made to grow more crystalline complexes from reactions of **3d** with other pyridine substrates (excluding 4-methoxypyridine) because it was assumed that **3q** would be representative of a common structural motif. All of these new potassium pyridylzincates were characterised by single-crystal X-ray crystallography, and solutions of the potassium-zincates, as well as reaction filtrates (following removal of the crystalline products), were analysed by ^{1}H and ^{13}C NMR spectroscopy. These results are now discussed in turn.

3.3.2.1) Solid-state Analysis

The diethyl-zincate family (**3j-3o**) and their dibutyl analogue **3q** share a common dimeric structural motif (**figure 3.10**). Structures **3j-3o** and **3q** can be viewed as heterocyclic 9,10-dihydroanthracene mimics, each with a central diazadicarbadizinca (ZnCN)$_2$ ring, capped on either side by a potassium cation, which is complexed with a PMDETA ligand. All these discrete molecules sit on crystallographically imposed inversion centres. Note there are two, nearly identical, independant molecules of **3o** in the asymmetric unit of the crystal structure (only one of these molecules is shown in **figure 3.10**). Across the series, the central hexagonal (ZnCN)$_2$ ring is essentially planar and lies in the same plane as the two outer pyridyl rings as illustrated by the small dihedral angles between the pyridyl ring plane and the central (ZnCN)$_2$ ring plane [the range for **3j-3n** and **3q** is 1.0(8)-2.93(15) and 1.2(4)^o, respectively], although the values for **3o** are slightly larger [5.80(19) and 12.52(14)^o]. In **3o** the phenyl rings are also twisted out of the pyridine ring plane [torsion angles for C2-C3-C6-C7 and C26-C27-C30-C31 (associated angle for the second independant molecule of **3o**, not shown in **figure 3.10**) are 34.4(5)^o and 39.0(5)^o, respectively]. Within each structure, the monomeric unit of the anthracene-like dianionic system comprises a pyridine molecule substituted at the 2-position by a diethylzinc molecule (indicative of the zinc-hydrogen exchange process inherent in AMM*Zn*), with the dimerisation junction being comprised of antiparallel (head-to-tail) dative Zn–N(pyr) bonds (pyr = pyridine). Overall, zinc occupies a modestly distorted tetrahedral C$_3$N environment (with a range of the mean bond

Figure 3.10: Molecular structures of pyridyl zincates of general formula [{2-Zn(Et)$_2$-μ-4-R-C$_5$H$_3$N}$_2$·2{K(PMDETA)}] {R = H (3j), Me$_2$N (3k), Et (3l), ^{i}Pr (3m), ^{t}Bu (3n) and Ph (3o)} and [{2-Zn(^{n}Bu)$_2$-μ-4-^{t}Bu-C$_5$H$_3$N}$_2$·2{K(PMDETA)}], 3q. Minor disorder components and hydrogen atoms are omitted for clarity.

angles across the series from 109.22 to 109.34°). Nine atoms (C × 4 and N × 5) fill the coordination sphere of the larger potassium cation containing two non-equivalent η^2-N,C interactions with the pyridyl rings (involving the anionic deprotonated C centre), which leads to an unsymmetrically bound tridentate PMDETA ligand, and contacts to two α-C atoms of two Et or ^{n}Bu ligands. Remarkably little variation is observed in the comparative dimensions of structures **3j-3o**. The mean lengths of the Zn–C bonds cover the narrow range 2.067-2.1007 Å (Δ = 0.0337 Å), all of which are shorter than the Zn–N dative bonds [in the range 2.167(4)-2.280(16) Å; Δ 0.061 Å]. Interactions between the potassium ion and the central $(ZnCN)_2$ ring are generally biased towards one N, C unit and form shorter contacts [for example, in **3k**, K–N, 3.036(13) Å; K–C, 3.1139(16) Å) than with the other [K–N, 3.2905(13) Å; K–C, 3.2791(15) Å]. Potassium also engages in long, weak, electron-deficient interactions with the zinc-bound ethyl ligands [K–C_α lengths in the range 3.140(2)-3.3896(17) Å]. Significantly shorter are the dative K–N (PMDETA) bonds, which cover the range 2.8422(14)-3.0512(19) Å.
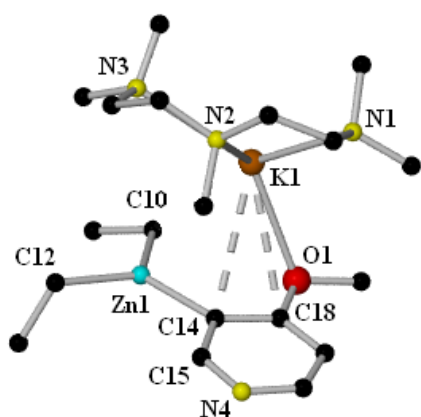
Figure 3.11: Asymmetric unit of 3p with out hydrogen atoms.

The structure of **3p**, [*catena*-{PMDETA·K[3-Zn(Et)$_2$-4-MeO-C$_5$H$_3$N]}$_\infty$], is remarkably different to those of **3j-3o**. In its asymmetric unit (**figure 3.11**), Zn occupies a trigonal C_3 environment comprising two Et and one 3-pyr ligands, and lying above the pyr ring plane [2.367(7) Å out of the plane] K occupies an irregular N$_3$O polyhedron comprising a MeO group and a PMDETA ligand. Through an intermolecular K–N(pyr) bond (making K 5-coordinate overall, excluding some long contacts to C atoms), with K coplanar to the pyridine ring plane, the asymmetric unit propagates to form an infinite stepladder structure (**figure 3.12**).

Curiously there are no Zn–N(pyr) bonds in **3p** making zinc coordinatively-deficient in comparison to the four-coordinate zinc in structures **3j-3o** and **3q** which forms dimerisation-defining Zn–N(pyr) bonds. An interesting aspect to note is that substituting the Me$_2$N substituent (in **3k**) to the isoelectronic MeO functional group, not only redirects the orientation of the

zincation reaction, it also reprograms the pyridine to function as a nitrogen σ-donor towards potassium, rebuffing zinc. Also, this reveals the accessibility of the O lone pairs and the inaccessibility of the NMe₂ lone pair due to conjugation with the aromatic π-system. Selected dimensions in **3p** are listed in **table 3.6**.
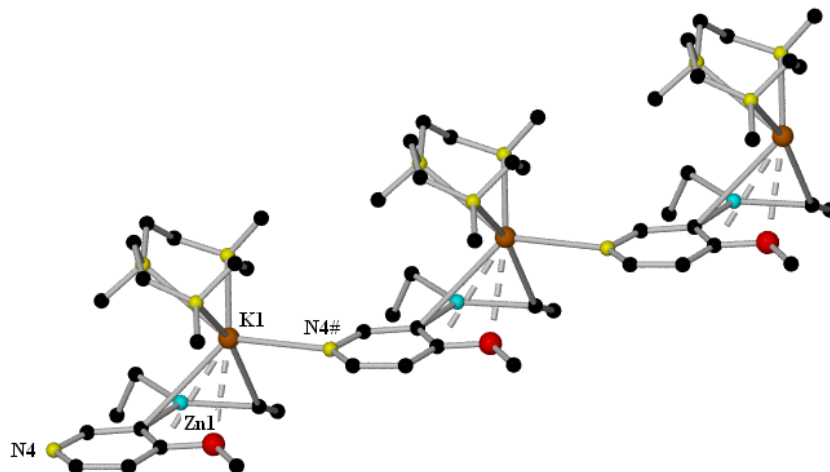
Figure 3.12: Trimeric section of the infinite stepladder structure 3p.

Table 3.6: Key bond lengths (Å) and bond angles (°) for 3p

K1–C14	3.404(4)	Zn1–C12	2.023(5)	N1–K1–N2	62.64(12)
K1–C18	3.334(4)	Zn1–C14	2.062(4)	N1–K1–N3	112.18(13)
K1–O1	2.796(3)	C10–Zn1–C12	123.5(2)	N2–K1–N3	62.43(12)
K1–N1	2.913(4)	C10–Zn1–C14	121.85(18)	O1–K1–N1	114.09(11)
K1–N2	2.926(4)	C12–Zn1–C14	114.67(19)	O1–K1–N2	121.70(11)
K1–N3	2.884(4)	K1–C14–Zn1	70.76(12)	O1–K1–N3	98.43(11)
Zn1–C10	2.025(5)	K1–C18–Zn1	55.6(2)	O1–K1–N4#	89.13(11)

The shortening of the Zn–C bonds (mean, 2.036 Å) in **3p** compared to those in **3k** (2.070 Å), for example, is not pronounced given the lower Zn coordination number involved. Also, situated far from the anionic pyr C atom [3.404(4) Å; *c.f.* 3.1139(16) Å in **3k**], potassium has a coordination sphere primarily involving dative bonding.

The molecular architecture shared by structures **3j-3o** and **3q** appears to be unique compared with any previously reported metallated pyridine derivative. However, there are a handful of literature compounds that possess a somewhat similar dihydroanthracene-type polycyclic arrangement. For example, *p*-block dimethylaluminium and –gallium complexes of unsubstituted pyridine, [Me$_2$E(μ-{2-pyr})]$_2$ (E = Al or Ga). have central (NCE)$_2$ shallow boat rings.[51] The *d*-block complex [(Br)(PPh$_3$)Pd(μ-{2-pyr})]$_2$ [52] and the *s*-block complex [(Br)(THF)Mg(μ-{2-pyr})]$_2$·(μ-THF)] [53] also share this dimeric tricyclic motif. For specific comparison to **3k**, metallated 4-(dimethylamino)pyridine structures are limited to two neutral Al complexes exhibiting a (NCAl)$_2$ flattened chair conformation.[54] However, none of these pyridyl dimers are heterobimetallic or ate complexes, nor do they show any type of face-capping akin to that observed here with potassium, because their (NCE)$_2$ faces lie vacant. Moreover, structurally defined 2-zincated pyridines are especially rare. [{Zn[Si(NMe$_2$)$_2$(NH^{t}Bu)(N^{t}Bu)](μ-NC$_5$H$_4$)}$_2$] is the one previous example (**scheme 3.8**), which was made by an indirect metathetical approach
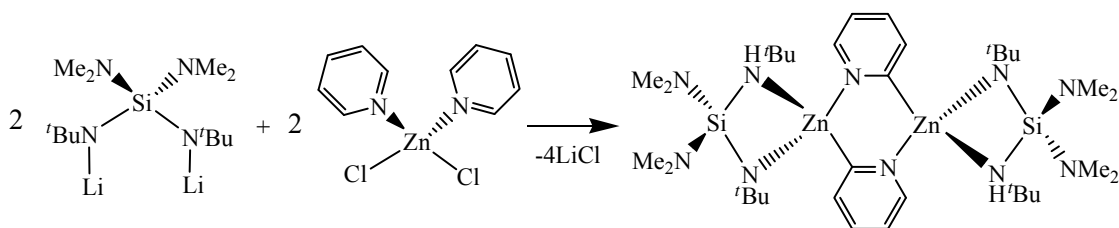
Scheme 3.8: Metathetical reaction forming a 2-zincated pyridine.

and not *via* direct zincation, and also displays an uncapped (NCE)$_2$ (E = Zn) tricyclic arrangement.[50] Without extra coordination provided by metallic caps, the (mean) Zn–C and Zn–N(pyr) bonds are predictably shorter (by 0.163 and 0.089 Å respectively) in this neutral zinc complex compared to that in the ate example **3j**. To the best of our knowledge, there are no previous crystal structures for zincated, or indeed any metallated, 4-ethyl-, 4-isopropyl-, 4-phenylpyridines or 4-methoxypyridines, thus structures **3l**, **3m**, **3o** and **3p** represent the first of their type. The previous dearth of crystallographic structural information markedly contrasts with the large body of studies in which metallated pyridines have been quenched (for example, in electrophilic trapping reactions) and thus studied indirectly without isolation. Advantages of AMM*Zn* are clearly evident from this comparison: first, that the method often facilitates the

formation of crystalline intermediates, and second, that the higher stability of zincated pyridines in relation to more polar metallated pyridines (typically lithiopyridines) makes them more amenable to isolation from solution under mild conditions without decomposing, which enables their crystallographic characterisation. In addition, the greater covalency and strength of Zn–C(pyr) bonds compared to Li–C(pyr) bonds makes them less prone to isomerisation processes. At the very least, these crystal structures represent resting states of possible solution structures.

3.3.2.2) Solution Studies

Potassium-zincates **3j-3o and 3q** are highly soluble in arene solvents, enabling the recording of their ^{1}H and ^{13}C NMR spectra from deuterated benzene (C_6D_6) solution at room temperature. Complex **3p** is soluble in the deuterated ethereal solvent d_8-THF. In all cases only one set of resonances, consistent with the crystallographically determined formulae, were observed. **Table 3.7** compares the ^{1}H NMR chemical shifts of the aliphatic resonances of the diethyl-zincates **3j-3o** with standards of the base **3b**, diethylzinc and PMDETA. Without exception, the CH_2 and CH_3 (Et) resonances of the potassium-zincates shift upfield and downfield respectively, in comparison to those of neutral diethylzinc. Bimetallic base **3b** retains much of its parent zinc character because its CH_2 (Et) resonance (0.47 ppm) lies close to that of diethylzinc (0.55 ppm), whereas those of **3j-3o** lie more upfield in the narrow range 0.15-0.24 ppm. More remote from the zinc centre, the CH_3 (Et) resonances of **3b** and **3j-3o** are grouped together in the range 2.03-2.15 ppm. PMDETA resonances for **3b** and **3j-3o** shift upfield (in the range 1.71-2.01 ppm) compared to those of the free ligand (2.11-2.46 ppm), which is indicative of the PMDETA–K$^+$ chelation observed in the crystal structure. Consistent with a pyridine zincated in the 2-position, only four aromatic resonances at 8.93, 8.05, 7.03, and 6.66 ppm are found in the ^{1}H NMR spectrum of **3j**. The ^{13}C NMR spectrum concurs with this, with the 2-zincated C resonance appearing downfield at 150.55 ppm. In general, there is little discrimination between the common resonances in the ^{13}C NMR spectra of **3j-3o** with, for example, the CH_2 (Et) resonance covering the small range (3.87 in **3l** to 6.12 ppm in **3o**). These are substantially shifted downfield compared with that in the diethylzinc standard (-2.12 ppm), which reflects both aggregative dimer/monomer and zinc coordination-sphere (C_3N versus C_2) differences. Displaying a unique trigonal planar (C_2N) zinc geometry within the series, the diethyl-TMP-zincate **3b** exhibits the

most downfield CH$_2$ (Et) signal of all at δ = 8.99 ppm. The complete assignment of ^{1}H and ^{13}C NMR spectra is listed in the Experimental Section, where assignment of the spectra was assisted by ^{1}H-^{1}H and ^{1}H-^{13}C coupling NMR spectroscopic techniques (COSY and HSQC respectively).

Table 3.7: Selected ^{1}H NMR chemical shifts of the starting materials, the zincate base 3b and zincated pyridine products 3j-3o in C$_6$D$_6$ solutions.

Compound	Et–C*H*$_2$ (ppm)	Et–C*H*$_3$ (ppm)	4 × C*H*$_3$ PMDETA (ppm)	1 × C*H*$_3$ PMDETA (ppm)	4 × C*H*$_2$ PMDETA (ppm)
Et$_2$Zn	0.55	1.51	-	-	-
PMDETA	-	-	2.11	2.18	2.46, 2.35
3b	0.47	2.03	1.81	1.74	1.77
3j	0.15	2.05	1.77	1.95	1.90
3k	0.22	2.13	1.88	2.01	1.96
3l	0.19	2.05	1.83	1.97	1.89
3m	0.17	2.08	1.78	1.98	1.92
3n	0.15	2.07	1.71	1.96	1.88
3o	0.24	2.15	1.71	1.94	1.88-1.81

Some of the modest to poor yields of the new crystalline potassium-zincates (for example, 16 and 7 % for **3j** and **3l**, respectively) suggest that the AMMZn reactions may not be clean, so the reaction filtrates that remained after isolating the crystalline products were also probed by NMR spectroscopy. In the case of **3j**, ^{1}H NMR spectra indicated that the oily filtrate appeared to contain a complicated mixture of products. The aromatic region revealed several overlapping resonances in the range 9.0–6.6 ppm, which proved to be indecipherable. Utilising Caubere's base ("BuLiLiDMAE") [DMAE = dimethylaminoethanol], 4-methylpyridine (γ-picoline) can be regioselectively metallated at the 2-position.[55] Therefore it was of interest for us to see what product(s) would be obtained from the reaction of base **3b** with 4-methylpyridine. Using a 1:1

mixture of base to pyridine, crystals of a product from the attempted metallation reaction of 4-methylpyridine could not be grown, thus an aliquot of the reaction mixture (**3r**) was removed for ^{1}H NMR analysis. Instead of signals for ring metallation, resonances indicative of lateral metallation alone were observed, a major difference from the reaction with Caubere's reagent. The obvious signals of lateral metallation were seen from the integration and chemical shift change of the CH$_2$ group from 1.84 to 3.33 ppm. The pair of doublets for the untouched ring also shift upfield as a result of the lateral metallation, from 8.44 and 5.63 ppm to 7.05 and 5.71 ppm respectively. The exact molecular structure of **3r** can only be predicted as no X-ray structure has so far been obtained. A potassium cation almost certainly exists in the structure as the resonances for the PMDETA ligand have changed significantly from that of the free tridentate amine. The four terminal CH$_3$ groups (2.02 ppm), the four CH$_2$ (1.99 ppm) and the central CH$_3$ (1.96 ppm) are all shifted upfield in comparison to free PMDETA by 0.09, 0.47/0.36 and 0.22 ppm respectively. Resonances for the ethyl groups of the diethylzinc part of the molecule can be identified from the ^{1}H NMR spectrum of the reaction mixture aliquot. With chemical shifts of 0.38 ppm (ethyl CH_2) and 1.74 ppm (ethyl CH_3), considerably different from those of the free zinc reagent (see **table 3.7**) thus perhaps the diethylzinc is part of the metallated 4-methylpyridine intermediate. With this information, a possible intermediate can be proposed (**figure 3.13**).
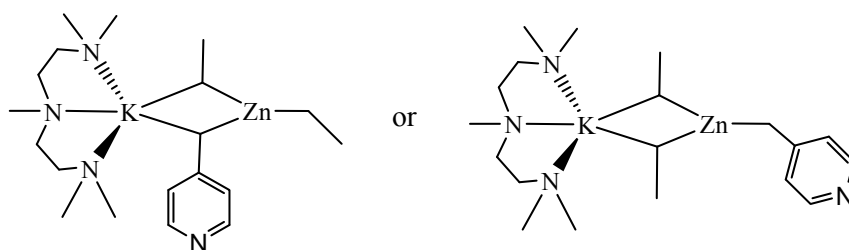
Figure 3.13: Proposed structures of product 3r from ^{1}H NMR spectral analysis.

With respect to KM*Zn* of 4-ethylpyridine, complex **3l** was found to be a minor product, with the major component of the oily, viscous filtrate a laterally metallated pyridine product (**scheme 3.9**). In **3l**, the methylene CH$_2$ of the Et pyridine substituent had been metallated to a methyne CH$^-$, with the resonance appearing significantly downfield (3.98 ppm) compared to the CH$_2$ resonance in 4-ethylpyridine (2.20 ppm). This movement of the CH resonance is similar to those

seen in ^{1}H NMR spectra of the isolated lithiated intermediates of the reactions between 4-(dimethylaminomethyl)pyridine and 4-(trimethylsilylmethyl)pyridine with lithium diisopropylamide in THF or Et$_2$O.[56] It is likely, given that this lateral metallation of 4-ethylpyridine has metal-bound PMDETA (4 × CH$_3$ at 2.03, 1 × CH$_3$ at 2.00, and 4 × CH$_2$ at 1.96 ppm) and Et (CH$_2$ at 0.30 and CH$_3$ at 1.85 ppm) resonances associated with it, that this major product could be formulated as [(PMDETA)·K(μ-4-CH$_3$CHC$_5$H$_4$N)(μ-Et)Zn(Et)] or [(PMDETA)·K(μ-Et)$_2$Zn(4-CH$_3$CHC$_5$H$_4$N)] (**3s**) and would adopt the same template design as
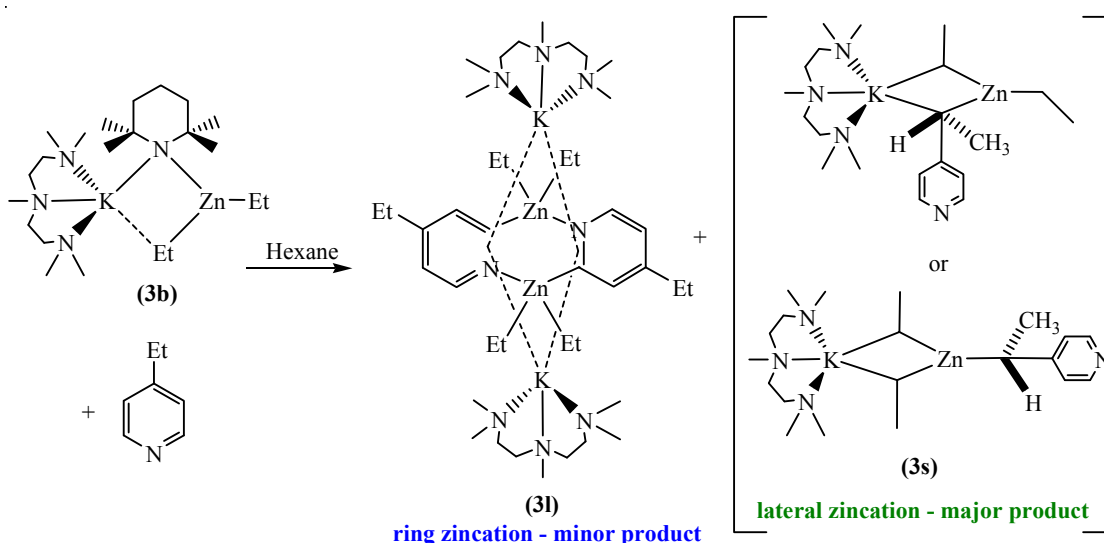
Scheme 3.9: Ring and lateral metallated products from KMZ*n* of 4-ethylpyridine.

3b. This result is not surprising because there has been a previous report of the metallation of the side chain of 4-ethylpyridine by using the sodium reagent NaNH$_2$ in liquid ammonia though no metallated intermediates were isolated in this study.[57] On the basis of similar NMR spectroscopic evidence, the reaction of 4-isopropylpyridine with **3b** follows a similar course, with the minor product being crystalline **3m** (23% yield) and the major product (found in the oily filtrate) being a laterally metallated pyridine compound, presumably [(PMDETA)·K(μ-Et)$_2$Zn(4-Me$_2$C-C$_5$H$_4$N)] (**3t**). There have also been precedents for C*H*(^{i}Pr) metallation of 4-isopropylpyridine with lithium, sodium, or potassium metal, the intermediates of which were used to carry out side-chain alkenylation and aralkylation reactions with conjugated dienes or styrenes.[58] Lateral metallation of 4-*tert*-butylpyridine is a much more challenging task, so

unsurprisingly **3n** was the only metallated product in crystalline form (67% yield) or in the reaction filtrate. The treatment of **3b** with 4-phenylpyridine also appeared to be a clean reaction giving a crystalline yield of **3o** of 51%, with more **3o** present in the reaction filtrate. Considering this result was achieved using a base/pyridine stoichiometry of 1:1, it favourably compares with the previous report by Gros and Fort of lithiation of the same substituted pyridine using Caubére's base (**scheme 3.10**), which give excellent yields (>80%) of the 2-substituted pyridine following electrophilic quenching, but only upon addition of four molar equivalents of the base.[59] Note that no metallated intermediates were characterised in this earlier study and that the reaction solution has to be cooled to below room temperature, unlike the potassium-mediated zincation of 4-phenylpyridine which is carried out successfully at room temperature.

(i) 4 eq. BuLi-LiDMAE, hexane, 0°C
(ii) MeSSMe or CBr$_4$ (4.8 eq.), hexane, -78°C

FG = SMe (80%)
FG = Br (83%)
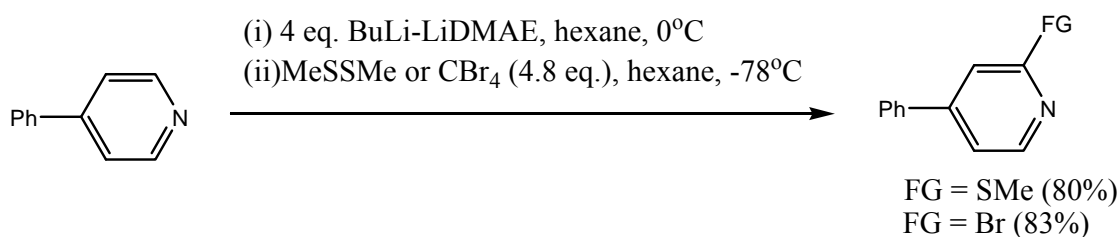
Scheme 3.10: Lithiation of 4-phenylpyridine using Caubére's base, followed by electrophilic quenching.

Perhaps the most interesting example of the potassium-mediated zincation of pyridines is shown in our reaction of the base **3b** with the acylation catalyst 4-(dimethylamino)pyridine (4-DMAP). This produces the 2-zincated pyridine **3k** in an isolated crystalline yield of 53%. Earlier PM3 calculations on DMAP indicate C3 is the most acidic site, and this is where the superbasic Me$_3$SiCH$_2$Li-LiDMAE [LiDMAE = Me$_2$N(CH$_2$)$_2$OLi] combination selectively deprotonates in hexane-THF solution.[60] In contrast BuLi-LiDMAE was found to give exclusive C2 lithiation (**scheme 3.11**). The distinction was attributed to an electronically-driven deprotonation in the former case and a pyridyl N atom assisted deprotonation in the latter case.[61] Extrapolating these ideas to **3k** suggests that base **3b** might operate through a precoordination step with a pyridyl N–metal bond, following elimination of TMP(H) and concomitant formation of a C2–Zn bond.

97
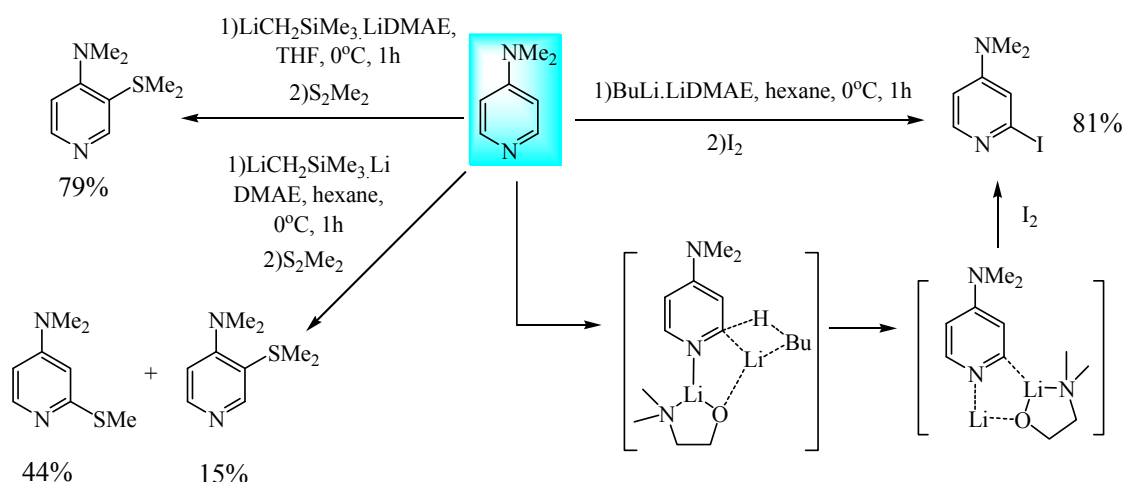
Scheme 3.11: Various lithiation/quenching reactions, with conditions, of 4-(dimethylamino)pyridine.

With respect to the deprotonation of 4-methoxypyridine, its lithiation has been reported with the organolithium bases phenyl- or mesityllithium.[62,63] Subsequent quenching reactions with a variety of electrophiles shows that these bases metallate regioselectively at the 3-position though no information was obtained on the lithiopyridine intermediates involved. In our work the potassium-zincate base **3b** reacts with 4-methoxypyridine to yield the 3-zincated complex **3p** (52% yield) [which is poorly soluble in deuterated benzene, but dissolves in d$_8$-THF solution]. This contrasts with the 2-zincation of 4-DMAP and can be rationalised by the greater DoM (directed *ortho*-metallation) ability of MeO$^-$ over isoelectronic Me$_2$N$^-$, which in part reflects accessibility of the O lone pairs and inaccessibility of the Me$_2$N lone pair due to its conjugation with the aromatic π-system.

Although AMMZn has been accomplished with all of the substrates studied and valuable structural information has been gathered, selectivity is an issue. Ring zincation competes with lateral zincation (in the cases of pyridine R = H, Et and ^{i}Pr) and base **3b** is not satisfactory because it gives a mixture of products. On the other hand, when R = Me$_2$N, ^{t}Bu, Ph, MeO and Me, base **3b** is a highly effective zincator, achieving 2-zincation (R = Me$_2$N, ^{t}Bu and Ph), 3-zincation (R = MeO) and lateral zincation (R = Me) selectively under mild (ambient temperature) conditions.

3.3.2.3) Ligand Transfer and Catalytic Considerations:

Because it possesses a heteroleptic formulation, **3b** could, in theory, function as an amido (TMP) or alkyl (Et) base (or both). This ambibasicity is one of the endearing features of this class of alkyl-amido reagent. Despite this possibility, all of the evidence accumulated from this study implies that **3b** is exclusively a TMP base. Thus, no anionic TMP ligands are found in structures **3j-3p**, while the proton-capturing residue TMP(H) is observed in the reaction filtrates. This appears to contrast with AMMZn reactions in which AM = Li or Na, which generally, although not exclusively, ultimately act as alkyl bases. By exploiting key structures previously elucidated by X-ray crystallography to build models for theoretical investigation, Uchiyama *et al.* showed through DFT (density functional theory) calculations that lithium- or sodium-TMP-dialkyl-zincate reagents deprotonate substrates in two steps: in step 1, TMP abstracts a proton from the substrate to form TMP(H); in step 2, TMP(H) is deprotonated to anionic TMP, which forms part of the deprotonated substrate complex, and alkane is concomitantly and irreversibly released (**scheme 3.12**).

It should be emphasised that this is not a direct comparison with the pyridine substrate investigations because the theoretical approach considered only anisole,[9] benzene,[64] benzonitrile,[65] methyl benzoate,[65] and *N,N*-diisopropylbenzamide [66] substrates. It appears that the potassium-zincate reactions reported here stop at step 1, and there could be several different contributing factors behind this such as the higher carbophilicity and softer character of potassium versus lithium or sodium [67] combined with the high covalent character of zinc, which could stabilise the KZnR$_2$(pyr) intermediates and preclude any subsequent reaction with TMP(H). However, the dominant factor is probably largely structural, because in contrast with the lithium- and sodium-zincate systems, which are dinuclear and monomeric, the potassium zincates **3j-3o** and **3q** are tetranuclear and dimeric. Assuming that aggregation occurs faster than TMP(H) "re-coordination", a PMDETA-wrapped, coordinatively saturated K$^+$ centre does not have a coordination site available for TMP(H) to rejoin the bimetallic complex, and consequently, no mutual alkyl-alkane/TMP(H)-TMP reaction can take place. Moreover, in contrast with lithium- and sodium-zincate systems in which zinc occupies a relatively exposed trigonal planar, 3-coordinate environment, in compounds **3j-3o** and **3q** the zinc exhibits a

99
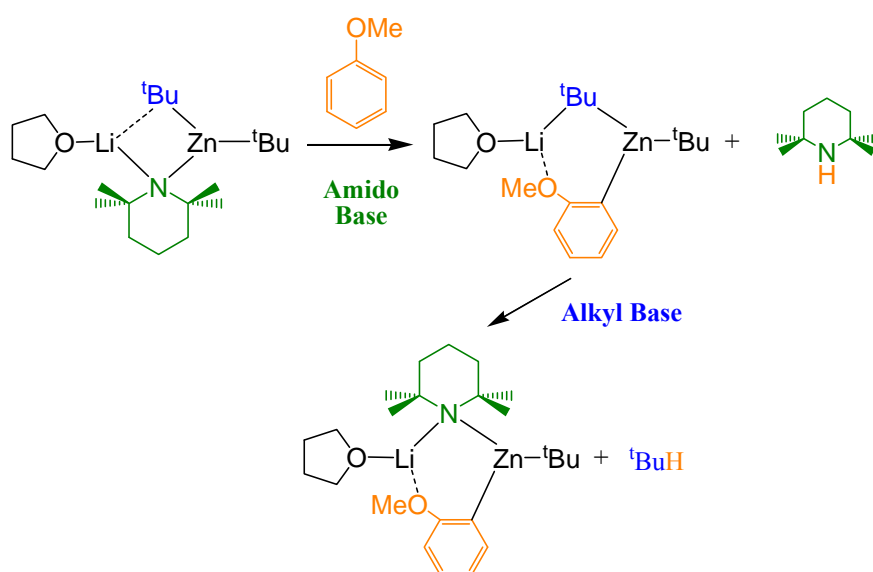
Scheme 3.12: Proposed two-step process for AMMZn of anisole.

tetrahedral, 4-coordinate environment comprising three Zn–C bonds and one Zn–N bond. Therefore, the zinc centre in **3j-3o** and **3q** is coordinately saturated, and as a result, is of diminished Lewis acidity compared with the coordinatively unsaturated zinc centres in the lithium- and sodium-zincates (**scheme 3.13**). This distinction may not necessarily be an alkali metal (K versus Li or Na) effect because it depends on the structures of the deprotonated
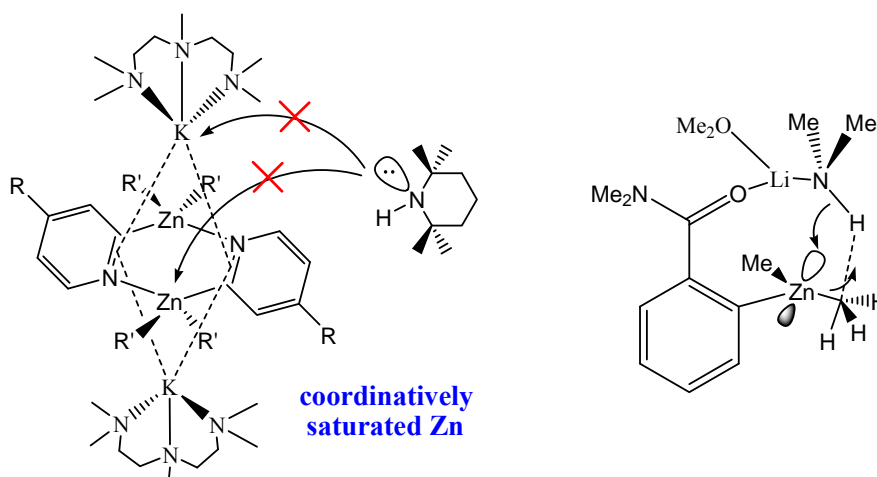
Scheme 3.13: Contrasting coordination-number dependent reactivity of zincates with amines.

substrate complexes formed, which are determined by several factors among them the nature of the alkyl ligand, the nature of the amide ligand, the nature of the Lewis-base supporting ligand, as well as the identity of the substrate undergoing deprotonation. Hence, it is essential to determine the structure of the metal-containing deprotonated substrate complex to gain a full explanation for the ligand transfer chemistry taking place. Uchiyama recently reported that the TMP-aluminate ^{i}Bu$_3$Al(TMP)Li behaves fundamentally differently from TMP-zincates with respect to the *ortho* metallation of aromatic substrates, in which ^{i}Bu$_3$Al(TMP)Li acts as a TMP base in a single step compared with the two-step ultimate alkyl basicity of the TMP-zincates.[68] Similarly, the idea of diminished Lewis acidity at coordinately saturated four-coordinate Al centres, which was supported by DFT calculations, was invoked to explain the distinction mentioned above. Hence, by analogy, the Zn centres in **3j-3o** and **3q** can be viewed as pseudo Al centres, and it can be stated that the mechanism followed by TMP-metallates (1 or 2 step) is not due to any inherent difference between Al and Zn, but is dictated by the molecular arrangement of the metal-containing deprotonated substrate complex formed in step 1.

The fact that the participation of TMP (and by implication of Zn–N bonds) is essential for the effective formation of AMM*Zn* was confirmed by qualitative experiments employing 4-*tert*-pyridine as a reference substrate. Thus bases **3b** and **3d** were found to 2-zincate the pyridine standard (1:1 molar equivalents in hexane solution) almost quantitatively in approximately one hour and a few minutes, respectively, as determined by NMR spectroscopic analysis of reaction aliquots at various time intervals (see **figures 3.14** and **3.15**). Upon substituting TMP by the alkyl ligand Me$_3$SiCH$_2$ to generate *in situ* [(PMDETA)·K(μ-Et)(μ-CH$_2$SiMe$_3$)Zn(Et)] and [(PMDETA)·K(μ-^{n}Bu)(μ-CH$_2$SiMe$_3$)Zn(^{n}Bu)] formulations devoid of any Zn–N bonding, the degree of metallation was low, even after a week,[69] amounting to only about 4 and 16% for the former and latter, respectively. Upon addition of 10 mol % of TMP(H) to these trialkyl-zincate formulations, the metallation levels significantly increased to about 49 and 79% respectively, although the reactions were still extremely slow with these conversions obtained after approximately eight and four days, respectively. These results suggest that TMP(H) reacts very slowly with trialkyl-zincates in a rate-determining step, because the products **3b** and **3d** react comparatively quickly with the pyridine substrate. It should be noted that because these
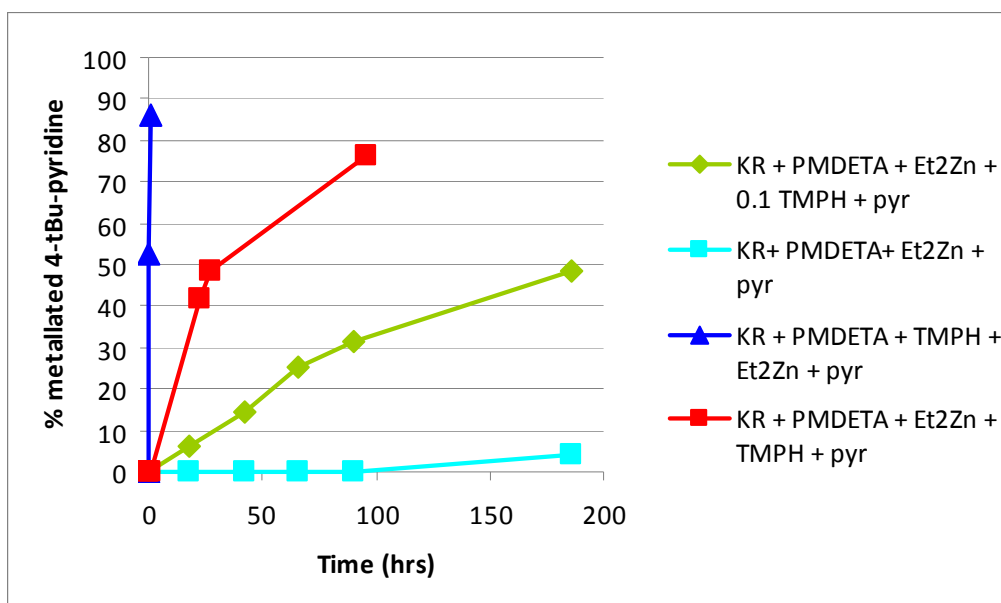
Figure 3.14: Equimolar and catalytic TMP(H) reactions of the diethyl K/Zn base with 4-*tert*-butylpyridine.
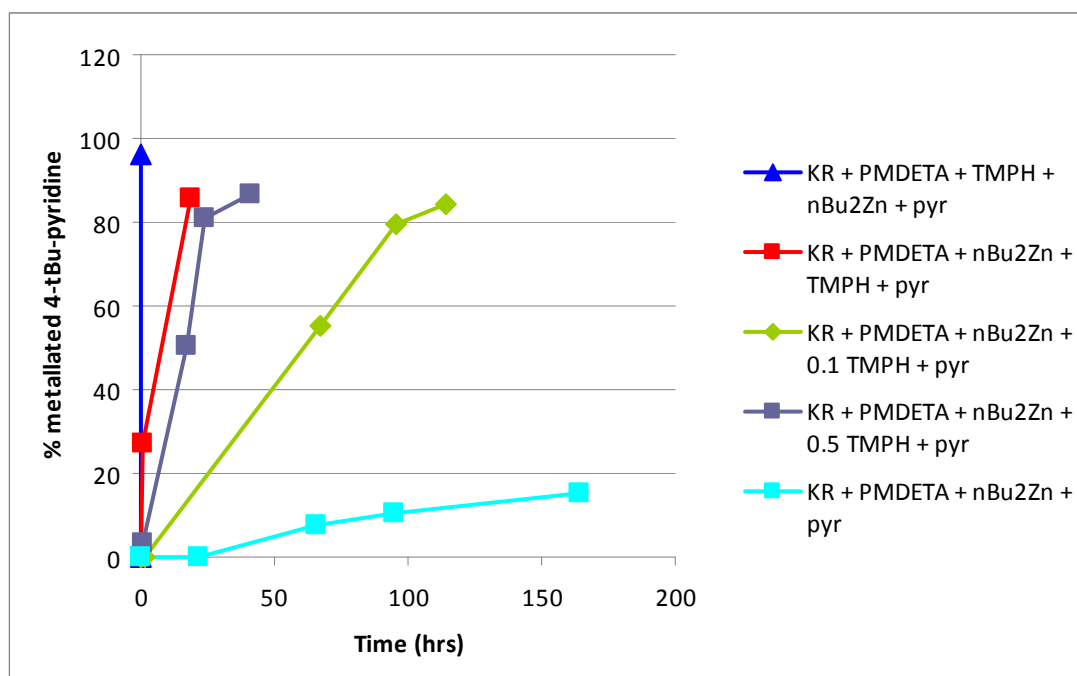
Figure 3.15: Equimolar and catalytic TMP(H) reactions of the di-*n*-butyl K/Zn base with 4-*tert*-butylpyridine.

metallation levels greatly exceed 10%, TMP(H) must be acting catalytically (**scheme 3.14**). Labile Zn–N bonds clearly hold the key to these enhanced metallating rates. The superior
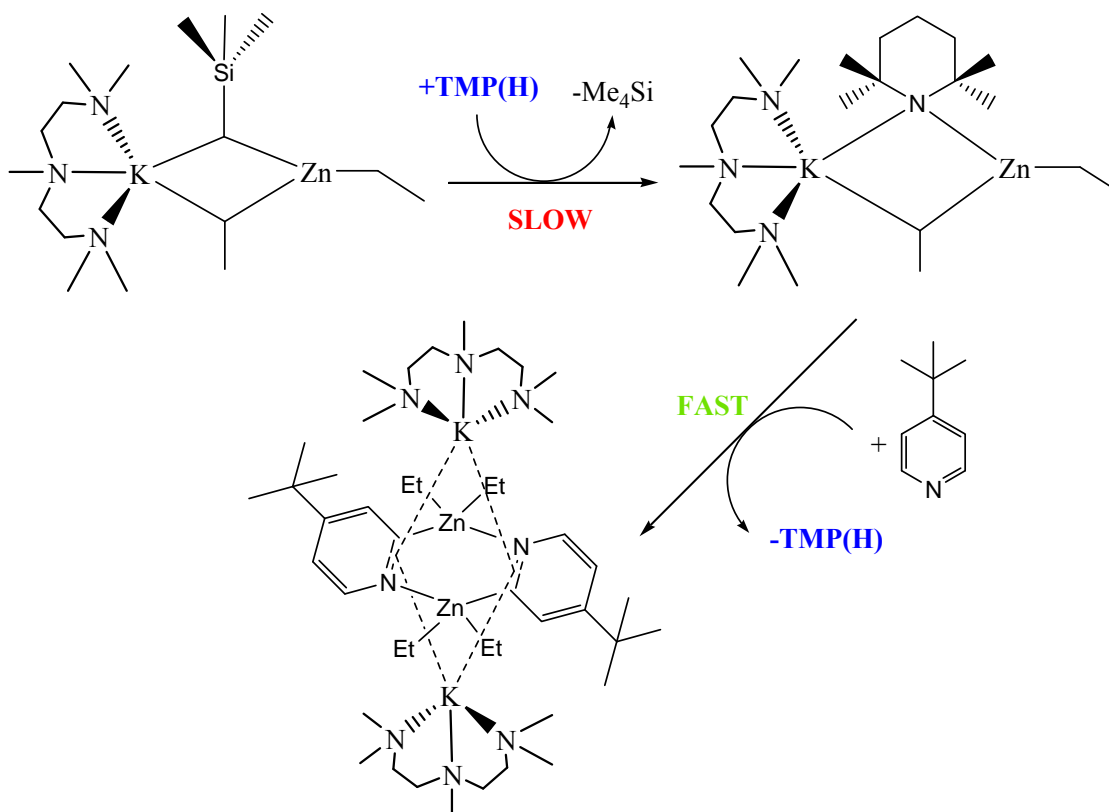
Scheme 3.14: Catalytic cycle with respect to the amine TMP(H).

reactivity of Zn–N bonds versus Zn–C bonds has also been recently documented by Hagadorn, who revealed that simple secondary amines (for example, morpholine, pyrrolidine) in stoichiometric or catalytic quantities greatly increased the rate of Zn–H exchange between Ph_2Zn and a range of relatively non-acidic carbon substrates (for example, *N,N*-diethylacetamide and trimethylphosphane oxide).[70] The proposed reactive intermediates are neutral aryl-amido zinc $PhZn(NR_2)$ formulations, although none were structurally defined in the study. Hagadorn notes that sterically demanding amines, such as $^iPr_2N(H)$ and $(Me_3Si)_2NH$, are ineffective promoters of Zn–H exchange because they do not form zinc amides with Ph_2Zn at a reasonable rate; a limitation comparable with the slow TMP(H)-trialkyl-zincate reactions observed here. When the trialkyl-zincates were treated with one molar equivalent of TMP(H), similar metallation levels were achieved (49 and 86%, respectively) and, although still slow, the reaction rates to obtain

these conversions (about 27 and 19 hours, respectively) were much improved in comparison to those obtained by using substoichiometric amounts of TMP(H). A final point to note is that co-complexation of Me_3SiCH_2K with Et_2Zn actually leads to a diminishment of the metallating power of the potassium alkyl, because on its own it reacts with TMP(H) almost instantaneously to form KTMP.[71]

3.4) Potassium-mediated Zincation of Metallocenes

3.4.1) *Ferrocene*

Published in 1951, Pauson and Kealy reported a ground-breaking paper on the synthesis of "a new type of organo-iron compound" which they named dicyclopentadienyliron, $Fe(C_5H_5)_2$.[72] The isolation of this new type of compound was, however, not the product they were initially intending to synthesise. Attempting the synthesis of fulvalene (a highly unsaturated hydrocarbon that was suggested to be aromatic) *via* the coupling of two molecules of the Grignard reagent cyclopentadienylmagnesium bromide, in the presence of ferric chloride ($FeCl_3$), to form dihydrofulvalene, an orange crystalline compound of element composition $C_{10}H_{10}Fe$ with a "remarkable stability" was instead isolated (**scheme 3.15**). This high stability is evident from its resistance to attributed to high temperatures and its ability to withstand decomposition in the presence of air, water, strong acids or strong bases. This epochal result was subsequently documented in the prestigious science journal *Nature*.[72]
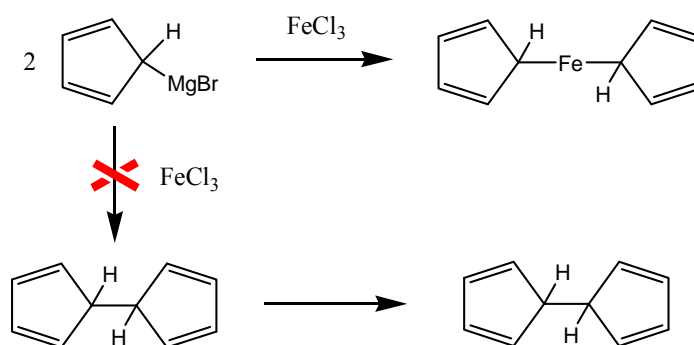
Scheme 3.15: Pauson's attempted synthesis of fulvalene and his initial depiction of ferrocene.

Although this was the first report of the isolation of this unprecedented organoiron compound, Miller, Tebboth and Tremaine of the British Oxygen Company (BOC) also published the preparation of dicyclopentadienyliron in the February 1952 issue of the *Journal of the Chemical Society*.[73] This paper, was in fact, submitted prior to that of Pauson and Kealy's isolation of the organometallic compound, as the members of the BOC group had prepared this compound three years earlier, albeit by a radically different route. Their alternative method to generate dicyclopentadienyliron involved passing cyclopentadiene over a heated iron-containing ammonia catalyst. Although these two reports were published with very little time between them, they were probably not the first to prepare this compound. Pauson [74] noted, after a personal communication with E. O. Brimm (Linde Air Products), that some years earlier, Union Carbide workers noticed that "a yellow sludge" formed in the iron pipes during the cracking of dicyclopentadiene to monocyclopentadiene. A sample of this sludge was later found to be dicyclopentadienyliron. Nevertheless, Pauson and Kealy were strictly the first to report the isolation of this complex, which subsequently stimulated major interest and activity in research laboratories all across the world.

Many chemists believed that Pauson's representation of dicyclopentadienyliron was incorrect. Two different research groups, namely that of Woodward, Whiting, Rosemblum and Wilkinson [75] and that of Fischer and Pfab [76] repeated the measurements carried out by Pauson and Kealy, and also performed physical measurements that seemed to support a 'sandwich' structure. These measurements included preliminary X-ray data, which suggested that the molecules were centrosymmetric. Also, only a single frequency was noted in the infra-red spectrum and the complex was deduced to be diamagnetic. The confirmation of the sandwich structure of dicyclopentadienyliron arrived *via* two separate publications containing X-ray structural determinations: one by Eiland and Pepinsky [77] and the second by Dunitz and Orgel [78] (**figure 3.16**). After these unequivocal structural studies on this compound were reported, the chemistry of this new organometallic compound was explored. Initial

Figure 3.16: Molecular structure of dicyclopentadienyliron.

investigative work by Woodward, Whiting and Rosenblum revealed that dicyclopentadienyliron was in fact aromatic in nature, and that it could undergo aromatic reactions such as Friedel-Crafts acylation.[79,80] This prompted Whiting to suggest the name 'ferrocene' for dicyclopentadienyliron – with the 'ene' ending denoting its aromaticity.[81] Since the first report of ferrocene (the first metallocene), the synthesis of many others quickly followed.[82-84] Such is the importance of metallocene chemistry, Wilkinson and Fischer jointly won the Nobel Prize of Chemistry in 1973 for "their pioneering work performed independently, on the chemistry of the organometallic, so called sandwich compounds". Woodward had earlier won the prize in 1965 "for his outstanding achievements in the art of organic synthesis".

The modern synthesis of ferrocene involves the metathetical reaction of $FeCl_2$ with two molar equivalents of sodium cyclopentadienide (NaCp) in a THF or DME (DME = dimethylether) solution, eliminating the salt NaCl in the process (**scheme 3.16**).

Scheme 3.16: Modern synthetic route to ferrocene.

Ferrocene can be bought commerically from chemical companies such as Aldrich for example, and is relatively inexpensive thus to save time most research laboratories would buy in ferrocene instead of preparing it *in situ*.

3.4.2) Ruthenocene

The 4d homologue of ferrocene, ruthenocene (Cp_2Ru), was first prepared by Wilkinson (1952) soon after the discovery of ferrocene.[84] Although ruthenocene has been known for over half a century, where ferrocene chemistry has flourished, much less attention has been paid to this substantially more expensive group 8 analogue (at the time of writing this thesis: 1 g of Cp_2Ru = £103.10; 1 g of Cp_2Fe = £0.32).[85] The X-ray crystal structure of ruthenocene was elucidated in

1959 by Hardgrove and Templeton.[86] It shows an eclipsed conformation of the Cp rings (**figure 3.17**), as opposed to the staggered conformation present within ferrocene (**figure 3.16**). This difference is due to the larger ionic radius of ruthenium, which increases the separation distance between the cyclopentadienyl rings, decreasing steric repulsions and allowing an eclipsed conformation to exist.

Ruthenocene can be prepared in a number of ways. For example, the following reactions form Cp_2Ru in high yields: i) ruthenium(III) acetylacetonate with excess cyclopentadienyl magnesium bromide; ii) ruthenium(III) chloride with cyclopentadienyl sodium; iii) ruthenium(III) chloride and Cp(H) in ethanol in the presence of zinc as a mild reducing agent; and iv) $[\{\eta^4\text{-}C_8H_{12}\}(RuCl_2)]$, where C_8H_{12} is cycloocta-1,5-diene, and tributyl(cyclopentadienyl)tin in ethanol at $80^{\circ}C$.
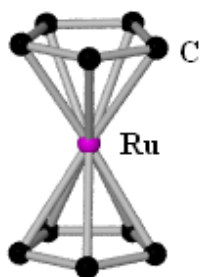
Figure 3.17: Molecular structure of ruthenocene, showing eclipsed arrangement of rings.

Ruthenocene is a crystalline solid with a pale yellow appearance, and like ferrocene, is insoluble in water but dissolves in most organic solvents. It is the most thermally stable of all metal dicyclopentadienyls. Ruthenocene is also not affected by bases or acids. However, oxidation can occur by several methods, for example, by bromine, iodine, aqueous Ag^+ or electrochemically. Since ruthenocene has larger, more diffuse orbitals than ferrocene, the metal's valence electrons can interact better with ring orbitals, resulting in stronger metal-ring bonds.

3.4.3) Metallation of Ferrocene and Ruthenocene

Deprotonation reactions involving ferrocene were studied soon after its discovery.[87] An important synthetic method which is still widely used today involves the deprotonation of

ferrocene with an alkali-metal alkyl compound RM (where R = ^{n}Bu, ^{t}Bu or ^{n}Pe and M = Li, Na or K), with the alkyl component forming the alkane by-product in the process.

Lithiation of ferrocene is a very common synthetic step. Reacting superfluous ferrocene (at 0°C in THF solution) with one molar equivalent of *tert*-butyllithium generates monolithioferrocene, $Fe(C_5H_4Li)(C_5H_5)$, in a direct lithiation synthetic step in high yields (70%).[88] Note that the same procedure using *n*-butyllithium produces monolithiated ferrocene in yields no greater than 25%.[89] Another method to produce monolithiated ferrocene involves the indirect metal-halogen exchange reaction of 1-bromoferrocene and *n*-butyllithium in diethylether solution.[90] In addition, the transmetallation reaction involving chloromercuriferrocene and *n*-butyllithium, again in diethylether solution, yields the desired product, $Fe(C_5H_4Li)(C_5H_5)$.[91,92] These two latter methods of incorporating a single lithium atom onto the ferrocene scaffold do produce high yields of the lithiated metallocene; however, the requirement of an extra synthetic step and the costs and toxicity involved with the starting materials involved hinder their application in general synthetic chemistry.

An issue when utilising direct lithiation techniques concerns the unavoidable generation of dilithioferrocene. A study by Kagan shows that this problem can be overcome by first lithiating ferrocene with *t*-butyllithium in a THF/hexane solvent system, and next adding ^{n}Bu$_3$SnCl to the reaction mixture to yield unreacted ferrocene, mono- and the distannylated product.[93] Ferrocene can be removed be sublimation (80°C at reduced pressure) and the mono-substituted ferrocene product can be separated from the disubstituted congener *via* vacuum distillation (temperature, 140°C; pressure, 0.1 mmHg). To make the monolithiated compound once more, the monostannylated ferrocene can be reacted with *n*-butyllithium (THF, -78°C) to yield the desired product, $Fe(C_5H_4Li)(C_5H_5)$.

Monolithiated ferrocene can also be obtained in high yields after metallation with the superbasic mixture of ^{t}BuLi and ^{t}BuOK at -78°C (90.7% yield, based on ferrocene and electrophilic quenching with DMF producing the carboxaldehyde ferrocene complex).[94]

It has long been known that ruthenocene is much more reactive towards lithiation than ferrocene. This has been theoretically calculated,[95] and relatively recently this notion has been proved experimentally.[94] To elaborate, ruthenocene and ferrocene were added in equimolar quantities and after lithiation and subsequent quenching with DMF, more of the free ferrocene was present compared to that of unreacted ruthenocene. This evidence suggests that ruthocenyl protons are comparatively more acidic than the ferrocenyl protons.

Ferrocene, and to a much lesser extent, its group 8 homologue, ruthenocene, have a very rich metallation chemistry, which includes a large variety of structural types.[96,97] Poorly represented in this category are the synthetically useful polar monometallated derivatives, which can be subsequently utilised for framework functionalisation. Many monometallated ferrocenes and ruthenocenes in the Cambridge Structural Database (CSD) [17] involve metals (for example, Al,[98] Ge,[99] Sn,[100] W,[101] and Zr [102]) that have been synthesised *via* reaction of a preformed polar intermediate and a metal salt *via* an indirect metathetical approach. Such is the sparse volume of definitive structural data available on these types of monometallated metallocenes, there are no examples at all of structurally defined molecules where an alkali metal or alkaline-earth metal is directly attached to the Cp ring. Earlier our group reported the lithium triferrocenylzincate $[Li(THF)_4]^+\{Zn(Fc)_3\}]^-$ (where Fc is $C_5H_5FeC_5H_4$) (see **scheme 3.17**), but this has a solvent(THF)-separated structure in which there are no Li⋯C(Fc) contacts.[4] Though bimetallic formulations of organometallic chemistry were laid over 150 years ago,[103] their status as versatile chemical reagents has risen remarkably over the past few years with many notable innovations made in organic synthesis,[104,105] host-guest macrocyclic chemistry,[106,107] structural science,[3,108] and polymerisation chemistry.[109] Applying bimetallic formulations to metallocene chemistry, our group previously reported the application of lithium-mediated zincation to ferrocene metallation, and although, as mentioned above, lithium ferrocenylzincate compounds were produced, no examples were obtained in which both metals (lithium and zinc) are involved in the coordination of the ferrocenyl anion. In his book "Organometallics in Synthesis" Schlosser reminds us that "the individuality of the metal is the most critical parameter for designing tailor-made organometallic reactions", so by extrapolation this must be even more significant in the context of bimetallic formulations.[110]
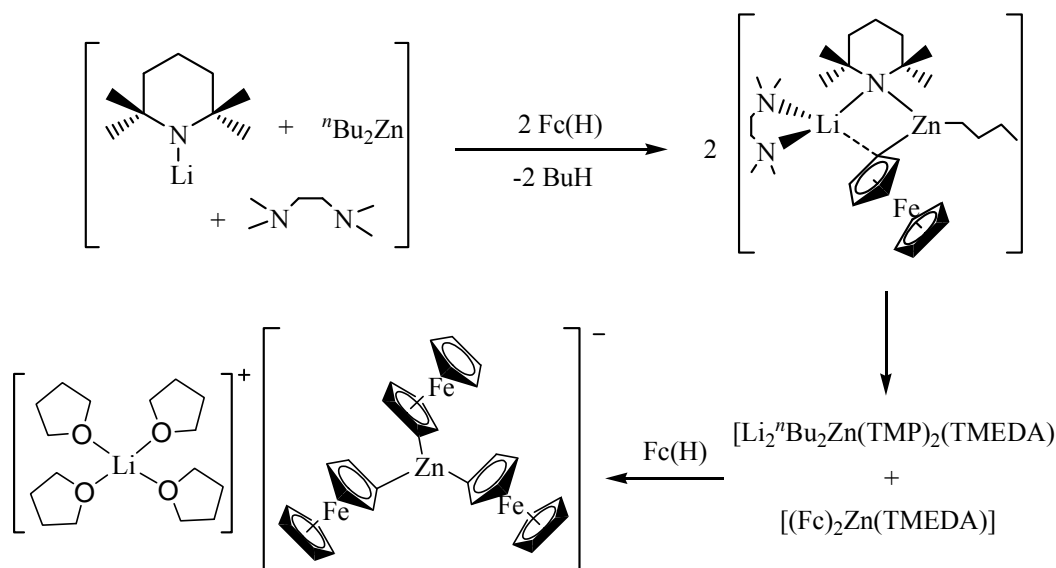
Scheme 3.17: Proposed pathway to generate the lithium zincate [Li(THF)$_4$]$^+${Zn(Fc)$_3$}]$^-$.

Therefore, in this section, potassium-mediated zincation (KMZn) is introduced to metallocene chemistry and, echoing Schlosser's comments, find that the reactions yield potassium ferrocenylzincate and potassium ruthenocenylzincate products with unique structures compared to the aformentioned lithium ferrocenylzincate, and in some cases, to each other.

Turning to the experimental work, the potassium zincate base [PMDETA·K(μ-TMP)(μ-Me)Zn(Me)] **3a**, prepared *in situ* in hexane solution was treated with one molar of ferrocene or ruthenocene. These reactions yielded [{PMDETA·K(μ-Me)$_2$Zn(Fc)}$_\infty$] (**3u**) and [{PMDETA·K(μ-Me)$_2$Zn(Rc)}$_2$] (**3v**) in isolated yields of 46 and 39% respectively (**scheme 3.18**). The ethyl congener of base **3a**, [PMDETA·K(μ-TMP)(μ-Et)Zn(Et)] (**3b**) reacts with ferrocene to generate the monozincated complex [{PMDETA·K(μ-Et)$_2$Zn(Fc)}$_\infty$] (**3w**) in an isolated yield of 40%. Dizincation of ferrocene was achieved by the base [PMDETA·K(μ-TMP)(μ-^{t}Bu)Zn(^{t}Bu] (**3e**) with half a molar equivalent of the metallocene to generate the product [THF·{(PMDETA)K}$_2$·(C$_5${1-Zn(^{t}Bu)$_2$}H$_4$)Fe(C$_5${1'-Zn(^{t}Bu)$_2$}H$_4$)] (**3x**) in a yield of 31%.

When a 1:1 mixture of ferrocene and the bimetallic base [when base = **3b** (Et), **3d** (^{n}Bu) and **3e** (^{t}Bu)] is prepared in bulk hexane solution in the presence of THF, compounds of formula

[(PMDETA)(THF)·K(Fc)$_2$Zn(R)] {where R = Et (**3y**), ^{n}Bu (**3z**) or ^{t}Bu (**3aa**)} are produced. The ruthenocene analogue [(PMDETA)(THF)·K(Rc)$_2$Zn(Et)] (**3ab**) [Rc = (C$_5$H$_5$)Ru(C$_5$H$_4$)] can be isolated under the same hexane/THF conditions with base **3b**. A major problem when adding THF to the reaction mixtures is that a mixture of products is obtained and reproducibility of compounds **3y-3ab** is very difficult, thus in this PhD thesis, with respect to complexes **3y-3ab**, only the X-ray structural data will be discussed and compared.
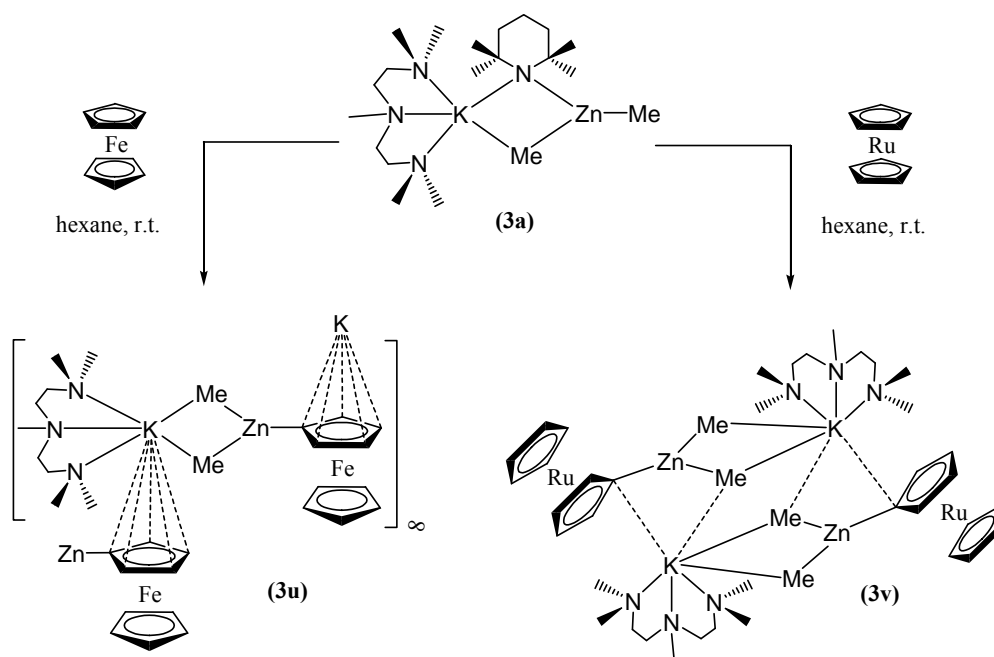
Scheme 3.18: Potassium-mediated zincations of ferrocene and ruthenocene.

3.4.4) Solid-state Analysis

Base **3a** was first tested on ferrocene to quantify its ability as a zincating reagent, producing a set of orange crystals of **3u** in an isolated yield of 46%. In the monomer unit, unlike **3a**, where the TMP is bridging the potassium and zinc metal centres, the monozincated ferrocene in **3u** is now at the terminal position with two smaller methyl groups bridging the distinct metals, generating a new planar KCZnC metallocycle. Trigonal Zn makes three Zn–C bonds, to bridging methyl ligands [bond lengths: Zn(1)–C(11) {2.037(3) Å} and Zn(1)–C(12) {2.027(3) Å}] and a slightly shorter bond to the deprotonated carbon atom of ferrocene [Zn(1)–C(1), 2.002(3) Å] (**figure 3.18**). The potassium cation has a coordination sphere consisting of two K–C(Me) bonds

[lengths, 3.091(3) Å {K(1)–C(11)} and 3.141(3) Å {K(1)–C(12)}] and three shorter K–N donor interactions with the tridentate PMDETA ligand [average K–N bond length, 2.872 Å]. The remainder of the coordination sphere of potassium is made up of intermolecular η^5-interactions

with the π-surface of a zincated ferrocene ring from a neighbouring monomer unit to create an unprecedented supramolecular step-ladder [average K–C(Fc) distance, 3.198 Å; K–C(Fc) range, 3.031(3)–3.371(3) Å] (**figure 3.19**). For K to achieve this η^5-π interaction with the metallocenyl ring, the zincated ferrocene carbon atom has a modestly distorted trigonal environment (mean bond angle around C1, 118.5°) The ligation of ferrocene onto

Figure 3.18: Asymmetric unit of 3u with hydrogen atoms omitted for clarity.

potassium has been documented before in potassium magnesiate chemistry in [{K(ferrocene)$_2$(toluene)$_2$}$^+${Mg(HMDS)$_3$}$^-$] [HMDS = 1,1,1,3,3,3-hexamethyldisilazide].[111] However, in this example ferrocene has not been metallated but instead acts as a neutral π-donating ligand to the potassium cation to form the discrete ion-pair compound [mean K–C(Fc) distance, 3.195 Å]. The average K–C(Fc) bond distances compare favourably with those of the monozincated ferrocene compound **3u**. Thus, the Fe···Cp(centroid) distances are found to be 1.635 Å (metallated Cp ring) and 1.634 Å (unsubstituted Cp ring).
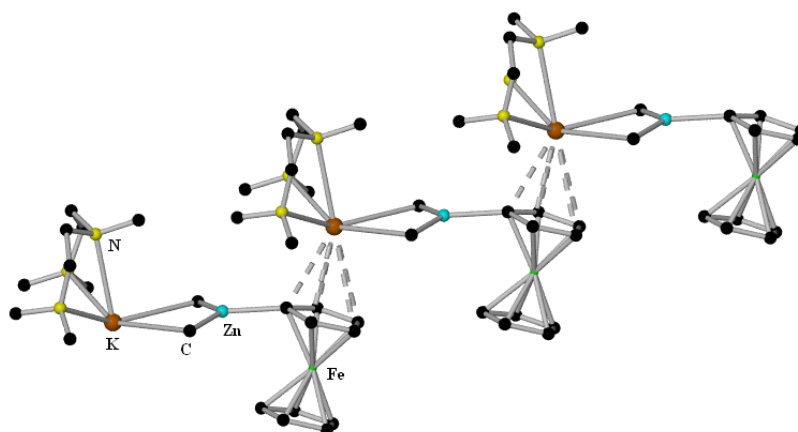
Figure 3.19: Section of the infinite step ladder of 3u. The intermolecular π-interactions are displayed as dashed lines.

Currently there is a dearth of solid-state structures of metallated ruthenocenes within the CSD. There are only four examples of monometallated ruthenocene structures,[112,113] two of which were pre-lithiated with excess *n*-butyllithium (2.4 molar equivalents in THF at -50°C) and reacted onwards with metal salts to make platinum derivatives.[112] Therefore KMZ*n* seemed an ideal vehicle from which to increase the number of informative crystal structures of this type. Carried out with the purpose of obtaining crystalline material as opposed to reaction optimisation, base **3a** was reacted with one molar equivalent of ruthenocene in hexane solution. Crystallisation was duly realised in the form of the pale yellow product **3v**, in a clean first batch yield of 39%. To the best of our knowledge, the molecular structure of **3v** represents the first crystallographically-characterised ruthenocene structure containing zinc made *via* any synthetic procedure (either indirect metathesis or direct zincation). It is a centrosymmetric molecular dimer (**figure 3.20**). The monomeric unit of **3v** closely matches that of **3u**, comprising a PMDETA-chelated K$^+$ cation bridged through two Me ligands to zinc [K–C(Me) bond lengths:
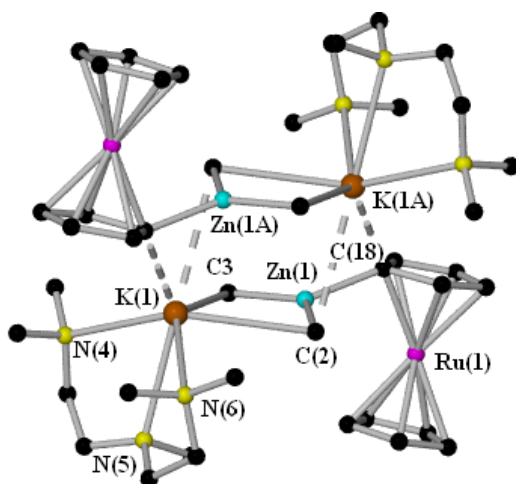
Figure 3.20: Molecular structure of dimeric 3v with hydrogen atoms omitted for clarity. Intermolecular contacts shown as dashed lines. Symmetry operation A: 2-x, 1-y, -z.

K(1)–C(2) {3.2546(18) Å} and K(1)–C(3) {3.1179(19) Å}; Zn–C(Me) bond distances, 2.0174(16) Å {Zn(1)–C(2)} and 2.0358(17) Å {Zn(1)–C(3)}], which has the largest anion, the monodeprotonated ruthenocene, in a terminal position [Zn(1)–C(18) bond length, 2.0192(15) Å]. Dimerisation is achieved *via* the K centre engaging inter-monomer with one Me C atom, C(3A) [3.3226(19) Å] and η^1 with the deprotonated C atom of the ruthenocene, C(18A) [3.2775(15) Å].

113

The average K–C bond length to the rest of the carbon atoms of the zincated Cp ring [average distance, 4.559 Å, range, 3.6162(15)– 5.2850(16) Å] highlights this η^1 interaction. For this type of interaction to occur, the zincated ruthenocene carbon deviates from planarity with an average bond angle of 116.8°, resulting in a distorted trigonal arrangement. The Ru···Cp(centroid) distances in **3v** [1.807 Å (metallated Cp ring) and 1.818 Å (unsubstituted Cp ring)] are larger than those for iron in **3u**. The Cp rings in **3v** have a near-eclipsed conformation, with an average Cp_C–$Cp_{(centroid)}$–$Cp_{(centroid)}$–Cp_C torsion angle of 9.0°.
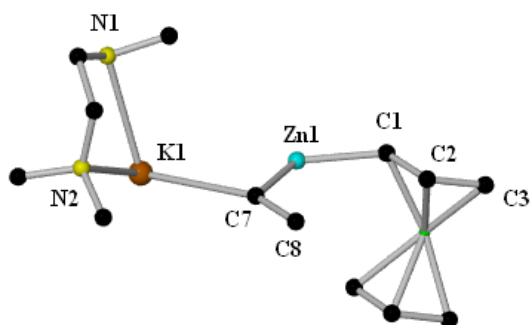
Figure 3.21: The asymmetric unit of 3w.

Applying the diethyl-TMP potassium zincate base, **3b**, to ferrocene, a batch of orange crystalline product **3w** (**figure 3.21**) (40% yield) could be isolated. Single-crystal X-ray diffraction reveals the same structural motif as step-ladder complex **3u**. However, the structure of **3w** does differ slightly in comparison due to the centre of symmetry which runs through the K Zn backbone of the complex. It could be said that the asymmetric unit is half of the complex.

The asymmetric unit of this compound grows to form the monomeric unit of the polymeric step-ladder structure (**figure 3.22**).
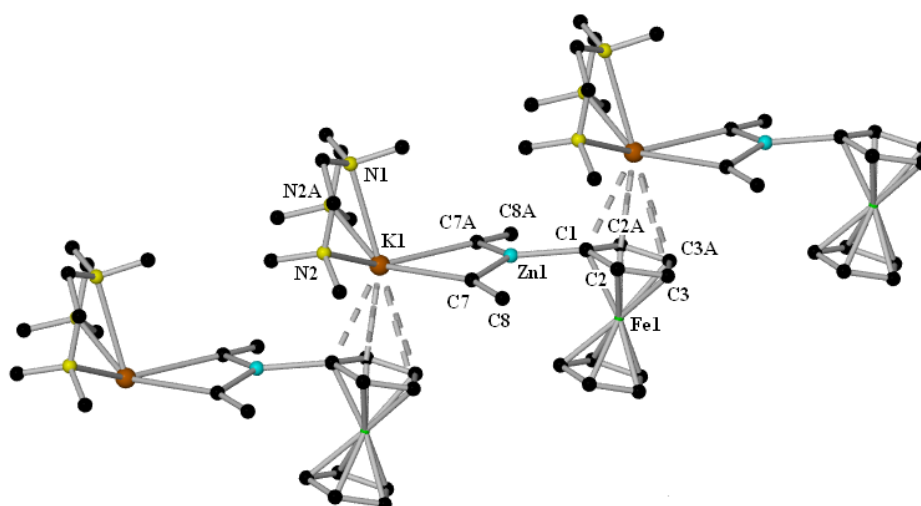
Figure 3.22: Section of the infinite step ladder architecture of 3w.

Trigonal planar, the zinc centre in **3w** forms three metal–carbon bonds, two equivalent Zn–C bonds to the ethyl groups [Zn(1)–C(7) and Zn(1)–C(7A) bond distance, 2.0583(17) Å] and one marginally shorter bond to a framework carbon atom of ferrocene [Zn(1)–C(1), 2.027(2) Å]. The potassium cation again has a coordination sphere which includes three $N_{(PMDETA)}$ [K(1)–N(1), 2.921(2) Å; K(1)–N(2) and K(1)–N(2A), 2.8535(17) Å] and two $C_{(ethyl)}$ contacts [K(1)–C(7) and K(1)–C(7A), 3.1157(18) Å]. To satisfy the potassium coordination environment, η^5-π-interactions are formed between it and the zincated ferrocene ring of a nearby monomeric unit [mean K–C(Fc) distance, 3.245 Å; range = 3.018(2)–3.4351(19) Å]. A comparison of the bond lengths in the dimethyl step-ladder complex **3u** to those in the polymer **3w** shows very little discrimination with respect to the mean K–C(alkyl) and K–N bond distances (**table 3.8**). However, the average Zn–C bond length in the dimethyl-based complex is slightly shorter than

Table 3.8: Comparison of selected bond lengths in complexes 3u and 3w.
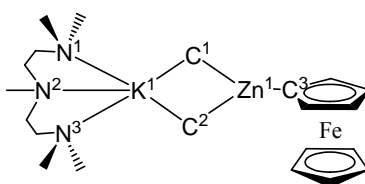
Complex	K1–C1	K1–C2	K1–N1	K1–N2
3u	3.141(3) Å	3.091(3) Å	2.860(3) Å	2.885(3) Å
3w	3.1157(18) Å	3.1157(18) Å	2.8535(17) Å	2.921(2) Å
Complex	**K1–N3**	**Zn1–C1**	**Zn1–C2**	**Zn1–C3**
3u	2.872(3) Å	2.027(3) Å	2.037(3) Å	2.002(3) Å
3w	2.8535(17) Å	2.0583(17) Å	2.0584(17) Å	2.027(2) Å
Complex	**Ave. Zn–C bond length**	**Ave. K–C bond length**	**Ave. K–N bond length**	**Ave. K–C(Fc) bond length**
3u	2.022 Å	3.116 Å	2.872 Å	3.198 Å
3w	2.048 Å	3.116 Å	2.876Å	3.245 Å

those in the diethyl-based congener. Also, the average K–C(Fc) bond distance is longer in **3w** compared to their associated bonds in **3u** by almost 0.05 Å. A comparison in the range in K–

C(Fc) distances in **3u** [3.031(3)–3.371(3) Å] shows that there is a smaller difference from the shortest to the longest bond length (0.34 Å) than those in **3w** (0.42 Å) [3.018(2)–3.4351(19) Å].

A problem which exists with the KMZ*n* of metallocenes using these bases arises with the choice of solvent mixture. Complexes **3u**, **3v** and **3w** were isolated from a pure hexane solvent system. Crystals of **3v**, obtained from the reaction of the potassium zincate base **3b** with one molar equivalent of ferrocene, were achieved by placing the Schlenk tube in the freezer at -28°C almost immediately after the addition of ferrocene [at the time a transparent solution was produced]. However, if the reaction mixture within the Schlenk tube is left for several minutes then an insoluble mixture arises. Addition of a small volume of THF solvent to the reaction components resulted in a transparent solution. A set of crystals were afforded from this solvent choice after a period of time in the freezer; however, the crystal analysed by X-ray diffraction produced the surprising result [(PMDETA)(THF)·K(Fc)$_2$Zn(Et)] **3y**, as only complex **3w** was expected to be present in the reaction mixture. Subsequent reactions with the ^{n}Bu$_2$Zn and ^{t}Bu$_2$Zn bases (**3d** and **3e** respectively), utilising hexane and THF solvents, yielded the *n*-butyl and *t*-butyl congeners, [(PMDETA)(THF)·K(Fc)$_2$Zn(^{n}Bu)] **3z** and [(PMDETA)(THF)·K(Fc)$_2$Zn(^{t}Bu)] **3aa** respectively. The ruthenocene analogue of **3y**, [(PMDETA)(THF)·K(Rc)$_2$Zn(Et)] **3ab**, can also be generated using the hexane/THF solvent mix, however like **3y**, these were single crystals picked out at random from the reaction mixture. ^{1}H NMR spectroscopic analysis gave a more complete picture revealing that a mixture of products were formed in the reactions where **3y**, **3z**, **3aa** and **3ab** were crystallographically characterised. It should be noted that these crystallographically characterised compounds were very difficult to reproduce, for example, crystals of **3aa** could only be grown once after many attempts (the actual goal was to isolate the *t*-butyl analogue of **3u**, containing two ^{t}Bu groups and one monozincated ferrocene unit) and they took several weeks (in one case months) to form in a freezer (-28°C). The crystal data collected of compounds **3y**, **3z**, **3aa** and **3ab** are of reasonable quality (**figure 3.23**), allowing their bond lengths and angles to be compared (**table 3.9**).

Dimetallocenylzincates **3y**, **3z**, **3aa** and **3ab** share a common structural motif. Each of the complexes structural make-up consists of two molecules of mono-deprotonated metallocene and

(3y)   **(3z)**

(3aa)   **(3ab)**
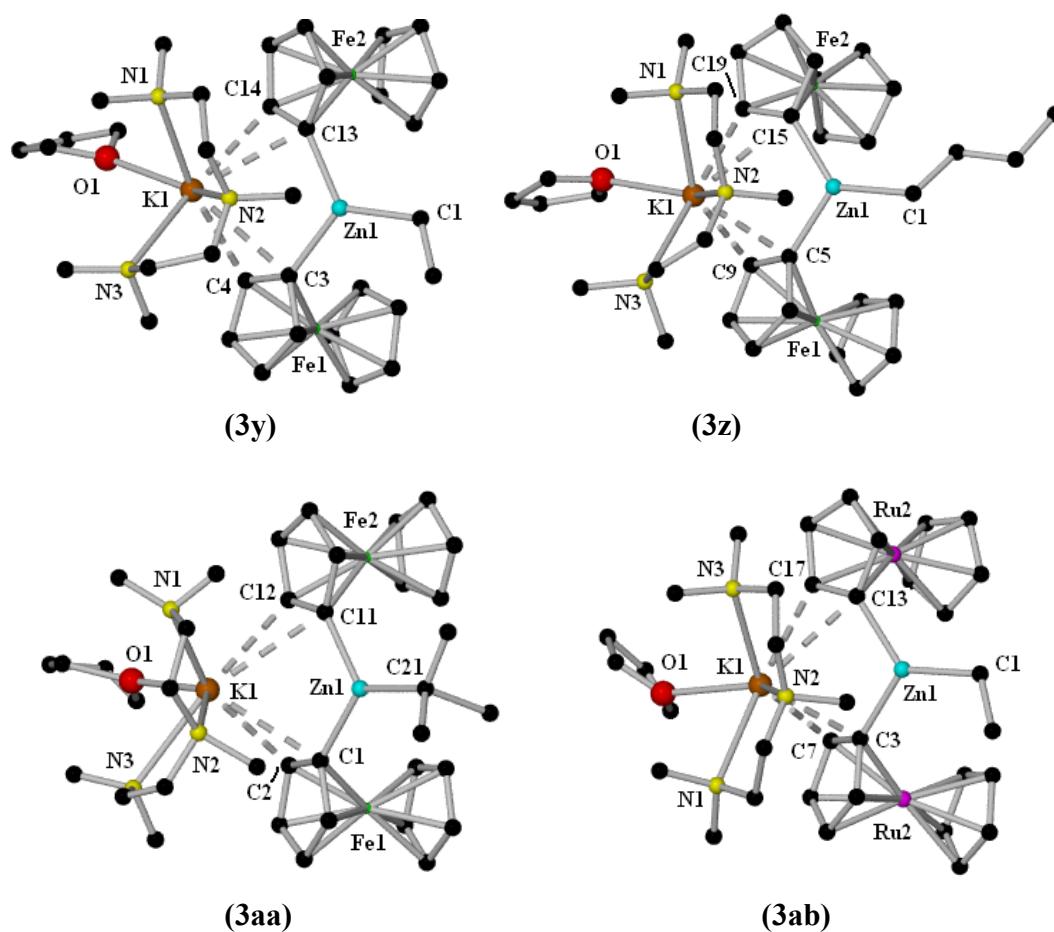
Figure 3.23: Molecular structures of dimetallocenylzincates 3y, 3z, 3aa and 3ab. Hydrogen atoms and minor disorder components are omitted for clarity.

an alkyl component on zinc, with a PMDETA- and THF-ligated potassium cation completing their structural design. It could be said that their respective potassium zincate metallating reagents have all reacted with dual basicity losing one amido group (TMP) as the free amine TMP(H) and one alkyl arm as alkane (ethane, butane or isobutane), although it cannot be ruled out that a dismutation reaction has occurred after the loss of the TMP anion, possibly forming a potassium-zinc trialkyl species as the co-product. Nevertheless the zinc centre, in all four compounds lies in a modestly distorted trigonal geometry and forms a Zn–C σ-bond to both molecules of ferrocene or ruthenocene and one Zn–C bond to the alkyl group. The potassium cation has a coordination sphere remarkably different to those in monozincated ferrocene complexes **3u** and **3v**. Instead of having 3 × N dative bonds and 2 × C(alkyl) anionic contacts, as

Table 3.9: Comparison of selected bond lengths (Å) and bond angles (°) in zincates 3y, 3z, 3aa and 3ab.
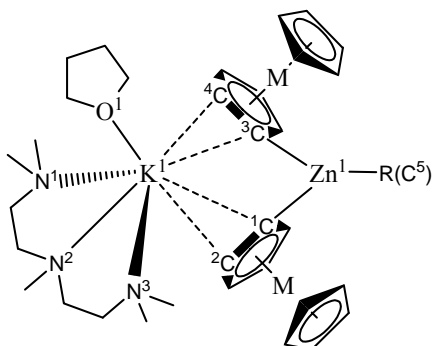
when M = Fe and R = Et (**3y**), ^{n}Bu (**3z**) or ^{t}Bu (**3aa**);

when M = Ru and R = Et (**3ab**)

Bond length (Å) or angle (°)	3y (Et, Fc)	3z (^{n}Bu, Fc)	3aa (^{t}Bu, Fc)	3ab (Et, Rc)
K1–O1	2.7457(14)	2.718(5)	2.7938(18)	(disorder)
K1–N1	2.9141(16)	2.997(3)	2.8491(16)	2.894(3)
K1–N2	2.8486(15)	2.854(3)	2.8820(17)	2.852(3)
K1–N3	2.8223(16)	2.875(3)	2.8656(17)	2.905(3)
Average K–N	2.8620	2.909	2.866	2.884
K1–C1	3.1074(18)	3.358(3)	3.124(3)	3.067(3)
K1–C2	3.2175(17)	3.345(4)	3.181(3)	3.511(3)
K1–C3	3.1074(18)	3.013(4)	3.281(3)	3.238(3)
K1–C4	3.1589(18)	3.242(4)	3.251(3)	3.316(3)
Average K–C	3.1478	3.2395	3.2093	3.283
Zn1–C1	2.0207(18)	2.042(4)	2.031(3)	2.028(3)
Zn1–C3	2.0247(18)	2.015(4)	2.037(3)	2.027(3)
Zn1–C5	2.0183(19)	2.032(7)	2.042(4)	2.005(3)
Average Zn–C	2.021	2.030	2.037	2.020
K1–C1–Zn1	81.60(6)	85.61(11)	82.85(8)	82.46(10)
K1–C3–Zn1	82.99(6)	76.34(10)	78.74(8)	78.11(9)
C1–Zn1–C3	117.41(7)	113.36(14)	114.49(10)	112.82(12)
C1–Zn1–C5	121.79(8)	(disorder)	120.02(13)	124.33(14)
C3–Zn1–C5	120.80(8)	(disorder)	125.28(13)	122.85(14)

well as η^5-π-interactions with a neighbouring metallated ferrocene monomer, the potassium atom (in all of the four structures) adopts a coordination sphere made up of four dative bonds (3 × N and 1 × O) and two non-equivalent η^2-interactions with the π-system (of the zincated Cp ring) of two molecules of metallated metallocene (ferrocene in **3y**, **3z** and **3aa**; ruthenocene in **3ab**) to form a structural motif which contains features of both solvent-separated and contact ion-pair complexes. Comparing the bond lengths in structures **3y**, **3z**, **3aa** and **3ab**, in all cases the O from the THF molecule forms a shorter bond to K than do the N atoms of PMDETA [range: K1–O1, 2.718(5)–2.7938(18) Å; K1–N$_{(PMDETA)}$, 2.8223(16)–2.997(3) Å]. However, these K–N bonds lengths are still shorter than the K–C$_{(metallocene)}$ bond distances [range: K(1)–C$_{(metallocene)}$, 3.013(4)–3.511(3)]. It is noteworthy that the smaller the average K–C$_{(metallocene)}$ {only with carbons associated with the η^2-π-interaction} bond distance becomes [mean K–C bond (Å): 3.283, **3ab**; 3.2395, **3z**; 3.2093, **3aa**; 3.1478, **3y**], the larger the C(Fc)–Zn(1)–C(Fc) angle [C1–Zn1–C3 bond angle (°): 112.82(12), **3ab**; 113.36(14), **3z**; 114.49(10), **3aa**; 117.41(7), **3y**]. The Zn–C bonds are stronger and shorter in comparison [range: Zn–C, 2.005(3)–2.042(4) Å] to those of the alkali metal-carbon interactions. Also, as the steric bulk of the R group increases (in the sequence Et, ^{n}Bu, ^{t}Bu), the average Zn–C bond lengthens (2.021, 2.030, 2.037 Å respectively). A direct comparison between **3y** and **3ab** can be carried out as the only difference in their associated structures is the transition metal within the metallocene [Fe in (**3y**); Ru in (**3ab**)]. The most significant distinction between the two complexes is that the potassium cation forms weaker bonds to the metallated ruthenocene rings than in the iron analogue, as mentioned above, which results in a tighter C(Fc)–Zn–C(Fc) bond angle. The differences in mean K–C [average K(1)–N$_{(PMDETA)}$ bond lengths: 2.8620 Å, **3y**; 2.884 Å, **3ab**] and Zn–C bond distances [average Zn(1)–C bond lengths: 2.021 Å, **3y**; 2.020 Å, **3ab**] are negligible.

The only other example where zinc bridges between two ferrocene units was reported in the lithium-mediated zincation reaction of ferrocene mentioned earlier [products (TMEDA)ZnFc$_2$ and [Li(THF)$_4$]$^+$[Zn(Fc)$_3$]$^-$], reported by our own group.[4] There are only a small number of structures (six in total) within the CSD where any type of metal bridges between two ferrocenes (the specific metals are Al,[98] Ga,[114] Hg,[115] Sn,[116] Ti [117] and W [118]). All of these literature complexes are neutral, non-ate compounds, and all require pre-lithiation of ferrocene at some stage of their synthesis, unlike the complexes **3y**, **3z**, **3aa** and **3ab**, which are all products of

119

direct zincation. With respect to ruthenocene, there are no examples at all in the CSD of structures in which ruthenocene has been metallated similar to that in **3ab**.

With the successful monometallation of ferrocene using the bases **3a** and **3b**, in hexane solution, dizincation of the metallocene was achieved using the ^{t}Bu variant, **3e**. Reacting the base with half of a molar equivalent of ferrocene, initially in hexane solution, generates the compound [THF·{(PMDETA)K}$_2$·(C$_5$\{1-Zn(^{t}Bu)$_2$\}H$_4$)Fe(C$_5$\{1'-Zn(^{t}Bu)$_2$\}H$_4$)] (**3x**) [as can be deduced from ^{1}H NMR spectroscopic data in deuterated cyclohexane solution (see later)] in a yield of 31%. However, when the solid is redissolved in deuterated benzene solution, recrystallisation with solvent exchange takes place to form the benzene adduct [C$_6$D$_6$·{(PMDETA)K}$_2$·(C$_5$\{1-Zn(^{t}Bu)$_2$\}H$_4$)Fe(C$_5$\{1'-Zn(^{t}Bu)$_2$\}H$_4$)] (**3ac**). The X-ray structure of this dizincated product (with the benzene ring present) is shown in **figure 3.24**.

Structure **3ac** reveals a dideprotonated ferrocene molecule substituted at the 1,1′-positions by zinc atoms. Two *t*-butyl groups complete the modestly distorted trigonal geometry around the zinc centres, but do not interact with the potassium cations. Surrounded by three N atoms from
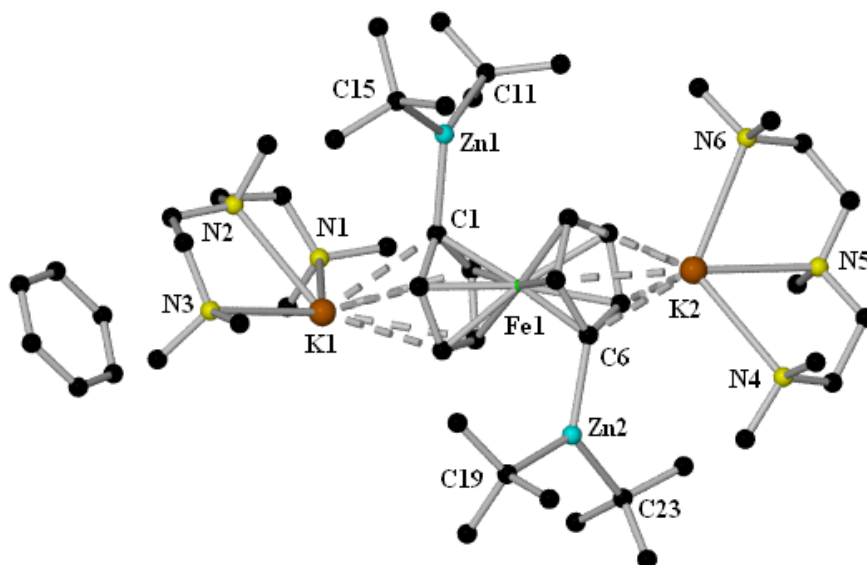
Figure 3.24: Molecular structure of 3ac. Hydrogen atoms have been removed for clarity. Interactions between potassium and the ferrocene π-surface are indicated by dashed lines.

the tridentate PMDETA ligand, the coordination sphere of each potassium is completed by forming a η^5-interaction with the π-surface of a metallated Cp ring at either end of the dizincated ferrocene molecule. The zinc-carbon bonds of Zn(1) to the two *t*-butyl groups [that is Zn(1)–C(11) and Zn(1)–C(15)] cannot be discussed due to disorder. However, the Zn(1)–C(1) bond length of the metal–ferrocene bond [2.031(2) Å] compares favourably with the Zn(2)–C(ferrocene) and the two Zn(2)–C(^{t}Bu) bond distances [Zn(2)–C(6), 2.025(2) Å; Zn(2)–C(19), 2.059(2) Å; Zn(2)–C(23), 2.079(2) Å respectively]. These bond lengths represent some of the shortest metal–carbon distances within structure **3ac**. Comparing the values and range of the K–C bond lengths [range: K(1)–C(ferrocene), 3.012(2)–3.165(2) Å; K(2)–C(ferrocene), 2.984(2)–3.371(2) Å] shows that this bonding interaction is weak, and also the difference between the longest and shortest K–C bond distances highlights that K(1) [Δ, 0.153 Å] is positioned more central over its associated Cp ring than K(2) [Δ, 0.387 Å]. Reinforcing the fact that the potassium atoms are not aligned perfectly, the K(1)···Fe(1)···K(2) bond angle (167.21°) is found to be non-linear. To achieve this π-interaction, the zincated carbon on ferrocene forms a mildly distorted trigonal planar geometry [mean angle around: C(1), 118.79°; C(6), 119.07°]. PMDETA interacts with the potassium cation in a tridentate manner. The K–N bonds [mean bond distance, 2.8648 Å; range, 2.7839(19)–2.930(2) Å] are more contracted in comparison to the K–C π-interactions [mean K–C bond length, by 3.1168 Å] by an average 0.252 Å.

A search of the literature reveals only one example of a structure containing dizincated ferrocene. Wagner reported the isolation of the complex [Fe(η^5-C$_5$H$_4$)$_2$]$_2$Zn$_2$(TMEDA)$_2$ (**3ad**) (**scheme 3.19**), which was prepared by salt metathesis from [Fe(η^5-C$_5$H$_4$)$_2$]$_3$Li$_6$(TMEDA)$_2$ and
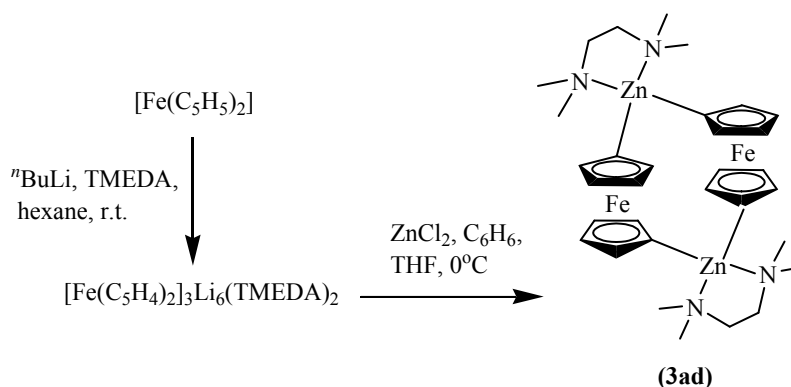
Scheme 3.19: Literature method to generate the doubly zincated ferrocene complex 3ad.

zinc chloride.[119] This reaction is an example of an indirect zincation, in contrast to the product of direct dizincation of ferrocene shown with zincator **3e** and half a molar equivalent of ferrocene. **3ad** is a neutral compound, containing homometallic zinc, whereas **3ac** is a zincate consisting of a 1:1 ratio of potassium and zinc.

3.4.5) Solution Studies

Potassium zincates **3u** and **3v** are poorly soluble in deuterated benzene solution; however, they readily solubilise on addition of a few drops of d_8-THF to the bulk arene solvent. On the other hand, **3w** dissolves in C_6D_6 solution alone, as does the dizincated ferrocene compound **3ac**, although **3ac** is not completely soluble in d_{12}-cyclohexane solution, hence it requires a few drops of d_8-THF to gain a homogeneous solution. Thus, ^{1}H and ^{13}C NMR spectroscopic characterisation was completed for these four isolated complexes.

The ^{1}H and ^{13}C NMR spectra for **3u** and **3v** are expectedly very similar. The largest difference between their ^{1}H NMR spectra (**figures 3.25 and 3.26**) is the chemical shift of the methyl groups. Where the two methyl groups come as a singlet at -0.36 ppm for compound **3u**, the corresponding singlet in the ^{1}H NMR spectrum of **3v** resides further upfield at -0.69 ppm, a
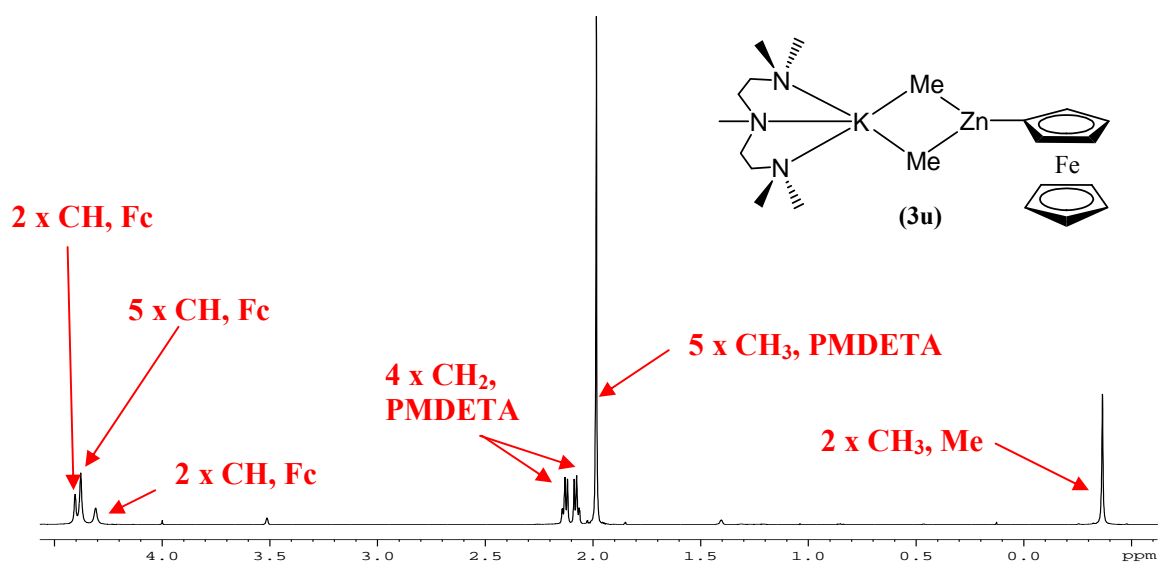
Figure 3.25: ^{1}H NMR spectrum of (3u) in deuterated benzene solution (containing a few drops of d_8-THF).

significant difference of 0.33 ppm. In contrast, the PMDETA resonances in both ^{1}H NMR spectra are fixed at similar positions [(4 × CH$_2$: **3u**, 2.13 and 2.08 ppm; **3v**, 2.33 and 2.23 ppm), (1 × CH$_3$: **3u**, 2.00 ppm; **3v**, 2.10 ppm), (4 × CH$_3$: **3u**, 2.00 ppm; **3v**, 2.05 ppm)]. The resonances associated with metallated ferrocene in **3u** move in a downfield direction [2 × CH, 4.41 ppm; 5 × CH (untouched Cp ring), 4.38 ppm; 2 × CH, 4.31 ppm] from those of ferrocene (δ 4.0 ppm). The peaks due to metallated ruthenocene [2 × CH, 4.71 ppm; 5 × CH (untouched Cp ring), 4.58 ppm; 2 × CH, 4.46 ppm] in the ^{1}H NMR spectrum of **3v**, also reside downfield compared to those of the free metallocene (4.43 ppm).

The filtrate of the reaction that generated **3u** revealed no further monometallated ferrocene; however, free ferrocene and resonances associated with unreacted base **3a** were observed. In contrast, analysis of the filtrate of the reaction to zincate ruthenocene identified a small amount of the monometallated product, along with characteristic resonances of the free metallocene and
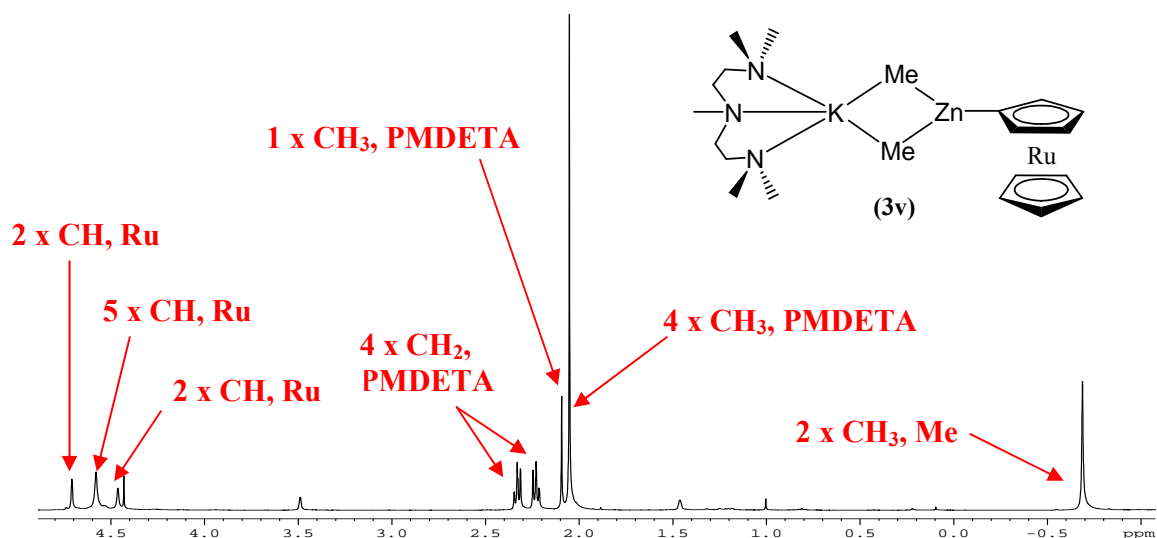
Figure 3.26: ^{1}**H NMR spectrum of (3v) in deuterated benzene solution (containing a few drops of d$_8$-THF).**

base **3a**. In both cases, as the Schlenk tube containing the filtrates were subjected to vacuum for a long period of time, free TMP(H) was not observed as the amine can be removed by this process.

123

The ^{1}H NMR spectrum of the diethyl monozincated ferrocene compound **3w (figure 3.27)** shows a slightly different pattern to the methyl congener **3u**, perhaps due to the solvent system utilised (that is pure C_6D_6 for **3w**, and a C_6D_6/d_8-THF mix for **3u**). A major difference can be seen with respect to the resonances of metallated ferrocene. The integration ratio in the ^{1}H NMR spectrum of **3w** is 5:2:2, whereas for **3u**, it is 2:5:2. The ethyl groups in compound **3w** may be sterically hindered and therefore not freely rotating, as the resonance for the metal-CH_2 hydrogens is relatively broad, giving a poorly defined quartet and triplet (for the CH_3 resonance of the ethyl group) in the process. In comparison to free Et_2Zn in deuterated benzene solution (^{1}H NMR resonances: CH_2, 0.55 ppm; CH_3, 1.51 ppm) and the ethyl groups in base **3b** (CH_2, 0.47 ppm; CH_3, 2.03 ppm), the resonances linked to the ethyl limbs in compound **3w** (CH_2, δ 0.48 ppm; CH_3, δ 2.04 ppm) show that the complex retains much of its parent zinc character. Without the presence of a potentially competitive donor to the potassium cation (for example, THF), the PMDETA resonances (range, 1.76-1.85 ppm) are all shifted upfield in comparison to the free tridentate ligand resonances (range, 2.11-2.46 ppm).
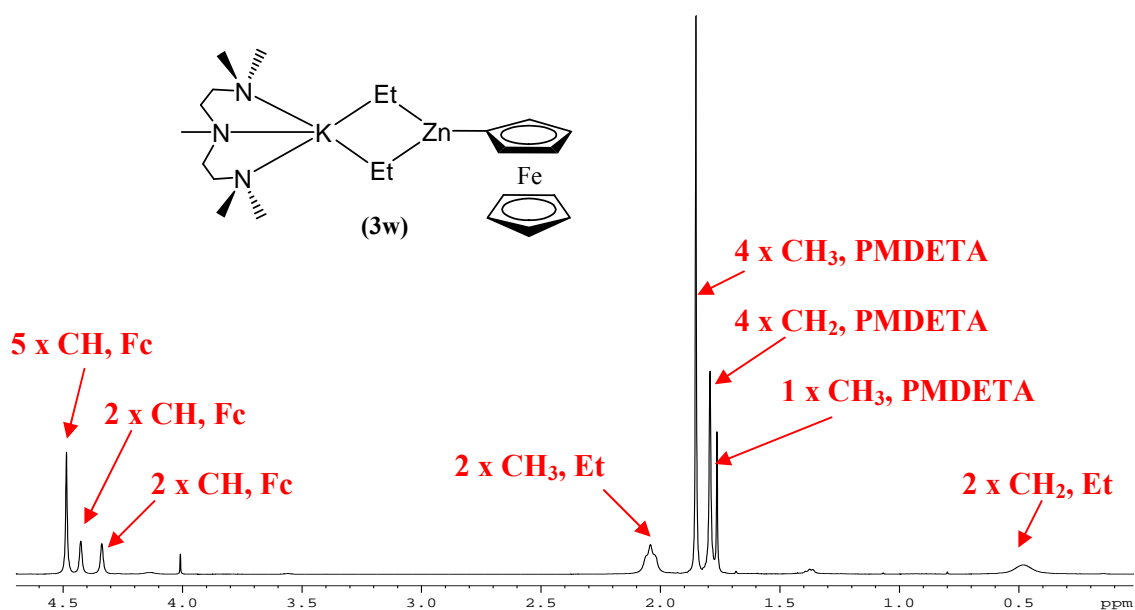
Figure 3.27: ^{1}H **NMR spectrum of (3w) in C_6D_6 solution.**

$[C_6D_6\cdot\{(PMDETA)K\}_2\cdot(C_5\{1\text{-}Zn(^tBu)_2\}H_4)Fe(C_5\{1'\text{-}Zn(^tBu)_2\}H_4)]$ (**3ac**) was crystallised by dissolving the solid formed from the reaction of 2:1 mix of base **3e** to ferrocene in deuterated

benzene solution. The ^{1}H NMR spectrum of this isolated compound is straightforward (**figure 3.28**). Only two sets of signals are present for the hydrogen atoms of the dimetallated ferrocene
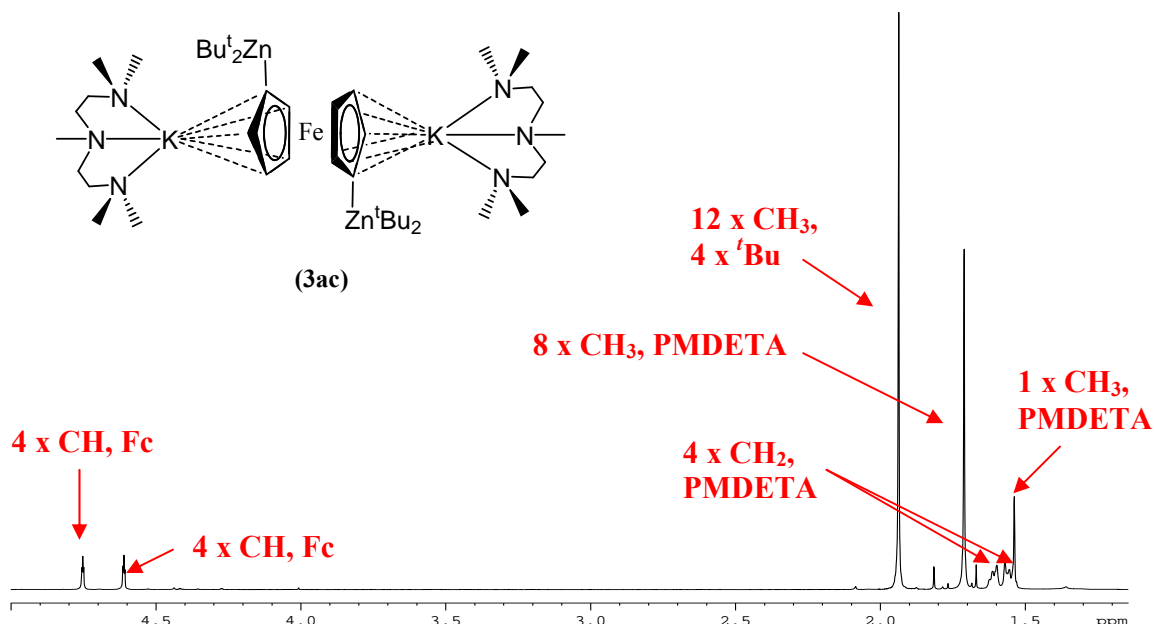
Figure 3.28: ^{1}H NMR spectrum of 3ac in C$_6$D$_6$ solution.

fragment, which appear as very narrow triplets (4.75 and 4.61 ppm). The four *t*-butyl groups appear equivalent in the ^{1}H NMR spectrum, with their resonance peak residing at 1.94 ppm. The resonances connected with PMDETA show the largest upfield shift [8 × CH$_3$, 1.71 ppm; 4 × CH$_2$, 1.62 ppm; 4 × CH$_2$, 1.57 ppm; 2 × CH$_3$, 1.53 ppm] of all the metallocenyl complexes discussed (**3u-3ab**), compared to those of the free ligand (range, 2.11-2.46 ppm). Initially, analysis of the ^{1}H NMR spectrum of the solid isolated from the original reaction involving the base **3e** and half a molar equivalent of the metallocene was confusing (**figure 3.29**). There seemed to be two species of dizincated ferrocene present, as well as resonances associated with THF. The ^{1}H–^{1}H coupling NMR technique, Correlated Spectroscopy (COSY), was used to confirm the identity of the two types of dizincated product. The resonance at 4.61 ppm was found to couple to that at 4.75 ppm (exactly the same as the ^{1}H NMR spectrum of **3ac)**, and the resonance at 4.70 ppm also couples with the hydrogens at 4.75 ppm. Also, the sum of the integration of the resonances at 4.70 and 4.61 ppm match that of the integration of the peak at 4.75 ppm. An explanation for the two sets of dizincated ferrocene could be that the initial

compound contains a THF molecule, with the predicted formula [THF·{(PMDETA)K}$_2$·(C$_4$H$_4$)Fe(C$_4$H$_4$)(Zn^{t}Bu$_2$)$_2$)], and that on dissolving this compound in C$_6$D$_6$ solution, a mixture of the THF solvate and the benzene product **3ac** exists.
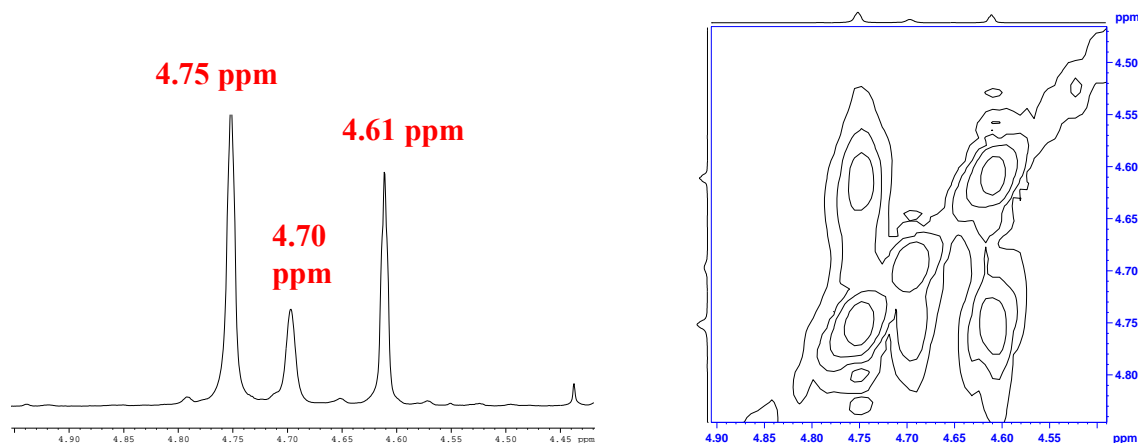
Figure 3.29: Left, metallocene region of the ^{1}H NMR spectrum of the original isolated compound 3x; right, the COSY NMR spectrum of the same region.

To back up this suggestion, the original reaction solid (**3x**) was dissolved in d$_{12}$-cyclohexane (containing a few drops of d$_8$-THF to allow the compound to dissolve). Its ^{1}H NMR spectrum (**figure 3.30**) appears to show only one set of resonances associated with the dizincation of ferrocene at 4.26 and 4.09 ppm. Resonances for non-deuterated THF can also be seen at 3.61 and 1.76 ppm. The remaining PMDETA and *t*-butyl groups can be identified by the resonances between 2.37-2.11 ppm and the singlet at δ 1.10 ppm respectively.

In all the cases of direct zincation of metallocenes shown in this section by KMZ*n*, the reagents **3a**, **3b**, **3d** and **3e** all act as an amido base with the concomitant evolution of TMP(H) into the reaction mixture. Mentioned in previous chapters, Uchiyama et al. suggests through DFT calculations on zincate chemistry that the free amine generated from the initial metallation step could react onwards, in a second step, with the alkyl substituent (in these cases methyl, ethyl, *n*-butyl and *t*-butyl to eliminate methane, ethane, *n*-butane or *iso*-butane respectively) and reincorporate a TMP anion into the structures.[9,64-66] In the isolated crystalline species obtained, no TMP is found within the structures, indicating the possibility that the metals in these

126

structures are so sterically encumbered that there is no room for TMP(H) to re-ligate to either K or Zn and to expel the alkyl group.
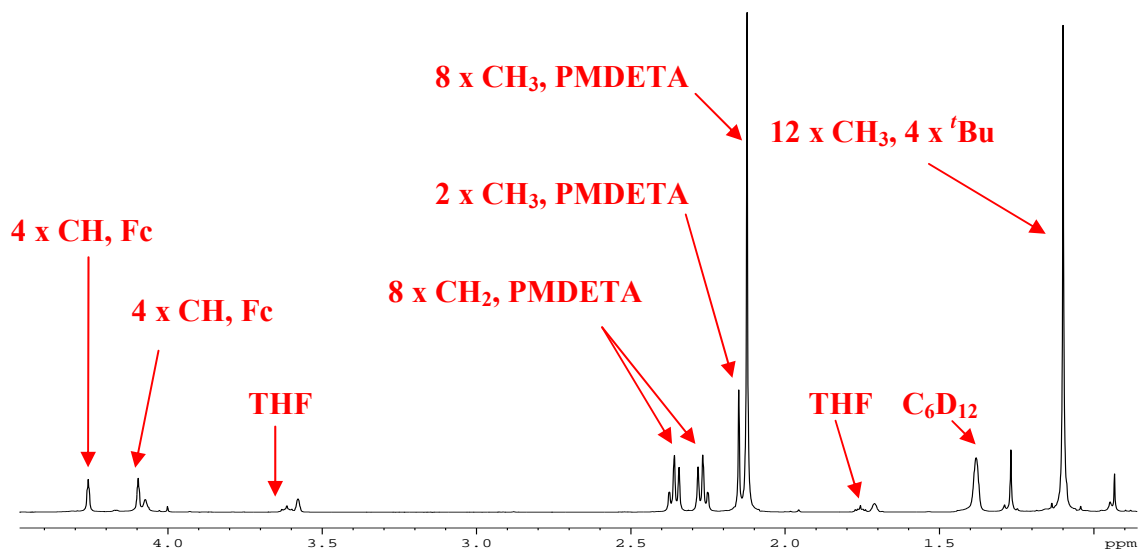
Figure 3.30: ^{1}H NMR spectrum of 3x in C_6D_{12} solution (and a few drops of d_8-THF).

In summary, ferrocene and ruthenocene can be monozincated by potassium-mediated zincation. The role of potassium in the aggregation of monomer units of the structures **3u** and **3v** is critical. Interacting with the zincated ferrocene Cp ring in a η^5-π-contact results in a supramolecular step-ladder, whereas dimerisation is the aggregation of choice with the monozincated ruthenocene compound *via* η^1 (Cp) and C(Me) intermolecular contacts to K. Dizincation of ferrocene can also be realised by KM*Zn*, with zincate **3e** acting as an amido base towards the metallocene. The solvent choice in these deprotonation reactions is crucial. It has been shown that the addition of THF to bulk hexane reaction mixtures (involving the bases **3b**, **3d** and **3e** and the substrates ferrocene and ruthenocene) results in the formation bis-(monozincated metallocene) complexes as a co-product, therefore only hexane should be used when the target complex contains only one molecule of monozincated metallocene. The profound influence of potassium on these unique structures calls for a systematic study of how alkali metals the supramolecularity of alkali-metal-mediated metallated (by Zn, Mg, Mn *etc.*) metallocenes.

3.5) Experimental Section:

Synthesis of [PMDETA·K(μ-TMP)(μ-Me)Zn(Me)] (3a)

0.24 g (2 mmol) of $KCH_2Si(CH_3)_3$ was suspended in 10 mL of hexane. 0.42 mL (2 mmol) of PMDETA was added, followed by 0.34 mL (2 mmol) of TMPH to afford a clear orange solution. Next, 2 mL (2 mmol) of 1M Me_2Zn (in heptanes) was added to the reaction mixture. The Schlenk tube was next placed in the freezer at -28°C overnight to afford colourless crystals (0.54 g, 60 % yield). ^{1}H NMR (400.13 MHz, 298K, C_6D_6): δ 2.01 [2H, m, γH TMP], 1.88 [12H, s, 4 × CH_3 PMDETA], 1.86 [8H, s, 4 × CH_2 of PMDETA], 1.82 [3H, s, 1 × CH_3 of PMDETA], 1.57 [4H, t, 2 × βCH_2 of TMP, *J* = 6.0 Hz], 1.41 [12H, s, 4 × CH_3 of TMP], -0.35 [6H, s, 2 × Zn−CH_3]. Some free TMPH found at δ 1.53, 1.22 and 1.06. ^{13}C{^{1}H} NMR (100.62 MHz, 298K, C_6D_6): δ 56.5 [2 × CH_2 of PMDETA], 54.9 [2 × CH_2 of PMDETA], 53.3 [tertiary C TMP], 45.1 [4 × CH_3 of PMDETA], 41.5 [1 × CH_3 of PMDETA], 41.2 [2 × βCH_2], 34.8 [4 x CH_3 of TMP], 20.4 [1 × γCH_2 of TMP], -2.9 ppm [2 × Zn−CH_3]. Some free TMPH was present at 38.2, 31.8 and 18.8 ppm.

Synthesis of [(PMDETA)·K(μ-TMP)(μ-Et)Zn(Et)] (3b)

0.24 g (2 mmol) of $KCH_2Si(CH_3)_3$ was suspended in 10 mL of hexane. 0.84 mL (4 mmol) of PMDETA was added to afford a clear orange solution. 0.34 mL (2 mmol) of TMPH was added, followed by 2 mL (2 mmol) of 1M Et_2Zn. The Schlenk tube was next placed in the freezer (−28°C) overnight to afford colourless crystals (0.58 g, 61% yield). ^{1}H NMR (400.13 MHz, 298K, C_6D_6): δ 2.06–1.98 [8H, m, 2 × CH_3 of Et and γH TMP], 1.81 [12H, s, 4 × CH_3, PMDETA], 1.77 [11H, m, 4 × CH_2 and 1 × CH_3 PMDETA], 1.58 [4H, m, βH TMP], 1.36 [12H, s, 4 × CH_3 TMP], 0.47 [4H, 2 × CH_2 of Et]. ^{13}C{^{1}H} NMR (100.62 MHz, 298K, C_6D_6): δ 56.9 [2 × CH_2 of PMDETA], 55.2 [2 × CH_2 of PMDETA], 53.4 [tertiary C TMP], 45.2 [4 × CH_3 of PMDETA], 41.6 [1 × CH_3 of PMDETA], 41.2 [2 × βC of TMP], 35.1 [4 × CH_3 of TMP], 20.8 [1 × γC of TMP], 15.1 [2 × CH_3 of Et], 9.0 ppm [2 × CH_2 of Et]. Calculated Microanalysis for

$C_{22}H_{51}KN_4Zn$: C 55.49%, H 10.80%, N 11.77%. Experimental Microanalysis: C   55.49%,   H 11.09%, N 11.39%.

Synthesis of [(PMDETA)·K(μ-TMP)(μ-^{i}Pr)Zn(^{i}Pr)] (3c)

0.24 g (2 mmol) of $KCH_2Si(CH_3)_3$ was suspended in 10 mL of hexane. 0.42 mL (2 mmol) of PMDETA was added to afford a homogeneous orange solution. 0.34 mL (2 mmol) of TMPH was added, followed by 2 mL (2 mmol) of 1M ^{i}Pr$_2$Zn. The Schlenk tube was next placed in the refrigerator at -4^oC overnight to afford colourless crystals. ^{1}H NMR (400.13 MHz, 298K, C_6D_6): δ = 1.98 [m, 2H, 1 × γCH$_2$ TMP], 1.97 [d, 12H, 4 × CH$_3$ ^{i}Pr, J = 7.9 Hz], 1.91 [m, 8H, 4 × CH$_2$ PMDETA], 1.88 [s, 12H, 4 × CH$_3$ PMDETA], 1.83 [s, 3H, 1 × CH3 PMDETA], 1.59 [t, 4H, 2 × βCH$_2$ TMP, J = 6.4 Hz], 1.31 [s, 12H, 4 × CH$_3$ TMP], 0.41 ppm [septet, 2H, 2 × CH of ^{i}Pr, J = 8.2 Hz].

Synthesis of [(PMDETA)·K(μ-TMP)(μ-^{n}Bu)Zn(^{n}Bu)] (3d)

0.24 g (2 mmol) of $KCH_2Si(CH_3)_3$ was suspended in 10 mL of hexane. 0.42 mL (2 mmol) of PMDETA was added to afford a clear orange solution. 0.34 mL (2 mmol) of TMPH was added, followed by 2 mL (2 mmol) of 1M ^{n}Bu$_2$Zn. The Schlenk tube was next placed in the freezer at -28^oC overnight to afford colourless crystals (0.21 g, 20 % yield). ^{1}H NMR (400.13 MHz, 298K, C_6D_6): δ = 2.25 [4H, m, 2 × CH$_2$ of ^{n}Bu], 2.01 [2H, m, γH TMP], 1.87–1.78 [15H, m, 4 × CH$_2$ PMDETA, 1 × CH$_3$ PMDETA, 2 × CH$_2$ ^{n}Bu], 1.76 [12H, s, 4 × CH$_3$ PMDETA], 1.58 [4H, m, 2 × βCH$_2$ TMP], 1.36 [12H, s, 4 × CH$_3$ TMP], 1.27 [6H, t, 2 × CH$_3$ of ^{n}Bu, J = 7.3 Hz], 0.41 ppm [4H, t, 2 × CH$_2$-Zn of ^{n}Bu, J = 8.0 Hz]. ^{13}C{^{1}H} NMR (100.62 MHz, 298K, C_6D_6): δ 56.9 [2 × CH$_2$ of PMDETA], 55.1 [2 × CH$_2$ of PMDETA], 53.5 [tertiary C TMP], 45.1 [4 × CH$_3$ of PMDETA], 41.6 [1 × CH$_3$ of PMDETA], 41.2 [2 × βC of TMP], 35.1 [4 × CH$_3$ of TMP], 34.0 [2 × CH$_2$ of ^{n}Bu], 31.3 [2 × CH$_2$ of ^{n}Bu], 20.8 [1 × γC of TMP], 19.3 [2 × Zn-CH$_2$ of ^{n}Bu], 14.9 ppm [2 × CH$_3$ of ^{n}Bu].

Synthesis of [(PMDETA)·K(μ-TMP)(μ-^{t}Bu)Zn(^{t}Bu)] (3e)

0.24 g (2 mmol) of KCH$_2$Si(CH$_3$)$_3$ was suspended in 10 mL of hexane. 0.42 mL (2 mmol) of PMDETA was added to afford a clear orange solution. 0.34 mL (2 mmol) of TMPH was added. This solution was transferred *via* a canula to a second Schlenk tube containing 0.36 g (2 mmol) of freshly prepared ^{t}Bu$_2$Zn dissolved in 10 mL of hexane. The Schlenk tube was next placed in the freezer at −28°C overnight to afford colourless crystals (0.74 g, 70 % yield). ^{1}H NMR (400.13 MHz, 298K, C$_6$D$_{12}$): δ = 2.40 [m, 8H, 4 × CH$_2$ PMDETA], 2.25 [s, 12H, 4 × CH$_3$ PMDETA], 2.23 [s, 3H, 1 × CH$_3$ PMDETA], 1.74 [m, 2H, γCH$_2$ TMP], 1.37 [t, 4H, 2 × βCH$_2$ TMP, *J* = 8.4 Hz], 1.11 [s, 12H, 4 × CH$_3$ TMP], 1.02 ppm [s, 12H, 6 × CH$_3$ ^{t}Bu]. ^{13}C{^{1}H} NMR (100.62 MHz, 298K, C$_6$D$_{12}$): δ = 56.9 [2 × CH$_2$ of PMDETA], 55.4 [2 × CH$_2$ of PMDETA], 51.9 [tertiary C TMP], 44.9 [4 × CH$_3$ of PMDETA], 41.6 [1 × CH$_3$ of PMDETA], 39.4 [2 × βC of TMP], 35.5 [6 × CH$_3$ ^{t}Bu], 34.2 [4 × CH$_3$ of TMP], 19.5 ppm [1 × γC of TMP].

Synthesis of [TMEDA·K(μ-TMP)(μ-Et)Zn(Et)]$_2$ (3f)

0.24 g (2 mmol) of KCH$_2$Si(CH$_3$)$_3$ was suspended in 10 mL of hexane. 0.6 mL (4 mmol) of TMEDA was added to afford a transparent yellow/orange solution. 0.34 mL (2mmol) of TMPH was added, followed by 2 mL (2 mmol) of 1M Et$_2$Zn. The Schlenk tube was next placed in the freezer at -28°C overnight to afford colourless crystals (0.59 g, 70 %).

Synthesis of [PMDETA·K(μ-HMDS)(μ-Me)Zn(Me)] (3g)

To a Schlenk tube containing 10 mL of hexane, 2 mL (2 mmol) of 1M KHMDS solution was added, followed by 0.42 mL (2 mmol) of PMDETA and then 2 mL (2 mmol) of 1M Me$_2$Zn (in hexane) was injected into the reaction mixture. The Schlenk tube was next placed in the freezer at −28°C to afford colourless crystals (0.54 g, 58 % yield). ^{1}H NMR (400.13 MHz, 298K, C$_6$D$_6$): δ = 1.85 [s, 12H, 4 × CH$_3$ PMDETA], 1.81 [m, 11H, 4 × CH$_2$ and 1 × CH$_3$ PMDETA], 0.35 [s, 18H, 6 × CH$_3$ HMDS], -0.28 ppm [s, 6H, 2 × Zn-CH$_3$]. ^{13}C{^{1}H} NMR (100.62 MHz, 298K,

C_6D_6): δ = 56.6 [2 × CH_2 of PMDETA], 55.0 [2 × CH_2 of PMDETA], 45.3 [4 × CH_3 of PMDETA], 41.9 [1 × CH_3 of PMDETA], 6.0 [6 × CH_3 HMDS], -5.3 ppm [2 × Zn-CH_3].

Synthesis of [{PMDETA·K[2-Zn(Et)$_2$-C$_5$H$_4$N]}$_2$] (3j)

0.24 g (2 mmol) of $KCH_2Si(CH_3)_3$ was suspended in 10 mL of hexane. 0.84 mL (4mmol) of PMDETA was added to afford a transparent orange solution. Subsequently 0.34 mL (2mmol) of TMPH was added, followed by 2 mL (2 mmol) of 1M Et_2Zn. 0.16 mL (2 mmol) of pyridine was added to form a yellow solution. After 2 hr of continuous stirring, an oil and solution bilayer was produced after leaving the reaction mixture to stand. The solution was transferred to another Schlenk tube *via* a canula, discarding the oil. The Schlenk tube containing the solution was placed in the freezer at −28°C for 4 days resulting in a small crop of colourless crystals (0.13 g, 16% yield). ^{1}H NMR (400.13 MHz, 298K, C_6D_6): δ = 8.93 [1H, broad singlet, aromatic H], 8.05 [1H, broad singlet, aromatic H], 7.03 [1H, broad singlet, aromatic H], 6.66 [1H, broad singlet, aromatic H], 2.05 [6H, t, *J* = 7.9 Hz, 2 × CH_3 of Et], 1.95 [3H, s, CH_3 of PMDETA], 1.90 [8H, m, 4 × CH_2 of PMDETA], 1.77 [s, 12H, 4 × CH_3 of PMDETA], 0.15 ppm [4H, q, *J* = 7.9 Hz, 2 × CH_2 of Et]. ^{13}C{^{1}H} NMR (100.62 MHz, 298K, C_6D_6): δ 150.7 = [aromatic C] 150.6 [metallated C], 136.7 [aromatic C], 129.8 [aromatic C], 118.4 [aromatic C], 57.4 [2 × CH_2 of PMDETA], 55.9 [2 × CH_2 of PMDETA], 45.2 [4 × CH_3 of PMDETA], 42.3 [1 × CH_3 of PMDETA], 16.2 [2 × CH_3 of Et], 6.0 ppm [2 × CH_2 of Et].

Synthesis of [{PMDETA·K[2-Zn(Et)$_2$-4-Me$_2$N-C$_5$H$_3$N]}$_2$] (3k)

0.24 g (2 mmol) of $KCH_2Si(CH_3)_3$ was suspended in 10 mL of hexane. 0.84 mL (4 mmol) of PMDETA was added to afford a clear orange solution. 0.34 mL (2mmol) of TMPH was added, followed by 2 mL (2 mmol) of 1M Et_2Zn. 0.244 g (2 mmol) of 4-(dimethylamino)-pyridine was added to form a yellow solution. After 4 hr the solution turned cloudy and 2 mL of THF was added to form a clear solution. The Schlenk tube was next placed in the freezer at −28°C for 3 hrs to afford colourless crystals (0.48 g, 53% yield). ^{1}H NMR (400.13 MHz, 298K, C_6D_6): δ = 8.74 [1H, broad singlet, aromatic H], δ 7.41 [1H, broad singlet, aromatic H], 6.09 [1H, broad singlet, aromatic H], 2.55 [6H, s, 2 × N-CH_3] 2.13 [6H, t, *J* = 7.8 Hz, 2 × CH_3 of Et], 2.01 [3H, s,

CH$_3$ of PMDETA], 1.96 [8H, m, 4 × CH$_2$ of PMDETA], 1.88 [s, 12H, 4 × CH$_3$ of PMDETA], 0.22 ppm [4H, q, *J* = 7.8 Hz, 2 × CH$_2$ of Et]. A trace amount of free DMAP was observed at 8.29, 6.28 and 2.27 ppm. ^{13}C{^{1}H} NMR (100.62 MHz, 298K, C$_6$D$_6$): δ 154.1 [aromatic C] 150.6 [aromatic C], 150.3 [aromatic C], 119.6 [aromatic C], 103.6 [aromatic C], 57.5 [2 × CH$_2$ of PMDETA], 56.1 [2 × CH$_2$ of PMDETA], 45.8 [4 × CH$_3$ of PMDETA], 42.3 [1 × CH$_3$ of PMDETA], 38.6 [2 x N-CH$_3$ of DMAP], 16.6 [2 × CH$_3$ of Et], 5.9 ppm [2 × CH$_2$ of Et]. Calculated Microanalysis C$_{40}$H$_{84}$K$_2$N$_{10}$Zn$_2$: C 52.56%, H 9.26%, N 15.32%. Experimental Microanalysis: C 52.56%,   H 9.02%,   N 16.35%.

Synthesis of [{PMDETA·K[2-Zn(Et)$_2$-4-Et-C$_5$H$_3$N]}$_2$] (3l)

0.24 g (2 mmol) of KCH$_2$Si(CH$_3$)$_3$ was suspended in 10 mL of hexane. 0.84 mL (4mmol) of PMDETA was introduced to afford a transparent orange solution. 0.34 mL (2mmol) of TMPH was added, followed by 2 mL (2 mmol) of 1M Et$_2$Zn. 0.23 mL (2 mmol) of 4-ethylpyridine was next added to form a yellow solution. After 0.5 hr of continuous stirring, an oil and solution bilayer was produced after leaving the reaction mixture to stand. The solution was transferred to another Schlenk tube *via* a canula, discarding the viscous oil. The Schlenk tube containing the solution was then placed in the freezer at −28°C overnight yielding a crop of colourless crystals (0.06 g, 7% yield). ^{1}H NMR (400.13 MHz, 298K, C$_6$D$_6$): δ = 8.90 [1H, broad singlet, aromatic H], δ 7.95 [1H, broad singlet, aromatic H], 6.58 [1H, broad singlet, aromatic H], 2.35 [2H, q, *J* = 7.3 Hz, CH$_2$ of pyr Et], 2.05 [6H, t, *J* = 7.9 Hz, 2 × CH$_3$ of Et], 1.97 [3H, s, CH$_3$ of PMDETA], 1.89 [8H, m, 4 × CH$_2$ of PMDETA], 1.83 [s, 12H, 4 × CH$_3$ of PMDETA], 1.11 [3H, t, *J* = 7.6 Hz, CH$_3$ of pyr Et], 0.19 ppm [4H, q, *J* = 8.0 Hz, 2 × CH$_2$ of Et]. Some product of lateral metallation (viscous oil) is found at δ 7.04, 6.81, 5.70, 5.60, 3.99 and under multiplet at 1.89. ^{13}C{^{1}H} NMR (100.62 MHz, 298K, C$_6$D$_6$): δ = 150.2 [aromatic C], 136.1 [aromatic C], 118.0 [aromatic C], 56.8 [2 × CH$_2$ of PMDETA], 55.6 [2 × CH$_2$ of PMDETA], 44.8 [4 × CH$_3$ of PMDETA], 41.1 [1 × CH$_3$ of PMDETA], 28.5 [1 × CH$_2$ of pyr Et], 15.4 [2 × CH$_3$ of Et], 14.7 [1 × CH$_3$ of pyr Et], 3.9 ppm [2 × CH$_2$ of Et]. Some product of lateral metallation (viscous oil) is found at 143.9, 141.3, 111.5, 104.0, 80.9 and 12.7. **Filtrate:** ^{1}H NMR (400.13 MHz, 298K, C$_6$D$_6$): δ = 7.04 [1H, d, *J* = 5.3 Hz aromatic H], δ 6.82 [1H, d, *J* = 5.6 Hz aromatic H], 5.66 [1H,

d, J = 6.6 Hz aromatic H], 5.57 [1H, d, J = 5.1 Hz aromatic H], 3.98 [1H, m, CH of met pyr Et], 2.03 [s, 12H, 4 × CH$_3$ of PMDETA], 2.00 [3H, s, CH$_3$ of PMDETA], 1.96 [8H, m, 4 × CH$_2$ of PMDETA], 1.85 [6H, t, J = 8.0 Hz, 2 × CH$_3$ of Et], 1.78 [3H, d, J = 6.7 Hz, CH$_3$ of pyr Et], 0.30 ppm [4H, q, J = 7.8 Hz, 2 × CH$_2$ of Et]. For comparison, free 4-ethylpyridine gives signals at 8.47 (d), 6.71 (d), 2.20 (q) and 0.90 (t) under the same NMR conditions.

Synthesis of [{PMDETA·K[2-Zn(Et)$_2$-4-^{i}Pr-C$_5$H$_3$N]}$_2$] (3m)

0.24 g (2 mmol) of KCH$_2$Si(CH$_3$)$_3$ was suspended in 10 mL of hexane. 0.84 mL (4mmol) of PMDETA was added to afford a transparent orange solution. 0.34 mL (2mmol) of TMPH was added, followed by 2 mL (2 mmol) of 1M Et$_2$Zn. 0.26 mL (2 mmol) of 4-isopropylpyridine was added to form a cloudy suspension. After 2 hr of continuous stirring, 3 mL of THF was added which resulted in a clear solution. The Schlenk tube containing the solution was placed in the freezer at −28°C yielding a crop of colourless crystals (0.21 g, 23% yield). ^{1}H NMR (400.13 MHz, 298K, C$_6$D$_6$): δ = 8.92 [1H, broad singlet, aromatic H], δ 7.95 [1H, broad singlet, aromatic H], 6.57 [1H, broad singlet, aromatic H], 2.57 [1H, septet, J = 6.7 Hz, CH of ^{i}Pr], 2.08 [6H, t, J = 7.8 Hz, 2 × CH$_3$ of Et], 1.98 [3H, s, CH$_3$ of PMDETA], 1.92 [8H, m, 4 × CH$_2$ of PMDETA], 1.78 [s, 12H, 4 × CH$_3$ of PMDETA], 1.15 [6H, d, J = 6.9 Hz, 2 × CH$_3$ of ^{i}Pr], 0.17 ppm [4H, q, J = 8.0 Hz, 2 × CH$_2$ of Et]. ^{13}C{^{1}H} NMR (100.62 MHz, 298K, C$_6$D$_6$): δ = 150.7 [aromatic C], 150.3 [tertiary or metallated C], 149.6 [tertiary or metallated C], 135.2 [aromatic C], 116.7 [aromatic C], 57.0 [2 × CH$_2$ of PMDETA], 55.5 [2 × CH$_2$ of PMDETA], 45.0 [4 × CH$_3$ of PMDETA], 42.1 [1 × CH$_3$ of PMDETA], 33.9 [1 × CH of ^{i}Pr], 23.1 [2 × CH$_3$ of ^{i}Pr], 16.0 [2 × CH$_3$ of Et], 5.4 ppm [2 × CH$_2$ of Et]. **Filtrate:** ^{1}H NMR (400.13 MHz, 298K, C$_6$D$_6$): Key resonances representing lateral metallated 4-isopropylpyridine: 6.89 [2H, d, J = 6.4 Hz, aromatic H], δ 5.58 [2H, d, J = 6.5 Hz, aromatic H], 1.75 [6H, s, 2 × CH$_3$ of ^{i}Pr]. For comparison, free 4-isopropylpyridine gives signals at δ 8.50 (d), 6.68 (d), 2.42 (septet) and 0.90 (d) under the same NMR conditions.

Synthesis of [{PMDETA·K[2-Zn(Et)$_2$-4-^{t}Bu-C$_5$H$_3$N]}$_2$] (3n)

0.24 g (2 mmol) of KCH$_2$Si(CH$_3$)$_3$ was suspended in 10 mL of hexane. 0.84 mL (4mmol) of PMDETA was added to afford a transparent orange solution. 0.34 mL (2mmol) of TMPH was added, followed by 2 mL (2 mmol) of 1M Et$_2$Zn. 0.29 mL (2 mmol) of 4-^{t}butylpyridine was added to form a clear solution. After 0.25 hr of continuous stirring, the Schlenk tube containing the solution was placed in the freezer at −28°C yielding a crop of colourless crystals (0.63 g, 67% yield). ^{1}H NMR (400.13 MHz, 298K, C$_6$D$_6$): δ = 8.89 [1H, broad singlet, aromatic H], δ 8.11 [1H, broad singlet, aromatic H], 6.70 [1H, broad singlet, aromatic H], 2.07 [6H, t, *J* = 8.0 Hz, 2 × CH$_3$ of Et], 1.96 [3H, s, CH$_3$ of PMDETA], 1.88 [8H, m, 4 × CH$_2$ of PMDETA], 1.71 [s, 12H, 4 × CH$_3$ of PMDETA], 1.25 [9H, s, 3 × CH$_3$ of ^{t}Bu], 0.15 ppm [4H, q, *J* = 8.0 Hz, 2 × CH$_2$ of Et]. ^{13}C{^{1}H} NMR (100.62 MHz, 298K, C$_6$D$_6$): δ = 151.5 [tertiary or metallated C], 150.4 [aromatic C], 133.3 [aromatic C], 115.8 [aromatic C], 57.3 [2 × CH$_2$ of PMDETA], 55.9 [2 × CH$_2$ of PMDETA], 45.2 [4 × CH$_3$ of PMDETA], 42.3 [1 × CH$_3$ of PMDETA], 34.1 [tertiary C of ^{t}Bu], 30.8 [3 × CH$_3$ of ^{t}Bu], 16.4 [2 × CH$_3$ of Et], 5.7 ppm [2 × CH$_2$ of Et].

Synthesis of [{PMDETA·K[2-Zn(Et)$_2$-4-Ph-C$_5$H$_3$N]}$_2$] (3o)

0.24 g (2 mmol) of KCH$_2$Si(CH$_3$)$_3$ was suspended in 10 mL of hexane. 0.84 mL (4mmol) of PMDETA was added to afford a transparent orange solution. 0.34 mL (2mmol) of TMPH was added, followed by 2 mL (2 mmol) of 1M Et$_2$Zn. 0.31 g (2 mmol) of 4-phenylpyridine was added to form a clear solution. After 1.5 hr of continuous stirring, 3 mL of THF was added to the Schlenk tube, which was then placed in the freezer at −28°C overnight, yielding a crop of colourless crystals (0.50 g, 51% yield). ^{1}H NMR (400.13 MHz, 298K, C$_6$D$_6$): δ = 9.13 [1H, broad singlet, pyr H], 8.46 [1H, broad singlet, pyr H], 7.67 [2H, d, *J* = 7.4 Hz, 2 × phenyl H], 7.23 [2H, t, *J* = 7.4 Hz, 2 × phenyl H], 7.15 [1H, d, *J* = 7.3 Hz, phenyl H], 7.02 [1H, broad singlet, pyr H], 2.15 [6H, t, *J* = 8.0 Hz, 2 × CH$_3$ of Et], 1.94 [3H, s, CH$_3$ of PMDETA], 1.88–1.81 [8H, m, 4 × CH$_2$ of PMDETA], 1.71 [s, 12H, 4 × CH$_3$ of PMDETA], 0.24 ppm [4H, q, *J* = 8.0 Hz, 2 × CH$_2$ of Et]. ^{13}C{^{1}H} NMR (100.62 MHz, 298K, C$_6$D$_6$): δ = 151.2 [aromatic C], 141.1 [tertiary pyr C or tertiary Ph C], 141.0 [tertiary pyr C or tertiary Ph C], 134.0 [aromatic C],

134

129.3 [aromatic C], 127.9 [aromatic C], 127.3 [aromatic C], 116.5 [aromatic C], 57.30 [2 × CH$_2$ of PMDETA], 56.0 [2 × CH$_2$ of PMDETA], 45.1 [4 × CH$_3$ of PMDETA], 42.1 [1 × CH$_3$ of PMDETA], 16.6 [2 × CH$_3$ of Et], 6.1 ppm [2 × CH$_2$ of Et].

Synthesis of [catena-{PMDETA·K[3-Zn(Et)$_2$-4-MeO-C$_5$H$_3$N]}$_\infty$] (3p)

0.24 g (2 mmol) of KCH$_2$Si(CH$_3$)$_3$ was suspended in 10 mL of hexane. 0.84 mL (4 mmol) of PMDETA was added to afford a clear orange solution. 0.34 mL (2mmol) of TMPH was added, followed by 2 mL (2 mmol) of 1M Et$_2$Zn. 0.20 mL (2 mmol) of 4-methoxypyridine was added to form a yellow solution, which turned into a suspension within 5 minutes. After 2 hr the solvent was removed *in vacuo* and 20 mL of toluene was introduced to form a clear orange solution. The Schlenk tube was next placed in the refrigerator (-4°C) overnight to afford colourless crystals (0.46 g, 51.8 % yield). ^{1}H NMR (400.13 MHz, 298K, deuterated THF): δ = 8.34 [1H, broad singlet], 7.84 [1H, broad doublet, aromatic H], 6.43 [1H, broad doublet, aromatic H], 3.76 [3H, s, O-CH$_3$] 2.44 [4H, m, 2 × CH$_2$ of PMDETA] 2.37 [4H, m, 2 × CH$_2$ of PMDETA] 2.22 [3H, s, CH$_3$ of PMDETA], 2.18 [12H, s, 4 × CH$_3$ of PMDETA], 1.21 [6H, t, *J* = 8.0 Hz, 2 × CH$_3$ of Et], 0.22 ppm [4H, m, 2 × CH$_2$ of Et]. ^{13}C{^{1}H} NMR (100.62 MHz, 298K, deuterated THF): δ = 172.1 [aromatic C] 158.6 [aromatic C], 144.4 [aromatic C], 128.6 [aromatic C], 108.4 [aromatic C], 57.5 [2 × CH$_2$ of PMDETA], 56.2 [2 × CH$_2$ of PMDETA], 52.7 [1 × O-CH$_3$], 44.9 [4 × CH$_3$ of PMDETA], 42.0 [1 × CH$_3$ of PMDETA], 14.2 [2 × CH$_3$ of Et], 4.6 [2 × CH$_2$ of Et]. Calculated Microanalysis for C$_{19}$H$_{39}$KN$_4$OZn: C 51.39%, H 8.85%, N 12.62%. Experimental Microanalysis: C 51.39%, H 8.99%, N 12.41%.

Synthesis of [{PMDETA·K[2-Zn(^{n}Bu)$_2$-4-^{t}Bu-C$_5$H$_3$N]}$_2$] (3q)

0.24 g (2 mmol) of KCH$_2$Si(CH$_3$)$_3$ was suspended in 10 mL of hexane. 0.42 mL (2mmol) of PMDETA was added to afford a transparent orange solution. 0.34 mL (2mmol) of TMPH was added, followed by 2 mL (2 mmol) of 1M ^{n}Bu$_2$Zn. 0.29 mL (2 mmol) of 4-^{t}butylpyridine was added to form a clear solution. After 10 minutes of continuous stirring a suspension was formed. 2 mL of THF was added resulting in a clear solution and the Schlenk tube containing the solution was placed in the freezer at −28°C yielding a crop of colourless crystals (0.61 g, 58% yield) after

4 days. ^{1}H NMR (400.13 MHz, 298K, C$_6$D$_6$): δ = 8.89 [1H, broad singlet, aromatic H], δ 8.10 [1H, broad singlet, aromatic H], 6.68 [1H, broad singlet, aromatic H], 2.31 [4H, m, 2 × CH$_2$ of ^{n}Bu], 1.95–1.83 [15H, m, 4 × CH$_2$ PMDETA, 1 × CH$_3$ PMDETA, 2 × CH$_2$ ^{n}Bu], 1.70 [s, 12H, 4 × CH$_3$ of PMDETA], 1.33 [6H, t, 2 × CH$_3$ of ^{n}Bu, J = 7.3 Hz], 1.26 [9H, s, 3 × CH$_3$ of ^{t}Bu], 0.10 ppm [4H, t, 2 × CH$_2$-Zn of ^{n}Bu, J = 7.9 Hz]. ^{13}C{^{1}H} NMR (100.62 MHz, 298K, C$_6$D$_6$): δ 216.9 [metallated C of pyr], 151.5 [tertiary C of ^{t}Bu], 150.6 [aromatic C], 133.1 [aromatic C], 115.9 [aromatic C], 57.3 [2 × CH$_2$ of PMDETA], 56.0 [2 × CH$_2$ of PMDETA], 45.4 [4 × CH$_3$ of PMDETA], 42.1 [1 × CH$_3$ of PMDETA], 35.3 [2 × CH$_2$ of ^{n}Bu], 34.2 [tertiary C of ^{t}Bu], 31.7 [2 × CH$_2$ of ^{n}Bu], 30.8 [3 × CH$_3$ of ^{t}Bu], 16.2 [2 × Zn-CH$_2$ of ^{n}Bu], 15.1 ppm [2 × CH$_3$ of ^{n}Bu].

Aliquot of reaction mixture of [PMDETA·K(Et)(TMP)Zn(Et)] with 4-methylpyridine, (3r).

0.24 g (2 mmol) of KCH$_2$Si(CH$_3$)$_3$ was suspended in 10 mL of hexane. 0.42 mL (2mmol) of PMDETA was added to afford a clear orange solution. 0.34 mL (2mmol) of TMPH was added, followed by 2 mL (2 mmol) of 1M Et$_2$Zn. 0.20 mL (2 mmol) of 4-methylpyridine was added to form a yellow solution containing a brown oil. After 0.5 hr of continuous stirring, 3 mL of THF was added to the reaction mixture and an aliquot was removed for ^{1}H NMR analysis. ^{1}H NMR (400.13 MHz, 298K, C$_6$D$_6$): δ = 7.05 [2H, d, aromatic H], δ 5.71 [2H, doublet, aromatic H], 3.33 [2H, s, pyr CH$_2$] 2.02 [12H,s, 4 × CH$_3$ of PMDETA], 1.99 [8H, m, 4 × CH$_2$ of PMDETA], 1.96 [3H, s, CH$_3$ of PMDETA], 1.74 [6H, t, J = 8.1 Hz, 2 × CH$_3$ of Et], 0.38 [4H, q, J = 8.1 Hz, 2 × CH$_2$ of Et]. A small quantity of starting materials can also be seen: free TMPH at 1.53, 1.22 and 1.06 ppm; free 4-methylpyridine at 8.38 (d) and 6.71 (d) and 1.87 (s); and free THF at 3.55 and 1.51 ppm.

Synthesis of [{PMDETA·K(μ-Me)$_2$Zn(Fc)}$_∞$] (3u)

0.24 g (2 mmol) of KCH$_2$Si(CH$_3$)$_3$ was suspended in 10 mL of hexane. 0.42 mL (2 mmol) of PMDETA was added, followed by 0.34 mL (2 mmol) of TMPH to afford a transparent orange solution. Next, 2 mL (2 mmol) of 1M Me$_2$Zn (in heptanes) was added to the reaction mixture. In a separate Schlenk tube, 0.37 g (2 mmol) of ferrocene was dissolved in 10 mL of hexane. The base mixture was then transferred to the ferrocene-containing Schlenk tube *via* a canula and left

to stir overnight. An orange suspension was formed and was isolated as an orange crystalline solid (0.45 g, 46% yield). ^{1}H NMR (500.13 MHz, 298K, C_6D_6 plus a few drops of deuterated THF to aid solubility): δ = 4.41 [2H, broad s, 2 × CH of metallated Cp ring], 4.38 [5H, broad s, 5 × CH of untouched Cp ring], 4.31 [2H, broad s, 2 × CH of metallated Cp ring], 2.13 [4H, m, 2 × CH_2 of PMDETA], 2.08 [4H, m, 2 × CH_2 of PMDETA], 2.00 [15H, s, 5 × CH_3 of PMDETA], -0.36 ppm [6H, s, 2 × Zn-CH_3]. THF signals can be seen at δ 3.52 and 1.41. A trace amount of free ferrocene is seen at 4.00 ppm. ^{13}C{^{1}H} NMR (100.62 MHz, 298K, C_6D_6 plus a few drops of deuterated THF to aid solubility): δ = 77.6 [2 × CH from metallated Cp], 70.4 [2 × CH from metallated Cp], 67.3 [5 × CH of untouched Cp], 57.4 [2 × CH_2 of PMDETA], 55.9 [2 × CH_2 of PMDETA], 45.3 [4 × CH_3 of PMDETA], 42.1 [1 × CH_3 of PMDETA], -6.6 ppm [2 × Zn−CH_3]. Solvent THF signals are seen at 66.7 and 24.5 ppm.

Synthesis of [{PMDETA·K(μ-Me)$_2$Zn(Rc)}$_2$] (3v)

0.24 g (2 mmol) of $KCH_2Si(CH_3)_3$ was suspended in 10 mL of hexane. 0.42 mL (2 mmol) of PMDETA was added, followed by 0.34 mL (2 mmol) of TMPH to afford a transparent orange solution. Next, 2 mL (2 mmol) of 1M Me_2Zn (in heptanes) was added to the reaction mixture. In a separate Schlenk tube, 0.46 g (2 mmol) of ruthenocene was dissolved in 20 mL of hexane. The base mixture was then transferred to the ruthenocene-containing Schlenk tube *via* a canula and left to stir overnight. A pale yellow suspension formed and was isolated as a pale yellow crystalline solid (0.42 g, 39% yield). ^{1}H NMR (500.13 MHz, 298K, C_6D_6 plus a few drops of deuterated THF to aid solubility): δ = 4.71 [2H, broad s, 2 × CH of metallated Cp ring], 4.58 [5H, broad s, 5 × CH of untouched Cp ring], 4.46 [2H, broad s, 2 × CH of metallated Cp ring], 2.33 [4H, m, 2 × CH_2 of PMDETA], 2.23 [4H, m, 2 × CH_2 of PMDETA], 2.10 [3H, s, 1 × CH_3 of PMDETA], 2.05 [12H, s, 4 × CH_3 of PMDETA], -0.69 ppm [6H, s, 2 × Zn-CH_3]. THF signals can be seen at δ 3.49 and 1.46. A trace quantity of free ruthenocene (from slight hydrolysis) can be seen at δ 4.43. ^{13}C{^{1}H} NMR (100.62 MHz, 298K, C_6D_6 plus a few drops of deuterated THF to aid solubility): δ = 79.3 [2 × CH from metallated Cp], 72.1 [2 × CH from metallated Cp], 68.8 [5 × CH of untouched Cp], 58.0 [2 × CH_2 of PMDETA], 56.6 [2 × CH_2 of PMDETA], 45.6 [4 ×

CH$_3$ of PMDETA], 42.6 [1 × CH$_3$ of PMDETA], -6.9 ppm [2 × Zn−CH$_3$]. THF signals are seen at 66.8 and 24.6 ppm. A minor amount of ruthenocene is seen at 70.1 ppm.

Synthesis of [{PMDETA·K(μ-Et)$_2$Zn(Fc)}$_∞$] (3w)

0.24 g (2 mmol) of KCH$_2$Si(CH$_3$)$_3$ was suspended in 10 mL of hexane. 0.42 mL (2mmol) of PMDETA was added, followed by 0.34 mL (2 mmol) of TMPH to afford a transparent orange solution. Next, 2 mL (2 mmol) of 1M Et$_2$Zn (in hexanes) was added to the reaction mixture, followed by 0.37 g (2 mmol) of ferrocene. Almost immediately, the Schlenk tube containing a clear orange solution was placed in the freezer at -28°C to yield a set of orange crystals (0.42 g, 40% yield). ^{1}H NMR (400.13 MHz, 298K, C$_6$D$_6$): δ = 4.48 [5H, s, 5 × CH of unsubstituted Cp ring], 4.42 [2H, s, 2 × CH of metallated Cp ring], 4.34 [2H, s, 2 × CH of metallated Cp ring], 2.04 [6H, broad t, 2 × CH$_3$ of Et], 1.85 [12H, s, 4 × CH$_3$ of PMDETA], 1.79 [8H, s, 4 × CH$_2$ of PMDETA], 1.76 [3H, s, 1 × CH$_3$ of PMDETA], 0.48 ppm [4H, broad q, 2 × CH$_2$ of Et]. ^{13}C{^{1}H} NMR (100.62 MHz, 298K, C$_6$D$_6$): δ = 77.4 [2 × CH of metallated Cp], 70.4 [2 × CH of metallated Cp], 66.6 [5 × CH of unsubstituted Cp ring], 56.7 [2 × CH$_2$ of PMDETA], 55.2 [2 × CH$_2$ of PMDETA], 44.8 [4 × CH$_3$ of PMDETA], 41.3 [1 × CH$_3$ of PMDETA], 15.1 [2 × CH$_3$ of Et], 5.3 ppm [2 × CH$_2$ of Et].

Synthesis of [THF·{(PMDETA)K}$_2$·(C$_5${1-Zn(^{t}Bu)$_2$}H$_4$)Fe(C$_5${1′-Zn(^{t}Bu)$_2$}H$_4$)] (3x)

0.24 g (2 mmol) of KCH$_2$Si(CH$_3$)$_3$ was suspended in 20 mL of hexane. 0.84 mL (4 mmol) of PMDETA was added, followed by 0.34 mL (2 mmol) of TMPH to afford a transparent orange solution. In a separate Schlenk tube, 0.36 g (2 mmol) of ^{t}Bu$_2$Zn was dissolved in 10 mL of hexane, which was subsequently added *via* a canula to the initial Schlenk tube. 0.186 g (1 mmol) of ferrocene was then added to the reaction mixture to afford an orange solution containing a red oil. 3 mL of THF was added to form a clear solution, which was stirred for 1 hr and placed in the freezer at -28°C to yield red crystals (0.29 g, 31%). ^{1}H NMR (400.13 MHz, 298K, C$_6$D$_{12}$ plus a few drops of deuterated THF to aid solubility): δ = 4.23 [4H, s, 4 × CH of metallated Cp ring], 4.09 [4H, s, 4 × CH of metallated Cp ring], 3.63 [m, THF], 2.37 [8H, m, 4 × CH$_2$ of PMDETA],

2.28 [8H, m, 4 × CH$_2$ of PMDETA], 2.16 [6H, s, 2 × CH$_3$ of PMDETA], 2.11 [24H, s, 8 x CH$_3$ of PMDETA], 1.76 [m, THF], 1.10 ppm [36H, s, 12 × CH$_3$ of 4 ^{t}Bu]. ^{13}C{^{1}H} NMR (100.62 MHz, 298K, C$_6$D$_{12}$ plus a few drops of deuterated THF to aid solubility): δ = 88.3 [2 × met C of ferrocene], 79.7 [4 × CH of metallated Cp ring], 70.0 [4 × CH of metallated Cp ring], 67.8 [THF], 55.5 [4 × CH$_2$ of PMDETA], 57.1 [4 × CH$_2$ of PMDETA], 46.0 [8 × CH$_3$ of PMDETA], 42.8 [2 × CH$_3$ of PMDETA], 36.3 [12 × CH$_3$ of 4 ^{t}Bu], 25.9 [THF], 22.6 ppm [4 × quarternary C of ^{t}Bu].

Synthesis of [(PMDETA)(THF)·K(Fc)$_2$Zn(Et)] (3y)

0.24 g (2 mmol) of KCH$_2$Si(CH$_3$)$_3$ was suspended in 10 mL of hexane. 0.42 mL (2 mmol) of PMDETA was added to afford a transparent orange solution. 0.34 mL (2 mmol) of TMPH was added, followed by 2 mL (2 mmol) of 1M Et$_2$Zn. 0.372 g (2 mmol) of ferrocene was added to the reaction mixture, along with 1 mL of THF to generate a clear homogeneous solution. The Schlenk tube was placed in the freezer at -28°C generating a batch of red crystals (0.46 g). The reaction yield is not given due to the presence of one or more unidentifiable product(s).

Synthesis of [(PMDETA)(THF)·K(Fc)$_2$Zn(^{n}Bu)] (3z)

0.24 g (2 mmol) of KCH$_2$Si(CH$_3$)$_3$ was suspended in 10 mL of hexane. 0.84 mL (4 mmol) of PMDETA was added to afford a clear orange solution. 0.34 mL (2 mmol) of TMPH was added, followed by 2 mL (2 mmol) of 1M ^{n}Bu$_2$Zn. 0.372 g (2 mmol) of ferrocene was added to the reaction mixture, along with 1 mL of THF to create a clear homogeneous solution. After 20 minutes stirring, the Schlenk tube was placed in the refrigerator at -4°C affording a batch of red crystals (0.42 g). The reaction yield is not given due to the presence of one or more unidentifiable product(s).

Synthesis of [(PMDETA)(THF)·K(Fc)$_2$Zn(^{t}Bu)] (3aa)

0.24 g (2 mmol) of KCH$_2$Si(CH$_3$)$_3$ was suspended in 20 mL of hexane. 0.84 mL (4 mmol) of PMDETA was added, followed by 0.34 mL (2 mmol) of TMPH to afford a transparent orange

solution. In a separate Schlenk tube, 0.36 g (2 mmol) of $^{t}Bu_2Zn$ was dissolved in 10 mL of hexane, which was subsequently added *via* a canula to the initial Schlenk tube. 0.372 g (2 mmol) of ferrocene was then added to the reaction mixture to yield an orange solution containing a red oil. 5 mL of THF was added to form a clear solution, which was stirred for 1 hr and placed in the freezer at -28°C to yield red crystals after 3 months (0.09 g). The reaction yield is not given due to the presence of one or more unidentifiable product(s).

Synthesis of [(PMDETA)(THF)·K(Rc)$_2$Zn(Et)] (3ab)

0.24 g (2 mmol) of $KCH_2Si(CH_3)_3$ was suspended in 10 mL of hexane. 0.84 mL (4 mmol) of PMDETA was added to afford a clear orange solution. 0.34 mL (2 mmol) of TMPH was added, followed by 2 mL (2 mmol) of 1M Et_2Zn. In a separate Schlenk tube, 0.46 g (2 mmol) of ruthenocene was dissolved in 5 mL of toluene, which was subsequently added *via* a canula to the initial Schlenk tube, to yield a white suspension. Upon addition of 2 mL of THF a clear solution was obtained, which was stirred for 2 hrs, and then placed in the freezer at -28°C to yield large pale yellow hexagonal crystals (0.32 g). The reaction yield is not given due to the presence of one or more unidentifiable product(s).

Synthesis of [C$_6$H$_6$·{(PMDETA)K}$_2$·(C$_5${1-Zn(^{t}Bu)$_2$}H$_4$)Fe(C$_5${1′-Zn(^{t}Bu)$_2$}H$_4$)] (3ac)

Solid **3x** was dissolved in several mL's of C_6D_6 solution, resulting in red hexagonal crystals at room temperature. ^{1}H NMR (400.13 MHz, 298K, C_6D_6): δ = 4.75 [4H, t, 4 × CH of metallated Cp ring], 4.61 [4H, s, 4 × CH of metallated Cp ring], 1.94 [36H, s, 12 × CH_3 of 4 ^{t}Bu], 1.71 [24H, s, 8 x CH_3 of PMDETA], 1.62 [8H, m, 4 × CH_2 of PMDETA], 1.57 [8H, m, 4 × CH_2 of PMDETA], 1.53 [6H, s, 2 × CH_3 of PMDETA]. ^{13}C{^{1}H} NMR (100.62 MHz, 298K, C_6D_6): δ = 88.5 [2 × met C of ferrocene], 79.7 [4 × CH of metallated Cp ring], 70.3 [4 × CH of metallated Cp ring], 56.6 [4 × CH_2 of PMDETA], 55.3 [4 × CH_2 of PMDETA], 44.9 [8 × CH_3 of PMDETA], 40.9 [2 × CH_3 of PMDETA], 36.8 [12 × CH_3 of 4 ^{t}Bu], 23.1 ppm [4 × quarternary C of ^{t}Bu].

Chapter 3 – References:

[1]   R. E. Mulvey, *Organometallics* **2006**, *25*, 1060.

[2]   R. E. Mulvey, F. Mongin, M. Uchiyama, Y. Kondo, *Angew. Chem. Int. Ed*. **2007**, *46*, 3802.

[3]   R. E. Mulvey, *Acc. Chem. Res*. **2009**, *42*, 743.

[4]   H. R. L. Barley, W. Clegg, S. H. Dale, E. Hevia, G. W. Honeyman, A. R. Kennedy, R. E. Mulvey, *Angew. Chem. Int. Ed*. **2005**, *44*, 6018.

[5]   P. C. Andrikopoulos, D. R. Armstrong, H. R. L. Barley, W. Clegg, S. H. Dale, E. Hevia, G. W. Honeyman, A. R. Kennedy, R. E. Mulvey, *J. Am. Chem. Soc*. **2005**, *127*, 6184.

[6]   W. Clegg, S. H. Dale, E. Hevia, G. W. Honeyman, R. E. Mulvey, *Angew. Chem. Int. Ed*. **2006**, *45*, 2370.

[7]   A. Seggio, A. Jutand, J. Priem, F. Mongin, *Synlett* **2008**, 2955.

[8]   J. -M. L'Helgoual'ch, A. Seggio, F. Chevallier, M. Yonehara, E. Jeanneau, M. Uchiyama, F. Mongin, *J. Org. Chem*. **2008**, *73*, 177.

[9]   Y. Kondo, M. Shilai, M. Uchiyama, T. Sakamoto, *J. Am. Chem. Soc*. **1999**, *121*, 3539.

[10]   M. Uchiyama, Y. Matsumoto, D. Nobuto, T. Furuyama, K. Yamaguchi, K. Morokuma, *J. Am. Chem. Soc*. **2006**, *128*, 8748.

[11]   Z. Dong, G. C. Clososki, S. H. Wunderlich, A. Unsinn, J. Li, P. Knochel, *Chem. Eur. J*. **2009**, *15*, 457.

[12]   J. A. Wanklyn, *Proc. R. Soc. London*, **1858**, 341.

[13]   For an excellent historical account of zincate chemistry, see D. Seyferth, *Organometallics,* **2001**, *20*, 2940.

[14]   E. Weiss, R. Wolfrum, Chem. Ber. **1968**, *101*, 35.

[15]   D. J. Linton, P. Schooler, A. E. H. Wheatley, *Coord. Chem. Rev.* **2001**, *223*, 53.

[16]   E. Álvarez, A. Grirrane, I. Resa, D. del Rio, A. Rodriguez, E. Carmona, *Angew. Chem. Int. Ed.* **2007**, *46*, 1296.

[17]   F. H. Allen, *Acta Crystallogr., Sect. B: Struct. Sci*. **2002**, *58*, 380.

[18]   D. J. Darensberg, S. A. Niezgoda, J. D. Draper, J. H. Reibenspies, *Inorg. Chem.* **1999**, *38,* 1356.

[19]   E. Rijnberg, B. Richter, K.-H. Thiele, J. Boersma, N. Veldman, A. L. Spek, G. Van Koten, *Inorg. Chem*. **1998**, *37*, 56.

[20]   C. K. Gren, T. P. Hanusa, A. L. Rheingold, *Organometallics* **2007**, *26*, 1643.

[21]   K. Merz, S. Block, R. Schoenen, M. Driess, *Dalton Trans.* **2003**, 3365.

[22]   R. M. Fabicon, M. Parvez, H. G. Richey Jr., *J. Am. Chem. Soc*. **1991**, *113*, 1412.

[23]   A. P. Purdy, C. F. George, *Polyhedron* **1994**,*13*, 709.

[24]   S. E. Baillie, E. Hevia, A. R. Kennedy, R. E. Mulvey, *Organometallics* **2007**, *26*, 204.

[25]   G. C. Forbes, A. R. Kennedy, R. E. Mulvey, B. A. Roberts, R. B. Rowlings, *Organometallics* **2002**, *21*, 5115.

[26]   A. P. Purdy, C. F. George, *Organometallics* **1992**, *11*, 1955.

[27]   U. Cremer, I. Pantenburg, U. Ruschewitz, *Inorg. Chem*. **2003**, *42*, 7716.

[28]   E. Rijnberg, J. Boersma, J. T. B. H. Jastrzebski, M. T. Lakin, A. L. Spek, G. Van Koten, *Organometallics*, **1997**, *16*, 3158.

[29]   E. Rijnberg, J. Boersma, J. T. B. H. Jastrzebski, M. T. Lakin, A. L. Spek, G. Van Koten, *Chem. Commun*. **1995**, 1839.

[30]   W. Clegg, G. C. Forbes, A. R. Kennedy, R. E. Mulvey, S. T. Liddle, Chem. Commun. **2003**, 406.

[31]   Based on data on hydration of aqueous group 1 ions, see: F. A. Cotton, G. Wilkinson, C. A. Murillo, M. Bochmann, *Advanced Inorganic Chemistry, 6th Ed.*, Wiley-VCH, Weinheim, **1999**, chap.3.

[32]   D. R. Armstrong, D. Barr, W. Clegg, R. E. Mulvey, D. Reed, R. Snaith, K. Wade, *J. Chem. Soc., Chem. Commun*. **1986**, 869.

[33]   For several examples of laddering, see: M. Lappert, A. Protchenko, P. Power, A. Seeber, *Metal Amide Chemistry*, Wiley-VCH, Weinheim, **2009**, chap.2.

[34]   D. R. Armstrong, E. Herd, D. V. Graham, E. Hevia, A. R. Kennedy, W. Clegg, L. Russo, *Dalton Trans*. **2008**, 1323.

[35]   J. A. Joule, K. Mills, *Heterocyclic Chemistry, 4th Ed.*, Blackwell Publishing, Oxford, **2000**, chap. 5.

[36]   M. Schlosser, F. Mongin, *Chem. Soc. Rev*. **2007**, *36*, 1161.

[37]   L. A. Summers, *The bipyridinium herbicides*, Academic Press, London, **1980**.

[38]   D. Gaskell, *Drugs against drugs, Chem. Brit*. **1998**, 27.

[39]   F. Marsais, G. Queguiner, *Tetrahedron* **1983**, *39*, 2009.

[40]   P. C. Gros, Y. Fort, *Eur. J. Org. Chem*. **2009**, 4199.

[41] P. C. Gros, Y. Fort, P. Caubère, *J. Chem. Soc., Perkin Trans. 1* **1997**, 3597.

[42] G. Quéguiner, F. Marsais, V. Snieckus, J. Epsztajn, *Adv. Heterocyclic Chem.* **1991**, *52*, 187.

[43] A. J. Clarke, S. McNamara, O. Meth-Cohn, *Tetrahedron Lett.* **1974**, 2373.

[44] S. L. Taylor, D. Y. Lee, J. C. Martin, *J. Org. Chem.* **1983**, *48*, 4156.

[45] S. V. Kessar, P. Singh, K. N. Singh, M. Dutt, *J. Chem. Soc., Chem. Commun.* **1991**, 570.

[46] S. V. Kessar, P. Singh, *Chem. Rev.* **1997**, *97*, 721.

[47] E. Vedejs, X. Chen, *J. Am. Chem. Soc.* **1996**, *118*, 1809.

[48] J. Verbeek, A. V. E. George, R. L. P. de Jong, L. Brandsma, *J. Chem. Soc., Chem. Commun.* **1984**, 257.

[49] J. Verbeek, L. Brandsma, *J. Org. Chem.* **1984**, *49*, 3857.

[50] J. Engering, M. Jansen, *Z. Anorg. Allg. Chem.* **2003**, *629*, 109.

[51] F. Garcia, A. Hopkins, R. A. Kowenicki, M. McPartlin, J. S. Silvia, J. M. Rawson, M. C. Rodgers, D. S. Wright, *Chem. Commun.* **2007**, 586.

[52] K. Nakatsu, K. Kinoshitu, H. Kanda, K. Isobe, Y. Nakamura, S. Kawaguchi, *Chem. Lett.* **1980**, 913.

[53] A. V. Churakov, D. P. Krut'ko, M. V. Borzov, R. S. Kirsanov, S. A. Belov, J. A. K. Howard, *Acta Crystallogr. Sect. E* **2006**, *62*, m1094.

[54] S. Schulz, F. Thomas, W. M. Priesmann, M. Nieger, *Organometallics* **2006**, *25*, 1392.

[55] T. Kaminski, P. Gros, Y. Fort, *Eur. J. Org. Chem.* **2003**, 3855.

[56] E. Anders, A. Opitz, W. Bauer, *Synthesis*, **1991**, 1221.

[57] H. C. Brown, W. A. Murphey, *J. Am. Chem. Soc.* **1951**, *73*, 3308.

[58] W. M. Stalick, H. Pines, *J. Org. Chem.* **1970**, *35*, 1712.

[59] P. Gros, Y. Fort, *J. Org. Chem.* **2002**, *67*, 2028.

[60] P. C. Gros, A. Doudouh, C. Woltermann, *Chem. Commun.* **2006**, 2673.

[61] Pyridine metallation in general is a complicated affair involving both thermodynamic and kinetic factors. For a general discussion, see J. Clayden, *Organolithiums: Selectivity for Synthesis*, Elsevier Science Ltd., Oxford, **2002**, pp. 59-70.

[62] D. L. Comins, D. H. LaMunyon, *Tetrahedron Lett.*, **1988**, *29*, 773.

[63] F. Trécourt, M. Mallet, F. Mongin, B. Gervais, G. Quéguiner, *Tetrahedron*, **1993**, *49*, 8373.

[64]   D. Nobuto, M. Uchiyama, *J. Org. Chem*. **2008**, *73*, 1117.

[65]   M. Uchiyama, Y. Matsumoto, S. Usui, Y. Hashimoto, K. Morokuma, *Angew. Chem. Int. Ed.* **2007**, *46*, 926.

[66]   Y. Kondo, J. V. Morey, J. C. Morgan, H. Naka, D. Nobuto, P. R. Raithby, M. Uchiyama, A. E. H. Wheatley, *J. Am. Chem. Soc*. **2007**, *129*, 13360.

[67]   N. D. R. Barnett, W. Clegg, A. R. Kennedy, R. E. Mulvey, S. Weatherstone, *Chem. Commun*. **2005**, 375.

[68]   H. Naka, J. V. Morey, J. Haywood, D. J. Eisler, M. McPartlin, F. Garcia, H. Kudo, Y. Kondo, M. Uchiyama, A. E. H. Wheatley, *J. Am. Chem. Soc*. **2008**, *130*, 16193.

[69]   The lack of basicity of alkyl-zincates has been previously noted, see: T. Furuyama, M. Yonehara, S. Arimoto, M. Kobayashi, Y. Matsumoto, M. Uchiyama, *Chem. Eur. J*. **2008**, *14*, 10348.

[70]   M. L. Hlavinka, J. F. Greco, J. R. Hagadorn, *Chem. Commun*. **2005**, 5304.

[71]   A similar reaction in reactivity has been noted in the comparison of NaMgBu$_3$ with BuNa in reactions with toluene, see: P. C. Andrikopoulos, D. R. Armstrong, E. Hevia, A. R. Kennedy, R. E. Mulvey, C. T. O'Hara, *Chem. Commun.* **2005**, 1131.

[72]   T. J. Kealy, P. L. Pauson, *Nature* **1951**, *168,* 1040.

[73]   S. A. Millar, J. A. Tebboth, J. F. Tremaine, *J. Chem. Soc*. **1952**, 633.

[74]   P. L. Pauson, *J. Organomet. Chem*. **2001**, *637-639*, 3.

[75]   G. Wilkinson, M. Rosenblum, M. C. Whiting, R. B. Woodward, *J. Am. Chem. Soc*. **1952**, *74*, 2125.

[76]   E. O. Fischer, W. Pfab, *Z. Naturforch. Teil* **1952**, *B7*, 377.

[77]   P. F. Eiland, R. Pepinsky, *J. Am. Chem. Soc*. **1952**, *74*, 4971.

[78]   J. D. Dunitz, L. E. Orgel, *Nature* **1953**, *171*, 121.

[79]   M. Rosenblum, *J. Organomet. Chem*. **2001**, *637-639*, 13.

[80]   P. L. Pauson, *Quart. Revs. (London)* **1955**, 9.

[81]   R. B. Woodward, M. Rosenblum, M. C. Whiting, *J. Am. Chem. Soc*. **1952**, *74*, 2125.

[82]   G. Wilkinson, P. L. Pauson, J. M. Birmingham, F. A. Cotton, *J. Am. Chem. Soc*. **1953**, *75*, 1011.

[83]   F. A. Cotton, R. O. Whipple, G. Wilkinson, *J. Am. Chem. Soc*. **1953**, *75*, 3586.

[84]   G. Wilkinson, *J. Am. Chem. Soc*. **1952**, *74*, 6146.

[85]   Based on quotations form Aldrich Chemical company, January **2010**.

[86]   G. L. Hardgrove, D. H. Templeton, *Acta Crystallogr.* **1959**, *12*, 28.

[87]   R. A. Benkesser, D. Goggin, G. Scholl, *J. Am. Chem. Soc.* **1954**, *76*, 4025.

[88]   F. Rebiere, O. Samuel, H. B. Kagan, *Tetrahedron Lett.* **1990**, *31*, 3121.

[89]   D. W. Slocum, T. R. Englemann, C. Ernst, C. A. Jennings, W. Jones, B. Koonsvitsky, J. Lewis, P. Shenkin, *J. Chem. Ed.* **1969**, *46*, 144.

[90]   F. C. Hedberg, H. Rosenberg, *Tetrahedron Lett.* **1969**, *10*, 4011.

[91]   D. Seyferth, H. P. Huffman, R. Burton, J. F. Helling, *Inorg. Chem.* **1962**, *1*, 414.

[92]   M. D. Rausch, *Inorg. Chem.* **1962**, *1*, 227.

[93]   D. Guillaneux, H. B. Kagan, *J. Org. Chem.* **1995**, *60*, 2502.

[94]   R. Sanders, U. T. Mueller-Westerhoff, *J. Organomet. Chem.* **1996**, *512*, 219.

[95]   M. D. Rausch, E. O. Fischer, H. Grubert, *J. Am. Chem. Soc.* **1960**, *82*, 76.

[96]   P. Štěpnička, *Ferrocenes: Ligands, Materials and Biomolecules,* VCH: Weinheim, Germany, **2008**.

[97]   N. J. Long, *Metallocenes: An introduction to Sandwich Compounds, 1ˢᵗ edn*, Blackwell Science, Oxford, **1998**.

[98]   B. Wrackmeyer, E. V. Klimkina, T. Ackermann, W. Milius, *Inorg. Chem. Commun.* **2007**, *10*, 743.

[99]   K. H. Pannell, R. N. Kappor, F. Cervantes-Lee, *Z. Kristallogr.-New Cryst. Struct.* **2000**, *215*, 123.

[100]   B. M. Yamin, Hoon-Kun Fun, Boon-Chuan Yip, O. B. Shawkataly, Siang-Guan Teoh, *Acta Crystallogr., Sect. C: Cryst. Struct. Commun.* **1994**, *50*, 1551.

[101]   M. Herberhold, H. Kniesel, L. Haumaier, A. Gieren, C. Ruiz-Perez, *Z. Naturforch., B: Chem. Sci.* **1986**, *41*, 1431.

[102]   M. Wedler, H. W. Roesky, F. T. Edelmann, U. Behrens, *Z. Naturforch., B: Chem. Sci.* **1988**, *43*, 1461.

[103]   J. A. Wanklyn, *Justus Liebigs Ann. Chem.* **1858**, *107*, 125.

[104]   C. J. Rohbogner, S. H. Wunderlich, G. C. Clososki, P. Knochel, *Eur. J. Org. Chem.* **2009**, 1781.

[105]   M. Hatano, S. Suzuki, K. Ishihara, *J. Am. Chem. Soc.* **2006**, *128*, 9998.

[106] P. C. Andrikopoulos, D. R. Armstrong, W. Clegg, C. J. Gilfillan, E. Hevia, A. R. Kennedy, R. E. Mulvey, C. T. O'Hara, J. A. Parkinson, D. M. Tooke, J. *Am. Chem. Soc.* **2004**, *126*, 11612.

[107] M. Westerhausen, *Dalton Trans.* **2006**, 4755.

[108] V. L. Blair, A. R. Kennedy, J. Klett, R. E. Mulvey, *Chem. Commun.* **2008**, 5426.

[109] T. Furuyama, M. Yonehara, S. Arimoto, M. obeyashi, Y. Matsumoto, M. Uchiyama, *Chem. Eur. J.* **2008**, *14*, 10348.

[110] M. Schlosser, *Organometallics in Synthesis, 2ⁿᵈ edn*, VCH, Weinheim, Germany, **2002**.

[111] G. W. Honeyman, A. R. Kennedy, R. E. Mulvey, D. C. Sherrington, *Organometallics* **2004**, *23*, 1197.

[112] T. Yoshida, T. Shinohara, K. Onitsuka, F. Ozawa, K. Sonogashira, *J. Organomet. Chem.* **1999**, *574*, 66.

[113] M. N. Nefedova, I. A. Mamed'yarova, V. I. Sokolov, E. I. Symslova, L. G. Kuz'mina, K. I. Grandverg, *Izv. Akad. Nauk SSSR, Ser. Khim. (Russ.) (Russ. Chem. Bull.)* **1994**, 1335.

[114] Boasheng Lee, W. T. Pennington, J. A. Laske, G. H. Robinson, *Organometallics* **1990**, *9*, 2864.

[115] Longgen Zhu, L. M. Daniels, L. M. Peerey, N. M. Kostic, *Acta Crystallogr., Sect. C: Cryst. Struct. Commun.* **1988**, *44*, 1727.

[116] N. G. Bokii, Yu. T. Struchkov, V. V. Korolkov, T. P. Tolstaya, *Koord. Khim. (Russ.)(Coord. Chem.)* **1975**, *1*, 1144.

[117] L. N. Zakharov, Yu. T. Struchkov, V. V. Sharutin, O. N. Suvorova, *Cryst. Struct. Commun.* **1979**, *8*, 439.

[118] M. Herberhold, H. Kniesel, L. Haumaier, U. Thewalt, *J. Organomet. Chem.* **1986**, *301*, 355.

[119] A. S. Perucha, J. Heilmann-Brohl, M. Bolte, H.-W. Lerner, M. Wagner, *Organometallics* **2008**, *27*, 6170.

Chapter 4: Unravelling the Hidden Mechanism behind Potassium Magnesiate bases

4.1) Introduction

Magnesiation (a metal–hydrogen exchange process) is currently going through a period of remarkable reassessment with regard to its effectiveness (previously poor but presently exceptionally good) in directly metallating aromatic and heteroaromatic substrates.[1-3] Eaton's enterprising employment of [Mg(TMP)$_2$] for executing direct *ortho*-magnesiation of representative aromatic amides and esters marked an early pivotal development in this transformation.[4,5] TMP was also a key factor in a later 1999 report presented by our own group of the dimagnesiation of arenes achieved *in situ* with sodium-magnesium alkyl-TMP mixtures, which coincidentally opened up a new aspect of inverse crown chemistry.[6] The seeds of these initial results have since grown into the idea of "alkali-metal-mediated magnesiation (AMM*Mg*)" and blossomed further to lowly electropositive metals such as zinc,[7-9] cadmium,[10] aluminium,[11-13] and manganese,[14-16] so promoting the general designation "alkali-metal-mediated metallation (AMM*M*)". Knochel and co-workers have demonstrated that TMP-driven magnesiation of, for example, chlorinated pyrimidines [17] can also be effected by alkyl-free halide compositions, "turbo-Grignard reagents", such as "TMPMgCl·LiCl".[18-24]

To date, nearly all AMM*Mg* chemistry has involved lithium or sodium exponents. Potassium, the common utility heavier alkali metal, has received only meagre attention, which is surprising given its prominence in Lochmann-Schlosser mixed-metal superbase chemistry.[25-29] A search of the CSD [30] highlights that the first structure elucidated of a compound containing both K and Mg in a complex was only reported in 1999. Reported by our own group, the inverse crown ether complex [{Me$_3$Si)$_2$N]$_4$K$_2$Mg$_2$(O$_2$)}$_\infty$] was generated from the reaction of "unrefined" *n*-butylpotassium, *n,s*-dibutylmagnesium, and HMDS(H) [HMDS(H) = 1,1,1,3,3,3-hexamethyldisilizane] in a ratio of 1:1:3.[31] Oxygen was not deliberately added to this reaction mixture, therefore the generation of this inverse crown ether complex was the result of adventitious oxygen, possibly present in the solvents or the amine as both were not deoxygenated before their employment. Many of the structures containing K and Mg, mostly reported by our

own group, were formed using the core reactants: a potassium source (*n*-butyl or benzyl); one molar equivalent of *n,s*-dibutylmagnesium; and three molar equivalents of an amine. Using this reaction mixture, when the amine is HMDS(H), generating the homoleptic magnesiate "KMg(HMDS)$_3$" (**4a**), many structural variants of this ate compound can be synthesised depending on the donor complexing to the alkali metal. For example, when **4a** is treated with one molar equivalent of the metal π-arene compound bis(benzene)chromium, in hexane, the one-dimensional chain complex [{K·[Cr(C$_6$H$_6$)$_2$]$_2$}$^+$[Mg(HMDS)$_3$]$^-$}$_\infty$] is isolated, where no metallation of the π-arene complex was identified, reflecting the limited basic character of HMDS.[32] Instead, one of the benzene rings from two distinct bis(benzene)chromium units ligates to the potassium cation, along with K···CH$_3$Si(Me)$_2$ agostic interactions to two methyl groups of the HMDS ligand, forming an ion-pair ate complex with the trigonal [Mg(HMDS)$_3$]$^-$ ion. In addition, one of the bis(benzene)chromium molecules forms a bridge to the K cation of a neighbouring molecule. However, when excess mesitylene (Mes) is added, a variant of this complex [{K·[Cr(C$_6$H$_6$)$_2$]$_{1.5}$·(Mes)}$^+${Mg(HMDS)$_3$$^-$}]$_\infty$ was formed in hexane, where the extended structure produces two-dimensional 6^3-nets with [Mg(HMDS)$_3$]$^-$ anions occupying the interstitial spaces between the ridged layers of adjacent sheets.[33] In contrast, when the cyclopentadienyl-based metallocene, ferrocene, was added to **4a** in a molar ratio of 1:1, in a hexane/toluene solvent environment, the discrete ion-pair complex [{K(η^5-ferrocene)$_2$(η^3-toluene)$_2$}$^+${Mg(HMDS)$_3$]$^-$}] was isolated (**scheme 4.1**).[34] Again, no metallation of the
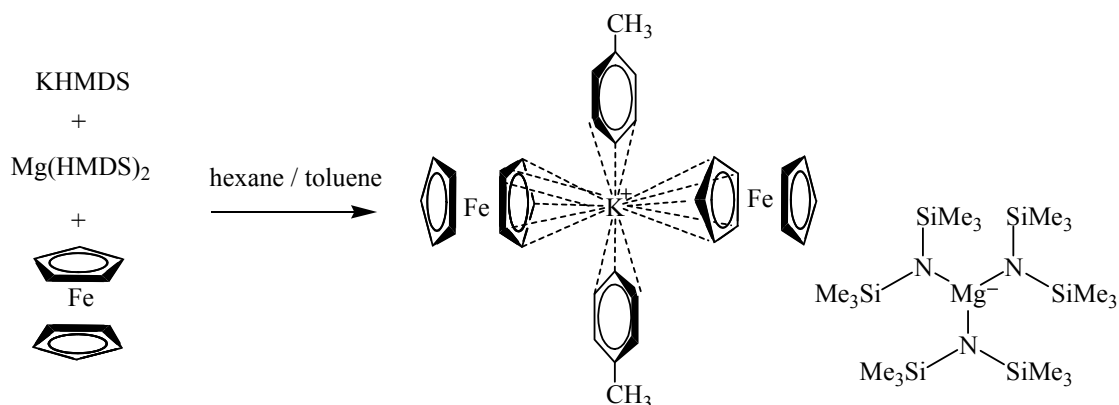
Scheme 4.1: Preparation of the discrete ion pair complex [{K(η^5-ferrocene)$_2$(η^3-toluene)$_2$}$^+${Mg(HMDS)$_3$}$^-$].

metallocene or the arene was observed; however, preliminary studies investigating the potential uses of this compound found that it could act as an initiator for the anionic polymerisation of methyl methacrylate (MMA).

Subjecting the ate mixture **4a** to excess benzene, toluene or *para*-xylene (in hexane solutions) was found to generate an array of solvated potassium magnesiate structures with formulae $[\{K(ar)_2\}^+\{Mg(HMDS)_3\}^-]_\infty$ (ar = arene).[35] Addition of benzene yielded a polymeric, linear chain, where each potassium atom bridges between two magnesiate anions *via* a K⋯Me interaction to one HMDS ligand from each anion. Also, two benzene molecules coordinate to the alkali metal to complete its coordination sphere. In the case of toluene, two supramolecular isomers could be isolated (**figure 4.1**). One is very similar to the benzene analogue, however, the potassium cation forms three K⋯Me interactions in total: one to magnesiate anion and two contacts to the other. Two toluene molecules further coordinate to each K atom. The other toluene analogue forms a discrete $[\{K(toluene)_2\}\{Mg(HMDS)_3\}]_2$ ring complex rather than a linear chain, linking *via* two K⋯Me contacts for each potassium atom. With respect to the para-xylene compound, its molecular structure is identical to the polymeric linear chain formed by toluene. As for the previously mentioned donor-solvated **4a** complexes, no metallation of the arene rings was observed.
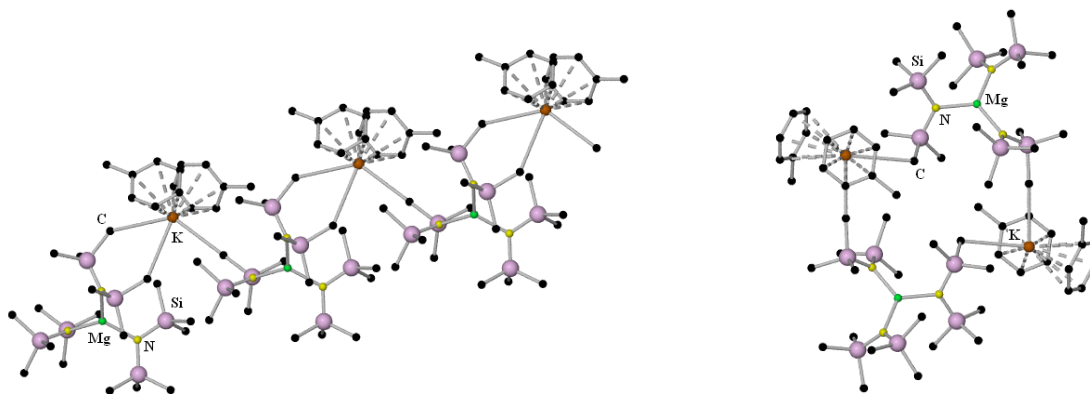
Figure 4.1: Two supramolecular isomers generated from toluene solvation of "KMg(HMDS)₃".

Moving to the less sterically encumbered amine diisopropylamine (DAH), it was reported that when benzylpotassium was reacted with *n,s*-dibutylmagnesium and DAH (1 and 3 molar

equivalents respectively), the unsolvated polymer $[K(\mu\text{-}DA)_2Mg(DA)]_\infty$ could be isolated and characterised by single crystal X-ray diffaction, as well as the TMEDA-solvate [TMEDA·K(μ-DA)$_2$Mg(DA)] (**figure 4.2**).[36] No metallation of toluene (which is produced by the protonation
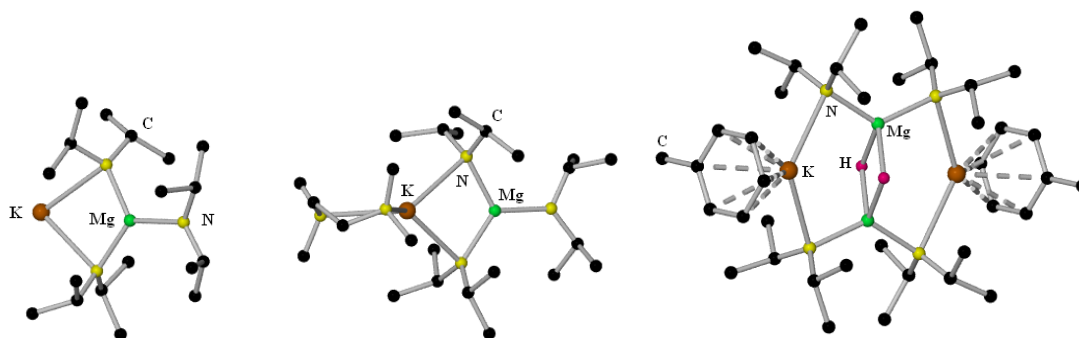
Figure 4.2: Molecular structures of the monomeric unit of the solvent-free DA polymer (LHS); TMEDA-solvated complex (central); and hydrido inverse crown (RHS).

of the basic benzylic group) was noted, hence the DA ligands in these complexes were shown to display weak basicity. Upon heating the KMg(DA)$_3$ reaction mixture, the hydrido inverse crown complex $[K_2Mg_2(N^iPr_2)_4(\mu\text{-}H)_2\cdot(toluene)_2]$ (**figure 4.2**) was produced and subsequently isolated in crystalline form.[37] It was suggested in the report that concomitant loss of the imine Me$_2$C=N^{i}Pr (upon heating the reaction mixture) leads to an attenuation of the steric crowding about the magnesium atom, thus clearing the way for dimerisation (**scheme 4.2**).
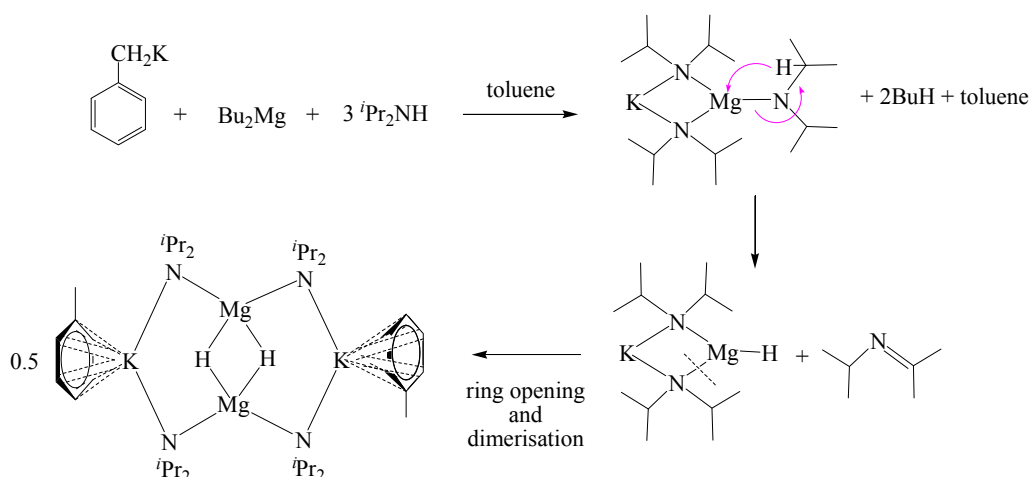
Scheme 4.2: Postulated intramolecular β-hydride transfer pathway.

In 2000, one of the most spectacular outcomes of AMM*Mg* arrived in the form of the 24-atom inverse crown ring complexes [(TMP)$_{12}$K$_6$Mg$_6$(C$_6$H$_4$R)$_6$] (R = H or CH$_3$) (**figure 4.3**).[38] This potassium-mediated magnesiation was accomplished through the action of *in situ* mixtures of
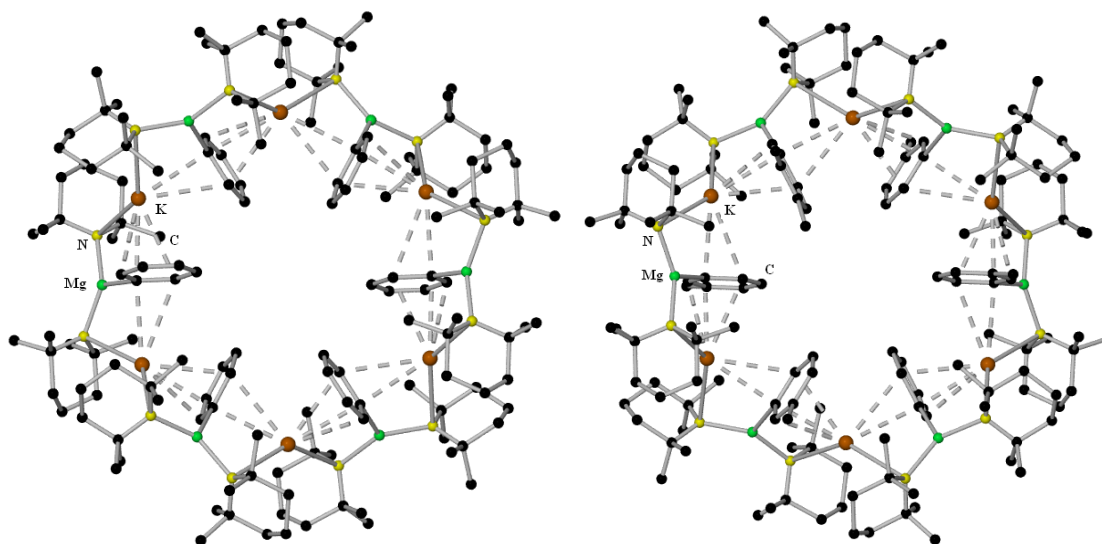
Figure 4.3: Molecular structures of the metallated benzene (LHS) and toluene (RHS) inverse crowns.

n-butylpotassium, *n,s*-dibutylmagnesium, and the amine TMP(H) on the relevant arene (benzene or toluene). These hexapotassium-hexamagnesium dodecaamide rings are the largest inverse crowns synthesised to date, and unlike the sodium/magnesium inverse crown (see Chapter 1, pages 35-38) structures where dideprotonation takes place, only a single deprotonation occurs with the potassium magnesium reagent (*meta*-magnesiation exclusively for toluene). One further example of a potassium magnesiate acting as a base (**figure 4.4**) occurs with the reaction mixture *n*-benzyl potassium, *n,s*-dibutylmagnesium, the amine TMP(H), and the bidentate ligand TMEDA, in a reactant ratio of

Figure 4.4: Molecular structure of [KMg{Cr(C$_6$H$_5$)(C$_6$H$_6$)}(TMP)$_2$·(TMEDA)].

1:1:3:1 respectively. In a report by our own group in 2005, upon addition of four molar equivalents of bis(benzene)chromium to the "[TMEDA·KMg(TMP)$_3$]" basic mixture, the compound [KMg{Cr(C$_6$H$_5$)(C$_6$H$_6$)}(TMP)$_2$·(TMEDA)] was generated.[32] Astonishingly, even a ratio of 1:10 of substrate to base results in the isolation of the monomagnesiated metal π-arene, with no twofold or higher deprotonation.

As recently as 2009, Zheng and co-workers reported the synthesis of potassium magnesiate complexes with a bulky diamido ligand.[39] From the reaction of silanediamine H$_2$[Me$_2$Si(Ndipp)$_2$]$_2$ (Dipp = 2,6-^{i}Pr$_2$C$_6$H$_3$) with ^{n}Bu$_2$Mg in *n*-hexane, the homometallic dimer [(μ-Mg){η^2:η^1-Me$_2$Si(Ndipp)$_2$}]$_2$ was isolated. This dimeric complex was then treated with two molar equivalents of potassium graphite (C$_8$K) in a reduction reaction step to afford the highly coordinated potassium magnesiate complexes [(η^6:η^6-K)$^+$]$_2$[Mg{η^2-MeSi(Ndipp)$_2$}$_2$]$^{2-}$ and [{η^6:η^6-K(THF)}{η^6:η^6-K(THF)$_2$]$^{2+}$[Mg{η^2-MeSi(Ndipp)$_2$}$_2$]$^{2-}$ (the latter complex was produced from the recrystallisation of the former compound in THF solution) (**scheme 4.3**).
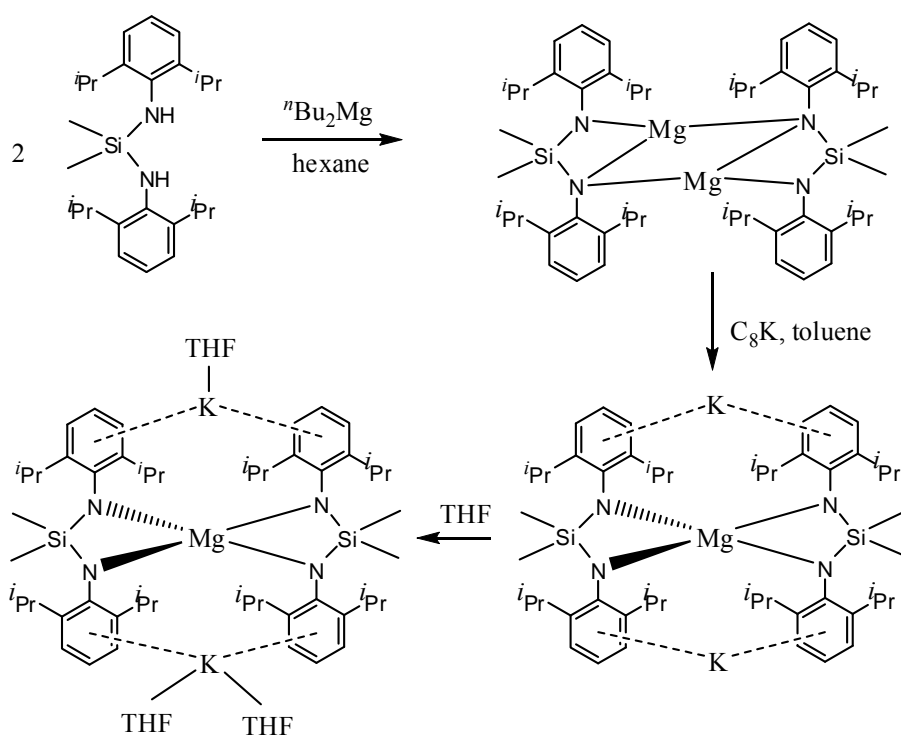
Scheme 4.3: Preparation of highly coordinated potassium silylamido magnesiate complexes.

In contrast to alkali-metal-mediated zincation (AMM*Zn*), which through more extensive study, has produced several examples of mixed alkyl-amido bases that have been prepared in solid form and structurally defined,[40,41] until this present work no potassium magnesiate base has been similarly prepared, characterised, or applied in metallation chemistry. Successful attempts to isolate and characterise K/Mg bases will now be discussed.

4.2) Synthesis of Potassium Magnesiate bases

As a starting point in this chapter, we fill this gap in knowledge by introducing the first examples of such mixed alkyl-amido potassium magnesiates characterised spectroscopically and X-ray crystallographically. The heteroleptic bases [PMDETA·K(μ-TMP)(μ-R)Mg(TMP)] {R = ^{n}Bu (**4b**) or CH$_2$SiMe$_3$ (**4c**)} were synthesised by two slightly different cocomplexation approaches in hexane solution (**scheme 4.4**) and each base was isolated, in crystalline form, in yields of 54%. It is noteworthy here that the addition of a further molar equivalent of TMP(H) to both **4b** and **4c** resulted in the recrystallisation of the bases, even after reflux conditions were applied.
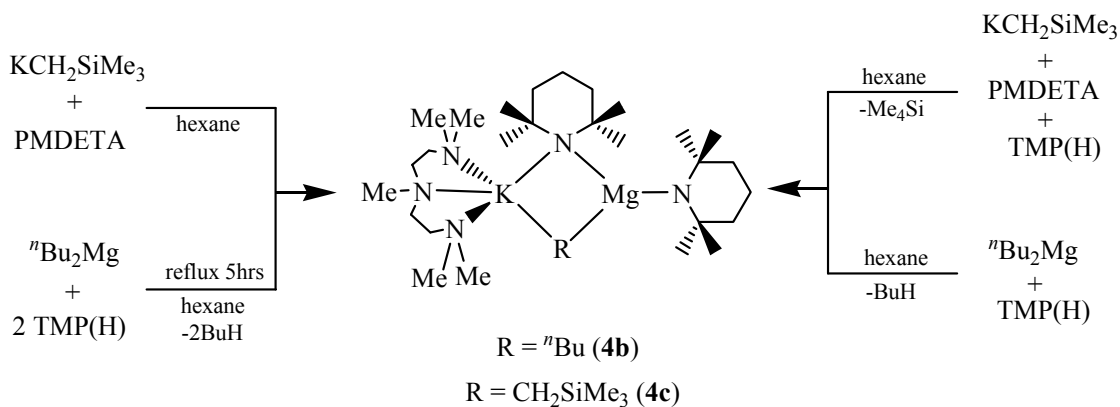
Scheme 4.4: Preparation of new potassium magnesiate bases 4b and 4c.

To fill in some of the gaps in the literature with regard to advances in potassium tris(amido)magnesiate chemistry, the complexes [PMDETA·KMg(amide)$_3$] were synthesised [where amide = DA (diisopropylamide) (**4d**) or the ligand DMP (*cis*-2,6-dimethylpiperidide) (**4e**)] using the reaction mixture of KCH$_2$SiMe$_3$, one molar equivalent of ^{n}Bu$_2$Mg and three molar

equivalents of the relevant amine, along with one molar equivalent of the tridentate ligand PMDETA (**scheme 4.5**). The isolated yields of **4d** and **4e** were both 54%. In a reversal of reactivity compared to the formation of TMP-based **4b** and **4c**, the addition of only two molar equivalents of either DA(H) or DMP(H) resulted in the isolation of the tris(amido) complexes. The Na congener of **4e**, [TMEDA·Na(μ-DMP)$_2$Mg(DMP)] (**4h**), was also synthesised as a comparison, and was isolated in a yield of 55%.
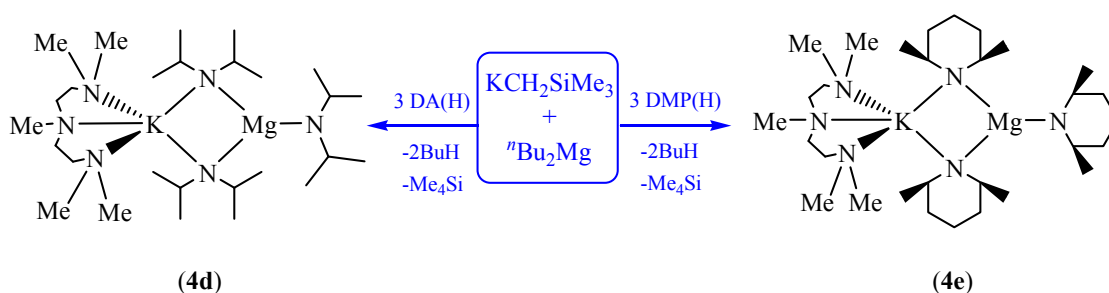
Scheme 4.5: Route to the PMDETA-solvated potassium tris(amido)magnesiates 4d and 4e.

4.2.1) Solid-State Analysis

Unfortunately the precision of the single crystal X-ray diffraction data of **4b** is relatively low, due to disorder both in the butyl arm and in the PMDETA ligand, limiting detailed comparison of bond lengths and dimensions; however, the molecular connectivity of this structure is unambiguous. A four element KNMgC ring, with a mixed TMP-^{n}Bu or TMP-CH$_2$SiMe$_3$ ligand set forms the central feature of the molecular structures of **4b** and **4c** respectively (**figure 4.5**). The structures are completed by a terminal TMP on Mg and a chelating PMDETA ligand on K. There exists significant disorder on the PMDETA ligand on **4c**, and as such only the remainder of the molecular structure will be discussed. In complex **4c**, the Mg anchors the anionic ligand set into a trigonal planar framework (sum of bond angles, 359.33°) through strong bonds of relatively high covalency, offering one triangular edge for the weaker, more electrostatic ancillary bonding of K. The significant difference in bond lengths of K to C and N [K(1)–C(1), 3.056(6) Å; K(1)–N(2), 2.927(4) Å] compared to Mg–C and Mg–N bond distances [Mg(1)–C(1), 2.065(4) Å; Mg(1)–N(2), 2.065(4) Å] is consistent with this picture. The geometry of the trigonal

planar Mg is distorted due to the steric bulk of the two TMP groups, resulting in a wide N(1)–Mg(1)–N(2) angle [128.83(16)°] which is counterbalanced by a constricted N(2)–Mg(1)–C(1) endocyclic bond angle [111.5(2)°].
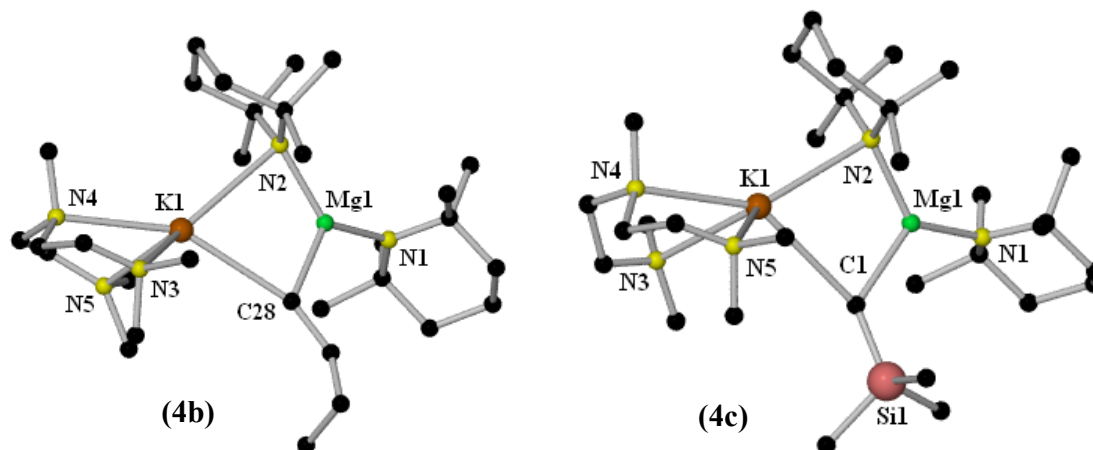
Figure 4.5: Molecular structures of 4b and 4c. Hydrogen atoms and disorder components are omitted for clarity.

Due to the fact of significant disorder displayed in the PMDETA ligand within **4c**, the structure of **4c** was optimised computationally by Dr. Jörg Sassmannshausen and Dr. Tell Tuttle to clarify its connectivity. The solid state structure was used as an initial starting geometry. The supplied structure showed severe disorder in the PMDETA ligand. This disorder was carefully removed with the Mercury program. The obtained structure was used as an input for the TURBOMOLE 6.0 program.[42] Two calculations were conducted, both with the def2-TZVP basis set for all atoms and the BP86 functional. In order to account for any dispersion effects, the second calculation was performed with the BP86-D [43-46] functional. The obtained structures were used for the generation of the wavefunction files by using the same basis set/functional approach.

The modelled structure **4c(a)** from the BP86 calculation is in reasonable agreement with the solid state structure (**figure 4.6**). As expected, the largest deviation is within the PMDETA part of the molecule. This can be easily explained by crystal packing effects. This assumption is further

corroborated by the observed large dislocation at that part of the molecule in the solid state structure. Indeed, the RMSD (root mean square deviation) values for the calculated and solid
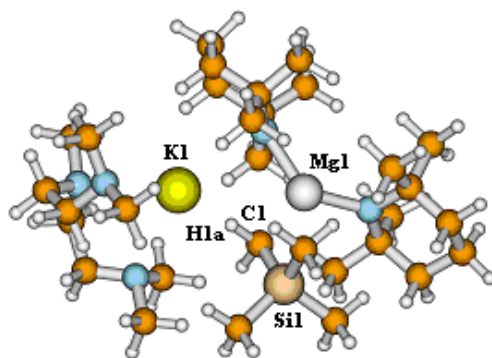
Figure 4.6: Graphical representation of 4c(a).

state structures are 0.6021 (all atoms), however neglecting the PMDETA part of the ligand gives a better value of 0.1817 (all atoms minus PMDETA). The Mg-C1 bond distance of 2.23 Å is in good agreement with the observed value of 2.202(5) Å. The K-H1a bond distance of 2.57 Å, together with the K-H1a-C1 angle of 106.02°, are indicative of an agostic interaction. Indeed, Bader analysis [47-50] confirmed this possibility. A bond critical point is defined as a local maximum in two directions and is a local minimum in the third, i.e. a *saddle point* in three dimensions. A bond critical point appears between every pair of neighbouring bonded atoms, and its position on the *bond path* reflects the polarity of a bond). A bond critical point [bcp1] ($\rho(r)$ = 0.0125 and $\nabla^2\rho(r)$ = -0.01278 between K and H1a was obtained, together with a bonding path between K and H1a (*cf.* **figure 4.7**). These values are indicative of an agostic bond. For comparison, the values of the bond critical point between Mg-C1 are $\rho(r)$ = 0.0412 and $\nabla^2\rho(r)$ = -0.04114. Judging from the plot of the Laplacian, no charge concentrations on either C1, H1a or K were observed (**figure 4.8**).

Turning to the BP86-D calculation, The modelled structure **4c(b)** (**figure 4.9**) is in reasonable agreement with the structure obtained via the X-ray crystallographic studies. The calculated structure is similar to **4c(a)**, however, probably the most interesting difference is the slightly shorter bond distance between C1 and Mg (2.19 Å). The RMSD values (all atoms) are 0.5635 for

the complete molecule and 0.1813 for the PMDETA ligand removed. Thus the obtained structure is slightly in better agreement with the solid state structure. The K-H1a bond distance of 2.48 Å
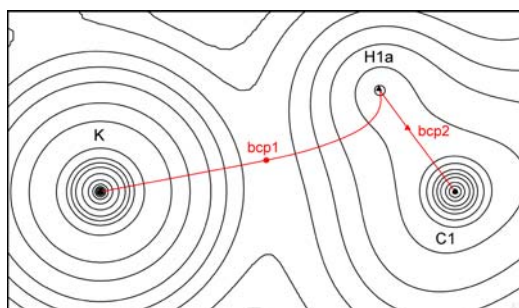
Figure 4.7: Electron density map of 4c(a).
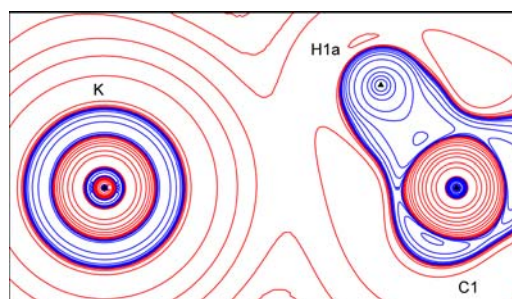
Figure 4.8: Laplacian map of 4c(a), standard values uses. Red: positive, blue: negative values.

and the K-H1a-C bond angle of are similar to the ones in **4c(a)** and are indicative for an agostic interaction. This was further corroborated by Bader analysis (cf. **figure 4.10**). Similar to **4c(a)**, a bond critical point bcp1 ($\rho(r)$ = 0.0145 and $\nabla^2\rho(r)$ = -0.01463) was obtained between K and H1a (**figure 4.10**). For comparison, the values of the bond critical point between Mg-C1 are
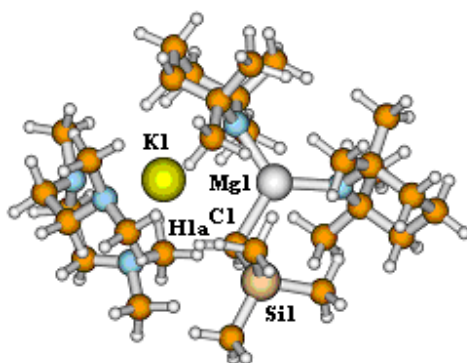
Figure 4.9: Graphical representation of 4c(b).

$\rho(r)$ = 0.0439 and $\nabla^2\rho(r)$ = -0.04626. NBO [51] (NBO = Natural Bond Orbital) analysis was carried out on **4c(b)**, using the BP86 functional in combination with the def2-TZVP basis set. An interaction was observed between the C-H bond consisting of 59.28% C($sp^{3.08}$) and 40.72% H(s)

and the empty K(s) orbital with a second order perturbation energy of E_{2P} of 1.87 kcal/mol (**figures 4.12-4.14**).
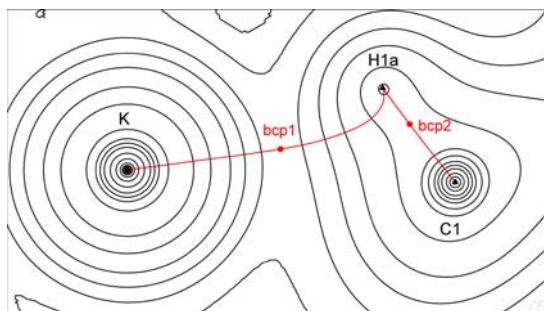
Figure 4.10: Electron density map of 4c(b).
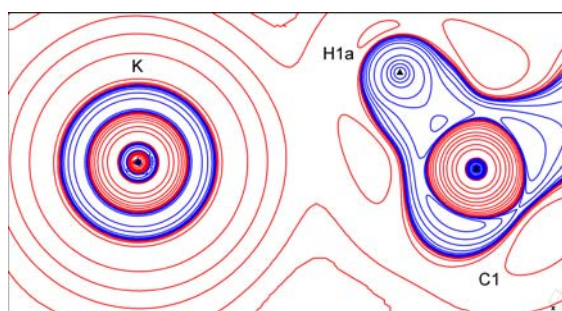
Figure 4.11: Laplacian map of 4c(b), standard values uses. Red: positive, blue: negative.

With regard to the calculations on complex **4c**, it can be concluded that in both cases evidence for an agostic interaction between K and H1a were obtained. The BP86-D functional appears to give slightly better results than the BP86 functional (without dispersion correction). Judging from Bader analysis and NBO calculations, there is strong evidence for the formation of an agostic bond between C1-H1a and K.
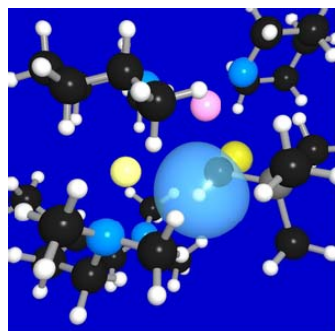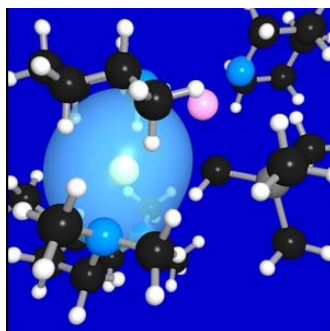
Figure 4.12: C—H bond.   **Figure 4.13: empty K(s) orbital.**   **Figure 4.14: CH -> K.**
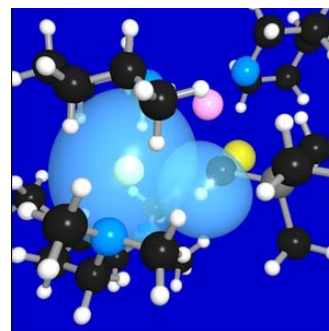
The molecular structures of the potassium tris(amido)magnesiates **4d** and **4e** closely resemble each other (**figure 4.15**). The bonding in these discrete molecular arrangements follows a similar pattern, as K forms a coordination sphere of 5 nitrogen atoms ($3 \times N_{PMDETA}$ and $2 \times N_{amide}$),

whereas Mg forms a trigonal planar geometry marked by shorter Mg–N$_{terminal}$ bonds [**4d**: Mg(1)–N(2), 1.9751(11) Å; **4e**: Mg(1)-N(1), 2.012(3) Å, Mg(1A)-N(1), 2.017(10) – due to disorder] in comparison to the longer Mg-(μ-N) bonds bond distances [**4d**: Mg(1)–N(1), 2.0517(11) Å; Mg(1)–N(3), 2.0565(12) Å. **4e**: Mg(1)–N(2), 2.0519(15) Å; Mg(1)–N(3), 2.0486(17) Å] in line with coordination number differences (that is, 3 for the terminal amide N and 4 for the bridging amide N). The longer K–N$_{amide}$ bonds [mean K–N$_{amide}$ bond lengths: **4d**, 2.960 Å; **4e**, 2.981 Å]
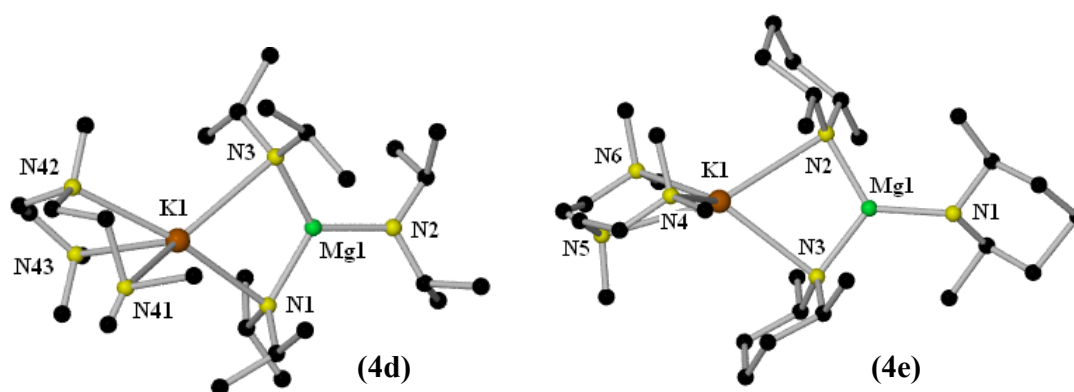
Figure 4.15: Molecular structures of 4d and 4e. Hydrogen atoms are omitted for clarity. Disorder components for the PMDETA ligand in 4d has been removed for simplicity.

represent the weak points of the tris-amido motif given that their Mg-(μ-N) counterparts are on average 0.932 and 0.949Å shorter, respectively. In the case of **4e**, the tridentate ligand fulfils the donor responsibility with dative K–N bonds (mean, 2.969Å) of the same magnitude as their anion-containing K-(μ-N) bond lengths. For comparison, as shown in **figure 4.2**, the unsolvated polymer [K(μ-DA)$_2$Mg(DA)]$_\infty$ (**4f**) and its TMEDA-solvate, [TMEDA·K(μ-DA)$_2$Mg(DA)] (**4g**), have already been crystallographically characterised (**table 4.1**).[36]

There is very little difference between the three structures, though not surprisingly, the bond properties of the PMDETA-solvate are closer to that of the TMEDA-bound ate complex. The major difference between **4d**, **4f,** and **4g** is the N$_{bridge}$–Mg–N$_{bridge}$ bond angle [118.03(5)^o, 112.74(8)^o and 113.87(6)^o respectively]. The N–Mg–N internal bond angle is widest in **4d**,

Table 4.1: Comparison of the metal–N$_{TMP}$ bond distances in 4d, 4f and 4g.

Compound (donor)	Mg–N$_{(bridging)}$ (Å)	Mg–N$_{(terminal)}$ (Å)	K–N$_{(bridging)}$ (Å)
4f (no donor)	2.0395(18), 2.0340(19)	2.0340(19)	2.9332(19), 2.9215(17)
4g (TMEDA)	2.0381(13), 2.0454(13)	1.9722(13)	2.8630(13), 2.9169(13)
4d (PMDETA)	2.0517(11), 2.0565(12)	1.9751(11)	2.9720(11), 2.9470(11)

possibly due to the weaker interactions that K plays with the bridging N of the DA ligands (as can be seen in **table 4.1**) as a result of the extra stability of the potassium cation by PMDETA.
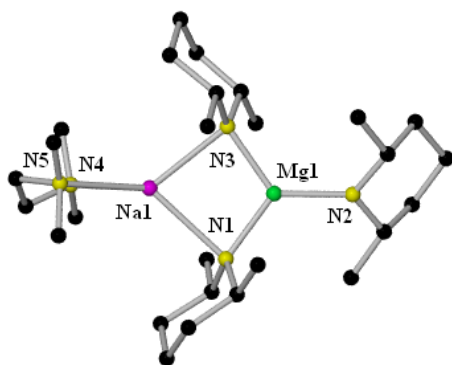
Figure 4.16: Molecular structure of (4h).

As a comparison for **4e**, the TMEDA-solvated sodium congener [TMEDA·Na(μ-DMP)$_2$Mg(DMP)] (**4h**) was investigated.[52] This complex was synthesised from the reaction of *n*-butylsodium, *n*-dibutylmagnesium, 2,6-*cis*-dimethylpiperidine and TMEDA in a molar ratio of 1:1:3:1, and could be isolated in a crystalline yield of 55% (**figure 4.16**). The metal–N core of the structure is a planar NaN$_{DMP}$MgN$_{DMP}$ ring (sum of endocyclic bond angles, 359.91°).

Three of the internal angles are acute and range from 81.09(4) – 86.59(4)°. The remaining internal angle N(1)–Mg(1)–N(3) is significantly wider [108.74(5)°], to accommodate the distorted trigonal planar geometry of the Mg centre [the associated angle in **4e** is larger, 112.76(6)°]. Four coordinate, the Na atom binds only to N atoms (two belong to N$_{DMP}$ anions and two to the bidentate TMEDA ligand). The coordination environment around Na is best described as highly distorted tetrahedral (sum of bond angles, 665.14°). As expected, the majority of this distortion is caused by the tight TMEDA bite-angle [71.13(4)°]. Turning to the bond distances, the Mg-N$_{bridging}$ bonds are longer (mean length, 2.050 Å) than the Mg-N$_{terminal}$ one [length, 1.9840(11) Å] – this is in accordance with the pattern seen in the K congener **4e** (with similar bond lengths noted). Perhaps counterintuitively, the two Na-N$_{bridging}$ bonds [Na(1)–N(1) and Na(1)–N(3)] have very different lengths [2.6263(12) and 2.4982(12) Å respectively; hence, Δ =

0.1281 Å]. Indeed, this former bond is essentially identical in length to the Na–N$_{TMEDA}$ dative bonds (mean distance, 2.6262 Å). The Na–N$_{DMP}$ bond distances in **4h** [mean, 2.562 Å] are expectedly much shorter than the K–N$_{DMP}$ bond lengths in **4e** [mean, 2.981 Å], and the pattern of one bond being longer than the other is common to this structure also [K(1)–N(2), 3.031 Å; K(1)–N(3), 2.932 Å]. Comparison of the Na–N$_{bridging}$ bonds with their aforementioned Mg–N$_{bridging}$ counterparts, the latter are more uniform (difference in length, 0.0119 Å) and are shorter (by on average 0.512 Å) implying that these are stronger bonds.

4.2.2) *Solution Studies*

Bases **4b**, **4d** and **4h** are soluble in arene solvents such as deuterated benzene, as is complex **4c** (this base was also analysed in deuterated d$_{12}$-cyclohexane solution as hydrolysis of the base was observed in every NMR spectrum run in C$_6$D$_6$ solution). The tris(amido) complex **4e** was analysed in deuterated d$_8$-THF solution. Hence, ^{1}H and ^{13}C NMR spectroscopic characterisation was obtained for these five isolated complexes.

The ^{1}H NMR spectrum of **4b** shows one set of resonances, which matches with the X-ray crystal structure data (**figure 4.17**). The resonance for the K–CH$_2$–Mg of the *n*-butyl group resides upfield at a high negative chemical shift of -0.69 ppm as a triplet. The other resonances associated with the alkyl ligand appear at 2.16 (CH$_2$, multiplet), 1.75 (CH$_2$, multiplet) and 1.26 (CH$_3$, triplet) ppm. The bridging and terminal TMP ^{1}H NMR resonances appear equivalent as only one set of TMP signals were observed in the spectrum, at 2.03 (2 × γCH$_2$), 1.64 (8 × CH$_3$) and 1.53 (4 × βCH$_2$) ppm, all without exception shifting downfield from the resonances of the free amine [at 1.53, 1.22 and 1.06 ppm for the γCH$_2$, βCH$_2$, CH$_3$ hydrogen atoms respectively]. This equivalency suggests that the structure is fluxional, with rapid exchange of the TMP ligand at room temperature. Another possibility is that the structure is separating in benzene solution into cation and anion pairs, that is with a discrete [Mg(^{n}Bu)(TMP)$_2$]$^-$ species. Resonance signals representing PMDETA complete the spectrum, located at δ = 1.84 (4 × CH$_3$, PMDETA) and 1.76-1.71 (1 × CH$_3$ and 4 × CH$_2$ of PMDETA) ppm, are found at a lower frequency in comparison to the chemical shifts of the free ligand resonances (range, 2.11–2.46 ppm).
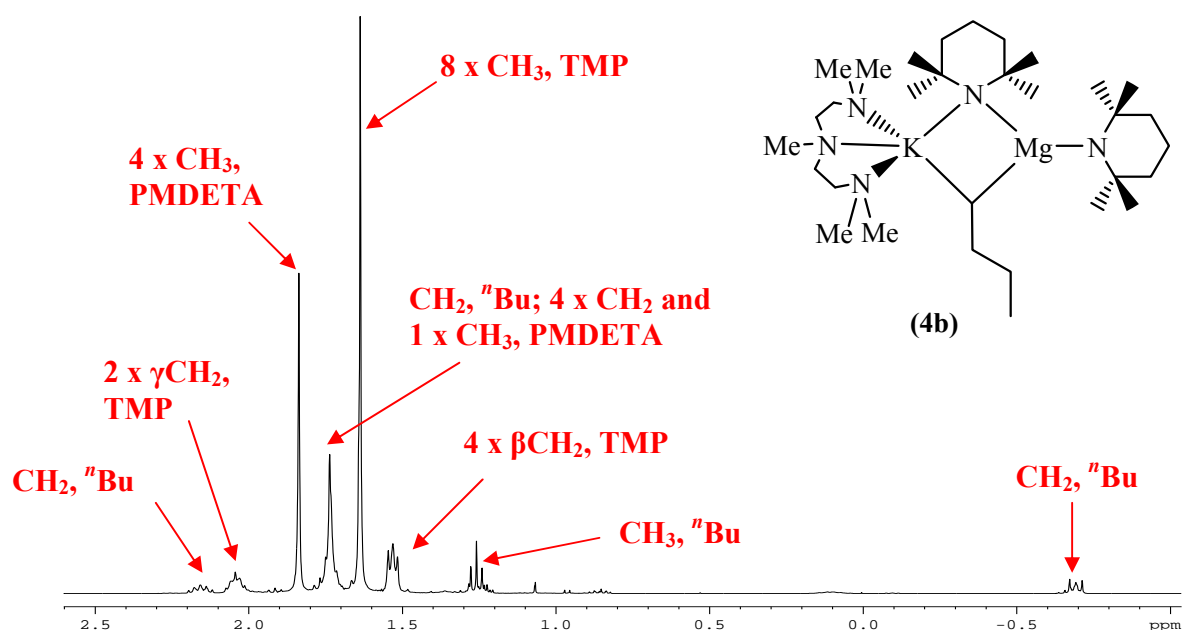
Figure 4.17: ^{1}H NMR spectrum of base 4b in C$_6$D$_6$ solution.

^{1}H and ^{13}C NMR spectroscopy of **4c** in deuterated d$_{12}$-cyclohexane solution produced well resolved spectra. Again, as for magnesiate **4b**, ^{1}H NMR spectroscopic analysis of **4c** reveals a pattern consistent with one type of compound (**figure 4.18**). The R group, in this case Me$_3$SiCH$_2$, produces two resonances, one at -2.11 ppm (CH$_2$) and the other at 0.01 ppm (3 × CH$_3$). The PMDETA ligand resonances [δ = 2.36, 2.23 and 2.22 ppm for the CH$_2$, terminal CH$_3$ and the central CH$_3$ hydrogen atoms respectively] lie very close to those of the free tertiary amine [^{1}H NMR chemical shift values of PMDETA standard in d$_{12}$-Cy solution: 2.40 and 2.29 (4 × CH$_2$), 2.19 (1 × CH$_3$) and 2.14 (4 × CH$_3$)]. As for the spectrum of **4b**, the resonances of the two TMP ligands (one bridging, one terminal in the crystalline structure) appear as one set of resonances in the ^{1}H NMR spectrum of **4c**, located downfield [1.72 (2 × γCH$_2$), 1.25 (8 × CH$_3$)] and upfield [1.21 (4 × βCH$_2$) ppm] in comparison to free TMP(H) [1.62 (2 × γCH$_2$), 1.06 (8 × CH$_3$) and 1.29 (4 × βCH$_2$) ppm].

The ^{1}H and ^{13}C NMR spectra of the tris(amido) complex **4d** are relatively straightforward to assign (**figure 4.19**). All of the amido ligands appear equivalent in the ^{1}H NMR spectrum. The resonances assigned to the diisopropylamide groups reside at 3.60 ppm (septet) and 1.44 ppm

162

(doublet) representing the CH and CH_3 components of the amide respectively. The PMDETA ligand displays resonance peaks at 1.88 ($4 \times CH_3$), 1.82 ($4 \times CH_2$) and 1.79 ($1 \times CH_3$) ppm in the ^{1}H NMR spectrum, consistent with the cation-bound amine.
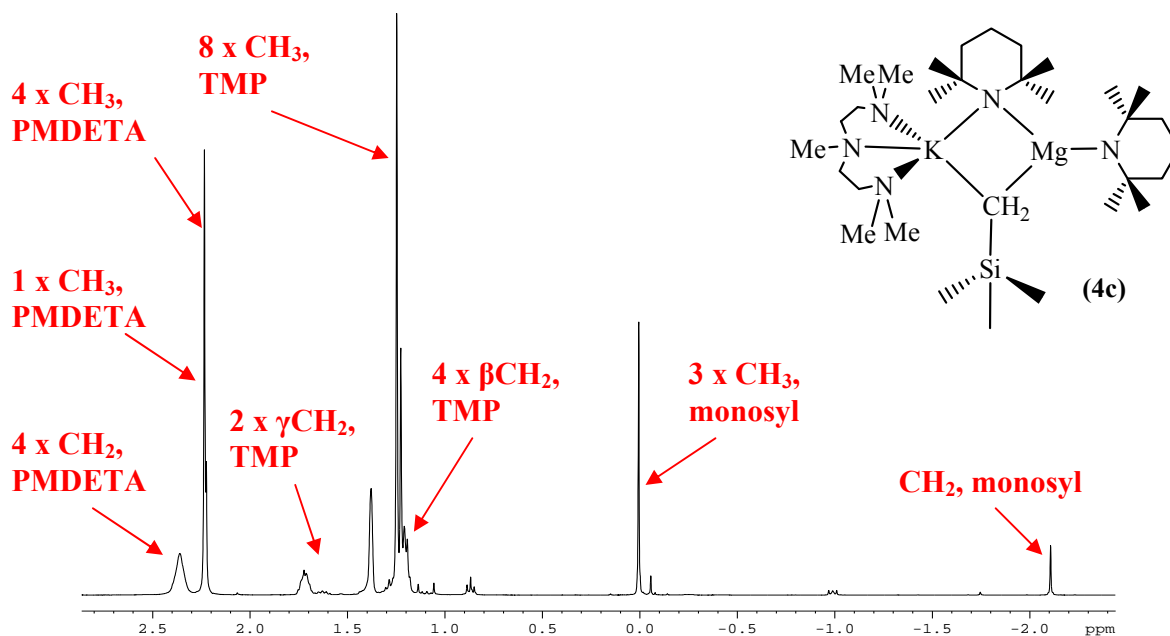
Figure 4.18: ^{1}H NMR spectrum of base 4c in d_{12}-cyclohexane solution.
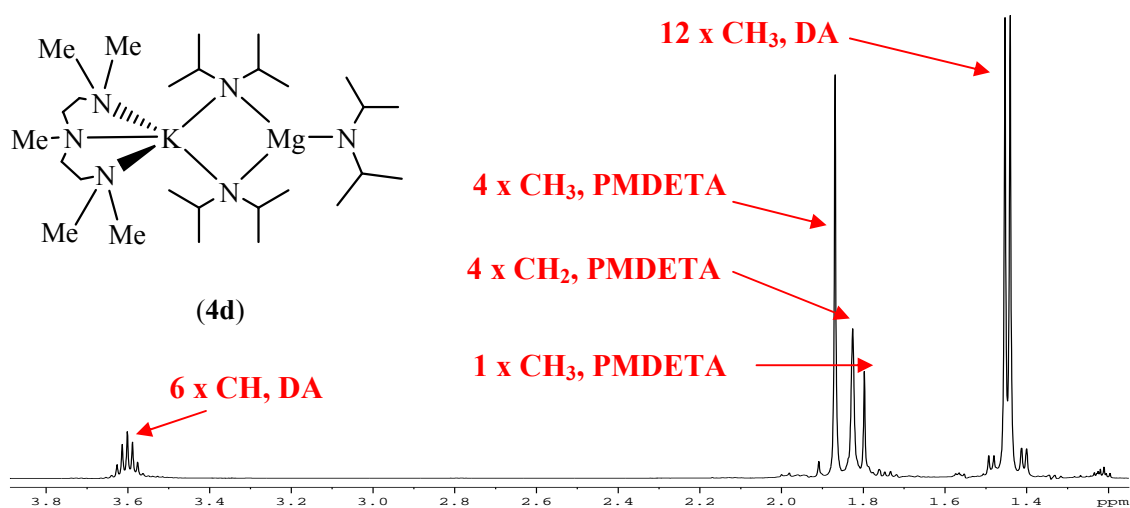
Figure 4.19: ^{1}H NMR spectrum of the ate complex 4d in C_6D_6 solution.

In comparison, the ^{1}H NMR spectrum of the chiral tris(amido) magnesiate **4e** is more complicated to assign. Insoluble in deuerated benzene and cyclohexane solution, the crystalline compound was dissolved in the ethereal solvent d$_8$-THF, which subsequently allowed NMR spectroscopic analysis (**figure 4.20**). For the assignment of the ^{1}H NMR spectrum of **4e**, two-dimensional (COSY and HSQC) techniques were used. Due to the chair conformation adopted by *cis*-DMP, four resonances are observed for the four chemically distinct β- and γ-H atoms. When deprotonated (and incorporated within the K/Mg framework), the resonances associated with *cis*-DMP show a downfield shift of the α-*H* (2.65 ppm), C*H*$_3$ (1.20 ppm), and γ-*H* (1.69 and 1.35 ppm) atoms and an upfield shift of the β-*H* atoms (1.26 and 0.74 ppm) compared to those of the free amine [α-*H*, 2.57 ppm; C*H*$_3$, 0.96 ppm; γ-*H*, 1.69 and 1.29 ppm; β-*H*, 1.48 and 0.90 ppm]. The resonances associated with PMDETA complete the spectrum, residing in the frequency range 2.47–2.17ppm. These resonances are almost identical for those of free PMDETA in d$_8$-THF solution, 2.48–2.15 ppm, and hence it could be said that the THF molecules replace the tridentate ligand on potassium.
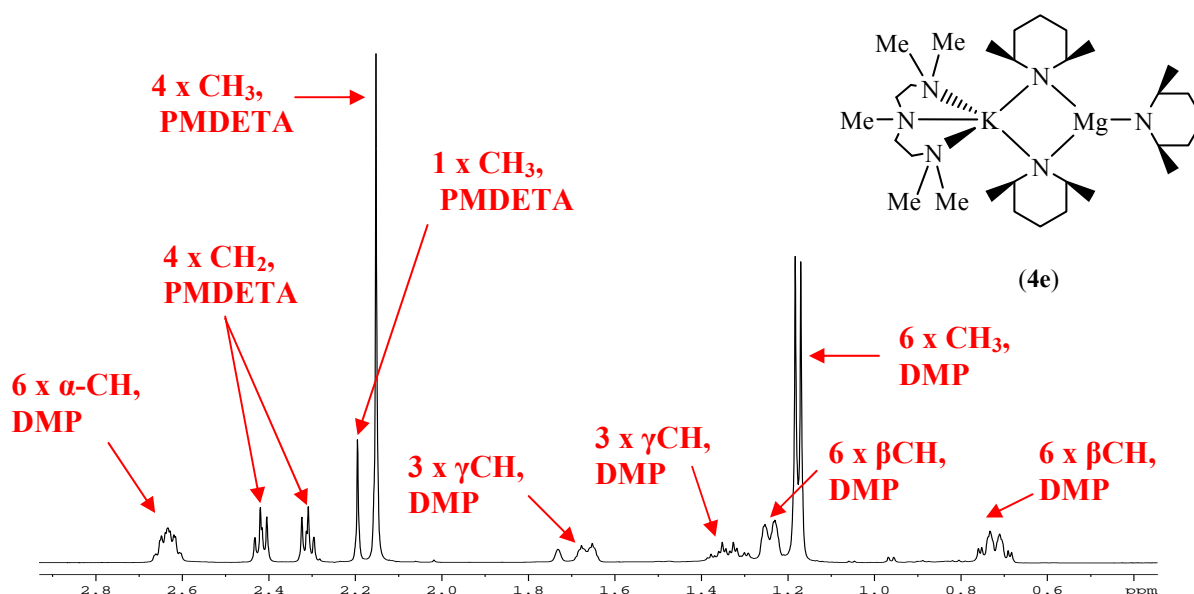
Figure 4.20: ^{1}**H NMR spectrum of complex 4e in d$_8$-THF solution.**

The ^{1}H NMR spectrum (**figure 4.21**) of the sodium congener **4h** (in C$_6$D$_6$ solution) exhibits broader resonances compared to those of **4e** [pattern of resonance shifts of DMP compared to

DMP(H): downfield shift of the α-*H*, C*H*$_3$, one β-*H* and one γ-*H* protons, and upfield shifts of the other β-*H* and γ-*H* protons are observed]. The C$_6$D$_6$ solution of magnesiate **4h** contains only one set of broad amido signals in the ^{1}H NMR spectrum suggesting that its solid-state structure may not be retained in solution (two distinct sets of signals, due to bridging and terminal amido ligands, would have been expected). This observation suggests that the chemically distinct *cis*-DMP ligands in **4h** undergo a dynamic fast exchange process in arene solution, or alternatively that **4h** forms a solvent-separated ion pair consisting of [Na·(arene)$_x$]$^+$ and [Mg(*cis*-DMP)$_3$]$^-$ moieties. To gain more insight into the solution behaviour of **4h** [and perhaps establish of how these tris(amido) magnesiates act in general] a low temperature ^{1}H NMR spectroscopic study of the magnesiate in d$_8$-toluene was conducted (**figure 4.22**). The main focus of the study was on the resonance for the α-C*H* protons. At 300 K, the resonance (3.05 ppm) was relatively broad. On cooling to 273 K, the resonance (3.03 ppm) broadened further without any sign of decoalescence. However, at 253 K, two distinct resonances (3.43 and 2.96 ppm) are present in a 1 : 2 ratio which can be attributed to terminal and bridging *cis*-DMP ligands respectively. These data suggest that in arene solution, **4h** does indeed undergo a fast dynamic exchange at ambient temperature, which is sufficiently slowed on cooling to 253 K.
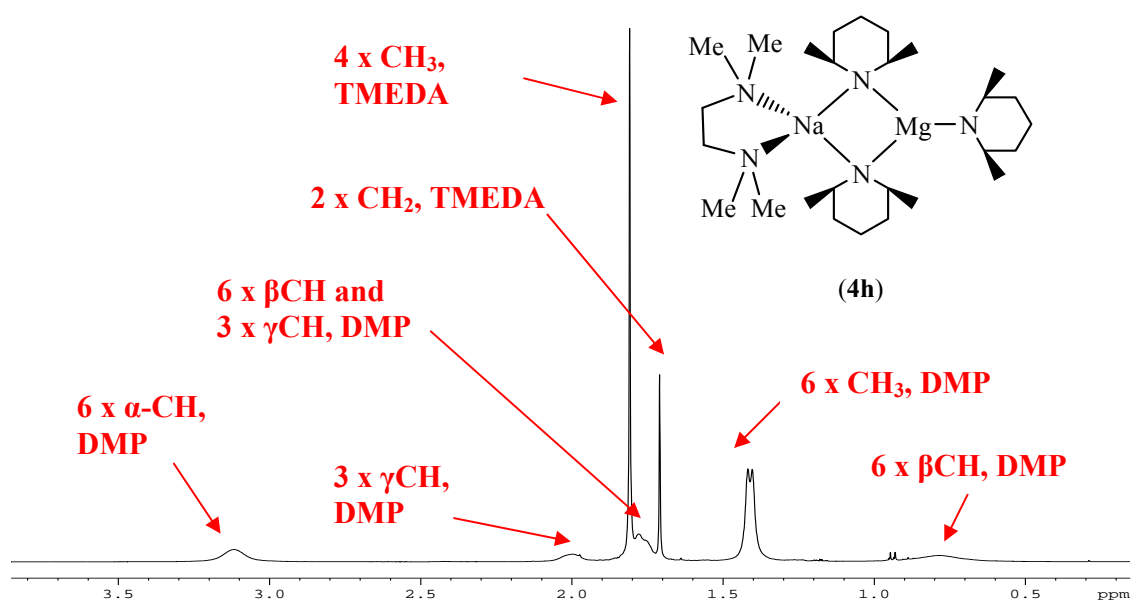
Figure 4.21: ^{1}H NMR spectrum of complex 4h in C$_6$D$_6$ solution.
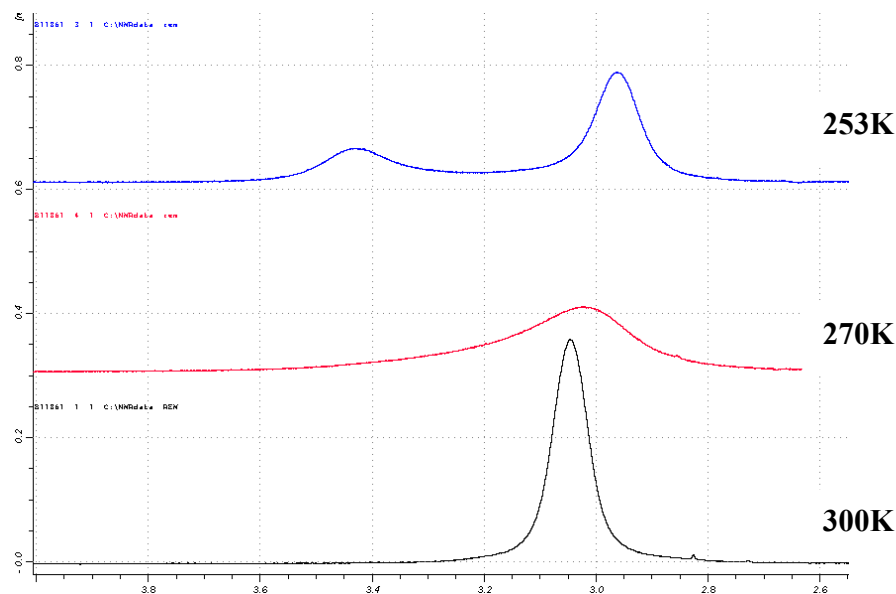
Figure 4.22: Variable temperature ^{1}H NMR spectra of complex 4h in $C_6D_5CD_3$ solution.

The attempted isolation of the PMDETA-solvated tris(HMDS) potassium magnesiate complex using the reactant ratio of 1:1:3:1 of KCH_2SiMe_3 : $^nBu_2Mg$: HMDS(H) : PMDETA, yielded a crystalline solid with a ^{1}H NMR spectrum (in d_8-THF solution) as shown in **figure 4.23**. Its integrals correspond to a ratio of 2 PMDETA : 3 HMDS, thus indicating that the isolated product is likely to have a discrete solvent-separated ion pair structure of formula $[\{(PMDETA)_2{\cdot}K\}^+\{Mg(HMDS)_3\}^-]$ (**4i**).
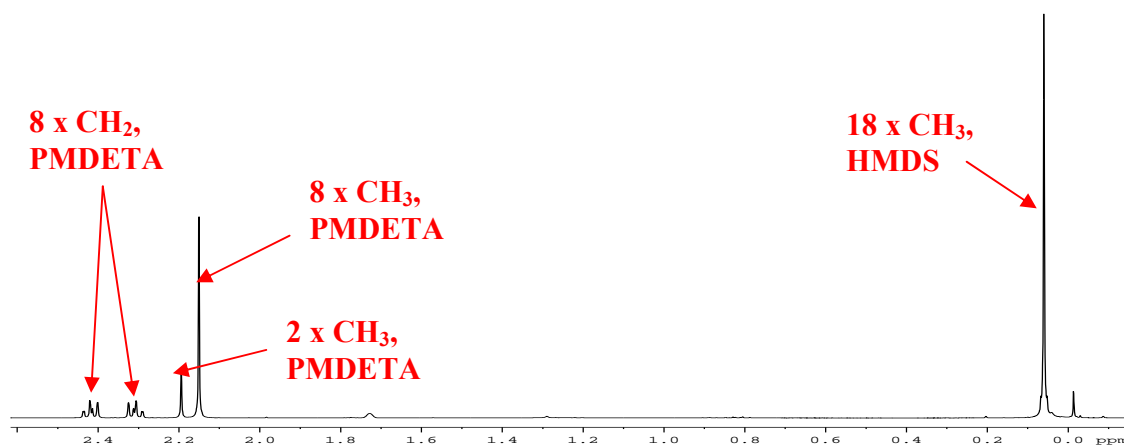
Figure 4.23: ^{1}H NMR spectrum of the isolated complex 4i in d_8-THF solution.

The successful isolation and characterisation of these potassium magnesiate (potential) bases allowed test deprotonation reactions to be carried out on functionalised aromatic substrates to quantify their metallation properties. These reactions are now discussed.

4.3) Deprotonation Reactions Using New Potassium Magnesiate Bases

The new base [PMDETA·K(μ-TMP)(μ-CH$_2$SiMe$_3$)Mg(μ-TMP)] **4c** was prepared *in situ* and reacted with the arene *N,N*-diisopropylbenzamide (an example of an arene with a strong electron-withdrawing amide group). This reaction deposited the crystalline product monoalkyl-monoamido complex [(PMDETA)·K(μ-TMP)(*o*-C$_6$H$_4$C(=O)N^{i}Pr$_2$)Mg(CH$_2$SiMe$_3$)] (**4j**). The bulk of the isolated product from this deprotonation reaction is **4j**, and reasoning for other minor products will be discussed in the solution study section. Depending on conditions, two distinct crystalline *ortho*-magnesiated anisole (an arene with an electron-donating methoxy group) complexes were produced from the reaction of anisole with **4c**, namely monoalkyl-monoamido [(PMDETA)·K(μ-TMP)(*o*-C$_6$H$_4$OMe)Mg(CH$_2$SiMe$_3$)] (**4k**) and bisamido [(PMDETA)·K(μ-TMP)(*o*-C$_6$H$_4$OMe)Mg(TMP)] (**4l**). The kinetic product is **4k** since it is the major product of the reactions carried out over a shorter timescale (about 2 h), although small amounts of **4l** are also detectable in the mixture. Over a longer timescale (4 days), **4l** predominates, marking it as the thermodynamic product, while the amount of kinetic **4k** in the mixture is considerably diminished. The reaction of **4c** with 4-methoxybiphenyl generated crystalline material of [(PMDETA)·K(μ-TMP){2-C$_6$H$_3$(1-OMe)(4-Ph)}Mg(TMP)] (**4m**), as determined by ^{1}H NMR spectroscopy, in a clean batch, isolated yield of 57%.

4.3.1) Solid-State Analysis

The molecular structure of **4j** (**figure 4.24, table 4.2**) can be classified as a contacted ion pair, displaying an unusual distorted tetrahedral Mg(C,C,N,O) coordination comprising two terminal (*C*H$_2$SiMe$_3$ and *ortho*-metallated C) and two bridging ligands (TMP N and benzamide O). Defining the metallation as a magnesiation, the deprotonated *ortho*-C atom forms a strong σ bond with the Mg atom, but does not interact with the Na atom. Instead the aryl ligand bridges to
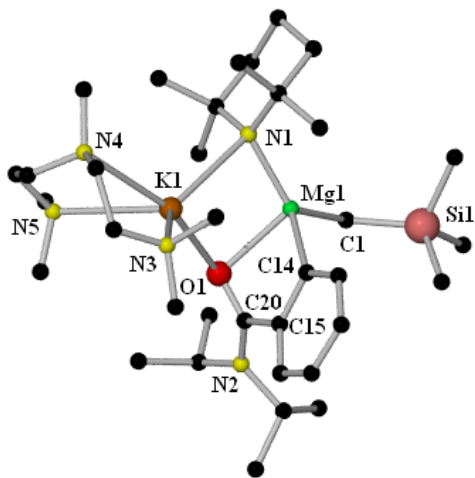
Figure 4.24: Molecular structure of the *ortho*-magnesiated product 4j.

K (and chelates to Mg) through its O-heteroatom. The bridging mode that O takes up establishes a structural core that is made up of a tricyclic arrangement consisting of three fused rings made up of two distinctly non-planar rings, one a four-atom, four-element KNMgO ring and the other a pentacyclic OMgCCC ring [sum of internal angles, 342.6° and 516.8° respectively], with the third having a planar benzene ring. These rings are fused at the Mg(1)–O(1) and C(14)-C(15) junctions, to generate an 11-membered outer ring. A tridentate PMDETA ligand completes the all-

heteroatom 5-membered coordination sphere (4 × N, 1 × O) of potassium. Magnesium occupies an unusual bonding environment made up of a N atom from the bridging TMP ligand [Mg(1)–

Table 4.2: Selected bond lengths (Å) and angles ($^{\circ}$) in complex 4j.

Mg1–O1	2.286(5)	Mg1–C1	2.193(6)	Mg1–C14	2.225(6)
Mg1–N1	2.059(5)	K1–N1	2.904(5)	K1–O1	2.827(4)
K1–N3	2.852(6)	K1–N4	3.021(5)	K1–N5	2.906(6)
K1–O1–Mg1	81.98(14)	K1–O1–C20	122.1(4)	Mg1–O1–C20	102.1(4)
K1–N1–Mg1	83.96(16)	N1–K1–O1	73.12(13)	N1–Mg1–O1	103.49(18)
N1–Mg1–C1	123.8(2)	N1–Mg1–C14	120.1(2)	C1–Mg1–C14	113.1(2)
C1–Mg1–O1	106.1(2)	C14–Mg1–O1	75.43(19)	O1–C20–C15	116.3(5)
C20–C15–C14	114.3(5)	C15–C14–Mg1	108.7(4)		

N(1) 2.059(5) Å], an alkyl C [Mg(1)–C(1) bond length, 2.193(6) Å], an aromatic C [Mg(1)–C(14) bond length, 2.225(6) Å] and an O [Mg(1)–O(1) bond length, 2.286(5) Å] completing a distorted tetrahedral environment [mean angle subtended at Mg, 107.0°]. A search of the CSD revealed only two other examples where magnesium has a ligand set of two C's, a N and an O, in

the complexes [DABCO·{THF·MgMe$_2$}$_2$] [53] [DABCO = 1,4-diazabicyclo{2.2.2}octane] and [THF·Mg(^{n}Bu){C(SiMe$_3$)$_2$Si(Me)$_2$NMe$_2$}].[54] However, in these examples the O came from THF ligation and the N from a tertiary amine, meaning that these compounds are neutral, non-ate, species unlike the ate complex **4j**. A search of structures within the CSD where *N,N*-diisopropylbenzamide has been *ortho*-metallated yielded eight hits, seven of which were ate in origin (the other is a homometallic lithium dimer [55]). In all seven accounts (where the alkali metal is Li or Na, and the lower polarity metal is Al,[12,56,57] Zn,[58,59] or Mn [15]), the O atom of the metallated benzamide ligates to the alkali metal exclusively. In partial reversal of this trend, in the molecular structure **4j** the O atom ligates to both K and Mg with a size derived preference to the less polar divalent metal, as the heteroatom forms a substantially shorter metal–O dative bond by 0.541 Å in length [bond lengths: K(1)–O(1), 2.827(4) Å; Mg(1)–O(1), 2.286(5) Å]. Bonding around K consists of four longer K–N bonds in comparison to those to oxygen, three from PMDETA [lengths: K(1)–N(3), 2.852(6) Å; K(1)–N(4), 3.021(5) Å; K(1)–N(5), 2.906(6) Å] and one from a TMP bridge [K(1)–N(1), 2.904(5) Å]. Complex **4j** is the first structurally characterised *ortho*-magnesiated *N,N*-diisopropylbenzamide complex; however, there is one example of a manganated compound very similar to **4j**.[15] As mentioned previously in Chapter 1, reported by our own group, the bimetallic sodium-manganese base [(TMEDA)·Na(µ-TMP)(µ-CH$_2$SiMe$_3$)Mn(TMP)] reacts with the same benzamide [as an amido base releasing TMP(H)] generating an isolated crystalline product with the formula [(TMEDA)·Na(µ-TMP)(*o*-C$_6$H$_4$C(=O)N^{i}Pr$_2$)Mn(CH$_2$SiMe$_3$)] (**4m**) (**figure 4.25**). The major difference between the molecular structure of this manganated benzamide complex and that of **4j**, is that the O of the benzamide ligates exclusively to Na [Na–O bond length, 2.313(6) Å], rebuffing Mn, whereas O bridges between K and Mg, forming a closer interaction to Mg in **4j**. The other examples of alkali-metal-mediated metallation of *N,N*-diisopropylbenzamide involve the alkali

Figure 4.25: Molecular structure of the *ortho*-manganated benzamide complex 4m.

metals Li and Na combined with lower polarity metals such as Mn, Zn, and Al, however neither K, nor Mg, feature in any of these structures, thus complex **4j** represents the first structurally defined example of any magnesiation reaction of *N,N*-diisopropylbenzamide.

Anisole, a favourable substrate to test potential bases with,[60-67] was subjected to KM*Mg* (potassium-mediated magnesiation) with base **4c**. Coupled with the crystallographic characterisation of base **4c**, the isolation and characterisation of the kinetic intermediate [(PMDETA)·K(μ-TMP)(*o*-C$_6$H$_4$OMe)Mg(CH$_2$SiMe$_3$)] (**4k**) and the thermodynamic final product [(PMDETA)·K(μ-TMP)(*o*-C$_6$H$_4$OMe)Mg(TMP)] (**4l**) provide three still frames of the structural manoeuvres accompanying the reactions taking place in solution (see later). These last two molecular structures are shown in **figure 4.26**.

In both examples anisole is *ortho*-magnesiated. In **4k** and **4l**, Mg adopts its usual (in the context of AMM*Mg* bases and products) distorted trigonal-planar geometry and lies essentially coplanar with the aryl ring. The mean Mg-C$_{ortho}$ bond length (2.198 Å) lies at the top end of the range of corresponding bonds [2.132(6)–2.199(7) Å] in the unsymmetrical dimer [Mg{bis(ortho-anisyl)}(THF)]$_2$, the only previously reported C-magnesiated anisole structure – not made by direct magnesiation but through transmetallation from the mercury analogue (**scheme 4.6**).[68] Corresponding bonds within **4k** and **4l** show little variation [for example, K–N$_{TMP}$ bond
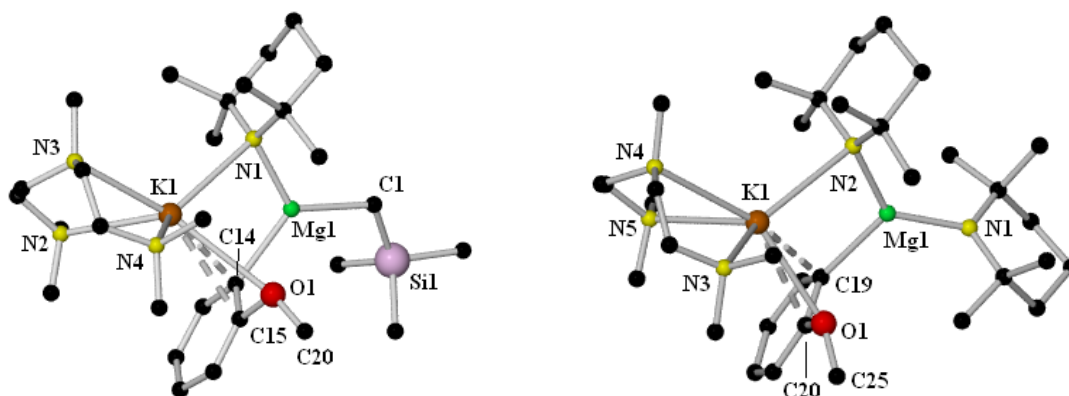
Figure 4.26: Molecular structures kinetic product 4k (left) and thermodynamic product 4l (right). Hydrogen atoms are omitted for clarity.

distances, 2.948(4) Å and 3.005(6) Å, respectively; mean K–N$_{PMDETA}$ bond distances, 2.907 Å and 2.893 Å respectively] with the exception of the dative K–O bonds [distances, 3.071(5) Å and 2.843(6) Å, respectively]. Probably as an artefact of the making of these ring closing K–O bonds, close topological contacts exist between K and the *ipso/ortho*(-magnesiated) C atoms of the anisole ligands [distances: K(1)–C(15) {3.187(5) Å} and K(1)–C(14) {3.216(5) Å} for **4k**; K(1)–C(20) {3.190(8) Å} and K(1)–C(19) {3.162(8) Å} for **4l**]. Structures **4k** and **4l** represent the first examples of structurally defined alkali-metal-mediated magnesiations of anisole. In addition, these are the first examples of direct magnesiation of this functionalised aromatic.
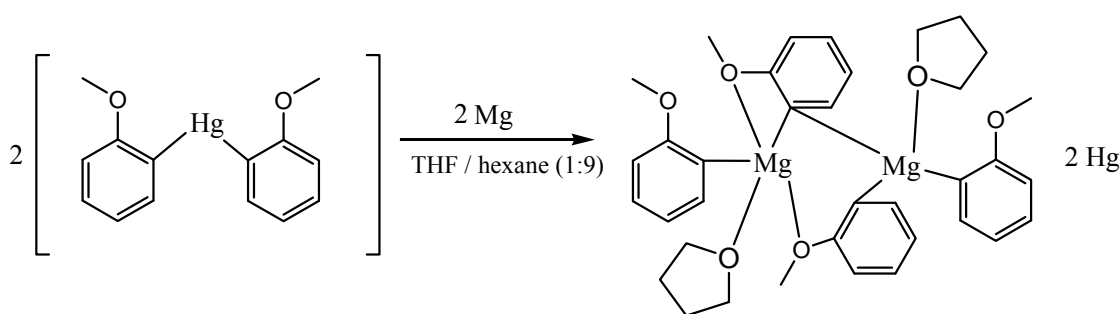
Scheme 4.6: Literature preparation of [Mg{bis(ortho-anisyl)}(THF)]$_2$.

4.3.2) *Solution Studies*

Compounds **4j–4m** are all soluble in deuterated benzene and, relatively unusually for highly polar potassium organometallics, deuterated cyclohexane solutions, which allows these complexes to be analysed by ^{1}H and ^{13}C NMR spectroscopic studies. The ^{1}H NMR spectrum (in C$_6$D$_6$ solution) of the isolated crystalline solid deposited from the reaction of **4c** with *N,N*-diisopropylbenzamide (**figure 4.27**) shows a mixture of several metallated aromatic products, however, **4j** is the major intermediate. Complex **4j** can be identified by the characteristic low frequency shift of the CH$_2$SiMe$_3$ group [at -1.28 (CH$_2$ attached to Mg) and 0.41 ppm (3 × CH$_3$)] . Resonances for the PMDETA ligand bound to K can be seen at 1.84 [4 × CH$_3$], 1.78 [4 × CH$_2$] and 1.75 ppm [1 × CH$_3$] and those attributed to TMP reside at 2.01 [1 × γCH$_2$], 1.58 [4 × CH$_3$] and 1.53 ppm [2 × βCH$_2$]. The ^{1}H NMR resonances associated with the ^{i}Pr methyl groups and the methine hydrogen atoms of the metallated benzamide substrate appear extremely broad coming in the range 1.55–0.70 and 5.13–2.55 ppm respectively. This broadening may be due to
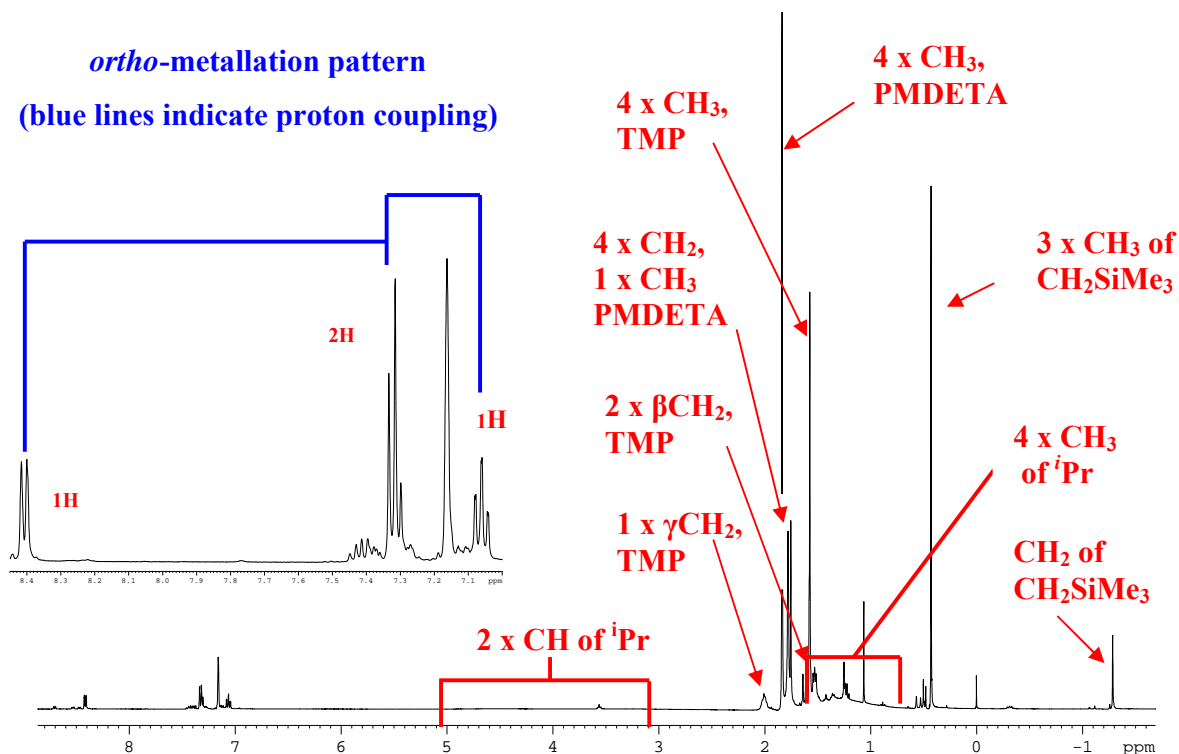
Figure 4.27: ^{1}H NMR spectrum of 4j in C_6D_6 solution, with inset showing the aromatic region.

the steric constraints of the benzamide unit bonding to K and Mg *via* dative interactions from O as seen in the solid state structure, hindering rotation of the ^{i}Pr groups. Resonances for the aromatic hydrogens of the metallated aryl ring can be identified at 8.41 (one H), 7.32 (two H) and 7.06 ppm (one H). Utilising two-dimensional (COSY and HSQC) techniques, an *ortho*-substituted pattern can be assigned (highlighted by the blue lines in **figure 4.27**). There are, however, extra resonances in the aromatic region, indicting that the isolated compound retains small quantities of another metallated species. Repeating the reaction of **4c** with *N,N*-diisopropylbenzamide and, leaving the reaction mixture to stir for three days, resulted in an oily reaction mixture which, upon loss of bulk solvent *in vacuo*, yielded a surprising ^{1}H NMR spectrum (in C_6D_6 solution). The *ortho*-metallation pattern was retained, yet no resonances attributed to the CH_2SiMe_3 group were observed. This suggested that perhaps a two-step reaction had taken place: in step 1, free TMP(H) is ejected by the deprotonation of the benzamide

substrate by base **4c**; then in step 2, the free amine becomes deprotonated, once more, by the alkyl ligand CH$_2$SiMe$_3$ with concomitant loss of tetramethylsilane (Me$_4$Si) to form bisamido [(PMDETA)·K(μ-TMP)(*o*-C$_6$H$_4$C(=O)N^{i}Pr$_2$)Mg(TMP)] (**4n**) (**Scheme 4.7**). To investigate this possibility, an NMR experiment (**figures 4.28 and 4.29**) was devised, dissolving the purest source of **4j** available in C$_6$D$_6$ and then subsequently adding one molar equivalent of TMP(H) into the NMR tube containing the dissolved base, under an inert atmosphere. Over a period of 21 hours, several ^{1}H NMR spectra were taken of the reaction mixture. Initially, only the resonances of **4j** could be observed, indicating that the reaction was slow. After 2 h had elapsed, resonances for **4n** could be seen in the aromatic region [δ = 8.43, 7.41 and 7.12 ppm; *cf.* 8.41, 7.32 and 7.06 ppm for **4j**] and the integration of the Me$_4$Si resonance had began to increase in relation to the alkyl group resonances (lowering in relative integration values). Over time this pattern continued, and after 21 h the resonances attributed to the aromatic region of **4j**, as well as those associated with the CH$_2$SiMe$_3$ group had almost disappeared, while a set of resonances indicative of an *ortho*-metallated product were still retained.

⬤ = [(PMDETA)·K(μ-TMP)(*o*-C$_6$H$_4$C(=O)N^{i}Pr$_2$)Mg(CH$_2$SiMe$_3$)] (**4j**)   ⬤ = [(PMDETA)·K(μ-TMP)(*o*-C$_6$H$_4$C(=O)N^{i}Pr$_2$)Mg(TMP)] (**4n**)
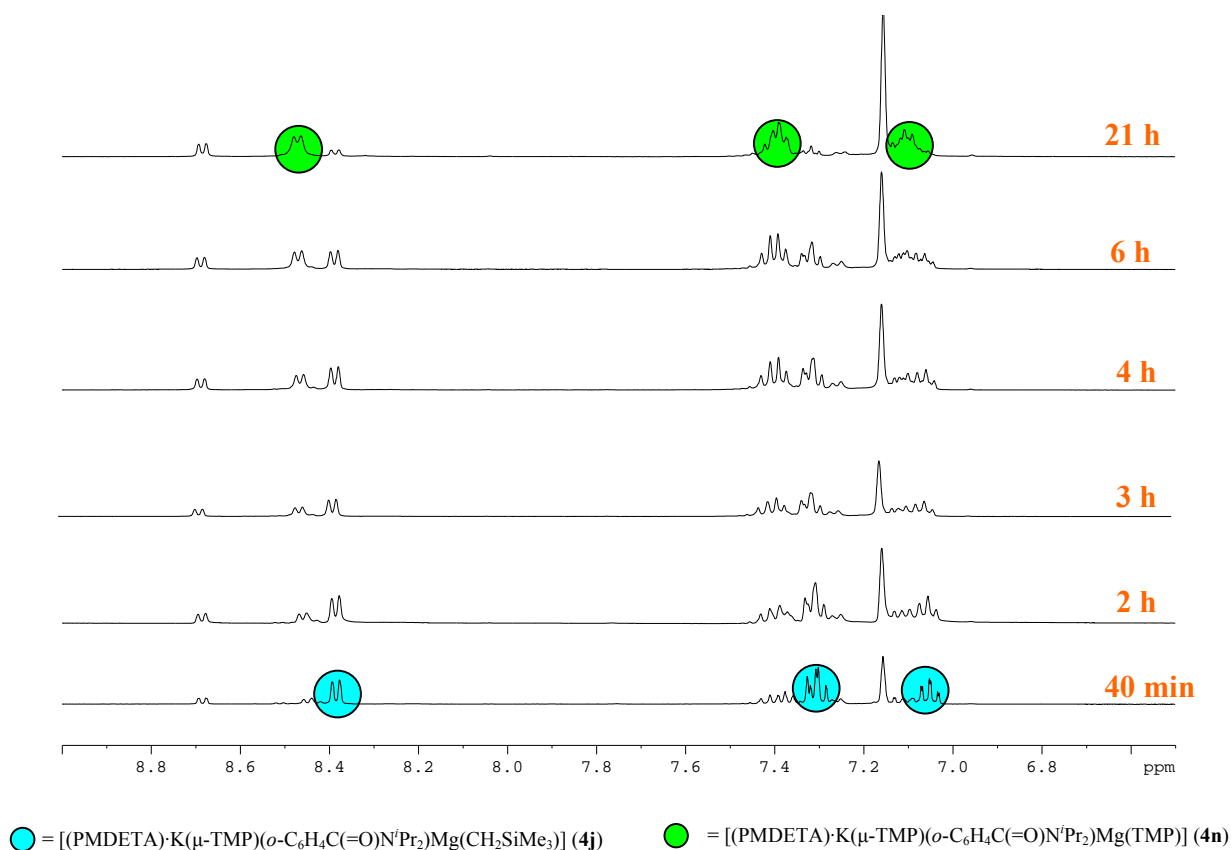
Figure 4.28: ^{1}H NMR study over 21 hrs. Aromatic region, C$_6$D$_6$ resonance at 7.16 ppm.
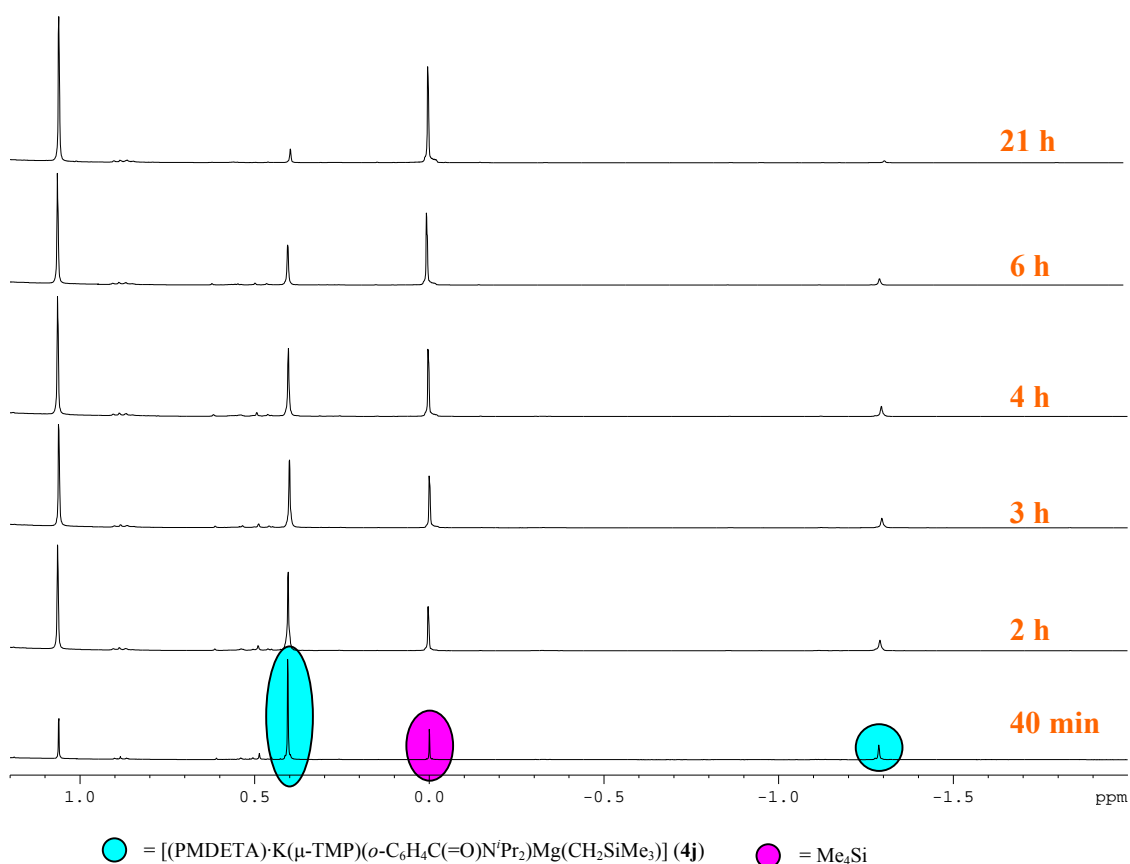
Figure 4.29: ^{1}H **NMR study over 21 hrs. Alkyl region, highlighting the gradual demise of** CH$_2$SiMe$_3$ **to Me$_4$Si over time.**
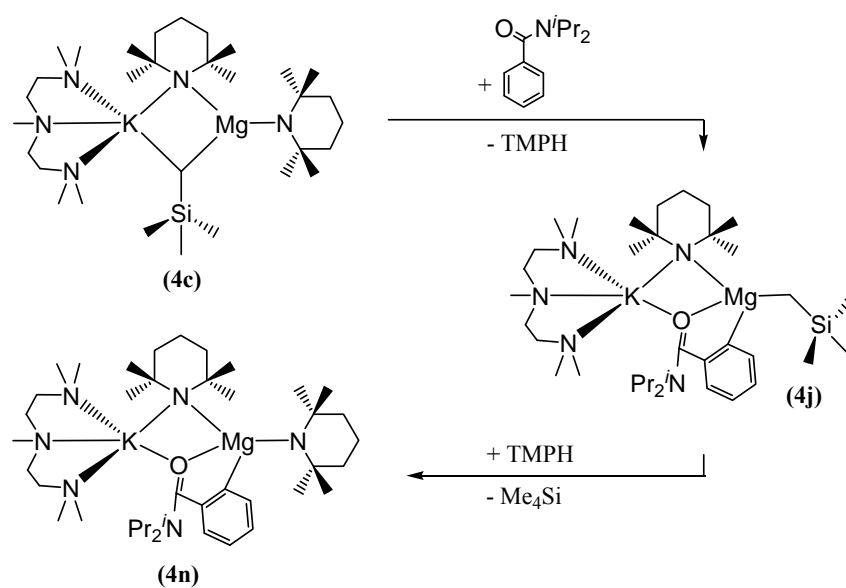
Scheme 4.7: Proposed two-step reaction of the KM*Mg* of *N*, *N*-diisopropylbenzamide.

With **4c**, **4k** and **4l** having distinct diagnostic resonances in their respective ^{1}H NMR spectra (see experimental section for full ^{1}H and ^{13}C NMR characterisation), a more comprehensive NMR experiment was attempted on the potassium-mediated magnesiation of anisole. This metallation reaction could be followed easily by recording spectra at different time intervals, similar to the previous NMR study discussed. Reactions of 1:1 mixtures of the base and anisole (0.15 mmol of each) were performed in NMR tubes under inert atmosphere with spectra recorded after 5 min, then at periods of 1, 3, 7, and 22 h (**figures 4.30 and 4.31**). After 5 min at ambient temperature, no reaction has taken place as best evidenced by resonances at 7.12 ppm (triplet of *meta*-H) and -2.11 ppm (singlet of CH_2SiMe$_3$) characteristic of unreacted anisole and base **4c**, respectively.

= [PMDETA·K(μ-TMP)(*o*-anisole)Mg(CH$_2$SiMe$_3$)] (**4k**)

= [PMDETA·K(μ-TMP)(*o*-anisole)Mg(TMP)] (**4l**)

= anisole
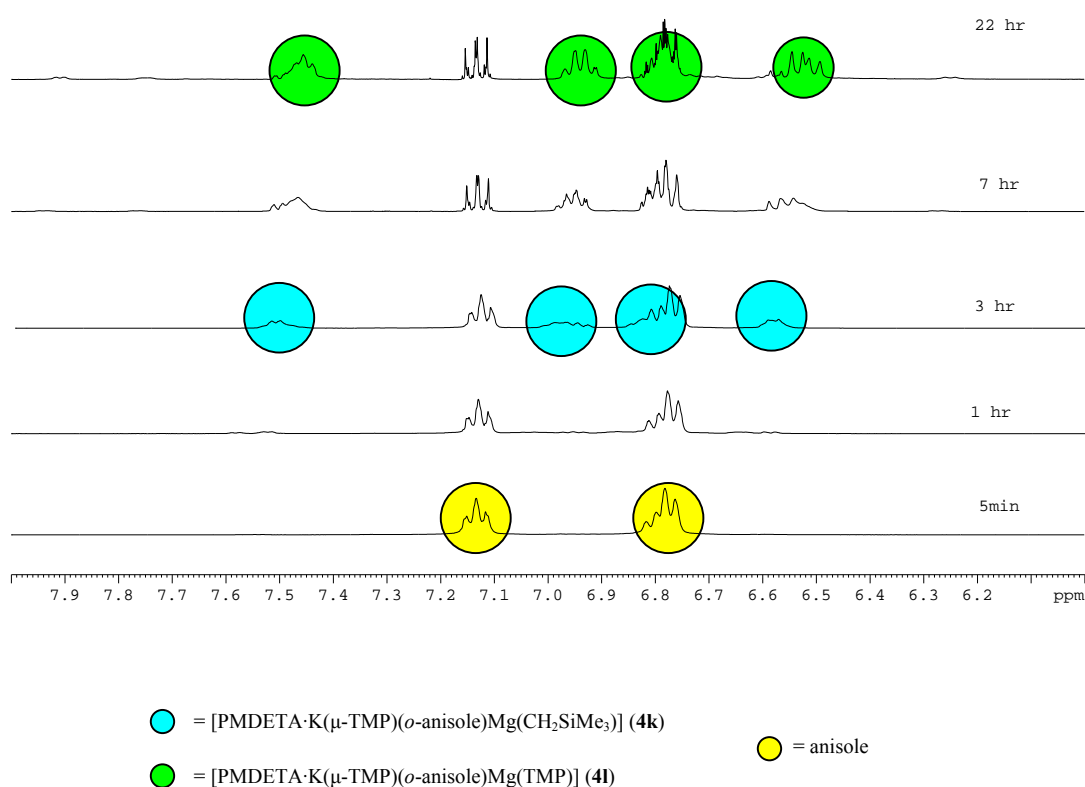
Figure 4.30: ^{1}H NMR study over 22 hrs in d$_{12}$-cyclohexane. Aromatic region.

After an hour, some of the starting materials are still present but **4k** has started to form, as seen in the emergence of a singlet resonance at -0.28 ppm (associated with CH$_2$Si*Me*$_3$, see 0.01 ppm in **4c**) and new anisole-derived aromatic resonances centred at 7.53, 6.94, 6.81, and 6.58 ppm. Concomitantly, characteristic resonances of free TMP(H), most prominently a singlet at 1.06

175

ppm denoting its CH_3 groups, also appears. This confirms the kinetic reaction is underway with base **4c** magnesiating anisole at the *ortho*-position to generate the alkyl-amido-arylmagnesiate product **4k** and at the same time releasing the amine TMP(H). After 3 h have elapsed the relative proportions of **4k** and TMP(H) grow substantially and at the same rate in comparison to the diminishing amounts of **4c** and anisole present. Reaching 7 h, **4k** is joined by the bisamido-arylmagnesiate product **4l** with a concomitant appearance of tetramethylsilane (Me$_4$Si), the product of protonating the alkyl ligand Me$_3$SiCH$_2^-$. Recorded after 22 h, the final spectrum establishes the dominance of the thermodynamic reaction with the major aromatic anisole resonances centred at 7.47, 6.96, 6.81, and 6.52 ppm denoting a high proportion of **4l** (accompanied by an increasing amount of Me$_4$Si), whereas there is a significantly reduced proportion of **4k**. **Scheme 4.8** summarises this dynamic reaction sequence.

⬤ = [PMDETA·K(µ-TMP)(µ-CH$_2$SiMe$_3$)Mg(TMP)] **(4c)**   ⬤ = 4 CH$_3$ of TMP(H)

⬤ = [PMDETA·K(µ-TMP)(*o*-anisole)Mg(CH$_2$SiMe$_3$)] **(4k)**   ⬤ = Me$_4$Si
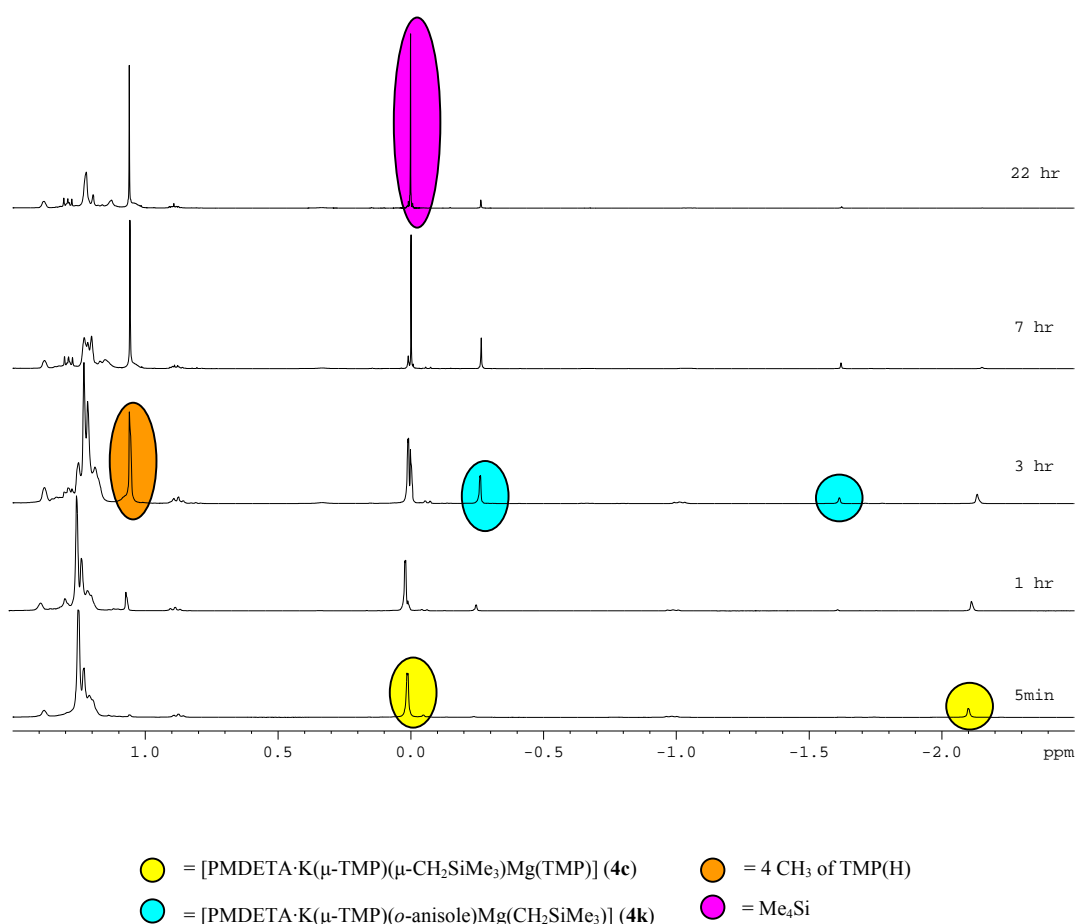
Figure 4.31: ^{1}H NMR study over 22 hrs in d$_{12}$-cyclohexane. Alkyl region
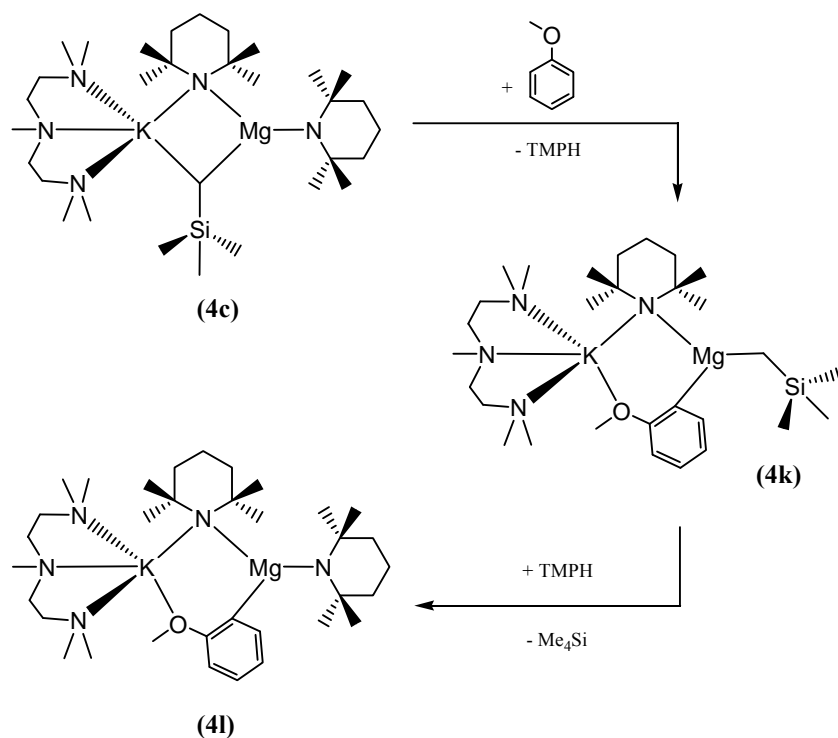
Scheme 4.8: Proposed two-step reaction for the KM*Mg* of anisole with base 4c.

The reaction of base **4c** with 4-methoxybiphenyl deposited long, thin needle-like crystals which were too narrow for X-ray crystollographic analysis. After stirring the solution (containing hexane predominately but also some THF) for 2hr, the Schlenk tube was placed in the refrigerator (at -4°C) to generate [(PMDETA)·K(μ-TMP){2-C$_6$H$_3$(1-OMe)(4-Ph)}Mg(TMP)] (**4m**) in an isolated yield of 57% (**scheme 4.9**). **4m** is readily soluble in arene solvents, therefore its ^{1}H (**figure 4.32**) and ^{13}C NMR spectra were obtained *via* NMR spectroscopic analysis of the sample in C$_6$D$_6$ solution.

The ^{1}H NMR spectrum of **4m** shows an *ortho*-metallation pattern, where the resonances associated with the untouched phenyl ring reside at 7.71 (2H, doublet of doublets, ^3J = 7.9 Hz), 7.29 (2H, triplet, ^3J = 7.2 Hz) and 7.13 ppm (1H, triplet, ^3J = 7.9 Hz). Resonances of the two coupling hydrogen atoms of the metallated ring are present at 7.35 (doublet of doublets, ^3J = 8.6 Hz) and 6.56 ppm (doublet, ^3J = 8.6 Hz). The last remaining aromatic hydrogen lies at the highest frequency in comparison to the other aromatic hydrogens, with its resonance lying at

8.19 ppm as a very narrow doublet (^4J = 2.4 Hz) due to coupling with the second *meta*-H (with respect to the methoxy group).
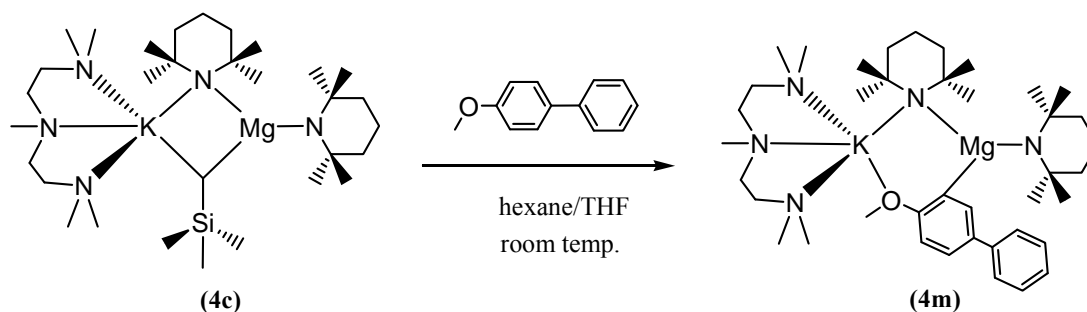
Scheme 4.9: KM*Mg* of 4-methoxybiphenyl with base 4c.
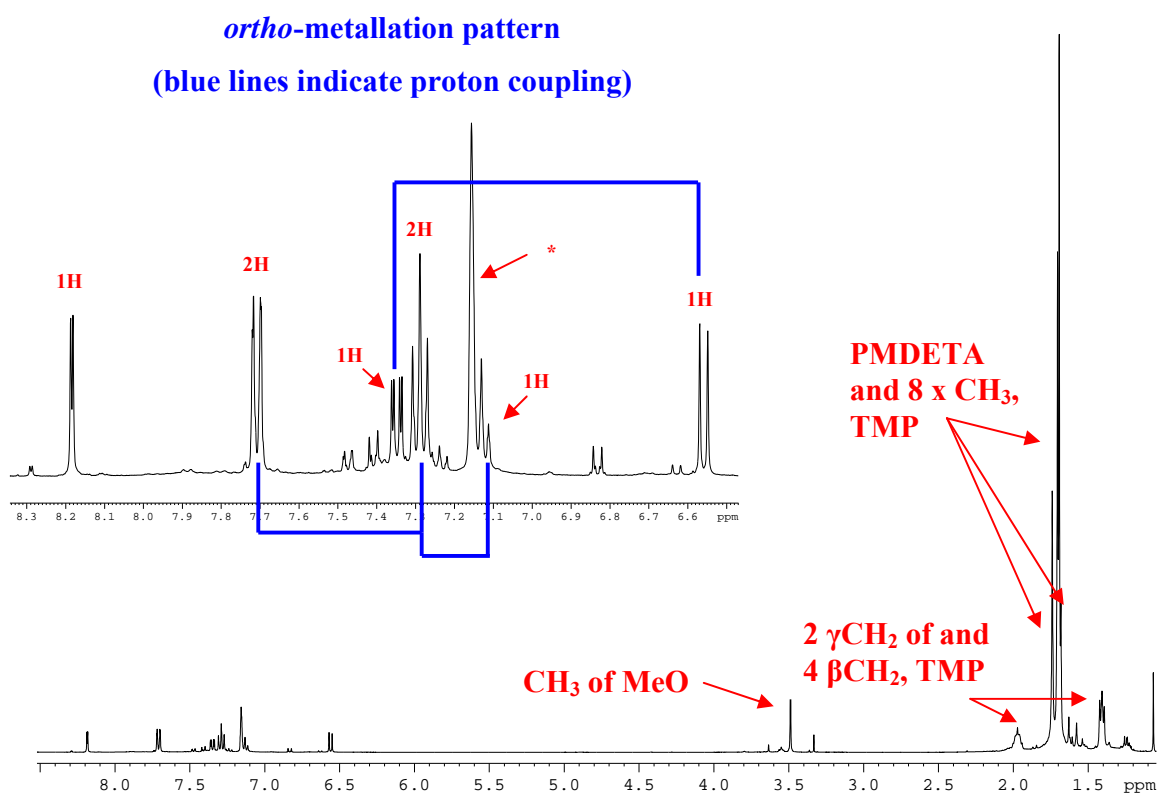
Figure 4.32: ^{1}H NMR spectrum of 4m in C$_6$D$_6$ solution. * represents the solvent resonance.

Within the ^{1}H NMR spectrum, resonances attributed to a small amount of the free biphenyl present in the aromatic region are visable, probably due to slight hydrolysis of the sample. The OMe resonance of **4m** occurs at 3.49 ppm, a downfield shift of 0.17 ppm compared to the equivalent resonance of free 4-methoxybiphenyl (3.32 ppm). Spanning the narrow region of 1.77–1.64 ppm in the ^{1}H NMR spectrum, the resonances of PMDETA and all the methyls of the TMP ligands can be found crowded together, with the remaining resonances of the γCH$_2$ and βCH$_2$ protons located at either side of this resonance pack, at 1.88 ppm and 1.41 ppm, respectively. The ^{1}H NMR spectrum of the reaction filtrate revealed a thick forest of resonances, some of which were attributed to **4m** and free 4-methoxybiphenyl; however, there are many unidentified resonances, possibly supporting the idea that the intermediate with formula [(PMDETA)·K(μ-TMP){2-C$_6$H$_3$(1-OMe)(4-Ph)}Mg(CH$_2$SiMe$_3$)] could be present.

Base **4c** appears to have acted ultimately as an alkyl base towards the arene substrate, however, from previous NMR studies on anisole and *N,N*-diisopropylbenzamide, it is likely that **4m** is the thermodynamic product, with the kinetic product being aforementioned "[(PMDETA)·K(μ-TMP){2-C$_6$H$_3$(1-OMe)(4-Ph)}Mg(CH$_2$SiMe$_3$)]". A search of the CSD revealed no examples of metallated 4-methoxybiphenyl (at any position). There is, however, a report of the *ortho*-lithiation (at -78°C) of the substituted arene with ^{s}BuLi and TMEDA leading to 3-hydroxy-4-methoxybiphenyl (in yields of 81-90%) after boronation and then oxidative work up (with H$_2$O$_2$) of the lithiated intermediate (**scheme 4.10**).[69] The major drawback of this earlier reaction involves the use of subambient temperatures, a complete contrast to the ambient temperature KM*Mg* approach introduced here. It should also be noted that unlike the work here no characterisation of any kind was performed on the lithiated intermediate.
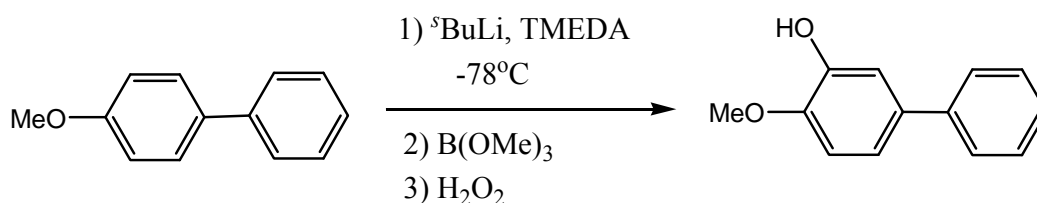
Scheme 4.10: Lithiation of 4-methoxybiphenyl at -78°C, followed by boronation and oxidative work-up.

The structural tracking and time-dependent NMR studies of the KM*Mg* of anisole carried out here represents the most complete study of any alkali-metal-mediated metallation to date, and has greatly improved fundamental knowledge of how such reactions work (that is, by a two step reaction as seen in AMM*Zn* chemistry) and will help towards the rational design of new synthetic applications in the future. An important consideration that this study brings out is that the timing of any subsequent electrophilic quench of the base-substrate reaction mixture may be critical to the outcome given the presence of different *ortho*-magnesiated products, though both should yield the same functionalised anisole product on electrophilic quenching.

The ability of the *n*-butyl base **4b** to act as a deprotonator towards the arenes *N, N*-diisopropylbenzamide, anisole and 4-methoxybiphenyl was investigated. For each substrate, metallation was observed in the ^{1}H and ^{13}C NMR spectra of the isolated material from the reaction mixture, however, a mixture of products (as well as unreacted base) was commonly found, therefore, for brevity, KM*Mg* with **4b** will not be discussed in any more detail. Further detailed NMR studies on the mechanism of base **4b** would be desirable to ascertain if this base acts, like **4c** (where liquid Me$_4$Si is eliminated in the final step), in a two-step manner, affording a closer comparison for the Na/Mg work,[32, 70-73] where it has always been perceived that a one step, gaseous alkane (*n*-butane) elimination occurs with the base [(TMEDA)·Na(μ-TMP)(μ-^{n}Bu)Mg(TMP)] towards a variety of organic substrates.

4.4) *Experimental Section*

Synthesis of [PMDETA·K(μ-TMP)(μ-^{n}Bu)Mg(TMP)] (4b)

Hexane (10 mL) was added to an oven-dried Schlenk tube containing 0.24 g (2 mmol) of KCH$_2$SiMe$_3$. 0.42 mL (2 mmol) of PMDETA, followed by 0.68 mL (4 mmol) of TMP(H) were injected into the reaction mixture to form a homogeneous solution. 2 mL (2 mmol) of 1M ^{n}Bu$_2$Mg (in hexane solution) were finally added to the Schlenk tube, which was stirred vigorously for 30 min before being placed in the freezer at -28°C to yield a crop of colourless crystals (0.63 g, 54%). ^{1}H NMR (400.13 MHz, 298K, C$_6$D$_6$): δ = 2.16 [2H, m, 1 × CH$_2$ of ^{n}Bu], 2.03 [4H, m, 2 × γCH$_2$ of TMP], 1.84 [12H, s, 4 × CH$_3$ of PMDETA], 1.77-1.70 [13H, m, 1 ×

CH$_2$ of ^{n}Bu, 1 × CH$_3$ of PMDETA and 4 × CH$_2$ of PMDETA], 1.64 [24H, s, 8 × CH$_3$ of TMP], 1.53 [8H, t, J = 6.0 Hz, 4 × βCH$_2$ of TMP], 1.26 [3H, t, J = 7.3 Hz, 1 × CH$_3$ of ^{n}Bu], -0.69 ppm [2H, t, J = 8.2 Hz, 1 × metal-CH$_2$ of ^{n}Bu]; ^{13}C{^{1}H} (100.62 MHz, 298K, C$_6$D$_6$): δ = 56.7 [2 × CH$_2$ of PMDETA], 55.1 [2 × CH$_2$ of PMDETA], 52.6 [4 × quaternary C of TMP], 44.7 [4 × CH$_3$ of PMDETA], 41.8 [4 × βCH$_2$ of TMP], 41.5 [1 × CH$_3$ of PMDETA], 35.4 [8 × CH$_3$ of TMP], 33.5 [1 × CH$_2$ of ^{n}Bu], 32.7 [1 × CH$_2$ of ^{n}Bu], 20.5 [2 × γCH$_2$ of TMP], 19.1 [1 × metal-CH$_2$ of ^{n}Bu], 14.5 ppm [1 × CH$_3$ of ^{n}Bu].

Synthesis of [PMDETA·K(μ-TMP)(μ-CH$_2$SiMe$_3$)Mg(TMP)] (4c)

Hexane (10 mL) was added to an oven-dried Schlenk tube followed by 2mL (2 mmol) of 1M ^{n}Bu$_2$Mg (in hexane solution) and 0.68 mL (4 mmol) of TMP(H). The reaction mixture was placed under reflux conditions for 5 h, and was then transferred, through a canula, to a separate Schlenk tube containing 0.24 g (2 mmol) of KCH$_2$SiMe$_3$. Next 0.42 mL (2 mmol) of PMDETA was added to produce a transparent yellow solution. The Schlenk tube was placed in the freezer at -28°C to yield colourless crystals (0.65 g, 54% yield). ^{1}H NMR (400.13 MHz, 298K, C$_6$D$_{12}$): δ = 2.36 [8H, m, 4 × CH$_2$ of PMDETA], 2.23 [12H, s, 4 × CH$_3$ of PMDETA], 2.22 [3H, s, 1 × CH$_3$ of PMDETA], 1.72 [4H, m, 2 × γCH$_2$ of TMP], 1.25 [24H, m, 8 × CH$_3$ of TMP], 1.21 [8H, t, J = 6.1 Hz, 4 × βCH$_2$ of TMP], 0.01 [9H, s, 3 × CH$_3$ of Me$_3$Si], -2.11 ppm [2H, s, metal-CH$_2$-Si]; ^{13}C{^{1}H} (100.62 MHz, 298K, C$_6$D$_{12}$): δ = 57.1 [2 × CH$_2$ of PMDETA], 55.3 [2 × CH$_2$ of PMDETA], 52.1 [4 × quaternary C of TMP], 45.0 [4 × CH$_3$ of PMDETA], 41.7 [1 × CH$_3$ of PMDETA], 41.1 [4 × βCH$_2$ of TMP], 34.9 [8 × CH$_3$ of TMP], 19.9 [2 × γCH$_2$ of TMP], 4.1 [metal-CH$_2$-Si], 4.0 ppm [3 × CH$_3$ of Me$_3$Si].

Synthesis of [PMDETA·K(μ-DA)$_2$Mg(DA)] (4d)

Hexane (10 mL) was added to an oven-dried Schlenk tube containing 0.24 g (2 mmol) of KCH$_2$SiMe$_3$. 0.42 mL (2 mmol) of PMDETA, followed by 0.84 mL (6 mmol) of DA(H) were injected into the reaction mixture. Finally, 2 mL (2 mmol) of 1M ^{n}Bu$_2$Mg (in hexane solution) was added to form a homogeneous solution. Note that heat was observed to be given off at this

point. The Schlenk tube was then placed in the freezer at -28°C to afford a set of colourless crystals (0.58 g, 54%). ^{1}H NMR (500.13 MHz, 298K, C_6D_6): δ = 3.60 [6H, septet, J = 6.3 Hz, 6 × CH of [i]Pr], 1.88 [12H, s, 4 × CH_3 of PMDETA], 1.82 [8H, m, 4 × CH_2 of PMDETA], 1.79 [3H, s, 1 × CH_3 of PMDETA], 1.44 ppm [36H, d, J = 6.7 Hz, 12 × CH_3 of [i]Pr]; [13]C{[1]H} (100.62 MHz, 298K, C_6D_6): δ = 56.8 [2 × CH_2 of PMDETA], 55.0 [2 × CH_2 of PMDETA], 49.6 [6 × CH of [i]Pr], 45.2 [4 × CH_3 of PMDETA], 41.7 [1 × CH_3 of PMDETA], 27.9 ppm [12 × CH_3 of [i]Pr].

Synthesis of [PMDETA·K(μ-DMP)₂Mg(DMP)] (4e)

Hexane (10 mL) was added to an oven-dried Schlenk tube containing 0.24 g (2 mmol) of KCH_2SiMe_3. 0.42 mL (2 mmol) of PMDETA, followed by 0.81 mL (6 mmol) of DMP(H) were injected into the reaction mixture. Finally, 2 mL (2 mmol) of 1M $^nBu_2Mg$ (in hexane solution) was added to form an opaque yellow solution, which upon stirring turned into a yellow suspension 15 min later. Note that heat was given off at this point. After 1.5 h stirring, 1.5 mL of THF were injected into the reaction mixture forming a homogeneous solution. The Schlenk tube was then placed in the freezer at -28°C to yield a crop of colourless crystals (0.46 g, 54%). ^{1}H NMR (500.13 MHz, 298K, d_8-THF): δ = 2.65 [6H, m, 6 × αCH of DMP], 2.43 [4H, m, 2 × CH_2 of PMDETA], 2.33 [4H, m, 2 × CH_2 of PMDETA], 2.21 [3H, s, 1 × CH_3 of PMDETA], 2.17 [12H, s, 4 × CH_3 of PMDETA], 1.69 [3H, m, 3 × γC(H)₂ of DMP], 1.35 [3H, m, 3 × γC(H)₂ of DMP], 1.26 [6H, m, 6 × βC(H)₂ of DMP], 1.20 [18H, d, J = 6.4 Hz, 6 × CH_3 of DMP], 0.74 ppm [6H, m, 6 × βC(H)₂ of DMP]; [13]C{[1]H} (100.62 MHz, 298K, d_8-THF): δ = 56.5 [2 × CH_2 of PMDETA], 56.1 [2 × CH_2 of PMDETA], 50.4 [6 × αCH of DMP], 43.4 [4 × CH_3 of PMDETA], 40.5 [1 × CH_3 of PMDETA], 32.4 [6 × $βCH_2$ of DMP], 24.5 [3 × $γCH_2$ of DMP], 20.6 ppm [6 × CH_3 of DMP].

Synthesis of [TMEDA·Na(μ-DMP)₂Mg(DMP)] (4h)

Hexane (10 mL) was added to an oven-dried Schlenk tube containing 0.16 g (2 mmol) of ^nBuNa, to which 2 mL (2 mmol) of 1M $^nBu_2Mg$ (in hexane solution) was added, followed by 0.81 mL (6

mmol) of DMP producing a yellow suspension. Addition of 0.30 mL (2 mmol) of TMEDA generated a homogeneous yellow solution. After 30 min stirring at room temperature, the Schlenk tube was placed in the freezer at -28°C which subsequently deposited a batch of colourless crystals (0.55 g, 55%).^{1}H NMR (400.13 MHz, 298K, C$_6$D$_6$): δ = 3.12 [6H, m, 6 × αCH of DMP], 2.00 [3H, m, 3 × γC(*H*)$_2$ of DMP], 1.81 [12H, s, 4 × CH$_3$ of TMEDA], 1.78 [9H, m, 3 × γC(*H*)$_2$ of DMP and 6 × βC(*H*)$_2$ of DMP], 1.76 [4H, s, 2 × CH$_2$ of TMEDA], 1.41 [18H, d, 6 × CH$_3$ of DMP], 0.79 ppm [6H, m, 6 × βC(*H*)$_2$ of DMP]; [13]C{[1]H} (100.62 MHz, 298K, C$_6$D$_6$): δ = 58.0 [6 × αCH of DMP], 57.6 [2 × CH$_2$ of TMEDA], 47.0 [4 × CH$_3$ of TMEDA], 38.6 [6 × βCH$_2$ of DMP], 27.4 [3 × γCH$_2$ of DMP], 27.2 [6 × CH$_3$ of DMP].

Synthesis of [{(PMDETA)$_2$·K}$^+${Mg(HMDS)$_3$}$^-$] (4i)

Hexane (10 mL) was added to an oven-dried Schlenk tube containing 0.24 g (2 mmol) of KCH$_2$SiMe$_3$. 0.42 mL (2 mmol) of PMDETA, followed by 1.26 mL (6 mmol) of HMDS(H) were injected into the reaction mixture. Finally, 2 mL (2 mmol) of 1M ^{n}Bu$_2$Mg (in hexane solution) was added to form a homogeneous solution. Note that heat appeared to be evolved at this point. After 5 h of stirring, the solution became opaque so 3 mL of THF was added and the Schlenk tube was placed into the freezer at -28°C. The next day a bilayer was observed, therefore all of the solvent was removed *in vacuo* and 5 mL of hexane was added to the residue, resulting in a white suspension. This suspension was filtered to reveal a white solid (0.20 g, 32%). ^{1}H NMR (400.13 MHz, 298K, d$_8$-THF): δ = 2.44 [8H, m, 4 × CH$_2$ of PMDETA], 2.33 [8H, m, 4 × CH$_2$ of PMDETA], 2.21 [6H, s, 2 × CH$_3$ of PMDETA], 2.17 [24H, s, 8 × CH$_3$ of PMDETA], 0.08 [54H, s, 18 × CH$_3$ of HMDS].

Synthesis of [(PMDETA)·K(μ-TMP)(*o*-C$_6$H$_4$C(=O)N^{i}Pr$_2$)Mg(CH$_2$SiMe$_3$)] (4j)

Hexane (10 mL) was introduced to an oven-dried Schlenk tube followed by 2mL (2 mmol) of 1M ^{n}Bu$_2$Mg (in hexane solution) and 0.68 mL (4 mmol) of TMP(H). The reaction mixture was placed under reflux conditions for 5 h, and was then transferred, through a canula, to a separate Schlenk tube containing 0.24 g (2 mmol) of KCH$_2$SiMe$_3$. Next 0.42 mL (2 mmol) of PMDETA was added to produce a clear yellow solution. 0.41 g (2 mmol) of *N,N*-diisopropylbenzamide was

also added to the reaction mixture, followed by 1 mL of THF to generate a homogeneous solution. After 1 h, the Schlenk tube was placed in the freezer at -28°C which yielded a batch of yellow crystals (0.73 g). ^{1}H NMR (400.13 MHz, 298K, C_6D_6): δ = 8.41 [1H, d, J = 6.9 Hz, 1 × aromatic CH], 7.32 [2H, m, 2 × aromatic CH], 7.06 [1H, t, J = 7.4 Hz, 1 × aromatic CH], 5.13–2.55 [2H, very broad m, 2 × CH of ^{i}Pr], 2.01 [2H, m, 1 × γCH$_2$ of TMP], 1.84 [12H, s, 4 × CH$_3$ of PMDETA], 1.78 [8H, m, 4 × CH$_2$ of PMDETA], 1.75 [3H, s, 1 × CH$_3$ of PMDETA], 1.58 [12H, s, 4 × CH$_3$ of TMP], 1.55–0.70 [12H, broad m, 4 × CH$_3$ of ^{i}Pr], 1.53 [4H, m, 2 × βCH$_2$ of TMP], 0.41 [9H, s, 3 × CH$_3$ of Me$_3$Si], -1.28 ppm [2H, s, 1 × metal-CH$_2$-Si]. ^{13}C{^{1}H} (100.62 MHz, 298K, C_6D_6): δ = 190.2 [1 × carbonyl C or metallated aromatic C], 180.1 [1 × carbonyl C or metallated aromatic C], 145.0 [1 × C$_{ipso}$], 142.4 [1 × aromatic CH], 128.1 [1 × aromatic CH], 124.4 [1 × aromatic CH], 122.5 [1 × aromatic CH], 57.3 [2 × CH$_2$ of PMDETA], 55.6 [2 × CH$_2$ of PMDETA], 53.1 [2 × quaternary C of TMP], 45.5 [4 × CH$_3$ of PMDETA], 43.0 [2 × βCH$_2$ of TMP], 42.1 [1 × CH$_3$ of PMDETA], 36.1 [4 × CH$_3$ of TMP], 21.8 [4 × CH$_3$ of ^{i}Pr], 21.2 [1 × γCH$_2$ of TMP], 5.7 [3 × CH$_3$ of Me$_3$Si], -1.3 ppm [1 × metal-CH$_2$-Si]. Note that the carbon resonances of the ^{i}Pr *C*H units could not be detected.

Synthesis of [(PMDETA)·K(μ-TMP)(*o*-C$_6$H$_4$OMe)Mg(CH$_2$SiMe$_3$)] (4k)

Hexane (10 mL) was added to an oven-dried Schlenk tube followed by 2mL (2 mmol) of 1M ^{n}Bu$_2$Mg (in hexane solution) and 0.68 mL (4 mmol) of TMP(H). The reaction mixture was placed under reflux conditions for 5 h, and was then transferred, through a canula, to a separate Schlenk tube containing 0.24 g (2 mmol) of KCH$_2$SiMe$_3$. Next 0.42 mL (2 mmol) of PMDETA was added to produce a clear yellow solution. 0.22 mL (2 mmol) of anisole was subsequently added to the reaction mixture, which was stirred for 2 h. The Schlenk tube was then placed in the freezer at -28°C to yield colourless crystals (0.41 g). ^{1}H NMR (400.13 MHz, 298K, C_6D_{12}): δ = 7.53 [1H, d, J = 6.4 Hz, 1 × aromatic CH], 6.94 [1H, t, J = 7.6 Hz, 1 × aromatic CH], 6.81 [1H, t, J = 6.5 Hz, 1 × aromatic CH], 6.58 [1H, d, J = 8.0 Hz, 1 × aromatic CH], 3.72 [3H, s, CH$_3$ of OMe], 2.27-2.23 [8H, m, 4 × CH$_2$ of PMDETA], 2.06 [15H, s, 5 × CH$_3$ of PMDETA], 1.72 [2H, m, 1 × γCH$_2$ of TMP], 1.35 [4H, t, J = 6.0 Hz, 2 × βCH$_2$ of TMP], 1.22 [12H, s, 4 × CH$_3$ of TMP], -0.28 [9H, s, 3 × CH$_3$ of Me$_3$Si], -1.60 ppm [2H, s, metal-CH$_2$-Si]; ^{13}C{^{1}H} (100.62 MHz,

298K, C_6D_{12}): δ = 163.0 [1 × C_{ipso}], 141.4 [1 × aromatic CH], 126.8 [1 × aromatic CH], 123.2 [1 × aromatic CH], 109.7 [1 × aromatic CH], 57.9 [2 × CH_2 of PMDETA], 56.5 [2 × CH_2 of PMDETA], 56.3 [1 × CH_3 of OMe], 52.7 [2 × quaternary C of TMP], 45.6 [4 × CH_3 of PMDETA], 42.2 [1 × CH_3 of PMDETA], 41.4 [2 × βCH_2 of TMP], 35.3 [4 × CH_3 of TMP], 20.9 [1 × γCH_2 of TMP], 4.3 [3 × CH_3 of Me_3Si], -3.8 ppm [metal-CH_2-Si].

Synthesis of [(PMDETA)·K(μ-TMP)(o-C_6H_4OMe)Mg(TMP)] (4l)

Hexane (10 mL) was added to an oven-dried Schlenk tube followed by 2mL (2 mmol) of 1M ^{n}Bu$_2$Mg (in hexane solution) and 0.68 mL (4 mmol) of TMP(H). The reaction mixture was placed under reflux conditions for 5 h, and was then transferred, through a canula, to a separate Schlenk tube containing 0.24 g (2 mmol) of KCH_2SiMe_3. Next 0.42 mL (2 mmol) of PMDETA was added to produce a clear yellow solution. 0.22 mL (2 mmol) of anisole was added to the reaction mixture, which was stirred for 4 days. The Schlenk tube was then placed in the freezer at -28°C to yield colourless crystals (0.44 g). ^{1}H NMR (400.13 MHz, 298K, C_6D_{12}): δ = 7.47 [1H, broad d, 1 × aromatic CH], 6.96 [1H, t, J = 7.2 Hz, 1 × aromatic CH], 6.81 [1H, t, J = 6.4 Hz, 1 × aromatic CH], 6.52 [1H, d, J = 7.8 Hz, 1 × aromatic CH], 3.60 [3H, s, 1 × CH_3 of OMe], 2.29-2.22 [8H, m, 4 × CH_2 of PMDETA], 2.09 [3H, s, 1 × CH_3 of PMDETA], 2.02 [12H, s, 4 × CH_3 of PMDETA], 1.67 [4H, m, 2 × γCH_2 of PMDETA], 1.24 [24H, s, 8 × CH_3 of TMP], 1.06 ppm [8H, m, 4 × βCH_2 of TMP]; $^{13}C\{^1H\}$ (100.62 MHz, 298K, C_6D_{12}): δ = 139.7 [1 × aromatic CH], 126.1 [1 × aromatic CH], 122.8 [1 × aromatic CH], 109.1 [1 × aromatic CH], 58.2 [2 × CH_2 of PMDETA], 56.9 [2 × CH_2 of PMDETA], 55.2 [1 × CH_3 of OMe], 52.7 [4 × quaternary C of TMP], 45.7 [4 × CH_3 of PMDETA], 42.7 [4 × βCH_2 of TMP], 42.5 [1 × CH_3 of PMDETA], 36.0 [8 × CH_3 of TMP], 20.6 ppm [2 × γCH_2 of TMP].

Synthesis of [(PMDETA)·K(μ-TMP){2-C_6H_3(1-OMe)(4-Ph)}Mg(TMP)] (4m)

Hexane (10 mL) was syringed into an oven-dried Schlenk tube followed by 2mL (2 mmol) of 1M ^{n}Bu$_2$Mg (in hexane solution) and 0.68 mL (4 mmol) of TMP(H). The reaction mixture was placed under reflux conditions for 5 h, and was then transferred, through a canula, to a separate

Schlenk tube containing 0.24 g (2 mmol) of KCH_2SiMe_3. Next 0.42 mL (2 mmol) of PMDETA was added to produce a clear yellow solution. 0.37 g (2 mmol) of 4-methoxybiphenyl was added to the reaction mixture, followed by 2 mL of THF after 1 h stirring. The Schlenk tube was placed in the refrigerator at -4°C to yield a crop of long, thin needle crystals (0.80 g, 57%). ^{1}H NMR (400.13 MHz, 298K, C_6D_6): δ = 8.19 [1H, d, J = 2.4 Hz, 1 × aromatic CH], 7.71 [2H, d, J = 7.9 Hz, 2 × aromatic CH], 7.35 [1H, d, J = 8.6 Hz, 1 × aromatic CH], 7.29 [2H, t, J = 7.2 Hz, 2 × aromatic CH], 7.13 [1H, t, J = 7.9 Hz, 1 × aromatic CH], 6.56 [1H, d, J = 8.6 Hz, 1 × aromatic CH], 3.49 [3H, s, 1 × CH_3 of OMe], 1.88 [4H, m, 2 × γCH_2 of TMP], 1.77-1.64 [35H, m, 5 × CH_3 of PMDETA, 4 × CH_2 of PMDETA and 4 × CH_3 of TMP], 1.41 ppm [8H, t, J = 5.9 Hz, 4 × βCH_2 of TMP]; $^{13}C\{^1H\}$ (100.62 MHz, 298K, C_6D_6): δ = 166.6 [1 × quaternary C], 164.3 [1 × quaternary C], 143.8 [1 × quaternary C], 140.5 [1 × aromatic CH], 134.8 [1 × quaternary C], 128.9 [2 × aromatic CH], 127.3 [2 × aromatic CH], 126.1 [1 × aromatic CH], 125.3 [1 × aromatic C], 108.7 [1 × aromatic C], 57.0 [2 × CH_2 of PMDETA], 55.5 [2 × CH_2 of PMDETA], 55.2 [4 × quaternary C of TMP], 52.6 [1 × CH_3 of MeO], 45.1 [4 × CH_3 of PMDETA], 42.2 [4 × βCH_2 of TMP], 41.6 [1 × CH_3 of PMDETA], 36.0 [8 × CH_3 of TMP], 20.6 ppm [2 × γCH_2 of TMP].

Chapter 4 – References:

[1]   R. E. Mulvey, *Organometallics* **2006**, *25*, 1060.

[2]   R. E. Mulvey, F. Mongin, M. Uchiyama, Y. Kondo, *Angew. Chem. Int. Ed.* **2007**, *46*, 3802.

[3]   R. E. Mulvey, *Acc. Chem. Res.* **2009**, *42*, 743.

[4]   P. E. Eaton, C. H. Lee, Y. Xiong, *J. Am. Chem. Soc.* **1989**, *111*, 8016.

[5]   W. Schlecker, A. Huth, E. Ottow, J. Mulzer, *J. Org. Chem.* **1995**, *60*, 8414.

[6]   D. R. Armstrong, A. R. Kennedy, R. E. Mulvey, R. B. Rowlings, *Angew. Chem. Int. Ed.* **1999**, *38*, 131.

[7]   W. Clegg, S. H. Dale, E. Hevia, G. W. Honeyman, R. E. Mulvey, *Angew. Chem. Int. Ed.* **2006**, *45*, 2370.

[8]   J.-M. L'Helgoual'ch, A. Seggio, F. Chevallier, M. Yonehara, E. Jeanneau, M. Uchiyama, F. Mongin, *J. Org. Chem.* **2008**, *73*, 177.

[9]   W. Clegg, B. Conway, E. Hevia, M. D. McCall, L. Russo, R. E. Mulvey, *J. Am. Chem. Soc.* **2009**, *131*, 2375.

[10]   G. Bentabed-Ababsa, F. Blanco, A. Derdour, F. Mongin, F. Trecourt, G. Queguiner, R. Ballesteros, B. Abarca, *J. Org. Chem.* **2009**, *74*, 163.

[11]   B. Conway, J. García-Álvarez, E. Hevia, A. R. Kennedy, R. E. Mulvey, S. D. Robertson, *Organometallics* **2009**, *28*, 6462.

[12]   B. Conway, E. Hevia, J. García-Álvarez, D. V. Graham, A. R. Kennedy, R. E. Mulvey, *Chem. Commun.* **2007**, 5241.

[13]   H. Naka, M. Uchiyama, Y. Matsumoto, A. E. H. Wheatley, M. McPartlin, J. V. Morey, Y. Kondo, *J. Am. Chem. Soc.* **2007**, *129*, 1921.

[14]   V. L. Blair, L. M. Carrella, W. Clegg, B. Conway, R. W. Harrington, L. M. Hogg, J. Klett, R. E. Mulvey, E. Rentschler, L. Russo, *Angew. Chem. Int. Ed.* **2008**, *47*, 6208.

[15]   V. L. Blair, W. Clegg, B. Conway, E. Hevia, A. R. Kennedy, J. Klett, R. E. Mulvey, L. Russo, *Chem. Eur. J.* **2008**, *14*, 65.

[16]   V. L. Blair, L. M. Carrella, W. Clegg, J. Klett, R. E. Mulvey, E. Rentschler, L. Russo, *Chem. Eur. J.* **2009**, *15*, 856.

[17]   M. Mosrin, M. Petrera, P. Knochel, *Synthesis* **2008**, 3697.

[18]   A. Krasovskiy, V. Krasovskaya, P. Knochel, *Angew. Chem. Int. Ed.* **2006**, *45*, 2958.

[19]   W. Lin, O. Baron, P. Knochel, *Org. Lett*. **2006**, *8*, 5673.

[20]   N. Boudet, J. R. Lachs, P. Knochel, *Org. Lett*. **2007**, *9*, 5525.

[21]   N. Boudet, S. R. Dubbaka, P. Knochel, *Org. Lett*. **2008**, *10*, 1715.

[22]   A. H. Stoll, P. Knochel, *Org. Lett*. **2008**, *10*, 113.

[23]   M. Mosrin, P. Knochel, *Org. Lett*. **2008**, *10*, 2497.

[24]   L. Melzig, C. B. Rauhut, P. Knochel, *Chem. Commun*. **2009**, 3536.

[25]   L. Lochmann, J. Pospíšil, J. Vodnansky, J. Trekoval, D. Lim, *Collect. Czech. Chem. Commun*. **1965**, *61*, 2187.

[26]   L. Lochmann, J. Pospíšil, D. Lim, *Tetrahedron Lett*. **1966**, *7*, 257.

[27]   M. Schlosser, *J. Organomet. Chem.* **1967**, *8*, 9.

[28]   M. Schlosser, F. Faigl, L. Franzini, H. Geneste, G. Katsoulos, G.-F. Zhong, *Pure Appl. Chem.* **1994**, *66*, 1439.

[29]   L. Lochmann, *Eur. J. Inorg. Chem*. **2000**, 1115.

[30]   F. H. Allen, *Acta Crystallogr., Sect. B: Struct. Sci*. **2002**, *58*, 380.

[31]   A. R. Kennedy, R. E. Mulvey, C. L. Raston, B. A. Roberts, R. B. Rowlings, *Chem. Commun*. **1999**, 353.

[32]   E. Hevia, G. W. Honeyman, A. R. Kennedy, R. E. Mulvey, D. C. Sherrington, *Angew. Chem. Int. Ed*. **2005**, *44*, 68.

[33]   J. J. Morris, B. C. Noll, G. W. Honeyman, C. T. O'Hara, A. R. Kennedy, R. E. Mulvey, K. W. Henderson, *Chem. Eur. J*. **2007**, *13*, 4418.

[34]   G. W. Honeyman, A. R. Kennedy, R. E. Mulvey, D. C. Sherrington, *Organometallics* **2004**, *23*, 1197.

[35]   G. C. Forbes, A. R. Kennedy, R. E. Mulvey, B. A. Roberts, R. B. Rowlings, *Organometallics* **2002**, *21*, 5115.

[36]   E. Hevia, F. R. Kenley, A. R. Kennedy, R. E. Mulvey, R. B. Rowlings, *Eur. J. Inorg. Chem*. **2003**, 3347.

[37]   P. C. Andrikopoulos, D. R. Armstrong, A. R. Kennedy, R. E. Mulvey, C. T. O'Hara, R. B. Rowlings, *Eur. J. Inorg. Chem*. **2003**, 3354.

[38]   P. C. Andrews, A. R. Kennedy, R. E. Mulvey, C. L. Raston, B. A. Roberts, R. B. Rowlings, *Angew. Chem. Int. Ed*. **2000**, *39*, 1960.

[39]   C. Pi, L. Wan, Y. Gu, H. Wu, C. Wang, W. Zheng, L. Weng, Z. Chen, X. Yang, L. Wu, *Organometallics* **2009**, *28*, 5281.

[40] B. Conway, D. V. Graham, E. Hevia, A. R. Kennedy, J. Klett, R. E. Mulvey, *Chem. Commun.* **2008**, 2638.

[41] W. Clegg, B. Conway, D. V. Graham, E. Hevia, A. R. Kennedy, R. E. Mulvey, L. Russo, D. S. Wright, *Chem. Eur. J.* **2009**, *15*, 7074.

[42] TurboMole, Program for Ab Initio Electronic Structure Calculations, TurboMole GmbH, Germany, **2007**.

[43] A. D. Becke, *Phys. Rev. A* **1988**, *38*, 3098.

[44] J. P. Perdew, *Phys. Rev. B* **1986**, *33*, 8822.

[45] J. P. Perdew, *Phys. Rev. B* **1986**, *34*, 7406.

[46] S. Grimme, *J. Comput. Chem.* **2006**, *27*, 1787.

[47] R. W. F. Bader, *Atoms in Molecules. A Quantom Theory,* Clarendon Press, Oxford, **1990**.

[48] R. W. F. Bader*, Chem. Rev.* **1991**, *91*, 893.

[49] F. Biegler-König, J. Schönbohm, D. Bayles, *J. Comput. Chem.* **2001**, *22*, 545.

[50] F. Biegler-König, J. Schönbohm, *J. Comput. Chem.* **2002**, *23*, 1489.

[51] NBO 5.G., E. D. Glendening, J. K. Badenhoop, A. E. Reed, J. E. Carpenter, J. A. Bohmann, C. M. Morales, F. Weinhold, Theoretical Chemistry Institute, University of Wisconsin, Madison, **2001**.

[52] R. Campbell, B. Conway, G. S. Fairweather, P. García-Álvarez, A. R. Kennedy, J. Klett, R. E. Mulvey, C. T. O'Hara, G. M. Robertson, *Dalton Trans.* **2010**, 511.

[53] R. I. Yousef, B. Walfort, T. Ruffer, C. Wagner, H. Schmidt, R. Herzog, D. Steinborn, *J. Organomet. Chem.* **2005**, *690*, 1178.

[54] S. S. Al-Juaid, A. G. Avent, C. Eaborn, S. M. El-Hamruni, S. A. Hawkes, M. S. Hill, M. Hopman, P. B. Hitchcock, J. D. Smith, *J. Organomet. Chem.* **2001**, *631*, 76.

[55] J. Clayden, R. P. Davies, M. A. Hendy, R. Snaith, A. E. H. Wheatley, *Angew. Chem. Int. Ed.* **2001**, *40*, 1238.

[56] J. García-Álvarez, D. V. Graham, A. R. Kennedy, R. E. Mulvey, S. Weatherstone, *Chem. Commun.* **2006**, 3208.

[57] H. Naka, J. V. Morey, J. Haywood, D. J. Eisler, M. McPartlin, F. Garcia, H. Kudo, Y. Kondo, M. Uchiyama, A. E. H. Wheatley, *J. Am. Chem. Soc.* **2008**, *130*, 16193.

[58] W. Clegg, S. H. Dale, R. W. Harrington, E. Hevia, G. W. Honeyman, R. E. Mulvey, *Angew. Chem. Int. Ed.* **2006**, *45*, 2374.

[59] Y. Kondo, J. V. Morey, J. C. Morgan, H. Naka, D. Nobuto, P. R. Raithby, M. Uchiyama, A. E. H. Wheatley, *J. Am. Chem. Soc.* **2007**, *129*, 12734.

[60]   H. Gilman, R. L. Bebb, *J. Am. Chem. Soc*. **1939**, *61*, 109.

[61]   G. Wittig, G. Fuhrman, *Chem. Ber*. **1940**, *73*, 1197.

[62]   S. Harder, J. Boersma, L. Brandsma, J. A. Kanters, *J. Organomet. Chem*. **1988**, *339*, 7.

[63]   W. Bauer, P. von R. Schleyer*, J. Am. Chem. Soc*. **1989**, *111*, 7191.

[64]   J. M. Saa, P. M. Deyà, G. A. Suner, A. Frontera, *J. Am. Chem. Soc*. **1992**, *114*, 9093.

[65]   M. Stratakis, *J. Org. Chem*. **1997**, *62*, 3024.

[66]   R. A. Rennels, A. J. Maliakal, D. B. Collum, *J. Am. Chem. Soc*. **1998**, *120*, 421.

[67]   S. T. Chadwick, R. A. Rennels, J. L. Rutherford, D. B. Collum, *J. Am. Chem. Soc*. **2000**, *122*, 8640.

[68]   P. R. Markies, G. Schat, A. Villena, O. S. Akkermann, F. Bickelhaupt, W. J. J. Smeets, A. L. Spek, *J. Organomet. Chem*. **1991**, *411*, 291.

[69]   M. Kauch, V. Snieckus, D. Hoppe, *J. Org. Chem*. **2005**, *70*, 7149.

[70]   E. Hevia, D. J. Gallagher, A. R. Kennedy, R. E. Mulvey, C. T. O'Hara, C. Talmard, *Chem. Commun*. **2004**, 2422.

[71]   P. C. Andrikopoulos, D. R. Armstrong, D. V. Graham, E. Hevia, A. R. Kennedy, R. E. Mulvey, C. T. O'Hara, C. Talmard, *Angew. Chem. Int. Ed*. **2005**, *44*, 3459.

[72]   D. R. Armstrong, W. Clegg, S. H. Dale, D. V. Graham, E. Hevia, L. M. Hogg, G. W. Honeyman, A. R. Kennedy, R. E. Mulvey, *Chem. Commun*. **2007**, 598.

[73]   P. C. Andrikopoulos, D. R. Armstrong, E. Hevia, A. R. Kennedy, R. E. Mulvey, *Organometallics*, **2006**, *25*, 2415.

Chapter 5: Alkali-Metal-Aluminates – Alumination (Al-H exchange) Traps for TMEDA, PMDETA and TMP

5.1) Introduction

First reported in 2004 by Uchiyama *et al.*, lithium TMP-aluminate "^{i}Bu$_3$Al(TMP)Li" (**5a**) [prepared by mixing triisobutylaluminium (^{i}Bu$_3$Al) with lithium 2,2,6,6-tetramethylpiperidide (LiTMP) in THF] was found to be an excellent base in THF solutions, realising high chemo- and regioselective deprotonative aluminations of functionalised aromatic and hetero-aromatic compounds as well as of functionalised allylic compounds.[1] Previous to this discovery, aromatic aluminium chemistry had not been developed to a significant extent, mainly due to the lack of efficient preparation methods which would leave the functional groups on the arene ring untouched. To generate aliphatic aluminium compounds, a simple transmetallation procedure involving organolithiums or Grignard reagents to the corresponding aluminium compounds can be used.[2] Extending this metathetical approach for the synthesis of functionalised aromatic aluminium compounds suffers from significant limitations. The aromatic lithium or Grignard intermediates are generally too reactive to coexist with several species of electrophilic functional groups, such as amide, halogen or cyano groups.[3] A second method to form aliphatic aluminium compounds involves the hydro- or carbo-alumination reaction of unsaturated bonds, however, this method was deemed ineffective in aromatic chemistry.[4] Furthermore, neither metal-halogen exchange, nor oxidative addition reactions, of aluminium on aromatic frameworks has been realised. Therefore, the introduction of ^{i}Bu$_3$Al(TMP)Li (**5a**) was a key new development to the field of organoaluminium reagents.

Uchiyama initially tested base **5a,** as well as a host of other organoaluminium reagents, in aluminium-halogen exchange reactions of haloaromatics. This application proved to be completely unsuccessful. Turning their attentions to the deprotonation of functionalised benzenes, using anisole (C$_6$H$_5$OMe) as the model substrate, base **5a** was found to be the best reagent to induce metallation of the arene ring (**scheme 5.1**). The direct *ortho*-alumination of anisole was achieved with this lithium aluminate, and a subsequent electrophilic quench of the metallated intermediate with D$_2$O or I$_2$ resulted in the isolation of the desired *o*-deuterio- or *o*-

iodoanisole, respectively, in high yields (95 and 88%, respectively). **5a** was found to selectively deprotonate various aromatics containing amide, cyano, ether or halogen functionalities (**table 5.1**), which are all prone to side reactions with conventional organolithium or Grignard reagents.
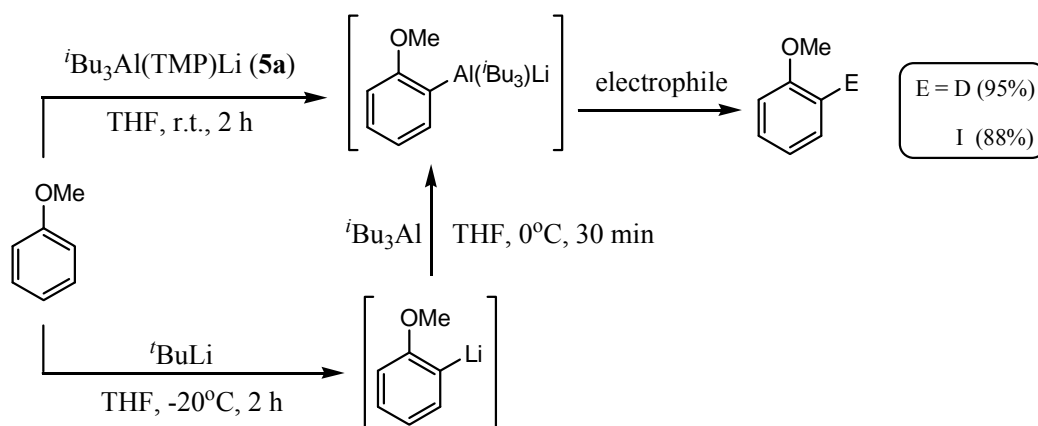
Scheme 5.1: *ortho*-Metallation/quench reactions of anisole with 5a.

Table 5.1: Deprotonative alumination of functionalised aromatics.

Substrate	Product	Yield	Substrate	Product	Yield
OMe	OMe I	99 % (rt, 3 h)	OMe OMe (meta)	OMe I OMe	92 % (0°C, 4 h)
CN	CN I	100 % (-78°C, 2 h)	OMe OMe	OMe OMe I	74 % (0°C, 4 h)
CON^{i}Pr$_2$	CON^{i}Pr$_2$ I	94 % (rt, 3 h)	Cl Cl	Cl I Cl	74 % (-78°C, 12 h)
I OMe	I OMe I	83 % (rt, 3 h)	Cl Cl	Cl Cl I	72 % (-78°C, 5 h)
I CN	I CN I	90 % (-78°C, 2 h)	indole N-Boc	indole 2-I N-Boc	64 % (-78°C, 1 h)
CF$_3$	CF$_3$ 10/20/10	40 % (0°C, 7 h)	N OMe (pyridine)	N I OMe	82 % (-78°C, 5 h)

Uchiyama also tested the ability of some of these aluminated intermediates to undergo copper- and palladium-catalysed C–C bond-forming reactions [such as allylation (with allyl bromide), phenylation (with iodobenzene), and benzoylation (with benzoylchloride)]. The results showed that these types of reactions are highly successful, giving high chemo- and regioselectivities, in impressive yields (79-100%).

At room temperature, base **5a** reacts with the substrate *N, N*-diisopropyl-3-bromobenzamide, generating a benzyne intermediate that can be treated with 1,3-diphenylisobenzofuran to give the corresponding Diels-Alder adduct in a quantitative yield. At -78°C, in contrast, the intermediate created from the initial deprotonation of the arene can be trapped with an electrophilic I$_2$ quench, producing *N, N*-diisopropyl-3-bromo-2-iodobenzamide in a 65% isolated yield (**scheme 5.2**).
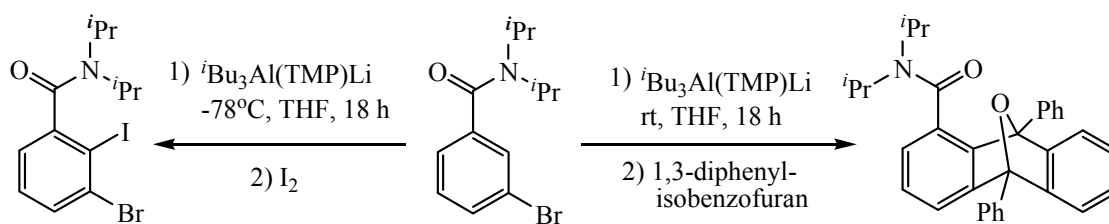
Scheme 5.2: Generation and suppression of 3-functionalised benzyne via temperature control.

In 2007, Uchiyama *et al.* published a full paper on lithium aluminate chemistry, an extention of their 2004 communication.[5] Using anisole and benzonitrile as selected model aromatic compounds (reflecting arenes with electron-donating and electron-withdrawing functional groups respectively), the *^{i}*Bu base worked just as well as the Et congener with respect to the *ortho*-metallation of anisole (88% and 87% isolated yield respectively after I$_2$ quench), whereas Me$_3$Al(TMP)Li was found to act as a poor base (12% yield). Toward benzonitrile, the TMP–aluminates of formula R$_3$Al(TMP)Li [where R = Me, Et or *^{t}*Bu] provided no signs of ring metallation, though significant decomposition of the cyano group was observed. Only the *^{i}*Bu analogue was found to achieve *ortho*-deprotonation, in a quantative yield after an electrophilic quench with I$_2$, leaving the CN group untouched.

As well as including more examples of arene metallation, Uchiyama introduced the concept of deprotonative alumination of functionalised allylic compounds with base **5a**. Various oxygen-substituted allylic substrates were studied and deprotonation was found to be regioselective and tolerant of carbamates and ethers under mild conditions (**scheme 5.3**).
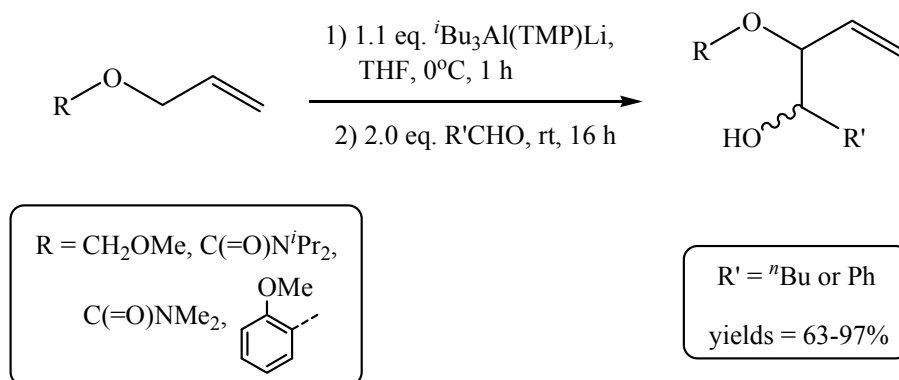
Scheme 5.3: Deprotonative alumination of functionalised allylic compounds.

The mechanism of the base in its reactions was investigated using DFT calculations (at the B3LYP/6-31+G* level of theory), that is whether **5a** acts as an alkyl [*iso*-butyl to *iso*-butane] or an amido [TMP to TMP(H)] base towards organic substrates. Two structural isomers of **5a** are possible: i) where Li^+ is connected to two alkyl groups (**A**) or ii) where Li^+ is connected to one alkyl and one TMP group (**B**) (**figure 5.1**). Initially, using the simplified theoretical model where
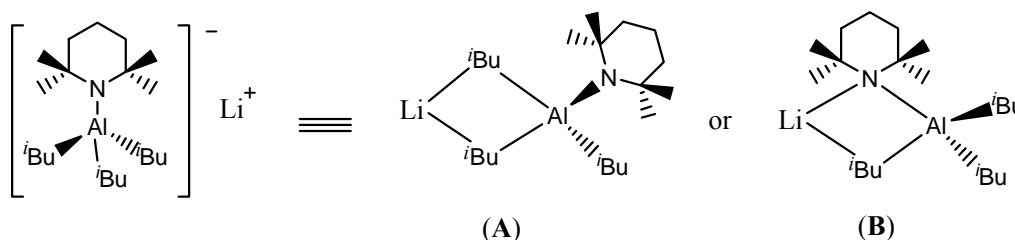
Figure 5.1: Two possible isomers of the aluminate base 5a.

$Me_3Al(Me_2N)Li$ represented **5a** and Me_2O signified THF, motif **B** was found to be more stable than its isomer **A** (by 10-13 kcal/mol). This result was found independant of whether one or two molecules of Me_2O ligated to the lithium cation. Full optimisations of $^iBu_3Al(TMP)Li$ were also

carried out, with the same pattern observed as before, no matter whether zero, one or two solvent ligands were present. From these calculations, the monosolvated lithium aluminate was found to be the most stable structure, which was backed up by the elucidation of the molecular structure of the isolated complex [THF·Li(μ-TMP)(μ-^{i}Bu)Al(^{i}Bu)$_2$] (from hexane solution). In mixed amido/alkyl aluminium systems, as noted in Chapter 1, nitrogen anions are generally more reactive than carbanions in these mixed ligand systems, thus it was suggested that TMP-mediated deprotonation was the more likely process to occur (**scheme 5.4**). DFT calculations (B3LYP/6-
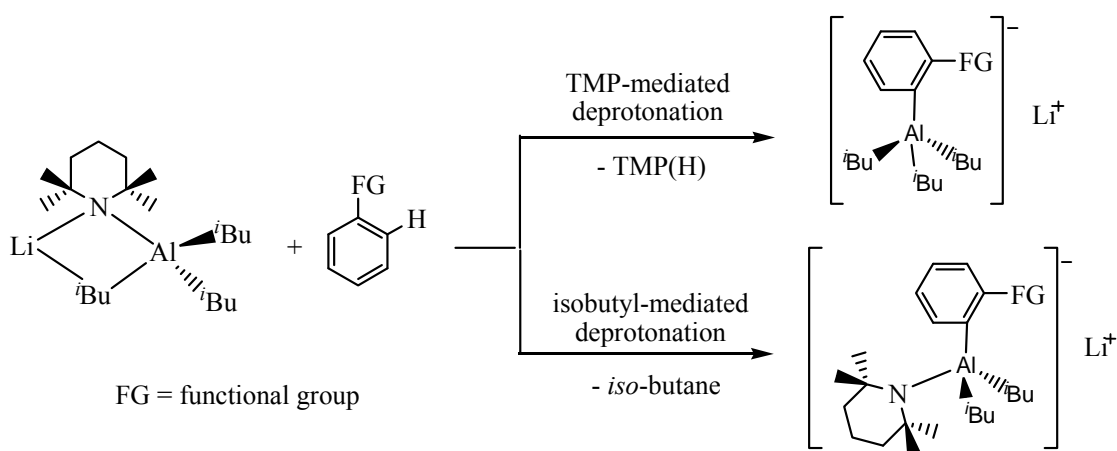
Scheme 5.4: Two potential pathways for *ortho*-deprotonation to occur.

31+G* level of theory), modelling **5a** as Me$_3$Al(Me$_2$N)Li, revealed that deprotonation of anisole at the *ortho*-position by the Me ligand was found to be kinetically unfavourable (due to a high activation energy of 47.9 kcal/mol) when compared to the smaller activation barrier of 29.8 kcal/mol for the NMe$_2$ base to perform the deprotonation. Within the calculated transition state, the nitrogen atom forms a relaxed tetrahedral geometry, providing a perfect alignment for the lone pair of the N to interact in an almost linear fashion with the unoccupied aromatic σ_{C-H}* orbital. The corresponding Me transition state generates an unfavourable distorted, five coordinate carbon geometry in which the aromatic σ_{C-H}* orbital interacts with the poorly directed sp^3-like orbitals, resulting in a transition step with a high energy barrier. In 2008, Uchiyama reported further calculations stating that **5a** acts as an amido base towards *N, N*-diisopropylbenzamide, removing the *ortho*-hydrogen to form the compound "[2-(^{i}Bu$_3$Al)C$_6$H$_4$C(=O)N(^{i}Pr)$_2$]$^-$Li$^+$", in a favourable reaction step.[6] It was also reported that the

reincorporation of the TMP ligand into the complex, releasing *iso*-butane as a result, is a disfavoured process (**scheme 5.5**).
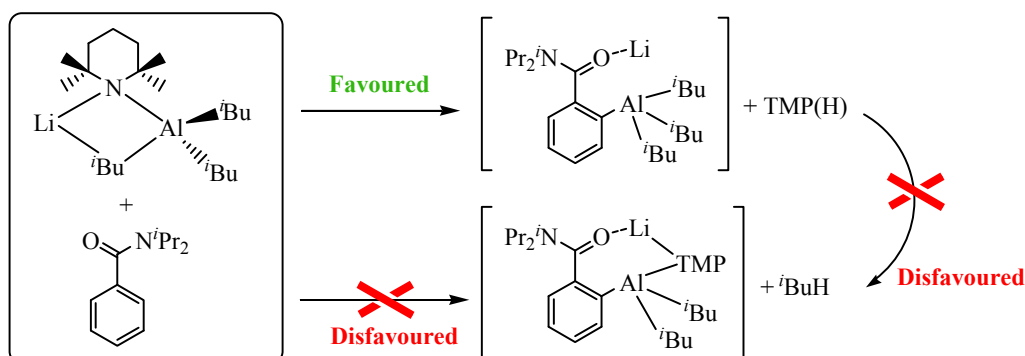
Scheme 5.5: Computationally predicted reactivity of 5a towards *N*, *N*-diisopropylbenzamide.

Another application of base **5a** in synthesis is the regioselective functionalisation of unsymmetrical ketones was observed with **5a** in THF solution at 0°C. Using the example of methyl isopropyl ketone, the kinetically preferred enolate was selectively synthesised after treatment with **5a**, elucidated by the retrieval of the product upon an electrophilic quench of the aluminated intermediate with benzaldehyde (**scheme 5.6**). This regioselective reaction step was found to be common in several examples of unsymmetrical ketones, the success of which was reasoned to be due to the highly controllable nature of the kinetic base, **5a**, used in these deprotonation reactions.
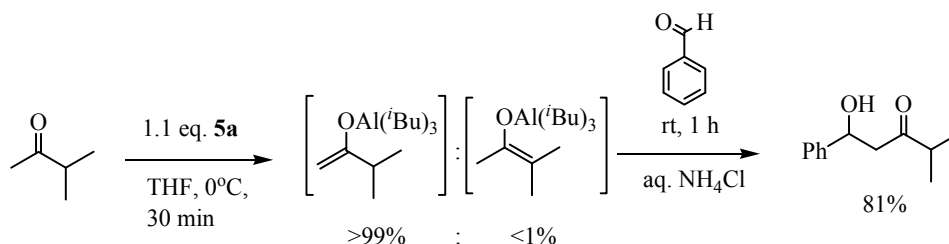
Scheme 5.6: Regioselective deprotonation of methyl isopropyl ketone using 5a.

Our research group has also explored the area of alkali-metal aluminate chemistry. In 2006, the first sodium alkyl(TMP)aluminate reagent was synthesised (from hexane solution) and

crystallographically characterised as [TMEDA·Na(μ-TMP)(μ-^{i}Bu)Al(^{i}Bu)$_2$] **5b**.[7] This complex was found to react as an amido base, akin to the lithum aluminate **5a**. Reaction of **5b** with phenylacetylene generated crystalline [(TMEDA)$_2$·Na(μ-C≡CPh)(μ-^{i}Bu)Al(^{i}Bu)$_2$] (**figure 5.2**) in an isolated yield of 21%, with the elimination of TMP(H) as a co-product. Crystals of the Li
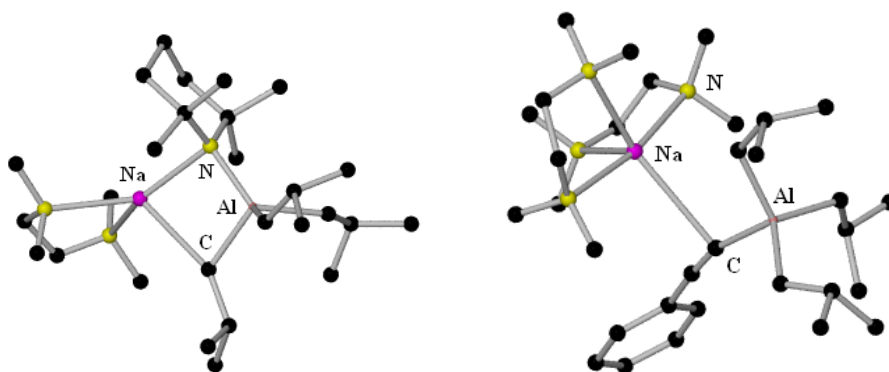
Figure 5.2: Molecular structures of base 5b (left) and the product of alumination of phenylacetylene (right).

congener (**5c**) of base **5b** could not be grown, as it was stated a white oily product was obtained. Using an *in situ* mixture of **5c** with *N, N*-diisopropylbenzamide, an unexpected crystalline product was isolated, namely [{PhC(=O)N(^{i}Pr)$_2$}·Li{2-[1-C(=O)N(^{i}Pr)$_2$]C$_6$H$_4$}{Me$_2$NCH$_2$CH$_2$N(Me)CH$_2$}Al(^{i}Bu)$_2$] (**5d**). A reaction pathway was proposed for the formation of this product (**scheme 5.7**), where it was suggested that, initially,
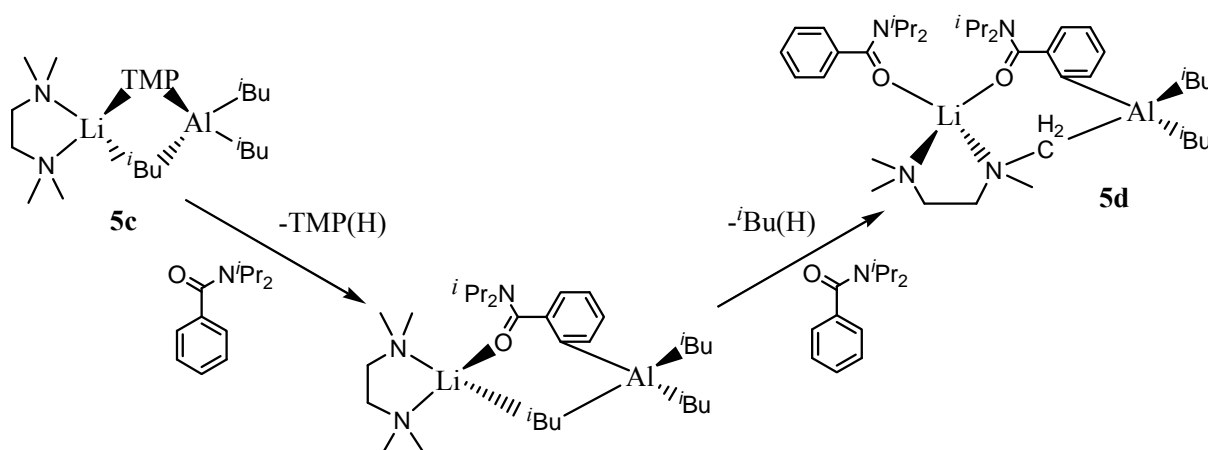
Scheme 5.7: Proposed two-step pathway for the formation of 5d.

the benzamide substrate is *ortho*-aluminated by TMP, followed by the intramolecular deprotonation of one methyl sidearm of the TMEDA ligand (with concomitant elimination of *iso*-butane) on complexation of a second benzamide molecule to Li. It is important to note that ^{i}Bu$_3$Al alone was found to be ineffective in the attempted deprotonation of TMEDA or the benzamide, therefore the two distinct deprotonations taking place were deemed synergic in origin (that is requiring both Li and Al metals). In addition, this work highlighted that TMP-aluminates could function as dual TMP/alkyl bases, which had not been mentioned previously.

Our group has also reported several derivatives of the THF-solvated lithium aluminate [THF·Li(μ-TMP)(μ-^{i}Bu)Al(^{i}Bu)$_2$]. Three Lewis base variations, with the formula [L·Li(μ-TMP)(μ-^{i}Bu)Al(^{i}Bu)$_2$] [where L is TMP(H), Et$_3$N or PhC(=O)N^{i}Pr$_2$ (**5e**)] were unveiled (**figure 5.3**) in a 2007 communication.[8]
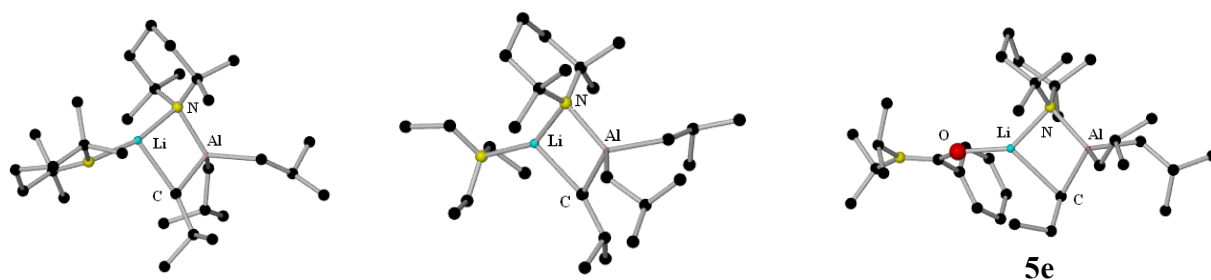
Figure 5.3: Molecular structures of the three Lewis base variations of 5a.

In the formation of **5e** no metallation of the benzamide ring was observed, thus as LiTMP alone deprotonates this substrate (even at subambient temperatures), combining the lithium amide with ^{i}Bu$_3$Al to generate this mixed-metal system appears to retard the basicity of the TMP anion. Deprotonation of *N, N*-diisopropylbenzamide was attempted by the addition of dioxane to **5e**, as Uchiyama had stated that a 94 % yield of the *ortho*-metallated benzamide could be achieved with **5a** in THF solution (determined indirectly by the isolation of the I$_2$-quenched product). The resultant product, [{PhC(=O)N(^{i}Pr)$_2$}·Li[OCH$_2$)$_2$OC(H)=CH$_2$]Al(^{i}Bu)$_3$}$_2$·(1,4-dioxane)] (**5f**), isolated in a 38% crystalline yield, showed a surprising preference for ether cleavage over the *ortho*-metallation of the benzamide (coordinating to Li as a neutral ligand within **5f**). The reaction mechanism put forward (**scheme 5.8**) proposed that the complex **5e** first acts as a TMP

base towards a ligated dioxane molecule (on the lithium atom). Secondly, the ring of the deprotonated ether molecule opens up and rearranges to form a vinylic arrangement with the final step involving the attack of the electrophilic Al by the alkoxy nucleophile, bridging between the two metals. This co-operation effect of the two metals in this contacted ion-pair system was deemed to override the acidity effect of the benzamide (which undergoes *ortho*-lithation at even -78°C with organolithium reagents).
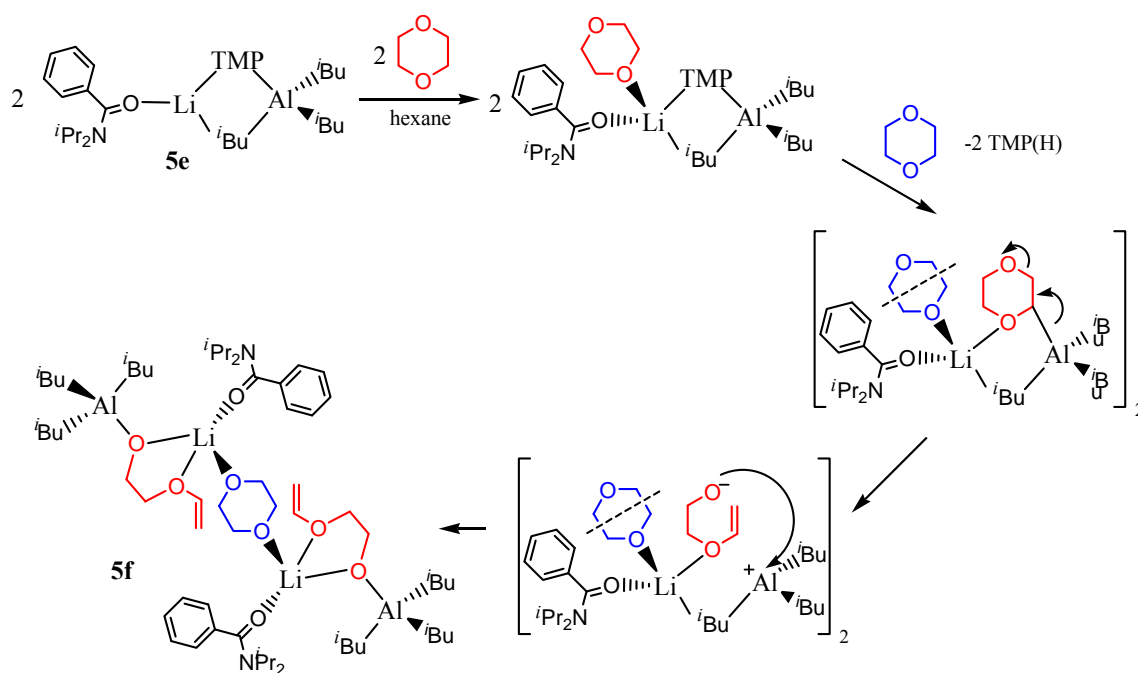
Scheme 5.8: Proposed reaction mechanism to generate the dioxane fragmentation complex 5f.

Attention within our group next turned to attempts to identify the true base within the reaction mixture that Uchiyama used in his reports of successful deprotonations of functionalised aromatic substrates. Uchiyama concluded that the active base was the aforementioned THF-solvated complex of **5a**, [THF·Li(μ-TMP)(μ-*i*Bu)Al(*i*Bu)₂] (**5g**). However, some confusion arose since Uchiyama stated within the main body of the paper that crystalline **5g** was obtained from bulk THF solution, whereas within the supporting material complex **5a** was said to be synthesised in hexane solution first with the addition of one molar equivalent of THF, generating a batch of **5g** for X-ray crystallographic characterisation. Within our group, "base" **5g** could not

be isolated in crystalline form from neat THF solution, but was readily isolated using the synthetic procedure in the supporting material mentioned above, in hexane solution. Surprisingly, in our hands **5g** was ineffective at deprotonating *N, N*-diisopropylbenzamide in a hexane medium.[9] The implication of this failure was that excess THF is necessary for metallation efficiency, and therefore doubts surfaced about **5g** being the true active base.

Following the original literature procedure, Dr. Joaquín Garica-Álvarez of our research group treated the benzamide with 2.2 molar equivalents of $^{i}Bu_3Al(TMP)Li$ in neat THF solution, which deposited a colourless crystalline solid identified as the solvent-separated ionic aluminate $[\{Li \cdot (THF)_4\}^{+}\{Al(^{i}Bu)_4\}^{-}]$ (**5h**) by ^{1}H, ^{7}Li and ^{13}C NMR spectroscopic techniques (and indirectly by comparison with its known crystallographically characterised dioxane analogue $[\{Li \cdot (dioxane)_4\}^{+}\{Al(^{i}Bu)_4\}^{-}]$). **5h** was also observed in THF solutions of **5a** in the absence of the benzamide substrate, which indicated that a dismutation of putative $^{i}Bu_3Al(TMP)Li$ could be responsible (**scheme 5.9**). Complex **5h** was subsequently tested as a base, unsuccessfully, against
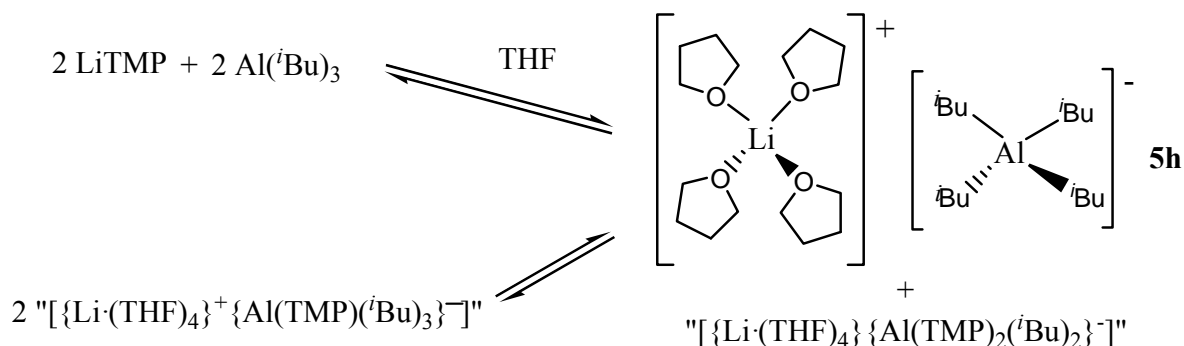
Scheme 5.9: Dismutation of putative $^{i}Bu_3Al(TMP)Li$ in neat THF solution.

the benzamide, and the presence of this inactive component of the $^{i}Bu_3Al(TMP)Li$ THF-solution was offered as an explanation for why 2.2 molar equivalents of the base was required to effect 94% metallation. From the filtrate that deposited **5h**, a second crystallised product was isolated and characterised by ^{1}H, ^{7}Li and ^{13}C NMR spectroscopy, and X-ray crystallography, as the tris(THF)-solvated lithium trialkyl-mono*ortho*arylaluminate $[(THF)_3 \cdot Li\{O(=C)N(^{i}Pr)_2(C_6H_4)\}Al(^{i}Bu)_3]$ (**5i**) (**scheme 5.10**), representing the first tangible metallo intermediate of a direct alumination reaction (performed in THF solution) of a

benzamide, or indeed of any functionalised aromatic compound, to be structurally defined and well characterised. A year later, in 2008, Uchiyama *et al* reported (**figure 5.4**) the same molecular structure (within experimental error) of **5i**, as well as the product of metallation of *N,N*-diisopropylnaphthamide, $[2-(^iBu_3Al)-C_{10}H_6C(=O)N(^iPr)_2]Li\cdot3THF$.[6]
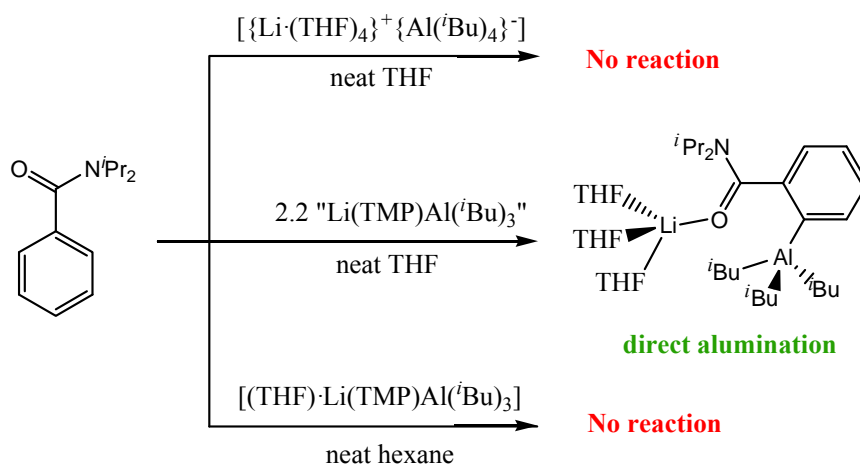
Scheme 5.10: Reactivity of various aluminates with *N, N*-diisopropylbenzamide.

This next section of this chapter will focus on attempts to synthesise species similar to the type "$[\{Li\cdot(THF)_n\}^+\{Al(TMP)_2(^iBu)_2\}^-]$" (postulated as a potential base in **scheme 5.9**). In addition, endeavours to synthesise new potassium-based aluminium reagents with formula $[L\cdot K(\mu-amide)(\mu-^iBu)Al(^iBu)_2]$, where L = ligand, will be disclosed.
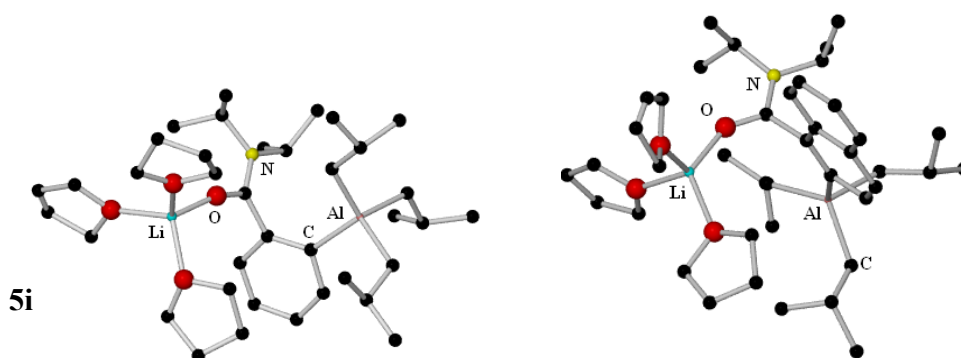
Figure 5.4: Molecular structures of the isolated products of alumination of *N,N*-diisopropylbenzamide (left) and −naphthamide (right) by 5a in THF solutions.

5.2)   *Attempted Isolation of Alkali-Metal Bis(amido)-bis(alkyl)aluminates*

The initial step in the attempted generation of alkali-metal bis(amido)-bis(alkyl)aluminates was the formation of a bis(alkyl)-(TMP)aluminium starting reagent. Using the metathetical approach adopted by Yamamoto,[10] LiTMP [formed from ^{n}BuLi and the amine TMP(H)] was reacted with ^{i}Bu$_2$AlCl, in hexane solution, at room temperature to produce the oily compound ^{i}Bu$_2$Al(TMP) (**5j**) in quantitative yields (elucidated by ^{1}H and ^{13}C NMR analysis of the reaction mixture), releasing insoluble LiCl co-product in the process. With the initial goal of isolating an almost pure source of monoamido-(bisalkyl)alumane, **5j**, complexation with several alkali-metal amides could be tested, together with donor ligands for solvation of the alkali metal.

Initial investigations centred on pairing LiTMP with **5j** in the presence of one molar equivalent of TMEDA. This reaction mixture produced the crystalline heterobimetallic-heterotrianionic complex [Li{Me$_2$NCH$_2$CH$_2$N(Me)CH$_2$}(TMP)Al(^{i}Bu)$_2$] (**5k**) in an isolated yield of 55%. In this unexpected product where a methyl of the bidentate ligand has been selectively deprotonated (**scheme 5.11**). Under the same reaction conditions, adding a further molar equivalent of TMEDA resulted in the isolation of **5k** exclusively (even after reflux conditions were employed). Changing the tertiary amine ligand from bidentate TMEDA to tridentate PMDETA (also just one molar equivalent) resulted in the deposition of crystals identified as [Li{Me$_2$NCH$_2$CH$_2$N(Me)CH$_2$CH$_2$N(Me)CH$_2$}(TMP)Al(^{i}Bu)$_2$] (**5l**). These were obtained in an isolable yield of 47%. As in the previous case, α-alumination of a terminal methyl group on the

M = Li (**5k**)   M = Li (**5l**) or Na (**5n**)
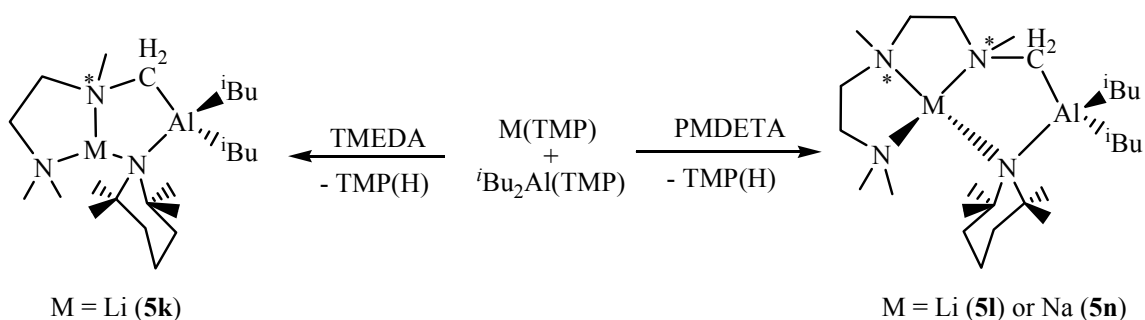
Scheme 5.11: Intramolecular alumination (Al–H exchange) traps for TMEDA and PMDETA.

chelate ligand takes place. Again, the reaction of excess PMDETA generated **5l** only. Substituting LiTMP by the less sterically encumbered lithium amide LiDMP [DMP = *cis*-2,6,-dimethylpiperidide], in the presence of one molar equivalent of TMEDA, a bis(alkyl)-bis(amido)aluminate can be produced, proved by the isolation of the solvent-separated complex [{Li·(TMEDA)$_2$}$^+${Al(DMP)$_2$(^{i}Bu)$_2$}$^-$] (**5m**), although initial experiments have only generated isolated **5m** in low yields due to the presence of several other products (see later).

Moving down Group 1 from lithium to sodium, NaTMP was added to **5j**, producing a suspension (suggesting that these two compounds might not complex without a donor ligand, as NaTMP in hexane is also a suspension). Addition of PMDETA generated a clear solution from which a crystalline material was isolated and characterised as the sodium analogue of **5l**, [Na{Me$_2$NCH$_2$CH$_2$N(Me)CH$_2$CH$_2$N(Me)CH$_2$}(TMP)Al(^{i}Bu)$_2$] (**5n**) (crystalline yield, 28%). Repetition of the reaction substituting PMDETA by TMEDA does not produce the sodium analogue of **5k**, but has a completely different outcome. At subambient temperature (-28°C), a solid could be isolated (in 18% yield) from the reaction mixture, identified by ^{1}H and ^{13}C NMR spectroscopic methods as [(TMEDA)·Na(μ-TMP*)(μ-^{i}Bu)Al(^{i}Bu)] (**5o**) {where TMP* = NC(Me)$_2$(CH$_2$)$_3$C(Me)(CH$_2$)}, where remarkably the TMP anion has been deprotonated on a methyl group. Continuing down the alkali-metal series, the reaction of KTMP, **5j** and TMEDA (in a 1:1:1 molar ratio) deposited crystalline material, in an isolable yield of 49%. Note that KTMP (suspension in hexane) does not seem to form a complex with **5j**, akin to NaTMP, as only on addition of TMEDA does a homogeneous solution occur. These crystals were of good enough quality for X-ray crystallography, and were characterised as [(TMEDA)·K(μ-TMP*)(μ-^{i}Bu)Al(^{i}Bu)] (**5p**), confirming that TMP can actually exist as a N,C–twofold deprotonated dianionic variant (**scheme 5.12**).

M = Na (**5o**) or K (**5p**)
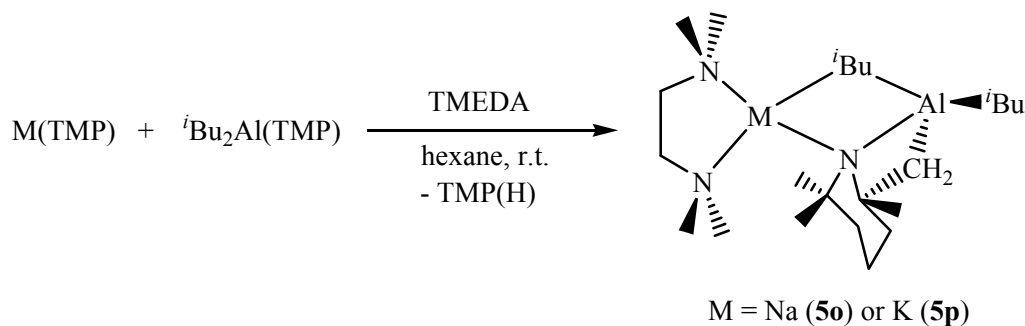
Scheme 5.12: Production and trapping of a TMP dianion.

5.2.1) Solid-State Analysis

The molecular structure of **5k** (**figure 5.5**) features a five-atom, four element LiNCAlN ring, with a mixed NCH$_2$-TMP bridging ligand set, and is completed by two terminal ^{i}Bu ligands on Al and a chelating metallated TMEDA (*N,N*-attached) to Li. Overall, the Al and Li centres are held together in an irregularly shaped octa-LiNCCNCAlN bicyclic ring, with a Li–N hinge. The
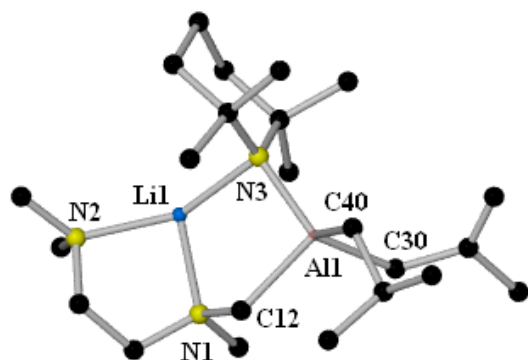
Figure 5.5: Molecular structure of [Li{Me$_2$NCH$_2$CH$_2$N(Me)CH$_2$}(TMP)Al(^{i}Bu)$_2$] (5k).
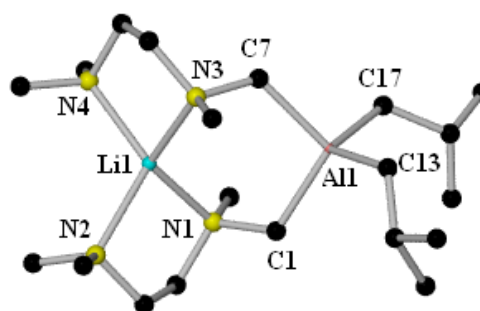
Figure 5.6: Molecular structure of the heterobimetallic bis-(deprotonated TMEDA) complex 5q.

Al centre displays a distorted tetrahedral geometry [subtending bond angles from 99.57(6)^o {N(3)–Al(1)–C(12)} to 121.47(6)^o {N(3)–Al(1)–C(30)}] made up of three carbon atoms, from two terminal ^{i}Bu ligands [with shortest Al–C bonds {Al(1)–C(40), 2.0319(17) Å; Al(1)–C(30), 2.0340(16) Å}] and one deprotonated TMEDA molecule [with longest Al–C bond, {Al(1)–C(12), 2.0658(17) Å}], with the fourth atom the N of TMP [Al(1)–N(3), 1.9869(13) Å], with a bond length in the same range as the Al–N distances found in other structures of general formula [donor·Li(TMP)Al(^{i}Bu)$_3$] [for example when donor *N, N*-diisopropylbenzamide, 1.974(2) Å].

Dr Joaquin García-Álvarez, formerly of our research group, isolated the crystalline product [Li{Me$_2$NCH$_2$CH$_2$N(Me)CH$_2$}$_2$Al(^{i}Bu)$_2$] (**5q**) (**figure 5.6**, isolated crystalline yield, 48%) from the reaction of LiTMP with two molar equivalents of TMEDA and one molar equivalent of the tris(alkyl)aluminium reagent, ^{i}Bu$_3$Al. This product, derived from the dual basicity of the lithium

TMP aluminate ^{i}Bu$_3$Al(TMP)Li, was formed even when one molar equivalent of the bidentate tertiary amine was utilised (15% isolated yield). Its molecular structure contains two molecules of methyl-aluminated TMEDA, which bridge both metals in a contacted ion-pair type complex, with both N atoms of the metallated junction of TMEDA chiral as each is attached to four different substituents, although overall the crystals are racemic. On comparison of structure **5q** with **5k**, the wide Al(1)–C(12)–N(1) bond angle at 116.86^o is marginally less than those in **5q** [Al(1)–C(1)–N(1), 118.28(13)^o; Al(1)–C(7)–N(3), 120.06(13)^o] and these fall in a similar range to those reported in the closely related terminally dialuminated TMEDA complexes R$_2$AlCH$_2$N(Me)CH$_2$CH$_2$N(Me)CH$_2$AlR$_2$ [R = Me, 113.9(1)^o; R = ^{t}Bu, 116.3(2)/116.2(2)^o], which in contrast to **5k** and **5q** were prepared by a conventional metathesis approach from the corresponding dilithium complex.[11] Note that an even wider Al–C(H)$_2$–N bond angle [121.5(2)^o] is found in (^{t}BuAlCH$_2$N^{i}Pr$_2$·LiCl)$_2$.[12] Contact from aluminium to the lithium atom in **5k** is through one amido (TMP) nitrogen atom [Li(1)–N(3), 2.035(3)Å] and one nitrogen of the metallated junction of TMEDA [Li(1)–N(1), 2.000(3)Å]. The remaining nitrogen atom of TMEDA also binds to Li, displaying the longest Li–N distance within the structure [Li(1)–N(2), 2.086(3)Å] to complete a distorted coordination sphere of N atoms [subtending bond angles from 88.58(12)^o {N(1)–Li(1)–N(2)} to 151.45(15)^o {N(2)–Li(1)–N(2)}].

Very few structural examples exist exhibiting metallation of the popular ligand TMEDA (there are only five structures within the CSD). One of these structures arises from the direct lithiation of TMEDA with ^{t}BuLi at -78°C (in *n*-pentane solution), to generate the tetrameric ring complex [(Me)$_2$NCH$_2$CH$_2$N(Me)CH$_2$Li]$_4$.[13] Three complexes can be classed as mixed aggregates (containing either dilithiated 2-methyl-6-*tert*-butylphenol,[14] thiolphenol [15] or 2-trimethylsilylthiolphenol) [15] as well as lithiated TMEDA. All of these structures are homometallic (all lithium), non-ate compounds. The final complex in the database hit list was synthesised within our own group (see **Scheme 5.7**) namely aforementioned complex **5d**, made by the reaction of "[TMEDA·Li(TMP)Al(^{i}Bu)$_3$]" with two equivalents of *N,N*-diisopropylbenzamide.[7]

Exchanging the amide ligand TMP by the less sterically hindered (via removal of two methyl groups for two hydrogen atoms) amide DMP in the reaction mixture, leads to the formation of

the complex [{Li·(TMEDA)$_2$}$^+$ {Al(DMP)$_2$(^{i}Bu)$_2$}$^-$] (**5m**). As can be seen from its crystal
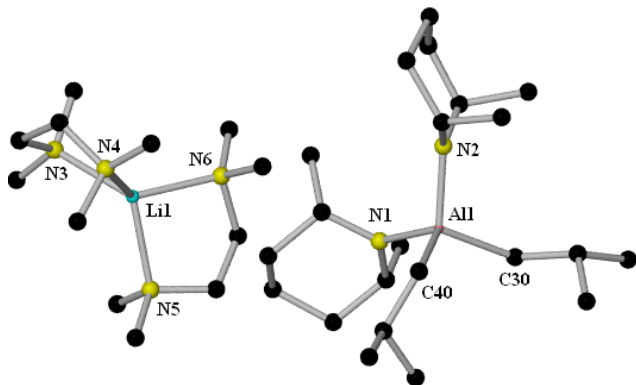
Figure 5.7: Molecular structure of the solvent-separated lithium bis(DMP)-bis(*iso*-butyl)aluminate 5m.

structure (**figure 5.7**), **5m** is a discrete solvent-separated ion-pair, with the lithium cation sitting in a modestly distorted tetrahedral environment [mean Li–N bond angle, 110.1^o] surrounded by two molecules of normal, unmetallated TMEDA, where the nitrogens form the longest bonds to Li within the complex [Li–N bond range, 2.102(5)-2.146(5)Å; mean bond length, 2.126Å]. The anionic moiety consists of a distorted tetrahedral Al centre [mean bond angle around Al, 109.5^o; range, 102.69(11)^o{N(1)–Al(1)–C(30)}–115.51(11)^o{C(40)–Al(1)–C(30)}], where the metal forms two shorter Al–N bonds [Al(1)–N(1), 1.860(2)Å; Al(1)-N(2), 1.880(2)Å] compared to two longer Al–C bonds [Al(1)–C(30), 2.036(3)Å; Al(1)–C(40), 2.028(3)Å] by an average of 0.162Å. This difference in bond length is a marked increase on the difference of 0.037Å in bond length between the average Al–C (1.990Å) and Al–N (1.953Å) bond lengths retrieved from the CSD. A search of analogous lithium aluminates containing a [Li·(TMEDA)$_2$]$^+$ cation found no examples of a mixed alkyl/amido ligand set on Al, though there is an example of a fully amido-ligated aluminate, in [{Li·(TMEDA)$_2$}$^+${Al(N(^{t}Bu)CH$_2$CH$_2$N(^{t}Bu))$_2$}$^-$], formed from the reaction of Al{N(^{t}Bu)CH$_2$CH$_2$N(^{t}Bu)}{HN(^{t}Bu)CH$_2$CH$_2$N(^{t}Bu)} with one molar equivalent ^{n}BuLi and excess TMEDA.[16] Other documented ligands on aluminium, in complexes where the lithium cation is solvated by two molecules of TMEDA, include for example alkyl,[17] hydrido,[18-20] thiol [21] or phosphide [22] examples.

After the successful, albeit unexpected, result in the α-metallation of TMEDA by means of "LiAl(TMP)$_2$(^{i}Bu)$_2$", we decided to extend this chemistry to the tridentate ligand PMDETA, which is commonly used to break up organolithium aggregates and thus to aid their solubility and reaction kinetics. A low resolution crystal structure of the isolated product

[Li{Me$_2$NCH$_2$CH$_2$N(Me)CH$_2$CH$_2$N(Me)CH$_2$}(TMP)Al(^{i}Bu)$_2$] (**5l**) (**figure 5.8**) was determined, and therefore bond angles and angular dimensions of this complex cannot be discussed. In contrast, a good quality crystal structure was obtained for the sodium congener [Na{Me$_2$NCH$_2$CH$_2$N(Me)CH$_2$CH$_2$N(Me)CH$_2$}(TMP)Al(^{i}Bu)$_2$] (**5n**) (**figure 5.8**), allowing a detailed analysis of its structural architecture to be made. The molecular structures of both **5l** and **5n** feature an undeca MNCCNCCNCAlN tricyclic ring (M = Li or Na), containing two five-atom, three element LiNCCN rings and a five-atom four-element LiNCAlN ring, with a mixed NCH$_2$-TMP bridging ligand set completed by two terminal ^{i}Bu ligands on Al and a chelating metallated PMDETA (*N,N,N*-attached) to the alkali metal M. In complex **5n**, Al displays a distorted tetrahedral geometry [mean bond angle around Al, 109.32^o; range, 94.10(6)^o {C(20)–Al(1)–C48)} – 122.15(5)^o {N(1)–Al(1)–C(20)}], displaying a ligand set of three carbon atoms, one from the deprotonated PMDETA molecule [Al(1)–C(48), 2.0479(14) Å] and two from the dormant terminal ^{i}Bu arms [bond lengths: Al(1)–C(20), 2.0342(13) Å; Al(1)–C(30), 2.0381(15) Å], and a N of the amido TMP, with the shortest bond length of 1.9704(11) Å [Al(1)–N(1)]. The wider bond Al(1)–C(48)–N(4) bond angle [124.46(9)^o], in comparison to the associated angle found in the Li/TMEDA complex **5k** [116.86(10)^o], is probably due primarily to the difference in denticity between TMEDA and PMDETA. Also, Na$^+$ has a larger ionic radius than Li$^+$ (relative differences in ionic radii of Li$^+$ and Na$^+$, Δ 0.26 Å [23]), therefore the ligand has to open up around the metal more to compensate for this change in size, resulting in the increase in bond angle. Contact to the sodium atom from aluminium in **5n** is through one amido (TMP) nitrogen atom [Na(1)–N(1), 2.4962(12) Å] and one nitrogen (shortest Na–N bond) of the metallated junction of PMDETA [Na(1)–N(4), 2.3906(12) Å]. The remaining nitrogen atoms of PMDETA also bind to Na [bond lengths: Na(1)–N(2), 2.5311(13) Å; Na(1)–N(3), 2.4682(13) Å], with bond lengths close to the mean K–N one calculated from the CSD [2.521 Å], completing a drastically distorted tetrahedral [mean bond angle around Na, 106.49^o; range 75.35(4)^o {N(3)–Na(1)–N(2)} – 141.66^o {N(3)–Na(1)–N(1)}] geometry around Na.

X-ray crystallographically determined structures of metallated derivatives of PMDETA are even rarer than those of TMEDA. Indeed only one hit was found in the CSD. As recently as 2007, it was reported by Strohmann that PMDETA can be lithiated (with ^{n}BuLi at -78°C) on a terminal

methyl to generate the crystalline dimeric complex [(Me)$_2$NCH$_2$CH$_2$N(Me)CH$_2$CH$_2$N(Me)CH$_2$Li]$_2$.[24]
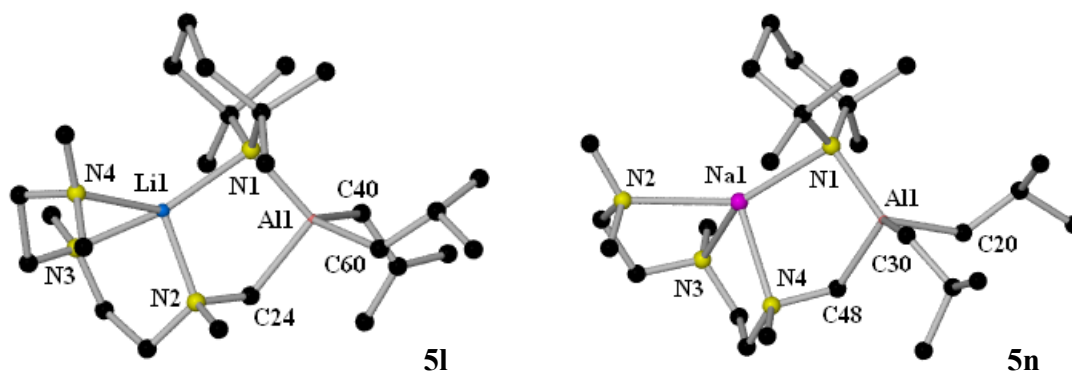
Figure 5.8: Molecular structures of lithium and sodium aluminates, 5l and 5n respectively.

When the heavier alkali metal amide KTMP was employed together with ^{i}Bu$_2$Al(TMP), in the presence of one molar equivalent of TMEDA, the unexpected product [(TMEDA)·K(μ-TMP*)(μ-^{i}Bu)Al(^{i}Bu)] (**5p**) was isolated. The molecular structure of **5p** (**figure 5.9**) is very different to complex **5k** (where LiTMP was utilised). The monomeric unit of **5p** consists of three fused rings, all non-planar [one a four element (KNAlC) ring (sum of bond angles, 356.67^o); a four-atom, three-element (NAlCC) ring (sum of bond angles, 353.96^o); and one six-membered
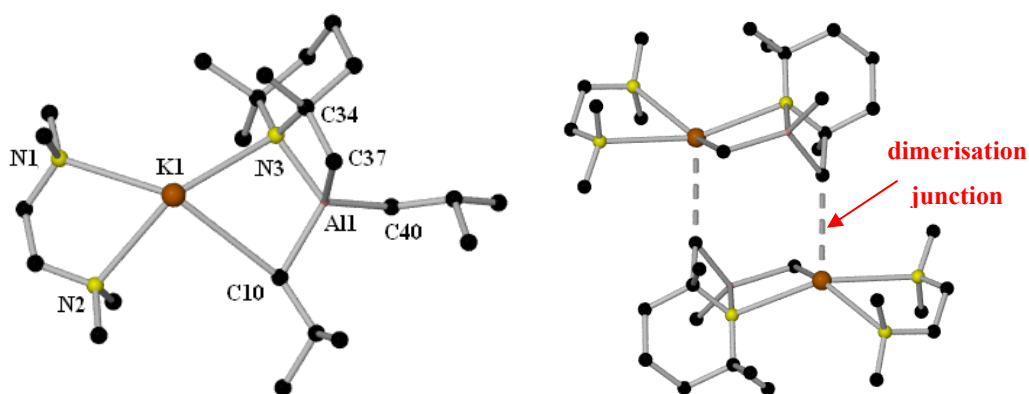
Figure 5.9: Molecular structures of the monomeric unit of trapped TMP* dianion complex 5p (left), and the dimeric form it produces (right) [the CH(Me)$_2$ of ^{i}Bu groups have been removed for clarity].

CCCCCN ring from the chair-shaped modified TMP* ligand]. The architecture of the monomeric unit also includes a mixed TMP*–^{i}Bu bridging set, unlike any of the other structures mentioned, and is completed by one terminal ^{i}Bu ligand on Al and a chelating TMEDA (*N,N*-attached) to K. The Al centre displays a distorted tetrahedral geometry [mean bond angle around Al, 108.87^o, where the smallest bond angle is that involving N and C from the dideprotonated TMP molecule {N(3)–Al(1)–C(37), 73.54(8)^o}] made up of one carbon atom from each ^{i}Bu group [terminal ^{i}Bu ligand {bond length: Al(1)–C(40), 2.015(2) Å}; bridging ^{i}Bu {length: A(1)–C(10), 2.023(2) Å}] and a carbon, nitrogen atom pair from the chelating TMP* ligand [lengths: Al(1)–C(37), 2.010(2) Å; Al(1)–N(3), 1.8975(17) Å]. As a consequence, both N(3) and C(34) become stereogenic centres. As the space group is centrosymmetric, these atoms exist as (*S,R*) and (*R,S*) enantiomeric pairs within the crystal. Contact to K from Al in the monomer is through one amido (TMP) nitrogen bridge [K(1)–N(3), 2.8253(16) Å] and one ^{i}Bu carbon bridge [K(1)–C(10), 3.184(2) Å]. Completing a distinctly distorted tetrahedral geometry around K [mean angle, 105.16^o], the N atoms of normal TMEDA (that is having its full complement of hydrogen atoms) bind in a bidentate fashion to K [bond lengths: K(1)–N(1), 2.8978(19) Å; K(1)–N(2), 2.8242(18) Å]. The reason for the distortion of the tetrahedral coordination sphere [subtending bonds angles from 64.30(6)^o {N(1)–K(1)–N(2)} to 146.28(5)^o {N(2)–K(1)–N(3)}] around the potassium cation is due in the main to the acute bite angle from the bidentate ligand, and also because of dimerisation. Potassium from each monomeric unit forms a relatively weak interaction with the aluminated methyl group (C37) of a neighbouring molecule from the TMP* ligand [K(1)-C(37'), 3.413(2) Å] (**figure 5.9**), and hence the result of this contact, making K five coordinate overall, is that a loose dimer is formed.

Reflecting the high novelty of structure **5p**, as far as we can ascertain, there are no structural examples, or indeed any reported syntheses, of TMP* dianion formation. Formally the reaction leading to **5p** an be regarded as a self-deprotonation, with one TMP anion reacting with another. This unusual reactivity emphasises the greater scope of mixed-metal chemistry as TMP self-deprotonation/metallation is unlikely to be reproduced (in a controlled manner) in a homometallic system. While this reaction is unprecedented, TMP dispensed as Mg(TMP)$_2$ has been reported to deprotonate LiHMDS at a Si(CH_3) site,[25] though this is a much less challenging task as several examples of Si(CH$_3$) deprotonation have appeared.[26] For example,

the reaction of the lanthanide amides $Ln(HMDS)_3$ [where Ln = Y or Yb] with the hypersilanide $KSi(SiMe_3)_3$ results in the ate complexes $[K]^+[CH_2Si(Me)_2N(SiMe_3)Ln\{N(SiMe_3)_2\}_2]$, where one of the methyl groups of the amide has been deprotonated, forming a dianion of HMDS.[27] Similar compounds have been isolated when the base utilised is $LiN(SiMe_3)_2$, $NaN(SiMe_3)_2$, KH or ^nBuLi.[28-31] Given that the TMP anion has been used as a base for about forty years in a wide range of deprotonative reactions (when attached to a metal, especially lithium, see Chapter 1), the second deprotonation of this amide (by a further TMP anion) is extraordinary, and potentially synthetically useful as an entry to unsymmetrical methyl-substituted TMP adducts.

5.2.2) Solution Studies

All of the compounds mentioned in this section are soluble in d_{12}-cyclohexane (d_{12}-Cy) solution, enabling their ^1H and ^{13}C NMR spectroscopic analysis. For $^iBu_2Al(TMP)$ (**5j**), even though it was previously found to act as a mild deprotonative metallating base (see Chapter 1, pages 20–23), to the best of our knowledge no NMR spectroscopic data has been hitherto reported for it. In d_{12}-Cy solution, **5j** gave a very clean ^1H NMR spectrum (**figure 5.10**), even though the oil was not purified, highlighting that the synthetic reaction to generate **5j** should be almost quantitative when used *in situ*. Within this spectrum, two well-defined sets of signals are present, one for the
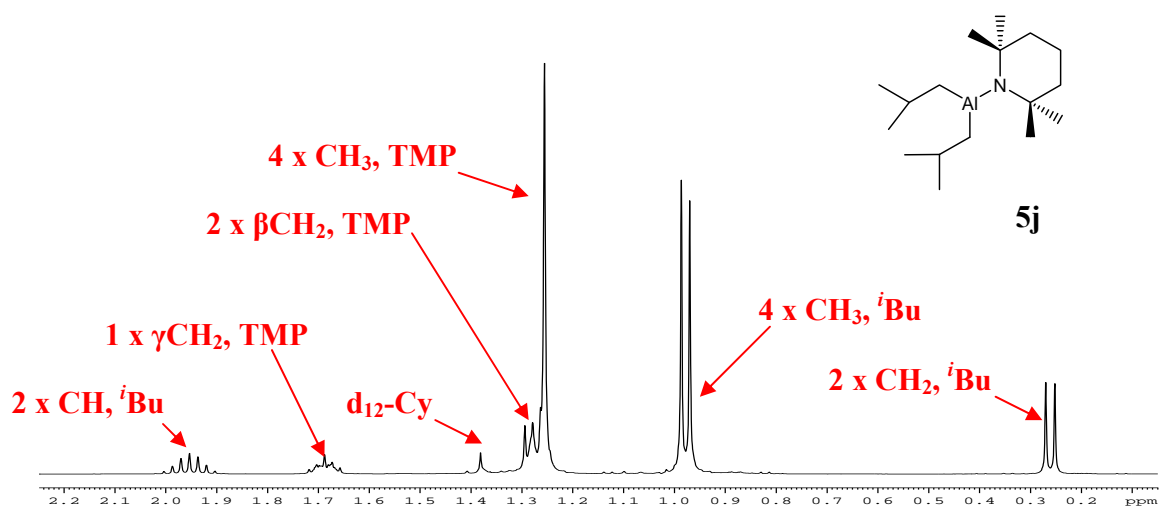
Figure 5.10: ^1H NMR spectrum of the neutral alumane 5j in d_{12}-Cy solution.

210

^{i}Bu groups [2 × CH, 1.96 ppm; 4 × CH$_3$, 0.98 ppm; and 2 × CH$_2$, 0.26 ppm] and the other for TMP [1 × γCH$_2$, 1.69 ppm; 2 × βCH$_2$, 1.28 ppm; and 4 × CH$_3$, 1.26 ppm], in a 2:1 ratio.

The lithium aluminate complex [Li{Me$_2$NCH$_2$CH$_2$N(Me)CH$_2$}(TMP)Al(^{i}Bu)$_2$] (**5k**), which was isolated in a yield of 55%, was characterised by ^{1}H, ^{13}C and ^{7}Li NMR spectroscopy. Although at first glance the ^{1}H NMR spectrum (**figure 5.11**) looks complicated, utilising ^{1}H–^{1}H and ^{1}H–^{13}C correlation techniques, the resonances can be fully assigned. The most significant feature of this spectrum is the two doublet signals (AB spin system, $J_{HA, HB}$ = 14.4 Hz) at 1.36 and 1.55 ppm for both hydrogen atoms of the metallated NCH_2 unit of TMEDA. The Me$_2$N and Me'N resonances appear at 2.37, 2.34 and 2.22 ppm, while all four H atoms of the two unique CH$_2$ groups are inequivalent, having separate resonances at 2.92, 2.71 and within the multiplet of 2.06-1.84 ppm, consistent with the rigid, bicyclic conformation of the structure. This ^{1}H NMR spectrum also reveals the presence of two ^{i}Bu groups and one TMP ligand. The resonances attributed to the former cover a wide chemical shift range, for example the metal–CH$_2$ resonances spread from 0.33–(-0.06) ppm [a marked difference from the narrow range of 0.28–0.25 ppm in **5j**]. The CH$_3$ and CH resonances appear as doublets [0.98 and 0.97 ppm (with $^3J_{HH}$ values of 6.4 Hz); and 0.91 and 0.87 ppm, with $^3J_{HH}$ values of 6.6 Hz] and as septets [one at 1.78 ppm ($^3J_{HH}$ = 6.7 Hz) and
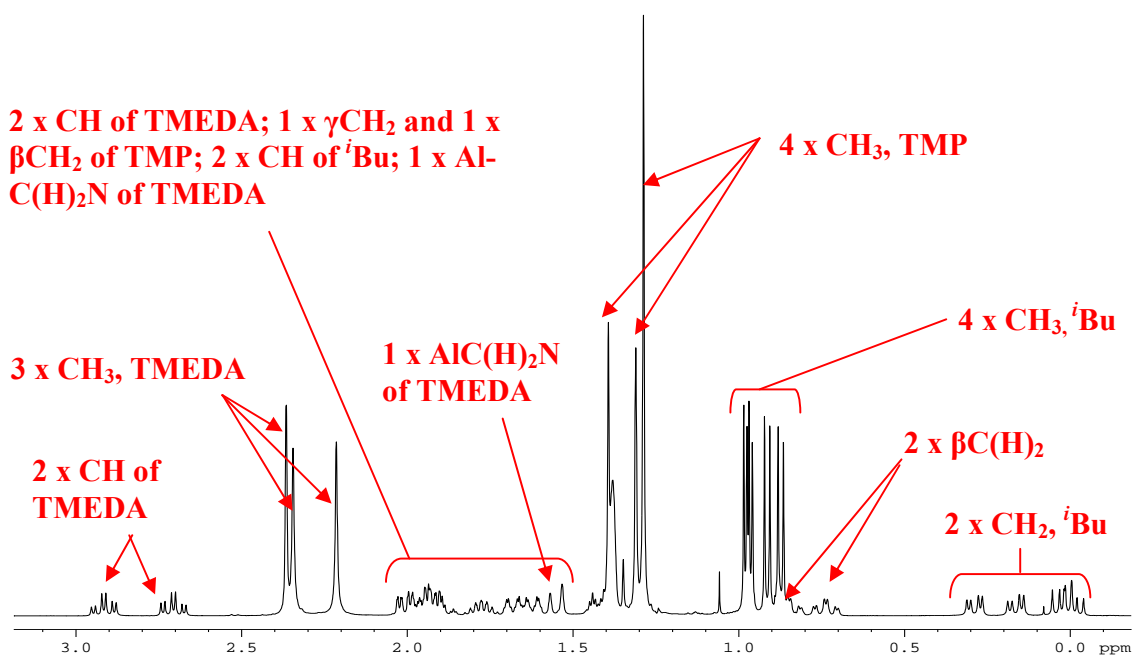
Figure 5.11: ^{1}H NMR spectrum of 5k in d$_{12}$-Cy solution.

the other resides within the multiplet between 2.06-1.84 ppm], respectively. Thus it seems that although both ^{i}Bu groups are terminal, they are magnetically inequivalent. Confirming the rigidity of the bicyclic ring system in solution, the TMP resonances spread out due to the different magnetic environments of the hydrogen atoms. Unlike in the spectrum of the neutral aluminium starting material **5j**, where only one singlet (at 1.25 ppm) represents all four TMP methyl groups, in the ^{1}H NMR spectrum of **5k**, three singlets at 1.39 (1 × CH$_3$), 1.31 (1× CH$_3$) and 1.29 (2 × CH$_3$) ppm are observed. The βC(H)$_2$ atoms are all inequivalent, residing at a lower frequency (0.74 and 0.85 ppm) and a higher frequency (1.72-1.58 ppm) compared to those in **5j** (1.28 ppm). Appearing within the multiplet between 2.06-1.84 ppm, the resonances of the γCH$_2$ hydrogens of TMP appear shifted downfield by at least 0.15 ppm in comparison to corresponding resonances in **5j**. The ^{7}Li NMR spectrum of **5k** reveals a resonance at 1.20 ppm, and the ^{13}C NMR has been fully assigned, showing a set of resonances consistent with structure **5k**. ^{1}H NMR spectroscopic analysis of the reaction filtrate revealed resonances of only **5k** and free TMP(H) [at 1.62 (1 × γCH$_2$), 1.29 (2 × βCH$_2$) and 1.06 (4 × CH$_3$) ppm], and with the ^{7}Li NMR spectrum confirming the presence of only one species it can be assumed that this deprotonation reaction of TMEDA is quantitative.

As previously remarked by Clayden,[32] "direct C–H deprotonation α to nitrogen is usually impossible to achieve (except for superbasic reagents) unless the lone pair is involved in conjugation with a carbonyl group or delocalised around an aromatic ring". This general process, direct α-metallation of tertiary amines, is a desirable synthetic route to polar heteroatom-containing organometallics but is hampered due to the destabilisation of the developing carbanions caused by the repulsion with the lone pair electron density of the adjacent nitrogen atom.[33-35] Usually multi-step procedures such as BF$_3$-activation of amines,[36] transmetallation (in particular, tin/lithium exchange),[11,12,37-40] or C–S/C–Te bond breakages [41-44] are necessary to access these useful synthetic reagents, but generally these provide only moderate yields. Only a few examples exist for which direct deprotonation of otherwise non-functionalised amines has been demonstrated. Although TMEDA's primary role in organometallic chemistry [45,46] is as a bidentate N donor ligand, it does, on prolonged contact to certain organoalkali reagents, undergo different direct α-metallation reactions, the regioselectivity of which depends on the identity of the deprotonating agent. Thus, by means of ^{t}BuLi [47] or ^{n}BuLi,[14,15] lithiation of TMEDA at the

terminal methyl group is achieved, while alternative methylene metallation followed by elimination of potassium dimethylamide is observed when the superbase LICKOR is used.[47] Only a select few methods have been proven to be effective in direct deprotonation of other non-functionalised bidentate amines. As examples, 1,3-dimethyl-1,3,diazacyclohexane can be deprotonated/lithiated at the disfavoured position between the two nitrogen atoms with ^{t}BuLi [48,49] and *N,N,N′,N′*-tetramethylcyclohexane-1,2-diamine [(*R,R*)-TMCDA] can also be deprotonated/lithiated, at a terminal CH_3 group, by the powerful base ^{t}BuLi.[50] In terms of regioselectivity and yield, the formation of **5k** by the process described (metallation occurs only on the methyl group) is quantitative (as proven by ^{1}H NMR spectroscopy) and the synthetic procedure takes place at room temperature in a relatively short period of time (30 minutes), making it a very attractive synthetic route.

In structural terms, one of the closest compounds to **5k** is **5q** (**figure 5.12**). Though not a complete comparison, as the ^{1}H NMR data of **5q** were recorded in C_6D_6 solution, the most significant common resonance is the presence of a pair of doublets, showing an AB spin system with a $J_{HA, HB}$ coupling of 12.9 Hz. A second molar equivalent of TMEDA was added to the *in situ* reaction mixture of **5k**, to ascertain whether the TMP anion would deprotonate the bidentate
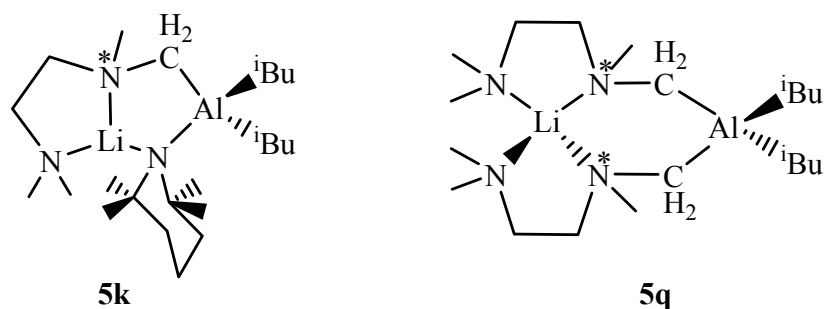
Figure 5.12: Structures of deprotonated TMEDA complexes 5k and 5q.

ligand to form **5q**. This reaction, at room temperature or even under reflux conditions, was unsuccessful since ^{1}H NMR analysis of the reaction mixture revealed **5k** and free TMEDA only. The ^{7}Li NMR spectrum also showed one resonance, that of **5k**. Therefore, from the results of this reaction, a reaction sequence for the formation of **5q** can be proposed (**scheme 5.13**). In the first step, TMEDA is intramolecularly α-aluminated by activated TMP, with concomitant elimination

of TMP(H) to yield intermediate **A** (not isolated or detected), which is more reactive than the initial lithium TMP-aluminate "^{i}Bu₃Al(TMP)Li" as **5q** was still obtained even when a deficiency of TMEDA was employed. This putative intermediate can react in two different possible ways: (i) with an additional equivalent of TMEDA (pathway x), where the chelating diamine could coordinate to lithium, because the Li···^{i}Bu contact in **A** can be expected to be relatively weak,
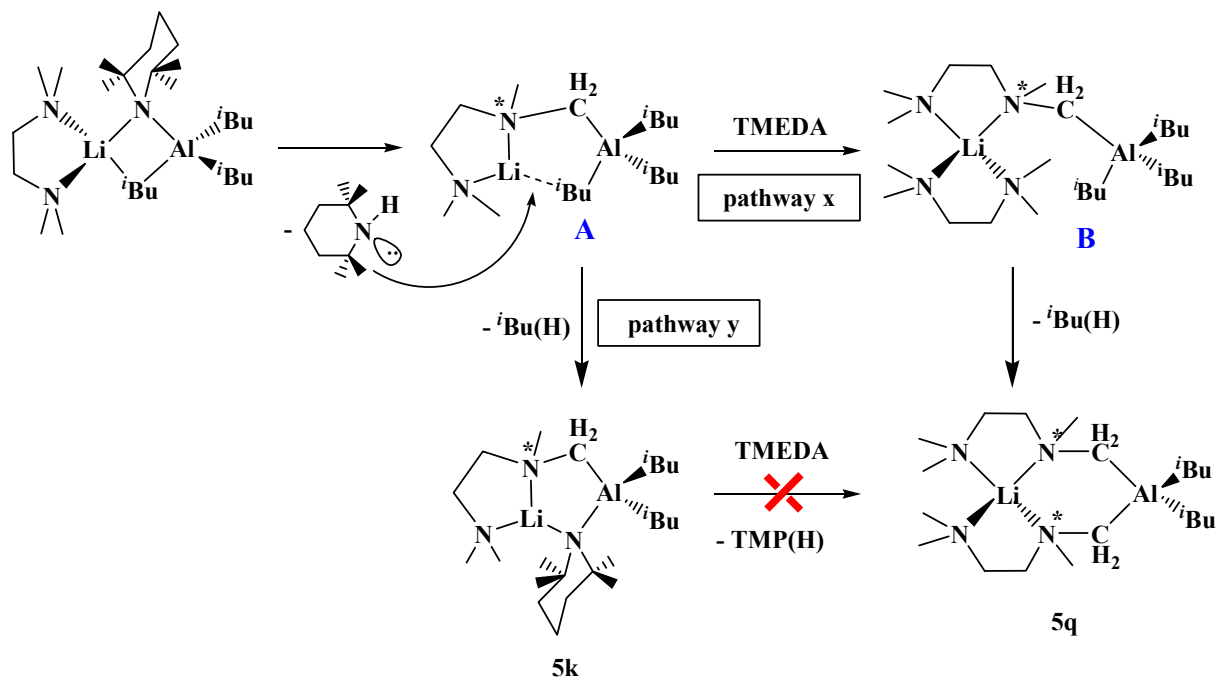
Scheme 5.13: Proposed stepwise reaction pathway for the formation of 5q.

allowing the formation of intermediate **B** (not isolated or detected). In a final step, one of the neighbouring ^{i}Bu groups attached to Al intramolecularly deprotonates one NMe₂ arm of the TMEDA, to close a six-atom {LiNCAlCN} ring, affording compound **5q** and releasing ^{i}Bu(H). (ii) alternatively, **A** could react with the TMP(H) formed during the metallation of the first equivalent of TMEDA (pathway y), affording compound **5k**. In this compound the TMP ligand forms a strong bridge between Li and Al, which is retained in solution as evidenced by the inequivalence of the four TMP methyl groups in the ^{1}H and ^{13}C NMR spectra. The failure to metallate a second equivalent of TMEDA, as mentioned previously, can be rationalised in terms of the coordination sphere of Li, which forms three strong Li–N bonds [Li–N bond distances:

2.00(3), 2.086(3) and 2.0340(16) Å], making the alkali-metal coordinatively and electronically saturated, leaving no place for the coordination of an additional molecule of TMEDA. Because this precoordination seems to be crucial for the deprotonation to take place, the formation of **5q** must occur through the alternative reaction pathway x. The stronger Lewis basicity of TMEDA versus that of bulky TMP(H) and also its bidentate nature may be important factors in favouring this unexpected reaction pathway.

The story behind the formation of solvent-separated $[\{Li \cdot (TMEDA)_2\}^+\{Al(DMP)_2({}^iBu)_2\}^-]$ (**5m**) is more complex. **5m** was first isolated in crystalline form from the initial reaction of LiDMP and one molar equivalent of both ${}^iBu_2Al(DMP)$ and TMEDA. Only 0.05 g of isolated crystalline material was recovered, with ${}^1H$ and ${}^{13}C$ NMR resonances confirming it as **5m**, but at least one other compound can be seen in the NMR spectra (highlighted in blue) (**figure 5.13**).
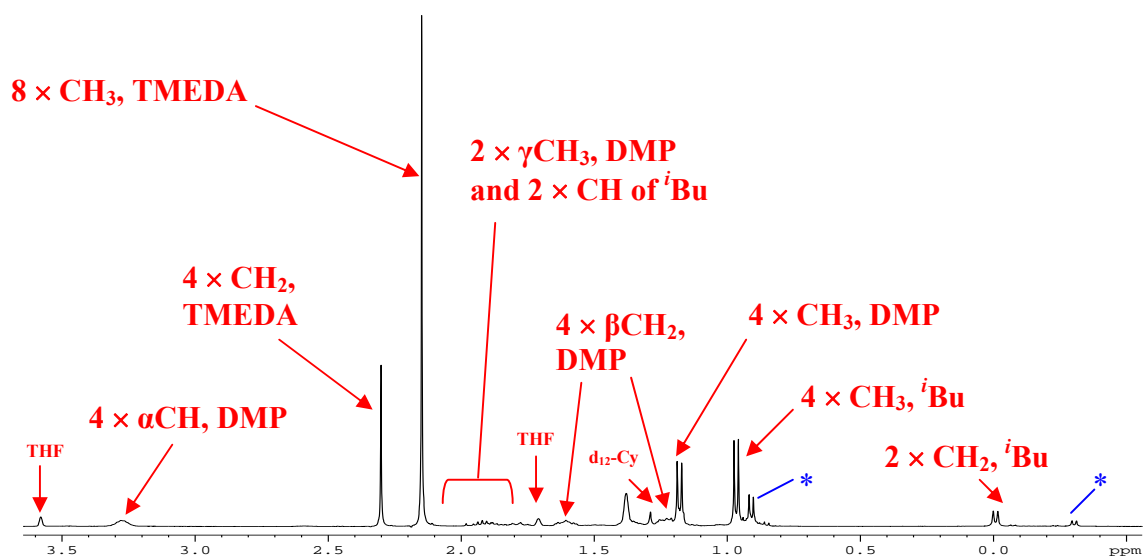
Figure 5.13: ${}^1H$ **NMR spectrum of the initial crystalline material of 5m (in d_{12}-Cy and a few drops of d_8-THF to give a homogeneous solution).**

The ${}^7Li$ NMR spectrum of this crystalline solid shows one relatively broad resonance at 0.69 ppm, hinting that perhaps two (or more) compounds could be present, reflecting the low quantity of **5m** recovered. The small resonances highlighted in blue in **figure 5.13** could be from the species $[(TMEDA)_nLi.]^+[Al({}^iBu)_4]^-$ (n = 0, 1 or 2), as it seems that the unassigned peaks

represent [i]Bu groups only (as seen from ^{1}H-^{1}H coupling NMR experiments) which do not correlate with the ^{1}H NMR standard of [i]Bu$_3$Al in d$_{12}$-Cy solution. Lithium tetraalkylaluminates have been seen before, for example [Li(μ-Et)$_2$Al(Et)$_2$]$_\infty$ is known as linear, polymeric chains in the solid state,[51] and more significantly [Li(dioxane)$_4$]$^+$[Al([i]Bu)$_4$]$^-$ has been reported by our own group.[8] Attempts to synthesise **5m** by the rational route of using two molar equivalents of TMEDA with respect to [i]Bu$_2$Al(DMP) and Li(DMP) produced a suspension in hexane solution in every case. ^{1}H, ^{13}C and ^{7}Li NMR spectroscopic analysis of this isolated solid (0.15 g) confirmed only one product was present. However, no resonances that can be assigned to [i]Bu groups were observed (**figure 5.14**). In fact, only resonances for DMP and TMEDA were witnessed, in a ratio of 4:1 respectively, and thus the formula of this compound has been tentatively proposed as [(TMEDA)·Li(μ-DMP)$_2$Al(DMP)$_2$] (**5r**). The possibility of a ladder-type structure with the formula "[(TMEDA)$_2$Li$_8$(DMP)$_8$]" was ruled out due to the isolation of the previously reported hemi-solvated complex [(TMEDA)·{Li(DMP)}$_2$]$_\infty$ [52] from the reaction mixture of four molar equivalents of LiDMP to one molar equivalent of TMEDA. The ^{7}Li NMR
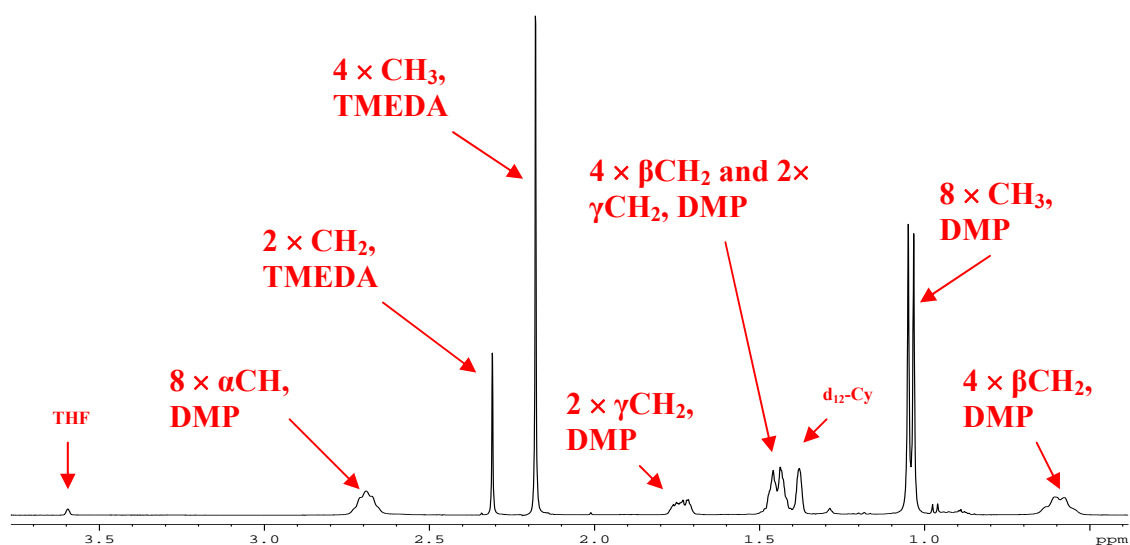
Figure 5.14: ^{1}H NMR spectrum of 5r in d$_{12}$-Cy (with a few drops of d$_8$-THF for solubility).

spectrum of **5r** showed one resonance at 1.95 ppm, which was not observable in the ^{7}Li NMR spectrum of the filtrate of this reaction mixture [resonances, 0.65 (major) and 0.19 ppm]. The ^{1}H NMR spectrum of the filtrate is complex showing overlapping resonances, reflecting a mixture

of products; however, several distinctive chemical shifts of **5m** can be identified. Combined with the ^{7}Li NMR resonance of 0.65 ppm, NMR spectroscopic evidence suggests that **5m** is present in significant quantities, along with other products of disproportionation (**scheme 5.14**).

The ^{1}H and ^{13}C (and ^{7}Li, for **5l**) NMR spectra of **5l,** and its sodium congener **5n (figure 5.15)**, reveals only one set of resonances, supporting the diastereoselective formation of these
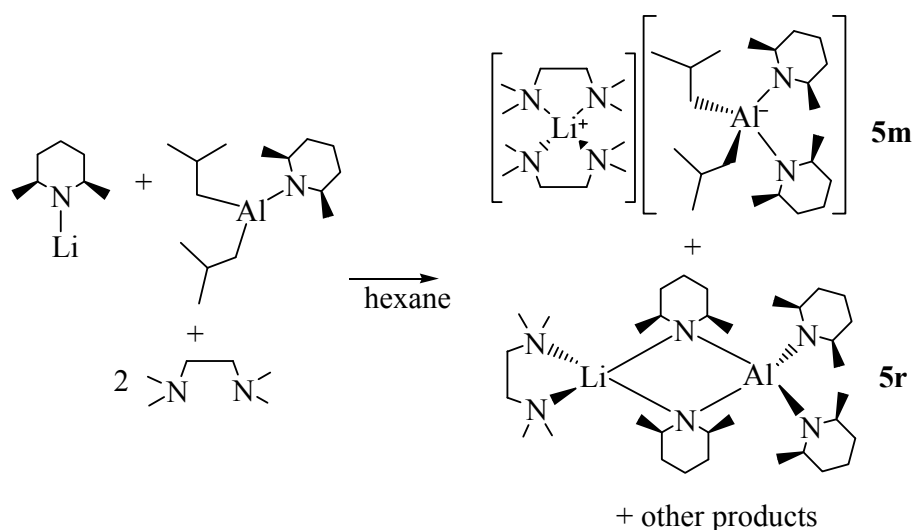
Scheme 5.14: Proposed products generated in the directed synthesis of 5m.

compounds (note that for each complex, two stereogenic centers are generated, namely the two N atoms of the metallated junction of PMDETA). The ^{1}H NMR spectra clearly shows the expected patterns for methyl-aluminated PMDETA, similar to that for TMEDA previously described for **5k**. For each compound, their ^{1}H NMR spectra (**figure 5.16**) reveals the AB spin system [**5l**, doublets at 1.04 and 1.79 ppm ($J_{HA, HB}$ = 13.4 Hz); **5n**, a doublet within the mutiplet between 1.01-0.84 ppm and a doublet at 1.66 ppm ($J_{HA, HB}$ = 13.2 Hz)]. The presence of two inequivalent ^{i}Bu groups and one TMP ligand can be identified, and their ^{1}H NMR spectra have the similar pattern observed in comparison to **5k** (see experimental section for full ^{1}H and ^{13}C NMR characterisation). It is noteworthy here that the resonances associated with the TMP methyl groups can be observed in the ^{1}H NMR spectrum for **5n** (at δ 1.32 and 1.29 ppm); however, the
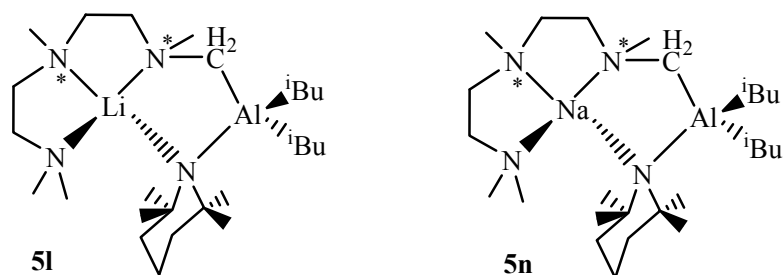
Figure 5.15: Structures of the mono-deprotonated PMDETA complexes 5l and 5n.

βCH_2 and γCH_2 hydrogen atoms could not be assigned. Utilising ^{13}C NMR spectroscopy, revealed the resonance of the γCH_2 carbon at 19.3 ppm and the βCH_2 carbon resonance was tentatively assigned at 46.9 ppm (on comparison with the chemical shift of 45.3 ppm for the βCH_2 (TMP) carbon of **5l**), though none of these resonances showed ^1H–^{13}C coupling signals. All of the other resonance signals associated with compound **5n** can be fully assigned by NMR spectroscopy.
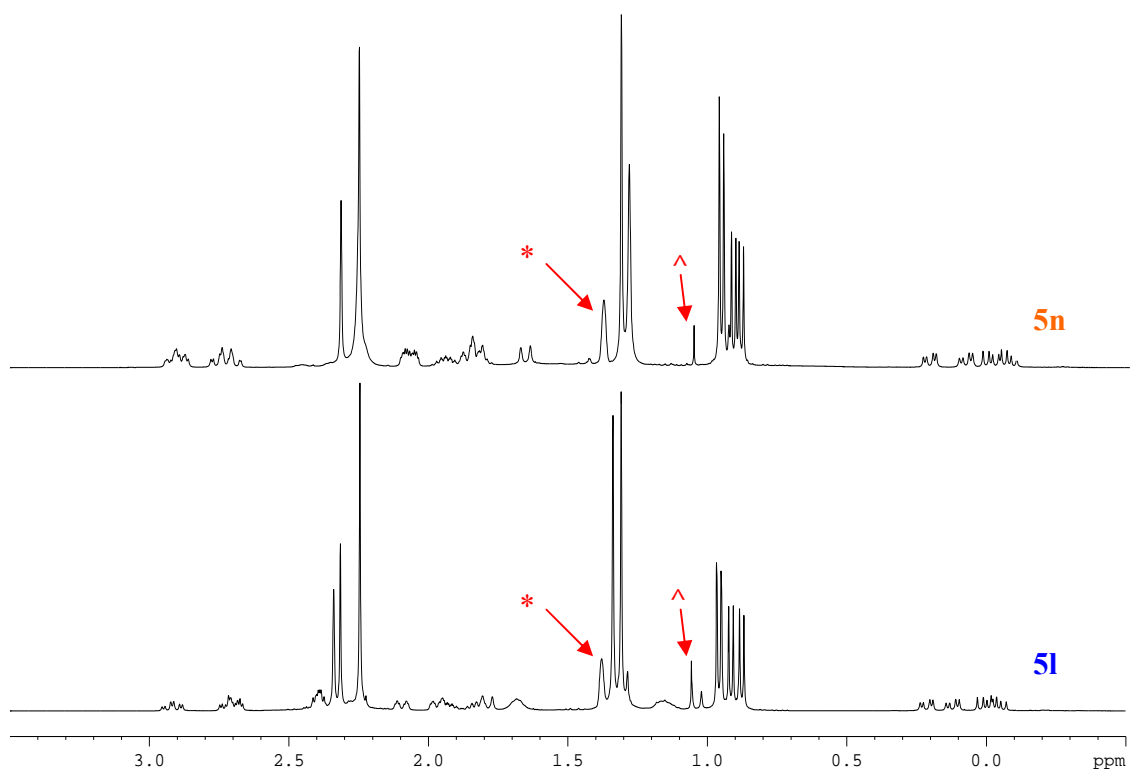
Figure 5.16: Comparison between the ^1H NMR spectra of the Li complex 5l and its Na analogue 5n. * and ^ represent d$_{12}$-Cy and TMP(H) respectively.

As mentioned previously, PMDETA deprotonation is an extremely rare occurrence. It is known that after prolonged exposure to alkyllithium reagents, the terminal or central methyl group can be lithiated depending on the concentration of the metallating reagent.[24,53-55] Other non-functionalised triamines can also be deprotonated. *N,N',N''*-trimethyl-1,4,7-triazacyclononane is lithiated at a CH_3 position by ^{n}BuLi,[56] whereas 1,3,5-trimethyl-1,3,5-triazacyclohexane (TMTAC) is deprotonated at a methylenic (CH_2) group between two nitrogen atoms with ^{t}BuLi.[48,49]

A second molar equivalent of PMDETA was added to the reaction mixture of **5l** to ascertain whether this second tridentate molecule could be metallated. The ^{1}H NMR spectrum of the reaction mixture revealed resonances of only free PMDETA and **5l**, with no evidence of a second deprotonation. Even after reflux conditions, the solution shows the same ^{1}H NMR spectrum. This mirrors the attempted reaction of a further equivalent of TMEDA to **5k**, which also failed in its goal, of generating a bis-(deprotonated TMEDA) complex.

With the Na / PMDETA reaction concoction yielding the same type of reactivity as the Li / PMDETA reaction, it was thought that the Na / TMEDA combination would follow the trend, that is showing metallation of the terminal carbon α to nitrogen as observed in complex **5k**. The homogeneous reaction mixture that followed from the mixing of NaTMP, ^{i}Bu$_2$Al(TMP) and TMEDA deposited a modest quantity of an off-white solid (**5o**) (0.15 g) after the Schlenk tube was left at -28°C. ^{1}H (**figure 5.17**) and ^{13}C NMR spectroscopic analysis of this highly soluble (in hexane solution) product revealed spectra unlike those of **5k**. Most significantly, the ^{1}H NMR spectrum revealed no resonances attributed to metallated TMEDA. In fact, unmetallated TMEDA resonances were observed [at 2.40 (CH_2) and 2.32 ppm (CH_3)]. Although no metallation had occurred on the bidentate ligand, an AB spin system is nonetheless present through resonances at 0.52 and -0.21 ppm [$J_{HA,HB}$ = 13.9 Hz], thus another type of metallation must have occurred. The site of metallation is a TMP methyl group, as the integration ratio of TMEDA to ^{i}Bu resonances [CH, 2.02-1.86 ppm; CH_3, 0.89 ppm; CH_2, 0.10-(-0.81) ppm] is 1:2, and from integration comparisons it seems that there is only one TMP ligand, where its resonances are spread across a relatively large chemical shift range. Only resonances for three of the four TMP methyl groups can be detected [two methyls at 0.89 ppm and one methyl at 1.19

ppm], and the βCH_2 and γCH_2 hydrogens of TMP cover the range 1.72-1.24 ppm], therefore the resonances at 0.52 and 0.21 ppm must be due to a metallated TMP methyl group. Analysis of the
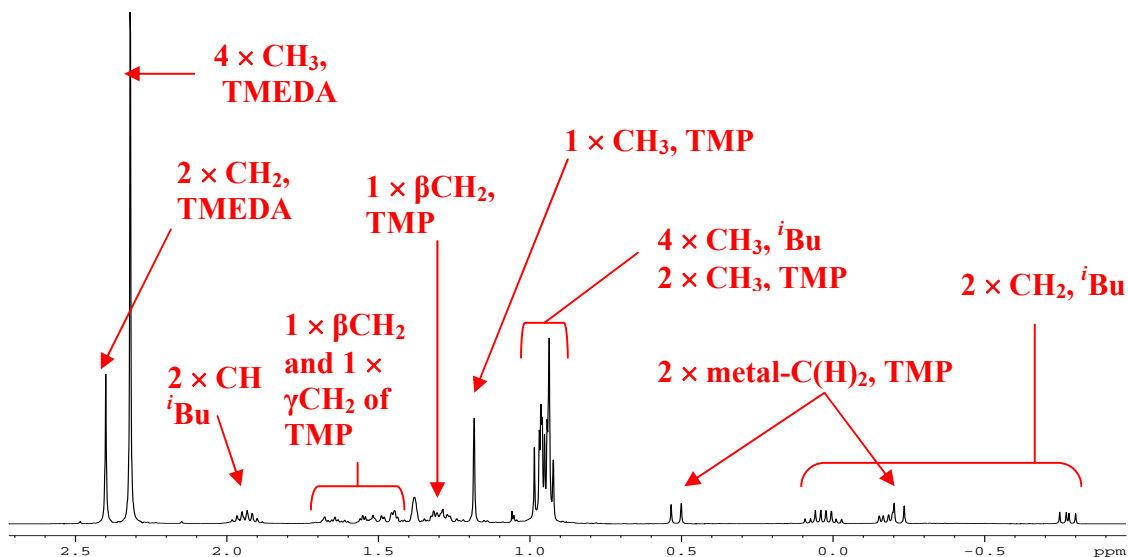
Figure 5.17: ^{1}H NMR spectrum of 5o in d$_{12}$-Cy solution.

^{13}C NMR spectrum shows that the carbon associated with the metallated methyl (31.8 ppm) is found close to the area, albeit at a lower frequency, of the untouched methyl groups (39.7, 39.1 and 38.0 ppm). The two ^{i}Bu groups appear magnetically inequivalent. The ^{13}C NMR data of **5o** confirm this assignment, as two separate resonances for the CH$_2$ carbons of the ^{i}Bu groups are identified at 31.0 and 26.1 ppm. The ^{1}H NMR spectrum filtrate of this reaction mixture showed only resonances for **5o**, as discussed, and free TMP(H), consequently this reaction can be considered to be quantitative. Many attempts to grow crystals of this compound suitable for X-ray crystallography were made; however, due to its high degree of solubility no success was forthcoming (even at -72°C).

Substituting the metal amide from NaTMP to KTMP, the reaction of this amide with one molar equivalent of ^{i}Bu$_2$Al(TMP) and TMEDA generated crystals of the TMP-dianion complex [(TMEDA)·K(μ-TMP*)(μ-^{i}Bu)Al(^{i}Bu)] (**5p**), which was characterised by X-ray crystallography. It is noteworthy to mention that before TMEDA was added, the reaction mixture consisted of a pale yellow suspension, similar to that of the KTMP starting material, indicating that the

homometallic reagents may not complex together in the absence of a suitable donor ligand. Complex **5o** should have an analogous structure to **5p** (**figure 5.18**), as its NMR spectra suggests a similar dianion structure, as mentioned previously. ^{1}H and ^{13}C NMR spectroscopy confirmed the dianionic TMP constitution of complex **5p**. Comparisons with the spectra of **5o** reveal an almost identical pattern (**figure 5.19**), confirming that the molecular structures should be essentially equivalent. The characteristic AB spin system of the hydrogen atoms of the
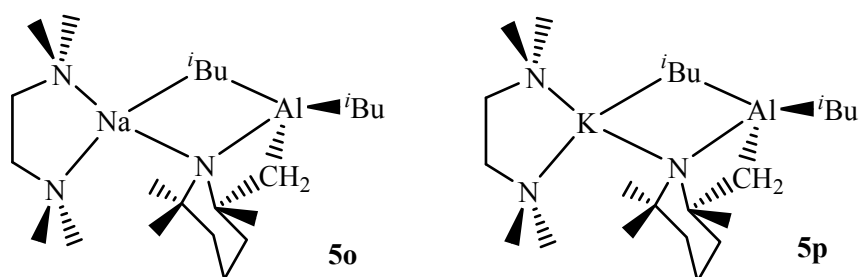
Figure 5.18: Structures of the TMP*-dianion complexes 5o and 5p.
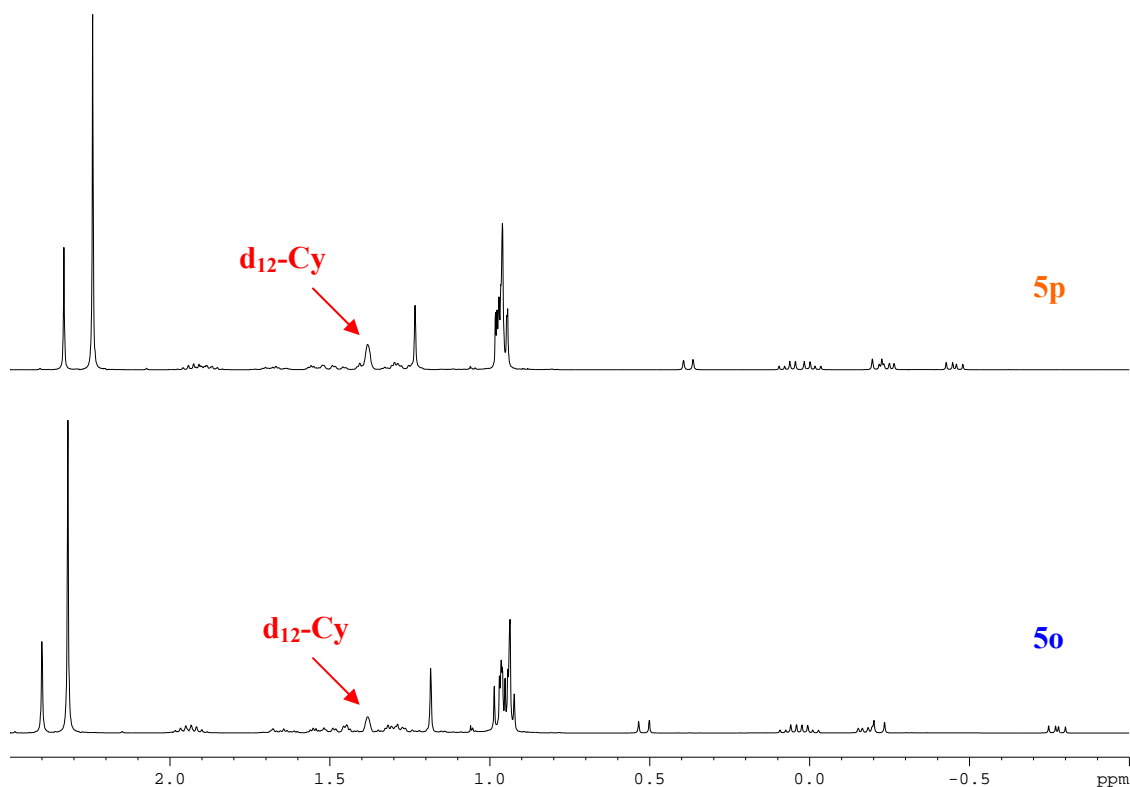
Figure 5.19: Comparison between the ^{1}H NMR spectra of the Na complex 5o and that of its K congener 5p.

aluminated methyl group, can be seen at 0.38 and -0.19 ppm (*c.f.* 0.52 and -0.21 ppm respectively for **5o**) with an associated ^{1}H–^{1}H coupling value of 12.5 Hz. Again, no deprotonation of the TMEDA ligand can be seen, as the integrations of the resonance peaks confirm that there are two ^{i}Bu groups and one TMP ligand. Reflecting the notion that complex **5p** retains its structure in solution, there are two ^{13}C NMR resonances associated with the CH$_2$ of the ^{i}Bu groups, at 31.8 and 27.3 ppm, confirming that the differences between bridging and terminal ^{i}Bu groups apparent in the solid state structure remain in solution. The effect of the direct alumination of the methyl group results in the generation of two distinct αC atoms of the TMP ligand, which is evident in the ^{13}C NMR spectrum by the appearance of two signals at 57.2 and 50.6 ppm [αC of free TMP(H) comes at 50.0 ppm in d$_{12}$-Cy solution]. The C resonance of the aluminated methyl (32.9 ppm) in **5p** follows the same pattern in the ^{13}C NMR of **5o**, as it resides close to the resonances of the untouched methyls (36.9, 36.6 and 31.5 ppm). The filtrate of the reaction mixture was analysed by ^{1}H NMR spectroscopy, which established that further **5p** and free TMP(H) were present.

To complete this mini-series of reactions, PMDETA was added to the insoluble brew of KTMP and ^{i}Bu$_2$Al(TMP). Upon addition of the tridentate ligand, a homogeneous solution was afforded, from which no solid material could be obtained (after numerous attempts). Removal of the solvent *in vacuo* yielded an oily substance (**5s**) that was soluble in d$_{12}$-Cy solution. The ^{1}H NMR spectrum (**figure 5.20**) of the crude reaction mixture revealed a surprising result. It was
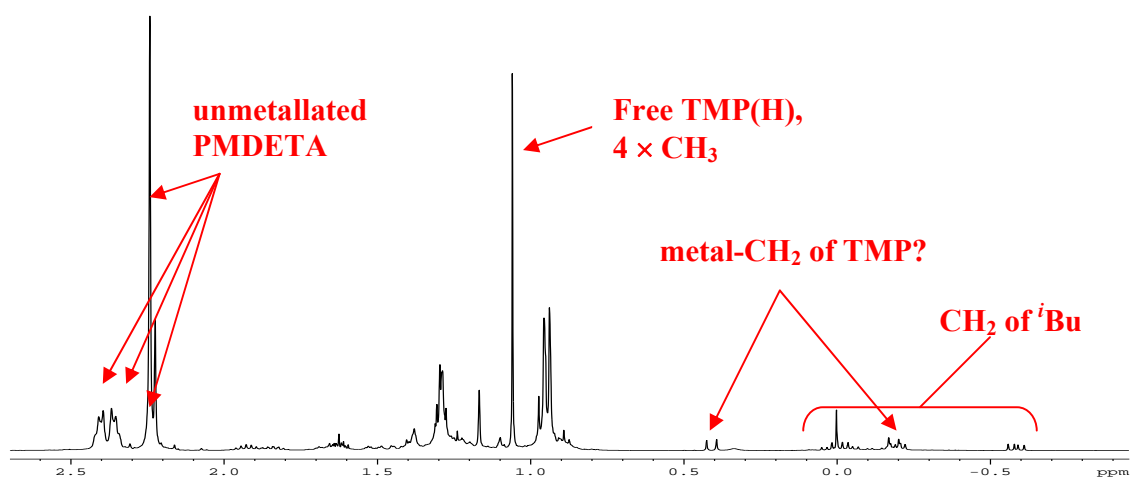
Figure 5.20: Crude ^{1}H NMR spectrum of the reaction mixture of 5s in d$_{12}$-Cy solution. Key resonances are labelled in red.

anticipated that a terminal methyl of the PMDETA would have been deprotonated, as the reactions involving LiTMP and NaTMP produced the mono-aluminated PMDETA complexes **5l** and **5n** respectively. However, significantly the resonances of the tridentate amine appear to be those of ligated, non-metallated, PMDETA [4 × CH$_2$, 2.44-2.34 ppm; 4 × CH$_3$, 2.25 ppm; 1 × CH$_3$, 2.23 ppm] by comparison to free PMDETA in d$_{12}$-Cy solution [2 × CH$_2$, 2.42-2.39 ppm; 2 × CH$_2$, 2.31-2.28ppm; 1 × CH$_3$, 2.19 ppm; 4 × CH$_3$, 2.14 ppm]. Supplying evidence for the formation of a TMP dianion, the resonances now indicative of an AB spin system, seen in the ^{1}H NMR spectra for compounds **5o** and **5p**, can be observed in the ^{1}H NMR spectrum of **5s**, at 0.41 and -0.19 ppm ($J_{HA,HB}$ = 12.8 Hz), and the resonance pattern associated with the CH$_2$ hydrogens of the ^{i}Bu groups [0.04-(-0.62)] ppm is very similar to those in the spectra of **5o** and **5p**. The presence of these mentioned resonances indicate that a TMP dianion compound could be present in the reaction mixture, though may be not exclusively as there are a small number of peaks which have not been assigned (the ^{13}C NMR spectrum is also crowded from unidentified resonances). However, there appears to be no evidence for PMDETA metallation.

Analysis of the products isolated from this metallation study, both in the solid and solution state, indicates a point where metallation of the ligand on the alkali-metal is disfavoured in preference to the deprotonation of the TMP ligand. This can be rationalised by the close proximity effect of the ligands, and the relative sizes of the coordination spheres of the alkali metal cations. For lithium, bidentate TMEDA and tridentate PMDETA more than sufficiently fulfils its coordination requirements, and hence acts as a "cap" on the metal. The terminal methyl groups therefore lie very close to the sterically-encumbered TMP ligands as the neutral co-ligand wrap around Li, such that one TMP can deprotonate a methyl group of the ligand, resulting in structures **5k** and **5l**, and eliminating TMP(H) as a co-product in each case. This reaction must be energetically favourable, as NMR spectroscopic studies proves that these reactions are quantitative. In the case of sodium, a larger cation in comparison to lithium, the PMDETA ligand acts in the same manner as for Li, due to its tridentate chelating nature, extending around a large area of the coordination sphere of sodium. However, TMEDA does not cover the Na coordination environment to the same extent, and therefore stays at one side of the Na cation, away from the TMP ligands. Therefore, one TMP ligand deprotonates another in an intramolecular metallation process to yield the dianion product **5o**. The same self-deprotonation

occurs for the yet larger K cation, where even PMDETA cannot get close enough to the TMP anions to afford methyl PMDETA alumination, therefore TMP deprotonation seems to take place preferentially. Following these precedents, other unlikely dianion or deprotonated ligand complexes should be achievable using the right metal/ligand combinations, as these bimetallic motifs seem ideal for carrying out special intramolecular reactions.

5.3)   Isolation of Potassium Mono(amido)-Tris(alkyl)aluminates

Uchiyama previously isolated and characterised the lithium aluminate [(THF)·Li(μ-TMP)(μ-^{i}Bu)Al(^{i}Bu)$_2$] (**5t**) from a hexane solution with one molar equivalent of THF.[5] Within our group, other aluminate species similar to **5t** have been made and isolated (as noted in pages 197-199) utilising either lithium or sodium.[7-9] Attempts to generate related mixed K / Al reagents have been unsuccessful in their initial goals. For example, attempting to synthesise the mono-alkoxy tris-alkyl complexes from Me$_3$Al and KO^{t}Bu in the presence of a chelating donor ligand, complexes of the type [K·(Sol)$_n$]$^+$[AlMe$_4$]$^-$ [sol = TMEDA, PMDETA, 18-crown-6] were formed through a disproportionation reaction and subsequently isolated. The reaction of TMEDA with one molar equivalent of KTMP (prepared by metathesis from LiTMP and KO^{t}Bu) and ^{i}Bu$_3$Al generated the unexpected homoalkyl product [(TMEDA)$_2$·K(μ-^{i}Bu)$_2$Al(^{i}Bu)$_2$] (**scheme 5.15**) in extremely limited yields (6%), where the expected product was [TMEDA·K(μ-TMP)(μ-^{i}Bu)Al(^{i}Bu)$_2$]. Our reasoning for this product of disproportionation was due to the relative size of the potassium atom in comparison to that of lithium and sodium. It was thought that because
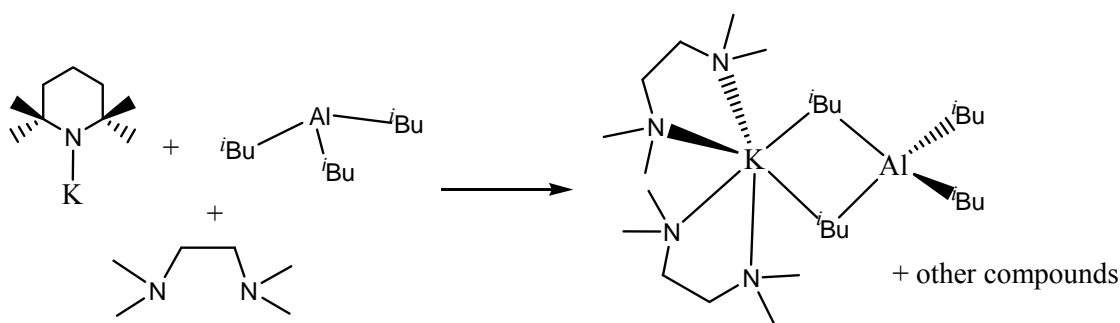
Scheme 5.15: A potassium aluminate isolated from a disproportionation reaction.

potassium prefers a larger coordination number (depending on ligand sizes normally greater than 4) in comparison to either of the smaller alkali-metals, it forms bonds to two molecules of TMEDA, and two to a [Al(^{i}Bu)$_4$]$^-$ unit. It is also reasoned that the lack of TMP in the molecular structure of the isolated complex is down to the tendency for potassium to favour K–C bonds over K–O or K–N. The aim of this section was to isolate and characterise potassium mono(amido)-tris(alkyl)aluminate species, mainly by altering the donor ligand attached to K.

Using PMDETA as the ligand for potassium, the mono(amido)-tris(*iso*-butyl)aluminates [synthesised via the cocomplexation of the relevant potassium amide, PMDETA and ^{i}Bu$_3$Al (scheme 5.16)] of general formula [PMDETA·K(μ-amide)(^{i}Bu)Al(^{i}Bu)$_2$] [where amide = TMP (**5u**), DMP (**5v**), or HMDS (**5w**)] can be isolated in yields of 17, 33, and 52 % respectively. The lower than expected yields can be explained by a high solubility of these compounds in hexane solution rather than by unclean reactions. ^{1}H NMR spectroscopic analysis of the filtrates reveals further quantities of the base in each case, with no resonances of disproportionation products observed.
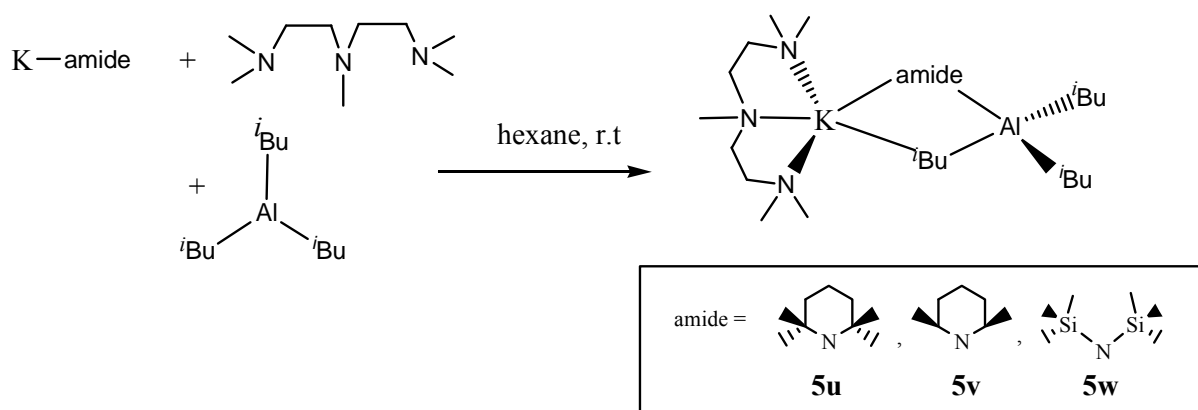
Scheme 5.16: Cocomplexations of the potassium mono(amido)-tris(*iso*-butyl)aluminates 5u, 5v, and 5w.

5.3.1) Solid-State Analysis

The three potassium aluminates **5u**, **5v**, and **5w** share a common structural motif (**figure 5.21**). At the centre of their molecular structures lies a four-element (KNAlC) ring. Only the central

ring of **5u** is planar (sum of internal angles, 360°), whereas those in **5v** (335.32^o) and **5w**
(353.38^o) are distinctly non-planar, forming a folded geometry. This core ring of each complex
contains a mixed ^{i}Bu-amide bridging set, and the molecular structures are completed by two
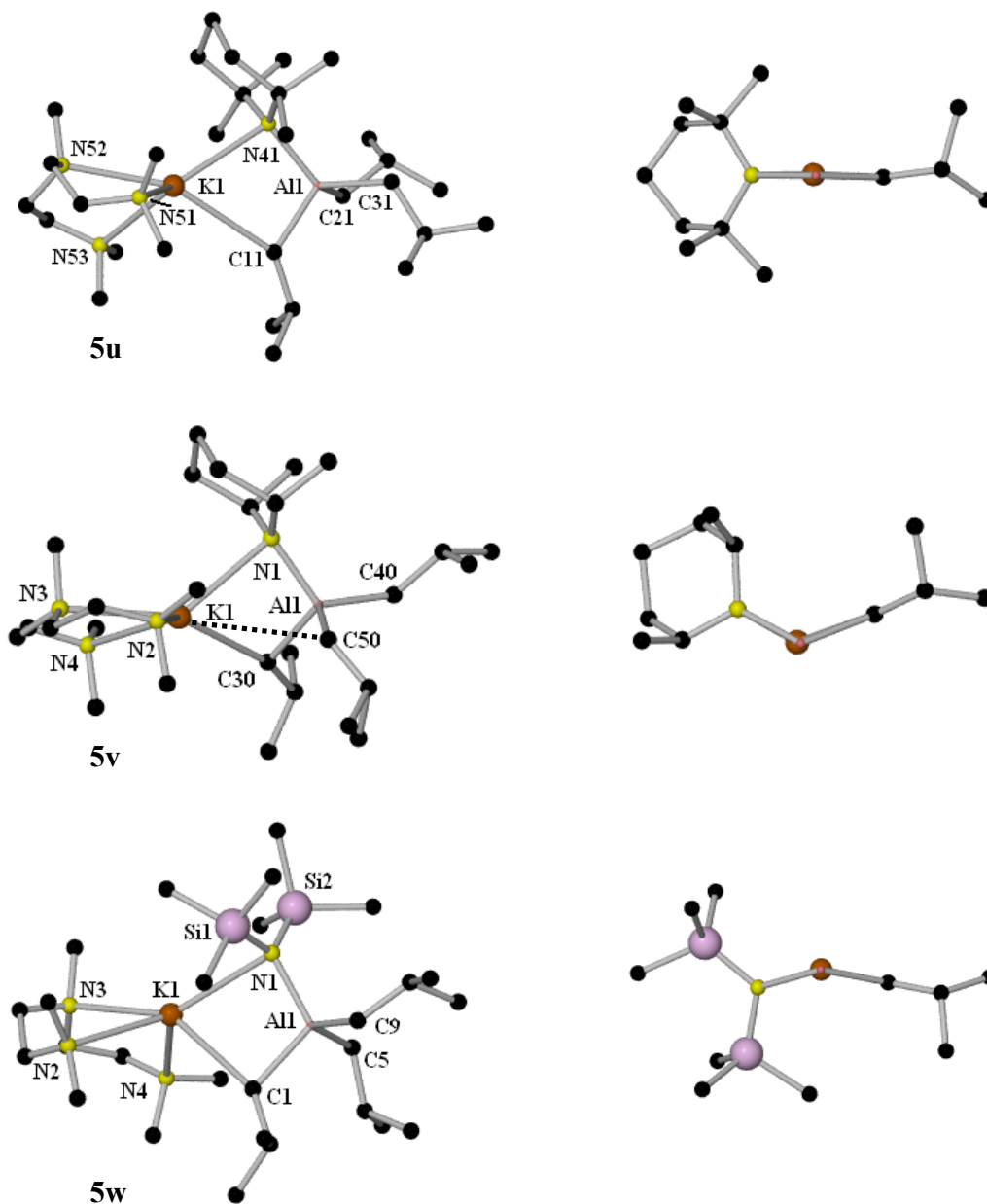
**Figure 5.21: Molecular structures of potassium aluminates 5u, 5v, and 5w. Their respective
central rings, minus terminal ^{i}Bu groups and PMDETA ligand, are also shown.**

terminal *i*Bu ligands on Al and a chelating PMDETA (*N,N,N*-attached) on K. In each complex, Al displays a distorted tetrahedral geometry [mean angle around Al: **5u**, 109.5°; **5v**, 109.3°; **5w**, 109.4°] with bond angles ranging from 99.0(4)-120.0(4)° in **5u**, 104.83(7)-117.35(7)° in **5v** and 101.12(8)-116.83(8)° in **5w**. In every case, Al forms shorter bonds to the amido nitrogen [**5u**, 1.996(8) Å; **5v**, 1.8918(14) Å; **5w**, 1.9626(14) Å] than to the α-carbon atom of either the bridging or terminal *i*Bu groups by at least 0.037 Å, 0.132 Å, and 0.050 Å in complexes **5u**, **5v** and **5w** respectively. This trend follows that of the difference [0.037Å] in bond lengths of Al–N bonds [mean bond length, 1.953 Å] and the modestly longer Al–C bonds [mean bond length, 1.990 Å] calculated from the many aluminium complexes within the CSD.[57] Within the molecular structure of complex **5v**, the Al–N bond is notably shorter than the mean bond distance, probably due to the less steric hinderance associated with the DMP amide in comparison to the bulkier TMP and HMDS amides. Potassium forms weaker interactions with the nitrogen atom of the amide and the carbon atom of the bridging *i*Bu group, in comparison to those of aluminium, with the K–N$_{(amide)}$ bonds being shorter in length [in complexes **5u** and **5v**, by 0.156 Å and 0.181 Å respectively] compared to the K–C$_{(iBu)}$ bond; however in complex **5w**

Table 5.2: Comparison of bond lengths (Å) and angles (°) within complexes 5u, 5v and 5w.

Parameter	5u	5v	5w
Al–N$_{(amide)}$	1.996(8)	1.8918(14)	1.9626(14)
Al–C$_{(bridging)}$	2.033(11)	2.0470(17)	2.0489(19)
Al–C$_{(terminal)}$	2.036(11), 2.045(10)	2.0236(17), 2.0344(18)	2.0122(19), 2.0292(18)
K–N$_{(amide)}$	2.955(8)	2.8675(15)	3.0164(15)
K–N$_{(PMDETA)}$	2.829(7), 2.855(9), 2.869(9)	2.8386(15), 2.8720(16), 2.9446(15)	2.8192(16), 2.8341(16), 2.9260(16)
K–C$_{(bridging)}$	3.111(8)	3.0483(17)	3.0184(17)
K–N$_{(amide)}$–Al	100.0(3)	86.55(5)	90.25(5)
N$_{(amide)}$–Al–C$_{(bridging)}$	103.1(3)	105.56(6)	109.01(7)
Al–C$_{(bridging)}$–K	94.3(3)	79.22(5)	88.58(6)
C$_{(bridging)}$–K–N$_{(amide)}$	62.6(2)	63.99(4)	65.54(4)

these bonds are indistinguishable in length [difference in bond lengths, 0.002 Å]. In each structure, the K–N bond lengths associated with the PMDETA ligand are the shortest interactions that the K cation forms and are also relatively similar to one another in length, as identified from the narrow range of K–N$_{(PMDETA)}$ bond lengths [2.829(7)–2.9260(16) Å], and are on average 0.081 Å shorter than the K–N(amide) bond lengths. With respect to the bond angles within the three structures, the biggest difference can be seen in the K–N$_{(amide)}$–Al and K–C$_{(bridging)}$–Al junctions. The greater the folding in the central ring, the more these angles decrease to compensate. Closer inspection of the molecular structure of **5v** reveals an interesting feature. The CH$_2$ of one of the terminal ^{i}Bu groups [C(50)] makes a long, weak interaction with K [K(1)–C(50) separation length, 3.567(2) Å {for comparison, K(1)···C(40) separation = 5.323(2) Å}], as the methyl atoms of the DMP ligand point away from K. The result of this conformation that the DMP ligand adopts is that a gap appears on the coordination sphere of K, into which the CH$_2$ of a terminal ^{i}Bu group can encroach. This long interaction in turn destroys the planarity [335.32°] of the KNAlC ring as consequence. TMP, in comparison, has two methyl groups pointing towards K and two away from it. These extra methyl groups (*c.f.* DMP) prevent either of the CH$_2$ of the terminal ^{i}Bu groups from forming any interactions with the K cation due to their more extreme steric presence, forcing them to stay a large distance away, which in turn provides a planar central ring as a result. Space filling models of these two complexes highlights these interactions (**figure 5.22**).

CH$_3$ of DMP

2 × CH$_3$ of TMP

Interaction point of terminal ^{i}Bu with K

Interaction point blocked by CH$_3$ of TMP
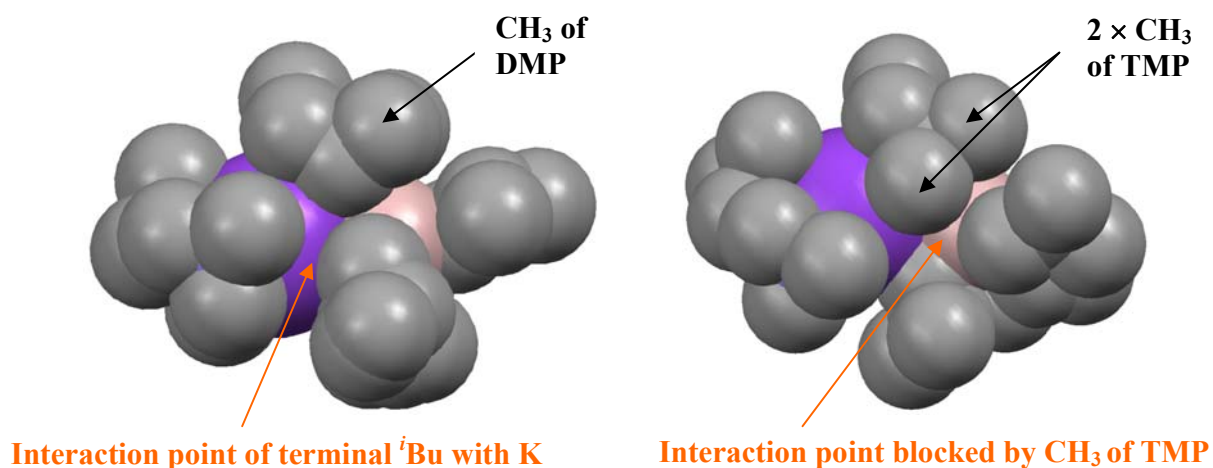
Figure 5.22: Space filling models of structures 5v (left) and 5u (right). K = purple, Al = pink, C = Grey. Hydrogen atoms are omitted for clarity.

The slight deviation from planarity in the central ring [353.38°] in **5w** can be attributed in part to inequivalent long range interactions of the methyl groups of HMDS to potassium [K–C$_{(HMDS)}$ bond lengths from Si(1): K(1)–C(13), 3.719(2) Å; K(1)–C(14), 3.488(2) Å; K(1)–C(15), 5.373(2) Å. K–C$_{(HMDS)}$ bond lengths from Si(2): K(1)–C(16), 3.480(2) Å; K(1)–C(17), 5.447(2) Å; K(1)–C(18), 5.037(2) Å]. From analysis of these bond lengths, K forms very weak contacts to two methyl groups of one SiMe$_3$ unit and one to the other SiMe$_3$, and these inequivalent interactions helps to distort the plane of the ring to a small, but noticeable degree.

There is only one other documented structural example where aluminium is connected to three carbons and one nitrogen atom, in the presence of K in a 1:1 metal molar ratio. Roesky reported the transmetallation reaction between [2,6-^{i}Pr$_2$C$_6$H$_3$N(SiMe$_3$)AlCl$_2$]$_2$ and potassium phenylacetylide (KC≡CPh) in THF solution at 50°C, yielding the mixed-metal complex [THF{K}$^+$·{2,6-^{i}Pr$_2$C$_6$H$_3$N(SiMe$_3$)Al(C≡CPh)$_3$}$^-$]$_2$ (**scheme 5.17**).[58] This structure was produced from a metathetical reaction approach, whereas aluminates **5u**, **5v,** and **5w** were synthesised by a cocomplexation route using the individual components PMDETA, K-amide and ^{i}Bu$_3$Al.
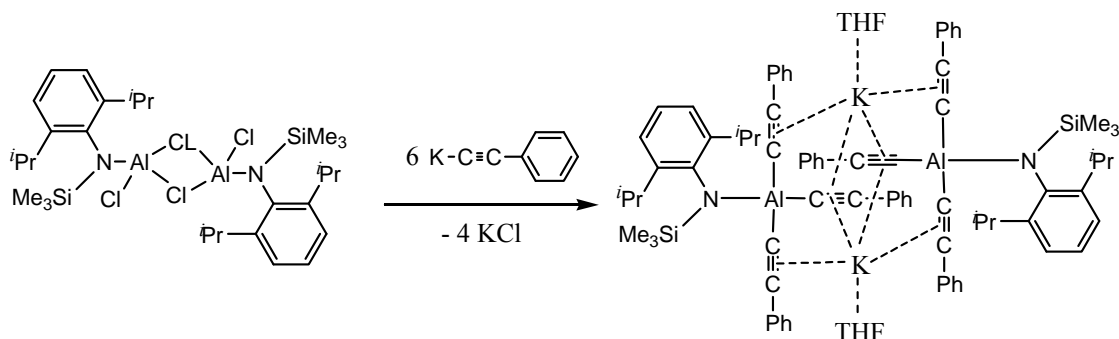
Scheme 5.17: Literature procedure for formation of a potassium aluminate containing one N and three C bonds to aluminium.

5.3.2) Solution Studies

Complexes **5u** and **5v** exhibit good solubility in deuterated d$_{12}$-cyclohexane [d$_{12}$-Cy] solution. However, **5w** was found to be insoluble in d$_{12}$-Cy, but in contrast readily dissolved in C$_6$D$_6$ solution. Thus, all three complexes could be characterised by ^{1}H and ^{13}C NMR spectroscopy. As

compounds **5u** and **5v** were dissolved using the same solvent-system, their NMR signals can be compared directly to each other to determine what effect the amide group has on the resonance patterns observed. The ^{i}Bu resonances (**table 5.3**) in the ^{1}H NMR spectra (**figures 5.23** and **5.24** for complexes **5u** and **5v** respectively) show that these alkyl groups are chemically equivalent in

Table 5.3: ^{1}H NMR chemical shift values of ^{i}Bu groups in compounds 5u and 5v.

Compound	CH$_2$ of ^{i}Bu	CH of ^{i}Bu	CH$_3$ of ^{i}Bu
5u	-0.17 ppm	1.92 ppm	0.94 ppm
5v	-0.31 ppm	1.92 ppm	0.94 ppm

solution as only one set of resonances is observed. The major difference between the two spectra is that the resonance attributed to the ^{i}Bu CH$_2$ group is found at a lower frequency in **5v** than in **5u** (by 0.14 ppm), indicating that the electron density on the CH$_2$ carbon in complex **5v** is modestly greater than on that in **5u**. A difference in chemical shift can be seen in the ^{13}C NMR spectra, where the CH$_2$ carbon resides at 32.4 ppm for **5u** and at a lower frequency (27.3 ppm) for **5v**, mirroring the direction of chemical shift change in the ^{1}H NMR spectra. The resonances for the CH and CH$_3$ groups, significantly further away from the attached metal centres, have exactly the same ^{1}H NMR resonance values (1.92 and 0.94 ppm respectively), and almost
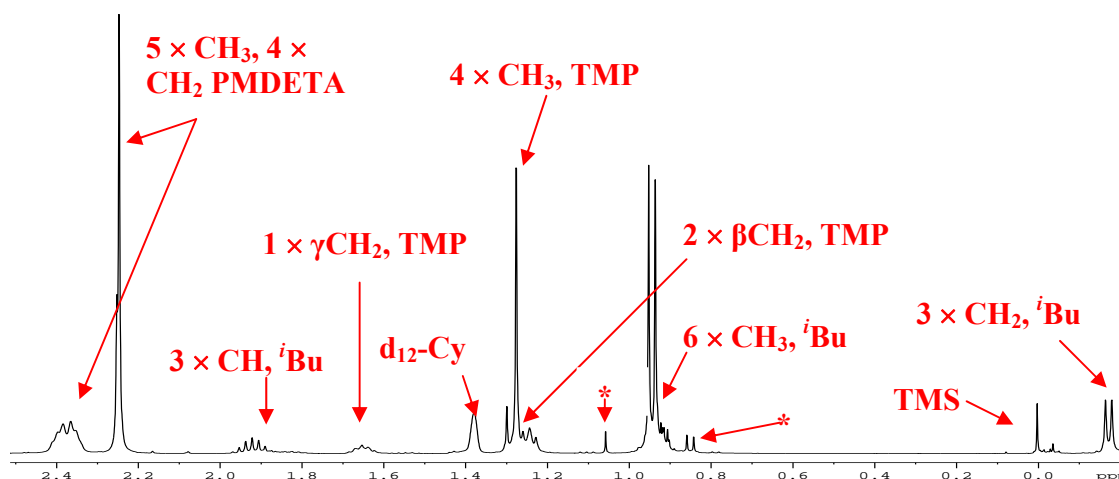
Figure 5.23: ^{1}H NMR spectrum of the TMP complex 5u in d$_{12}$-Cy solution. * = protic impurity.

identical ^{13}C NMR chemical resonances (**5u**: 28.1 and 30.0 ppm respectively. **5v**: 28.2 and 29.8 ppm respectively). The resonances attributed to the amides (TMP and DMP) and PMDETA move in the expected directions for metallated and cation-bound amines respectively (*c.f.* ^{1}H and ^{13}C NMR spectra of the free amines).
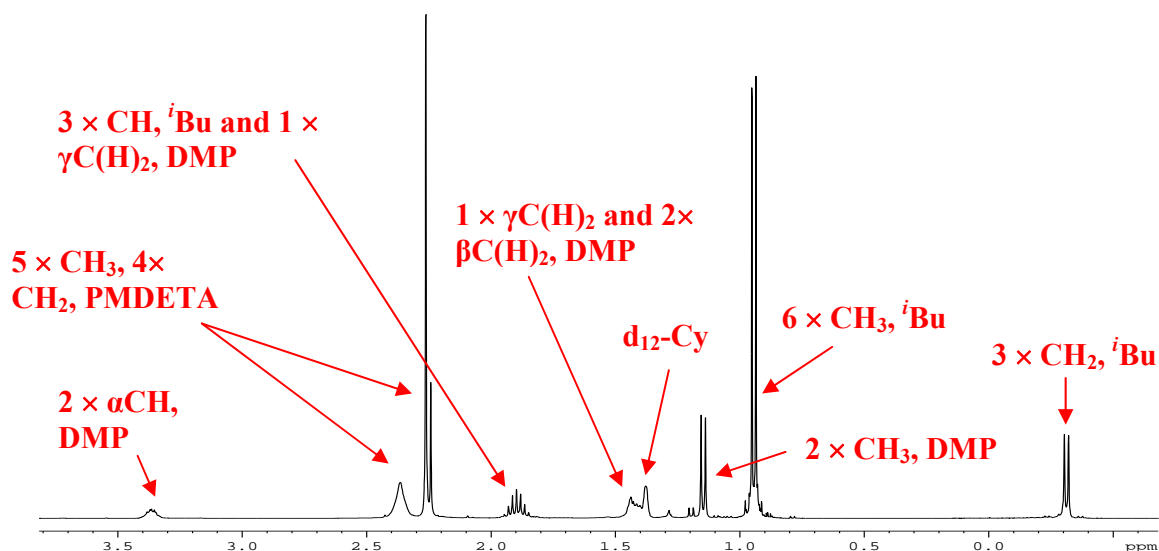
Figure 5.24: ^{1}H NMR spectrum of the DMP potassium aluminate 5v, in d$_{12}$-Cy solution.

Although not a direct comparison as the [1]H (**figure 5.25**) and ^{13}C NMR spectra of **5w** were recorded in C$_6$D$_6$ solution, it is the only complex out of the three mentioned where the CH$_2$ resonance of the chemically equivalent [i]Bu groups resides at a positive chemical shift value [0.15 ppm]. In comparison to ^{1}H and ^{13}C NMR data of other known literature alkali-metal aluminates (with a similar structural motif, see **table 5.4**), the resonance of 0.15 ppm is within the reported chemical shift range of 0.38-0.14 ppm for the CH$_2$ hydrogen atoms of the [i]Bu groups, as are the values obtained for the CH [2.43 ppm, range = 2.45-2.28 ppm] and CH$_3$ components of the [i]Bu ligands [1.42, range = 1.43-1.33 ppm]. Interestingly, the ^{13}C NMR chemical shift of the CH$_2$ carbon has never been witnessed in the NMR data of the literature comparisons, however, in the ^{13}C NMR spectrum of **5w**, coupled with evidence from ^{1}H–^{13}C coupling NMR techniques, the CH$_2$ carbon resonance was identified under methyl resonance of the [i]Bu groups [at 30.0 ppm].
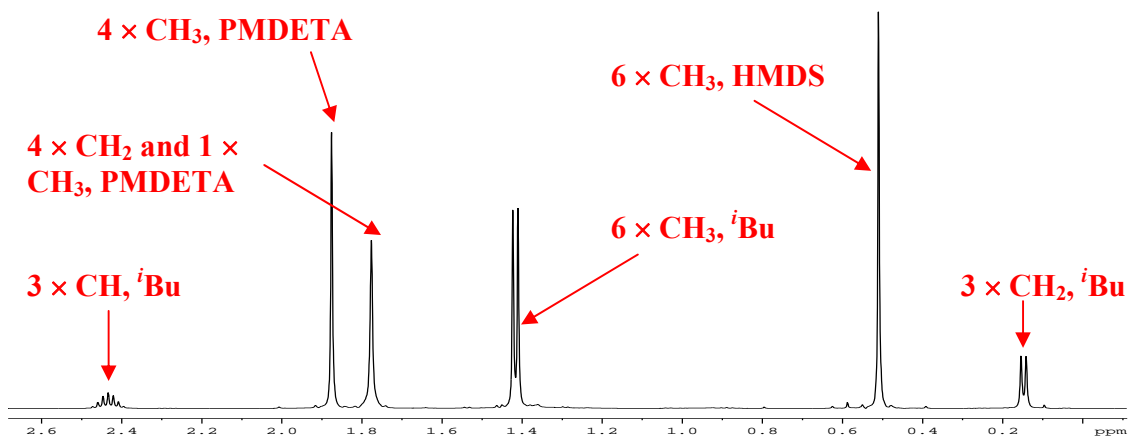
Figure 5.25: ^{1}H HMR spectrum of compound 5w in C$_6$D$_6$ solution.

Table 5.4: Comparison of ^{1}H and ^{13}C NMR values (ppm, in C$_6$D$_6$ solutions) of complex 5w with literature alkali-metal aluminates of similar structural motif.

Alkali metal	ligand	Amide	^{1}H NMR CH$_2$	^{1}H NMR CH	^{1}H NMR CH$_3$	^{13}C NMR CH$_2$	^{13}C NMR CH	^{13}C NMR CH$_3$
Li	TMP(H)	TMP	0.14	2.28	1.33	-	28.4	30.2
Li	NEt$_3$	TMP	0.20	2.36	1.36	-	28.3	30.1
Li	*N,N*-diisopropyl benzamide	TMP	0.38	2.35	1.36	-	28.2	30.0
Na	TMEDA	TMP	0.21	2.45	1.43	-	27.9	29.9
K	PMDETA	HMDS	0.15	2.43	1.42	30.0	27.8	30.0

The next stage in the development of these potassium aluminates would be to access how these complexes react with organic substrates. Do these aluminates act as amido or alkyl bases (or both), or do they even react at all, as [THF·Li(μ-TMP)(μ-^{i}Bu)Al(^{i}Bu)$_2$] was found to be wholly ineffective against *N, N*-diisopropylbenzamide; whereas in marked contrast [TMEDA·Na(μ-TMP)(μ-^{i}Bu)Al(^{i}Bu)$_2$] smoothly deprotonates phenylacetylene?

5.4) *Experimental Section*

Synthesis of ^{i}Bu$_2$Al(TMP) (5j)

10 mL of hexane was added to an oven dried Schlenk tube. Next, 1.25 mL (2 mmol) of 1.6 M solution of ^{n}BuLi were added, followed by 0.34 mL of TMP(H) at room temperature. The reaction mixture was left to stir for 30 min and then 0.38 mL (2 mmol) of ^{i}Bu$_2$AlCl were injected into the Schlenk tube, producing a white suspension almost immediately. The reaction was left to stir for 45 min and was then filtered through Celite and glasswool, which was then washed with a further 10 mL of hexane. The solvent was then removed in vacuo to yield a transparent oil (quantitative yield from NMR data). ^{1}H NMR (400.13 MHz, 298K, C$_6$D$_{12}$): δ = 1.95 [2H, septet, J = 6.8 Hz, 2 × CH of ^{i}Bu], 1.69 [2H, m, 1 × γCH$_2$ of TMP], 1.28 [4H, t, J = 6.0 Hz, 2 × βCH$_2$ of TMP], 1.25 [12H, s, 4 × CH$_3$ of TMP], 0.98 [12H, d, J = 6.6 Hz, 4 × CH$_3$ of ^{i}Bu], 0.26 ppm [4H, d, J = 7.4 Hz, 2 × CH$_2$ of ^{i}Bu]. ^{13}C{^{1}H} (100.62 MHz, 298K, C$_6$D$_{12}$): δ = 51.7 [2 × quaternary C of TMP], 40.1 [2 × βCH$_2$ of TMP], 33.4 [4 × CH$_3$ of TMP], 29.4 [2 × CH$_2$ of ^{i}Bu], 28.6 [4 × CH$_3$ of ^{i}Bu], 26.8 [2 × CH of iBu], 19.8 ppm [1 × γCH$_2$ of TMP].

Synthesis of [Li{Me$_2$NCH$_2$CH$_2$N(Me)CH$_2$}(μ-TMP)Al(^{i}Bu)$_2$] (5k)

10 mL of hexane was added to an oven dried Schlenk tube. Next, 1.25 mL (2 mmol) of 1.6 M solution of ^{n}BuLi were added, followed by 0.34 mL of TMP(H) at room temperature. The reaction mixture was left to stir for 30 min and then 0.38 mL (2 mmol) of ^{i}Bu$_2$AlCl were then injected into the Schlenk tube, producing a white suspension almost immediately. The reaction solution was stirred for 45 min and was then filtered through Celite and glasswool, which was then washed with a further 10 mL of hexane. In a separate Schlenk tube, a solution of freshly prepared LiTMP in 10 mL of hexane [from a mixture of 1.25 mL (2 mmol) of 1.6 M ^{n}BuLi and 0.34 mL (2 mmol) of TMPH], which was added *via* canula to the other Schlenk tube to give a homogeneous solution. Finally, 0.30 mL (2 mmol) of TMEDA were injected into the reaction mixture which was left to stir for 30 min before the Schlenk tube was placed in the freezer at -28°C. A crop of colourless crystals formed in solution (0.44 g, 55%). ^{1}H NMR (400.13 MHz, 298K, C$_6$D$_{12}$): δ = 2.92 [1H, triplet of doublets, ^3J = 12.6 Hz, ^2J = 5.1 Hz, 1 × C(H)$_2$ of

TMEDA], 2.71 [1H, triplet of doublets, ^3J = 13.5 Hz, ^2J = 5.0 Hz, 1 × C(H)$_2$ of TMEDA], 2.37 [3H, s, 1 × CH$_3$ of TMEDA], 2.34 [3H, s, 1 × CH$_3$ of TMEDA], 2.22 [3H, s, 1 × CH$_3$ of TMEDA], 2.06-1.84 [5H, m, 2 × C(H)$_2$ of TMEDA, 1 × γCH$_2$ of TMP and 1 × CH of ^{i}Bu], 1.78 [1H, septet, J = 6.7 Hz, 1 × CH of ^{i}Bu], 1.72-1.59 [2H, m, 2 × βC(H)$_2$ of TMP], 1.55 [1H, d, AB spin system, $J_{HB, HB}$ = 14.4 Hz, 1 × Al-C(H)$_2$N of TMEDA], 1.39 [3H, s, 1 × CH$_3$ of TMP], 1.36 [1H, d, 1 × Al-C(H)$_2$N of TMEDA], 1.31 [3H, s, 1 × CH$_3$ of TMP], 1.29 [6H, s, 2 × CH$_3$ of TMP], 0.98 [3H, d, J = 6.4 Hz, 1 × CH$_3$ of ^{i}Bu], 0.97 [3H, d, J = 6.4 Hz, 1 × CH$_3$ of ^{i}Bu], 0.91 [3H, d, J = 6.6 Hz, 1 × CH$_3$ of ^{i}Bu], 0.87 [3H, d, J = 6.6 Hz, 1 × CH$_3$ of ^{i}Bu], 0.85 [1H, triplet of doublets, ^3J = 13.3 Hz, ^2J = 3.5 Hz, 1 × βC(H)$_2$ of TMP], 0.74 [1H, triplet of doublets, ^3J = 13.1 Hz, ^2J = 4.3 Hz, 1 × βC(H)$_2$ of TMP], 0.33-(-0.06) ppm [4H, m, 2 × CH$_2$ of ^{i}Bu]. ^{13}C{^{1}H} (100.62 MHz, 298K, C$_6$D$_{12}$): δ = 60.1 [1 × CH$_2$ of TMEDA], 57.4 [1 × CH$_2$ of TMEDA], 53.3 [1 × quaternary C of TMP], 52.3 [1 × quaternary C of TMP], 49.0 [1 × CH$_3$ of TMEDA], 48.3 [1 × CH$_3$ of TMEDA], 47.4 [1 × βCH$_2$ of TMP], 46.3 [1 × βCH$_2$ of TMP], 42.2 [1 × CH$_3$ of TMEDA], 37.3 [1 × CH$_3$ of TMP], 36.3 [1 × CH$_3$ of TMP], 30.5 [1 × CH$_3$ of ^{i}Bu], 29.8 [1 × CH$_3$ of ^{i}Bu and 1 × CH$_3$ of TMP], 29.6 [1 × CH$_3$ of TMP], 28.6 [1 × CH$_3$ of ^{i}Bu], 28.4 [1 × CH$_3$ of ^{i}Bu], 28.1 [1 × CH of ^{i}Bu], 28.0 [1 × CH of ^{i}Bu], 19.1 ppm [1 × γCH$_2$ of TMP]. The resonances for the CH$_2$N and CH$_2$ of ^{i}Bu attached to aluminium could not be identified. ^{7}Li NMR (155.50 MHz, C$_6$D$_{12}$, 298K, reference LiCl in D$_2$O at 0.00 ppm): δ = 1.20 ppm.

Synthesis of [Li{Me$_2$NCH$_2$CH$_2$N(Me)CH$_2$CH$_2$N(Me)CH$_2$}(μ-TMP)Al(^{i}Bu)$_2$] (5l)

10 mL of hexane was added to an oven dried Schlenk tube. Next, 1.25 mL (2 mmol) of 1.6 M solution of ^{n}BuLi were added, followed by 0.34 mL of TMP(H) at room temperature. The reaction mixture was left to stir for 30 min and then 0.38 mL (2 mmol) of ^{i}Bu$_2$AlCl were then injected into the Schlenk tube, producing a white suspension almost immediately. The reaction was left to stir for 45 min and was then filtered through Celite and glasswool, which was then washed with a further 10 mL of hexane. In a separate Schlenk tube, a solution of freshly prepared LiTMP in 10 mL of hexane [from a mixture of 1.25 mL (2 mmol) of 1.6 M ^{n}BuLi and 0.34 mL (2 mmol) of TMPH], which was added *via* canula to the other Schlenk tube to give a homogeneous solution. Finally, 0.42 mL (2 mmol) of PMDETA were injected into the reaction

mixture, and it was stirred for 30 min before the Schlenk tube was placed in the freezer at -28°C. A crop of colourless crystals formed in solution (0.43 g, 47%). ^{1}H NMR (400.13 MHz, 298K, C_6D_{12}): δ = 2.92 [1H, triplet of doublets, ^{3}J = 12.3 Hz, ^{2}J = 4.1 Hz, 1 × C(H)$_2$ of PMDETA], 2.77-2.64 [2H, m, 2 × C(H)$_2$ of PMDETA], 2.43-2.36 [2H, m, 2 × C(H)$_2$ of PMDETA, 2.34 [3H, s, 1 × CH$_3$ of PMDETA], 2.31 [3H, s, 1 × CH$_3$ of PMDETA], 2.24 [7H, m, 2 × CH$_3$ of PMDETA and 1 × C(H)$_2$ of PMDETA], 2.13-2.05 [1H, m, 1 × C(H)$_2$ of PMDETA], 2.00-1.88 [2H, m, 1 × C(H)$_2$ of PMDETA and 1 × CH of ^{i}Bu], 1.83 [1H, m, 1 × CH of ^{i}Bu], 1.79 [1H, d, AB spin system, $J_{HA, HB}$ = 13.4 Hz, 1 × AlC(H)$_2$N], 1.68 [2H, broad signal, 2 × βC(H)$_2$ of TMP], 1.34 [6H, s, 2 × CH$_3$ of TMP], 1.31 [6H, s, 2 × CH$_3$ of TMP], 1.16 [2H, broad signal, 2 × βC(H)$_2$ of TMP], 1.04 [1H, d, AB spin system, $J_{HA, HB}$ = 13.4 Hz, 1 × AlC(H)$_2$N], 0.99-0.94 [6H, m, 2 × CH$_3$ of ^{i}Bu], 0.92 [3H, d, J = 6.5 Hz, 1 × CH$_3$ of ^{i}Bu], 0.88 [3H, d, J = 6.4 Hz, 1 × CH$_3$ of ^{i}Bu], 0.26-(-0.09) ppm [4H, m, 2 × CH$_2$ of ^{i}Bu]. ^{13}C{^{1}H} (100.62 MHz, 298K, C_6D_{12}): δ = 62.1 [1 × CH$_2$ of PMDETA], 59.9 [1 × CH$_2$ of PMDETA}, 58.2 [1 × CH$_2$ of PMDETA], 55.1 [1 × CH$_2$ of PMDETA], 52.9 [2 × quaternary C of TMP], 51.1 [Al-CH$_2$N of TMEDA], 49.6 [1 × CH$_3$ of PMDETA], 48.2 [1 × CH$_3$ of PMDETA], 47.4 [2 × CH$_3$ of PMDETA], 45.3 [2 × βCH$_2$ of TMP], 33.6 [2 × CH of ^{i}Bu and 4 × CH$_3$ of TMP], 30.8 [1 × CH$_3$ of ^{i}Bu], 30.1 [1 × CH$_3$ of ^{i}Bu], 28.7 [1 × CH$_3$ of ^{i}Bu], 28.5 [1 × CH$_3$ of ^{i}Bu], 28.2 [1 × CH of ^{i}Bu], 28.1 [1 × CH of ^{i}Bu], 19.3 [1 × γCH$_2$ of TMP]. ^{7}Li NMR (155.50 MHz, C_6D_{12}, 298K, reference LiCl in D_2O at 0.00 ppm): δ = 0.43 ppm.

Synthesis of [(TMEDA)$_2$·Li]$^{+}$[Al(DMP)$_2$(^{i}Bu)$_2$]$^{-}$ (5m)

10 mL of hexane was added to an oven dried Schlenk tube. Next, 1.25 mL (2 mmol) of 1.6 M ^{n}BuLi solution were added, followed by 0.27 mL of DMP(H) at room temperature. The reaction mixture was left to stir for 30 min and then 0.38 mL (2 mmol) of ^{i}Bu$_2$AlCl were then injected into the Schlenk tube, producing a white suspension almost immediately. The reaction was left to stir for 45 min and was then filtered through Celite and glasswool, which was then washed with a further 10 mL of hexane. In a separate Schlenk tube, a solution of freshly prepared LiDMP in 10 mL of hexane [from a mixture of 1.25 mL (2 mmol) of 1.6 M ^{n}BuLi and 0.27 mL (2 mmol) of DMP(H)], which was added *via* canula to the other Schlenk tube to give a

homogeneous solution. Completing the preparation, 0.30 mL (2 mmol) of TMEDA were injected into the reaction mixture, which was left to stir for 30 min before the Schlenk tube was placed in the freezer at -28°C. A crop of colourless crystals formed in solution (0.05 g). ^{1}H NMR (400.13 MHz, 298K, C_6D_{12}, plus a few drops of d_8-THF for a homogeneous solution): δ = 3.3 [4H, m, 4 × αCH of DMP], 2.30 [8H, s, 4 × CH_2 of TMEDA], 2.15 [24H, s, 8 × CH_3 of TMEDA], 1.98-1.72 [6H, m, 2 × CH of ^{i}Bu and 2 × γCH_2 of DMP], 1.66-1.58 [4H, m, 4 × βC(H)$_2$ of DMP], 1.28-1.20 [4H, m, 4 × βC(H)$_2$ of DMP], 1.18 [12H, d, J = 6.4 Hz, 4 × CH_3 of DMP], 0.97 [12H, d, J = 6.7 Hz, 4 × CH_3 of ^{i}Bu], -0.01 ppm [4H, d, J = 6.9 Hz, 2 × CH_2 of ^{i}Bu]. ^{13}C{^{1}H} (100.62 MHz, 298K, C_6D_{12}, plus a few drops of d_8-THF for a homogeneous solution): δ = 58.1 [4 × CH_2 of TMEDA], 47.6 [4 × αCH of DMP], 45.2 [8 × CH_3 of TMEDA], 33.6 [4 × βCH_2 of DMP], 28.7 [4 × CH_3 of ^{i}Bu], 27.1 [2 × γCH_2 of ^{i}Bu], 26.7 [2 × CH of ^{i}Bu], 26.0 ppm [4 × CH_3 of DMP]. ^{7}Li NMR (155.50 MHz, C_6D_{12}, plus a few drops of d_8-THF to obtain a homogeneous solution, 298K, reference LiCl in D_2O at 0.00 ppm): δ = 0.69 (broad signal) ppm.

Synthesis of [Na{Me$_2$NCH$_2$CH$_2$N(Me)CH$_2$CH$_2$N(Me)CH$_2$}(μ-TMP)Al(^{i}Bu)$_2$] (5n)

An oven dried Schlenk tube was filled with 10 mL of hexane. Next, 1.25 mL (2 mmol) of 1.6 M solution of ^{n}BuLi were introduced, followed by 0.34 mL of TMP(H). The reaction mixture was left to stir for 30 min and then 0.38 mL (2 mmol) of ^{i}Bu$_2$AlCl were injected into the Schlenk tube, producing a white suspension almost immediately. The reaction was stirred for an additional 45 min and subsequently filtered through Celite and glasswool, which was then washed with a further 10 mL of hexane. To a separate Schlenk tube containing a suspension of freshly prepared NaTMP in 10 mL of hexane [from a mixture of 0.16 g (2 mmol) of ^{n}BuNa and 0.34 mL (2 mmol) of TMP(H)], the solution was added *via* canula to give a pale yellow coloured suspension. Finally, 0.42 mL (2 mmol) of PMDETA were added and the reaction mixture quickly turned into a homogeneous solution which was left to stir for 30 min before the Schlenk tube was left in the refrigerator at -4°C . A crop (0.27 g, 28%) of colourless crystals formed in solution that were suitable for X-ray crystallographic analysis. ^{1}H NMR (400.13 MHz, 298K, C_6D_{12}): δ = 2.97-2.83 [2H, m, 1 × CH_2 of PMDETA], 2.81-2.65 [2H, m, 1 × CH_2 of PMDETA], 2.32 [3H, s, 1 × CH_3 of PMDETA], 2.25 [3H, s, 3 × CH_3 of PMDETA], 2.11-2.02 [2H, m, 1 ×

CH$_2$ of PMDETA], 2.00-1.75 [4H, m, 1 × CH$_2$ of PMDETA and 2 × CH of ^{i}Bu], 1.66 [1H, d, J = 13.2 Hz, 1 × NC(H)$_2$ of metallated PMDETA], 1.32 [6H, s, 2 × CH$_3$ of TMP], 1.29 [6H, s, 2 × CH$_3$ of TMP], 1.01-0.84 [13H, m, 1 × NC(H)$_2$ of metallated PMDETA and 4 × CH$_3$ of ^{i}Bu], 0.29-(-0.13) ppm [4H, m, 2 × CH$_2$ of ^{i}Bu]. Resonances for the βCH$_2$ and γCH$_2$ could not be identified, even with the help of 2D spectroscopic techniques. This could be due to very broad signals, like that seen in the lithium congener published in Organometallics,[59] although the degree of broadening was less in that example as the resonances could still be assigned. ^{13}C{^{1}H} (100.62 MHz, 298K, C$_6$D$_{12}$): δ = 61.2 [1 × CH$_2$ of PMDETA], 58.4 [1 × CH$_2$ of PMDETA], 56.8 [1 × CH$_2$ of PMDETA], 52.7 [2 × quaternary C of TMP], 52.2 [1 × CH$_2$ of PMDETA], 49.5 [1 × CH$_3$ of PMDETA], 46.9 [2 × CH$_3$ of PMDETA and possibly 2 × βCH$_2$ of TMP], 44.8 [1 × CH$_3$ of PMDETA], 30.8 [1 × CH$_3$ of ^{i}Bu], 30.2 [1 × CH$_3$ of ^{i}Bu], 28.9 [1 × CH$_3$ of ^{i}Bu], 28.7 [1 × CH$_3$ of ^{i}Bu], 28.2 [1 × CH of ^{i}Bu], 28.1 [1 × CH of ^{i}Bu], 19.3 ppm [1 × γCH$_2$ of TMP]. The resonances of the CH$_2$ carbons of the ^{i}Bu groups could not be observed. Also, those resonances attributed to the CH$_3$ groups of TMP may be obscured under the broad range from 30.8-28.9 ppm.

Synthesis of [(TMEDA)·Na(μ-TMP*)(μ-^{i}Bu)Al(^{i}Bu)] (5o)

Following the usual protocol, 10 mL of hexane was added to an oven dried Schlenk tube. Next, 1.25 mL (2 mmol) of 1.6 M solution of ^{n}BuLi were added, followed by 0.34 mL of TMP(H) at room temperature. The reaction mixture was left to stir for 30 min and then 0.38 mL (2 mmol) of ^{i}Bu$_2$AlCl were then injected into the Schlenk tube, rapidly producing a white suspension. The reaction was left to stir for 45 min and was then filtered through Celite and glasswool, which was then washed with a further 10 mL of hexane. To a separate Schlenk tube containing a suspension of freshly prepared NaTMP in 10 mL of hexane [from a mixture of 0.16 g (2 mmol) of ^{n}BuNa and 0.34 mL (2 mmol) of TMP(H)], the solution was added via canula to give a pale yellow coloured suspension. Finally, 0.30 mL (2 mmol) of TMEDA were introduced and the reaction mixture, which quickly turned into a homogeneous solution, was left to stir for 30 min before the Schlenk tube was left in the freezer at -28°C. An off-white solid (0.15 g, 18%) was isolated from the reaction mixture. ^{1}H NMR (400.13 MHz, 298K, C$_6$D$_{12}$): δ = 2.40 [4H, s, 2 × CH$_2$ of

TMEDA], 2.32 [12H, s, 4 × CH$_3$ of TMEDA], 2.02-1.86 [2H, m, 2 × CH of ^{i}Bu], 1.72-1.41 [4H, m, 1 × γCH$_2$ of TMP and 1 × βCH$_2$ of TMP], 1.34-1.24 [2H, m, 1 × βCH$_2$ of TMP], 1.19 [3H, s, 1 × CH$_3$ of TMP], 1.01-0.89 [18H, m, 2 × CH$_3$ of TMP and 4 × CH$_3$ of ^{i}Bu], 0.52 [1H, d, J = 13.9 Hz, 1 × metal-C(H)$_2$ of metallated TMP Me], 0.1-(-0.03) [2H, m, CH$_2$ of ^{i}Bu], -0.14-(-0.25) [2H, m, 1 × metal-C(H)$_2$ of metallated TMP Me (J = 13.9 Hz) and 1 × C(H)$_2$ of ^{i}Bu], -0.74-(-0.81) ppm [1H, m, 1 × C(H)$_2$ of ^{i}Bu]. ^{13}C{^{1}H} (100.62 MHz, 298K, C$_6$D$_{12}$): δ = 58.1 [2 × CH$_2$ of TMEDA], 57.2 [1 × quaternary C of TMP], 50.5 [1 × quaternary C of TMP], 46.7 [4 × CH$_3$ of TMEDA], 39.7 [1 × βCH$_2$ of TMP], 39.1 [1 × βCH$_2$ of TMP], 38.0 [1 × CH$_3$ of TMP], 36.5 [1 × CH$_3$ of TMP], 32.7 [1 × CH$_3$ of TMP], 31.8 [1 × metal-CH$_2$ of TMP], 31.0 [1 × CH$_2$ of ^{i}Bu], 30.4 [1 × CH$_3$ of ^{i}Bu], 29.3 [1 × CH$_3$ of ^{i}Bu], 28.4 [2 × CH$_3$ of ^{i}Bu], 28.1 [2 × CH of ^{i}Bu], 26.1 (hidden under solvent) [1 × CH$_2$ of ^{i}Bu], 20.9 ppm [1 × γCH$_2$ of TMP].

Synthesis of [(TMEDA)·K(μ-TMP*)(μ-^{i}Bu)Al(^{i}Bu)] (5p)

10 mL of hexane was added to an oven dried Schlenk tube. Next, 1.25 mL (2 mmol) of 1.6 M solution of ^{n}BuLi were added, followed by 0.34 mL of TMP(H) at room temperature. The reaction mixture was left to stir for 30 min and then 0.38 mL (2 mmol) of ^{i}Bu$_2$AlCl were then injected into the Schlenk tube, producing a white suspension almost immediately. The reaction mixture was left to stir for 45 min and was then filtered through Celite and glasswool, which was then washed with a further 10 mL of hexane. To a separate Schlenk tube containing a suspension of freshly prepared KTMP in 10 mL of hexane [from a mixture of 0.24 g (2 mmol) of KCH$_2$SiMe$_3$ and 0.34 mL (2 mmol) of TMP(H)], the solution was added via canula to give a tan coloured suspension. Finally, 0.30 mL (2 mmol) of TMEDA were injected and the reaction mixture quickly turned into a homogeneous solution which was left to stir for 30 min before the Schlenk tube was left in the refrigerator at -4°C. A crop (0.43 g, 49%) of colourless crystals formed in solution that were suitable for X-ray crystallographic analysis. ^{1}H NMR (400.13 MHz, 298K, C$_6$D$_{12}$): δ = 2.34 [4H, s, 2 × CH$_2$ of TMEDA], 2.24 [12H, s, 4 × CH$_3$ of TMEDA], 1.98-1.82 [2H, m, 2 × CH of ^{i}Bu], 1.75-1.60 [1H, m, 1 × γC(H)$_2$ of TMP], 1.58-1.24 [5H, m, 1 × γC(H)$_2$ of TMP and 2 × βCH$_2$ of TMP], 1.23 [3H, s, 1 × CH$_3$ of TMP], 1.01-0.91 [18H, m, 2 × CH$_3$ of TMP and 4 × CH$_3$ of ^{i}Bu], 0.38 [1H, d, J = 12.5 Hz, 1 × metal-C(H)$_2$ of metallated TMP

Me], 0.11-(-0.04) [2H, m, CH_2 of ^iBu], -0.17-(-0.28) [2H, m, 1 × metal-C(H)$_2$ of metallated TMP Me (J = 11.8 Hz) and 1 × C(H)$_2$ of ^iBu], -0.42-(-0.49) ppm [1H, m, 1 × C(H)$_2$ of ^iBu]. ^{13}C{^{1}H} (100.62 MHz, 298K, C_6D_{12}): δ = 58.1 [2 × CH_2 of TMEDA], 57.2 [1 × quaternary C of TMP], 50.6 [1 × quaternary C of TMP], 46.1 [4 × CH_3 of TMEDA], 40.6 [1 × βCH_2 of TMP], 39.6 [1 × βCH_2 of TMP], 36.9 [1 × CH_3 of TMP], 36.6 [1 × CH_3 of TMP], 32.9 [1 × metal-CH_2 of TMP], 31.8 [1 × CH_2 of ^iBu], 31.5 [1 × CH_3 of TMP], 30.2 [1 × CH_3 of ^iBu], 29.5 [1 × CH_3 of ^iBu], 29.3 [1 × CH_3 of ^iBu], 28.8 [1 × CH_3 of ^iBu], 28.5 [1 × CH of ^iBu], 28.4 [1 × CH of ^iBu], 27.3 [1 × CH_2 of ^iBu], 20.9 ppm [1 × γCH_2 of TMP].

Synthesis of [(TMEDA)·Li(μ-DMP)$_2$Al(DMP)$_2$] (5r)

10 mL of hexane was added to an oven dried Schlenk tube. Next, 1.25 mL (2 mmol) of 1.6 M solution of ^{n}BuLi were added, followed by 0.27 mL of DMP(H) at room temperature. The reaction mixture was left to stir for 30 min and then 0.38 mL (2 mmol) of $^iBu_2AlCl$ were then injected into the Schlenk tube, producing a white suspension almost immediately. The reaction was left to stir for 45 min and was then filtered through celite and glasswool, which was then washed with a further 10 mL of hexane and 0.60 mL (4 mmol) of TMEDA were added to the reaction mixture. In a separate Schlenk tube, a solution of freshly prepared LiTMP in 10 mL of hexane [from a mixture of 1.25 mL (2 mmol) of 1.6 M ^{n}BuLi and 0.27 mL (2 mmol) of DMP(H)], which was added *via* canula to the second Schlenk tube to give an initial homogeneous solution. After 5 min, a white solid deposited from solution (0.15 g). ^{1}H NMR (400.13 MHz, 298K, C_6D_{12}, plus a few drops of d_8-THF for a homogeneous solution): δ = 2.76-2.63 [8H, m, 4 × αCH of DMP], 2.31 [4H, s, 2 × CH_2 of TMEDA], 2.18 [12H, s, 4 × CH_3 of TMEDA], 1.79-1.67 [4H, m, 2 × γCH_2 of DMP], 1.50-1.40 [12H, m, 2 × γCH_2 and 4 × βCH_2 of DMP], 1.04 [24H, d, J = 6.9 Hz, 8 × CH_3 of DMP], 0.68-0.50 ppm [4 × βCH_2 of DMP]. ^{13}C{^{1}H} (100.62 MHz, 298K, C_6D_{12}, plus a few drops of d_8-THF for a homogeneous solution): δ = 60.5 [8 × αCH of DMP], 58.7 [2 × CH_2 of TMEDA], 46.4 [4 × CH_3 of TMEDA], 39.7 [8 × βCH_2 of DMP], 28.1 [4 × γCH_2 of DMP], 27.7 ppm [8 × CH_3 of DMP]. ^{7}Li NMR (155.50 MHz, C_6D_{12}, plus a few drops of d_8-THF for a homogeneous solution, 298K, reference LiCl in D_2O at 0.00 ppm): δ = 1.95 ppm.

Synthesis of oily product (5s)

10 mL of hexane was added to an oven dried Schlenk tube. Next, 1.25 mL (2 mmol) of 1.6 M solution of ^{n}BuLi were added, followed by 0.34 mL of TMP(H) at room temperature and the reaction mixture was left to stir for 30 min. Subsequently 0.38 mL (2 mmol) of ^{i}Bu$_2$AlCl were then injected into the Schlenk tube, producing a white suspension almost immediately. The reaction solution was left to stir for 45 min and was then filtered through Celite and glasswool, which was then washed with a further 10 mL of hexane. To a separate Schlenk tube containing a suspension of freshly prepared KTMP in 10 mL of hexane [from a mixture of 0.24 g (2 mmol) of KCH$_2$SiMe$_3$ and 0.34 mL (2 mmol) of TMP(H)], the solution was added via canula to give a tan coloured suspension. Finally, 0.42 mL (2 mmol) of PMDETA were injected into the reaction mixture which quickly turned into a homogeneous solution which was left to stir for 1 h. Next, all of the solvent was removed *in vacuo* yielding a brown oil. A ^{1}H NMR experiment was run in d$_{12}$-Cy solution, however, the obtained spectrum was impossible to assign accurately due to many overlapping resonances.

Synthesis of [(PMDETA)·K(μ-TMP)(μ-^{i}Bu)Al(^{i}Bu)$_2$] (5u)

An oven-dried Schlenk tube containing 0.24 g (2 mmol) of KCH$_2$SiMe$_3$ was filled with hexane (10 mL). 0.42 mL (2 mmol) of PMDETA, followed by 0.34 mL (2 mmol) of TMP(H) were then injected into the reaction mixture to form a homogeneous solution. Finally, 2 mL (2 mmol) of 1M ^{i}Bu$_3$Al solution were injected, and the Schlenk tube was placed in the freezer at -28°C to yield a crop of colourless crystals (0.19 g, 17 % yield). ^{1}H NMR (400.13 MHz, 298K, C$_6$D$_{12}$): δ = 2.43-2.33 [8H, m, 4 × CH$_2$ of PMDETA], 2.25 [15H, s, 5 × CH$_3$ of PMDETA], 1.92 [3H, septet, J = 6.5 Hz, 3 × CH of ^{i}Bu], 1.66 [2H, m, 1 × γCH$_2$ of TMP], 1.32-1.22 [16H, m, 4 × CH$_3$ and 2 × βCH$_2$ of TMP], 0.94 [18H, d, J = 5.4 Hz, 6 × CH$_3$ of ^{i}Bu], -0.17 ppm [6H, d, J = 9.3 Hz, 3 × CH$_2$ of ^{i}Bu]. ^{13}C{^{1}H} (100.62 MHz, 298K, C$_6$D$_{12}$): δ = 58.2 [2 × CH$_2$ of PMDETA], 56.3 [2 × CH$_2$ of PMDETA], 53.1 [2 × quaternary C of TMP], 46.0 [4 × CH$_3$ of PMDETA], 44.8 [2 × βCH$_2$ of TMP], 42.9 [1 × CH$_3$ of PMDETA], 34.8 [4 × CH$_3$ of TMP], 32.4 [3 × CH$_2$ of ^{i}Bu], 30.0 [6 × CH$_3$ of ^{i}Bu], 28.1 [3 × CH of ^{i}Bu], 19.3 [1 × γCH$_2$ of TMP].

Synthesis of [(PMDETA)·K(μ-DMP)(μ-^{i}Bu)Al(^{i}Bu)$_2$] (5v)

Hexane (10 mL) was added to an oven-dried Schlenk tube containing 0.24 g (2 mmol) of KCH$_2$SiMe$_3$. 0.42 mL (2 mmol) of PMDETA, followed by 0.27 mL (2 mmol) of DMP(H) were syringed into the reaction mixture to form a homogeneous solution. Finally, 2 mL (2 mmol) of 1M ^{i}Bu$_3$Al solution were added, and the Schlenk tube was placed in the freezer at -28°C to yield a crop of colourless crystals (0.35 g, 33 % yield). ^{1}H NMR (400.13 MHz, 298K, C$_6$D$_{12}$): δ = 3.37 [2H, m, 2 × αCH of DMP], 2.37 [8H, m, 4 × CH$_2$ of PMDETA], 2.26 [12H, s, 4 × CH$_3$ of PMDETA], 2.24 [3H, s, 1 × CH$_3$ of PMDETA], 1.98-1.82 [4H, m, 3 × CH of ^{i}Bu and 1 × γC(H)$_2$ of DMP], 1.47-1.40 [5H, m, 2 × βCH$_2$ and 1 × γC(H)$_2$ of DMP], 1.15 [6H, d, J = 6.8 Hz, 2 × CH$_3$ of DMP], 0.94 [18H, d, J = 6.6 Hz, 6 × CH$_3$ of ^{i}Bu], -0.31 ppm [6H, d, J = 6.8 Hz, 3 × CH$_2$ of ^{i}Bu]. ^{13}C{^{1}H} (100.62 MHz, 298K, C$_6$D$_{12}$): δ = 58.1 [2 × CH$_2$ of PMDETA], 56.3 [2 × CH$_2$ of PMDETA], 47.6 [2 × αCH of DMP], 45.8 [4 × CH$_3$ of PMDETA], 42.7 [1 × CH$_3$ of PMDETA], 34.2 [2 × βCH$_2$ of DMP], 29.8 [6 × CH$_3$ of ^{i}Bu], 28.2 [3 × CH of ^{i}Bu], 27.3 [2 × CH$_3$ of DMP and 3 × CH$_2$ of ^{i}Bu], 16.4 ppm [1 × γCH$_2$ of DMP].

Synthesis of [(PMDETA)·K(μ-HMDS)(μ-^{i}Bu)Al(^{i}Bu)$_2$] (5w)

Hexane (10 mL) was added to an oven-dried Schlenk tube containing 0.24 g (2 mmol) of KCH$_2$SiMe$_3$. 0.42 mL (2 mmol) of PMDETA, followed by 0.42 mL (2 mmol) of HMDS(H) were added to the reaction mixture to form a homogeneous solution. Finally, 2 mL (2 mmol) of 1M ^{i}Bu$_3$Al solution were added, and the Schlenk tube was placed in the freezer at -28°C to yield a crop of colourless crystals (0.59 g, 52 % yield). ^{1}H NMR (500.13 MHz, 298K, C$_6$D$_6$): δ = 2.43 [3H, septet, J = 6.3 Hz, 3 × CH of ^{i}Bu], 1.88 [12H, s, 4 × CH$_3$ of PMDETA], 1.77 [11H, s, 1 × CH$_3$ and 4 × CH$_2$ of PMDETA], 1.42 [18H, d, J = 6.7 Hz, 6 × CH$_3$ of ^{i}Bu], 0.51 [18H, s, 6 × CH$_3$ of HMDS], 0.15 ppm [6H, d, J = 7.1 Hz, 3 × CH$_2$ of ^{i}Bu]. ^{13}C{^{1}H} (100.62 MHz, 298K, C$_6$D$_6$): δ = 57.1 [2 × CH$_2$ of PMDETA], 55.1 [2 × CH$_2$ of PMDETA], 45.5 [4 × CH$_3$ of PMDETA], 42.3 [1 × CH$_3$ of PMDETA], 30.0 [6 × CH$_3$ and 3 × CH$_2$ of ^{i}Bu], 27.8 [3 × CH of ^{i}Bu], 7.4 ppm [6 × CH$_3$ of HMDS].

Chapter 5 – References:

[1]   M. Uchiyama, H. Naka, Y. Matsumoto, T. Ohwada, *J. Am. Chem. Soc*. **2004**, *126*, 10526.

[2]   G. Wilkinson, F. G. A. Stone, E. W. Abel, *In Comprehensive Organometallic Chemistry*, Pergamon Press, Oxford, **1982**, Vol. 6, chap. 6.

[3]   C. J. Upton, P. Beak, *J. Org. Chem*. **1975**, *40*, 1094.

[4]   B. M. Trost, *In Comprehensive Organic Synthesis*, Pergamon Press, Oxford, **1991**, Vol. 8, chap. 3.

[5]   H. Naka, M. Uchiyama, Y. Matsumoto, A. E. H. Wheatley, M. McPartlin, J. V. Morey, Y. Kondo, *J. Am. Chem. Soc*. **2007**, *129*, 1921.

[6]   H. Naka, J. V. Morey, J. Haywood, D. J. Eisler, M. McPartlin, F. Garcia, H. Kudo, Y. Kondo, M. Uchiyama, A. E. H. Wheatley, *J. Am. Chem. Soc*. **2008**, *130*, 16193.

[7]   J. García-Álvarez, D. V. Graham, A. R. Kennedy, R. E. Mulvey, S. Weatherstone, *Chem. Commun*. **2006**, 3208.

[8]   J. García-Álvarez, E. Hevia, A. R. Kennedy, J. Klett, R. E. Mulvey, *Chem. Commun.* **2007**, 2402.

[9]   B. Conway, E. Hevia, J. García-Álvarez, D. V. Graham, A. R. Kennedy, R. E. Mulvey, *Chem. Commun*. **2007**, 5241.

[10]   A. Yasuda, S. Tanaka, K. Oshima, H. Yamamoto, H. Nozaki, *J. Am. Chem. Soc*. **1974**, *96*, 6513.

[11]   X. Tian, R. Fröhlich, T. Pape, N. W. Mitzel, *Organometallics* **2005**, *24*, 5294.

[12]   X. Tian, R. Fröhlich, N. W. Mitzel, *Dalton Trans*. **2005**, 380.

[13]   V. H. Gessner, C. Strohmann, *J. Am. Chem. Soc*. **2008**, *130*, 14412.

[14]   S. Harder, M. Lutz, *Organometallics* **1994**, *13*, 5173.

[15]   A. Hildebrand, P. Lonnecke, L. Silaghi-Dumitrescu, I. Silaghi-Dumitrescu, E. Hey-Hawkins, *Dalton Trans*. **2006**, 967.

[16]   M. G. Gardiner, C. L. Raston, B. W. Skelton, A. H. White, *Inorg. Chem*. **1997**, *36*, 2795.

[17]   W. Uhl, *Z. Anorg. Allg. Chem*. **1989**, *579*, 75.

[18]   W. Uhl, E. Schnepf, J. Wagner, *Z. Anorg. Allg. Chem*. **1992**, *613*, 67.

[19]   S. S. Al-Juaid, C. Eaborn, I. B. Gorrell, S. A. Hawkes, P. B. Hitchcock, J. D. Smith, *J. Chem. Soc., Dalton Trans*. **1998**, 2411.

[20] M. M. Andrianarison, A. G. Avent, M. C. Ellerby, I. B. Gorrell, P. B. Hitchcock, J. D. Smith, D. R. Stanley, *J. Chem. Soc., Dalton Trans*. **1998**, 249.

[21] Wu-Yong Chen, C. Eaborn, I. B. Gorrell, P. B. Hitchcock, J. D. Smith, *J. Chem. Soc., Dalton Trans*. **2000**, 2313.

[22] G. Muller, J. Brand, *Organometallics* **2003**, *22*, 1463.

[23] Based on data on hydration of aqueous group 1 ions, see: F. A. Cotton, G. Wilkinson, C. A. Murillo, M. Bochmann, *Advanced Inorganic Chemistry, 6th Ed.*, Wiley-VCH, Weinheim, **1999**, chap.3.

[24] C. Strohmann, V. H. Gessner, *Angew. Chem. Int. Ed.* **2007**, *46*, 4566.

[25] L. Barr, A. R. Kennedy, J. G. MacLellan, J. H. Moir, R. E. Mulvey, P. J. A. Rodger, *Chem. Commun*. **2000**, 1757.

[26] P. C. Andrews, P. J. Nichols, *Organometallics* **2000**, *19*, 1277.

[27] M. Niemeyer, *Inorg. Chem*. **2006**, *45*, 9085.

[28] M. A. Putzer, J. Magull, H. Goesmann, B. Neumüller, K. Dehnicke, *Chem. Ber*. **1996**, *129*, 1401.

[29] M. Moore, S. Gambarotta, C. Bensimon, *Organometallics* **1997**, *16*, 1086.

[30] M. A. Putzer, B. Neumüller, K. Dehnicke, *Z. Anorg. Allg. Chem*. **1998**, *624*, 1087.

[31] M. Karl, K. Harms, G. Seybert, W. Massa, S. Fau, G. Frenking, K. Dehnicke, *Z. Anorg. Allg. Chem*. **1999**, *625*, 2055.

[32] J Clayden, *Organolithiums: Selectivity for Synthesis,* Tetrahedron Organic Chemistry Series, **2002**, *23*, p 14.

[33] G. Boche, J. C. W. Lohrenz, A. Opel, A.-M. Sapse, P. v. R. Schleyer, *Lithium Chemistry*, John Wiley & Sons: New York, **1995**, p. 195.

[34] N. R. Bordwell, R. Vanler, X. Zhang, *J. Am. Chem. Soc*. **1991**, *113*, 9856.

[35] M. Schlosser, *Organometallics in Synthesis – A Manual*, 2nd Ed., Wiley, New York, **2002**.

[36] S. V. Hessar, P. Singh, *Chem. Rev*. **1997**, *97*, 721.

[37] D. Seyferth, M. A. Weiner, *J. Org. Chem*. **1959**, *60*, 5763.

[38] D. J. Peterson, *J. Organomet. Chem*. **1970**, *21*, 63.

[39] D. J. Peterson, *J. Am. Chem. Soc*. **1971**, *93*, 4027.

[40] X. Tian, M. Woski, C. Lustig, P. Pape, R. Fröhlich, D. Le Van, K. Bergander, N. W. Mitzel, *Organometallics* **2005**, *24*, 82.

[41]   R. E. Gawley, Q. Zhang, *J. Org. Chem*. **1995**, *60*, 5763.

[42]   J.-P. Quintard, B. Elissondo, B. Jousseaume, *Synthesis* **1984**, 495.

[43]   B. Trost, I. Fleming, *Comprehensive Organic Synthesis*, Pergamon Press, New York, **1991**.

[44]   C. Strohmann, B. C. Abele, *Angew. Chem. Int. Ed*. **1996**, *35*, 2378.

[45]   D. B. Collum, *Acc. Chem. Rev*. **1992**, *25*, 448.

[46]   A. W. Langer, *Polyamine-Chelate Alkali Metal Compounds*, Advances in Chemistry Series, American Chemical Society, Washington, DC, **1974**, p 130.

[47]   F. H. Köhler, N. Hertkorn, J. Blümel, *Chem. Ber*. **1987**, *120*, 2081.

[48]   D. Bojer, I. Kamps, X. Tian, A. Hepp, T. Pape, R. Fröhlich, N. W. Mitzel, *Angew. Chem. Int. Ed*. **2007**, *46*, 4176.

[49]   R. D. Köhn, G. Seifert, G. Kociok-Köhn, *Chem. Ber*. **1996**, *129*, 1327.

[50]   C. Strohmann, V. H. Gesser, *Angew. Chem. Int. Ed*. **2007**, *46*, 8281.

[51]   R. L. Gerteis, R. E. Dickerson, T. L. Brown, *Inorg. Chem*. **1964**, *3*, 872.

[52]   W .Clegg, L. Horsburgh, S. A. Couper, R. E. Mulvey, *Acta Crystallogr., Sect. C* **1999**, *C55*, 867.

[53]   M. Schakel, M. P. Aarnts, G. W. Klumpp, *Recl. Trav. Chim. Pays-Bas* **1990**, *109*, 305.

[54]   G. W. Klumpp, H. Luitjes, M. Schakel, E. J. J. de Kanter, R. F. Schmitz, N. J. R. C. van Eikema Hommes, *Angew. Chem. Int. Ed*. **1992**, *31*, 633.

[55]   H. Luitjes, M. Schakel, M. P. Aarnts, R. F. Schmitz, E. J. J. de Kanter, G. W. Klumpp, *Tetrahedron* **1997**, *53*, 9977.

[56]   J. Arnold, V. Knapp, J. A. R. Schmidt, A. Shafir, *J. Chem. Soc., Dalton Trans*. **2002**, 3273.

[57]   F. H. Allen, *Acta Crystallogr., Sect. B: Struct. Sci*. **2002**, *58*, 380.

[58]   M. Schiefer, H. Hatop, H. W. Roesky, H.-G. Schmidt, M. Noltemeyer, *Organometallics* **2002**, *21*, 1300.

[59]   B. Conway, J. García-Álvarez, E. Hevia, A. R. Kennedy, R. E. Mulvey, S. D. Robertson, *Organometallics*, **2009**, *28*, 6462.

Chapter 6: General Experimental Techniques

6.1) Schlenk Techniques

Throughout the duration of this project, many metal-based reactants and isolated metal-based products were, in general, air and moisture sensitive. Hence, standard Schlenk techniques, involving the repeated use of a high-vacuum Schlenk line (**figure 6.1**), were employed as a matter of routine.

Figure 6.1: Typical Schlenk line in use.

A typical Schlenk line consists of two independent paths: one of which is connected to a vacuum pump; and another which supplies dry and oxygen-free argon gas. The one photographed in **figure 6.1** contains four connections to Schlenk apparatus, primarily Schlenk tubes. Each connection has a two-way tap which can be adjusted so that the apparatus can be subjected to a vacuum or to an argon source. Air can be removed from the Schlenk tubes by evacuating them, and then subsequently refilling with argon gas, and this process is repeated three times as standard practice. A trap, which is placed in a liquid nitrogen-filled Dewar flask, is included to condense any volatile substances just before reaching, and potentially damaging, the vacuum pump. Also incorporated into the Schlenk line is a pressure release Dreschel bottle. This ensures that there is no pressure build-up in the apparatus.

6.2) Use of a glove box

The manipulation of all solid reactants and products, for example, for the determination of weights of reactant solids and product yields, and also for NMR spectroscopic preparations, had to be carried out in an inert atmosphere to prevent decontamination or decomposition. Hence, an argon-filled glove box was the best apparatus at hand to achieve these manipulations safely. A typical glove box is shown in **figure 6.2**.

Figure 6.2: A typical research glove box with fitted argon gas recirculation and purification system.

The small port on the right-hand side of the box allows the transfer of chemicals and small pieces of apparatus in and out of the glove box. Once the item(s) of interest are placed in the port, the outer port door is closed and, as for the Schlenk line, a pattern of evacuating the port and then refilling with argon is followed twice. The inner port door can then be opened in the knowledge that no, or negligible quantities, of H_2O or O_2 has entered the main body of the glove box.

6.3) Solvent purification

To minimise the possibility of oxygen or water being present in the solvents, with the result of unwanted reactions taking place, all the solvents were dried and degassed before use. All of the

solvents used in the reactions stated in this report were distilled over nitrogen in the presence of sodium and benzophenone.[1] The purpose of these two substances is that they are used as an excellent self-indicating method of ensuring oxygen and water are absent from the solvent. Sodium reacts with benzophenone to yield an intensely blue ketyl radical. This species is extremely reactive to oxygen and water and if present will yield colourless or yellow products. This colour difference is a simple, yet effective method of determining whether oxygen and/or water was present. The dried solvent was then collected in a nitrogen atmosphere into a round bottomed flask containing 4Å molecule sieves (which was dried at a temperature of 130°C for several hours). The round bottomed flask was then sealed airtight using a Subaseal®. This rubber stopper is an effective way of removing solvent without letting any air into the system. The solvent was removed by a glass syringe and needle, which importantly had to be flushed three times with nitrogen prior. To prevent a negative pressure arising within the round bottomed flask, it was essential that a volume of nitrogen was injected into the flask via the Subaseal® before removal of the solvent. If a negative pressure was to occur, solvent removal would become increasingly difficult to achieve, which could lead, in turn, to a gradual pull of atmospheric gases into the round bottomed flask as the pressure gradient tries to re-equilibrate. This would result in a contamination of the solvent.

6.4) Purification of hygroscopic liquids

Some liquids used in the reactions within the project (amines or pyridines) were very hygroscopic. Therefore, to ensure no contaminant moisture was present in these liquids, they had to be distilled in the presence of a dessicant before being introduced to reactions. The liquid was placed in a round bottomed flask containing calcium hydride and was distilled for a couple of hours. The purified liquid was collected into a round bottomed flask filled with argon, and enclosed with a Subaseal® for subsequent use in reactions.

6.5) Standardisation of ^{n}BuLi and ^{n}Bu$_2$Mg

Standardisation of commercial organometallic solutions, such as ^{n}BuLi in hexane and ^{n}Bu$_2$Mg in heptane, is necessary to ensure that the solution has the correct molarity for the stoichiometry to

be used in subsequent reactions. This is necessary because the molarity of the solutions can change due to evaporation of the solvent, or reaction of the organometallic compound with air.

Standardisation of the organometallic compounds was carried out (as illustrated in **scheme 6.1**) by dissolving 0.6 g of salicylaldehyde phenylhydrazone (synthesis of salicylaldehyde phenylhydrazone is outlined in **scheme 6.2**) in 10 mL of THF to form a yellow solution, and then titrating this with either ^{n}BuLi solution until a persistent red colour is obtained.[2]
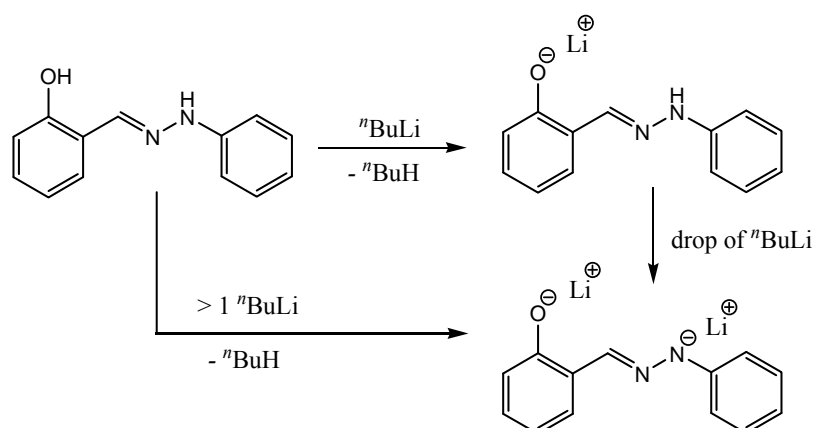
Scheme 6.1: Standardisation of ^{n}BuLi using salicylaldehyde phenylhydrazone.
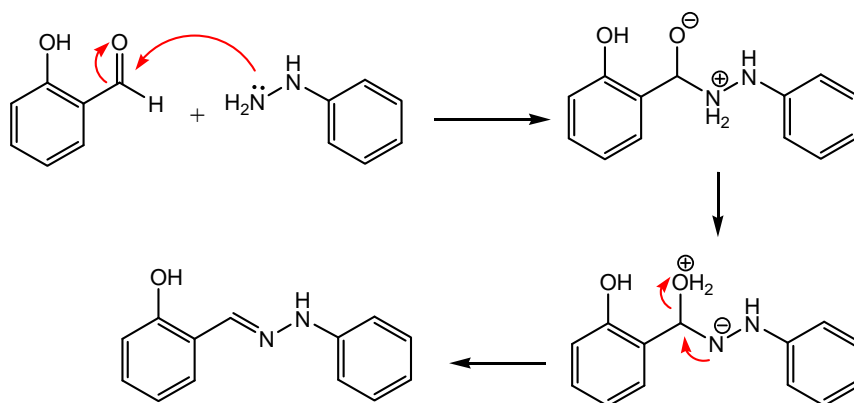
Scheme 6.2: Synthesis of salicylaldehyde phenylhydrazone.

The molarity of the ^{n}BuLi solution was then calculated using the formula in **eqn. 6.1**.

Weight of salicylaldehyde phenylhydrazone = X (g)

Volume of ^{n}BuLi needed to turn the solution red = Y (mL)

Z = X / 212.5   (where molecular weight of salicylaldehyde phenylhydrazone = 212.5)

Concentration of ^{n}BuLi   =   (Z / Y) x 1000   **(6.1)**

Dibutylmagnesium was standardised by diluting 2 mL of the organomagnesium compound in heptane with 10 mL of dried THF. Several crystals of 1, 10-phenanthroline were added to give a rust red colour. This was then titrated with *sec*-butanol in dry xylene to form a colourless solution.[3]

6.6) Analytical Procedures

^{1}H NMR spectra were recorded on either a Brüker DPX 400 or AV500 spectrometer, operating at 400.13 or 500.13 MHz respectively. The same instruments, operating at 100.62 MHz, were used to record ^{13}C NMR spectra. All ^{13}C NMR spectra were proton decoupled. The chemical shifts quoted are relative to TMS at 0.00 ppm. Correlations between protons and carbon atoms were obtained through COSY and HSQC NMR spectroscopic methods.

Single-crystal X-ray diffraction data were recorded on Nonius Kappa CCD or Oxford Diffraction Gemini A Ultra diffractometers using graphite-monochromated $Mo_{K\alpha}$ radiation (0.71073 Å).[4,5] The structures were solved by direct methods (SHELX-97 or SIR program package) and refined on all unique F^2 values (SHELX).[6,7]

Elemental analysis was carried out on a Perkin Elmer 2400 elemental analyser.

6.7) Computational Methods

The structure of **4c** was obtained from the crystallographic coordinates and the dislocations in the PMDETA ligand were removed manually. The structure was optimised at the BP86-D/def2-

TZVP level of theory by using TurboMole.[8] The converged wave-function file from the optimised structure was used for the subsequent Bader and NBO analyses. The Bader analysis was performed with the AIM2000 [9] program and the NBO perturbation study was carried out within the NBO 5.0 program.[10]

Chapter 6 – References:

[1]   D. F. Schriver, M. A. Derezdzon, *The Manipulation of Air-Sensitive Compounds*, 2nd ed., Wiley and Sons, New York, **1986**, p. 88.

[2]   B. E. Love, E. G. Jones, *J. Org. Chem.* **1999**, *64*, 3755.

[3]   Y. Aso, H. Yamashita, T. Otsubo, F. Ogura, *J. Org. Chem*. **1989**, *54*, 5627.

[4]   COLLECT, *Program for Data Collection*, Nonius BV, Delft (The Netherlands), **2000**.

[5]   CrysAlisPro, Program for Integration and Absorption Correction, Oxford Diffraction Ltd., Abingdon (UK), **2008**.

[6]   G. M. Sheldrick, *Acta Crystallogr. Sect. A* **2008**, *64*, 112.

[7]   G. M. Sheldrick, SHELXL93, *Program for the Refinement of Crystal Structures*, University of Göttingen, Göttingen (Germany), **1993**.

[8]   TurboMole, *Program for Ab Initio Electronic Structure Calculations*, TurboMole GmbH, Germany, **2007**.

[9]   F. Biegler-König, J. Schönbohm, AIM2000, *Program to Analyse and Visualise Atoms in Molecules*, Germany, **2002**.

[10]   NBO 5.G., E. D. Glendening, J. K. Badenhoop, A. E. Reed, J. E. Carpenter, J. A. Bohmann, C. M. Morales, F. Weinhold, Theoretical Chemistry Institute, University of Wisconsin, Madison, **2001**.

X-ray Crystallographic Data

252

4k

4l

5k

5l

5m

5n

5p

5u

5v

5w

254
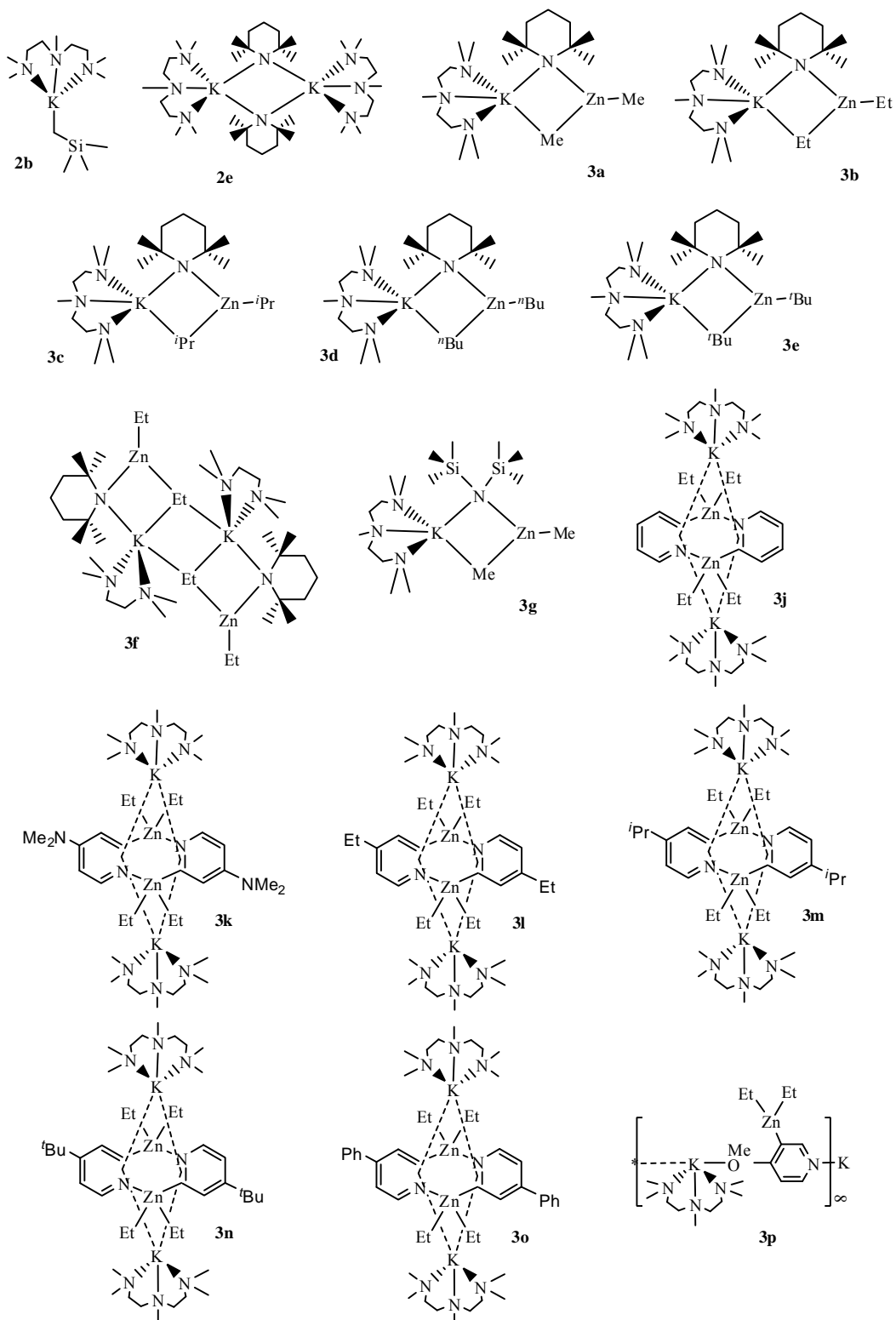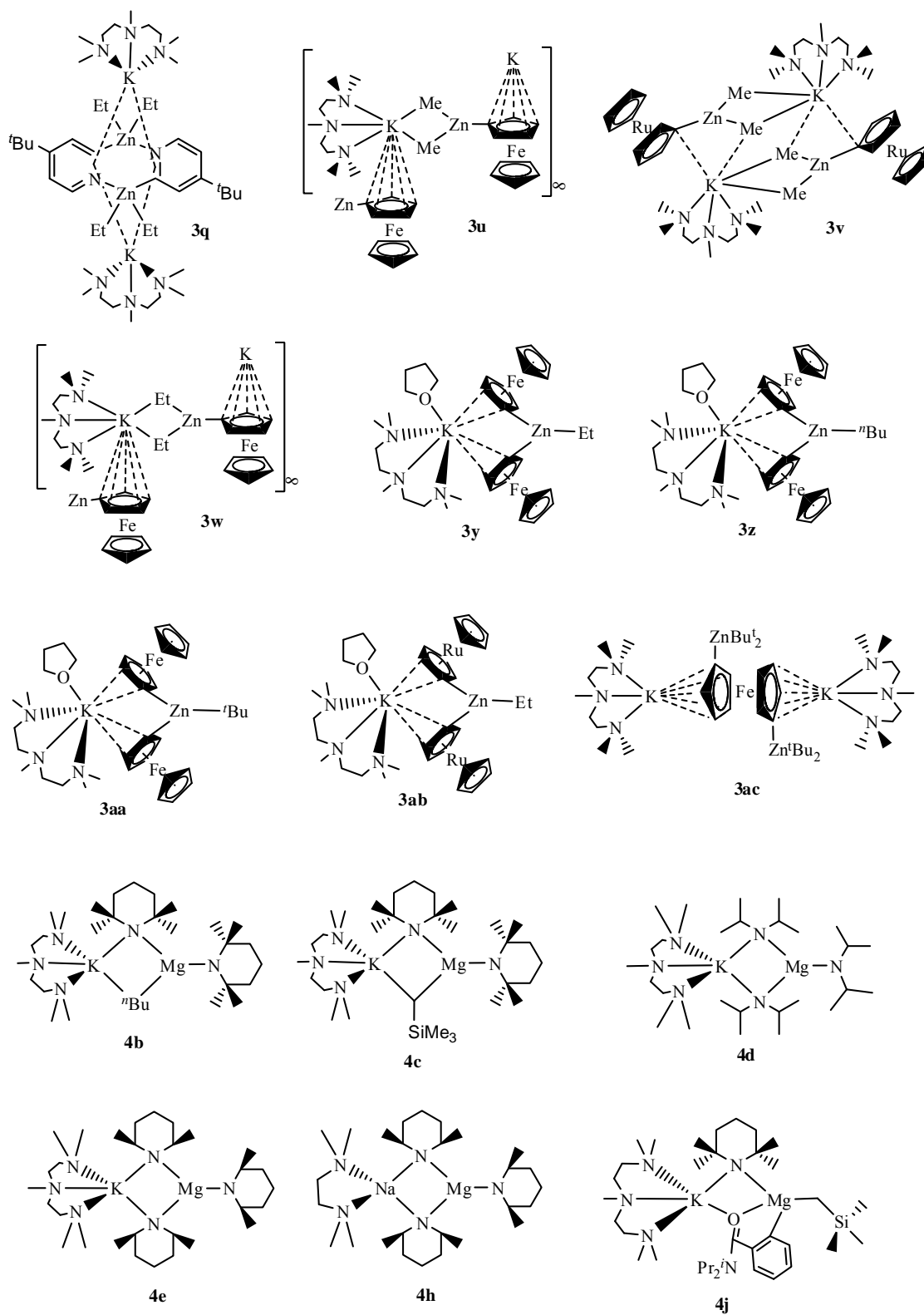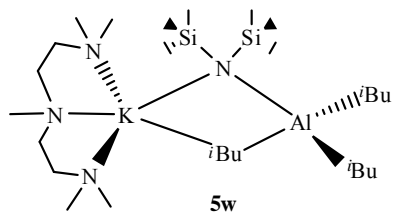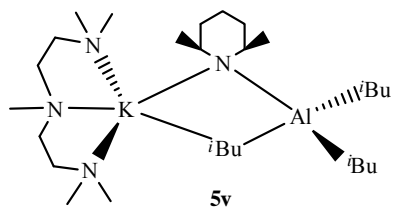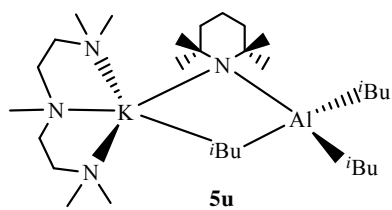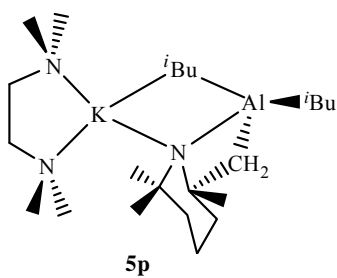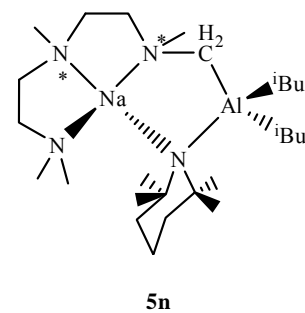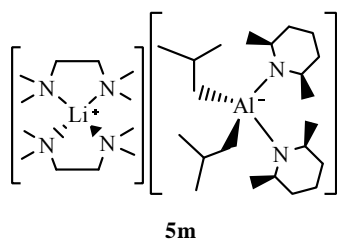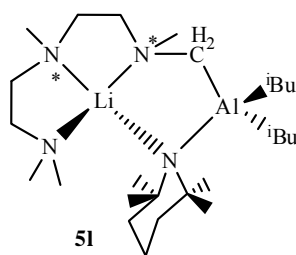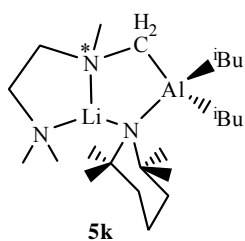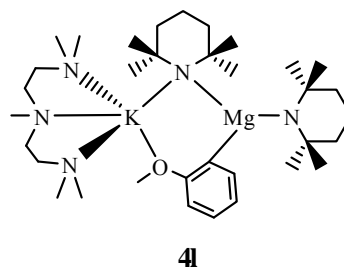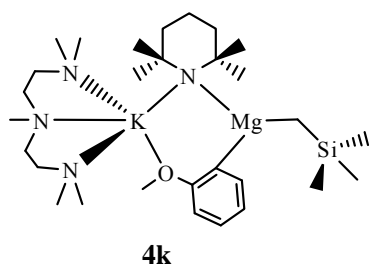
Crystal Data for 2b

Empirical formula	C13 H34 K N3 Si
Formula weight	299.62
Temperature	123(2) K
Wavelength	0.71073 Å
Crystal system	Trigonal
Space group	P3(2)
Unit cell dimensions	a = 10.77300(10) Å $\alpha = 90°$.
	b = 10.77300(10) Å $\beta = 90°$.
	c = 14.6261(3) Å $\gamma = 120°$.
Volume	1470.05(4) Å^3
Z	3
Density (calculated)	1.015 Mg/m^3
Absorption coefficient	0.324 mm^{-1}
F(000)	498
Crystal size	0.25 x 0.15 x 0.15 mm^3
Theta range for data collection	2.59 to 30.45°.
Index ranges	-15<=h<=7, -10<=k<=14, -20<=l<=20
Reflections collected	8954
Independent reflections	4955 [R(int) = 0.0184]
Completeness to theta = 27.00°	99.9 %
Absorption correction	Semi-empirical from equivalents
Max. and min. transmission	1.00000 and 0.95746
Refinement method	Full-matrix least-squares on F^2
Data / restraints / parameters	4955 / 1 / 183
Goodness-of-fit on F^2	0.913
Final R indices [I>2sigma(I)]	R1 = 0.0308, wR2 = 0.0495
R indices (all data)	R1 = 0.0388, wR2 = 0.0509
Largest diff. peak and hole	0.231 and -0.195 e.Å^{-3}

Crystal Data for 2e

Empirical formula	C36 H82 K2 N8
Formula weight	705.30
Temperature	123(2) K
Wavelength	0.71073 Å
Crystal system	Triclinic
Space group	P-1
Unit cell dimensions	$a = 11.8881(4)$ Å $\alpha = 69.405(2)°$.
	$b = 12.6209(4)$ Å $\beta = 75.270(2)°$.
	$c = 16.2808(3)$ Å $\gamma = 79.316(3)°$.
Volume	2199.03(11) Å^3
Z	2
Density (calculated)	1.065 Mg/m^3
Absorption coefficient	0.248 mm^{-1}
F(000)	784
Crystal size	0.2 x 0.2 x 0.1 mm^3
Theta range for data collection	2.53 to 30.49°.
Index ranges	-16<=h<=16, -17<=k<=17, -22<=l<=22
Reflections collected	44924
Independent reflections	12214 [R(int) = 0.0308]
Completeness to theta = 29.00°	99.3 %
Absorption correction	MULTISCAN
Max. and min. transmission	1.00000 and 0.94336
Refinement method	Full-matrix least-squares on F^2
Data / restraints / parameters	12214 / 0 / 515
Goodness-of-fit on F^2	0.978
Final R indices [I>2sigma(I)]	R1 = 0.0356, wR2 = 0.0796
R indices (all data)	R1 = 0.0610, wR2 = 0.0853
Largest diff. peak and hole	0.298 and -0.184 e.Å^{-3}

Crystal Data for 3a

Empirical formula	C20 H47 K N4 Zn
Formula weight	448.09
Temperature	150(2) K
Wavelength	0.71073 Å
Crystal system	Monoclinic
Space group	$P12_1/c1P-1$
Unit cell dimensions	a = 24.7840(7) Å $\quad$ $\alpha = 90°$.
	b = 8.4806(2) Å $\quad$ $\beta = 93.929(3)°$.
	c = 48.933(2) Å $\quad$ $\gamma = 90°$.
Volume	10260.7(6) Å^3
Z	16
Density (calculated)	1.160 Mg/m^3
Absorption coefficient	1.130 mm^{-1}
F(000)	3904
Crystal size	0.58 x 0.38 x 0.16 mm^3
Theta range for data collection	2.9 to 20.8°.
Index ranges	-24<=h<=24, -8<=k<=8, -47<=l<=48
Reflections collected	30421
Independent reflections	10705 [R(int) = 0.0684]
Completeness to theta = 20.8°	99.6 %
Absorption correction	semi-empirical from equivalents
Max. and min. transmission	0.8399 and 05602
Refinement method	Full-matrix least-squares on F^2
Data / restraints / parameters	10705 / 1619 / 981
Goodness-of-fit on F^2	1.079
Final R indices [I>2sigma(I)]	R1 = 0.0988, wR2 = 0.2038
R indices (all data)	R1 = 0.1461, wR2 = 0.2175
Largest diff. peak and hole	1.30 and -0.86 e.Å^{-3}

Crystal Data for 3b

Empirical formula	$C_{22} H_{51} K N_4 Zn$
Formula weight	476.14
Temperature	123(2) K
Wavelength	0.71073 Å
Crystal system	Orthorhombic
Space group	P212121
Unit cell dimensions	a = 8.0619(2) Å α = 90°.
	b = 15.9886(4) Å β = 90°.
	c = 21.2669(6) Å γ = 90°.
Volume	2741.27(12) Å^3
Z	4
Density (calculated)	1.154 Mg/m^3
Absorption coefficient	1.061 mm^{-1}
F(000)	1040
Crystal size	0.4 x 0.2 x 0.15 mm^3
Theta range for data collection	1.59 to 27.44°.
Index ranges	-10<=h<=10, -20<=k<=20, -27<=l<=27
Reflections collected	6220
Independent reflections	6220 [R(int) = 0.0000]
Completeness to theta = 27.44°	99.6 %
Absorption correction	none
Refinement method	Full-matrix least-squares on F^2
Data / restraints / parameters	6220 / 0 / 265
Goodness-of-fit on F^2	1.125
Final R indices [I>2sigma(I)]	R1 = 0.0840, wR2 = 0.1700
R indices (all data)	R1 = 0.1176, wR2 = 0.1876
Largest diff. peak and hole	2.339 and -1.476 e.Å^{-3}

Crystal Data for 3c

Empirical formula	C24 H55 K N4 Zn
Formula weight	504.19
Temperature	150(2) K
Wavelength	0.71073 Å
Crystal system	Monoclinic
Space group	$P2_1/n$
Unit cell dimensions	$a = 11.809(3)$ Å $\quad \alpha = 90°.$
	$b = 15.997(5)$ Å $\quad \beta = 94.019(4)°.$
	$c = 16.148(5)$ Å $\quad \gamma = 90°.$
Volume	3042.9(15) Å^3
Z	4
Density (calculated)	1.101 Mg/m^3
Absorption coefficient	0.959 mm^{-1}
F(000)	1104
Crystal size	0.68 x 0.56 x 0.34 mm^3
Theta range for data collection	5.1 to 25.0°.
Index ranges	-14<=h<=13, -18<=k<=19, -19<=l<=19
Reflections collected	21640
Independent reflections	5290 [R(int) = 0.0177]
Completeness to theta = 25.0°	99.1 %
Absorption correction	semi-empirical from equivalents
Max. and min. transmission	0.7362 and 0.5615
Refinement method	Full-matrix least-squares on F^2
Data / restraints / parameters	5290 / 293 / 374
Goodness-of-fit on F^2	1.013
Final R indices [I>2sigma(I)]	R1 = 0.0328, wR2 = 0.0836
R indices (all data)	R1 = 0.0378, wR2 = 0.0880
Largest and mean shift/su	0.001 and 0.000
Largest diff. peak and hole	0.60 and -0.36 e.Å^{-3}

Crystal Data for 3d

Empirical formula	C26 H59 K N4 Zn
Formula weight	532.24
Temperature	150(2) K
Wavelength	0.71073 Å
Crystal system	Triclinic
Space group	P1
Unit cell dimensions	$a = 10.5721(2)$ Å $\quad \alpha = 86.851(2)°.$
	$b = 10.7949(3)$ Å $\quad \beta = 78.881(2)°.$
	$c = 15.6143(4)$ Å $\quad \gamma = 64.329(2)°.$
Volume	1575.12(7) Å^3
Z	2
Density (calculated)	1.122 Mg/m^3
Absorption coefficient	0.930 mm^{-1}
F(000)	584
Crystal size	0.54 x 0.48 x 0.04 mm^3
Theta range for data collection	3.2 to 25.0°.
Index ranges	-10<=h<=12, -12<=k<=12, -18<=l<=18
Reflections collected	10981
Independent reflections	5500 [R(int) = 0.0154]
Completeness to theta = 25.0°	98.9 %
Absorption correction	semi-empirical from equivalents
Max. and min. transmission	0.9637 and 0.6336
Refinement method	Full-matrix least-squares on F^2
Data / restraints / parameters	5500 / 780 / 387
Goodness-of-fit on F^2	1.061
Final R indices [I>2sigma(I)]	R1 = 0.0270, wR2 = 0.0683
R indices (all data)	R1 = 0.0344, wR2 = 0.0700
Largest and mean shift/su	0.002 and 0.000
Largest diff. peak and hole	0.81 and -0.33 e.Å^{-3}

Crystal Data for 3e

Empirical formula	C26 H59 K N4 Zn
Formula weight	532.24
Temperature	123(2) K
Wavelength	0.71073 Å
Crystal system	Monoclinic
Space group	P21/n
Unit cell dimensions	a = 11.5804(3) Å $\quad\quad$ α = 90°.
	b = 24.0227(5) Å $\quad\quad$ β = 105.110(2)°.
	c = 11.9775(2) Å $\quad\quad$ γ = 90°.
Volume	3216.85(12) Å^3
Z	4
Density (calculated)	1.099 Mg/m^3
Absorption coefficient	0.911 mm^{-1}
F(000)	1168
Crystal size	0.47 x 0.44 x 0.37 mm^3
Theta range for data collection	2.76 to 25.02°.
Index ranges	-13<=h<=13, -28<=k<=27, -14<=l<=13
Reflections collected	19383
Independent reflections	5675 [R(int) = 0.0232]
Completeness to theta = 25.02°	99.8 %
Absorption correction	semi-empirical from equivalents
Max. and min. transmission	0.833 and 0.721
Refinement method	Full-matrix least-squares on F^2
Data / restraints / parameters	5675 / 0 / 304
Goodness-of-fit on F^2	1.000
Final R indices [I>2sigma(I)]	R1 = 0.0253, wR2 = 0.0628
R indices (all data)	R1 = 0.0352, wR2 = 0.0645
Largest diff. peak and hole	0.399 and -0.274 e.Å^{-3}

Crystal Data for 3f

Empirical formula	C19 H44 K N3 Zn
Formula weight	419.04
Temperature	123(2) K
Wavelength	0.71073 Å
Crystal system	Triclinic
Space group	P-1
Unit cell dimensions	$a = 8.5952(3)$ Å $\quad \alpha = 77.183(2)°$.
	$b = 11.2893(4)$ Å $\quad \beta = 71.892(2)°$.
	$c = 13.6711(6)$ Å $\quad \gamma = 70.794(2)°$.
Volume	1180.06(8) Å^3
Z	2
Density (calculated)	1.179 Mg/m^3
Absorption coefficient	1.223 mm^{-1}
F(000)	456
Crystal size	0.2 x 0.2 x 0.12 mm^3
Theta range for data collection	1.58 to 27.55°.
Index ranges	$-11 \leq h \leq 11, -14 \leq k \leq 14, -17 \leq l \leq 17$
Reflections collected	10533
Independent reflections	10533 [R(int) = 0.0000]
Completeness to theta = 27.55°	97.7 %
Absorption correction	none
Refinement method	Full-matrix least-squares on F^2
Data / restraints / parameters	10533 / 0 / 228
Goodness-of-fit on F^2	1.028
Final R indices [I>2sigma(I)]	R1 = 0.0644, wR2 = 0.1289
R indices (all data)	R1 = 0.1117, wR2 = 0.1522
Largest diff. peak and hole	1.151 and -0.563 e.Å^{-3}

Crystal Data for 3g

Empirical formula	C17 H47 K N4 Si2 Zn
Formula weight	468.24
Temperature	150(2) K
Wavelength	0.71073 Å
Crystal system	Monoclinic
Space group	$P12_1/c1$
Unit cell dimensions	a = 15.7664(12) Å $\quad$ α = 90°.
	b = 15.4286(16) Å $\quad$ β = 90.029(7)°.
	c = 22.7138(18) Å $\quad$ γ = 90°.
Volume	5525.2(8) Å^3
Z	8
Density (calculated)	1.126 Mg/m^3
Absorption coefficient	1.134 mm^{-1}
F(000)	2032
Crystal size	0.28 x 0.22 x 0.02 mm^3
Theta range for data collection	4.1 to 25.0°.
Index ranges	-18<=h<=17, -18<=k<=17, -26<=l<=27
Reflections collected	19088
Independent reflections	8632 [R(int) = 0.1315]
Completeness to theta = 25.0°	88.8 %
Absorption correction	semi-empirical from equivalents
Max. and min. transmission	0.9777 and 0.7419
Refinement method	Full-matrix least-squares on F^2
Data / restraints / parameters	8632 / 0 / 477
Goodness-of-fit on F^2	0.752
Final R indices [I>2sigma(I)]	R1 = 0.0630, wR2 = 0.1029
R indices (all data)	R1 = 0.2249, wR2 = 0.1340
Largest and mean shift/su	0.002 and 0.000
Largest diff. peak and hole	1.31 and -0.43 e.Å^{-3}

Crystal Data for 3j

Empirical formula	C36 H74 K2 N8 Zn2
Formula weight	827.97
Temperature	150(2) K
Wavelength	0.71073 Å
Crystal system	Monoclinic
Space group	P2$_1$/n
Unit cell dimensions	a = 11.436(2) Å α = 90°.
	b = 16.493(3) Å β = 97.27(3)°.
	c = 12.218(2) Å γ = 90°.
Volume	2286.0(8) Å^3
Z	2
Density (calculated)	1.203 Mg/m^3
Absorption coefficient	1.263 mm^{-1}
F(000)	888
Crystal size	0.36 x 0.24 x 0.06 mm^3
Theta range for data collection	5.1 to 25.0°.
Index ranges	-13<=h<=13, -19<=k<=19, -14<=l<=13
Reflections collected	15618
Independent reflections	3984 [R(int) = 0.0838]
Completeness to theta = 25.0°	99.0 %
Absorption correction	semi-empirical from equivalents
Max. and min. transmission	0.9281 and 0.6591
Refinement method	Full-matrix least-squares on F^2
Data / restraints / parameters	3984 / 298 / 233
Goodness-of-fit on F^2	1.047
Final R indices [I>2sigma(I)]	R1 = 0.0640, wR2 = 0.0819
R indices (all data)	R1 = 0.1326, wR2 = 0.0964
Largest and mean shift/su	0.001 and 0.000
Largest diff. peak and hole	0.46 and -0.37 e.Å^{-3}

Crystal Data for 3k

Empirical formula	C40 H84 K2 N10 Zn2
Formula weight	914.11
Temperature	123(2) K
Wavelength	0.71073 Å
Crystal system	Monoclinic
Space group	C2/c
Unit cell dimensions	$a = 28.3709(8)$ Å $\quad \alpha = 90°.$
	$b = 12.1545(3)$ Å $\quad \beta = 128.6170(10)°.$
	$c = 18.5001(5)$ Å $\quad \gamma = 90°.$
Volume	4984.5 (2) Å^3
Z	4
Density (calculated)	1.218 Mg/m^3
Absorption coefficient	1.166 mm^{-1}
F(000)	1968
Crystal size	0.3 x 0.3 x 0.1 mm^3
Theta range for data collection	2.01 to 27.49°.
Index ranges	-36<=h<=36, -15<=k<=15, -23<=l<=23
Reflections collected	10886
Independent reflections	5679 [R(int) = 0.0215]
Completeness to theta = 27.49°	99.4 %
Absorption correction	none
Refinement method	Full-matrix least-squares on F^2
Data / restraints / parameters	5679 / 0 / 269
Goodness-of-fit on F^2	1.062
Final R indices [I>2sigma(I)]	R1 = 0.0274, wR2 = 0.0617
R indices (all data)	R1 = 0.0396, wR2 = 0.0672
Largest diff. peak and hole	0.356 and -0.376 e.Å^{-3}

Crystal Data for 3l

Empirical formula	C40 H82 K2 N8 Zn2
Formula weight	884.08
Temperature	123(2) K
Wavelength	0.71073 Å
Crystal system	Monoclinic
Space group	P21/c
Unit cell dimensions	a = 13.4732(3) Å α = 90°.
	b = 12.6443(3) Å β = 97.405(2)°.
	c = 14.5974(3) Å γ = 90°.
Volume	2466.06(9) Å^3
Z	2
Density (calculated)	1.191 Mg/m^3
Absorption coefficient	1.175 mm^{-1}
F(000)	952
Crystal size	0.28 x 0.22 x 0.16 mm^3
Theta range for data collection	2.73 to 30.00°.
Index ranges	-18<=h<=18, -17<=k<=16, -20<=l<=20
Reflections collected	29148
Independent reflections	6670 [R(int) = 0.0247]
Completeness to theta = 26.00°	98.9 %
Absorption correction	Semi-empirical from equivalents
Max. and min. transmission	1.00000 and 0.92946
Refinement method	Full-matrix least-squares on F^2
Data / restraints / parameters	6670 / 0 / 259
Goodness-of-fit on F^2	1.039
Final R indices [I>2sigma(I)]	R1 = 0.0353, wR2 = 0.0853
R indices (all data)	R1 = 0.0610, wR2 = 0.0901
Largest diff. peak and hole	0.440 and -0.233 e.Å^{-3}

Crystal Data for 3m

Empirical formula	C21 H43 K N4 Zn
Formula weight	456.06
Temperature	123(2) K
Wavelength	0.71073 Å
Crystal system	Monoclinic
Space group	P21/c
Unit cell dimensions	a = 13.4980(5) Å α = 90°.
	b = 13.1963(4) Å β = 128.224(2)°.
	c = 18.1640(5) Å γ = 90°.
Volume	2541.75(14) Å^3
Z	4
Density (calculated)	1.192 Mg/m^3
Absorption coefficient	1.142 mm^{-1}
F(000)	984
Crystal size	0.3 x 0.1 x 0.1 mm^3
Theta range for data collection	2.46 to 27.47°.
Index ranges	-17<=h<=17, -13<=k<=17, -23<=l<=23
Reflections collected	9756
Independent reflections	5809 [R(int) = 0.0218]
Completeness to theta = 27.47°	99.5 %
Absorption correction	none
Refinement method	Full-matrix least-squares on F^2
Data / restraints / parameters	5809 / 0 / 268
Goodness-of-fit on F^2	1.088
Final R indices [I>2sigma(I)]	R1 = 0.0516, wR2 = 0.1174
R indices (all data)	R1 = 0.0779, wR2 = 0.1335
Largest diff. peak and hole	0.761 and -0.562 e.Å^{-3}

Crystal Data for 3n

Empirical formula	C44 H90 K2 N8 Zn2
Formula weight	940.18
Temperature	150(2) K
Wavelength	0.71073 Å
Crystal system	Monoclinic
Space group	$P2_1/n$
Unit cell dimensions	$a = 13.441(3)$ Å $\quad \alpha = 90°$.
	$b = 12.970(3)$ Å $\quad \beta = 92.67(3)°$.
	$c = 15.234(3)$ Å $\quad \gamma = 90°$.
Volume	2652.7(9) Å^3
Z	2
Density (calculated)	1.177 Mg/m^3
Absorption coefficient	1.096 mm^{-1}
F(000)	1016
Crystal size	0.43 x 0.41 x 0.11 mm^3
Theta range for data collection	5.1 to 25.0°.
Index ranges	-14<=h<=15, -15<=k<=13, -17<=l<=18
Reflections collected	15975
Independent reflections	4618 [R(int) = 0.0264]
Completeness to theta = 25.0°	98.8 %
Absorption correction	semi-empirical from equivalents
Max. and min. transmission	0.8889 and 0.6500
Refinement method	Full-matrix least-squares on F^2
Data / restraints / parameters	4618 / 136 / 312
Goodness-of-fit on F^2	1.096
Final R indices [I>2sigma(I)]	R1 = 0.0247, wR2 = 0.0534
R indices (all data)	R1 = 0.0374, wR2 = 0.0596
Largest and mean shift/su	0.001 and 0.000
Largest diff. peak and hole	0.29 and -0.22 e.Å^{-3}

Crystal Data for 3o

Empirical formula	C48 H82 K2 N8 Zn2
Formula weight	980.16
Temperature	123(2) K
Wavelength	0.71073 Å
Crystal system	Triclinic
Space group	P-1
Unit cell dimensions	a = 9.8074(6) Å $\quad$ α = 86.341(5)°.
	b = 13.1617(9) Å $\quad$ β = 88.833(5)°.
	c = 22.4372(15) Å $\quad$ γ = 69.464(6)°.
Volume	2706.7(3) Å^3
Z	2
Density (calculated)	1.203 Mg/m^3
Absorption coefficient	1.077 mm^{-1}
F(000)	1048
Crystal size	0.30 x 0.25 x 0.20 mm^3
Theta range for data collection	2.53 to 27.00°.
Index ranges	-12<=h<=12, -16<=k<=16, -28<=l<=28
Reflections collected	37589
Independent reflections	11451 [R(int) = 0.0533]
Completeness to theta = 26.00°	97.5 %
Absorption correction	Semi-empirical from equivalents
Max. and min. transmission	1.00000 and 0.95614
Refinement method	Full-matrix least-squares on F^2
Data / restraints / parameters	11451 / 0 / 577
Goodness-of-fit on F^2	0.872
Final R indices [I>2sigma(I)]	R1 = 0.0455, wR2 = 0.1013
R indices (all data)	R1 = 0.1004, wR2 = 0.1121
Largest diff. peak and hole	0.494 and -0.571 e.Å^{-3}

Crystal Data for 3p

Empirical formula	C19 H39 K N4 O Zn
Formula weight	444.01
Temperature	123(2) K
Wavelength	0.71073 Å
Crystal system	Orthorhombic
Space group	Pna21
Unit cell dimensions	a = 19.3708(11) Å $\alpha = 90°$.
	b = 7.6797(4) Å $\beta = 90°$.
	c = 16.2156(9) Å $\gamma = 90°$.
Volume	2412.3(2) Å^3
Z	4
Density (calculated)	1.223 Mg/m^3
Absorption coefficient	1.204 mm^{-1}
F(000)	952
Crystal size	0.2 x 0.2 x 0.1 mm^3
Theta range for data collection	2.10 to 27.49°.
Index ranges	-24<=h<=25, -9<=k<=9, -20<=l<=20
Reflections collected	5218
Independent reflections	5218 [R(int) = 0.0000]
Completeness to theta = 27.49°	99.7 %
Absorption correction	none
Refinement method	Full-matrix least-squares on F^2
Data / restraints / parameters	5218 / 1 / 244
Goodness-of-fit on F^2	1.050
Final R indices [I>2sigma(I)]	R1 = 0.0529, wR2 = 0.0884
R indices (all data)	R1 = 0.0967, wR2 = 0.1037
Largest diff. peak and hole	0.496 and -0.351 e.Å^{-3}

Crystal Data for 3q

Empirical formula	C52 H106 K2 N8 Zn2
Formula weight	1052.39
Temperature	150(2) K
Wavelength	0.71073 Å
Crystal system	monoclinic
Space group	C12/c1
Unit cell dimensions	$a = 27500(7)$ Å $\quad \alpha = 90°$.
	$b = 12.8693(10)$ Å $\quad \beta = 123.765(14)°$.
	$c = 20.695(3)$ Å $\quad \gamma = 90°$.
Volume	6088.7(18) Å^3
Z	4
Density (calculated)	1.148 Mg/m^3
Absorption coefficient	0.962 mm^{-1}
F(000)	2288
Crystal size	0.32 x 0.18 x 0.16 mm^3
Theta range for data collection	6.8 to 25.0°.
Index ranges	-32<=h<=27, -13<=k<=15, -24<=l<=24
Reflections collected	17368
Independent reflections	5223 [R(int) = 0.1214]
Completeness to theta = 27.49°	97.7 %
Absorption correction	semi-empirical from equivalents
Max. and min. transmission	0.8613 and 0.7483
Refinement method	Full-matrix least-squares on F^2
Data / restraints / parameters	5223 / 656 / 356
Goodness-of-fit on F^2	1.042
Final R indices [I>2sigma(I)]	R1 = 0.1077, wR2 = 0.2266
R indices (all data)	R1 = 0.1364, wR2 = 0.2390
Largest and mean shift/su	0.000 and 0.000
Largest diff. peak and hole	0.92 and -1.30 e.Å^{-3}

Crystal Data for 3u

Empirical formula	C21 H38 Fe K N3 Zn
Formula weight	492.86
Temperature	123(2) K
Wavelength	0.71073 Å
Crystal system	Orthorhombic
Space group	Pca21
Unit cell dimensions	$a = 18.2193(7)$ Å $\quad \alpha = 90°$.
	$b = 7.5981(4)$ Å $\quad \beta = 90°$.
	$c = 17.7793(7)$ Å $\quad \gamma = 90°$.
Volume	2461.23(19) Å^3
Z	4
Density (calculated)	1.330 Mg/m^3
Absorption coefficient	1.743 mm^{-1}
F(000)	1040
Crystal size	0.2 x 0.1 x 0.05 mm^3
Theta range for data collection	2.51 to 29.00°.
Index ranges	-24<=h<=24, -6<=k<=10, -23<=l<=24
Reflections collected	14510
Independent reflections	6300 [R(int) = 0.0517]
Completeness to theta = 27.50°	99.9 %
Absorption correction	Semi-empirical from equivalents
Max. and min. transmission	1.00000 and 0.93371
Refinement method	Full-matrix least-squares on F^2
Data / restraints / parameters	6300 / 1 / 270
Goodness-of-fit on F^2	0.799
Final R indices [I>2sigma(I)]	R1 = 0.0374, wR2 = 0.0448
R indices (all data)	R1 = 0.0717, wR2 = 0.0486
Largest diff. peak and hole	0.519 and -0.350 e.Å^{-3}

Crystal Data for 3v

Empirical formula	C42 H76 K2 N6 Ru2 Zn2
Formula weight	1076.17
Temperature	123(2) K
Wavelength	0.71073 Å
Crystal system	Triclinic
Space group	P-1
Unit cell dimensions	a = 8.8165(3) Å α = 114.673(4)°.
	b = 11.9380(4) Å β = 95.400(3)°.
	c = 12.9284(5) Å γ = 99.969(3)°.
Volume	1196.61(7) Å^3
Z	1
Density (calculated)	1.493 Mg/m^3
Absorption coefficient	1.817 mm^{-1}
F(000)	556
Crystal size	0.2 x 0.2 x 0.2 mm^3
Theta range for data collection	2.69 to 30.45°.
Index ranges	-12<=h<=12, -16<=k<=16, -18<=l<=18
Reflections collected	21909
Independent reflections	6756 [R(int) = 0.0246]
Completeness to theta = 27.00°	99.9 %
Absorption correction	Semi-empirical from equivalents
Max. and min. transmission	1.00000 and 0.84849
Refinement method	Full-matrix least-squares on F^2
Data / restraints / parameters	6756 / 0 / 284
Goodness-of-fit on F^2	0.990
Final R indices [I>2sigma(I)]	R1 = 0.0213, wR2 = 0.0472
R indices (all data)	R1 = 0.0289, wR2 = 0.0485
Largest diff. peak and hole	0.393 and -0.545 e.Å^{-3}

Crystal Data for 3w

Empirical formula	C23 H42 Fe K N3 Zn
Formula weight	520.92
Temperature	150(2) K
Wavelength	0.71073 Å
Crystal system	Monoclinic
Space group	Cm
Unit cell dimensions	$a = 11.714(2)$ Å, $\alpha = 90°$.
	$b = 14.980(3)$ Å, $\beta = 93.74(3)°$.
	$c = 7.5330(15)$ Å, $\gamma = 90°$.
Volume	1319.0(5) Å^3
Z	2
Density (calculated)	1.312 Mg/m^3
Absorption coefficient	1.630 mm^{-1}
F(000)	552
Crystal size	0.82 x 0.36 x 0.08 mm^3
Theta range for data collection	5.1 to 27.5°.
Index ranges	-15<=h<=15, -18<=k<=19, -9<=l<=6
Reflections collected	5301
Independent reflections	2526 [R(int) = 0.0246]
Completeness to theta = 27.5°	99.0 %
Absorption correction	Semi-empirical from equivalents
Max. and min. transmission	0.8807 and 0.3483
Refinement method	Full-matrix least-squares on F^2
Data / restraints / parameters	2526 / 2 / 148
Goodness-of-fit on F^2	1.020
Final R indices [I>2sigma(I)]	R1 = 0.0167, wR2 = 0.0393
R indices (all data)	R1 = 0.0185, wR2 = 0.0404
Largest diff. peak and hole	0.24 and -0.19 e.Å^{-3}

Crystal Data for 3y

Empirical formula	C35 H54 Fe2 K N3 O Zn
Formula weight	748.98
Temperature	150(2) K
Wavelength	0.71073 Å
Crystal system	Monoclinic
Space group	$P12_1/c1$
Unit cell dimensions	$a = 11.7414(2)$ Å $\alpha = 90°$.
	$b = 20.1551(3)$ Å $\beta = 109.588(2)°$.
	$c = 15.8707(3)$ Å $\gamma = 90°$.
Volume	$3538.43(10)$ Å^3
Z	4
Density (calculated)	1.406 Mg/m^3
Absorption coefficient	1.630 mm^{-1}
F(000)	1576
Crystal size	0.42 x 0.40 x 0.18 mm^3
Theta range for data collection	6.8 to 25.0°.
Index ranges	-13<=h<=13, -23<=k<=20, -18<=l<=18
Reflections collected	18154
Independent reflections	6086 [R(int) = 0.0228]
Completeness to theta = 25.0°	97.8 %
Absorption correction	Semi-empirical from equivalents
Max. and min. transmission	0.7580 and 0.5477
Refinement method	Full-matrix least-squares on F^2
Data / restraints / parameters	6086 / 47 / 394
Goodness-of-fit on F^2	1.052
Final R indices [I>2sigma(I)]	R1 = 0.0223, wR2 = 0.0549
R indices (all data)	R1 = 0.0300, wR2 = 0.0561
Largest and mean shift/su	0.002 and 0.000
Largest diff. peak and hole	0.46 and -0.43 e.Å^{-3}

Crystal Data for 3z

Empirical formula	C37 H58 Fe2 K N3 O Zn
Formula weight	777.03
Temperature	150(2) K
Wavelength	0.71073 Å
Crystal system	Monoclinic
Space group	$P2_1/n$
Unit cell dimensions	$a = 13.619(3)$ Å $\quad \alpha = 90°$.
	$b = 17.969(4)$ Å $\quad \beta = 101.06(3)°$.
	$c = 16.150(3)$ Å $\quad \gamma = 90°$.
Volume	3538.43(10) Å^3
Z	4
Density (calculated)	1.331 Mg/m^3
Absorption coefficient	1.489 mm^{-1}
F(000)	1640
Crystal size	0.16 x 0.14 x 0.12 mm^3
Theta range for data collection	5.1 to 25.0°.
Index ranges	-16<=h<=16, -21<=k<=21, -19<=l<=18
Reflections collected	32580
Independent reflections	6489 [R(int) = 0.0454]
Completeness to theta = 25.0°	95.0 %
Absorption correction	Semi-empirical from equivalents
Max. and min. transmission	0.8415 and 0.7965
Refinement method	Full-matrix least-squares on F^2
Data / restraints / parameters	6489 / 482 / 556
Goodness-of-fit on F^2	1.064
Final R indices [I>2sigma(I)]	R1 = 0.0397, wR2 = 0.0789
R indices (all data)	R1 = 0.0715, wR2 = 0.0913
Largest and mean shift/su	0.002 and 0.000
Largest diff. peak and hole	0.58 and -0.44 e.Å^{-3}

Crystal Data for 3aa

Empirical formula	C37 H58 Fe2 K N3 O Zn
Formula weight	777.03
Temperature	150(2) K
Wavelength	0.71073 Å
Crystal system	Triclinic
Space group	P$\bar{1}$
Unit cell dimensions	a = 10.3320(7) Å α = 96.555(14)°.
	b = 12.346(2) Å β = 99.940(12)°.
	c = 16.916(4) Å γ = 109.996(9)°.
Volume	1962.0(6) Å^3
Z	2
Density (calculated)	1.315 Mg/m^3
Absorption coefficient	1.472 mm^{-1}
F(000)	820
Crystal size	0.42 x 0.40 x 0.11 mm^3
Theta range for data collection	5.2 to 25.0°.
Index ranges	-12<=h<=12, -14<=k<=14, -20<=l<=20
Reflections collected	25622
Independent reflections	6786 [R(int) = 0.0248]
Completeness to theta = 25.0°	98.0 %
Absorption correction	Semi-empirical from equivalents
Max. and min. transmission	0.8548 and 0.5768
Refinement method	Full-matrix least-squares on F^2
Data / restraints / parameters	6786 / 540 / 567
Goodness-of-fit on F^2	1.049
Final R indices [I>2sigma(I)]	R1 = 0.0300, wR2 = 0.0672
R indices (all data)	R1 = 0.0448, wR2 = 0.0752
Largest and mean shift/su	0.001 and 0.000
Largest diff. peak and hole	0.65 and -0.42 e.Å^{-3}

Crystal Data for 3ab

Empirical formula	C39 H62 K N3 O2 Ru2 Zn
Formula weight	911.53
Temperature	150(2) K
Wavelength	0.71073 Å
Crystal system	Monoclinic
Space group	$P2_1/n$
Unit cell dimensions	$a = 13.713(3)$ Å $\quad \alpha = 90°$.
	$b = 18.688(4)$ Å $\quad \beta = 103.67(3)°$.
	$c = 16.432(3)$ Å $\quad \gamma = 90°$.
Volume	4091.7(14) Å^3
Z	4
Density (calculated)	1.480 Mg/m^3
Absorption coefficient	1.447 mm^{-1}
F(000)	1880
Crystal size	0.24 x 0.24 x 0.04 mm^3
Theta range for data collection	5.1 to 25.0°.
Index ranges	-16<=h<=11, -22<=k<=16, -18<=l<=19
Reflections collected	22708
Independent reflections	7075 [R(int) = 0.0238]
Completeness to theta = 25.0°	98.1 %
Absorption correction	Semi-empirical from equivalents
Max. and min. transmission	0.9444 and 0.7227
Refinement method	Full-matrix least-squares on F^2
Data / restraints / parameters	7075 / 239 / 485
Goodness-of-fit on F^2	1.133
Final R indices [I>2sigma(I)]	R1 = 0.0260, wR2 = 0.0551
R indices (all data)	R1 = 0.0423, wR2 = 0.0643
Largest and mean shift/su	0.002 and 0.000
Largest diff. peak and hole	0.62 and -0.44 e.Å^{-3}

Crystal Data for 3ac

Empirical formula	C50 H96 Fe K2 N6 Zn2
Formula weight	1046.12
Temperature	150(2) K
Wavelength	0.71073 Å
Crystal system	Monoclinic
Space group	$P2_1/c$
Unit cell dimensions	$a = 13.846(3)$ Å $\quad \alpha = 90°$.
	$b = 27.528(6)$ Å $\quad \beta = 91.71(3)°$.
	$c = 15.551(3)$ Å $\quad \gamma = 90°$.
Volume	5924(2) Å^3
Z	4
Density (calculated)	1.173 Mg/m^3
Absorption coefficient	1.220 mm^{-1}
F(000)	2248
Crystal size	0.64 x 0.62 x 0.08 mm^3
Theta range for data collection	5.1 to 25.0°.
Index ranges	$-16 \leq h \leq 16, -32 \leq k \leq 30, -16 \leq l \leq 18$
Reflections collected	49797
Independent reflections	10334 [R(int) = 0.0341]
Completeness to theta = 25.0°	98.9 %
Absorption correction	Semi-empirical from equivalents
Max. and min. transmission	0.9087 and 0.5091
Refinement method	Full-matrix least-squares on F^2
Data / restraints / parameters	10334 / 295 / 630
Goodness-of-fit on F^2	1.046
Final R indices [I>2sigma(I)]	R1 = 0.0289, wR2 = 0.0590
R indices (all data)	R1 = 0.0457, wR2 = 0.0650
Largest and mean shift/su	0.003 and 0.000
Largest diff. peak and hole	0.39 and -0.30 e.Å^{-3}

Crystal Data for 4b

Empirical formula	C32 H68 K Mg N5
Formula weight	586.32
Temperature	123(2) K
Wavelength	0.71073 Å
Crystal system	Triclinic
Space group	P-1
Unit cell dimensions	$a = 11.4644(6)$ Å $\quad\quad \alpha = 67.916(5)°.$
	$b = 12.2312(5)$ Å $\quad\quad \beta = 85.002(5)°.$
	$c = 16.2463(10)$ Å $\quad\quad \gamma = 69.662(5)°.$
Volume	1976.89(18) Å^3
Z	2
Density (calculated)	0.985 Mg/m^3
Absorption coefficient	0.174 mm^{-1}
F(000)	652
Crystal size	0.6 x 0.35 x 0.30 mm^3
Theta range for data collection	2.97 to 29.00°.
Index ranges	-15<=h<=15, -16<=k<=16, -20<=l<=22
Reflections collected	34238
Independent reflections	10096 [R(int) = 0.0247]
Completeness to theta = 26.00°	98.3 %
Absorption correction	Semi-empirical from equivalents
Max. and min. transmission	1.00000 and 0.90425
Refinement method	Full-matrix least-squares on F^2
Data / restraints / parameters	10096 / 0 / 441
Goodness-of-fit on F^2	1.069
Final R indices [I>2sigma(I)]	R1 = 0.0559, wR2 = 0.1634
R indices (all data)	R1 = 0.0826, wR2 = 0.1743
Largest diff. peak and hole	0.444 and -0.297 e.Å^{-3}

Crystal Data for 4c

Empirical formula	C31 H69.50 K Mg N5 Si
Formula weight	603.92
Temperature	123(2) K
Wavelength	0.71073 Å
Crystal system	Monoclinic
Space group	C2/c
Unit cell dimensions	a = 11.8644(4) Å $\alpha = 90°$.
	b = 20.0291(10) Å $\beta = 95.042(4)°$.
	c = 16.2840(6) Å $\gamma = 90°$.
Volume	3854.6(3) Å^3
Z	4
Density (calculated)	1.041 Mg/m^3
Absorption coefficient	0.210 mm^{-1}
F(000)	1342
Crystal size	0.12 x 0.12 x 0.04 mm^3
Theta range for data collection	3.09 to 27.00°.
Index ranges	-15<=h<=15, -24<=k<=23, -16<=l<=20
Reflections collected	15126
Independent reflections	6223 [R(int) = 0.0574]
Completeness to theta = 26.00°	97.1 %
Absorption correction	Semi-empirical from equivalents
Max. and min. transmission	1.00000 and 0.97658
Refinement method	Full-matrix least-squares on F^2
Data / restraints / parameters	6223 / 24 / 363
Goodness-of-fit on F^2	0.827
Final R indices [I>2sigma(I)]	R1 = 0.0613, wR2 = 0.1367
R indices (all data)	R1 = 0.1201, wR2 = 0.1511
Largest diff. peak and hole	0.329 and -0.372 e.Å^{-3}

Crystal Data for 4d

Empirical formula	C27 H65 K Mg N6
Formula weight	537.26
Temperature	123(2) K
Wavelength	0.71073 Å
Crystal system	Triclinic
Space group	P-1
Unit cell dimensions	a = 10.6458(4) Å $\quad$ α = 101.999(3)°.
	b = 11.1422(4) Å $\quad$ β = 103.143(3)°.
	c = 15.9544(6) Å $\quad$ γ = 104.920(3)°.
Volume	1707.89(11) Å^3
Z	2
Density (calculated)	1.045 Mg/m^3
Absorption coefficient	0.197 mm^{-1}
F(000)	600
Crystal size	0.4 x 0.3 x 0.1 mm^3
Theta range for data collection	2.70 to 30.43°.
Index ranges	-15<=h<=14, -14<=k<=15, -22<=l<=22
Reflections collected	35521
Independent reflections	9510 [R(int) = 0.0358]
Completeness to theta = 27.00°	99.9 %
Absorption correction	Semi-empirical from equivalents
Max. and min. transmission	1.00000 and 0.97734
Refinement method	Full-matrix least-squares on F^2
Data / restraints / parameters	9510 / 0 / 353
Goodness-of-fit on F^2	1.028
Final R indices [I>2sigma(I)]	R1 = 0.0467, wR2 = 0.0939
R indices (all data)	R1 = 0.0810, wR2 = 0.1026
Largest diff. peak and hole	0.256 and -0.224 e.Å^{-3}

Crystal Data for 4e

Empirical formula	C30 H65 K Mg N6
Formula weight	573.29
Temperature	123(2) K
Wavelength	1.54180 Å
Crystal system	Monoclinic
Space group	P 21/n
Unit cell dimensions	a = 11.5825(4) Å $\alpha = 90°$.
	b = 20.8412(7) Å $\beta = 92.503(3)°$.
	c = 14.5607(5) Å $\gamma = 90°$.
Volume	3511.5(2) Å^3
Z	4
Density (calculated)	1.084 Mg/m^3
Absorption coefficient	1.684 mm^{-1}
F(000)	1272
Crystal size	0.20 x 0.14 x 0.12 mm^3
Theta range for data collection	3.71 to 73.15°.
Index ranges	-13<=h<=14, -25<=k<=25, -17<=l<=16
Reflections collected	25345
Independent reflections	6913 [R(int) = 0.0749]
Completeness to theta = 73.15°	98.1 %
Absorption correction	None
Refinement method	Full-matrix least-squares on F^2
Data / restraints / parameters	6913 / 4 / 403
Goodness-of-fit on F^2	1.030
Final R indices [I>2sigma(I)]	R1 = 0.0498, wR2 = 0.1382
R indices (all data)	R1 = 0.0618, wR2 = 0.1448
Largest diff. peak and hole	0.696 and -0.381 e.Å^{-3}

Crystal Data for 4h

Empirical formula	C27 H58 Mg N5 Na
Formula weight	500.08
Temperature	123(2) K
Wavelength	0.71073 Å
Crystal system	Monoclinic
Space group	P21/n
Unit cell dimensions	a = 14.1862(4) Å $\alpha = 90°$.
	b = 15.1005(5) Å $\beta = 97.090(3)°$.
	c = 14.6621(4) Å $\gamma = 90°$.
Volume	3116.88(16) Å^3
Z	4
Density (calculated)	1.066 Mg/m^3
Absorption coefficient	0.093 mm^{-1}
F(000)	1112
Crystal size	0.16 x 0.10 x 0.06 mm^3
Theta range for data collection	2.52 to 30.47°.
Index ranges	-18<=h<=20, -21<=k<=17, -20<=l<=20
Reflections collected	25234
Independent reflections	8635 [R(int) = 0.0370]
Completeness to theta = 29.00°	98.7 %
Absorption correction	Semi-empirical from equivalents
Max. and min. transmission	1.00000 and 0.99393
Refinement method	Full-matrix least-squares on F^2
Data / restraints / parameters	8635 / 0 / 317
Goodness-of-fit on F^2	0.949
Final R indices [I>2sigma(I)]	R1 = 0.0475, wR2 = 0.0931
R indices (all data)	R1 = 0.0987, wR2 = 0.1045
Largest diff. peak and hole	0.428 and -0.183 e.Å^{-3}

Crystal Data for 4j

Empirical formula	C35 H70 K Mg N5 O Si
Formula weight	668.46
Temperature	150(2) K
Wavelength	0.71073 Å
Crystal system	Orthorhombic
Space group	Pbca
Unit cell dimensions	$a = 18.702(11)$ Å $\quad \alpha = 90°$.
	$b = 20.462(16)$ Å $\quad \beta = 90°$.
	$c = 22.053(16)$ Å $\quad \gamma = 90°$.
Volume	8439(10) Å^3
Z	8
Density (calculated)	1.052 Mg/m^3
Absorption coefficient	0.199 mm^{-1}
F(000)	2944
Crystal size	0.14 x 0.14 x 0.01 mm^3
Theta range for data collection	3.9 to 25.0°.
Index ranges	-22<=h<=22, -23<=k<=21, -23<=l<=26
Reflections collected	31479
Independent reflections	7144 [R(int) = 0.1437]
Completeness to theta = 25.00°	96.5 %
Absorption correction	Semi-empirical from equivalents
Max. and min. transmission	0.9980 and 0.9726
Refinement method	Full-matrix least-squares on F^2
Data / restraints / parameters	7144 / 0 / 413
Goodness-of-fit on F^2	1.136
Final R indices [I>2sigma(I)]	R1 = 0.1078, wR2 = 0.1862
R indices (all data)	R1 = 0.1944, wR2 = 0.2257
Largest diff. peak and hole	0.44 and -0.53 e.Å^{-3}

Crystal Data for 4k

Empirical formula	C29 H59 K Mg N4 O Si
Formula weight	571.30
Temperature	150(2) K
Wavelength	0.71073 Å
Crystal system	Monoclinic
Space group	$P2_1/n$
Unit cell dimensions	$a = 11.564(2)$ Å $\quad \alpha = 90°$.
	$b = 17.538(4)$ Å $\quad \beta = 91.61(3)°$.
	$c = 18.308(4)$ Å $\quad \gamma = 90°$.
Volume	3711.4(13) Å^3
Z	4
Density (calculated)	1.022 Mg/m^3
Absorption coefficient	0.216 mm^{-1}
F(000)	1256
Crystal size	0.18 x 0.14 x 0.03 mm^3
Theta range for data collection	3.9 to 25.0°.
Index ranges	-13<=h<=13, -20<=k<=20, -21<=l<=21
Reflections collected	22813
Independent reflections	6403 [R(int) = 0.1286]
Completeness to theta = 25.00°	98.4 %
Absorption correction	Semi-empirical from equivalents
Max. and min. transmission	0.9935 and 0.9621
Refinement method	Full-matrix least-squares on F^2
Data / restraints / parameters	6403 / 558 / 347
Goodness-of-fit on F^2	1.065
Final R indices [I>2sigma(I)]	R1 = 0.0908, wR2 = 0.1446
R indices (all data)	R1 = 0.1983, wR2 = 0.1815
Largest and mean shift/su	0.001 and 0.000
Largest diff. peak and hole	0.36 and -0.31 e.Å^{-3}

Crystal Data for 4l

Empirical formula	C34 H66 K Mg N5 O
Formula weight	624.33
Temperature	150(2) K
Wavelength	1.54178 Å
Crystal system	Orthorhombic
Space group	Pca2$_1$
Unit cell dimensions	a = 22.1578(13) Å α = 90°.
	b = 20.4943(13) Å β = 90°.
	c = 16.9487(13) Å γ = 90°.
Volume	7696.5(9) Å^3
Z	8
Density (calculated)	1.078 Mg/m^3
Absorption coefficient	1.588 mm^{-1}
F(000)	2752
Crystal size	0.22 x 0.06 x 0.02 mm^3
Theta range for data collection	2.2 to 66.7°.
Index ranges	-25<=h<=26, -22<=k<=24, -17<=l<=19
Reflections collected	21432
Independent reflections	9566 [R(int) = 0.0835]
Completeness to theta = 66.8°	98.4 %
Absorption correction	Semi-empirical from equivalents
Max. and min. transmission	0.9689 and 0.7214
Refinement method	Full-matrix least-squares on F^2
Data / restraints / parameters	9566 / 1322 / 786
Goodness-of-fit on F^2	0.865
Final R indices [I>2sigma(I)]	R1 = 0.0688, wR2 = 0.1593
R indices (all data)	R1 = 0.1477, wR2 = 0.1898
Largest and mean shift/su	0.001 and 0.000
Largest diff. peak and hole	0.67 and -0.48 e.Å^{-3}

Crystal Data for 5k

Empirical formula	C23 H51 Al Li N3
Formula weight	403.59
Temperature	123(2) K
Wavelength	0.71073 Å
Crystal system	Monoclinic
Space group	P21/n
Unit cell dimensions	a = 10.3165(4) Å $\alpha = 90°$.
	b = 15.3891(6) Å $\beta = 105.505(4)°$.
	c = 17.0248(7) Å $\gamma = 90°$.
Volume	2604.52(18) Å^3
Z	4
Density (calculated)	1.029 Mg/m^3
Absorption coefficient	0.090 mm^{-1}
F(000)	904
Crystal size	0.52 x 0.50 x 0.40 mm^3
Theta range for data collection	2.48 to 27.10°.
Index ranges	-13<=h<=13, -17<=k<=19, -21<=l<=21
Reflections collected	23211
Independent reflections	5742 [R(int) = 0.0441]
Completeness to theta = 27.10°	99.8 %
Absorption correction	Semi-empirical from equivalents
Max. and min. transmission	0.965 and 0.815
Refinement method	Full-matrix least-squares on F^2
Data / restraints / parameters	5742 / 0 / 287
Goodness-of-fit on F^2	0.999
Final R indices [I>2sigma(I)]	R1 = 0.0457, wR2 = 0.1053
R indices (all data)	R1 = 0.0785, wR2 = 0.1136
Largest diff. peak and hole	0.337 and -0.242 e.Å^{-3}

Crystal Data for 5l

Empirical formula	C26 H58 Al Li N4
Formula weight	460.68
Temperature	123(2) K
Wavelength	0.71073 Å
Crystal system	Monoclinic
Space group	Pbca
Unit cell dimensions	a = 10.578(2) Å $\alpha = 90°$.
	b = 17.746(4) Å $\beta = 90°$.
	c = 31.598(6) Å $\gamma = 90°$.
Volume	5932(2) Å^3
Z	8
Density (calculated)	1.032 Mg/m^3
Absorption coefficient	0.087 mm^{-1}
F(000)	2064
Crystal size	? x ? x ? mm^3
Theta range for data collection	2.59 to 30.39°.
Index ranges	-14<=h<=8, -24<=k<=18, -27<=l<=44
Reflections collected	15905
Independent reflections	6863 [R(int) = 0.0523]
Completeness to theta = 30.39°	76.5 %
Absorption correction	None
Refinement method	Full-matrix least-squares on F^2
Data / restraints / parameters	6863 / 0 / 301
Goodness-of-fit on F^2	1.650
Final R indices [I>2sigma(I)]	R1 = 0.1550, wR2 = 0.3631
R indices (all data)	R1 = 0.2862, wR2 = 0.3889
Largest diff. peak and hole	0.896 and -0.326 e.Å^{-3}

Crystal Data for 5m

Empirical formula	C34 H78 Al Li N6
Formula weight	604.94
Temperature	123(2) K
Wavelength	1.54180 Å
Crystal system	Monoclinic
Space group	P 21/c
Unit cell dimensions	a = 14.3637(6) Å $\alpha = 90°$.
	b = 10.4038(4) Å $\beta = 92.876(4)°$.
	c = 26.9515(11) Å $\gamma = 90°$.
Volume	4022.5(3) Å^3
Z	4
Density (calculated)	0.999 Mg/m^3
Absorption coefficient	0.634 mm^{-1}
F(000)	1360
Crystal size	0.50 x 0.40 x 0.35 mm^3
Theta range for data collection	6.12 to 61.65°.
Index ranges	-16<=h<=16, -11<=k<=11, -29<=l<=30
Reflections collected	18254
Independent reflections	6138 [R(int) = 0.0290]
Completeness to theta = 61.65°	97.9 %
Absorption correction	Semi-empirical from equivalents
Max. and min. transmission	1.00000 and 0.49957
Refinement method	Full-matrix least-squares on F^2
Data / restraints / parameters	6138 / 0 / 455
Goodness-of-fit on F^2	1.032
Final R indices [I>2sigma(I)]	R1 = 0.0624, wR2 = 0.1668
R indices (all data)	R1 = 0.0780, wR2 = 0.1745
Largest diff. peak and hole	0.351 and -0.172 e.Å^{-3}

Crystal Data for 5n

Empirical formula	C26 H58 Al N4 Na
Formula weight	476.73
Temperature	123(2) K
Wavelength	0.71073 Å
Crystal system	Monoclinic
Space group	P 1 21/n 1
Unit cell dimensions	$a = 10.5999(3)$ Å $\alpha = 90°$.
	$b = 15.7675(4)$ Å $\beta = 92.700(2)°$.
	$c = 18.2169(4)$ Å $\gamma = 90°$.
Volume	3041.28(13) Å^3
Z	4
Density (calculated)	1.041 Mg/m^3
Absorption coefficient	0.100 mm^{-1}
F(000)	1064
Crystal size	0.42 x 0.34 x 0.20 mm^3
Theta range for data collection	2.58 to 29.69°.
Index ranges	-14<=h<=14, -21<=k<=21, -25<=l<=24
Reflections collected	29534
Independent reflections	7829 [R(int) = 0.0407]
Completeness to theta = 27.50°	99.8 %
Absorption correction	Semi-empirical from equivalents
Max. and min. transmission	1.0000 and 0.8618
Refinement method	Full-matrix least-squares on F^2
Data / restraints / parameters	7829 / 0 / 325
Goodness-of-fit on F^2	1.013
Final R indices [I>2sigma(I)]	R1 = 0.0443, wR2 = 0.1020
R indices (all data)	R1 = 0.0765, wR2 = 0.1104
Largest diff. peak and hole	0.328 and -0.206 e.Å^{-3}

Crystal Data for 5p

Empirical formula	C23 H51 Al K N3
Formula weight	435.75
Temperature	123(2) K
Wavelength	1.54180 Å
Crystal system	Triclinic
Space group	P -1
Unit cell dimensions	a = 11.5698(9) Å $\quad$ $\alpha = 80.845(7)°$.
	b = 11.9773(9) Å $\quad$ $\beta = 68.551(8)°$.
	c = 12.2821(10) Å $\quad$ $\gamma = 62.341(8)°$.
Volume	1403.0(2) Å^3
Z	2
Density (calculated)	1.031 Mg/m^3
Absorption coefficient	2.030 mm^{-1}
F(000)	484
Crystal size	0.78 x 0.78 x 0.60 mm^3
Theta range for data collection	5.00 to 61.45°.
Index ranges	-13<=h<=13, -13<=k<=13, -12<=l<=13
Reflections collected	11013
Independent reflections	4263 [R(int) = 0.0402]
Completeness to theta = 61.45°	98.1 %
Absorption correction	Semi-empirical from equivalents
Max. and min. transmission	1.00000 and 0.03649
Refinement method	Full-matrix least-squares on F^2
Data / restraints / parameters	4263 / 0 / 288
Goodness-of-fit on F^2	1.077
Final R indices [I>2sigma(I)]	R1 = 0.0435, wR2 = 0.1187
R indices (all data)	R1 = 0.0463, wR2 = 0.1202
Largest diff. peak and hole	0.750 and -0.406 e.Å^{-3}

Crystal Data for 5u

Empirical formula	C30 H68 Al K N4
Formula weight	550.96
Temperature	123(2) K
Wavelength	1.54180 Å
Crystal system	Orthorhombic
Space group	Pna2(1)
Unit cell dimensions	$a = 16.505(3)$ Å $\quad \alpha = 90°$.
	$b = 11.562(3)$ Å $\quad \beta = 90°$.
	$c = 18.948(4)$ Å $\quad \gamma = 90°$.
Volume	3616.0(14) Å^3
Z	4
Density (calculated)	1.012 Mg/m^3
Absorption coefficient	1.665 mm^{-1}
F(000)	1232
Crystal size	0.4 x 0.3 x 0.05 mm^3
Theta range for data collection	6.59 to 64.98°.
Index ranges	-19<=h<=19, -12<=k<=13, -13<=l<=22
Reflections collected	8896
Independent reflections	4713 [R(int) = 0.0896]
Completeness to theta = 64.98°	96.2 %
Absorption correction	Semi-empirical from equivalents
Max. and min. transmission	1.00000 and 0.77546
Refinement method	Full-matrix least-squares on F^2
Data / restraints / parameters	4713 / 6 / 340
Goodness-of-fit on F^2	0.948
Final R indices [I>2sigma(I)]	R1 = 0.0773, wR2 = 0.1956
R indices (all data)	R1 = 0.1578, wR2 = 0.2561
Largest diff. peak and hole	0.661 and -0.879 e.Å^{-3}

Crystal Data for 5v

Empirical formula	C28 H64 Al K N4
Formula weight	522.91
Temperature	123(2) K
Wavelength	0.71073 Å
Crystal system	Monoclinic
Space group	P 21/n
Unit cell dimensions	a = 11.3887(5) Å $\quad\quad$ $\alpha = 90°$.
	b = 18.1965(8) Å $\quad\quad$ $\beta = 105.222(5)°$.
	c = 16.9006(8) Å $\quad\quad$ $\gamma = 90°$.
Volume	3379.5(3) Å^3
Z	4
Density (calculated)	1.028 Mg/m^3
Absorption coefficient	0.204 mm^{-1}
F(000)	1168
Crystal size	0.37 x 0.44 x 0.47 mm^3
Theta range for data collection	2.92 to 25.97°.
Index ranges	-13<=h<=13, -20<=k<=22, -16<=l<=20
Reflections collected	18993
Independent reflections	6485 [R(int) = 0.0446]
Completeness to theta = 25.97°	98.1 %
Absorption correction	Semi-empirical from equivalents
Max. and min. transmission	1.00000 and 0.27032
Refinement method	Full-matrix least-squares on F^2
Data / restraints / parameters	6485 / 0 / 336
Goodness-of-fit on F^2	0.985
Final R indices [I>2sigma(I)]	R1 = 0.0513, wR2 = 0.1234
R indices (all data)	R1 = 0.0615, wR2 = 0.1268
Extinction coefficient	0.056(3)
Largest diff. peak and hole	0.482 and -0.328 e.Å^{-3}

Crystal Data for 5w

Empirical formula	C27 H68 Al K N4 Si2
Formula weight	571.11
Temperature	123(2) K
Wavelength	0.71073 Å
Crystal system	Monoclinic
Space group	P21/n
Unit cell dimensions	$a = 11.5276(6)$ Å $\quad \alpha = 90°$.
	$b = 18.4028(8)$ Å $\quad \beta = 93.669(5)°$.
	$c = 17.3602(9)$ Å $\quad \gamma = 90°$.
Volume	3675.2(3) Å^3
Z	4
Density (calculated)	1.032 Mg/m^3
Absorption coefficient	0.254 mm^{-1}
F(000)	1272
Crystal size	0.18 x 0.10 x 0.05 mm^3
Theta range for data collection	3.03 to 29.00°.
Index ranges	-15<=h<=15, -25<=k<=25, -23<=l<=23
Reflections collected	49892
Independent reflections	9769 [R(int) = 0.0786]
Completeness to theta = 29.00°	99.9 %
Absorption correction	Semi-empirical from equivalents
Max. and min. transmission	1.00000 and 0.96303
Refinement method	Full-matrix least-squares on F^2
Data / restraints / parameters	9769 / 0 / 334
Goodness-of-fit on F^2	0.796
Final R indices [I>2sigma(I)]	R1 = 0.0414, wR2 = 0.0887
R indices (all data)	R1 = 0.0843, wR2 = 0.0984
Extinction coefficient	0.0176(6)
Largest diff. peak and hole	0.537 and -0.566 e.Å^{-3}

Overview, Conclusions, and Outlook

This PhD programme set out to extend the alkali-metal-mediated metallation strategy towards potassium-based reagents as the main target. Initial objectives of isolating and characterising suitable homometallic potassium precursors were met in the form of KCH_2SiMe_3 (**2a**), which could be synthesised in impressive yields with a high degree of purity. The successful generation of the PMDETA-solvate $[PMDETA \cdot KCH_2SiMe_3]_\infty$ (**2b**), and the related potassium-TMP complex $[PMDETA \cdot K(TMP)]_2$ (**2e**), allow for potassium-mediated metallations to be studied without the fear of an impure homometallic starting reagent, a problem which has hampered the use of this extremely reactive metal in synthesis in the past.

Lagging well behind the much studied lithium– and sodium–mediated zincation methodologies, potassium-zincate chemistry has been meagerly studied by comparison. Within this investigation, a systematic study revealed a series of potassium–dialkyl–TMP–zincate bases which could be synthesised *via* a simple cocomplexation approach combining (cocomplexing) the potassium amide **2e** with PMDETA and the relevant dialkylzinc reagent. These zincates could be isolated, structurally defined and characterised by NMR spectroscopic techniques. The work carried out within this investigation has already alluded to related research on zincate systems carried out by Dr. Jan Klett within our research group. Dr. Klett recently isolated the zincate base of formula $[PMDETA \cdot K(\mu\text{-}TMP)(\mu\text{-}CH_2SiMe_3)Zn(CH_2SiMe_3)]$ (utilising the same cocomplexation approach noted within this thesis), which remarkably deprotonates THF generating the complex $[PMDETA \cdot K(\mu\text{-}TMP)(\mu\text{-}C_5H_7O)Zn(CH_2SiMe_3)]$, stopping the problematic issue of ether cleavage in its tracks. This astonishing result was published in the highly prestigious *Science* journal in late 2009 (reference: A. R. Kennedy, J. Klett, R. E. Mulvey, D. S. Wright, *Science* **2009**, *326*, 706).

Potassium-mediated zincation has been studied in the context of pyridine metallation chemistry, using base $[PMDETA \cdot K(\mu\text{-}TMP)(\mu\text{-}Et)Zn(Et)]$ (**3b**) in most cases. Prior to this work, only one structural example of a zincated pyridine was present in the literature, synthesised through a pre-lithiation step and therefore classed as an indirect zincation. By utilising a potassium–diethyl–TMP–zincate base, zinc has been delivered regioselectively and directly to the 2-position of the

296

heterocyclic ring in substituted 4-R-pyridines, in which R is Me_2N, ^tBu, or Ph, but the new methodology is less successful when R is H, Et, or ^iPr, because mixtures of ring- and laterally zincated complexes are produced. When R is OMe, a completely different step-ladder type structural motif is generated via direct zincation at the alternative 3-position of the ring. Seven of the zincated pyridine intermediate (that is, existing before any electrophilic quenching protocol) complexes have been structurally defined here by single-crystal X-ray crystallography and NMR spectroscopy, were found to share a dimeric motif in which a central diazadicarbadizinca $(ZnCN)_2$ dianionic ring is capped on either side by a PMDETA-wrapped K^+ cation. The coordinative saturation of the distorted tetrahedral Zn centre within these structures appears to be a major factor in the inhibition of a subsequent alkyl–amine/alkane–amido ligand transfer that is commonly observed in lithium– and sodium–dialkyl–TMP–zincate reactions. An interesting aspect to note is that substituting the Me_2N substituent (in **3k**) for the isoelectronic MeO functional group (in **3p**), not only redirects the orientation of the zincation reaction, it also reprograms the pyridine to function as a nitrogen σ-donor towards potassium, and consequently rebuffing zinc. Also, this reveals the accessibility of the O lone pairs and the inaccessibility of the NMe_2 lone pair due to conjugation with the aromatic π-system. There is great scope for these potassium zincate bases to act towards other C=N containing substrates, such as quinolines, isoquinolines, pyrazines and imines for example. Also, perhaps the potassium atoms could be removed from the core structure by incorporating crown ethers or the alkali-metal could be replaced with other metals (such as rubidium, in a transmetallation procedure with RbO^tBu), potentially forming new structural motifs.

Ferrocene and ruthenocene can be readily monozincated by potassium-mediated zincation (KMZ*n*). The role of potassium in the aggregation of monomer units of the structures $[\{PMDETA \cdot K(\mu\text{-}Me)_2Zn(Fc)\}_\infty]$ (**3u**) and $[\{PMDETA \cdot K(\mu\text{-}Me)_2Zn(Rc)\}_2]$ (**3v**) is critical. Interacting with the zincated ferrocene Cp ring in a η^5-π-contact manner results in a supramolecular step-ladder, whereas dimerisation is the aggregation of choice with the monozincated ruthenocene compound *via* a combination of η^1 (Cp) and C(Me) intermolecular contacts to K. Dizincation of ferrocene can also be realised by KMZ*n*, with zincate $[PMDETA \cdot K(\mu\text{-}TMP)(\mu\text{-}^tBu)Zn(^tBu)]$ (**3e**) acting as an amido base towards the metallocene. The solvent choice in these deprotonation reactions is crucial. It has been shown that the addition of

THF to bulk hexane reaction mixtures (involving the bases **3b**, **3d** and **3e** and the substrates ferrocene or ruthenocene) results in the formation of bis-(monozincated metallocene) complexes as a co-product, therefore only hexane should be used when the target complex contains only one molecule of monozincated metallocene. The profound influence of potassium on these unique structures calls for a future systematic study of how alkali metals can influenece the supramolecularity of alkali-metal-mediated metallated (by Zn, Mg, Mn *etc.*) metallocenes.

An observation noted within KM*Zn* chemistry is that potassium zincate bases act as amido bases. This contrasts with the sodium-mediated zincation work with the base [TMEDA·Na(μ-TMP)(μ-^{t}Bu)Zn(^{t}Bu)] which ultimately (thermodynamically) acts as an alkyl base towards substrates, as noted in Chapter 1 (pages 41-43). Therefore, a much detailed study should be directed at the base **3e,** the PMDETA·K equivalent, to observe potential different reactivity and associated structural changes.

The synthesis, isolation and characterisation of the potassium magnesiate bases [PMDETA·K(μ-TMP)(μ-^{n}Bu)Mg(TMP)] (**4b**) and [PMDETA·K(μ-TMP)(μ-CH$_2$SiMe$_3$)Mg(TMP)] (**4c**) represent pivotal progress in potassium-mediated magnesiation chemistry. The structural tracking and time-dependent NMR studies of the KM*Mg* of anisole and *N, N*-diisopropylbenzamide carried out here represents the most complete study of any alkali-metal-mediated metallation to date, and has greatly improved fundamental knowledge of how such reactions operate (that is, by a two-step pathway as seen in AMM*Zn* chemistry) and will help towards the rational design of new synthetic applications in the future. An important consideration that this study brings out is that the timing of any subsequent electrophilic quench of the base-substrate reaction mixture may be critical to the outcome given the presence of different *ortho*-magnesiated products, though both products isolated here [(PMDETA)·K(μ-TMP)(*o*-C$_6$H$_4$OMe)Mg(CH$_2$SiMe$_3$)] (**4k**) and [(PMDETA)·K(μ-TMP)(*o*-C$_6$H$_4$OMe)Mg(TMP)] (**4l**) should yield the same functionalised arene product on electrophilic quenching.

Further detailed NMR studies on the mechanism of base **4b** and [(TMEDA)·Na(μ-TMP)(μ-^{n}Bu)Mg(TMP)] (**1a**) would be desirable to ascertain these bases acts like **4c** (where liquid Me$_4$Si is eliminated in the final step), in a two-step manner, affording a closer comparison for the

sodium-magnesium work, where it has always been assumed that a one-step, gaseous alkane (*n*-butane) elimination occurs with the base **1a** towards a variety of organic substrates (see Chapter 1, pages 37-40).

Lithium TMP aluminates can function as dual TMP/alkyl [for ^{i}Bu$_3$Al-(TMP)Li] or as mono amido bases [for ^{i}Bu$_2$Al(TMP)$_2$Li] exhibiting two-fold or single-fold AMM*Al* (alkali-metal-mediated alumination), respectively, toward TMEDA or PMDETA. On their own, ^{i}Bu$_3$Al or ^{i}Bu$_2$Al(TMP) are not sufficiently strong bases to metallate the relatively non-acidic TMEDA or PMDETA, so in [Li{Me$_2$NCH$_2$CH$_2$N(Me)CH$_2$}$_2$Al(^{i}Bu)$_2$] **(5q)**, [Li{Me$_2$NCH$_2$CH$_2$N(Me)CH$_2$}(TMP)Al(^{i}Bu)$_2$] **(5k)**, [Li{Me$_2$NCH$_2$CH$_2$N(Me)CH$_2$CH$_2$N(Me)CH$_2$}(TMP)Al(^{i}Bu)$_2$] **(5l)**, and [Na{Me$_2$NCH$_2$CH$_2$N(Me)CH$_2$CH$_2$N(Me)CH$_2$}(TMP)Al(^{i}Bu)$_2$] **(5n)** the R-deprotonations of TMEDA and PMDETA are synergic based, as the intramolecular communication between lithium (sodium for **5n**) and aluminium appears to activate the TMP and ^{i}Bu bases. It has also been established that by using AMM*Al* the normal patterns of reactivity can be reversed with a TMEDA nonacidic C-H bond breaking in preference to an acidic TMP(H) N-H bond. This special behavior can be attributed to intramolecular proximity effects between the active base component (TMP or ^{i}Bu) and the ligating TMEDA molecule. Remarkably the TMP anion can be metallated for a second time, unprecedented in the long 40 year history of TMP chemistry, using sodium- or potassium-TMP with ^{i}Bu$_2$Al(TMP) in the presence of TMEDA to generate the TMP* products [(TMEDA)·K(μ-TMP*)(μ-^{i}Bu)Al(^{i}Bu)] **(5p)** and [(TMEDA)·Na(μ-TMP*)(μ-^{i}Bu)Al(^{i}Bu)] **(5o)** respectively. Following these precedents, other unlikely dianion or deprotonated ligand complexes should be achievable using the correct metal/ligand combinations, as these bimetallic motifs seem ideal for carrying out special intramolecular reactions.

There is whole range of parameters that could be studied with regard to these alkali-metal bis(amido)-bis(alkyl)aluminates. For example, the donor ligand could be replaced for monodentate ligands, such as THF for example, in one or more molar equivalents to generate compounds with a mixed bound and metallated donor system. Also, utilising one molar equivalent of a monodentate ligand and one molar equivalent of a different substrate could lead

to structural evidence of direct aluminations not seen previously. The amines used in these systems could be replaced or mixed (only TMP has been studied within this investigation) with a chiral amide (such as DMP) or other amides (such as DA). Using the two examples suggested could potentially generate dianionic species akin to **5p** and **5o** as they both contain βCH_3 groups. Enantioselective synthesis could potentially be developed using a mixture of chiral and achiral amides in these alkali-metal bis(amido)-bis(alkyl)aluminates, as an amide bridge between the two metals appears necessary (TMP in all cases mentioned here), thus the chiral amide may be active towards a range of substrates (if for example paired with TMP).

 The isolation and charcterisation of the dianion **5o** opens the question whether even a trianion of TMP is possible. Perhaps synthesising the homometallic aluminium compound $TMP_2Al(R)$ (R = alkyl group, for example ^tBu or ^nBu) and reacting this bis(amido)-mono(alkyl)alumane with TMEDA and KTMP may achieve the previously unthinkable existence of a trianionic TMP species.

With respect to the homometallic starting reagent $(TMP)Al(^iBu)_2$, no structural information is known on mono-TMP bis-alkyl alumanes. Thus, by adding half a molar equivalent of a "synergic spacer" in the form of DABCO (DABCO = 1,4-diazabicyclo[2.2.2]octane) to this alumane could provide a structural framework to isolated crystalline material, as the alumane itself is an oil. Although the alumane has been shown to act as a mild base in a handful of studies, perhaps a synergic spacer could also activate the TMP group to react as a strong base towards substates.

Despite previous unsuccessful attempts to isolate mono-amido/tri-alkyl potassium aluminate bases, this investigation revealed a successful route to these types of aluminates. Utilising **2b**, TMP, DMP, and HMDS variations could be generated (from the cocomplexation of the potassium amide with PMDETA and $^iBu_3Al$), isolated and then characterised by X-ray and NMR spectroscopic techniques. The next stage in the development of these potassium aluminates would be to access how these complexes react with organic substrates. Do these aluminates act as amido or alkyl bases (or both), or do they even react at all, as [THF·Li(μ-TMP)(μ-^iBu)Al(^iBu)$_2$] was found to be wholly ineffective against *N, N*-diisopropylbenzamide; whereas in marked contrast [TMEDA·Na(μ-TMP)(μ-^iBu)Al(^iBu)$_2$] smoothly deprotonates phenylacetylene.

300

In summary, the concept of potassium-mediated metallation chemistry has been successfully applied to zinc, magnesium, and aluminium. Revealing regioselective deprotonations, mechanistic studies, new structural motifs, and the generation of previously unthinkable compounds, the work presented in this thesis has shown that potassium ate methodologies can deviate substantially from lithium and sodium ate chemistry, even though potassium sits directly below these metals in Group 1 of the periodic table. A plethora of avenues are yet to be explored with respect to potassium zincates, magnesiates, and aluminates, and should be extendable to other metals, such as the rapidly developing transition metal ate chemistry within our own research group.